
2010 NRL REVIEW

POWER
N
SYNERGY
R
G
Y



NAVAL RESEARCH LABORATORY
Washington, DC

NRL'S MISSION

To conduct a broadly based multidisciplinary program of scientific research and advanced technological development directed toward maritime applications of new and improved materials, techniques, equipment, systems, and ocean, atmospheric, and space sciences and related technologies.

The Naval Research Laboratory provides primary in-house research for the physical, engineering, space, and environmental sciences; broadly based applied research and advanced technology development programs in response to identified and anticipated Navy and Marine Corps needs; broad multidisciplinary support to the Naval Warfare Centers; and space and space systems technology, development, and support.

VIEW FROM THE TOP



DR. JOHN A. MONTGOMERY
Director of Research

CAPT PAUL C. STEWART, USN
Commanding Officer

NRL

is all about our people: the scientists, the engineers, and the support personnel who enable the Lab's research every day. They serve a vital role for the Department of the Navy, the Department of Defense, and the nation. They have a deep and broad understanding of the physical and engineering sciences, and of the operational needs of the U.S. Navy and Marine Corps. They explore today's unknowns of science to create tomorrow's new capabilities, some of which may prove to have a revolutionary impact on the future of the Navy and even the world. NRL's pioneering contributions to what is now the Global Positioning System is but one example of this.

NRL's scientists and engineers are highly respected and widely known throughout the world's scientific communities. They are the recipients of prestigious recognitions and awards, serve on influential boards and panels of scientific societies, government committees, and multinational scientific and engineering bodies that represent important Navy, DoD, and U.S. interests. They are truly the DoN's window on the world's science, with over 1100 scientific publications a year, nearly 1200 collaborations with colleges and universities around the world, and 1500 conference attendees or speakers each year. This robust level of participation is essential both to harvesting the rest of the world's science, which is growing rapidly, and to preventing technological surprise. Sustaining this workforce and preparing it for the future is essential if NRL is to continue to support the Navy as well in the future as it has in the past. This is a major area of focus for us as the Lab's leadership.

Today we are at the conjunction of three trends — the retirement of the post-Sputnik generation, the decline in clearance-eligible scientists and engineers (S&Es), and a diminishing of U.S. technological dominance due to the globalization of R&D and migration of the world's scientific/technical intellectual centroid towards Asia. The combination of these factors has made the development and growth of our workforce a critical requirement if the Navy's Corporate Laboratory is to provide revolutionary scientific and engineering products essential to meeting Naval requirements in an uncertain future. To meet this challenge we have embarked on a series of programs to encourage the growth and maturation of potential future NRL scientists and engineers.

We are making concerted efforts to reach out and encourage more students to enter the scientific, technical, engineering, and mathematics (STEM) fields. To this end, NRL has brought 399 students on board as employees, tutored another 544, and mentored another 25. We have maintained a vigorous postdoctoral researcher program with the National Research Council and the American

Society of Engineering Education, with 162 postdocs onboard during the past year. They are extremely productive scientifically, and are an exceptionally valuable source of new hires upon completion of their tenure.

The U.S. Congress has also recognized the need to reinvigorate the S&E workforce across the DoD laboratories by giving us effective new personnel management authorities. These include the direct hire authority and the Section 219 authorities of the 2009 National Defense Authorization Act. Under the Section 219 authority, funds have been made available to hire Karles Fellows, so-named in honor of renowned scientists Drs. Jerome and Isabella Karle, recipients of the Nobel Prize in chemistry and the National Medal of Science, respectively.

The Jerome and Isabella Karle Distinguished Scholar Fellowship program provides for hiring highly accomplished scientists and engineers at any degree level, within one year of receiving the degree, who have a GPA of at least 3.5/4.0, and it provides funds under the Section 219 authorities to pay their salaries for two years. They are hired to conduct a specific program of research appropriate to their individual scientific/engineering skills and research interests and the NRL division that has hired them. Two years provide sufficient time for new researchers to develop programs of their own, establish credentials based on accomplishments during the Fellowship, and integrate themselves into the Naval research community. In addition, Karles Fellowships will be available to superior NRL postdoctoral researchers if hired immediately upon completion of their postdoctoral appointments. So far we have hired 37 Karles Fellows. The average GPA for our Karles Fellows with advanced degrees has been 3.85/4.0 and they are students of high distinction from superb graduate programs across the country.

The direct hire authority has given NRL a streamlined, accelerated hiring process that has allowed us to provide firm job offers to candidates with advanced technical degrees in only 15 days on average, an astoundingly rapid time period compared with the government-wide average. In 2010 we had authority for 36 direct hires and for 2011 we have been authorized 93. Through these and other initiatives, the average age of the NRL S&E workforce has declined by more than a year, establishing an important new trend.

The Navy and the Marine Corps, within the Department of the Navy, are experiencing a time of unprecedented challenges fiscally, militarily, and technically. Fortunately the resolve to sustain our scientific and technical endeavors in the face of an uncertain future has held firm. The prospects for advancement in science and technology in support of our warfighters have never been more promising and, through our strengthening workforce, we will strive to see it realized. If history is any indication, the NRL will succeed.



p. 20



our people MAKE A BIG DIFFERENCE

p. 2

2010 NRL REVIEW



p. 16

FEATURES

- 2 Our People Make a Big Difference
- 7 Advances in Power and Energy Research at NRL
- 11 10 NRL-led Space Experiments Launched in 2009
- 16 The Ion Tiger Fuel Cell Unmanned Air Vehicle
- 19 Dr. Bhakta Rath Receives Honors of the Padma Bhushan Award
- 20 NRL Breaks Ground for Its Laboratory for Autonomous Systems Research
- 23 Father of GPS Inducted into the National Inventors Hall of Fame

THE NAVAL RESEARCH LABORATORY

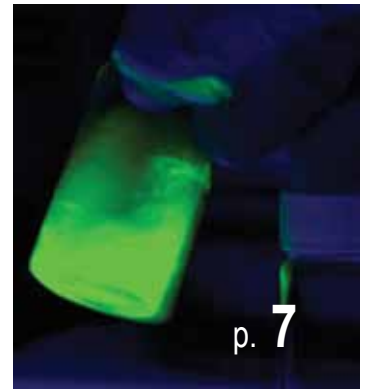
- 28 NRL – Our Heritage
- 29 Highlights of NRL Research in 2009
- 41 NRL Today

FEATURED RESEARCH

- 88 **What a Drag...But We Might Have the Cure**
Marine Biofouling: Grasping Barnacle Cement Curing from the Inside Out
- 97 **Let's show 'em what we're made of**
Structure–Property Relationships in a 3D Polycrystalline Microstructure
- 104 **It's Alive!...Sort of**
Monitoring Enzyme Activity with Hybrid Semiconductor Quantum Dot–Fluorescent Protein Assemblies
- 113 **Seismic Oceanography Allows a New View of the Ocean**
Seismic Oceanography — A New View of the Ocean
- 122 **Looking Hurricanes in the Eye**
The Impact of Ice Nuclei Concentration on Hurricane Modeling



p. 19



p. 7



p. 23



p. 11

RESEARCH ARTICLES

acoustics

- 132 Measurements and Modeling of Acoustic Scattering from Unexploded Ordnance (UXO) in Shallow Water
- 134 Scalable Wideband Frequency-Response for Free-Field, Littoral, and Seismic Applications

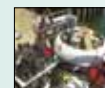
ON THE COVER



XFC – NRL's eXperimental Fuel Cell unmanned aerial vehicle.



Methane hydrates – frozen mixtures of water and hydrocarbon gas.



Field testing an oceanographic mooring powered by a benthic microbial fuel cell.



NIKE laser is a large angularly multiplexed KrF system that uses controlled spatial incoherence to achieve very uniform illumination of targets.

atmospheric science and technology

- 140** Optical Depth Assimilation for Operational Dust and Pollution Prediction
- 142** Measurements of Water Vapor from the Lower Stratosphere to the Upper Mesosphere
- 143** Long-Range Optical Communications Link

chemical/biochemical research

- 148** Elastomer-Steel Laminate Armor
- 151** Contaminant Monitoring in Ground and Surface Water
- 153** Synfuel from Seawater

electronics and electromagnetics

- 156** Improvements to Towed Decoys to Enhance Aircraft Survivability
- 159** Adaptive Jamming Cancellation in Radar
- 162** Laser System for Protection of Navy Ships
- 165** Particle Filters for Multipath Mitigation
- 167** A New Gallium Nitride-based Switch for High Efficiency Power Electronics

information technology and communications

- 172** CT-Analyst® Deployed for the 2009 Presidential Inauguration
- 174** Beyond-line-of-sight Tactical Communications Relay (BTCR)
- 176** Coastal Environmental Hyperspectral Imaging from the Space Station

materials science and technology

- 180** Nanostructured Magnets for Improved Energy Efficiency
- 181** High Performance Antireflection Structured IR Fibers
- 183** Broad-Spectrum Pathogen Surveillance
- 187** Plasma Processing of Ion Energy-sensitive Materials
- 189** Standoff Detection of Trace Explosive Residues by Resonant Infrared Photothermal Imaging

nanoscience technology

- 194** Spectral Tuning of Organic Nanocolloids
- 196** Spin Rotation for Quantum Information
- 198** Sheet of Carbon Atoms Points Way to Ultra-fast Transistors
- 200** Functionalized CMOS Nanomechanical Resonators for Chem-Bio Sensing

ocean science and technology

- 206** The ASW Reach-back Cell Ocean Analysis System
- 208** Marine Sediment Strength from Dynamic Probes
- 211** Characterizing River Environments by Combining Imagery and Models: What We Can Do Now and In the Future

optical sciences

- 216** Asymmetric Lasercom for Small Unmanned Aerial Systems
- 218** SWOrRD: Swept-Wavelength Optical resonance-Raman Detection of Bacteria, Chemicals, and Explosives
- 222** Single-shot Imaging Magnetometry and Spectroscopy Using Cold Atoms

remote sensing

- 226** Real-time Surface Wave Information by Coherent Radar
- 227** Shipboard AIS and Radar Contact Reporting (SARCR)

simulation, computing, and modeling

- 232** High-Yield Z-Pinch Thermonuclear Neutron Source
- 234** Rapid Air Traffic Modeling and Prediction

space research and satellite technology

- 238** Joint Milli-Arcsecond Pathfinder Survey (JMAPS) Fine Attitude Determination Approach
- 240** TacSat-4, Advanced UHF SATCOM
- 242** Integrating the Sun-Earth System for the Operational Environment (ISES-OE)
- 245** Origins of Solar Energetic Particle (SEP) Variability
- 248** Technology Development for High Integrity GPS (HiGPS)

SPECIAL AWARDS AND RECOGNITION

- 254** Special Awards & Recognition
- 268** Alan Berman Research Publication and NRL Edison (Patent) Awards
- 271** NRC/ASEE Postdoctoral Research Publication Awards

PROGRAMS FOR PROFESSIONAL DEVELOPMENT

- 274** Programs for NRL Employees — Graduate Programs, Continuing Education, Professional Development, Equal Employment Opportunity (EEO) Programs, and Other Activities
- 276** Programs for Non-NRL Employees — Recent Ph.D., Faculty Member, and College Graduate Programs, Professional Appointments, and College and High School Student Programs
- 278** Employment Opportunities

GENERAL INFORMATION

- 280** Technical Output
- 281** Key Personnel
- 282** Contributions by Divisions, Laboratories, and Departments
- 285** Subject Index
- 288** Author Index
- 289** Map/Quick Reference Telephone Numbers

Advances in POWER AND ENERGY

Research at NRL

The U.S. Department of Defense (DoD) consumed 889 trillion BTU of energy in FY08.¹ This represents 78% of Federal Government usage, and although this is less than 1.5% of overall U.S. usage, it makes the DoD the single largest energy user in the country.

As our nation struggles to convert from fossil fuel dependence to alternative energy sources, so too must the DoD. To help lead the way, Secretary of the Navy Ray Mabus recently set ambitious energy goals for the Navy and Marine Corps.² Meeting these goals will ensure a strong and flexible fighting force that is not solely dependent on fossil fuel, and will help reduce our national dependence on foreign oil. Specifically, Secretary Mabus set several targets that can be achieved only by advances in, and transition of, science and technology: (1) by 2015, reduce by 50 percent the petroleum use in the 50,000-strong shore-based commercial vehicle fleet by phasing in hybrid fuel and electric vehicles; (2) by 2016, create and deploy a fleet of ships powered by bio-fuels; (3) by 2020, produce half of the shore-based energy needs from renewable sources, such as

solar, wind, and ocean, generated by the base; and (4) by 2020, ensure at least 40 percent of the Navy's total energy consumption comes from alternative sources. These alone are lofty goals, and added to them is the need to provide lighter, smaller, and renewable sources of man-portable power for the Marine and Sailor.

There is clearly no single solution to the Navy's varied energy needs. The Naval Research Laboratory, with its broad base of expertise across numerous science and technology disciplines, is poised to provide a range of solutions to help meet the Navy's targets. Decades in the making, NRL's basic and applied research has provided the underpinnings of future energy technologies. This article highlights just a few of the energy research activities at the Laboratory — some key promising mature research and some higher-risk, high-payoff initiatives.

¹“Office of the Under Secretary of Defense, Installations and Environment, www.acq.osd.mil/ie/energy; www.congressional.energy.gov/documents/Final_Testimony.pdf; U.S. Energy Information Administration, www.eia.doe.gov/emeu/aer/overview.html.

²“SECNAV Outlines Five ‘Ambitious’ Energy Goals” (released Oct. 16, 2009), available at http://www.navy.mil/Search/display.asp?story_id=49044.

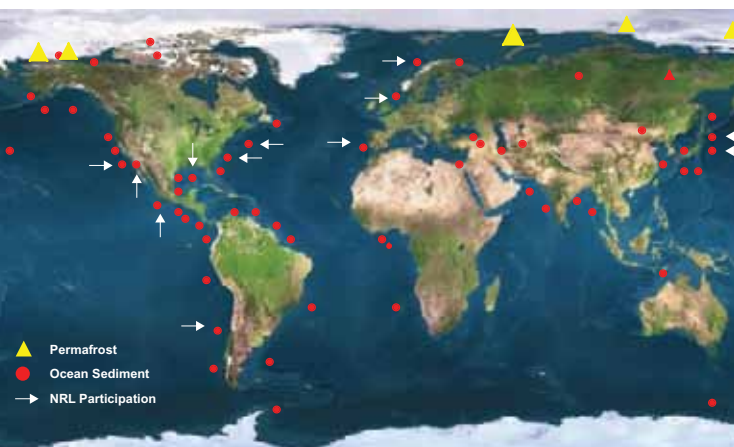
Energy Sources



NRL's Nike – the world's largest KrF laser facility.

LASER FUSION. Nuclear fusion has the promise to provide a clean, plentiful source of electrical power. Fusion energy does not produce greenhouse gases, and the fuel supply (lithium and deuterium feedstock) is sufficient for thousands of years. Fusion requires heating deuterium and tritium (D-T) to very high temperatures — on the order of 100 million °C — so they ignite and “burn” in a thermonuclear reaction. Two approaches are being pursued in international research efforts to harness fusion for power production. One approach is to confine the high-temperature D-T fuel by magnetic fields. The other approach is based on inertial confinement, where a pellet containing the D-T fuel mixture is compressed to very high density (~1000× solid) and then ignited; because the highly compressed fuel burns so rapidly, there is no need for external confinement. The technological and scientific challenges to inertial and magnetically confined fusion are quite different; pursuing both adds robustness to the fusion energy research effort.

NRL's long-established laser fusion program has concentrated on developing advanced laser technology and target designs for inertial fusion. The program has developed a krypton fluoride (KrF) laser technology that is predicted to greatly facilitate obtaining the high target gains (ratio of fusion energy output to laser energy input) needed for inertial fusion power. KrF lasers provide deeper UV ($\lambda = 248$ nm) and more uniform target illumination than any other high-energy laser technology. Simulations with NRL's FASTRAD3D hydro-code predict that the high target gains required for power plants can be attained with KrF laser energies of only 1 MJ. NRL has built the world's largest KrF laser facility, Nike, for target experiments, and uses its Electra KrF laser facility to develop the efficient and durable high-repetition-rate (5 Hz) technologies needed for fusion energy. In addition, NRL managed an external program (with researchers at universities, national labs, industries, and small businesses) that has advanced the other critical science and technologies needed to build a power plant, such as durable reaction chambers and low-cost target fabrication. This modular, KrF laser-based approach has the potential to put development of fusion energy on a faster track, possibly enabling the first fusion power plants to come on line in the 2030s.



Methane hydrate deposits around the globe.

METHANE HYDRATES. Abundant natural deposits of methane hydrates are embedded in the sea floor along most of the world's continental margins and in permafrost at high latitudes, representing a huge potential energy resource. The energy contained in methane hydrates — frozen mixtures of water and methane gas — is estimated to be double that contained in global reserves of coal, oil, and conventional natural gas combined. The resource potential in the United States alone is an estimated 200,000 trillion cubic feet; thus, at our current consumption rate of natural gas — about 22 trillion cubic feet annually — just a 1% recovery has the potential to fill the natural gas needs of the nation for the next 100 years. For direct fuel combustion, methane gas provides high energy density per weight and produces relatively low carbon dioxide emissions.

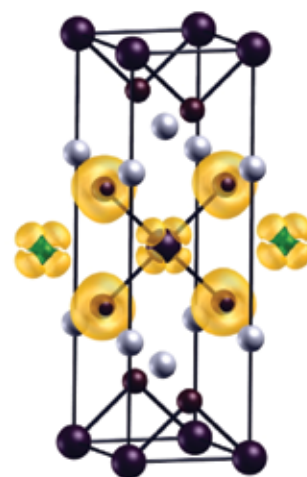
NRL has been conducting methane hydrate research for more than 20 years, joining international efforts to understand, locate, and evaluate the deposits, and extract the methane safely and economically. NRL's expertise is focused in several areas: geophysical and geochemical prediction of deep sediment hydrate deposits; evaluation of flux and cycling of methane in shallow sediments; the effect of deposits on acoustic profiles; ocean and sediment carbon models; methane contribution to climate change; and methane influence on microbial community diversity in sediment. NRL researchers have led and participated in international expeditions studying methane hydrate deposits off northern Alaska (most recently in September 2009), New Zealand, Chile, Canada, Norway, and the Gulf of Mexico; future investigations may include India, Russia, and Brazil. With concerted efforts in research and development by government and industry, methane from some regions could optimistically be extracted in as few as ten years.

Energy Storage

NANOSCALE ELECTRODE MATERIALS FOR BATTERIES. In order to fully exploit alternative energy sources such as solar, wind, and hydroelectric, better energy storage materials must be developed. For the military, the need for portable, high energy density batteries for communications, sensors, computing, and other electronics applications is one of its most pressing technological problems. Rechargeable lithium ion batteries store chemical energy and have enormous potential as power sources for such applications, but they need to show improvements in energy density and cycle life before their wide-scale use is practical. NRL is working to effect these improvements, conducting research to develop low-cost, high-capacity, high-power battery electrodes from nanoscale materials.

A primary characteristic of a good rechargeable electrode material is high capacity, that is, the ability to incorporate a large amount of lithium ions. The material must further be able to maintain its good capacity throughout a large number of recharges (cycles) and at high power (rate). Poor “capacity retention” as a function of cycle number and/or rate presently limits the use of many initially promising materials as practical electrodes.

NRL's recent research has shown that across a wide range of materials, nanoscale electrodes show a marked increase in lithium ion capacity retention compared to their bulk counterparts. Furthermore, the improvement depends sensitively on the particular nanoscale morphology — nanofilm, nanowire, nanoparticle, or nanoporous “foam,” for example. The observed improvement in retention holds even for materials such as Si, Co_3O_4 , or SnO_2 , whose atomic-scale structure changes drastically during electrochemical cycling. Nanostructured architectures for power storage provide many advantages over existing technologies to minimize power losses, improve charge/discharge rates, and enhance energy densities.



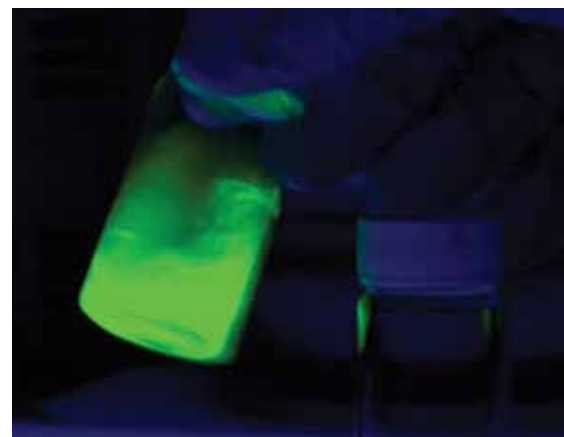
Structure of de-lithiated Li_2CuO_2 cathode material.

Energy Conversion

PHOTOVOLTAICS. The Sun is arguably the most plentiful source of energy available to us on Earth. Photovoltaics, or solar cells, convert sunlight into electricity, but often with low efficiency. NRL is engineering photovoltaic cells to more efficiently exploit solar energy for specific operational applications, such as in space, under water, and in man-portable devices.

For remote systems and portable applications, NRL is developing extremely high power density (W/kg) energy sources by incorporating quantum wells (QWs) into the active regions of a multijunction solar cell. QWs are nanostructures whose optoelectronic properties can be precisely controlled through choice of material system, doping, and internal structure to optimize them for specific operational conditions. Taking space as one of the most extreme and harsh remote environments, NRL is using quantum wells (QWs) to create solar cells designed for radiation resistance and space performance that exhibit greater than 35% efficiency and will not degrade after 15 years in geostationary Earth orbit. For portable power, NRL is using QWs to create solar cells that have efficiencies approaching 50% under concentrated terrestrial sunlight, to demonstrate a hand-held system capable of producing $\sim 20 \text{ W/cm}^2$.

NRL is also developing photovoltaics tuned to the filtered light underwater so they can provide continuous, long-term power for underwater unmanned vehicles (UUVs) and deployed sensors. Conventional solar cells are designed to take advantage of the broad solar spectrum, but suffer significant loss of efficiency in underwater applications, where the sunlight is filtered toward the blue end of the spectrum. NRL's photovoltaic cell is designed to efficiently exploit the blue-green transmission band-pass of littoral sea water, and to make use of low-intensity sunlight. The solar cell is formed out of InGaP (band gap of 1.8 eV) developed for high-efficiency space solar cells. InGaP is a mature solar cell technology that can produce monochromatic conversion efficiencies greater than 65% (under illumination by 570 nm light). NRL is aiming for power generation of 6 W/m^2 at depths of 20 meters in littoral waters.



Solution of nanocrystals that will be used to produce the layers of a photovoltaic device by spraying, spin-coating, or other solution-based process.



Field testing an oceanographic mooring powered by a benthic microbial fuel cell.

MICROBIAL FUEL CELLS. To create networked autonomous sensor systems for long-term deployment (>1 year), technologies that can harvest energy from the environment (biological, wave, piezoelectric) need to be incorporated into sensor design. Microbial fuel cells (MFCs) use naturally occurring nutrient sources, such as from the metabolic activities of microorganisms, to generate enough electricity to power such systems. NRL is developing the Littoral Autonomous Sensor System (LASS), a free-floating, self-contained sensor package that connects both passive and active flow microbial fuel cells in parallel to generate continuous power greater than $1 \mu\text{W}$ at voltages greater than 3.0 V utilizing a custom DC-DC boost converter. With this design, no additional power source (such as a battery) is needed to operate the sensor, and the modular MFC systems connected in parallel are smaller than systems connected in series. DC-DC boost conversion at a voltage less than 0.5 V has resulted in usable voltages generated from MFCs containing a total volume less than 10 mL.

NRL has also developed a benthic microbial fuel cell (BMFC), an oceanographic mooring that exploits natural microbial processes to generate persistent electrical power at a typical density of 0.38 W/m^2 . Remotely deployed Navy sensors engineered to use less power to extend their battery life, typically for just months, may be powered indefinitely by BMFCs. Other advantages of the BMFC include safety (there are no reactive catalysts or hydrogen generation) and design flexibility (they do not require oceanographic housings). In field demonstrations, BMFCs have powered hydrophones, a meteorological buoy with real-time RF data exfiltration, an acoustic vector sensor, and a bottom-resting UUV.

Power Delivery



NRL's Epicenter for Advanced Materials Growth and Characterization.

SUPERCONDUCTORS. Superconducting technology has matured over the past quarter century and now is establishing a growing role in meeting the energy challenges of the 21st century. From efficient, power-dense applications such as transmission lines for the smart grid or motors for industrial or transportation needs, to very low power quantum-level devices for sensing and logic elements, superconducting applications are offering unparalleled performance capable of meeting our growing energy needs. Key to progress will be continued development of new materials and advanced development of materials targeted for specific applications. System designs stressing reliable, long-term use that can compete economically with other technologies are a major focus of the superconducting industry as it grows its customer base.

Scientists at NRL are focused on discovering, understanding, and developing new superconducting materials to provide greater operational advantages for this new technology. Recent theoretic studies have focused on the newly discovered pnictide superconductors (e.g., LiFeAs compounds) that can have transition temperatures over 50 K. These compounds are the first-ever superconductors containing a dominant magnetic atom (Fe) and have led to new theories about the origin of superconductivity in these materials. A new synthesis facility allows NRL researchers to form compounds between metals of widely disparate melting temperatures (e.g., noble metal alloys containing Bi) by a synthetic chemistry approach. Other NRL programs are developing new fabrication techniques to coat high-temperature superconductors into both wire and sheet form for Navy applications (such as wires and shielding).

SIMPLEX VI & VII • ANDE-2 • SEITE I & II • HREP • HICO
RAIDS • HERSCHEL • CARE-I • SSULI • MISSE7

10

NRL-led Space Experiments Launched in 2009

Space research and space technology have been productive and vibrant activities at the Naval Research Laboratory from the 1940s to the present. The Laboratory is well known as one of the most successful designers and builders of spacecraft in the United States. More than 90 satellites encompassing a variety of purposes have been built and launched, with an enviable record of success. In addition, the Lab has performed numerous other space science and development activities in conjunction with the U.S. Air Force (USAF) and NASA, and has been called on to develop many hundreds of space instruments and subsystems. By any standard of measure — productivity, sponsor satisfaction, innovation, quality of personnel, archival publications — NRL's record compares most favorably with any major industrial, academic, national, or Government laboratory. The NRL space program is important to C4ISR, precision navigation and timing, orbital tracking, space situational awareness, maritime domain awareness, battlespace environmental awareness, and the fundamental understanding of geophysical phenomena and natural radiation sources.

In 2009, ten space activities spearheaded by NRL researchers were successfully launched and deployed (see Table 1). Eight militarily relevant experiments of very high technical value were integrated, launched, deployed, and operated by the Department of Defense (DoD) Space Test Program (STP), one cutting-edge instrument suite (the experimental

HERSCHEL imager) was launched by NASA on a sounding rocket, and one transitioning operational capability (the SSULI sensor) was launched on-board the Defense Meteorological Satellite Program (DMSP) F18 satellite. These ten space activities scientifically encompass a wide range of investigations and applications: investigation of hyperspectral spaceborne remote sensing of the Earth's coastal regions to demonstrate battlespace capabilities needed by the operational Navy and Marine Corps; the performance of in situ monitoring of materials and componentry exposure to the extreme space environment; the dynamics exploration and the combination of remote sensing and in situ measurements of the Earth's thermosphere and ionosphere for purposes of validating and improving both space weather models and orbit determination calculations; and the global simultaneous imaging of both helium and hydrogen in the Sun's corona as a crucial step toward increased predictive understanding of the solar wind.

Operational sensor SSULI launched by the Defense Meteorological Satellite Program. The Special Sensor Ultraviolet Limb Imager (SSULI) under the direction of instrument Principal Investigator (PI) Andrew Nicholas and Program Manager (PM) Sean Lynch was launched 18Oct09 on the DMSP F18 satellite and observed sensor first light on 01Dec09. SSULI cleanly measures vertical profiles of natural airglow radiation from atoms, molecules, and ions in

TABLE 1 – NRL-led Space Activities Launched in 2009

| Launch Date | Space Activity | Principal Investigator |
|-------------------|-----------------------------------------------------------------------------------------------------|--------------------------------|
| 15 March 2009 | Shuttle Ionospheric Modification with Pulsed Localized Exhaust (SIMPLEX VI and VII, K4, K5, K6, K7) | Paul Bernhardt |
| 15 July 2009 | Atmospheric Neutral Density Experiment 2 (ANDE-2) | Andrew Nicholas |
| 15 July 2009 | Shuttle Exhaust Ionospheric Turbulence Experiment (SEITE I and II) | Paul Bernhardt |
| 10 September 2009 | HICO/RAIDS Experiment Payload (HREP) | Davidson Chen |
| 10 September 2009 | Hyperspectral Imager for the Coastal Ocean (HICO) | Michael Corson |
| 10 September 2009 | Remote Atmospheric and Ionospheric Detection System (RAIDS) | Scott Budzien |
| 14 September 2009 | Helium Resonance Scattering in the Corona and Heliosphere (HERSCHEL) | J. Daniel Moses |
| 19 September 2009 | Charged Aerosol Release Experiment I (CARE-I) | Paul Bernhardt |
| 18 October 2009 | Special Sensor Ultraviolet Limb Imager (SSULI) | Andrew Nicholas and Sean Lynch |
| 16 November 2009 | Materials on the International Space Station Experiment #7 (MISSE7) | Phillip Jenkins |

the upper atmosphere and ionosphere by passively scanning the Earth's limb in the extreme ultraviolet (EUV) to far ultraviolet wavelength ranges, to provide necessary space environmental data in support of military and civilian systems. SSULI (Fig. 1) is the first operational atmospheric sensor to exploit the EUV spectrum. It is tailored to accommodate the unique requirements for flight aboard the DMSP satellite constellation and data processing at the Air

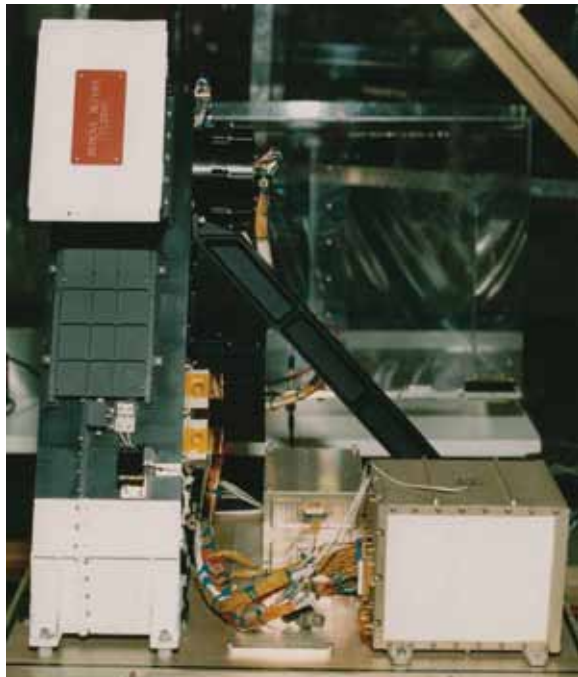


FIGURE 1. The SSULI instrument includes a high-resolution scanning spectrograph (left), control electronics (lower right), and high voltage power supplies (bottom middle behind harness).

Force Weather Agency (AFWA) including system redundancy, operational survivability, ground and flight software maintainability, and processing algorithm obsolescence. DMSP F18 SSULI data products, once calibrated and validated, will be used operationally at AFWA to support the warfighter. The DMSP is a DoD environmental monitoring spacecraft program led by the USAF Space and Missile Systems Center.

HREP, HICO, and RAIDS launched aboard the Japanese H-II Transfer Vehicle. Designed and built by NRL under the direction of PI Davidson Chen, the HICO/RAIDS Experiment Payload (HREP) launched 10Sep09 from Tanegashima Launch Center aboard the inaugural flight of the Japanese Aerospace Exploration Agency (JAXA) H-II Transfer Vehicle unmanned resupply ship under the auspices of the DoD STP. HREP (Fig. 2) is the first U.S. payload on the Japanese Experiment Module – Exposed Facility (JEM-EF), a component of the International Space Station (ISS). Following docking to the ISS, robotic payload installation, and initial testing, HREP entered the normal science operations phase of its unique mission on 19Oct09. HREP provides all structural support and attitude knowledge to the NRL-led HICO and RAIDS hyperspectral sensors, and serves as the control interface to the JEM-EF for HICO and RAIDS communication, data handling, monitoring, and power.

Following the 10Sep09 launch, NRL's Hyperspectral Imager for the Coastal Ocean (HICO) experiment, led by instrument PI Michael Corson, suc-



FIGURE 2. HREP (foreground) being prepared for installation aboard JAXA's H-II Transfer Vehicle (background). (Photo: JAXA)

launch, RAIDS completed on-orbit commissioning activities on 23Oct09 and entered the initial science operations phase of its mission. RAIDS collects the temperature and composition of the sparsely measured lower thermosphere and retrieves ionospheric electron densities. The new high-resolution results are being compared with predictions from applied and research quality global assimilative models relevant to military and civilian space-based systems, toward improved forecasting of satellite drag, specification of the ionosphere, and investigation of the surprisingly strong relationship between atmospheric dynamic processes and global-scale ionospheric morphology. RAIDS was built and is operating in a collaboration between NRL and The Aerospace



FIGURE 3. This HICO image over a coastal region of the South China Sea near Hong Kong, China, was taken 02Oct09. The image is approximately 43 km wide and 190 km long centered upon 22° 5'N, 114° 18'E, oriented from SW at the bottom to NE at the top.

cessfully completed commissioning activities on schedule and is currently in its science operations phase. From its vantage point on the ISS, HICO is collecting high-fidelity hyperspectral images of land and coastal scenes and is using this information to derive important environmental data products such as bathymetry and water clarity (Fig. 3). Under the Office of Naval Research Innovative Naval Prototype program, HICO is successfully demonstrating the viability of operating a commercial off-the-shelf (COTS)-based system in space as a pathfinder for responsive littoral environmental imaging that is relevant to Navy and Marine Corps operations.

The Remote Atmospheric and Ionospheric Detection System (RAIDS) experiment is a hyperspectral sensor suite now orbiting the Earth onboard the ISS (Fig. 4), studying the upper atmosphere with eight optical limb-scanning sensors that range from EUV to near-infrared wavelengths. Following the 10Sep09



FIGURE 4. The gold RAIDS scan head is visible at the open end of HREP on the International Space Station. (Photo: NASA)

Corporation under the leadership of RAIDS PI Scott Budzien. HICO/RAIDS was integrated and flown under the auspices of the DoD STP.

MISSE7 launched by Space Shuttle Atlantis to the International Space Station. The Materials on the International Space Station Experiment (MISSE) #7, designed and built by NRL at the direction of PI Phillip Jenkins, launched aboard NASA's STS-129 Space Shuttle Atlantis on 16Nov09 for transport to the ISS. MISSE7 consists of two Passive Experiment Carriers (PECs) and three experiments mounted to the EXPRESS Pallet Assembly and was the first payload to use the NASA-built EXPRESS Logistics Carrier (EXPRESS = EXPedite the PProcessing of Experiments to the Space Station). The numerous individual experiments on MISSE7 include in situ monitoring of materials sensitivities to space temperature ranges, atomic oxygen concentrations, and ionizing radiation dosages. MISSE7 results will provide a better understanding of the durability of advanced

materials and electronics when they are exposed to vacuum, solar radiation, atomic oxygen, and extremes of heat and cold. Upon completion of the MISSE7 evaluation phase, the technology readiness of successful experimental components will increase to the operational environment prototype level. ISS astronauts opened the MISSE7 PECs during an Extra Vehicular Activity on 24Nov09 to expose the experiments to the space environment. The MISSE7 PECs will remain on the ISS for approximately eight months and are scheduled to be returned to Earth during the STS-134 mission for post-exposure evaluation and analysis. MISSE7 was integrated and flown under the auspices of the DoD STP.

ANDE-2 microsattellites launched by Space Shuttle Endeavour. The NRL ANDE-2 twin experimental microsattellites (Fig. 5), utilizing DoD STP-developed and built deployment mechanisms, deployed on



FIGURE 5. The NRL ANDE-2 spacecraft, Castor and Pollux, shortly after deployment under the auspices of the DoD STP from NASA's Space Shuttle Endeavour STS-127 on 30Jul09, as photographed by the crew of the STS-127 from the flight deck. (Photo: NASA)

30Jul09 from NASA's STS-127 Space Shuttle Endeavour (launched 15Jul09) for ANDE project PI Andrew Nicholas. The ANDE-2 mission hardware centrally consists of two spherical microsattellites with the same size and drag coefficient but different masses, which are slowly separating into lead-trail orbits. ANDE-2 data is providing researchers with a direct opportunity to study small-scale spatial and temporal variations in drag associated with geomagnetic activity. The ANDE research products are being used to improve methods for the precision orbit determination of space objects and to calibrate the Space Fence, a radar system of the USAF 20th Space Control Squadron that tracks low-Earth-orbiting space objects. In addition to obtaining data for correcting deficiencies in upper atmospheric models,

the ANDE project is advancing miniaturization of sensor technologies that are pivotal for multi-point in situ space weather sensing.

CARE-I launched by a DoD STP sounding rocket.

Under the direction of NRL PI Paul Bernhardt, the Charged Aerosol Release Experiment I (CARE-I) was launched by the DoD STP from the NASA Wallops Flight Facility at dusk on 19Sep09 to investigate properties of charged dust in the ionosphere. The bright optical CARE-I upper atmospheric display,



FIGURE 6. On 19Sep09 after sunset, the CARE-I dust cloud release was the brightest object in the sky over NRL as viewed from Alexandria, Virginia, six minutes after launch. The CARE-I release, 200 km to the east of the Virginia coast, was produced by a solid rocket motor that remained at a fixed altitude of 290 km during the rocket engine burn.

easily seen from the ground along the East Coast of the United States (Fig. 6), was produced by sunlight scattered by concentrated rocket exhaust that was released at 290 km altitude by a delayed firing of the sounding rocket fourth stage. The exhaust material, composed of 1/3 aluminum oxide particles and 2/3 combustion product molecules, interacted with the ionosphere to create a dusty plasma with high-speed pick-up ions. Ground-based radars tracked the effects of CARE-I on the ionosphere for more than four hours, producing valuable data about how rocket motors affect ionospheric densities. CARE-I also provided a simulation of natural disturbances in the Earth's upper atmosphere.

HERSCHEL launched by a NASA sounding rocket.

Under the direction of NRL PI J. Daniel Moses, the NASA-sponsored Helium Resonance Scattering in the Corona and Heliosphere (HERSCHEL) suborbital sounding rocket launched successfully on 14Sep09 from the White Sands Missile Range. This joint mission with the NASA Living With a Star program,

NRL, and multiple institutions in Italy, France, and the United Kingdom, provided the first global images for the two most abundant elements of the solar corona, hydrogen and helium. HERSCHEL achieved three first-time measurements: simultaneous global imaging of the extended corona in EUV, ultraviolet, and visible light; global measurement of the ratio of helium to hydrogen in the corona; and global maps of solar wind outflow. Determination of the processes that generate and drive the solar wind will provide a fundamental advance in our understanding and forecasting of space weather effects at Earth.

SEITE I & II and SIMPLEX VI & VII fielded by Space Shuttles Discovery, Endeavour, and Atlantis. The Shuttle Exhaust Ionospheric Turbulence Experiment (SEITE) I & II and the Shuttle Ionospheric Modification with Pulsed Localized Exhaust (SIMPLEX) VI & VII were two Space Shuttle Orbital Maneuvering System (OMS) rocket burn ionospheric detection and theory validation experiments fielded by the DoD STP for NRL PI Paul Bernhardt. SEITE I & II were fielded on 30Jul09 by NASA's Space Shuttle mission STS-127 (launched 15Jul09) and on 26Nov09

by STS-129 (launched 16Nov09), respectively. SEITE I & II remotely detected OMS on-orbit burn from space collaboratively with the STP-launched USAF satellite C/NOFS (Communication/Navigation Outage Forecasting System). C/NOFS instruments successfully detected the SEITE OMS exhaust gases from 230 and 430 km away, validating the plasma physics theory and modeling that was used to explain the OMS burn in situ signatures. Ionospheric disturbance theory and modeling validation was also achieved by SIMPLEX VI & VII, fielded on 27Mar09 from NASA's STS-119 (launched 15Mar09) and on 10Sep09 from STS-128 (launched 28Aug09), respectively. The SIMPLEX team applied upper atmospheric neutral and plasma physics models to determine where and when to look for the OMS rocket burn signatures with high-frequency ground-based radars such as the SuperDARN radar at Wallops Island, and ultra-high-frequency radars at Millstone Hill, Massachusetts, and Kwajalein, Marshall Islands. The radar scatter experiments achieved long-range (700 km) detection of the OMS-driven radar turbulence consistent with predictions.

Space research brings together a set of core competencies that are required both in fundamental scientific investigations and for military applications: highly automatic sensor technologies; spacecraft development, launch, and communications; remote sensing, data handling and transmission; analysis and interpretation of data; and action taken in response to signal or event. As one of the handful of laboratories able to develop capabilities across all of these areas, NRL's most basic goals and products are hardware-oriented. The NRL space program melds the strengths resident throughout the Laboratory — in chemical diagnostics, materials science, applied optics, radiation survivability, high-performance computing simulation and modeling, electronic warfare, directed energy technology, and remote sensing — into a structure that helps the Navy multiply force combat effectiveness. NRL space researchers advance understanding and predictive capability of the space domain in order to exploit the extended operational environment and its impact on Navy and DoD activities. They envision, design, fabricate, integrate, test, launch, operate, and experiment with forefront assets that preserve, protect, and enhance space platforms in the performance of functions that are of critical importance to Navy Fleet operations. As exemplified by this successful and extensive portfolio of ten NRL-led space activities that were deployed in 2009, NRL's space work represents cost-effective coordination across the broader science and technology program of the Office of Naval Research and of other U.S. Government services and agencies, to achieve significant progress.

THE ION TIGER FUEL CELL UNMANNED AIR VEHICLE



The 35-lb Ion Tiger aircraft in flight.

NRL began research into fuel cell unmanned air vehicles (UAVs) in 2003. With a small, 100-W fuel cell from Protonex Technology Corporation in hand, the team assembled a series of commercial off-the-shelf parts, such as a paintball tank to hold the high-pressure hydrogen fuel and a radiator made from aluminum foil and tubes. The system was retrofitted into a sailplane kit and called the “Spider Lion.” The 6-lb Spider Lion demonstrated the first viable flight of a hydrogen/polymer fuel cell system in July 2005, and flew for 3.3 hr in November 2005 on 15 g, or half an ounce, of hydrogen in the

tank. Although the Spider Lion was far from a useful military vehicle — it did not fly a payload and it was capable of flying only in very calm conditions — it showed that fuel-cell-powered flight might be viable for unmanned air vehicles.

Fuel cell UAVs offer electric propulsion, which has numerous favorable attributes for these vehicles: near-silent operation, instant starting, increased reliability, ease of power control, reduced thermal signature, and

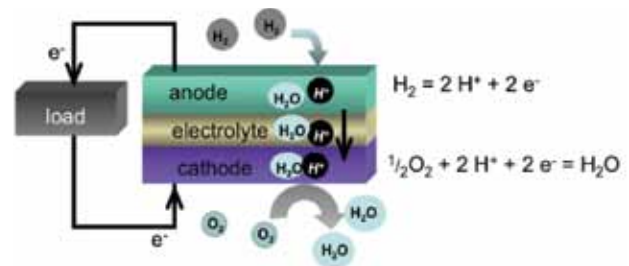
reduced vibration. There is no need for a generator, and payloads can be operated directly from the propulsion system. The only disadvantage of electric

propulsion has been the low capacity, or endurance, of the traditional battery electric power source. The low endurance can be overcome by using a fuel cell.

Fuel cells are energy conversion devices. Like engines, they convert fuel and air into useable energy, but fuel cells do so by electrochemical processes, so they make electricity directly. There are several types of fuel cells, and NRL is focusing on proton exchange membrane fuel cells (PEMFCs), or polymer fuel cells, which make electricity and water from hydrogen and oxygen. Polymer fuel cells are 40 to 50% efficient, or about two to four times more efficient than a combustion engine. They operate at 55 to 80 °C, below the boiling point of water. The only noise they make comes from the pumps that drive air and coolant through the fuel cell. The lightweight



The late James Kellogg with the 6-lb Spider Lion. The Spider Lion flew for 3 hr and 19 min on 15 g of hydrogen fuel in November 2005.



A polymer fuel cell combines hydrogen (H₂) at its anode and oxygen (O₂) at its cathode to make water (H₂O) and heat while providing electricity to a load. The reaction is catalyzed at the anode and cathode by platinum catalysts. The electrolyte is a solid polymer perfluorosulfonic membrane, Nafion.

hydrogen — one of the highest energy fuels available — is stored as a compressed gas in carbon/aluminum tanks. The result is a quiet, high-energy electrical production system with a low heat signature. The high energy and efficiency of the fuel cell system leads to seven times the endurance of a battery with

the same weight for this mission. The allure of high-efficiency, clean propulsion makes hydrogen-fueled polymer fuel cell systems the leading candidates for commercial automotive systems.

NRL's approach is to develop new unmanned air vehicle airframes around the new propulsion plant to take full advantage of the technology in two vehicles — the XFC and Ion Tiger. The XFC is a 16-lb air vehicle with a mission goal of 6 hr with a 2-lb payload.

The Ion Tiger is designed to fly for 24 hr with a 5-lb payload. A 5-lb payload was selected because it is the approximate weight of common payloads such as a day/night camera or a communication relay.

The Ion Tiger program was funded by the Office of Naval Research (ONR) in the fall of 2007, and concluded in the fall of 2009 with a successful 26-hr demonstration flight. NRL designed the Ion Tiger vehicle, determined the specifications for the propulsion system, and designed the hydrogen fueling systems (tanks and regulators) and the cooling (radiator) system. NRL also carried out basic research on how the fuel cell system would survive in heavily polluted air. NRL teamed with Protonex Technology Corporation to develop the fuel cell system, the University of Hawaii for systems testing and modeling, HyperComp Engineering to build the hydrogen tanks, and Arcturus UAV to build the airframes.

A 35-lb aircraft was designed that could achieve a 24-hr endurance with the 550-W fuel cell. The power demand of the vehicle is an average of 300 W. This low value is due to the vehicle's 17-ft wingspan, leading to a lift over drag ratio of approximately 17. A total of 3 lb was allocated for the fuel cell system and 9 lb for the hydrogen tank and regulator. The system was also designed to be throttled, so that it could fly continuously at maximum power into headwinds, or save energy by flying in thermals.

Protonex Technology Corporation developed the 2.2-lb, 550-W fuel cell system for the Ion Tiger, exceeding the original power goal by 10%. The full system includes a 36-cell fuel cell stack, an air blower, a coolant pump, humidifier, and control electronics. It converts 99% of the hydrogen fuel to electricity at 40 to 55% efficiency.

Fuel cells are energy conversion devices. Like engines, they convert fuel and air into useable energy, but fuel cells do so by electrochemical processes, so they make electricity directly.

NRL designed new hydrogen tanks capable of storing 12% hydrogen by weight, a factor of 6 better than was demonstrated on the Spider Lion. NRL also modeled the thermal system for the fuel cell and developed a new, compact, lightweight radiator system that enables the Ion Tiger fuel cell system to fly in hot conditions. NRL and University of Hawaii proved out an electrochemical process to recover the fuel cell performance in the event that it became contaminated with poisons released from munitions or diesel exhaust. The culmination of these accomplishments is a lightweight fuel cell propulsion system that can be flown on a tactical system for naval missions.

The Ion Tiger had three successful flights in the summer and fall of 2009: a 13-hr "dawn to dusk" flight in August, a 23⁺-hr flight with a 4-lb payload in October 2009, and finally a 26⁺-hr flight with a 5-lb payload in November 2009. Each of these successive flights set an unofficial flight duration record for fuel-cell powered flight. The October flight was shorter



2.2-lb, 550-W polymer fuel cell developed by Protonex Technology Corporation.



The Ion Tiger being launched for a 23-hr flight at Aberdeen Proving Ground in October 2009.

than the November flight because several hours of 40 mph winds were encountered overnight, forcing the vehicle to fly at full throttle and burn more fuel. Otherwise, all of the flights were uneventful, and ended with safe landings.

The Ion Tiger development was successful by drawing on the fuel cell and UAV expertise of NRL and other members of the Ion Tiger team, leading to a lightweight, efficient, and effective system.

Researchers at NRL are presently developing the next-generation Ion Tiger system with triple the flight time of the present system by using cryogenic liquid hydrogen; this system can store three times as much fuel as the present systems that use compressed hydrogen, for the same weight. A larger system with a 1.5 kW fuel cell and capable of carrying a 15-lb payload is also being explored. The present Ion Tiger system is being adapted to the XFC vehicle, which is poised for naval transition.

Stealthy, small (<100 lb) unmanned air vehicles capable of carrying 15-lb payloads are needed for the next generation of naval aviation. Fuel cell UAVs will be able to stay on station for long periods of time, undetected. Their quiet propulsion will allow them to fly at low altitudes, and thus do surveillance with lower-resolution imaging systems. The long endur-

ance will enable them to serve as communication relays. Although hydrogen is not a logistics fuel, it can be made by electrolyzing water into hydrogen and oxygen, as is presently done on Navy ships and submarines. Another option is to reform heavy fuels into hydrogen. The ultimate benefit is to replace big, manned air vehicles, with small, inexpensive unmanned vehicles, to decrease potential harm to sailors and pilots while increasing naval capability, all by using a "green," quiet, efficient, and affordable fuel cell system.

The Ion Tiger program was supported by the Office of Naval Research. Fuel cell UAV development at NRL is also funded by the Office of the Secretary of Defense (OSD) Office of Technology Transition and the OSD Rapid Reaction Technology Office.

PADMA BHUSHAN AWARD

Dr. Bhakta Rath receives honors of the Padma Bhushan Award

Dr. Bhakta Rath, Associate Director of Research and Head of the Materials Science and Component Technology Directorate at NRL, has been awarded the Padma Bhushan Award of Honors and Excellence bestowed by the President of India. The Padma Bhushan is a prestigious, civilian award that recognizes distinguished service of a high order in any field, in arts, sciences, and public service.

The award is the second in the hierarchy of civilian Padma awards in India. The President of India originated the award on January 2, 1954. The president traditionally awards medals and citations during the honorary ceremony. Many civilians receive honors in arts, medicine, civil service, public affairs, and science and engineering. Dr. Rath received recognition for excellence in the field of science and for his exceptional service toward the advancement of science. Following a tenured faculty appointment at Washington State University and stints at the corporate research labs of U.S. Steel and McDonnell Douglas, Dr. Rath began his career at NRL as Head of the Physical Metallurgy Branch in 1976, and was subsequently selected to head the Materials Science and Technology Division, followed by his appointment to his present position. In his current position, Dr. Rath manages multidisciplinary theoretical and experimental research to discover and exploit new, improved materials, generate new concepts associated with materials behavior, and develop advanced components based on these new and improved materials and concepts.

Following his undergraduate studies in India, Dr. Rath earned an M.S. in metallurgy from the Michigan Technological University and went on to earn his Ph.D. from the Illinois Institute of Technology.

He is recognized as a fellow of several engineering societies in the U.S. and abroad and has been honored by NRL, the Office of Naval Research, the Department of Defense, and numerous professional and scholarly organizations. He was elected to the U.S. National Academy of Engineering.

During recent years, Dr. Rath has received the 2008 Acta Materialia, Inc. J. Herbert Hollomon Award, an honorary doctorate in engineering from Michigan Technological University, the Department of Defense Distinguished Civilian Service Award, the 2005 Fred Saalfeld Award for Outstanding Lifetime Achievement in Science, the Presidential Rank Award for Distinguished Executive (2005), the NRL Lifetime Achievement Award (2004), National Materials Advancement Award from the Federation of Materials Societies (2001), and the Presidential Rank Award for Meritorious Executive (1999 and 2004). He served as the 2004-2005 President of the American Society for Materials. He also has served as a member of the Boards of Directors/Trustees of several technical societies and on the editorial boards of international materials research journals. He also served for the office of the Deputy Under Secretary of Defense as the Executive Chair of Materials and Processes Research Group, developing many collaborative research projects with the Defense Laboratories of US, Canada, UK, Australia, and New Zealand (TTCP Countries).



The President of India, Smt. Pratibha Devisingh Patil, presents the Padma Bhushan Award to Dr. Bhakta Rath. The award was presented at a ceremony held at the President's residence in New Dehli on April 14, 2009.



Dr. Rath stands before the President of India as he accepts the Padma Bhushan Award.

NRL breaks ground for its

LABORATORY FOR AUTONOMOUS SYSTEMS RESEARCH

NRL HELD A GROUNDBREAKING CEREMONY ON APRIL 8, 2010, TO MARK THE START OF CONSTRUCTION OF A MAJOR NEW FACILITY: THE **LABORATORY FOR AUTONOMOUS SYSTEMS RESEARCH**.

OPEN FOR BUSINESS IN 2012



FORGING THE TECHNOLOGY OF TOMORROW

This new, \$17.7M facility on the Washington, D.C., campus will become the nerve center for basic research in autonomous systems for the Navy and Marine Corps. Its unique combination of laboratory and high bay spaces will allow NRL's scientists and engineers to integrate science and technology components into research prototype systems for testing and demonstration. Construction of the nearly 50,000 ft² laboratory is scheduled for completion in May 2011.

The new laboratory's specialized facilities will support highly innovative, interdisciplinary research in autonomous systems, including intelligent autonomy, mobility, sensor systems, power and energy systems, human-system interaction, networking and communications, and platforms. The laboratory will consist of a Power and Energy Laboratory, a Sensor Laboratory, four Human-System Interaction laboratories, a Reconfigurable Prototyping High Bay, and three simulated environments: the Desert High Bay, the Littoral High Bay, and the Tropical High Bay (which also includes an upland forest environment). These areas will serve as adaptable test beds for system demonstration and validation prior to field testing, saving the Navy and Marine Corps significant funds.

The objective of NRL's new Laboratory for Autonomous Systems Research is to enable Navy and DoD scientific leadership in this complex, emerging area and identify opportunities for advances in future defense technology.



forging the technology of tomorrow...



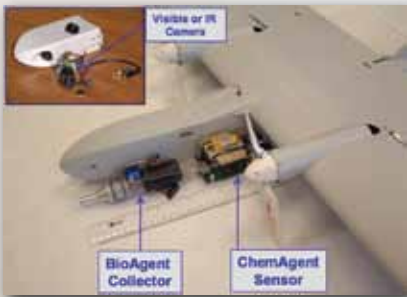
Because Autonomous Systems are not just vehicles, the building will contain a number of **Human-System Interaction Labs** to develop automated decision support tools and address critical communications and network issues.



The **Power and Energy Lab** will have a walk-in dry room for handling moisture-sensitive materials such as those used in lithium ion batteries.



Novel power sources such as fuel cells will be integrated into new systems and platforms.



The **Sensor Lab** will have facilities to calibrate and test many different types of chemical, biological, radiation, nuclear or explosives (CBRNE) sensors developed elsewhere at NRL and brought to this new building for integration into systems or platforms.

Intelligent Autonomy • Power and Energy • Sensors • Human-System Interaction **RESEARCH LABORATORIES**



NRL's Micro Tactical Expendable "MITE" air vehicle.



The **Reconfigurable High Bay** will allow real-time, accurate tracking of many entities (vehicles and humans) for experimental ground truth. Small UAVs and ground vehicles can simultaneously operate within the large high bay, which is viewable from four adjacent human-system interaction labs. The lab will also have pseudo-GPS and a surround sound system to allow emulation of environmental noises.



The **Tropical High Bay** will provide a simulated jungle terrain and rain forest including a flowing water feature in an enclosed greenhouse-type structure. An adjacent outdoor area features an upland forest.



The **Littoral High Bay** will provide a simulated coastal environment featuring mud/sediment pits (used to support the energy harvesting device shown in the picture), small flow and wave tanks, and a larger pool with a sloping floor.



The **Desert High Bay** will provide a simulated desert environment featuring a sand pit and rock wall plus variable levels of illumination, wind, and smoke.

Desert • Littoral • Tropical • Reconfigurable Prototyping **SIMULATED ENVIRONMENTS**



Father of GPS Inducted into the National Inventors Hall of Fame

Joining the likes of world-renowned inventors Thomas Edison and Alexander Graham Bell, former Naval Research Laboratory scientist Roger L. Easton was inducted into the National Inventors Hall of Fame in a ceremony on March 31, 2010. Easton is widely recognized for his pioneering achievements

in spacecraft tracking and time navigation (Easton's TIMATION) that were critical enabling technologies for the NAVSTAR Global Positioning System (GPS).

The award ceremony was hosted by Under Secretary of Commerce for Intellectual

Property and Director of the United States Patent and Trademark Office, David Kappos, and was held at the Department of Commerce Herbert C. Hoover Auditorium in Washington, D.C. Easton was cited for inventing the TIMATION Satellite Navigation System, U.S. Patent 3,789,409 ("Navigation System Using Satellites and Passive Ranging Techniques," January 29, 1974).

Easton developed and tested his revolutionary concept for a time-based navigation system over a long career at NRL.

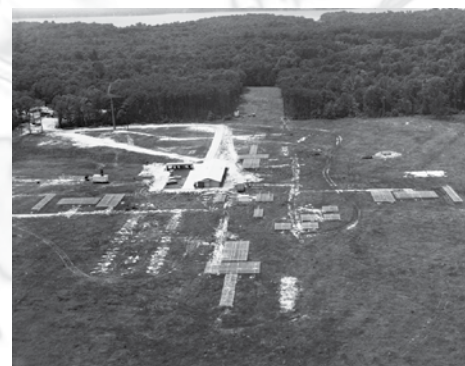
Taking the Guesswork Out of Satellite Tracking

Easton came to NRL in 1943 as a research physicist, and began by working on the development of radar beacons and blind landing systems at the Lab's Radio Division. In the 1950s, Easton collaborated with electrical engineer Milton Rosen to write NRL's Project Vanguard proposal for a scientific satellite program for the International Geophysical Year (IGY). The IGY was an unprecedented international effort to advance

scientific studies of Earth, extending from July 1, 1957, through December 31, 1958. In 1955, the Eisenhower Administration selected NRL's Vanguard program to represent the United States in the IGY and approved a plan to orbit a series of instrumented Earth satellites. Easton was one of the main scientists in the program.

NRL's Vanguard mission was to design, build, launch, and track a satellite carrying a scientific experiment. Easton not only helped to design the Vanguard I satellite (which launched March 17, 1958, and is still in orbit today), he and his colleagues also designed and built the first satellite tracking system.

The system was called MINITRACK, because it minimized the weight and power requirement of the satellite transmitter, which only needed to transmit a signal of a few milliwatts due to the very high sensitivity of the MINITRACK interferometer antenna design. Each MINITRACK ground station had pairs of interferometer antennas at right angles, with each measuring the angle to the transmitting satellite as it passed through its "fan beam" antenna pattern. There were six such stations located approximately along the 75th meridian stretching along the east coast of the United States to the west coast of South America with one other station near San Diego, California. This network of stations, each measuring the angle and time of passage overhead



MINITRACK ground station at Blossom Point, MD.

of the tiny Vanguard satellite, provided sufficient data to determine the precise orbit of the satellite.

When the Soviet Union launched Sputnik into orbit in October 1957, the United States could not track non-radiating satellites or determine if other launches occurred. Easton solved this problem by extending the



Mr. Roger Easton (left) supervising the placement of the Vanguard I satellite atop the Vanguard launch vehicle.

MINITRACK concept to actively follow unknown satellites orbiting Earth. Under his leadership, with sponsorship through the Department of Defense Advanced Research Projects Agency, now referred to as DARPA, this new tracking system became the Naval

Space Surveillance System (NAVSPASUR). This was the world's first system to detect and track all types of Earth-orbiting objects — a system that contributed to America's national security and sense of well-being during the Cold War.

Long-time colleague of Easton and current Director of NRL's Naval Center for Space Technology, Peter Wilhelm recalls Easton's work: "After seeing how well the very sensitive MINITRACK interferometer antenna field at Blossom Point, Maryland, detected and measured reflected 108-MHz radio frequency energy off the metallic shell of the Sputnik satellite, Roger quickly put together a proposal to build a new interferometer antenna system which, in a very short time frame, became the United States' most capable system for what we today call 'Space Situational Awareness' or SSA."



NTS-2 satellite team: (standing, left to right) Dr. Bruce Faraday, Mr. Richard Statler, Mr. Guy Burke, and Mr. Roger Easton; (seated, left to right) Mr. Al Bartholomew, CDR Bill Huston, Mr. Red Woosley, Mr. Ron Beard, Mr. Woody Ewen, and Mr. Pete Wilhelm.

NAVSPASUR stretched from the east coast of the U.S. to the west coast along a great circle path inclined at 32 degrees to the equator. It consisted of nine stations comprising a "fence": three on the eastern complex of receiver-transmitter-receiver, three in the center of the U.S., and three more on the western complex. The data from all six receivers was brought together at a central processing station in Dahlgren, Virginia, where the orbits of all objects passing through the fence, above a certain minimum radar cross section, could be calculated and stored in a catalog.

"As the number of objects in orbit grew, it became apparent to Roger that adding a 'second fence' south of the main fence, with an offset of about 480 miles, a 'one pass' solution could be provided to determine the object's orbit. Roger further improved the accuracy and utility of the data by adding ranging tones to the transmitted signal at the second fence. This, however, required that the receiving and transmitting sites, which were about 90 miles apart, had to be set precisely on the same time base," added Wilhelm. "Maintaining the required accuracy turned out to be difficult to accomplish, which led Roger to the vision that the way to do this was to put very good clocks, probably atomic clocks, in satellites," he said.

A Patent in Time

Easton conceived the idea of using satellite-carried precise atomic clocks for passive ranging. Starting in 1964, he conducted research, carried out space-based experiments, and published his findings that accurate, reliable, and instantaneous satellite navigation could be achieved with a combination of passive ranging, circular orbits, and a constellation of space-borne high-precision clocks synchronized to a master clock — the primary features of modern GPS.

His work exploiting space-based systems for geodesy, navigation, and timing laid the foundations for his visionary leap to the concept he dubbed TIMATION. Sponsored by the Naval Air Systems Command, Easton tested his concepts at NRL through the development and launch of four experimental satellites: TIMATION I (1967), TIMATION II (1969), TIMATION IIIA/Navigation Technology Satellite (NTS)-1 (1974), and TIMATION IV/NTS-2 (1977).

NTS-2, the first satellite to fly in the GPS 12-hour orbit and transmit GPS signals, flew the first cesium atomic frequency standard in space. Using time measurements from NTS-2, Easton experimentally verified Einstein's theory of relativity. A relativistic offset correction that he applied is still in use by every satellite in the GPS constellation. While initially designed for use by the military, GPS has been adapted for civilian use from commercial airline navigation to portable hand-held and wrist-worn devices. GPS today is a constellation of Earth-orbiting satellites providing precise naviga-



TIMATION I satellite (rectangular object) shown mounted on the side of its launch vehicle.

tion and timing data to military and civilian end-users around the globe.

A Legacy

Easton retired from NRL and federal service in 1980, going into public service in his home state of New Hampshire, and later serving as a consultant to NRL to assess industry proposals for upgrading the Naval Space Surveillance System and to explore his concept for improving GPS geolocational accuracy.

Easton has been awarded 11 patents, and has received several major awards and honors for his accomplishments. In 1978, he received the Institute of Navigation's Colonel Thomas L. Thurlow Award recognizing outstanding contributions to the science of navigation. In 1991, the Naval Space Surveillance Center established the Roger L. Easton Science and Engineering Award to mark the 30th anniversary of the Naval Space Surveillance System. The National Aeronautic Association presented its 1992 Robert J. Collier Trophy to the GPS Team composed of NRL, the U.S. Air Force, Aerospace Corp., Rockwell International, and IBM Federal Systems "for the most significant development for safe and efficient navigation and surveillance of air and spacecraft since the introduction of radio navigation 50 years ago." In 1995, the Naval Research Laboratory established the Roger L. Easton Award for Engineering Excellence "in recognition of the multiple contributions in engineering excellence achieved at NRL by and under the leadership of Roger Easton." In 1996, Easton was inducted into the GPS Joint Program Office GPS Hall of Fame "for his overwhelming contributions to engineering applications in navigation satellite technology [that] have made GPS a reality." In 1997, he received the American Philosophical Society's Magellanic Premium for Navigation "for essential contributions to creating the Global Positioning System, thereby making the tools for precision navigation available to everyone." Most recently, Easton was awarded the 2004 National Medal of Technology by President George W. Bush "for his extensive pioneering achievements in spacecraft

tracking, navigation, and timing technology that led to the development of the NAVSTAR-Global Positioning System."

Roger L. Easton joins 15 other new inductees into the National Inventors Hall of Fame. The National Inventors Hall of Fame honors the women and men responsible for the great technological advances that make human, social, and economic progress possible. Each year, the Selection Committee selects inventors for induction from those nominated by peers and



President George W. Bush awarded the 2004 National Medal of Technology to Roger Easton for his pioneering achievements in spacecraft tracking, navigation, and timing technology that led to the development of the NAVSTAR Global Positioning System.

the public for contribution to the nation's welfare and progress of science and useful arts. The Selection Committee includes representatives from leading national scientific and technical organizations. Including this year's honorees, 421 inventors have been inducted into the National Inventors Hall of Fame since its formation in 1973.

"His leap in vision led to the United States' first satellite tracking network, and his system of synchronized timing between spacecraft and user permitted 'passive ranging' which became the fundamental basis for GPS."

-- Pete Wilhelm
Director
NRL Naval Center for Space Technology

The Naval Research Laboratory

28

NRL – Our Heritage

29

Highlights of NRL Research in 2009

41

NRL Today

NRL — OUR HERITAGE

The Naval Research Laboratory's early 20th-century founders knew the importance of science and technology in building naval power and protecting national security. They equally knew that success depended on taking the long view, focusing on the long-term needs of the Navy through fundamental research. NRL began operations on July 2, 1923, as the United States Navy's first modern research institution.

Thomas Edison's Vision: The first step came in May 1915, a time when Americans were deeply worried about the great European war. Thomas Edison, when asked by a *New York Times* correspondent to comment on the conflict, argued that the Nation should look to science. "The Government," he proposed in a published interview, "should maintain a great research laboratory....In this could be developed...all the technique of military and naval progression without any vast expense." Secretary of the Navy Josephus Daniels seized the opportunity created by Edison's public comments to enlist Edison's support. He agreed to serve as the head of a new body of civilian experts — the Naval Consulting Board — to advise the Navy on science and technology. The Board's most ambitious plan was the creation of a modern research facility for the Navy. Congress allocated \$1.5 million for the institution in 1916, but wartime delays and disagreements within the Naval Consulting Board postponed construction until 1920.

The Laboratory's two original divisions — Radio and Sound — pioneered in the fields of high-frequency radio and underwater sound propagation. They produced communications equipment, direction-finding devices, sonar sets, and perhaps most significant of all, the first practical radar equipment built in this country. They also performed basic research, participating, for example, in the discovery and early exploration of the ionosphere. Moreover, the Laboratory was able to work gradually toward its goal of becoming a broadly based research facility. By the beginning of World War II, five new divisions had been added: Physical Optics, Chemistry, Metallurgy, Mechanics and Electricity, and Internal Communications.

World War II Years and Growth: Total employment at the Laboratory jumped from 396 in 1941 to 4400 in 1946, expenditures from \$1.7 million to \$13.7 million, the number of buildings from 23 to 67, and the number of projects from 200 to about 900. During WWII, scientific activities necessarily were concentrated almost entirely on applied research. New electronics equipment — radio, radar, sonar — was

developed. Countermeasures were devised. New lubricants were produced, as were antifouling paints, luminous identification tapes, and a sea marker to help save survivors of disasters at sea. A thermal diffusion process was conceived and used to supply some of the ^{235}U isotope needed for one of the first atomic bombs. Also, many new devices that developed from booming wartime industry were type tested and then certified as reliable for the Fleet.

Post-WWII Reorganization: The United States emerged into the postwar era determined to consolidate its significant wartime gains in science and technology and to preserve the working relationship between its armed forces and the scientific community. While the Navy was establishing its Office of Naval Research (ONR) as a liaison with and supporter of basic and applied scientific research, it was also encouraging NRL to broaden its scope and become, in effect, its corporate research laboratory. There was a transfer of NRL to the administrative oversight of ONR and a parallel shift of the Laboratory's research emphasis to one of long-range basic and applied investigation in a broad range of the physical sciences.

However, rapid expansion during WWII had left NRL improperly structured to address long-term Navy requirements. One major task — neither easily nor rapidly accomplished — was that of reshaping and coordinating research. This was achieved by transforming a group of largely autonomous scientific divisions into a unified institution with a clear mission and a fully coordinated research program. The first attempt at reorganization vested power in an executive committee composed of all the division superintendents. This committee was impracticably large, so in 1949, a civilian director of research was named and given full authority over the program. Positions for associate directors were added in 1954, and the laboratory's 13 divisions were grouped into three directorates: Electronics, Materials, and Nucleonics.

The Breadth of NRL: During the years since World War II, the Laboratory has conducted basic and applied research pertaining to the Navy's environments of Earth, sea, sky, space, and cyberspace. Investigations have ranged widely — from monitoring the Sun's behavior, to analyzing marine atmospheric conditions, to measuring parameters of the deep oceans. Detection and communication capabilities have benefitted by research that has exploited new portions of the electromagnetic spectrum, extended ranges to outer space, and provided a means of transferring information

reliably and securely, even through massive jamming. Submarine habitability, lubricants, shipbuilding materials, firefighting, and the study of sound in the sea have remained steadfast concerns, to which have been added recent explorations within the fields of virtual reality, superconductivity, biomolecular science and engineering, and nanotechnology.

The Laboratory has pioneered naval research into space — from atmospheric probes with captured V-2 rockets, through direction of the Vanguard project (America's first satellite program), to inventing and developing the first satellite prototypes of the Global Positioning System (GPS). Today, NRL is the Navy's lead laboratory in space systems research, as well as in fire research, tactical electronic warfare, microelectronic devices, and artificial intelligence.

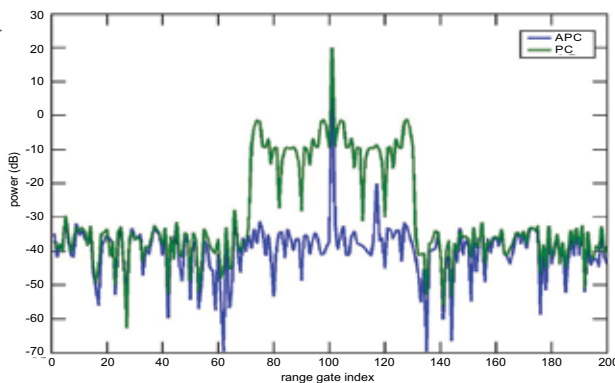
The consolidation of NRL and the Naval Oceanographic and Atmospheric Research Laboratory, with centers at Bay St. Louis, Mississippi, and Monterey, California, added critical new strengths to the Laboratory. NRL now is additionally the lead Navy center for research in ocean and atmospheric sciences, with

special strengths in physical oceanography, marine geosciences, ocean acoustics, marine meteorology, and remote oceanic and atmospheric sensing.

The Twenty-First Century: The Laboratory is focusing its research efforts on new Navy strategic interests in the 21st century, a period marked by global terrorism, shifting power balances, and irregular and asymmetric warfare. NRL scientists and engineers are working to give the Navy the special knowledge, capabilities, and flexibility to succeed in this dynamic environment. While continuing its programs of basic research that help the Navy anticipate and meet future needs, NRL also moves technology rapidly from concept to operational use when high-priority, short-term needs arise — for pathogen detection, lightweight body armor, contaminant transport modeling, and communications interoperability, for example. The interdisciplinary and wide-ranging nature of NRL's work keeps this "great research laboratory" at the forefront of discovery and innovation, solving naval challenges and benefiting the nation as a whole.

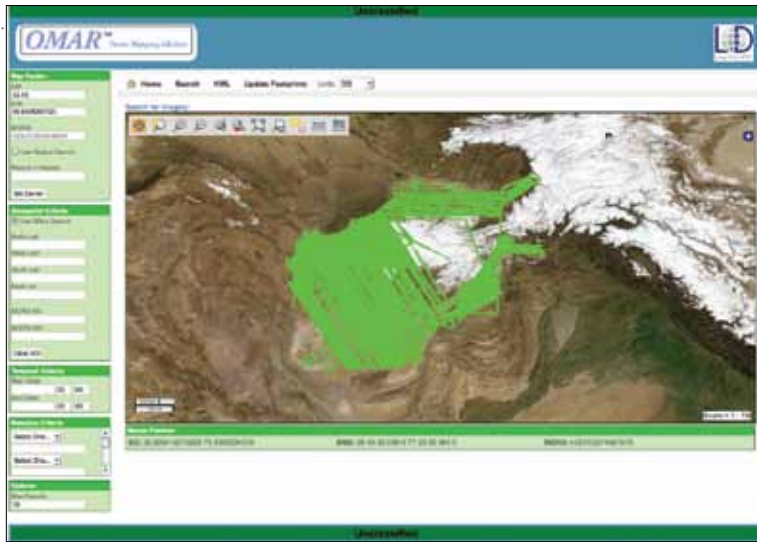
HIGHLIGHTS OF NRL RESEARCH IN 2009

The scientific community at NRL conducts innovative research across a wide spectrum of technical areas, much of it detailed in the *NRL Review* chapters ahead. The following is a selection of the many projects pursued during 2009.



Plot of received signal power after pulse compression processing for a series of range gates. Using traditional pulse compression (green), the sidelobes of the high RCS target at range gate 100 mask the presence of the low RCS target at range gate 120. The APC process (blue) suppresses the sidelobes, allowing detection of the smaller target.

ADAPTIVE PULSE COMPRESSOR: In a radar detection scenario in which a high radar cross section (RCS) threat and a low RCS threat are in close proximity, the application of standard radar pulse compression (PC) techniques on receive results in the high RCS threat masking the low RCS threat, rendering the low RCS threat undetectable. NRL's recently developed Adaptive Pulse Compressor (APC) algorithm greatly increases the radar's sensitivity to these smaller targets. In simulation, lab experimentation, and short-range, proof-of-concept experiments, the APC resolved and detected low RCS threats by lowering significantly the pulse compression range sidelobes of the nearby large threats. Experiments using a functional X-band APC test bed verified substantive sidelobe performance improvement (>20 dB) over the standard pulse compressor in an open-air configuration. When the APC was used to process data collected from the SPY-1 radar, it demonstrated greater than 10 dB sidelobe performance improvement over the standard pulse compressor.

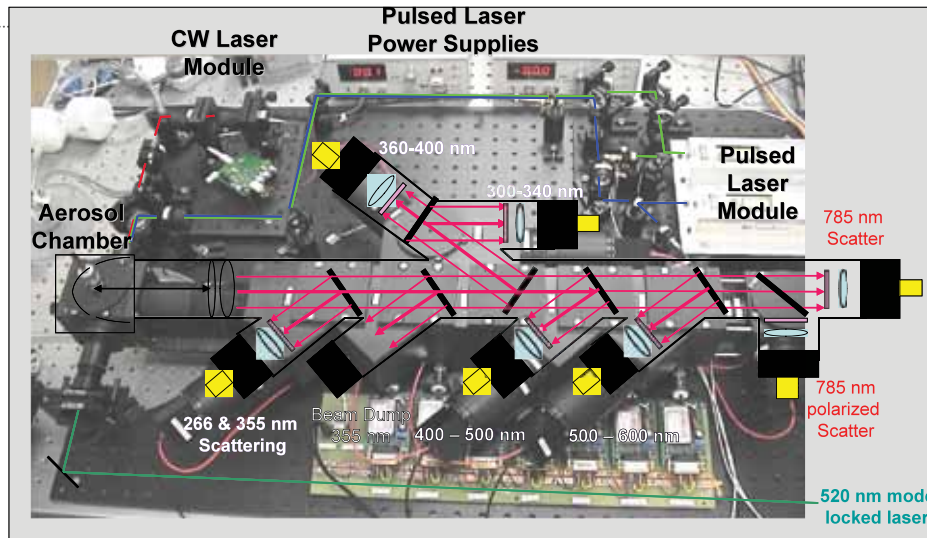


The Large Data OMAR tool provides dynamic web services for image and video large archive search.

LARGE DATA JOINT CAPABILITIES TECHNOLOGY DEMONSTRATION (JCTD):

The NRL Large Data JCTD addresses a number of formidable data dissemination challenges presently facing various branches of the Department of Defense. Chief among those challenges is the ability to gather vast amounts of raw

data from widely distributed sources, process that raw data into useful information, and make that information available to a wide range of global consumers with differing needs. The Large Data JCTD created technical solutions to enable large file and archive data sharing across a global enterprise, high performance access to data for applications, resilient continuity of operations, enhanced transport for 10 Gbps networks, and extremely dense shared storage in a highly efficient footprint. The result is faster access to critical data by warfighters and analysts. In 2009, the Large Data JCTD team was awarded Team of the Year by the Director of Defense Research and Engineering.



Optical layout of the bioaerosol detection system.

MEASUREMENT OF TWO-PHOTON EXCITATION EMISSION FROM SINGLE MICRON-SIZED BIO-AEROSOLS:

NRL researchers recently developed a test bed for investigating the optical spectra from single micron-sized aerosol particles. Using this test bed, they evaluated a new mode-locked fiber laser with a 40 MHz pulse repetition frequency and 500 femtosecond pulse duration as part of a bioaerosol detection system. The short pulse lengths have enabled the first observation of two-photon excitation fluorescence from individual aerosol particles made from biological warfare agent simulants. Previous methods of bioaerosol detection have used lasers with ultraviolet wavelengths as excitation for characteristic bioparticle emission. With the new two-photon excitation process, bioaerosols may be detected using lasers in the visible part of the spectrum. This could result in an increased range for sensors used for remote detection of biological aerosols.

316L Prop (15 min)
Fin perforation



LTIH-316L Prop (15 min)
No penetrating damage

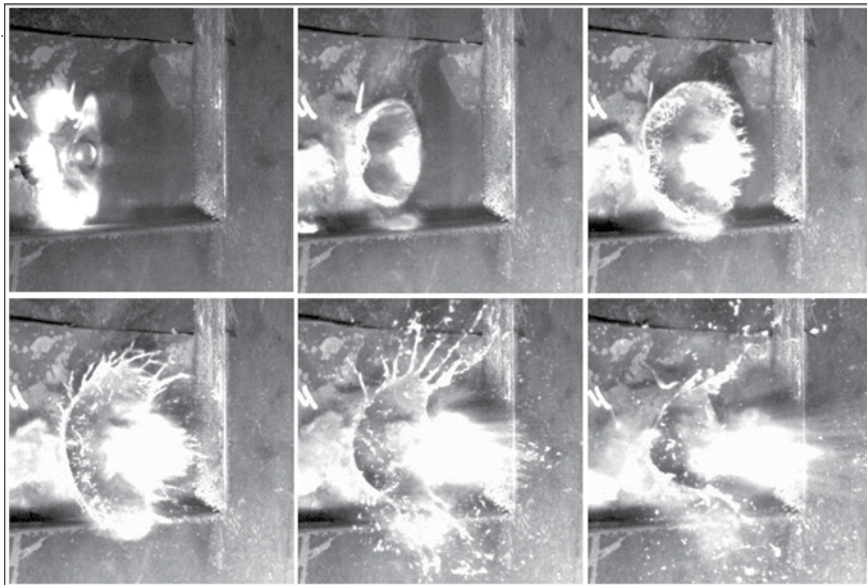


LTIH-316L Prop (60 min)
Fin perforation



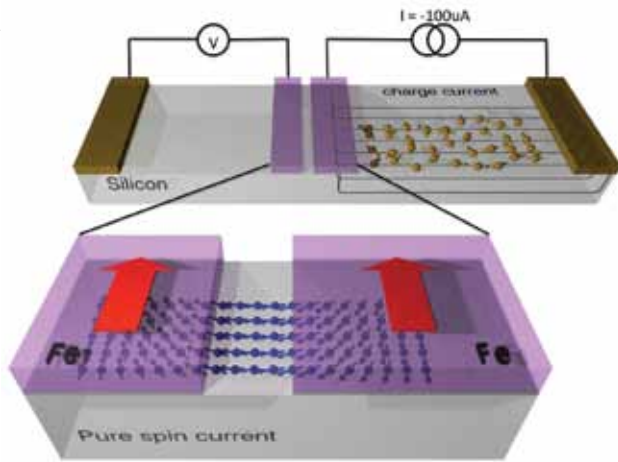
DEVELOPMENT OF CAVITATION-RESISTANT ALLOYS BY SURFACE HARDENING USING LOW-TEMPERATURE CARBURIZATION:

NRL demonstrated improved cavitation erosion resistance on stainless steel propellers using low-temperature interstitial hardening (LTIH), a technology that diffuses significant amounts of carbon into the stainless steel surface.



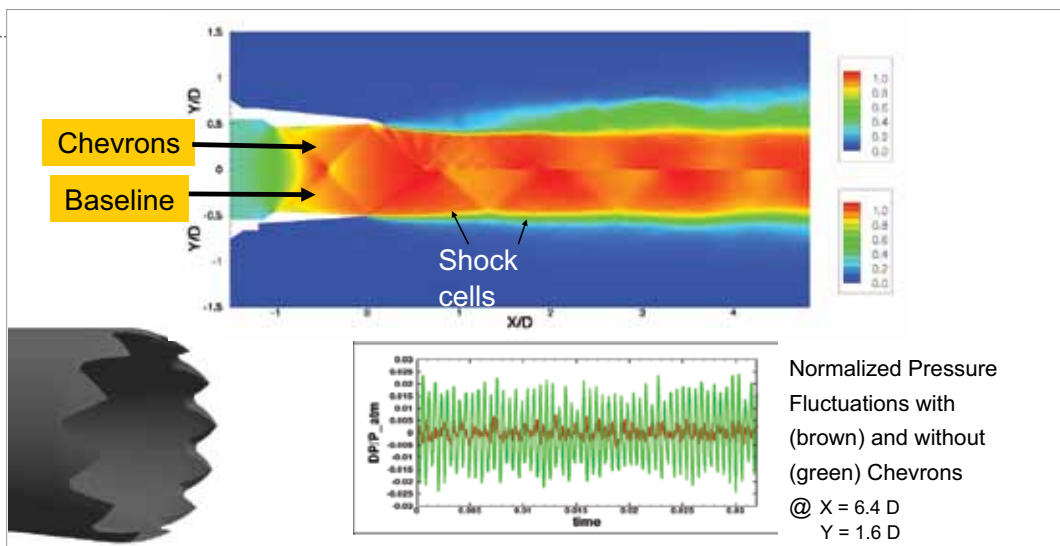
Viscoelastic phase transition induced in polyurea by impact of .50 caliber projectile. Repeated interactions with polymer/metal layers break the pressure wave into multiple, lower-amplitude waves.

HETEROGENEOUS LAMINATE ARMOR: A composite array of heterogeneous elastomer-steel panels has been found to substantially increase the penetration resistance (“ballistic limit”) of armor. The resulting structure is lighter and more effective than conventional armor, finding broad utility in both military applications and for the protection of civilian infrastructure. The elastomer laminate assemblies function by breaking up and dissipating the pressure wave created upon impact of a bullet or bomb fragment.

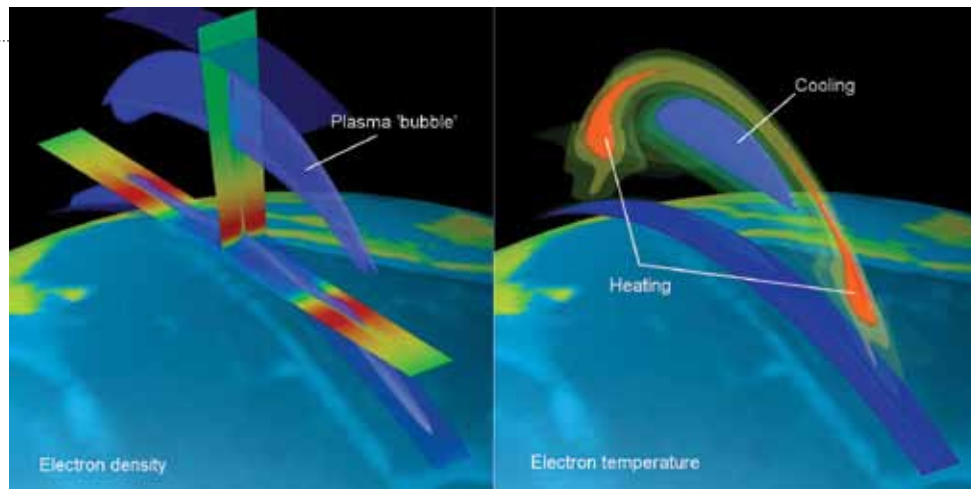


Silicon spin-valve. Spin-polarized electrons injected from the Fe/Al₂O₃ tunnel barrier form a charge current flowing to the right, and generate a pure spin current flowing to the left. This pure spin current produces a voltage at a second magnetic contact that is sensitive to the relative orientation of the spin in the silicon. The orientation of the spin in the silicon can be uniformly rotated by an applied magnetic field (coherent precession). Thus, information can be encoded on the spin system and read out as a voltage.

INFORMATION PROCESSING WITH PURE SPIN CURRENTS IN SILICON: NRL has demonstrated that information can be transmitted and processed with pure spin currents in silicon – an important step toward the realization of a functional silicon spintronic device. Fe/Al₂O₃ tunnel barrier contacts are used to produce significant electron spin polarization in the silicon, generating a spin current which flows outside of the charge current path. This pure spin current produces a voltage at a second magnetic contact that is sensitive to the relative orientation of the spin in the silicon. The spin orientation (and thus the output voltage) is controlled in one of three ways: (a) by switching the magnetization of the Fe contact, (b) by changing the polarity of the bias on the Fe/Al₂O₃ “injector” contact, which generates either majority or minority spin populations in the Si, providing a way to electrically manipulate the spin orientation without changing the magnetization of the contact itself, and (c) by inducing coherent spin precession through application of a small perpendicular magnetic field. This manipulation and detection of pure spin current was demonstrated in a planar silicon spin-valve device with output characteristics similar to those of non-volatile giant magnetoresistance metal spin-valve structures.

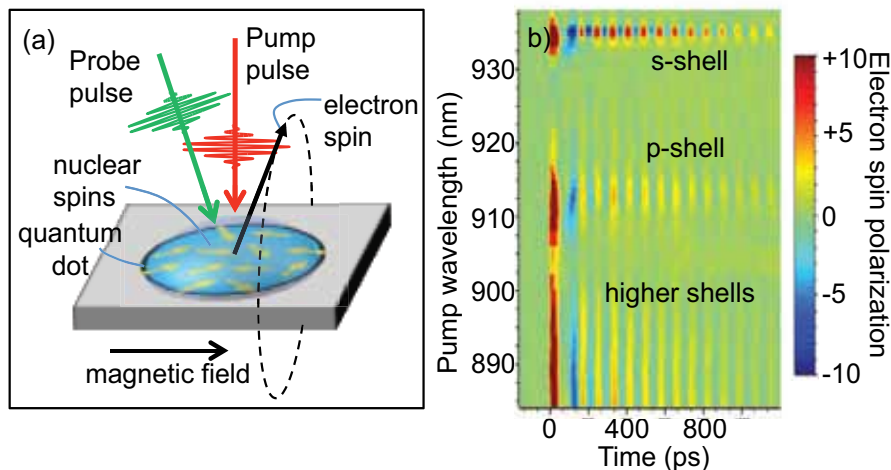


JET NOISE REDUCTION USING CHEVRONS: In a study to identify noise reduction techniques for military aircraft engines, NRL has conducted monotonically integrated large-eddy simulations (MILES) of the flow fields and acoustics of supersonic jet flows from military jet engine nozzles with and without flow modifiers called chevrons. A finite-element flow solver using unstructured grids allows us to accurately model the nozzle geometry with chevrons, and the MILES approach directly computes the large-scale turbulent flow structures. Our simulations have shown that significant reduction in pressure oscillations is possible using mechanical chevrons even in supersonic flows. The chevrons are observed to disrupt the shock waves and modify the shock cells to reduce the level of pressure fluctuations generated within the jet. This translates into a reduction in the noise.



Three-dimensional graphic of electron density (left) and electron temperature (right) based on SAMI3/ESF. The large blue isosurface in the left panel is the rising plasma “bubble” associated with ESF. In the right panel the blue isosurface shows the cooling of the electrons inside the bubble; the red isosurface shows the heating of the electrons by collisional coupling with the ions and by thermal conduction at higher altitudes.

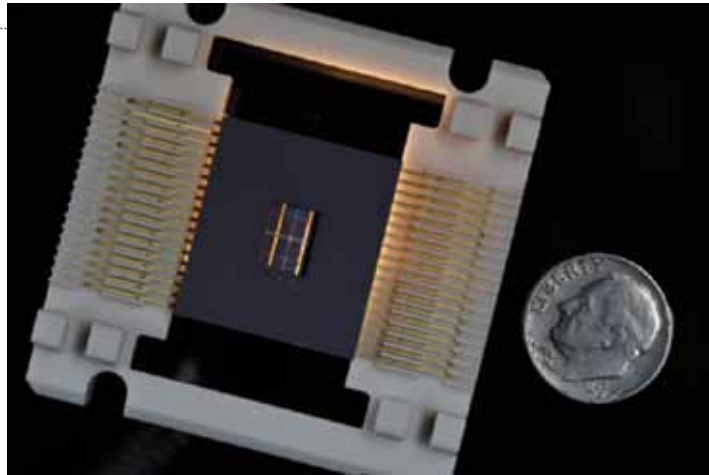
EQUATORIAL SPREAD F MODELING: Equatorial spread F (ESF) is a low-latitude ionospheric phenomenon that leads to the development of large-scale electron density depletions, or “bubbles,” that disrupt communication and navigation systems. The development of models to understand and predict the onset and evolution of ESF is critically important to a number of space-based systems. NRL has developed a three-dimensional code, SAMI3/ESF, to study the evolution of ESF. The model is based on the comprehensive, multi-ion ionosphere model SAMI3 that follows the dynamical and chemical evolution of seven ion species (H^+ , He^+ , N^+ , O^+ , N^{+2} , NO^+ , and O^+). Additionally, the SAMI3/ESF model solves the complete ion temperature equation for three ion species (H^+ , He^+ , and O^+), and the electron temperature equation. SAMI3/ESF is the most comprehensive 3D model of ESF in the world.



(a) Illustration of two laser pulses manipulating an electron spin in a quantum dot. (b) Color scale map of the electron spin polarization as a function of the pump pulse wavelength and time. The probe pulse wavelength is set to 935 nm, the s-shell of the quantum dot. Oscillations in time are due to electron spin precession in the magnetic field.

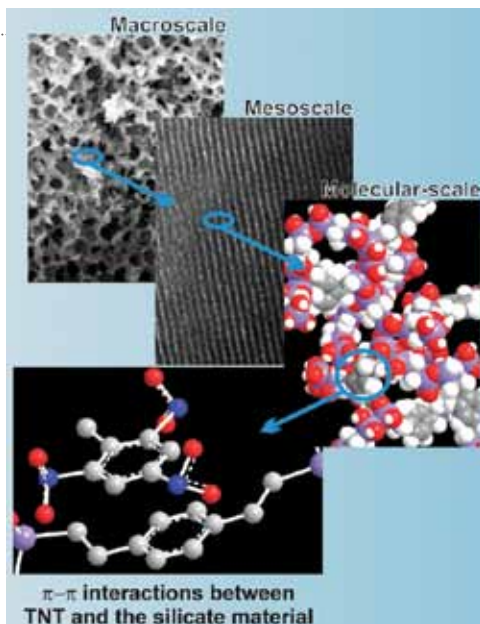
ULTRAFAST TWO-COLOR MANIPULATION OF SPINS IN QUANTUM DOTS FOR QUANTUM

INFORMATION: An electron spin in a quantum dot is of great interest for quantum information applications, which have the potential to revolutionize computation and secure communications. NRL has made key advances in very fast control of electron spins and their environment using two picosecond pulses at two different wavelengths. This ultrafast two-color technique was used to polarize electron spins through excited energy levels in quantum dots, giving control of the spin orientation and the spatial extent of its wavefunction. The laser pulses were also shown to adjust the nuclear spin environment depending on the pulse wavelength, providing a way to stabilize the nuclear spin polarization and lengthen the coherence lifetime of spins in quantum dots.



XeF₂-etched 4-Mbit CMOS/SOI SRAM in a package with an aperture, prior to boron-10 deposition.

LOW-POWER DIGITAL NEUTRON DETECTOR: NRL has demonstrated the world's first digital neutron detector. The low-power (< 1 mW) detector is based on memory state change. A 4 Mbit complementary metal-oxide-semiconductor/silicon-on-insulator (CMOS/SOI) static random access memory (SRAM) is loaded with a boron-10 neutron conversion layer after etching the thick silicon substrate down to the buried oxide of the SOI structure. The memory cells in this modified structure are then less than 0.2 microns away from the deposited boron-10 layer. Neutrons are converted by the boron-10 into charged alpha and lithium particles, which travel the short distance into the SRAM and cause memory state changes. This memory cell-based detection system has the potential to enable important new applications in health physics and homeland security.

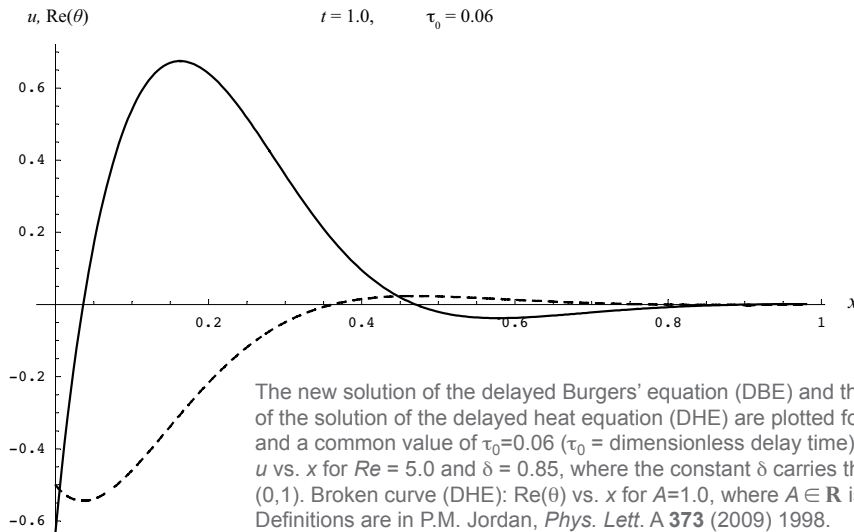


Heirarchical organosilicate materials. Macroscale structure allows rapid diffusion of targets to an organized mesoscale structure containing a high concentration of binding sites. Diethylenebenzene bridging groups in the material offer target binding capacity, and siloxane groups provide structural rigidity.

PERIODIC MESOPOROUS ORGANOSILICAS (PMOs) AS PRECONCENTRATION ELEMENTS FOR IMPROVED LONG-TERM MONITORING OF NITROENERGETICS IN GROUNDWATER:

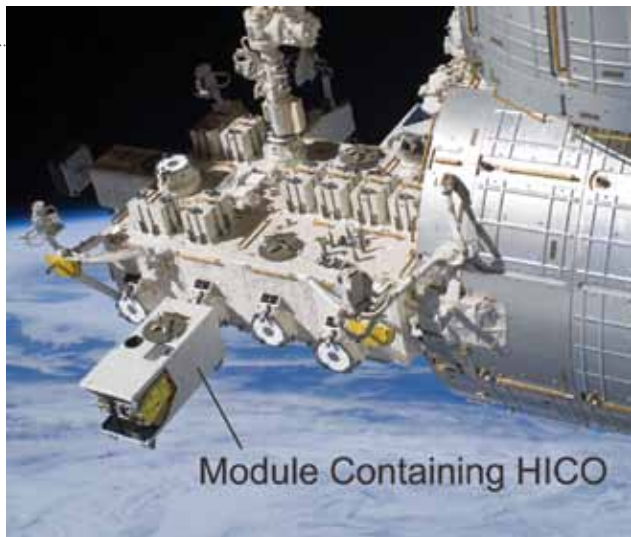
NRL has developed novel materials to aid in the field detection of traces of nitroenergetic compounds such as TNT, DNT, RDX, and HMX in groundwater. These contaminants are present at many DoD sites used for weapons testing and training; monitoring them with currently

available portable technologies usually requires preconcentration of the target compound to provide detectable levels. Preconcentration can be accomplished with target-selective sorbents made from periodic mesoporous organosilicas (PMOs), hybrid materials that combine organic groups and inorganic silica components to take advantage of the properties of both. The silicate component provides a high-surface-area, stable structure while the organic moieties offer favorable binding characteristics. NRL's new synthesis protocol creates PMOs with organizational structure on multiple length scales and allows imprinting of the materials for enhanced target selectivity. These new PMOs have shown order-of-magnitude enhancement in concentration of targets sampled from groundwater.



A NEW EXACT SOLUTION OF THE DELAYED BURGERS' EQUATION OF NONLINEAR ACOUSTICS VIA THE COLE-HOPF TRANSFORMATION:

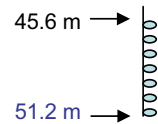
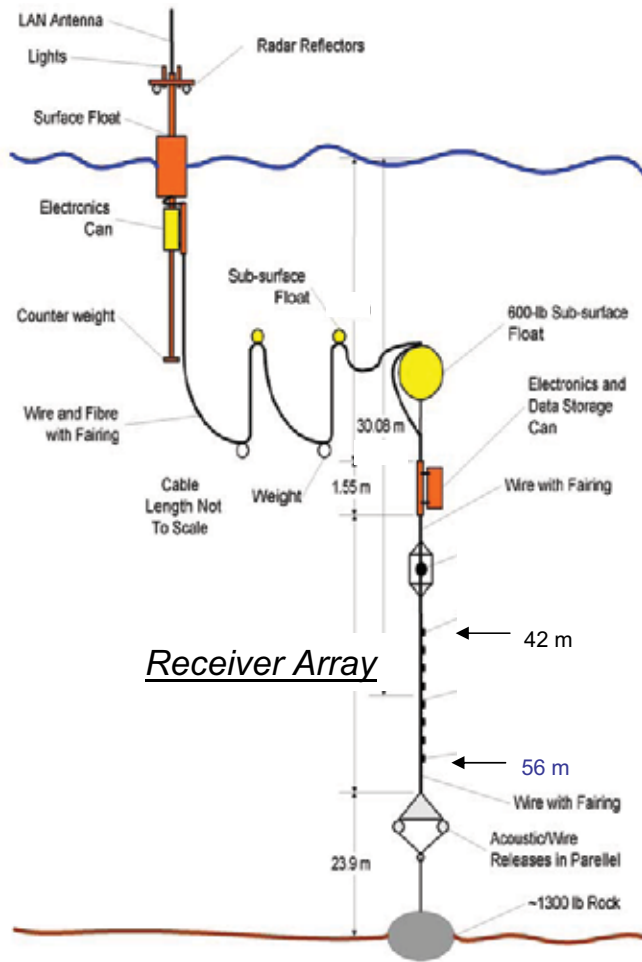
In problems involving large-amplitude acoustic signals, the usual linear theory of sound propagation is found to be inadequate as the effects of nonlinearity, being cumulative in nature, rapidly become felt over time and distance. As a result, while exotic and possibly useful acoustic phenomena emerge when nonlinearities are present, researchers are often forced to give up on the idea of obtaining analytical solutions, due to the inherent mathematical obstacles posed by nonlinear problems, and instead turn to numerical methods. NRL has shown that the Cole-Hopf transformation, a mathematical "trick" used to solve the famous Burgers' equation (a nonlinear partial differential equation), can also be used to obtain an exact solution to the more complicated time-delayed Burgers' equation. Equations of this type have arisen in the modeling of a wide range of physical phenomena including, but not limited to, acoustic propagation in thermo-viscous fluids (e.g., seawater), turbulence, waves in granular media, and even the flow of traffic on highways.



HICO was launched to the International Space Station in September 2009 and is shown attached to the Station in this NASA photograph.

DEVELOPMENT AND LAUNCH OF THE HYPERSPECTRAL IMAGER FOR THE COASTAL OCEAN (HICO):

NRL's Hyperspectral Imager for the Coastal Ocean, now operating on the International Space Station, is the first hyperspectral imager designed to demonstrate the ability to characterize coastal ocean environments using space imagery. HICO images of coastal zones are processed to produce maps of water depth, suspended and dissolved matter, and water optical properties. HICO was built and is operated by NRL under the sponsorship of the Office of Naval Research Innovative Naval Prototype program. As an Innovative Naval Prototype, HICO also demonstrated significant cost and schedule savings for this pathfinder instrument by using commercial off-the-shelf components, and was delivered only 16 months after program start.

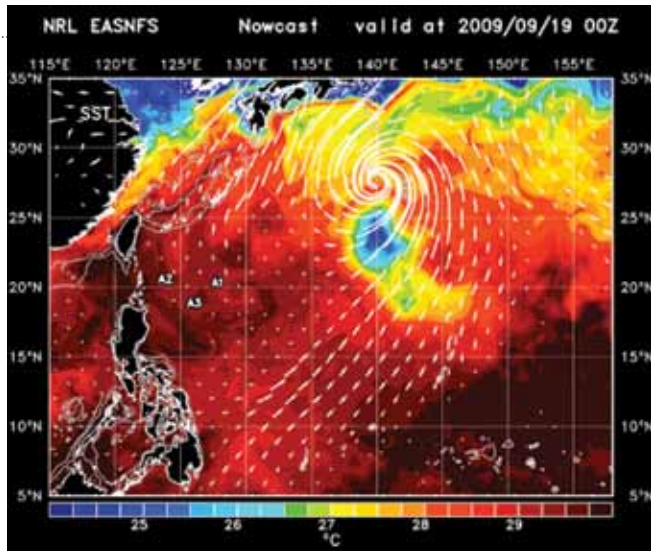


Source Array

Experimental setup for MIMO underwater acoustic communications at sea. An 8-element source array was used to transmit acoustic communications signals to an 8-element receiver array to demonstrate the increase in data rate (multiplicity).

MULTIPLICITY AND DIVERSITY OF MULTIPLE-INPUT MULTIPLE-OUT (MIMO) UNDERWATER

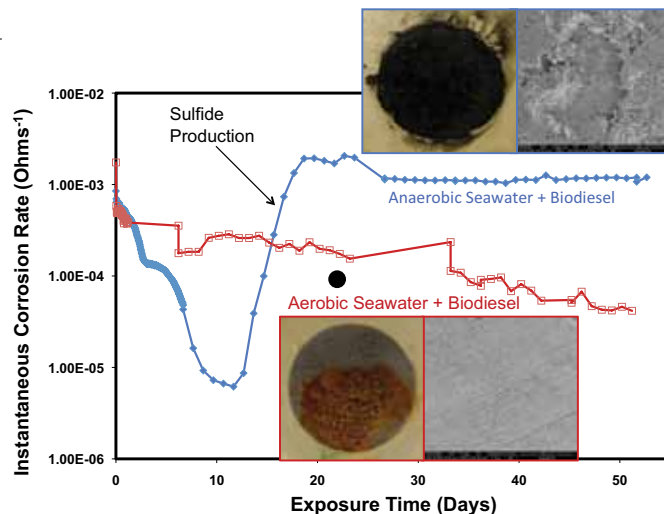
ACOUSTIC COMMUNICATIONS: NRL has demonstrated that the multiplicity of an 8x8 MIMO system is indeed 8. Using a direct-sequence code-division-multiple-access (DS-CDMA) communication scheme, in which we use de-spreading to remove the co-channel interference, we show that an 8x8 MIMO system has zero bit error rate. In other words, an 8x8 CDMA system has eight times the data rate of a 1x1 system.



The NRL EASNFS sea surface temperature prediction for 2009/09/19 00Z. The wind stresses from FNMOC NOGAPS showing Typhoon Melor are superimposed. The prediction shows an intense cold wake behind the typhoon over a cold eddy that is induced by strong wind-generated turbulence mixing. The moorings deployed by Taiwan ITOP investigators are indicated by A1, A2, and A3; these observations are used for evaluation of the ocean/wave/atmosphere models.

TOWARD A COUPLED OCEAN-WAVE-ATMOSPHERE MODEL OF TYPHOON IMPACTS ON THE WESTERN PACIFIC:

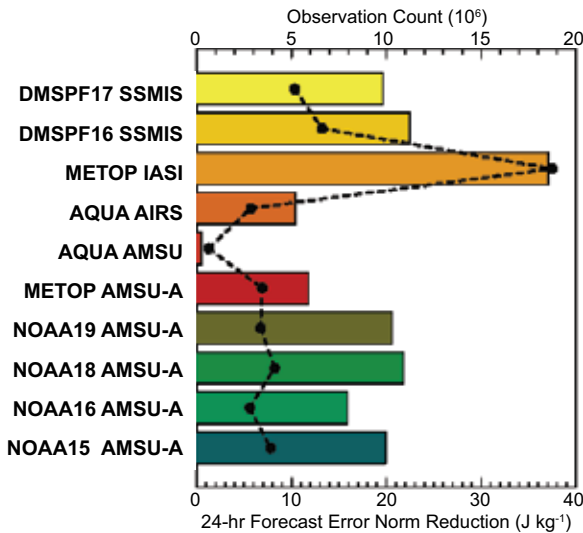
NRL has developed an ocean nowcast/forecast system to cover the study area of the Office of Naval Research Departmental Research Initiative (DRI) "Impact of Typhoons on the Ocean in the Pacific" (ITOP). In collaboration with other ITOP investigators and the TCS project (Tropical Cyclone Structure field experiment in the Western North Pacific), NRL studies the interaction between the ocean, waves, and atmosphere under typhoon conditions and applies the knowledge learned to improve Navy ocean prediction capability. In 2009, NRL conducted real-time ocean prediction experiments using its East Asian Seas Ocean Nowcast/Forecast System (EASNFS) and Intra-Americas Sea Ocean Nowcast/Forecast System (IASNFS) for both the Western Pacific and Atlantic regions. Daily ocean predictions as well as satellite remote sensing data and weather forecasts were provided to other investigators in the ITOP DRI to initialize their ocean/wave/atmosphere models and use the products for boundary conditions. Archived data supported virtual experiments in 2009 and will support a planned 2010 field experiment.



Carbon steel coupons (2 cm²) were exposed to natural seawater with biodiesel addition under anaerobic (blue) and aerobic (red) conditions. After 12 days, sulfide production in the anaerobic exposure resulted in a three-order-of-magnitude increase in corrosion rate. The carbon steel corrosion rate in anaerobic seawater without biodiesel addition (*) was the lowest. Aerobic exposure produced orange iron hydroxide corrosion products and slight etching of the carbon steel surface. Anaerobic exposure produced black iron sulfide corrosion products and deep localized pitting.

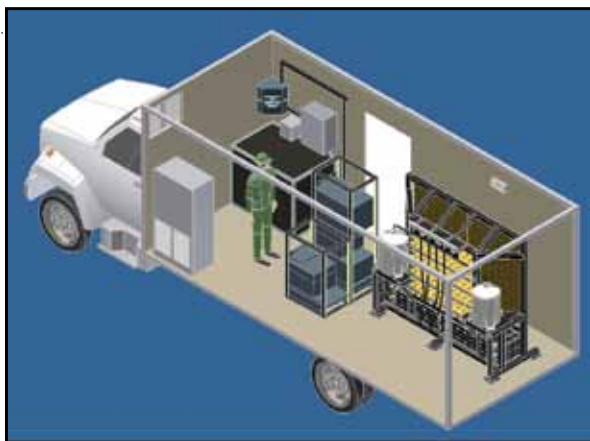
MICROBIAL AND ELECTROCHEMICAL CHARACTERIZATION OF ADVANCED DIESEL FUELS:

NRL experiments have clearly demonstrated that naturally occurring microorganisms in coastal seawater in the presence of biodiesel can influence metal corrosion under both aerobic and anaerobic conditions. Specific corrosion mechanisms may vary with chloride and oxygen concentration. Under anaerobic conditions (such as those typically found in pipes or storage tanks), microbial sulfide production is stimulated by the presence of biodiesel either as a separate phase or emulsified in water. Results indicate there may be risks in the storage and transportation of biodiesel in the presence of seawater.



Example of information derived from NAVOBS. This figure shows the cumulative reduction (horizontal bars) in 24-hr NOGAPS forecast error obtained by assimilating various types of satellite radiance observations in NAVDAS-AR from 17 Jan to 16 Feb 2009. Each instrument type (AMSU-A, AIRS, IASI, SSMIS) includes many radiance channels, for which impacts can also be separately evaluated using NAVOBS. The number of observations is shown by points on the dashed line.

TRANSITION OF NRL'S OBSERVATION IMPACT MONITORING SYSTEM: NRL developed the only computationally feasible technique to accurately quantify and evaluate the forecast impact of all assimilated observations in an operational numerical weather prediction framework. NAVOBS, the NRL OBServation impact monitoring System, was transitioned to Navy operations at Fleet Numerical Meteorology and Oceanography Center (FNMOC) in 2009, and is being implemented at other forecast centers around the globe, including the European Center for Medium-range Weather Forecasts, Environment Canada, the United Kingdom Meteorological Office, and the NASA Global Modeling and Assimilation Office. NAVOBS is based on the adjoints of NAVDAS-AR (NRL Atmospheric Variational Data Assimilation System–Accelerated Representer) and NOGAPS (Navy Operational Global Atmospheric Prediction System). On the NAVOBS web page (http://www.nrlmry.navy.mil/obsens/fnmoc/obsens_main_od.html), users can generate combinations of over 10,000 different graphical images and statistical results. Information about the impact of individual observations is used to improve data assimilation procedures and short-range forecast skill.



MISTI was developed for standoff detection of special nuclear materials, with funding from the Domestic Nuclear Detection Office of the Department of Homeland Security. The MISTI system is shown housed in a customized box truck.

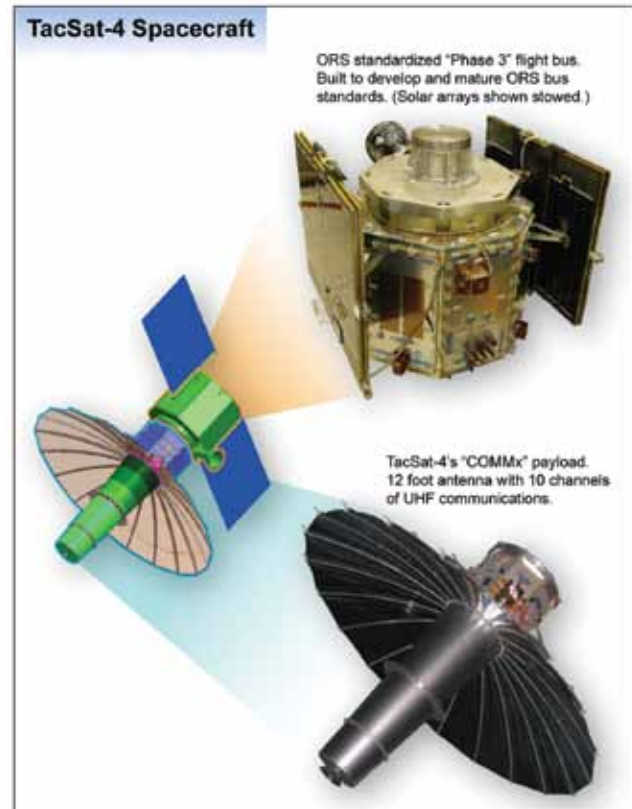
MOBILE IMAGING AND SPECTROSCOPIC THREAT IDENTIFICATION (MISTI):

NRL's MISTI system is a mobile, self-contained, gamma-ray spectroscopy and imaging system for detecting radiological threats. Gamma-ray

detection and imaging are difficult due to the low interaction probability and inability to focus high-energy photons. MISTI's hybrid system combines the exceptional spectroscopic capabilities of germanium detectors with the cost-effective collection power of an imaging array of sodium iodide detectors. The data from the sensor is analyzed in real time onboard the vehicle and is combined with optical and infrared images and data from other instruments to provide users with a visual location of the source. The system can detect nuclear materials (e.g., Cs-137) at distances up to 100 m in 20 seconds with a ±10 m accuracy in range determination. Its commercial off-the-shelf technology reduces total cost.



The TacSat-4 spacecraft.



TacSat-4 COMMx ADVANCED SATCOM EXPERIMENT: In 2009, NRL completed all flight hardware development and testing for the integrated space vehicle (payload and bus) for the TacSat-4 mission. TacSat-4 is a Navy-led joint mission to augment current satellite communications (SATCOM) capabilities and to advance Operationally Responsive Space (ORS) systems. TacSat-4 provides 10 ultra high frequency (UHF) channels available for any combination of communications, data exfiltration, or Friendly Force Tracking. The unique orbit augments geosynchronous SATCOM assets by providing near-global, but not continuous, coverage that includes the high latitudes. TacSat-4 provides communications-on-the-move (COTM) for existing radios without requiring users to point their antennas toward the satellite. Technologies that enable these capabilities on a small satellite (<500 kg) include the 12-foot deployable antenna, the payload's thermal subsystem, a standardized spacecraft bus, and the Virtual Mission Operations Center (VMOC). With the spacecraft complete, TacSat-4 is ready for its 2010 launch.

Celebration of NRL Continuous Service

August 19, 2010

On this day, CAPT Paul Stewart and Dr. John Montgomery recognized the loyalty of NRL employees who have completed from 5 to 50 years of continuous NRL service. The celebration included the presentation of lapel pins to representatives of each 5-year “Class” of employees. Each pin was designed to represent an NRL innovation of substantial significance both to the Navy and the Nation.

August has special importance in the history of NRL, for it was in August 1916 that Congress appropriated \$1,000,000 for the construction of the Naval Research Laboratory and an additional \$500,000 for the initial year of operation. Ground was broken for Building 1 in December 1920, and NRL began operations in July 1923.

COMMEMORATIVE SERVICE PINS



NRL Seal – 5 years

U.S. Radar – 10 years

Moon Radar – 15 years



Vanguard – 20 years

Molecular Structure Determination – 25 years

GRAB – 30 years



Deep Ocean Search – 35 years

GPS – 40 years

Specific Emitter Identification – 45 years

Custom Pin – 50 years

This pin will be custom designed to reflect the recipient’s most significant contribution to NRL over their 50 years of service.

NRL TODAY

ORGANIZATION AND ADMINISTRATION

The Naval Research Laboratory is a field command under the Chief of Naval Research, who reports to the Secretary of the Navy via the Assistant Secretary of the Navy for Research, Development and Acquisition.

Heading the Laboratory with joint responsibilities are CAPT Paul C. Stewart, USN, Commanding Officer, and Dr. John A. Montgomery, Director of Research. Line authority passes from the Commanding Officer and the Director of Research to three Associate Directors of Research, the Director of the Naval Center for Space Technology, and the Associate Director for Business Operations. Research divisions are organized under the following functional directorates:

- Systems
- Materials Science and Component Technology
- Ocean and Atmospheric Science and Technology
- Naval Center for Space Technology

The *NRL Fact Book*, published every two years, contains information on the structure and functions of the directorates and divisions.

NRL operates as a Navy Working Capital Fund (NWCF) Activity. All costs, including overhead, are charged to various research projects. Funding in FY09 came from the Chief of Naval Research, the Naval Systems Commands, and other Navy sources; government agencies such as the U.S. Air Force, the Defense Advanced Research Projects Agency, the Department of Energy, and the National Aeronautics and Space Administration; and several nongovernment activities.

PERSONNEL DEVELOPMENT

At the end of FY09, NRL employed 2669 persons — 37 officers, 70 enlisted, and 2562 civilians. In the research staff, there are 784 employees with doctorate degrees, 316 with master's degrees, and 442 with bachelor's degrees. The support staff assists the research staff by providing administrative support, computer-aided design, machining, fabrication, electronic construction, publication and imaging, personnel development, information retrieval, large mainframe computer support, and contracting and supply management services.

Opportunities for higher education and other professional training for NRL employees are available through several programs offered by the Employee Relations Branch. These programs provide for graduate work leading to advanced degrees, advanced training, college course work, short courses, continuing

education, and career counseling. Graduate students, in certain cases, may use their NRL research for thesis material.

For non-NRL employees, several postdoctoral research programs exist. There are also agreements with several universities for student opportunities under the Student Career Experience Program (formerly known as Cooperative Education), as well as summer and part-time employment programs. Summer and interchange programs for college faculty members, professional consultants, and employees of other government agencies are also available. These programs are described in the *NRL Review* chapter "Programs for Professional Development."

NRL has active chapters of Women in Science and Engineering (WISE), Sigma Xi, Toastmasters International, and the Federal Executive and Professional Association. An amateur radio club, a drama group, and several sports clubs are also active. NRL has a Recreation Club that provides gymnasium and weight-room facilities. NRL also has an award-winning Community Outreach Program. See "Programs for Professional Development" for details on all these programs and activities.

NRL has its very own credit union. Established in 1946, NRL Federal Credit Union (NRLFCU) is a sound financial institution that serves about 20,000 NRL employees, contractors, select employee groups, and their families. Focusing on its mission of *Trusted Partners for Life*, NRLFCU provides many free and low-cost products and services including free bill payer, great rates on deposits, credit cards, auto loans, mortgages and more. It offers direct deposit, online access, three local branches (one of them located in Bldg. 222) and nationwide access via the National Shared Branching Network. NRLFCU also offers full-service investment and brokerage services. For more information, call 301-839-8400 or log onto www.nrlfcu.org.

Public transportation to NRL is provided by Metrobus. Metrorail service is three miles away.

SITES AND FACILITIES

NRL's main campus in Washington, D.C., consists of 87 main buildings on about 130 acres. NRL also maintains 11 other research sites, including a vessel for fire research and a Flight Support Detachment. The many diverse scientific and technological research and support facilities are described here. More details can be found in the *NRL Major Facilities* publication at www.nrl.navy.mil.

Institute for Nanoscience



Nanoscience Cleanroom Facility

The revolutionary opportunities available in nanoscience and nanotechnology led to a National Nanotechnology Initiative in 2001. The NRL Institute for Nanoscience was established in that same year with a current annual budget of \$11 million in core research funds. The prospect for nanoscience to provide a dramatic change in the performance of materials and devices was the rationale for identifying this emerging field as one of the DoD strategic research areas for basic research funding on a long-term basis.

The mission of the NRL Institute for Nanoscience is to conduct highly innovative, interdisciplinary research at the intersections of the fields of materials, electronics, and biology in the nanometer size domain. The Institute exploits the broad multidisciplinary character of the Naval Research Laboratory to bring together scientists with disparate training and backgrounds to pursue common goals at the intersection of their respective fields in systems at this length scale. The Institute provides the Navy and DoD with scientific leadership in this complex, emerging area and

identifies opportunities for advances in future defense technology. NRL's nanoscience research programs and accomplishments directly impact nearly all Naval S&T focus areas.

The Institute's current research program emphasizes multidisciplinary, cross-division efforts in a wide range of science and technology applications:

- Ultra-low-power electronics
- Quantum information processing
- Chem/bio/explosive sensing
- Energy conversion/storage
- Photonics/plasmonics
- Multifunctional materials
- Biomimetics
- Biologically based complex assembly

The Institute for Nanoscience building, opened in October 2003, provides NRL scientists access to state-of-the-art laboratory space and fabrication facilities. The building has 5000 ft² of Class 100 clean room space for device fabrication, 4000 ft² of "quiet" space with temperature controlled to ± 0.5 °C, acoustic isolation at the NC35 standard (35 dB at 1 kHz), floor vibration isolation to <150 $\mu\text{m/s}$ rms at 10 to 100 Hz and <0.3

mOe magnetic noise at 60 Hz, and 1000 ft² of “ultra-quiet” laboratory space with temperature controlled to ± 0.1 °C and acoustic isolation at the NC25 standard (25 dB at 1 kHz). Clean room equipment includes a wide range of deposition and etch systems; optical mask aligners; an electron beam writer; a focused ion beam writer; an optical pattern generator for mask making; a plasma-enhanced atomic layer deposition system; a laser machining tool; a wide variety of characterization tools; and more. ♦



Metrology.



Electron beam lithography.



The Institute for Nanoscience research building.

Radar



The AMRFC testbed, located at NRL's CBD, was developed as a proof-of-principle demonstration system that is capable of simultaneously transmitting and receiving multiple beams from common transmit and receive array antennas for radar, electronic warfare, and communications.

NRL has gained worldwide renown as the birthplace of U.S. radar, and for more than half a century has maintained its reputation as a leading center for radar-related research and development. A number of facilities managed by NRL's Radar Division continue to contribute to this reputation.

A widely used major facility is the Compact Antenna Range (operated jointly with the Space Systems Development Department) for antenna design and development and radar cross section measurements. The range is capable of simulating far-field conditions from 1 to 110 GHz, with a quiet zone approximately 7 ft in diameter and 8 ft in length. Instrumentation covers from 1 to 95 GHz. Another strong division capability is in the Computational Electromagnetics (CEM) Facility, which has capabilities for complex electromagnetic modeling, including radar target and antenna structures. The Radar Signature Calculation Facility produces detailed computations of radar cross sections of various targets, primarily ships. The CEM facility includes multiple-CPU supercomputers that are also used to design phased array radar antennas.

The tremendous synergism between the CEM group and the Compact Antenna Range Facility provides the ability to design in the CEM environment, to test in the compact range, and to have immediate feedback between the theoretical and experimental aspects to shorten the development cycle for new designs.

In connection with airborne radar, the division operates a supercomputer-based Radar Imaging Facility and an inverse synthetic aperture radar (ISAR) deployed either in the air, on the ground, or aboard ship for radar imaging data collection. A P-3 aircraft equipped with the AN/APS-145 radar and cooperative engagement capability is also available for deploying experiments.

In connection with ship-based radar, the division operates the Radar Testbed Facility at the Chesapeake

Bay Detachment (CBD) near Chesapeake Beach, Maryland. The site has radars for long-range air search and surface search functions and features the newly developed W-band Advanced Radar for Low Observable Control (WARLOC), a fully operational high-power coherent millimeter-wave radar operating at 94 GHz. The WARLOC transmitter is capable of producing 10 kW average power with a variety of waveforms suitable for precision tracking and imaging of targets at long range. Waveforms with a bandwidth of 600 MHz can be transmitted at full power. A 6-ft Cassegrain antenna is mounted on a precision pedestal and achieves 62 dB of gain.

The Advanced Multifunction Radio Frequency Concept (AMRFC) testbed is a new installation at CBD operated by the Radar Division, with joint participation of several other NRL divisions as well. The goal of the AMRFC program is to demonstrate the integration of many sorts of shipboard RF functions, including radar, electronic warfare (EW), and communications, by utilizing a common set of broadband array antennas, signal and data processing, and signal generation and display hardware. The testbed consists of separate active transmit and receive arrays that operate over the 6 to 18 GHz band (nominally). Current functionality of the testbed includes a multimode navigation/surface surveillance Doppler radar, multiple communication links (line-of-sight and satellite), and passive and active EW capabilities. Testbed electronics are housed in seven converted 20-ft shipping containers and trailers. The arrays are mounted on a 15° tilt-back in the ends of two of the trailers overlooking the Chesapeake Bay, simulating a possible shipboard installation.

The division also has access to other radar systems: the Microwave Microscope (MWM); the Navy's relocatable over-the-horizon radar (AN/TPS-71); and an experimental Cooperative Aircraft Identification system. The internally developed MWM has a high-resolution (2 cm) ultrawideband capability that is used to investigate backscatter from surface and volumetric clutter, has through-wall detection capability, and characterizes the impulse responses of scattering objects. The division provides direct technical support for AN/TPS-71 and has direct access to data. The Cooperative Aircraft Identification system is used to explore system concepts and engineering developments in connection with target identification. ♦



Compact Range Facility.



Radar antennas in front of and on the roof of the Radar Test Facility.

Information Technology

The Navy Center for Applied Research in Artificial Intelligence is investigating learning and adaptation within teams of autonomous robots. Recent work has focused on a team of robots performing force protection.



NRL's Information Technology Division (ITD) conducts basic research, exploratory development, and advanced technology demonstrations in the collection, transmission, processing, dissemination, and presentation of information. ITD's research program spans the areas of artificial intelligence, autonomous systems, high assurance systems, computer networks, modeling and simulation, virtual and augmented reality, visual analytics, human/computer interaction, communication systems, transmission technology, and high performance computing.

A Voice Communication Laboratory supports the development of tactical voice technology, a Wireless Networking Testbed supports the development of Mobile Ad Hoc Networking (MANET) technology, and an Integrated Communications Technology Test Lab provides the capability to perform analysis, testing, and prototype development of high-speed wired and wireless networked data communication systems. A Freespace Laser Communications Laboratory supports the design and development of prototype technical solutions for Naval laser communications requirements. ITD research networks connect internal NRL

networks via high-speed links to the Defense Research and Engineering Network (DREN) and to an all-optical network that forms the DoD's Global Information Grid Evaluation Facility (GIG-EF). ITD's High Performance Computing Facilities and the Laboratory for Large Data provide an OC-192c based environment for experimentation and proof-of-concept development in high performance networking and the use and sharing of extremely large (petabytes and larger) data sets.

The Cryptographic Technology Laboratory supports the development of certifiable Communications Security (COMSEC) and Information Security (INFOSEC) products, including programmable cryptographic devices, cryptographic applications, and high assurance cross-domain solutions. The Naval Key Management Laboratory investigates electronic key management and networked key distribution technologies for the Navy and DoD. The Cyber Defense Development Laboratory provides direct support to the Fleet in the areas of computer network defense and visualization, cross-domain solutions, and reverse code analysis.

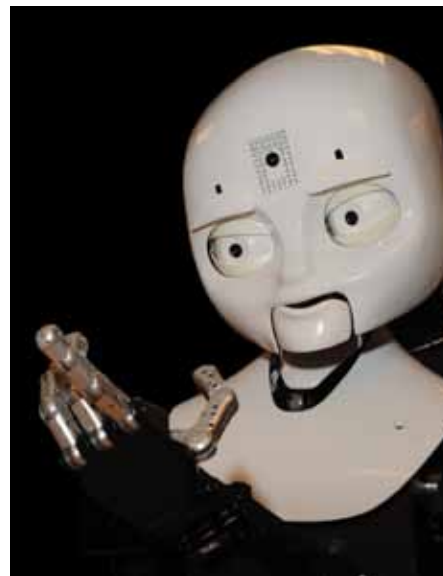
The Autonomous Systems and Robotics Laboratory provides the ability to develop and evaluate intelligent software and interfaces for autonomous vehicles. The Immersive Simulation Laboratory utilizes a collection of commercial off-the-shelf and specially

developed components to support R&D in interfaces for virtual simulators, ranging from fully immersive to desktop simulations. The Warfighter Human System Integration Laboratory maintains a range of Virtual Environment interface technologies as well as wearable, Wi-Fi physiological monitors and associated real-time processing algorithms for use in adaptive operational and training support technologies. The core of the new Visual Analytics Laboratory is a display wall composed



The newly installed 48-element loudspeaker array in NRL's audio lab provides a spherical, aurally detailed, 360-degree immersive listening space. Although primarily used for human performance studies in simulated, multisensory combat decision environments, the technology will also be used for training purposes and for research in treating post-traumatic stress disorder (PTSD). The installation is controlled by a powerful, state-of-the-art, 3D audio modeling and rendering package that provides physically accurate free-field sound propagation and concurrent, customizable multilistener support for headphone-based virtual auditory information displays.

of LCD tiles, which enable teams of analysts to explore massive, diverse streams of data, supporting research into the science of analytical reasoning facilitated by visual interfaces. The Service Oriented Architecture Laboratory is used to investigate, prototype, and evaluate flexible, loosely coupled Web services that can be rapidly combined to meet dynamically changing warfighter needs. The Behavioral Detection Laboratory supports the development of algorithms, processes, and sensor suites associated with behavioral indicators of deception. ✦



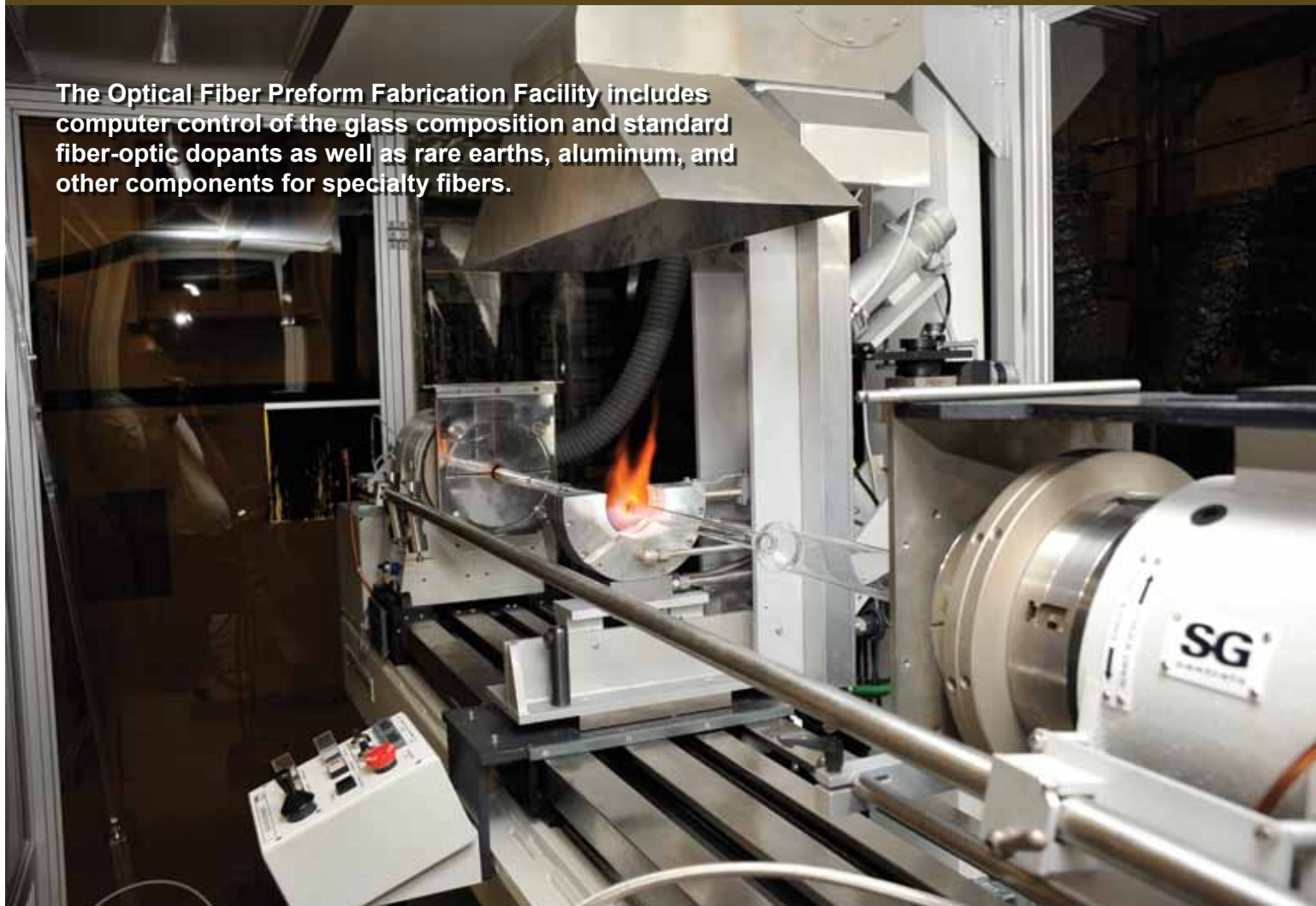
Octavia is one of three anthropomorphic robots used to study how humans and robots will work in teams.



The Pointman avatar controller, developed at NRL's Immersive Simulation Lab, allows users to employ correct tactical infantry movements. Left, Marine operates Pointman via a head tracker, gamepad, and rudder pedals. Right, the user's avatar rendered in Virtual Battlespace 2, a combined arms simulator used by the Marine Corps.

Optical Sciences

The Optical Fiber Preform Fabrication Facility includes computer control of the glass composition and standard fiber-optic dopants as well as rare earths, aluminum, and other components for specialty fibers.



The Optical Sciences Division conducts a broad program of basic and applied research in optics and electro-optics. Areas of concentration include fiber optics and fiber-optic sensing, materials and sensors in the visible and infrared (IR), integrated optical devices, signal processing, optical information processing, panchromatic and hyperspectral imaging for surveillance and reconnaissance, and laser development.

The division occupies some of the most modern optical facilities in the country. The newest facility in Optical Sciences is the Optical Fiber Preform Fabrication Facility, which includes computer control of the glass composition and standard fiber-optic dopants as well as rare earths, aluminum, and other components for specialty fibers. The facility is capable of making multi-mode, single-mode, multi-core, and photonic

crystal glass preforms at temperatures as high as 2300 °C, which are then drawn into fibers. This facility enables NRL scientists to prepare unique and novel glass optical fibers designed for advanced laser, modulator, and sensor applications. Optical fiber facilities also include draw towers, optical fiber coaters, and fiber splicers.

Two other recently added facilities include the Surface Characterization Facility for ultraviolet and X-ray photoemission spectroscopy, atomic force and scanning tunneling microscopy (STM), and STM-induced light emission measurements; and the molecular beam epitaxial growth system dedicated to infrared lasers and detectors based on GaSb/InAs/AlSb quantum well and superlattice structures. Several other laboratories allow development and testing of new laser and nonlinear frequency conversion concepts and evaluation of nondestructive test and evaluation

techniques. Fiber-optic sensor testing stations include acoustic test cells and a three-axis magnetic sensor test cell. There is also an Ultra-low-loss Infrared Fiber-Optic Waveguide Facility using high-temperature IR glass technology. The facilities for ceramic optical materials include powder preparation, vacuum presses, and a 50-ton hot press for sintering. The Focal Plane Array Evaluation Facility allows measurement of the

optical and electrical characteristics of infrared focal plane arrays being developed for advanced Navy sensors. The IR Missile-Seeker Evaluation Facility performs open-loop measurements of the susceptibilities of IR tracking sensors to optical countermeasures. An ultra-high-vacuum multichamber deposition apparatus is used for fabrication of electro-optical devices and can be interlocked with the Surface Characterization Facility. ♦



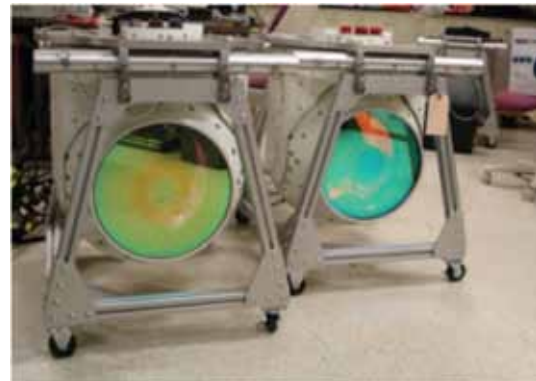
Fiber Fabrication Facility for Non-Oxide and Specialty Glasses.



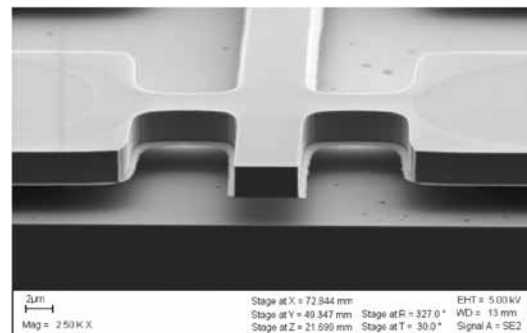
The Optical Sciences Surface Characterization Facility includes instrumentation for ultraviolet and X-ray photoemission spectroscopy (UPS and XPS), atomic force and scanning tunneling microscopy (AFM and STM), and STM-induced light emission (STM-LE) measurements.



Molecular beam epitaxy (MBE) system dedicated to quantum confined GaSb/InAs/AlSb structures for mid-wave infrared laser development.



MX-20SW hyperspectral sensors.



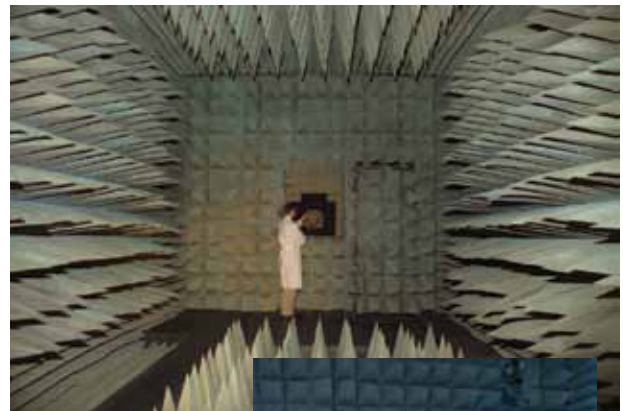
MBE growth, photo and e-beam lithography, and selective etches define a suspended semiconductor waveguide for polariton and nonlinear optical interactions.

Tactical Electronic Warfare

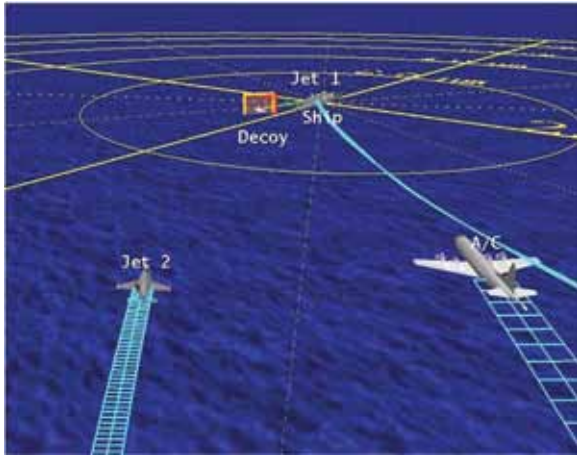


Learjet with simulators during RIMPAC exercises.

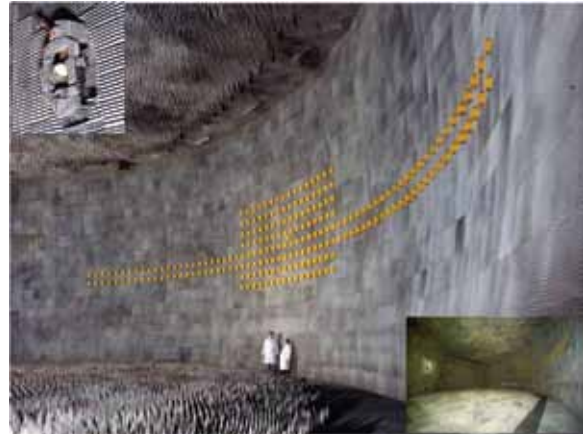
The Tactical Electronic Warfare (TEW) Division's program for electronic warfare (EW) research and development covers the entire electromagnetic spectrum. The program includes basic technology research and advanced developments and their applicability to producing EW products. The range of ongoing activities includes components, techniques, and subsystems development as well as system conceptualization, design, and effectiveness evaluation. The focus of the research activities extends across the entire breadth of the battlespace. These activities emphasize providing the methods and means to detect and counter enemy hostile actions — from the beginning, when enemy forces are being mobilized for an attack, through to the final stages of the engagement. In conducting this program, the TEW Division has an extensive array of special research and development laboratories, anechoic chambers, and modern computer systems for modeling and simulation work. Dedicated field sites, an NP-3D EW flying laboratory, and Learjets allow for the conduct of field experiments and operational trials. This assemblage of scientists, engineers, and specialized facilities also supports the innovative use of all Fleet defensive and offensive EW resources now available to operational forces. ♦



Radio Frequency Countermeasures anechoic chamber for EW testing.



TEWD develops and implements advanced visualization tools to support EW systems development and analysis.



A high-performance, hardware-in-the-loop simulator for real-time closed-loop testing and evaluation of electronic warfare (EW) systems and techniques to counter the anti-ship missile threats.



EATES — Electronic Attack Technique Evaluation System, a stand-alone portable EA testing system.



Deployed EW sub-system to improve emitter detection and classification based on conceptualization and development performed in TEW.



NRL's Vehicle Research Section (VRS) in the TEW Division develops technologies for autonomous, affordably expendable, unmanned systems that carry a wide variety of payloads for numerous mission scenarios. The VRS has developed more than 50 unmanned flying machines since the mid-1970s: fixed and rotary wing vehicles, ground, ship, and air deployed vehicles, EW decoys, reconnaissance aircraft, electric vehicles powered by fuel cells, unpowered vehicles, vehicles designed for planetary exploration, and more.





Fire test aboard ex- USS *Shadwell*: Quadruple 98 MW test fire prior to activation of HotFoam, a high-expansion foam system.

NRL has been a major center for chemical research in support of naval operational requirements since the late 1920s. The Chemistry Division continues this tradition. The Chemistry Division conducts basic research, applied research, and development studies in the broad fields of diagnostics, dynamics, synthesis, materials, surface/interfaces, environment, corrosion, combustion, and fuels. Specialized programs currently within these fields include the synthesis and characterization of organic and inorganic materials, coatings, composites, nondestructive evaluation, surface/interface modification and characterization, nanometer structure science/technology, chemical vapor processing, tribology, solution and electrochemistry, mechanisms and kinetics of chemical processes, analytical chemistry, theoretical chemistry, decoy materials, radar-absorbing materials/radar-absorbing structures (RAM/RAS) technology, chemical/biological warfare defense, atmosphere analysis and control,

environmental remediation and protection, corrosion science and engineering, marine coatings, personnel protection, and safety and survivability. The Division has several research facilities.

Chemical analysis facilities include a wide range of modern photonic, phononic, magnetic, electronic, and ionic based spectroscopic/microscopic techniques for bulk and surface analysis.

The Magnetic Resonance Facility includes advanced high-resolution solid-state nuclear magnetic resonance (NMR) spectroscopy techniques to observe nuclei across much of the periodic table and provides detailed structural and dynamical information.

The Synchrotron Radiation Facility has intense, monochromatic X-ray photon beams tunable from 10 eV to 35 KeV available from four beam lines developed by NRL at the National Synchrotron Light Source at the Brookhaven National Laboratory.

The Nanometer Characterization/Manipulation Facility includes fabrication and characterization capability based on scanning tunneling microscopy/

spectroscopy, atomic force microscopy, and related techniques.

The Materials Synthesis/Property Measurement Facility has special emphasis on polymers, surface-film processing, and directed self-assembly.

The Chemical Vapor and Plasma Deposition Facility is designed to study and fabricate materials such as diamond using in situ diagnostics, laser machining, and plasma deposition reactors.

The Navy Fuel Research Facility performs basic and applied research to understand the underlying chemistry that impacts the use, handling, and storage of current and future Navy mobility fuels.

Fire research facilities include a 11,400 ft³ fire-research chamber (Fire I) and the 457-ft ex-USS *Shadwell* (LSD 15) advanced fire research ship. Commensurate support has been devoted to survivability of the new classes of ships, DDX, LPD 17, LCS, CVNX, and LHA(R).



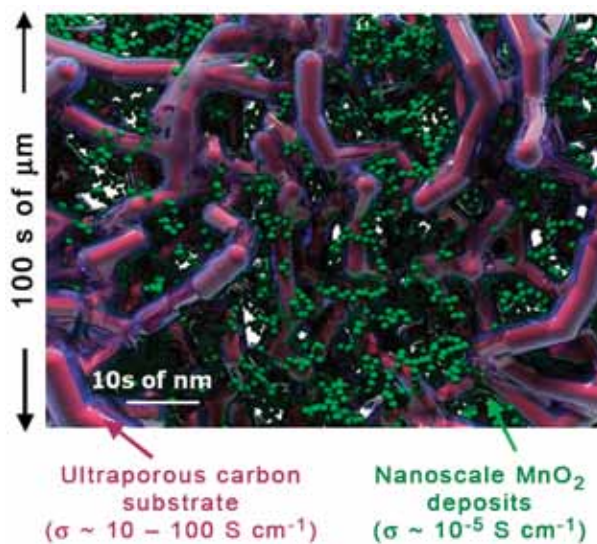
Marine Corrosion Facility, Key West, FL.

The Marine Corrosion and Coatings Facility located on Fleming Key at Key West, Florida, offers a “blue” ocean environment and unpolluted, flowing seawater for studies of environmental effects on materials. Equipment is available for experiments involving accelerated corrosion and weathering, general corrosion, long-term immersion and alternate immersion, fouling, electrochemical phenomena, coatings application and characterization, cathodic protection design, ballast water treatment, marine biology, and corrosion monitoring.

The Chemistry Division has focused on force protection/homeland defense (FP/HD) since September 11, 2001, especially on the development of improved detection techniques for chemical, biological, and explosive threats. As part of a multidivisional program



Peptide backbone structure of a β -helical supersecondary structure developed, synthesized, and characterized at NRL. Heterochiral peptides promise numerous potential applications as sensors, smart materials, and catalysts.



Redesigning electrode nanoarchitectures: schematic of the interior of a multifunctional nanoarchitecture comprising a carbon nanofoam or related ultraporous carbon coated with nanoscale deposits of MnO_2 .

to develop new technology systems, the Chemistry Division is a major contributor to the NRL Institute for Nanoscience. Nanoscience complements FP/HD in that nanoscience is expected to provide dramatic improvements to chemical/biological detection, protection, and neutralization. Chemistry will approach the nanoscale from the bottom up — building smaller atoms and molecules into nanostructures with new properties and developing the directed assembly of nanostructures into hierarchical systems. The NRL Nanoscience building is linked directly into the Chemistry building to provide controlled access and auxiliary space for work not requiring a “low noise” environment. ♦

Materials Science and Technology

The Magnetolectronics Fabrication Facility consists of a Class 1000 clean room equipped with tools for lithographic construction of magnetolectronic and spintronic devices.



The Materials Science and Technology Division at NRL conducts materials research using seven major division facilities.

The Magnetolectronics Fabrication Facility consists of a Class 1000 clean room equipped with tools for lithographic construction of magnetolectronic and spintronic devices. It provides pattern definition, metallization, dielectric layer deposition, and both reactive and Ar^+ ion etching of wafers and small pieces.

The Electrical, Magnetic, and Optical Measurement Facility contains several complementary instruments that allow for the magnetic, electrical, optical, and heat capacity characterization of materials and devices. SQUID (superconducting quantum interference device) magnetometry and vibrating sample magnetometry are used to determine important properties of superconducting, paramagnetic, diamagnetic, and ferromagnetic materials. The transport properties of materials, namely the temperature- and magnetic-field-dependent resistivity combined with heat-capacity measurements, allow for a fundamental physical understanding of electronic properties.

The Materials Processing Facility includes apparatuses for powder production by fluid atomization, thermal evaporation, and arc erosion, and a physical vapor deposition system designed to produce and coat submicron powders in situ. Facilities to process powder into bulk specimens by hot and cold isostatic pressing permit a variety of consolidation possibilities. The isothermal heat treatment facility and quenching dilatometer permit alloy synthesis and single crystal growth. Bulk alloys can be prepared by induction melting, while rapid solidified metals of thin cross section can be made by splat quenching and melt spinning. Ceramic and ceramic-matrix composites processing facilities include a wide variety of conventional, controlled atmospheric furnaces, hot presses, a ball milling apparatus, particle size determination capability, and sol-gel and organometallic coating processing capabilities.

The Mechanical Characterization Facility consists of various testing systems, many with automated computer control and data acquisition, for determining the mechanical response of materials under controlled loading/deformation and environmental conditions. Basic capabilities include quasi-static tensile and



NRL GelMan human surrogate technology is used to record and analyze dynamic responses to blast pressure and impacts. GelMan torso measurement systems assess pressure transmission directly into the body, and through body armor into the body. GelMan-Brain systems quantify headborne protective equipment performance with the aim of reducing traumatic brain injury.

fracture testing, dynamic storage and loss moduli as a function of frequency and temperature, cyclic fatigue crack growth and corrosion fatigue testing, and stress-corrosion cracking testing.

The Thin-Film Materials Synthesis and Processing Facility provides users a wide variety of techniques for growth and processing of thin films (thickness 1 μm or less). Sputter deposition offers a versatile method of depositing metallic and dielectric films and is a primary tool of this facility. Thermal evaporation of metals is implemented in both high-vacuum and ultra-high-vacuum systems. Pulsed laser deposition (PLD) with variable stage temperature and controlled atmosphere allows growth of oxides. Electrolytic deposition offers efficient growth of gold and silver films. Laser direct-write ablation and deposition processes provide unique methods for imposing CAD-defined features via ablation of a substrate film and ablative mass transfer to a substrate.

The 3-MV Tandem Pelletron Accelerator Facility uses two “pelletron” charging chains to produce a terminal voltage up to 3 MV in the accelerator. Negative ions are injected at 10 to 70 keV, accelerated up to the terminal where they undergo collisions with a stripper gas or a carbon stripper foil and lose electrons, then are accelerated as positive ions back to ground potential. Protons can be accelerated up to 6 MeV, He up to 9 MeV, and highly stripped Au (+12) up to 39 MeV. The lower limit of beam energy is about 400 keV. On the analysis beam line, the sample of interest is located at the end of the beam line, and

a signal generated by scattering of incident high-energy ions indicates the composition of the sample. Incident high-energy ions can also be used to damage the surface of a sample of interest, or to introduce a dopant.

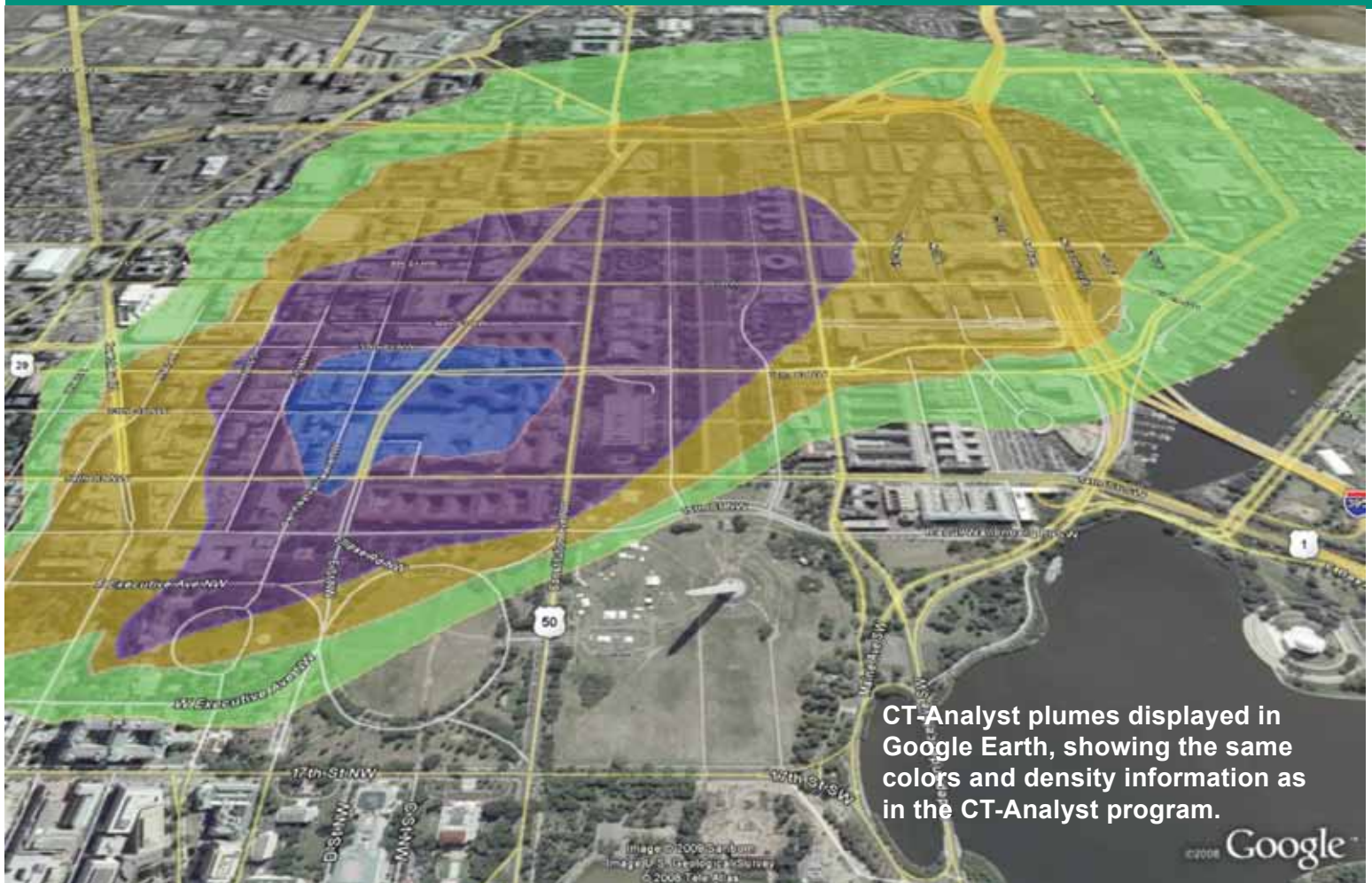
The Micro/Nanostructure Characterization Facility is capable of performing transmission electron microscopy (TEM), scanning transmission electron microscopy (STEM), atomic resolution transmission electron



3-MV Tandem Pelletron Accelerator Facility.

microscopy (ARTEM), electron energy loss spectroscopy (EELS), Z-contrast imaging, and spectral imaging through the use of a JEOL 2010F transmission electron microscope, a Phillips CM30 transmission electron microscope, and a Leo scanning electron microscope. Other standard microstructure characterization instruments are also available. ♦

Laboratory for Computational Physics and Fluid Dynamics



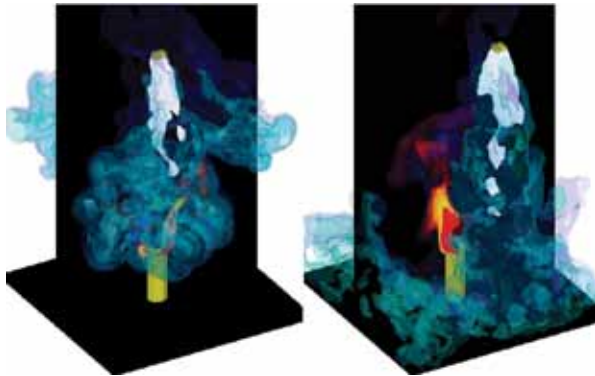
The Laboratory for Computational Physics and Fluid Dynamics (LCP&FD) is a division of physicists, engineers, and computer scientists who use high-performance computers to solve priority problems for the Navy, the DoD, and the nation when existing capabilities and readily available commercial software prove inadequate to the application. For example, the LCP&FD developed the CT-Analyst crisis management software (figure above) so first responders could have instant predictions of an airborne contaminant plume in a city.

The LCP&FD maintains a very powerful collection of computer systems applied to a broad range of research. There is currently a total of 320 shared memory Itanium processors, 1700 clustered x86 cores, and their associated support systems. In addition, there are more than 50 Apple computers in the group, most

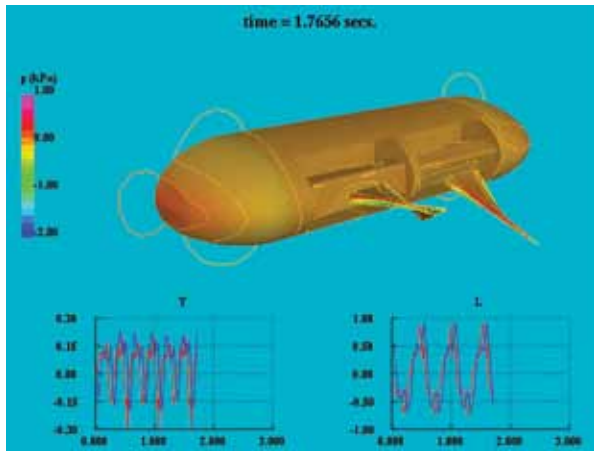
of which are capable of large calculations both independently and in parallel ad hoc clusters.

The shared memory computer systems are comprised of three 64-core and one 128-core Itanium 2 SGI Altix machines. There are three 64-bit x86 multi-core distributed memory clusters, each well coupled with Infiniband high speed switched interconnect. The GPU cluster is comprised of 48 NVIDIA Fermi GPUs tightly coupled to 24 x86 multi-core processor nodes connected with Infiniband.

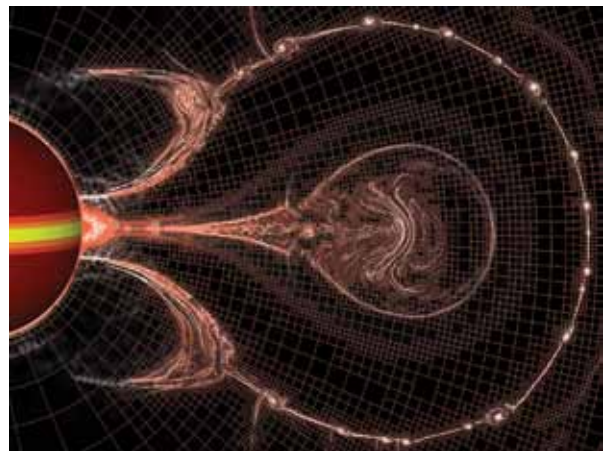
Each system has on the order of 72 terabytes of disk for storage during a simulation, and at least one gigabyte of memory per processor core. All unclassified systems share a common disk space for home directories as well as 1.4 terabytes of AFS space which can be used from any AFS-capable system throughout the allowed Internet. Each system is connected to NRL's network via 10 Gb Ethernet as well an internal Infiniband intranet. ♦



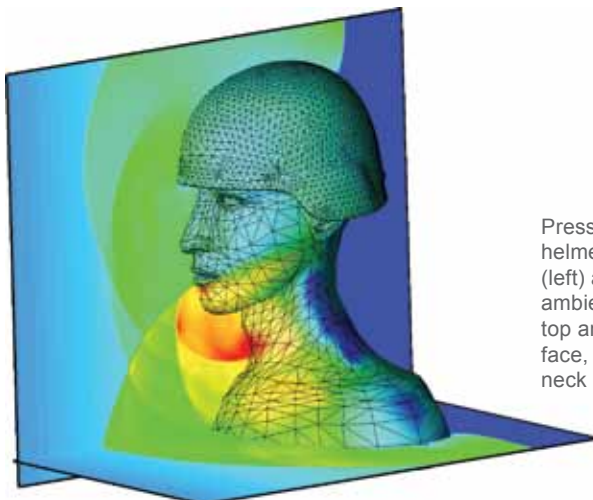
Simulations of fire suppression with different sprinkler locations, fuel flow rates, and under different gravitational environments allow us to understand the interaction of several different physical processes such as vaporization and buoyancy that are important for fast suppression of flames. The current Fire-Blast-Mitigation code uses parallel adaptive mesh refinement to handle detailed physics in large domains efficiently.



Flow past an unmanned underwater vehicle (UUV) propelled by flapping fins with controlled deformation.



Numerical simulation of an eruptive solar flare and coronal mass ejection using the Adaptively Refined Magnetohydrodynamics Solver (ARMS). The gradual accumulation of a strong longitudinal magnetic field concentrated near the Sun's equator (yellow band on sphere at left) powers the explosive eruption. Electric current sheets (white shading against the sky) separate regions of oppositely directed fields and highlight regions permeated by magnetohydrodynamic shock waves and strong magnetic forces. The computational grid (red lines against the sky) adaptively refines to capture all of this fine-scale structure.



Pressure contours resulting from blast interaction with a helmeted head. The shock wave approaches from the front (left) and envelopes the geometry; the boundary between ambient (dark blue) and post-shock (green) air is seen at the top and bottom right. Interacting shock reflections from the face, helmet, and torso generate high pressures (red) on the neck below the chin.

Plasma Physics



NRL's Materials Testing Facility railgun. This system is designed to perform experiments on bore materials under high-power launch conditions.

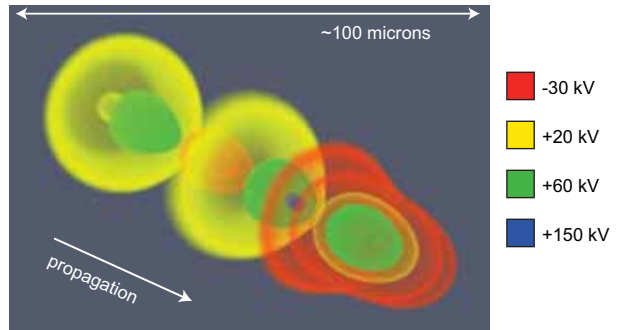
The Plasma Physics Division is the major center for in-house Navy and DoD plasma physics research. The Division conducts a broad program in laboratory and space plasma physics and related disciplines, including high power lasers, pulsed-power sources, intense particle beams, advanced radiation sources, materials processing, and nonlinear dynamics.

The two largest of the Division's lasers, Nike and Electra, are krypton fluoride (KrF) lasers operating at 0.25-micron wavelengths and are used for inertial confinement fusion (ICF) energy studies. Nike provides a single, 3-kJ pulse and is used primarily for ICF target physics. Electra is used to develop repetitively pulsed KrF technology. Three ultrashort-pulse, high-intensity lasers, the Table-Top Terawatt (T3) laser, the Ti:Sapphire Femtosecond Laser (TFL), and the new KiloHertz Ti:Sapphire Femtosecond Laser (KTFL) investigate intense laser-target interactions, laser-

driven accelerators, laser-triggered discharges, and laser propagation in air, plasmas, and water. The High Energy Laser Laboratory includes four multi-kilowatt, continuous-wave (CW) fiber lasers and investigates laser propagation in the atmosphere and incoherent beam combining for directed energy and power beaming applications. The SWOrRD facility uses resonant Raman spectroscopy based on illuminating a target at many wavelengths using a rapidly tunable laser, thus generating two-dimensional signatures of explosives and biological/chemical/nuclear threats.

The Division also has a number of pulsed-power, microwave, and laboratory plasma facilities. The Railgun Materials Testing Facility railgun focuses on materials issues for a major Navy effort to develop a long-range, electromagnetic launcher for a future electric ship. Two large, high-voltage, pulsed-power devices, Gamble II and Mercury, are used to produce intense electron and ion beams, flash X-ray sources,

and high-density plasmas. The microwave materials processing laboratory includes a 20-kW, CW, 83-GHz gyrotron. Laboratory plasma experiments include the Space Physics Simulation Chamber (SPSC), an 11 m³ space chamber capable of reproducing the near-Earth space plasma environment, and the Large Area Plasma Processing System (LAPPS), designed to study modification of polymers, graphene, and other sensitive materials. ♦



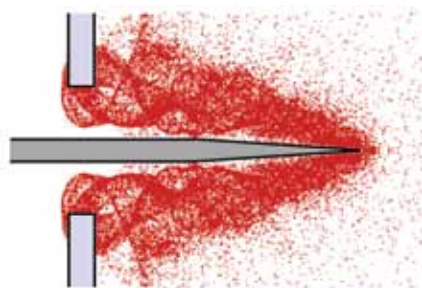
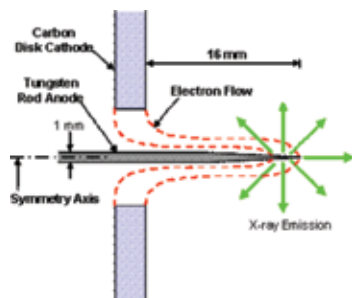
The scalar potential in a laser wakefield accelerator as computed by turboWAVE, a set of software modules used for simulating a wide range of phenomena involving plasmas.



Space Physics Simulation Chamber.



NRL's Nike target chamber, the largest krypton fluoride (KrF) laser facility in the world, where targets are accelerated to the velocities needed for fusion implosions.



Electron distribution at the tip of a rod-pinch diode.

Electronics Science and Technology



The Electronics Science and Technology Division's Advanced Silicon Carbide Epitaxial Research Laboratory (ASCERL).

The Electronics Science and Technology Division conducts a multidisciplinary basic and applied research program in solid-state electronics; electronic materials including growth, theory, and characterization of semiconductors and heterostructures; surface and interface science; microwave and millimeter-wave components and techniques; microelectronic device research and fabrication; nanoelectronics science and technologies; vacuum electronics; power electronics; and process modeling and simulation.

The Division operates seven major facilities: the Compound Semiconductor Processing Facility (CSPF), the Laboratory for Advanced Materials Synthesis (LAMS), the Ultrafast Laser Facility (ULF), the Epicenter, the Advanced Silicon Carbide Epitaxial Research Laboratory (ASCERL), the Space Solar Cell Characterization Facility (SSCCF), and the Millimeter-Wave Vacuum Electronics Synthesis Facility (MWVESF).

The CSPF processes compound semiconductor structures on a service basis, especially if advanced fabrication equipment such as electron beam lithography

or reactive ion etching is required. But most fabrication can be hands-on by NRL scientists to assure personal process control and history. The LAMS uses metallorganic chemical vapor deposition to synthesize a wide range of thin films, particularly wide bandgap semiconductors such as gallium nitride (GaN) and related alloys. The Epicenter (a joint activity of the Electronics Science and Technology, Materials Science and Technology, Optical Sciences, and Chemistry Divisions) is dedicated to the growth of multilayer nanostructures by molecular beam epitaxy (MBE). Current research involves the growth and etching of conventional III-V semiconductors, ferromagnetic semiconductor materials, 6.1Å II-V semiconductors, and II-VI semiconductors. The structures grown in this facility are analyzed via in situ scanning tunneling microscopy and angle resolved electron microscopy.

The ASCERL is the focal point of NRL efforts to develop thin film heterostructure materials needed for high-voltage, high-power silicon carbide (SiC) power electronic components in future naval systems. ASCERL employs an EPIGRESS reactor capable of growing thick, low-defect, ultra-high-purity SiC epitaxial layers. The SSCCF studies the effects of particle irradiation on new and emerging solar cell technologies for space applications. The ULF is optimized for the characterization of photophysical and photochemical processes on a timescale of tens of femtoseconds. It

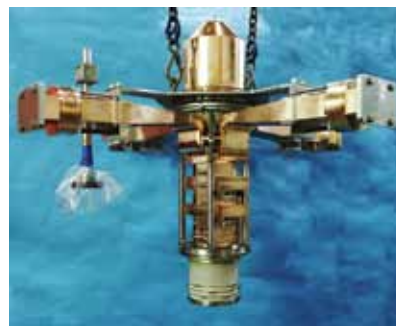


ISS021E031746

The MISSE7 experiment (upper center of photo) on the International Space Station, photographed by a space-walking STS-129 astronaut. MISSE7 is the latest in a series of experiments that expose materials to space for several months before they are returned for analysis. The results provide a better understanding of the durability of advanced materials and electronics when they are exposed to vacuum, solar radiation, atomic oxygen, and extremes of heat and cold. The project is a collaboration between the Electronics Science and Technology Division, Naval Center for Space Technology, and outside organizations. (Photo Credit: NASA, ISS021-E-031746, 23 Nov. 2009).

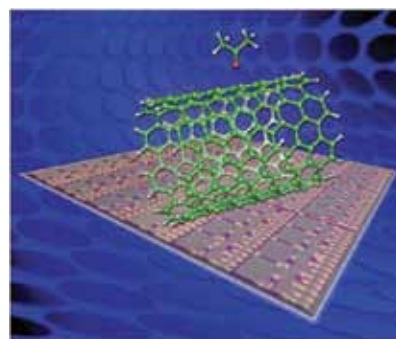


A microfabricated grating circuit made using deep reactive ion etching (DRIE) at NRL for a vacuum electronic traveling-wave amplifier driven by a sheet electron beam. The device is designed to generate up to 50 W at a center frequency of 220 GHz and has potential applications in extremely high data rate communication systems and high-resolution radar, with the added benefit of a drastically reduced antenna footprint.



The NRL eight-beam (45 kV, 30 A), 600-kW output power S-band multiple-beam klystron (MBK). MBKs produce coherent, broadband microwave radiation in a compact package. This promising device technology has the potential to provide the low-noise, high average power transmitter

performance required by shipboard radar systems to keep pace with evolving ballistic missile and anti-ship cruise missile threats in high clutter environments.



Acetone molecule and single-walled carbon nanotube over an array of nanotube transistor structures.

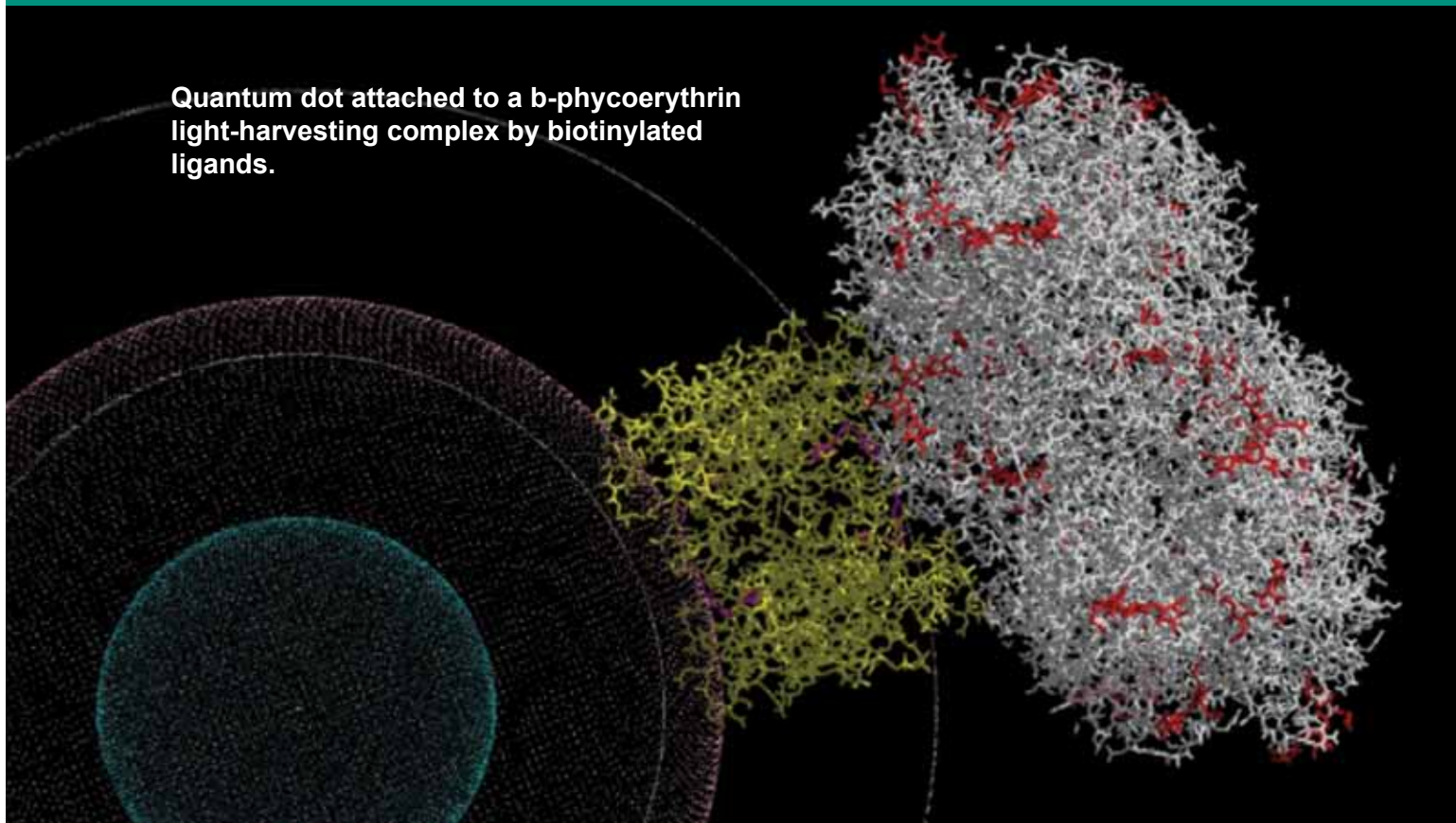
includes a synchronously pumped dye laser system for simulating the effects of charge deposited in semiconductors characteristic of space radiation.

The MWVESF contains a computer numerically controlled (CNC) milling machine and a CNC precision lathe capable of fabricating intricate millimeter-

wave vacuum electronic components and a wire electric discharge machining (EDM) tool for fabrication of submillimeter-wave components that cannot be fabricated by conventional rotary cutting tools. EDM offers a non-contact process for both hard and soft metals as well as SiC and doped silicon. ♦

Center for Bio/Molecular Science and Engineering

Quantum dot attached to a b-phycoerythrin light-harvesting complex by biotinylated ligands.



The Center for Bio/Molecular Science and Engineering conducts research and development to address problems relevant to the Navy and the DoD by exploiting biology's well-known ability for developing effective materials and sensing systems. The primary goal is to translate cutting-edge, bio-based discoveries into useful materials, sensors, and prototypes that can be scaled up, are robust, and lead to enhanced capabilities in the field. The challenges include identifying biological approaches with the greatest potential to solve Navy problems and provide new capabilities while focusing on bio-inspired solutions that have not otherwise been solved by conventional means.

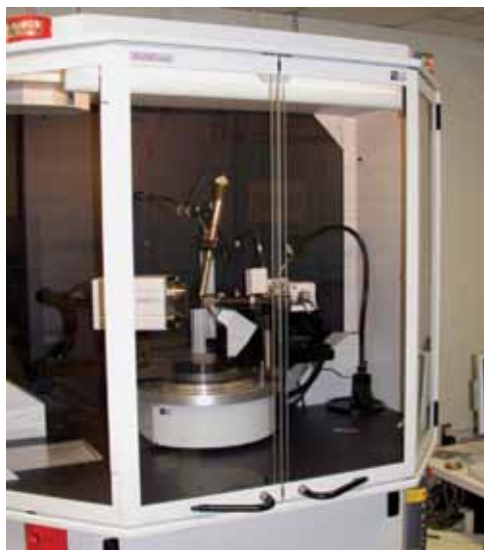
Studies involve biomaterial development for chemical/biological warfare defense, structural and functional applications, and environmental quality/cleanup. Program areas include optical biosensors, nanoscale manipulations, genomics and proteomics, bio/molecular and cellular arrays, surface modification, energy harvesting, systems biology, viral particles as scaffolds, and bioorganic materials from self-assembly.

The staff of the Center is an interdisciplinary team with expertise in biochemistry, surface chemistry, biophysics, molecular and cell biology, organic synthesis, materials science, and engineering. The Center also collaborates throughout NRL and with other government laboratories, universities, and industry.

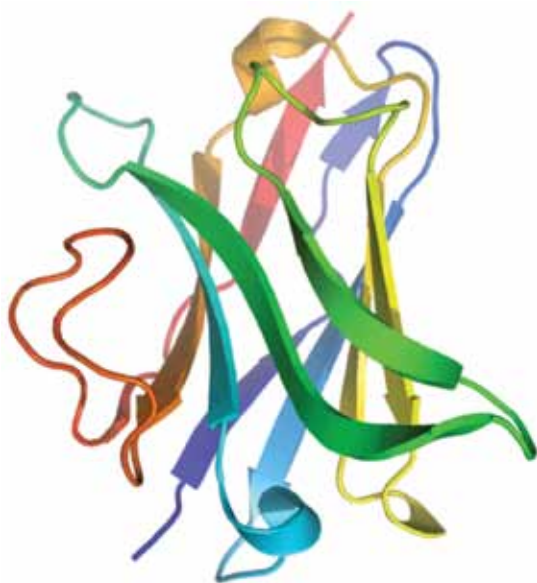
The Center's modern facilities include laboratories for research in chemistry, biochemistry, molecular biology, and physics. Specialized areas include an electron microscope facility, a scanning probe microscope laboratory, instrument rooms with access to a variety of spectrophotometers, a multichannel surface plasmon resonance (SPR) sensor, and an optical microscope facility including polarization, fluorescence, and confocal microscopes. Additional laboratories accommodate nuclear magnetic resonance spectroscopy, liquid chromatography-mass spectrometry (LCMS), and fabrication of microfluidic and micro-optical systems in polymers. The Center recently upgraded the X-ray diffraction system to a state-of-the-art MicroSTAR-H X-ray generator. In combination with new detectors and components, the system is ideal for data collection on proteins or very small single crystals of organic compounds and is also capable of collecting

data on films and powders. The Center's facilities were used to demonstrate the capabilities of a microarray system developed at NRL for broad-spectrum pathogen surveillance. The system detected multiple infectious and bioterrorism agents in a demonstration involving

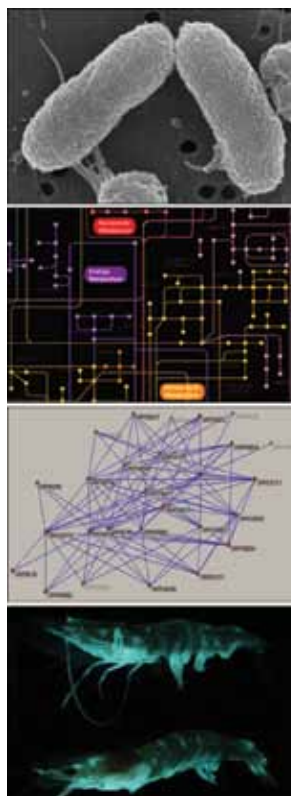
NRL staff, Air Force medical personnel, and contractors. A smaller-scale version of the genomics-based molecular diagnostic array was developed in the Center and is currently being validated in field trials. ♦



APEX-2 is the Center workhorse X-ray system configured for rapid and accurate single crystal X-ray data collection on compounds such as energetic materials, drugs, and other small molecules. The system is equipped with a "Monocap" X-ray optic and low temperature system.



Single-domain antibodies are small recombinant proteins that are being developed by the Center. These unique detection reagents possess both high affinity for biotreats, and the ability to rapidly refold after denaturation, recovering their activity.



Bacterial systems and synthetic biology. The Center's multidisciplinary and multidivisional team of scientists is working to develop a fundamental understanding of marine bacterial system architecture, regulation, and dynamics for the purpose of re-engineering synthetic constructs for Navy-relevant sensing and decontamination applications. These challenges are being addressed through a combination of genetic, functional genomic, proteomic, biochemical, physiological, and mathematical approaches using a bioluminescent marine bacterium, *Vibrio campbellii*, as a model. Research is also focused on understanding and re-engineering the quorum sensing subsystem in this bacterium and extending the systems biology tools to other members of the *Vibrio* core group.



Field testing an oceanographic mooring powered by a benthic microbial fuel cell.

Acoustics



A 21-inch-diameter AUV is used for detection and classification in mine hunting and antisubmarine warfare applications.

The Acoustics Division conducts a broad research and development program in underwater acoustics, atmospheric acoustics, and physical acoustics requiring laboratory and at-sea measurements.

Laboratory Facilities: The Division has three integrated structural acoustic facilities — two pools (one with a sandy bottom) and a large, in-air, semi-anechoic laboratory. These facilities support research in areas including mine detection and identification, antisubmarine warfare, and detection of improvised explosive devices (IEDs). These facilities have a number of measurement capabilities including compact range scattering, nearfield holography, and scanning laser Doppler vibrometry. The major pool facility is cylindrical (17 m dia. \times 15 m deep) and filled with approximately 1 million gallons of deionized water. Features include vibration and temperature control and anechoic interior walls to reduce reverberation.

The Salt Water Tank Facility provides a controlled environment for studying complex ocean processes under saline conditions, especially the acoustics of bubbly media. This $6 \times 6 \times 3$ m pool facility has large plexiglass windows on all four sides to permit imaging of processes inside the tank. Instrumentation includes acoustic sources, amplifiers, hydrophones, environmental sensors, a digital holographic imaging system, high-speed digital cameras, and a LabVIEW-based data acquisition system.

The Geoacoustic Model Fabrication Laboratory enables fabrication of rough topographical surfaces in various materials (usually plastics) for acoustic scattering and propagation measurements in the tank facilities. The facility consists of a three-axis computer-controlled milling machine capable of cutting with $100\text{-}\mu\text{m}$ accuracy over a 1.37×1.27 m region.

The SOnoMAGnetic LABoratory (SOMALAB) is used to study magnetic fields produced by acoustic motions in electrically conducting media, such as seawater. Two nested skins of HY-80 steel plate magneti-

cally shield this facility. Inside is a $3 \times 6 \times 3$ ft plexiglass experimental water tank on a vibration-insulating optical table equipped with three sets of mutually perpendicular Helmholtz coils to control the magnetic field. The tank is instrumented with a three-axis magnetometer, and acoustic signals are generated from an external transducer.

The Division also operates laboratories to study the structural dynamics and performance of high-Q oscillators and other micromechanical and nanomechanical systems. A super-resolution nearfield scanning optical microscope permits spatial mapping of the complex vibratory motion at resolutions of 100 nm. These laboratories can also measure the mechanical and electrical properties of micro-oscillators, and thin films applied to them.

At-Sea Research: The Division operates several systems to generate and receive sound in at-sea experiments. Sound sources include two XF-4 units, one ITC 2077 source with tow body, two battery-operated organ-pipes that can project single tones from off-board moorings, and a towable, vertically directional source array consisting of 10 individually controllable elements at frequencies of 1.5 to 9.5 kHz. In addition, the Division has several battery-operated, rubidium-clock controlled, programmable sound source moorings that can transmit sounds with arbitrary waveforms. The division has a 64-channel broadband source-receiver array with time reversal mirror functionality operating over 500–3500 Hz. The division operates high-frequency (up to 600 kHz) measurement systems to obtain scattering, target strength, and propagation data using bottom-moored instrumentation towers and a remotely operated vehicle.

The Division performs research to relate acoustic array gain variability to fluid dynamic variability and bottom heterogeneity in the littorals. Measurements are made with an autonomous acoustic data acquisition suite. Three independent, autonomous, 32-channel vertical arrays receive and store 24-bit data at 4 kHz for 22 days. Two autonomous sources operate at center frequencies of 300 and 500 Hz and generate programmable waveforms at 50% duty cycle for 22 days. The division also has seven Environmental Acoustic Recording Systems (EARS) buoys. The buoys are autonomous, self-recording, bottom-mounted acoustic acquisition systems. Each buoy can record four channels simultaneously at 25 kHz bandwidth per channel and has a storage capacity of 480 Gbyte. Each buoy has four hydrophones on a 22 m array.

Narrowbeam 200 and 350 kHz acoustic backscattering (flow visualization) systems are used to study

fine structure, internal wave, and larger-scale fluid dynamic perturbation of the density and sound speed field in the ocean. A 25 kW radar system is used in conjunction with the flow visualization system to record the surface expression of internal waves.

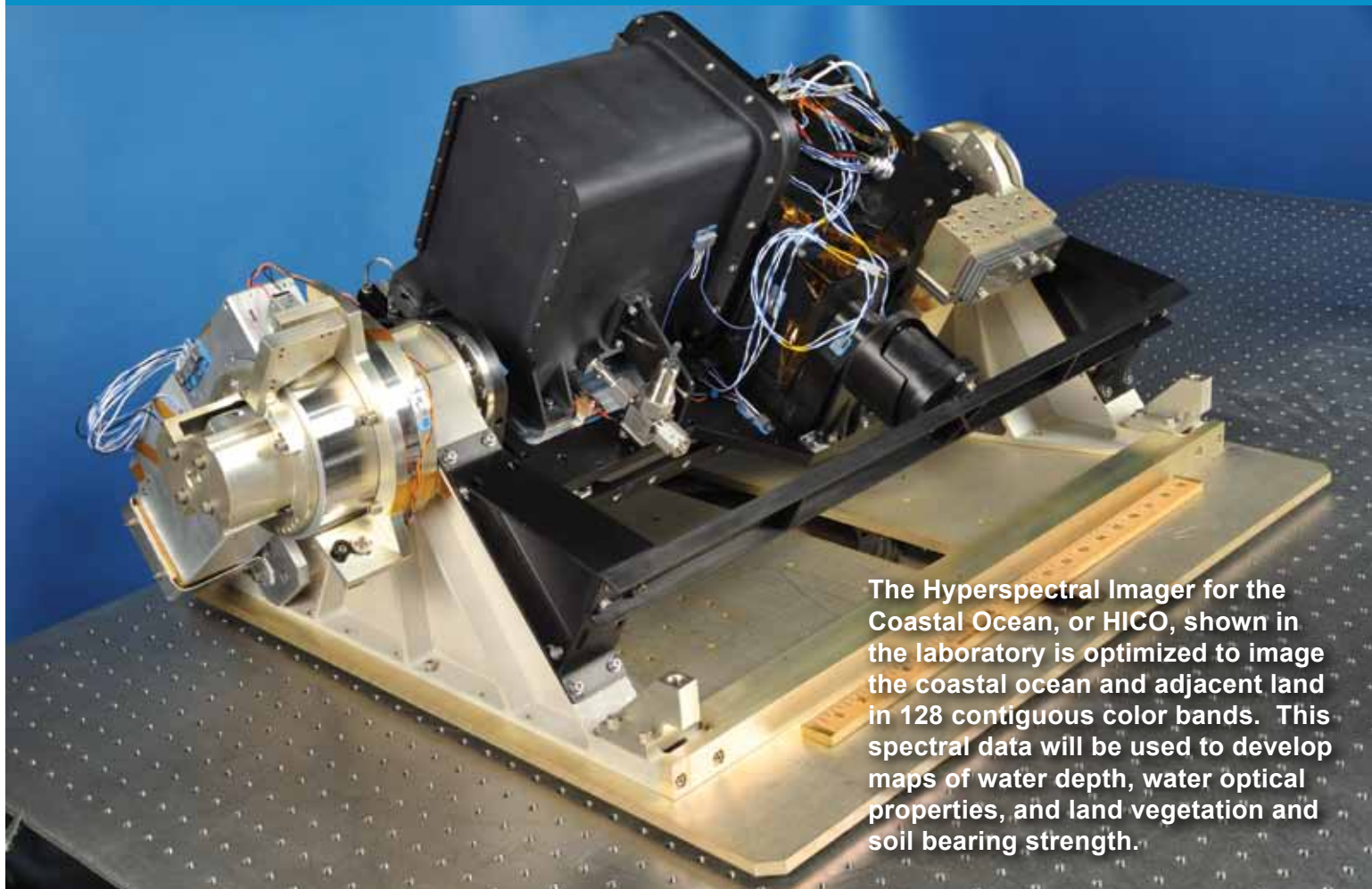


The Structural Acoustics In-Air Facility is instrumented with acoustic and vibration measurement systems for conducting ultra-high-precision, highly spatially sampled measurements on scaled submarine structures, satellite payload fairings, active and passive material systems for sound control, and new transducer and sensor systems.

The Division conducts research addressing the channel capacity of multi-node underwater acoustic communications networks. Two 8-channel acoustic communications data acquisition systems or modems, which can be moored or towed and remotely controlled, provide measurements in the 2–5 kHz, 6–14 kHz, and 10–14 kHz frequency bands.

NRL is developing and deploying AUV-based and rail-based systems for acquiring signature data at sea. The rail-based system has a 100 m horizontal robotic scanner used to collect synthetic aperture (SA) scattering data from proud and buried targets. The receiver system is used in conjunction with impulsive broadband projectors mounted on the scanner. The AUV-based system uses acoustic SA techniques to recover high-fidelity, quantitative broadband data over a large range of target aspect angles. ♦

Remote Sensing



The Hyperspectral Imager for the Coastal Ocean, or HICO, shown in the laboratory is optimized to image the coastal ocean and adjacent land in 128 contiguous color bands. This spectral data will be used to develop maps of water depth, water optical properties, and land vegetation and soil bearing strength.

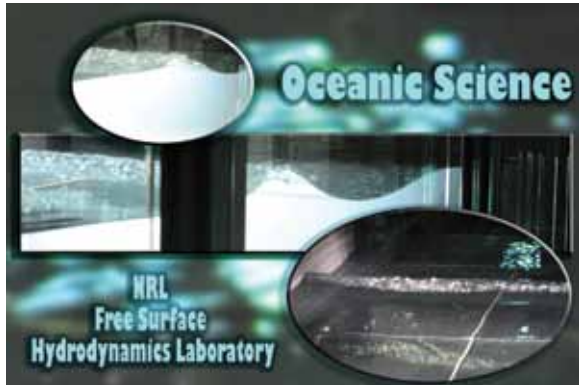
The Remote Sensing Division is the Navy's center of excellence for remote sensing research and development, conducting a broad program of basic and applied research across the full electromagnetic spectrum using active and passive techniques from ground-, air-, and space-based platforms. Current applications include earth, ocean, atmospheric, astronomy, astrometry, and astrophysical science, and surveillance/reconnaissance activities including maritime domain awareness, antisubmarine warfare, and mine warfare. Special emphasis is given to developing space-based platforms and exploiting existing space systems.

Research in ocean and earth science includes maritime hyperspectral imaging, radar measurements of the ocean surface for the remote sensing of waves and currents, model- and laboratory-based hydrodynamics, and land-based trafficability studies.

Current airborne sensors used for characterization of the littoral environment include visible/near-IR and shortwave hyperspectral imagers, a broadband, visible polarimetric sensor, long- and midwave IR thermal cameras, and an X-band, 2-channel interferometric synthetic aperture radar. As an outgrowth of our airborne sensing program, the Division developed the Hyperspectral Imager for the Coastal Ocean (HICO), the world's first spaceborne hyperspectral sensor specifically designed for coastal maritime environmental observations. HICO was launched to the International Space Station in September 2009 and is currently providing scientific imagery of varied coastal types worldwide. Ground-based instruments for maritime sensing include the NRL Focused Phased Array Imaging Radar (NRL FOPAIR), an X-band, high-frame-rate polarimetric radar system.

For radiometric and spectral calibration of the visible and IR imaging sensors, the Division operates a Calibration Facility that includes a NIST-traceable integrating sphere and a set of gas emission standards for wavelength calibration.

The Division's Free Surface Hydrodynamics Laboratory (FSHL) supports ocean remote sensing research. The lab consists of a 10 m wave tank equipped with a computer-controlled wave generator and a comprehensive set of diagnostic tools. Recent work focuses on



Snapshots of breakers generated in the Free Surface Hydrodynamics Laboratory. At lower right, a wave traveling toward the viewer is seen breaking across the width (approx. 3 m) of the tank. In the upper images, waves traveling from left to right are breaking and forming surface turbulence.

the physics of breaking waves, their infrared signature, and their role in producing aerosols. Experiments conducted in the FSHL are also used to test and validate numerical results and analytical theories dealing with the physics of the ocean's free surface.

Current atmospheric science research areas include the remote sensing of aerosols, measurement of ocean surface winds, and middle atmospheric research. The Division has developed a unique eye-safe volume-imaging lidar system to remotely characterize aerosol backscatter. NRL also developed the first spaceborne polarimetric microwave radiometer, WindSat, launched in January 2003 and still operational. Its primary mission was to demonstrate the capability to remotely sense the ocean surface wind vector with a passive system. WindSat provides major risk reduction for development of the microwave imager for the next-generation DoD operational environmental satellite program. WindSat data are processed at the Navy Fleet Numerical Meteorology and Oceanography Center (FNMOC), and operationally assimilated into the Navy global weather model, NOGAPS. In addition, the Remote Sensing Division is exploiting WindSat's unique data set for other environmental parameters such as sea surface temperature, soil moisture, and sea ice concentration.

The Water Vapor Millimeter-wave Spectrometer (WVMS) is a ground-based instrument designed to measure water vapor in the middle atmosphere. It

is part of the international ground-based Network for Detection of Atmospheric Composition Change (NDACC), with sensors based in Lauder, New Zealand, Mauna Loa, Hawaii, and Table Mountain, California.

The Division has research programs in astronomy and astrophysics ranging in wavelength from the optical to longwave radio, with an emphasis on interferometric imaging. Facilities include the Navy Prototype Optical Interferometer (NPOI), located near Flagstaff, Arizona, a joint project between the U.S. Naval Observatory and the NRL Remote Sensing Division. The NPOI is used for optical astrometry, to investigate unfilled aperture imaging technologies, and to conduct astrophysical research. When completed,



The NRL WindSat polarimetric radiometer prior to spacecraft integration.

it will be the highest-resolution ground-based optical telescope in the world. The Division is also at the forefront of research in low-frequency (<100 MHz) radio astronomy and associated instrumentation and interferometric imaging techniques. The Division developed and installed VHF receivers on the National Radio Astronomy Observatory's Very Large Array (VLA), and developed the imaging techniques to correct for ionospheric phase disturbances which had heretofore severely limited observational baselines and, thus, the utility of low-frequency astronomical imaging. The Division is also collaborating with the University of New Mexico and New Mexico Tech on the Long Wavelength Array, a prototype, next-generation, low-frequency imaging array with 200–300 km baselines. ♦

Oceanography



The Oceanography Division's Scanfish is used to measure the variability of temperature, salinity, and optical properties of the littoral environment.

The Oceanography Division is the major center for in-house Navy research and development in oceanography. It is known nationally and internationally for its unique combination of theoretical, numerical, experimental, and remotely sensed approaches to oceanographic problems. The Division's modeling focus is on a truly integrated global-to-coastal modeling strategy, from deep water up to the coast including straits, harbors, bays, inlets, and rivers. This requires emphasis on both ocean circulation and wave/surf prediction, with additional emphasis on coupling the ocean models to atmospheric, biological, optical, and sediment models. This includes processing and analysis of satellite and in-water observations, development of numerical model systems, and assimilation for predicting the ocean environment. This modeling is conducted on the Navy's and DoD's most powerful vector and parallel processing machines. The Division's in-house Ocean Dynamics and Prediction Computational Network Facility provides computer services to scientists for program development, graphics, data processing, storage, and backup. To study the results of this intense modeling effort, the Division operates a number of highly sophisticated graphic systems to visualize ocean and coastal dynamic processes. Problems addressed cover

a wide scope of physics including parameterization of oceanic processes, construction and analysis of ocean models and forecast systems, basic and applied research of ocean dynamics, surface waves, thermohaline circulation, nearshore circulation, estuarine and riverine modeling, Arctic ice modeling, internal waves, and ocean/atmosphere coupling. Additional emphasis is on optimization of underwater, airborne, and satellite observing systems, representation of ocean processes affecting temperature, salinity, and mixed-layer depth, uncertainty analysis in coupled systems, ensemble and probabilistic ocean forecasting, targeting ocean glider observations, representing probability in ocean/acoustic systems, and satellite-observed surface heat fluxes. The end goal is to build cutting-edge technology systems that transition to operational forecast centers.

The Division's Ocean Sciences Branch conducts basic and applied research in ocean physics, air-sea interaction, ocean optics, and marine microbially influenced corrosion. Emphasis of this research is on understanding the oceans' physical processes and their interactions with the atmosphere and biological/chemical systems at scales ranging from basin-scale to microscale. Numerical and analytical models are developed and tested in laboratory and field experiments. The results of this research support the Navy's operational capability for predictions of oceanic atmospheric exchanges, acoustic propagation/detection, light

transmission/emission, and influences of microbes on marine corrosion. The seagoing experimental programs of the Division range worldwide. Unique measurement systems include a wave measurement system to acquire in situ spatial properties of water waves; a salinity mapper that acquires images of spatial and temporal sea surface salinity variabilities in littoral regions; an integrated absorption cavity and optical profiler system, and towed optical hyperspectral array for studying ocean optical characteristics; self-contained, bottom-mounted, upward-looking acoustic Doppler current profilers (ADCPs) for measuring ocean variability; and an in situ volume scattering function measurement system to support remote sensing and in-water optical programs. NRL is working jointly with the NATO Undersea Research Center (NURC) for development and deployment of the SEPTR instrument, a trawl-resistant, bottom-mounted ADCP system that includes a pop-up profiling float for real-time observation and reporting.

Division operates an environmental scanning electron microscope for detailed studies of biocorrosion in naval materials.

The Division's remote sensing research focuses on radiative transfer theory, optical ocean instrumentation, lasers and underwater imaging and vision, satellite and aircraft remote sensing, remote sensing of bio-optical signatures, and coupled physical bio-optical modeling. The research includes applying aircraft and satellite ocean color and thermal infrared signatures for understanding the bio-geo-chemical cycles in the surface ocean. Additional emphasis is on algorithm and model development using satellite (SeaWiifs, MODIS, MERIS, NPOESS, OCM, HICO, GEOCAPE, ACE) and aircraft (CASI, AVIRIS, PHILLS) sensors to address the spatial and temporal variability of coastal optical properties. The Division has the capability to download MODIS data directly using an X-band receiving system and is a national leader in the development and analysis of MODIS ocean color data for oceanographic pro-



New capabilities for sensing the littoral environment. Left: Slocum Glider. Center: Vertical Microstructure Profiler. Right: SEPTR.

The Oceanography Division has acquired new capabilities for sensing the littoral environment. These include a Vertical Microstructure Profiler (VMP), a Scanfish, and four Slocum Gliders. The turbulent dissipation rate can be quickly obtained with very high accuracy from measurements collected by the VMP. The Scanfish allows efficient and rapid three-dimensional mapping of mesoscale oceanic features. The Gliders rely on a low-powered battery-induced change of buoyancy to glide autonomously through the coastal ocean collecting both physical and optical data that are uplinked to satellite and then relayed to the laboratory or ship in near real time. In the laboratory, the

cesses and naval applications in littoral areas. The Division conducts optical field experiments using advanced in situ and remote sensing instrumentation (ship-towed sensors, sea gliders, and bio-optical/physical moorings) to understand remotely sensed signatures for calibration, validation, and refinement of algorithms. The Division also conducts research addressing how remote sensing optical and biological signatures can be fused with in-water bio-optical profiles and assimilated into ocean process models, and includes developing methods and techniques to understand and forecast the ocean optical environment through the combined use of remote sensing products and models. ♦

Marine Geosciences



An international field experiment at Cassino Beach, Brazil, studied the impact of the mud seafloor in the damping of waves reaching the beach (right side of photo).

The Marine Geosciences Division is the major Navy in-house center for research and development in marine geology, geophysics, geodesy, geoacoustics, geotechnology, and geospatial information and systems.

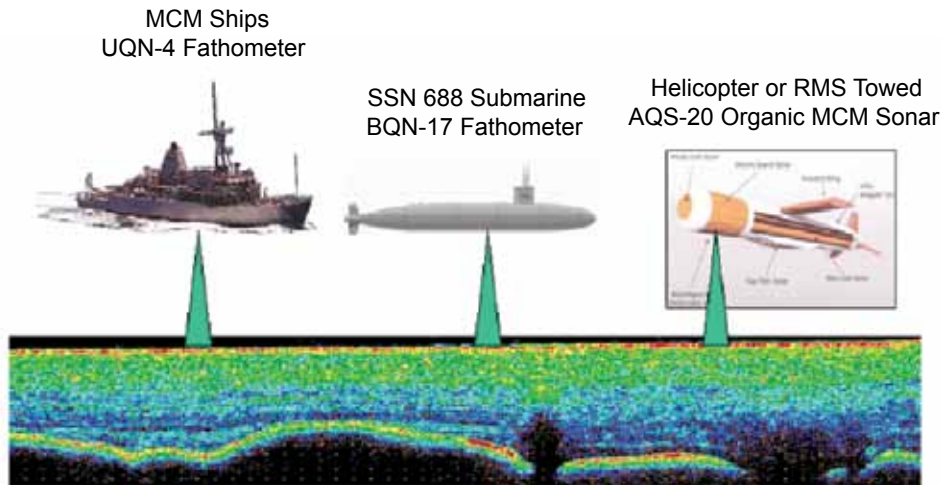
Instrumentation used in the field is deployable from aircraft, ships, submarines, remotely operated and unmanned vehicles, undersea platforms, and by divers. Instrumentation includes an integrated airborne geophysical sensor suite with gravity, magnetic, and sea/ice/land topographic profiling sensors, all based on centimeter-level KGPS aircraft positioning. Seafloor and subseafloor research uses the Deep-Towed Acoustics/Geophysics System (220 to 1000 Hz); a chirp sub-bottom profiler; high-resolution sidescan sonars (100 and 500 kHz); the Acoustic Seafloor Characterization System (15, 30, and 50 kHz); the In Situ Sediment Acoustic Measurement System, measuring

compressional and shear wave velocities and attenuation; a heat flow probe system; and underwater stereo photography and nearshore video imaging systems. Five instrumented, 8-ft-long, 2220-lb, mine-like cylinders are used to gather impact burial data (one system) and scour and sand wave burial data (four systems) for testing and validation of mine burial prediction models.

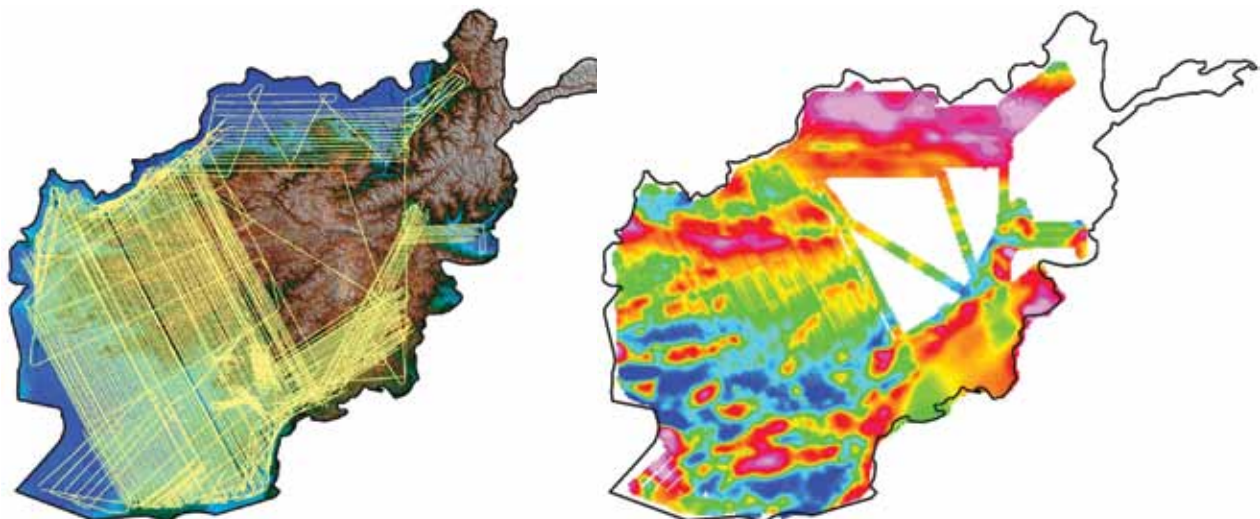
Laboratory facilities allow measurement of sediment physical, geochemical, and geotechnical properties. Equipment includes a photon correlation spectrometer and a laser Doppler velocimeter to measure size and electrostatic properties of submicrometer-size sediment particles. The Transmission Electron Microscopy Facility includes a 300 kVa transmission electron microscope with environmental cell enabling real-time observations of hydrated and gaseous experiments for research in microscale biological, chemical, and geological processes. A high-resolution industrial computed-tomography scanner provides capability for investigating volumetric heterogeneity of sediments.

The Moving Map Composer Facility is used to design and write mission-specific map coverages for F/A-18 and AV-8B tactical aircraft onto militarized optical disks. The Geospatial Information Data Base

capability provides Internet access to the Digital Nautical Chart data, mapping data, imagery, and other data types such as video and pictures used for planning, training, and operations. ♦



NRL is developing techniques that utilize the data stream from tactical systems to also extract ocean environmental measurements for near-real-time use (a through-the-sensor approach). Key components of the effort include fusion of dynamic with historical data to refresh the environmental picture, and delivery of the information to tactical decision aids. Current efforts include the demonstration of acoustic seafloor sediment classification, seafloor imaging, and seafloor bathymetry with sonars currently installed on fleet mine countermeasure ships, on nuclear attack submarines, and on helicopter-towed mine hunting sonars.



Rampant Lion I and II were multisensor aerogeophysical surveys of Afghanistan conducted in 2006 and 2008 by NRL and the U.S. Geological Survey to advance geospatial techniques, support military planners, and aid in economic infrastructure development. During Rampant Lion I, 40 mission flights produced more than 125,000 line-km of airborne survey tracks (left) and 330,000 km² of imagery. The magnetic anomaly map (right) provides data for oil, gas, and mineral exploration.

Marine Meteorology



NRL's Marine Meteorology Division has a direct downlink capability for real-time geostationary data from NOAA's GOES-E and GOES-W satellites.

The Marine Meteorology Division, located in Monterey, California, conducts basic and applied research in atmospheric sciences and develops meteorological analysis and prediction systems and other products to support Navy and other customers at the theater, operational, and tactical levels. The Division is collocated with the Fleet Numerical Meteorology and Oceanography Center (FNMOC), the Navy's operational production center for numerical weather prediction (NWP) and satellite data.

The Division's state-of-the-art Satellite Data Processing Laboratory allows direct downlink of real-time

NOAA geostationary data and data relays from three other geostationary satellites. Data from numerous polar orbiting platforms is also received in near real time; some data is received directly and some is provided through various interagency agreements. In total, NRL-Monterey processes satellite data from 31 low-Earth-orbit sensors and 7 geostationary platforms and uses that data to conduct research and development of multisensory data fusion products to support a variety of DoD operations. These activities range from monitoring and analyzing tropical cyclone characteristics to providing enhanced imagery in support of combat operations in Southwest Asia.

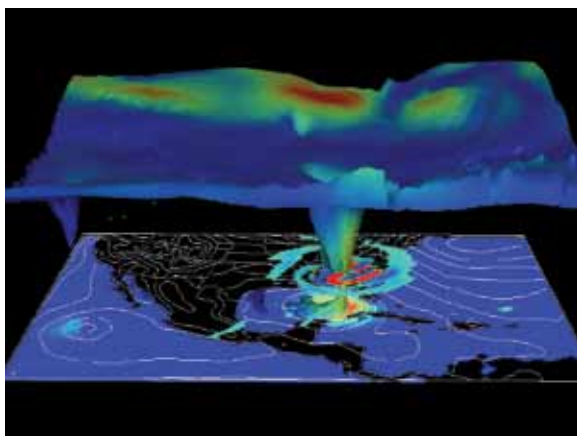
The Division's Atmospheric Prediction System Development Laboratory is built around two LINUX clusters (with 176 and 44 processors) supported by

a 200 TB RAID storage system and a 1000 TB tape library, as well as several smaller LINUX clusters, including a 22-processor cluster with SIPRNET connectivity. These systems enable the Division to efficiently develop, improve, and transition numerical weather analysis and prediction systems and coupled air/ocean systems to operational use, producing guidance which is used by Fleet forces around the globe. These systems also support basic research in atmospheric processes such as air-sea interaction, atmospheric dynamics, and cloud/aerosol physics.

The Mobile Atmospheric Aerosol and Radiation Characterization Observatory (MAARCO) is a set of climate-controlled containers with integrated suites of meteorological, aerosol, gas, and radiation instruments that can be rapidly deployed to operate in strategic areas around the globe, including remote regions, overseas locales, and onboard ships at sea. The instruments can also be removed and mounted on aircraft for added flexibility in field data collection, and are used to investigate boundary layer meteorology, aerosol microphysics, and electro-optical propagation. ♦



MAARCO is designed as a stand-alone facility for basic atmospheric research and the collection of data to assist in validating aerosol and weather models. Its purpose is to enable research on atmospheric aerosols, gases, and radiation (visible and IR light) in areas of key interest, including remote areas, overseas locales, and onboard ships. This complete mobile laboratory facilitates deployment in areas with limited facilities, and provides maximum flexibility for integration of additional instrumentation.



NRL developed a new version of the Navy's high-resolution operational mesoscale model, COAMPS® (Coupled Ocean/Atmospheric Prediction System), specifically for tropical cyclone (TC) prediction: COAMPS-TC. This COAMPS-TC three-dimensional depiction of hurricane Katrina (valid 29 August 2005) includes the 340K equivalent potential temperature isosurface, sea-level pressure (white), 10-m wind speed (color), and 2.5-km adjoint sensitivity.

Space Science



The VERIS sounding rocket instrument payload is being loaded for testing into a Space Science Division coronagraph test chamber.

The Space Science Division conducts a broad-spectrum RDT&E program in solar-terrestrial physics, astrophysics, upper/middle atmospheric science, and astronomy. Division researchers conceive, plan, and execute scientific research and development programs and transition the results to operational use. They develop instruments to be flown on satellites, sounding rockets and balloons; and ground-based facilities and mathematical models. Division major research thrusts include remote sensing of the upper and middle atmospheres, studies of solar activity and effects on the Earth's ionosphere, and studies of high-energy natural radiation and particles, for applications ranging from astrophysics through force protection.

The Division's Vacuum Ultraviolet Solar Instrument Test (SIT) facility is an ultra-clean solar instrument test facility designed to satisfy the rigorous contamination requirements of state-of-the-art solar spaceflight instruments. The facility has a 400 ft² Class 10 clean room and a large Solar Coronagraph Optical Test Chamber (SCOTCH). The SIT clean room is ideally suited for assembly and test of contamination-sensitive spaceflight instrumentation. It contains a large vibration-isolated optical bench and a 1-ton capacity overhead crane. The SCOTCH consists of a large vacuum tank and a precision instrument-pointing table. The division also maintains extensive facilities for supporting ultraviolet (UV) spectroscopy sounding rocket programs. These facilities include a dedicated Class 1000 instrument clean room, and a gray room area for assembling and testing the rocket payloads

that incorporates all of the fixtures required for safe handling of payloads. The Division rocket facilities also include a large UV optical test chamber that is additionally equipped with a large vibration- and thermal-isolated optical bench for telescope testing, which allows the laboratory area to be turned into a reasonable quality Schlieren facility. The Division also has a unique facility for developing Doppler Asymmetric Spatial Heterodyne (DASH) thermospheric wind sensors, which are currently being evaluated and tested in support of potential future space flight missions.

The division has a wide range of new satellite, rocket, balloon, and ground-based instruments under development. These include the SoloHI heliospheric imager that will image both the quasi-steady flow and transient disturbances in the solar wind when aloft on-board the Solar Orbiter; the Compact CORonagraph (CCOR), an elegant, externally occulted instrument that uses a single-stage optical design with two lens groups, a polarization analyzer, and a spectral filter to achieve performance comparable to the traditional three-stage Lyot coronagraph but with significantly lower mass and volume than the traditional design; VERIS (Very high angular resolution Imaging Spectrometer), a space experiment that is being designed to uncover the fundamental structure of the solar

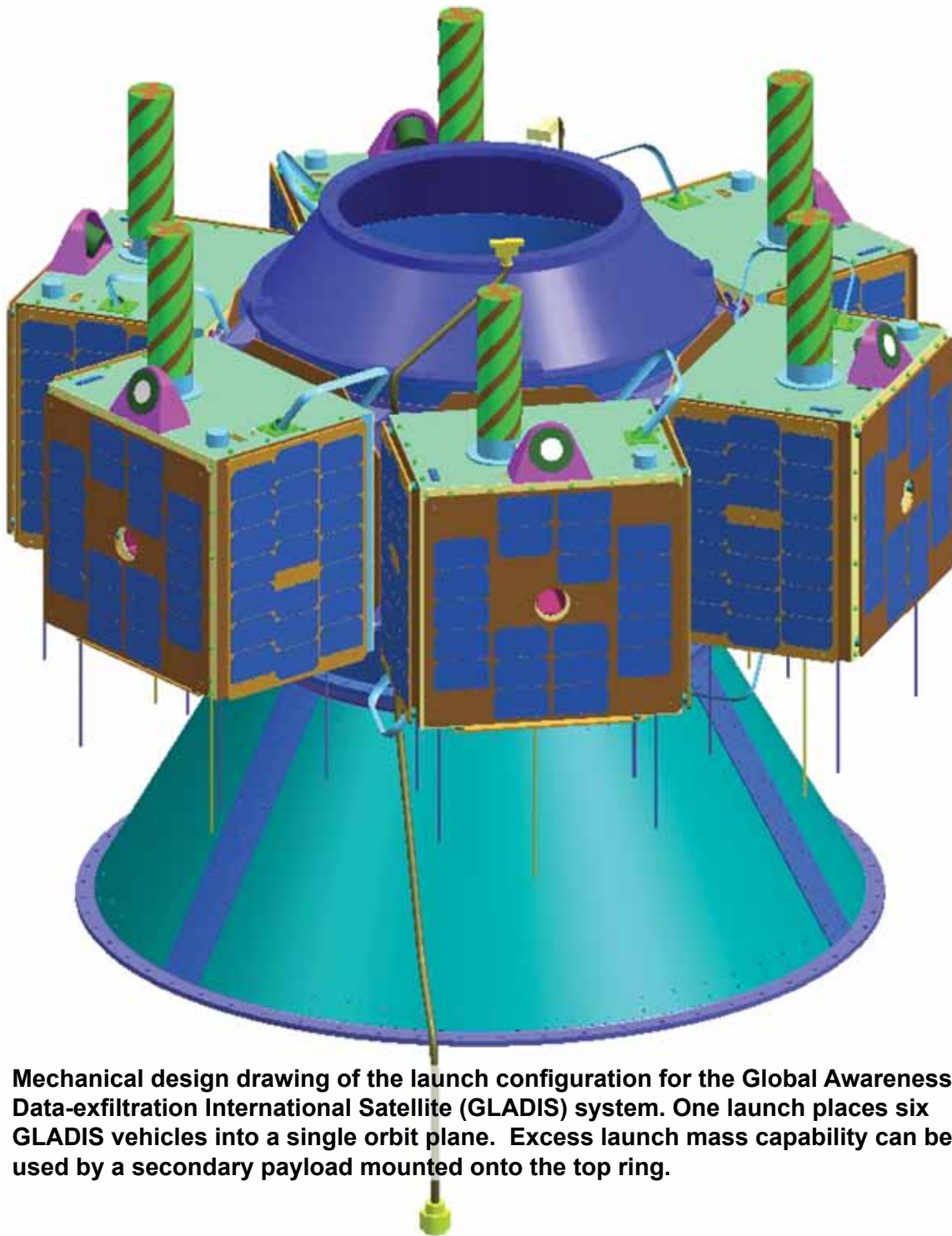
atmosphere, which is expected to launch on a sounding rocket in April 2011; and the NRL-led Large Area Scintillation Array (LASA), intended to demonstrate standoff detection of radiation/nuclear weapons of mass destruction (WMD) in maritime environments in support of the Office of Naval Research's Maritime WMD Detection program. Division scientists are also designing innovative high-resolution spectrometers and coronagraphs for a possible flight on the Japanese Solar-C mission that will provide unprecedented views of the solar atmosphere.

Division scientists, using the Division network of computers and workstations and other connected high performance computing assets, develop and maintain physical models in support of their research. These include NOGAPS-ALPHA, the Advanced Level Physics High Altitude middle atmosphere extension of the Navy Operational Global Atmospheric Prediction System; HiFi, a user-friendly, highly parallel, fully implicit adaptive spectral element code framework designed for model development, magnetohydrodynamics, and multi-fluid numerical modeling in two- and three-dimensional geometries; and GAIM (Global Assimilation of Ionospheric Measurements), a physics-based assimilative model of the ionosphere now operational at the Air Force Weather Agency. ♦



The NRL ANDE-2 twin experimental microsatellites, Castor and Pollux, shortly after deployment under the auspices of the DoD Space Test Program from NASA's Space Shuttle Endeavour (STS-127) on 30JUL09, as photographed by the crew of the STS-127 from the flight deck. ANDE research products are being used to improve methods for the precision orbit determination of space objects, and to calibrate the Space Fence, a radar system of the USAF 20th Space Control Squadron that tracks low-Earth-orbiting space objects.

Space Systems Development Department



Mechanical design drawing of the launch configuration for the Global Awareness Data-exfiltration International Satellite (GLADIS) system. One launch places six GLADIS vehicles into a single orbit plane. Excess launch mass capability can be used by a secondary payload mounted onto the top ring.

The Space Systems Development Department (SSDD) is responsible for the end-to-end definition, design, development, integration, test, and operation of space systems that satisfy naval and national defense requirements.

The total system engineering philosophy employed by the SSDD enables seamless sensor-to-shooter capabilities to be deployed that optimize the interfaces between command and control, on-orbit satellite collection, and onboard and ground processing functions; the dissemination of data to tactical and national users; and the design of tools that provide for the automated correlation and fusion of collected information with other sources.

Research and development is conducted in the areas of space system architectures; advanced mission data processing and data analysis techniques; advanced information systems concepts, including enterprise and cloud computing and networking of space, air, ground, and subsurface sensors; and mission simulation techniques. Intelligence collection, advanced RF, optical, and laser communication, satellite laser ranging, digital signal processing, data management, and space navigation systems are constantly improved upon to satisfy evolving requirements. These systems are engineered for maximum reuse and interoperability.

Having conceived of and developed the payload for the first Global Positioning System (GPS) satellite, the SSDD continues to be the world's center of excellence in the research and development of advanced GPS technology. Advanced theoretical and experimental investigations are applied to expanding the design and interoperability of systems used for a wide range of military, space, geodetic, and time dissemination applications. These investigations involve critical precise time generation and measurement technology for passive and active ranging techniques incorporating advanced data transmission and signal design. Precise time and time interval research conducted involves theoretical and experimental development of atomic time/frequency standards, instrumentation, and time-keeping to support highly precise and accurate time-scale systems in scientific and military use. Net-centric systems are critically dependent on highly accurate and stable time/frequency standards coordinated to a common timescale through the diverse dissemination comparison techniques developed within the SSDD.

In addition to a wide array of test tools and facilities, the Department operates several field sites including the Midway Research Center satellite calibration facility in Stafford, Virginia; the Blossom Point Satellite Command and Tracking Facility in Welcome, Maryland; and the Chesapeake Bay Detachment Radar Range in Chesapeake Beach, Maryland. ♦



Blossom Point Satellite Tracking and Command Facility in Welcome, Maryland.

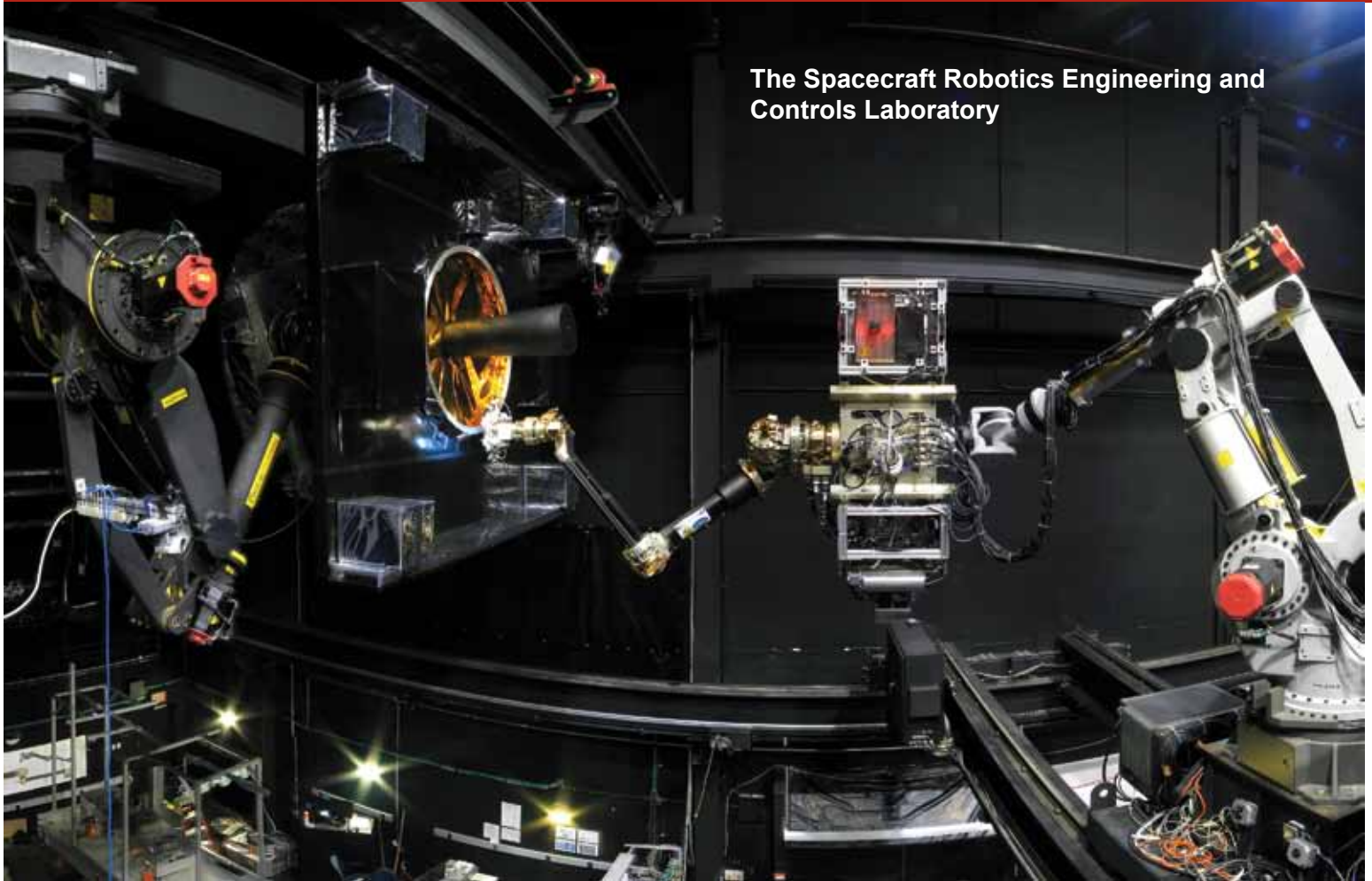


Midway Research Center satellite calibration facility in Stafford, Virginia.



Minuteman InfraLynx Communications System (MICS) – communications trucks designed to support the intercontinental ballistic missile (ICBM) fields in the remote upper midwest.

Spacecraft Engineering Department



The Spacecraft Robotics Engineering and Controls Laboratory

The Spacecraft Engineering Department (SED) and the Space Systems Development Department, together comprising NRL's Naval Center for Space Technology (NCST), cooperatively develop space systems to respond to Navy, DoD, and national mission requirements with improved performance, capacity, reliability, efficiency, and life cycle cost.

The SED facilities that support this work include integration and test highbays, large and small anechoic radio frequency chambers, varying levels of clean rooms, shock and vibration tables, an acoustic reverberation chamber, large and small thermal/vacuum test chambers, a thermal systems integration and test laboratory, a spin test facility, a static loads test facility, and a spacecraft robotics engineering and control system interaction laboratory.

Integration and Test Facilities

The Radio Frequency Anechoic Chamber supports electromagnetic compatibility/radio frequency interference (EMC/RFI) testing of flight hardware. It is also used to support custom RF testing up to 40 GHz. The facility consists of a 23 × 23 ft semi-anechoic main chamber with a 23 × 20 ft antechamber. It is a completely welded steel structure which provides a minimum of 120 dB of shielding effectiveness at 18 GHz and 100 dB up to 50 GHz. The main chamber uses a hybrid anechoic material consisting of wideband pyramidal absorbers and ferrite tiles for performance from 20 MHz to 50 GHz. A 10 ft high × 11 ft wide sliding bladder type door allows easy access of large test items to the main chamber.

The Laminar Flow Clean Room provides a Class 100 ultraclean environment for the cleaning, assembly, and acceptance testing of contamination-sensitive spacecraft components, and integration of complete spacecraft subsystems. The facility is used primarily to support spacecraft propulsion systems but has been

used to support all spacecraft electrical, electronic, and mechanical subsystems.

The Vibration Test Facility, which simulates the various vibration loading environments present during flight operations and demonstrates compliance to design specifications, consists of the following shakers: Unholtz-Dickie T5000 50K Flb random 2-in. DA stroke, Ling 4022 30K Flb random 2-in. DA stroke, Ling 2022 16K Flb random 2-in. DA stroke, and a Ling 335 16K Flb random 1-in. DA stroke.

The Acoustic Reverberation Simulation Facility is a 10,000 ft³ reverberation chamber that simulates the acoustic environment that spacecraft will experience during launch. The maximum capable sound pressure level is approximately 152 dB.

The Thermal Fabrication and Test Facility supports the design, fabrication, installation, and verification of spacecraft thermal control systems. It also provides for the analytical thermal design and analysis of any spacecraft. This includes conceptual design, analytical thermal model development, definition of requirements, worst-case environments and design conditions, and temperature predictions for all cases. The facility provides the means to go from design and analysis to hardware qualification and acceptance testing and then to orbit.

The Spin Test Facility contains two spin balancing machines (one horizontal and one vertical) to handle various types of balancing requirements. Both machines are provided with a plane separation network to obtain correction readings directly in the plane of correction. Moment of inertia (MOI) tables of various capacities are used to verify MOI and center of gravity for units under test.

The Static Loads Test Facility provides the capability to perform modal survey testing on a wide variety of spacecraft and structures. It consists of two 6-ft × 12-ft × 6-in.-thick, ~15,500-lb steel plates (attachable) with floating base, six 75-Flb stinger shakers (1/2-in. DA stroke), two 250-Flb stinger shakers (4-in. DA stroke), and a ~300-channel data acquisition system (expandable).

Spacecraft Robotics Engineering and Controls Laboratory

This facility, which is the largest dual-platform motion simulator of its kind, is operated by NCST in

collaboration with NRL's Naval Center for Applied Research in Artificial Intelligence. It supports research in the emerging field of space robotics including autonomous rendezvous and capture, remote assembly operations, and machine learning. It allows full-scale, hardware-in-the-loop testing of flight mechanisms, sensors, and logic of space robotic systems. ♦



Interim Control Module (ICM) in the Integration and Test Facility.



WindSat in the large thermal vacuum chamber.

RESEARCH SUPPORT FACILITIES

Technology Transfer Office

The NRL Technology Transfer Office (TTO) is responsible for NRL's implementation of the Federal Technology Transfer Act. It facilitates the transfer of NRL's innovative technologies for public benefit by marketing NRL technologies and by negotiating patent license agreements and Cooperative Research and Development Agreements (CRADAs).



TTO markets NRL technologies through its Web site, by the preparation of Fact Sheets to be distributed at trade shows and scientific conferences, and through DoD-contracted Partnership Intermediaries such as TechLink.

A license grants a company the right to make, use, and sell NRL technologies commercially in exchange for equitable licensing fees and royalties. Revenue is distributed among the inventors and NRL's general fund. Prior to granting a license, TTO reviews the commercialization plan submitted by the licensee in support of its application for license. The plan must provide information on the licensee's capabilities, proposed development expenditures, milestones, a time line to commercialization, and an assessment of the intended market.

A license may be exclusive, partially exclusive (exclusive for a particular field of use or geographic area), or non-exclusive. Once a license is executed, TTO monitors the licensee for timely payments and for its diligence in commercializing the licensed invention.

TTO also negotiates Government Purpose Licenses to transition NRL technologies for manufacture and sale solely for Navy and other U.S. Government purposes.

CRADAs provide a vehicle for NRL scientists and engineers to collaborate with their counterparts in industry, academia, and state and local governments. Under a CRADA, a company may provide funding for collaborative work between it and NRL and is granted an exclusive option to license technologies developed under that CRADA's Statement of Work (SOW). TTO works with the NRL scientist to develop a SOW that has sufficient detail to define the scope of the CRADA partner's rights.

Technical Information Services

The Technical Information Services (TIS) Branch combines publication, graphics, photographic, multimedia, exhibit, and video services into an integrated organization. Publication services include writing, editing, composition, publications consultation and production, and printing management. Quick turn-around digital black-and-white and color copying/printing services are provided. TIS uses digital publishing technology to produce scientific and technical reports that can be used for either print or Web. Graphics support includes technical and scientific illustrations, computer graphics, design services, photographic composites, display posters, and framing. The HP large format printers offer exceptional color print quality up to 600 dpi and produce indoor posters and signs with 56 inches being the limitation on one side. Lamination and mounting are available. Photographic services

include digital still camera coverage for data documentation, both at NRL and in the field. Photographic images are captured with state-of-the-art digital cameras and can be output to a variety of archival media. Photofinishing services provide custom printing and quick service color prints from digital files. Video services include producing video reports



Visual information specialist printing an exhibit on one of the large-format printers.

and technical videos, and capturing presentations of scientific and technical programs. TIS digital video editing equipment allows in-studio and on-location editing. The TIS Exhibits Program works with NRL's scientists and engineers to develop exhibits that best represent a broad spectrum of NRL's technologies, and promotes these technologies to scientific and nonscientific communities at conferences throughout the United States.

Administrative Services

The Administrative Services Branch is responsible for collecting and preserving the documents that comprise NRL's corporate memory. Archival documents include personal papers and correspondence, laboratory notebooks, and work project files — documents that are appraised for their historical or informational value and considered to be permanently valuable. The Branch provides records management services, train-



Employees of the Administrative Services Branch working in the mail room.

ing, and support for the maintenance of active records, including electronic records, as an important information resource. The Branch is responsible for processing NRL's incoming and outgoing correspondence and provides training and support on correct correspondence formats and practices. The Branch is responsible for NRL's Forms and Reports Management Programs (including designing electronic forms and maintaining a Web site for Lab-wide use of electronic forms), compiles and publishes the NRL Code Directory and Organizational Index, and is responsible for providing NRL postal mail services for first class and accountable mail and for mail pickup and delivery throughout NRL. The Branch also provides NRL Locator Service.

Ruth H. Hooker Research Library

NRL's Ruth H. Hooker Research Library continues to support NRL and ONR scientists in conducting their research by making a comprehensive collection of the most relevant scholarly information available and useable; by providing direct reference and research support; by capturing and organizing the NRL research portfolio; and by creating, customizing, and deploying a state-of-the-art digital library.

Traditional library resources include extensive technical report, book, and journal collections dating back to the 1800s housed within a centrally located research facility that is staffed by subject special-

ists and information professionals. The collections include 44,000 books; 80,000 bound historical journal volumes; more than 3,500 current journal subscriptions; and approximately 2 million technical reports in paper, microfiche, or digital format (classified and unclassified). Research Library staff members provide advanced information consulting; literature searches against all major online databases including classified databases; circulation of materials from the collection including classified literature up to the SECRET level; and retrieval of articles, reports, proceedings, or documents from almost any source around the world. Staff members provide scheduled and on-demand training to help researchers improve productivity through effective use of the library's resources and services.

The Research Library staff has developed and is continuing to expand the NRL Digital Library. The Digital Library currently provides desktop access to thousands of journals, books, and reference sources to NRL-DC; NRL-Stennis; NRL-Monterey; and the Office of Naval Research.

Library systems provide immediate access to scholarly information, including current issues of journals and conference proceedings that are fully searchable at the researcher's desktop (more than 4,000 titles). Extensive journal archives from all the major scientific publishers and scholarly societies are now available



Librarians working in the Ruth H. Hooker Research Library.

online. The breadth and depth of content available through TORPEDO, NRL's locally loaded digital repository, continues to grow and provides a single point of access to scholarly information by providing full text search against journals, books, conference proceedings, and technical reports from 19 publishers (12 million items by April 30, 2010). The NRL Online Bibliography, a Web-based publications information system, is ensuring that the entire research portfolio of written knowledge from all NRL scientists and engineers since the 1920s will be captured, retained, measured, and shared with current and future generations.

OTHER RESEARCH SITES AND FACILITIES

NRL has acquired or made arrangements over the years to use a number of major sites and facilities outside of Washington, D.C., for research. The largest facility is located at the Stennis Space Center (NRL-SSC) in Bay St. Louis, Mississippi. Others include a facility near the Naval Postgraduate School in Monterey, California (NRL-MRY), and the Chesapeake Bay Detachment (CBD) and Scientific Development Squadron One (VXS-1) in Maryland. Additional sites are located in Virginia, Alabama, and Florida.

Stennis Space Center (NRL-SSC)

The NRL Detachment at Stennis Space Center, Mississippi (NRL-SSC), consists of NRL's Oceanography Division and portions of the Acoustics and Marine Geosciences Divisions. NRL-SSC, a tenant activity at NASA's John C. Stennis Space Center (SSC), is located in the southwest corner of Mississippi, about 50 miles northeast of New Orleans, Louisiana, and 20 miles from the Mississippi Gulf Coast. Other Navy tenants at SSC include the Naval Meteorology and Oceanography Command, the Naval Oceanographic Office, the Navy Small Craft Instruction and Training Center, the Special Boat Team-Twenty-two, and the Human Resources Service Center Southeast. Other Federal and State agencies at SSC involved in marine-related science and technology are the National Coastal Data Development Center, the National Data Buoy Center, the U.S. Geological Survey, the Environmental Protection Agency's Gulf of Mexico Program and Environmental

Chemistry Laboratory, the Center of Higher Learning, University of Southern Mississippi, and Mississippi State University.

The Naval Meteorology and Oceanography Command and the Naval Oceanographic Office are major operational users of the oceanographic, acoustic, and geosci-

ences technology developed by NRL researchers. The Naval Oceanographic Office operates the Major Shared Resource Center (MSRC), one of the nation's High Performance Computing Centers, which provides operational support to the warfighter and access to NRL for ocean and atmospheric science and technology.



Slocum gliders, autonomous underwater vehicles, are equipped with temperature/salinity/pressure sensors and with real-time satellite connection to the Iridium network.

The Acoustics, Marine Geosciences, and Oceanography Divisions occupy more than 175,000 ft² of research, computation, laboratory, administrative, and warehouse space. Facilities include the sediment core laboratory, transmission electron microscope,



The JEOL JEM-3010 transmission electron microscope.

moving-map composer facility, underwater navigation control laboratory, computed tomography scanning laboratory, real-time ocean observations and forecast facility, ocean color data receipt and processing facility, environmental microscopy facility, maintenance and calibration systems, environmental modeling and simulation high-speed network, and numerous laboratories for acoustic, geosciences, and oceanographic computation, instrumentation, analysis, and testing. Special areas are available for constructing, staging, refurbishing, and storing seagoing equipment.

Monterey (NRL-MRY)

NRL's Marine Meteorology Division (NRL-MRY) is located in Monterey, California, on a 5-acre campus about one mile from the Naval

Postgraduate School (NPS) campus. This group has occupied this site since the early 1970s, when the U.S. Navy decided to collocate the

meteorological research facility with the operational center, now known as Fleet Numerical Meteorology and Oceanography Center (FNMOC). FNMOC was stood up in Monterey around 1960 to be able to share resources and expertise with NPS. This collocation of research, education, and operations continues to be a winning formula, as FNMOC remains the primary customer for the numerical weather prediction and satellite product systems developed by NRL-MRY. NRL scientists have direct access to FNMOC's large classi-



Antenna receiving geostationary satellite data.

fied supercomputers, allowing advanced development to take place using the real-time, on-site, global atmospheric and oceanographic databases, set in the same computational environment as operations. Such access offers unique advantages for successfully implementing new systems and system upgrades, and allows for rapid integration of new research results into the operational systems. Proximity to NPS also offers unique opportunities for collaborative research, as well as educational and teaching/mentoring opportunities for NRL staff.

Today, the NRL/FNMOC compound is comprised of four primary buildings — one dedicated to FNMOC supercomputer operations; two large shared buildings dedicated to NRL-MRY and FNMOC office spaces, computer laboratories, and conference facilities; and a fourth building now occupied by NOAA's local National Weather Service Forecast Office, which offers additional opportunities for interagency collaboration and data sharing. In addition to the main buildings, NRL-MRY also occupies two modular office buildings and a warehouse on the campus. Altogether, NRL-MRY occupies approximately 1500 ft² of storage space and 26,500 ft² of office/laboratory/conference space, which includes a research library, a computer center that supports the Atmospheric Prediction System Development Laboratory, the Atmospheric Composition Monitoring Station, and a small classified processing facility. A newly approved MILCON project will give NRL-MRY a new, state-of-the-art, "green" building that will replace the two modular buildings and will include an atmospheric aerosol laboratory. It is scheduled for completion in FY12.

Chesapeake Bay Detachment (CBD)

NRL's Chesapeake Bay Detachment (CBD) occupies a 168-acre site near Chesapeake Beach, Maryland, and provides facilities and support services for research in radar, electronic warfare, optical devices, materials, communications, and fire research.

Because of its location high above the western shore of the Chesapeake Bay, unique experiments can be performed in conjunction with the Tilghman Island site, 16 km across the bay from CBD. Some of these experiments include low-clutter and generally low-background



Aerial view of the Chesapeake Bay Detachment at Randle Cliff (Chesapeake Beach), Maryland.

radar measurements. Using CBD's support vessels, experiments are performed that involve dispensing chaff over water and characterizing aircraft and ship radar targets. Basic research is also conducted in radar antenna properties, testing of radar remote sensing concepts, use of radar to sense ocean waves, and laser propagation. A ship-motion simulator (SMS) that can handle up to 12,000 lb of electronic systems is used to test and evaluate radar, satellite communications, and line-of-sight RF communications systems under dynamic conditions (various sea states). CBD also hosts facilities of the Navy Technology Center for Safety and Survivability, which conducts fire research on simulated carrier, surface, and submarine platforms.



The Chesapeake Bay Detachment Radar Range facility overlooks the shipping channels in the Chesapeake Bay, in conjunction with the extensive Marine Navigation Radar (MNR) Test Range on Tilghman Island.

The Radar Range facility at CBD, together with the Maritime Navigation Radar (MNR) Test Range at Tilghman Island, provide the emitters and analysis tools for developing comprehensive Maritime Domain Awareness capabilities. The MNR consists of dozens of radars that represent a precise cross-section of today's actual MNR environment. An integrated suite of advanced sensors has been developed for data collection and processing to identify and classify vessels. A suite of similar sensors and processors has been integrated into a transportable shelter, the Modular Sensor System (MSS), that can be rapidly deployed to ports or other sites for enhanced maritime awareness reporting.

Scientific Development Squadron One (VXS-1)

Scientific Development Squadron ONE (VXS-1) located at Naval Air Station Patuxent River, Maryland, is manned by approximately 14 officers, 80 enlisted, and 9 civilians. VXS-1 is currently responsible for the maintenance, operations, and security of three uniquely configured NP-3D Orion aircraft and two RC-12 Beech King Air research aircraft. The squadron conducts numerous worldwide detachments in support of a wide range of scientific research projects. In FY08/09, VXS-1 provided flight support for several diverse research programs: Operation Rampant Lion II consisted of exploration, reconstruction, counternarcotics, and security efforts in Afghanistan, and provided airborne support to an emerging riverine mission set in Iraq; THORPEX

Pacific-Asian Regional Campaign (T-PARC) was a multinational endeavor collecting data directly from one tropical storm and three typhoons to increase the predictability of tropical cyclones in the Western Pacific region; Operation Rampant Lion III was a presidential priority mission in support of ongoing MIA recovery efforts, including data collection in the search to find the remains of CAPT Speicher lost in 1991 and a crew lost in a 1942 search and recovery effort; and Missile Defense Agency (MDA) testing and experimentation



Operation Rampant Lion III in Afghanistan.

vital to the success of global defense efforts included multinational land- and surface-based missile tracking and interceptor tests. In January 2009 while operating out of Curacao, Netherlands Antilles, the Rampant Lion SOUTH project supported SOUTHCOM Counter Drug operations by utilizing cutting-edge airborne geophysical sensor technology to provide quick turnaround analysis for intelligence applications. In summer 2009, the squadron deployed an RC-12 aircraft and crew to Alaska to conduct gravitational measurements in support of NOAA objectives, building on an already strong relationship with federal civilian agencies pursuing similar airborne scientific investigations. VXS-1 surpassed 47 years and 69,000 hours of Class “A” mishap-free operations in FY09.

Midway Research Center

The Midway Research Center (MRC) is a world-wide test range that provides accurate, known signals as standards for performance verification, validation, calibration, and anomaly resolution. In this role, the MRC ensures the availability of responsive and coordinated scheduling, transmission, measurement, and reporting of accurate and repeatable signals. The MRC, under the auspices of NRL’s Naval Center for Space Technology, provides NRL with state-of-the-art facilities dedicated to Naval communications, navigation, and basic research. The headquarters and primary site is located on 162 acres in Stafford County, Virginia. The main site consists of three 18.2-m, radome-enclosed precision tracking antennas and a variety of smaller antennas. The MRC has the capability to transmit precision test

signals with multiple modulation types. Its normal configuration is transmit but can be configured to receive as required. The MRC also provides cross-mission and cross-platform services from worldwide locations using a combination of fixed and transportable resources and a quick-reaction, unique signals capability. Assets include Pulstar Systems (several worldwide locations), a 45-m tracking antenna in Palo Alto, California, and a 25-m tracking antenna system on Guam. The MRC instrumentation suite includes nanosecond-level time reference to

the U.S. Naval Observatory, precision frequency standards, accurate RF and microwave power measurement instrumentation, and precision tracking methodologies. The MRC also contains an Optical

Test Facility with two specialized suites of equipment: a multipurpose Transportable Research Telescope (TRTEL) used for air-to-ground optical communications and for passive satellite tracking operations, and a Satellite Laser Ranging (SLR) system built around a 1-meter telescope as a tool for improving customer ephemeris validation processes.

Pomonkey Facility

The Naval Research Laboratory’s Pomonkey Facility is a field laboratory with a variety of ground-based antenna systems designed to support research and development of space-based platforms. Located 25 miles south of Washington, D.C., the facility sits on approximately 140 acres of NRL-owned land, which protect its systems from encroaching ground-based interferers.

Among its various precision tracking antennae, the facility hosts the largest high-speed tracking antenna in the United States. Boasting a diameter of 30 meters, its range of trackable platforms includes



Midway Research Center (MRC), Stafford County, Virginia.



The NRL Pomonkey Facility.

those in low Earth orbit through those designed for deep space missions. The facility's antenna systems are capable of supporting missions at radio frequencies from 50 MHz through 20 GHz and can be easily configured to meet a variety of mission requirements. The ease of system configuration is due to the facility's stock of multiple antenna feeds, amplifiers, and downconverters. Other facility assets include an in-house ability to design, fabricate, test, and implement a variety of radio frequency components and systems. The facility also hosts a suite of spectrum analysis instrumentation that when coupled to its antenna systems, provides a unique platform for a variety of research and development missions.

Blossom Point Satellite Tracking and Command Facility

The Blossom Point Satellite Tracking and Command Facility (BP) provides engineering and operational support to several complex space systems for the Navy and other sponsors. BP provides direct line-of-sight, two-way communications services with spacecraft in multiple bands and multiple orbits including LEO, HEO, GEO, and Lunar. Additionally, with BP as a node on the Air Force Satellite Control Network (AFSCN), it has the capability to provide coverage worldwide.

BP consists of a satellite mission operations center, multiple antennas, and an infrastructure capable of providing space system command, control, and management. Specific BP resources include the following:

Common Ground Architecture (CGA): CGA is government-owned software that provides infrastructure and reusable components facilitating construction of command, control, and monitoring systems for space vehicle development, integration, test, and operations. CGA with Automated Ground Operations (AGO) software allows for 5x8 (lights out) operations or 24x7 operations. Current missions include 13 satellites with 186 worldwide contacts per day. The GAO-10-55 report dated October 2009, titled *Challenges in Aligning Space Systems Components*, lauds BP with CGA as one facility that can control a variety of satellites.



Blossom Point Satellite Command and Tracking Facility.

Hardware Architecture: Based on RF, video, and matrix switching with net-centric control and processing, virtually any hardware asset can be “switched” into a path to create the correct capability required for any mission. This architecture supports both classified and unclassified operations and missions, and internal LANs support multiple simultaneous mission operations. Salient resources include antennas; receivers; telemetry, tracking, and command (TT&C); command encoder; front-end processors; operations automatic data processing (ADP) resources; and satellite health and monitoring/engineering evaluation and maintenance (SHM/EEM).

Research Platforms

Mobile research platforms contribute greatly to NRL's research. These include six P-3 Orion turbo-prop aircraft and one ship, the ex-USS *Shadwell* (LSD 15), berthed in Mobile Bay, Alabama. The *Shadwell* is used for research on aboard-ship fire suppression techniques.



Moored in Mobile Bay, Alabama, the ex-USS *Shadwell* is regularly set ablaze in a controlled environment to further the safety of operational Navy and civilian firefighting measures.

Marine Corrosion and Marine Coatings Facilities

The Chemistry Division's Marine Corrosion and Coatings Facility located in Key West, Florida, offers a “blue” ocean environment with natural seawater characterized by historically small compositional variation and a stable biomass. This continuous source of stable, natural seawater provides a site ideally suited for studies of marine environment



Demonstration of the removal of non-skid coating by heat induction at NRL Key West.

effects on materials, including accelerated and long-term exposure testing and materials evaluation. The site maintains

capabilities for extensive RDT&E of marine engineering and coatings technologies and supports a wide array of Navy and industrial sponsors. Equipment is available for experiments involving accelerated corrosion and weathering, general corrosion, long-term immersion and alternate immersion, fouling, electrochemical phenomena, coatings application and characterization, cathodic protection design, ballast water treatment, marine biology, and corrosion monitoring. In 2009, the facility received a comprehensive refurbishment due to hurricane damage.

88

Marine Biofouling: Grasping Barnacle Cement Curing from the Inside Out
K.J. Wahl, D.E. Barlow, R.K. Everett, G.H. Dickinson, B. Orihuela, and D. Rittschof

97

Structure-Property Relationships in a 3D Polycrystalline Microstructure
A.C. Lewis, D.J. Rowenhorst, G. Spanos, A.B. Geltmacher, and S.M. Qidwai

104

Monitoring Enzyme Activity with Hybrid Semiconductor Quantum Dot-Fluorescent Protein Assemblies
K. Boeneman, J.R. Deschamps, I.L. Medintz, and M.H. Stewart

113

Seismic Oceanography – A New View of the Ocean
W.T. Wood, D.A. Lindwall, J.W. Book, J. Wesson, S. Carniel, and R.W. Hobbs

122

The Impact of Ice Nuclei Concentration on Hurricane Modeling
Y. Jin, J.D. Doyle, Q. Zhao, S. Wang, and S.W. Chang

What a Drag...But We Might Have the Cure

Biofouling (the accumulation of biological matter, such as microorganisms, plants, algae, or animals on seagoing vessels) adds significant drag to ship hulls and it is really a drag that it increases the Navy's fuel and maintenance costs. Modern antifouling paints have helped but environmental and regulatory concerns regarding toxic leaching of chemicals from these paints make finding a better solution for use on Navy ships and underwater structures a major priority.

What's the cure? Well, one solution for hard foulants like barnacles is to figure out how barnacles' insoluble glue cures underwater – and then invent advanced marine coatings that can disrupt those specific chemical and biomechanical processes. To do this, a research team from NRL's Chemistry and Materials Science and Technology Divisions and the Duke University Marine Laboratory was assembled and has been looking at barnacles from the inside out. These researchers have been devising new methodologies and using such technologies as CAT scans (X-ray tomography), atomic force microscopy, and infrared and ultraviolet spectroscopy to find out how barnacles secrete and cure their amazing adhesive glue. And the team's own stick-to-itiveness has paid off: they've found that the curing may be accomplished via a process similar to blood clotting in mammals; that the barnacles' glue differs from clotted blood in that its proteins fold in ladder-like amyloid structures, similar to how Alzheimer's disease affects protein conformation; and that barnacles use many simultaneous methods to make the glue they secrete an insoluble adhesive.

Applying more than an ounce of prevention (which is worth at least a pound of cure) seems to be the key, so the push now is to design new coatings that prevent barnacles from curing their adhesives. That should reduce the barnacle bill for sailors!

Marine Biofouling: Grasping Barnacle Cement Curing from the Inside Out

K.J. Wahl and D.E. Barlow
Chemistry Division

R.K. Everett
Materials Science and Technology Division

G.H. Dickinson, B. Orihuela, and D. Rittschof
Duke University Marine Laboratory

Biofouling of Navy vessels substantially increases fuel and maintenance costs: the added drag increases fuel consumption, and the tenacious foulants are difficult to dislodge from hull surfaces. Understanding the biochemical and mechanical properties of biofoulants and their often insoluble adhesives will enable development of hull surface treatments that specifically target biofouling without resorting to materials or coatings that contain toxins. Our team from the Naval Research Laboratory and Duke University Marine Laboratory studied the barnacle *Balanus amphitrite* to learn how it secretes and cures its insoluble adhesive glue. We developed new in situ methods to examine the live barnacle/substrate interface, glue releasing structures, and adhesive curing chemistry. We used the first application of computer-aided X-ray tomography to image the shell structure in 3D where the glue is secreted; and used X-ray, UV, IR, and circular dichroism spectroscopy to elucidate the structure, hydration state, and curing mechanism of the adhesive protein. We discovered that curing proceeds, in part, by a coagulation process similar to blood clotting in mammals. In addition, we found that the adhesive consists of amyloid-like fibrils usually associated with disease in humans. Understanding how barnacles develop, apply, and cure the underwater adhesive protein will guide development of new coating formulations to prevent marine biofouling.

A CLINGY PROBLEM

For centuries, mariners and navies have battled biofoulants. These are the microorganisms, plants, algae, and animals that accumulate on ship hulls and other marine structures, sometimes attaching themselves tenaciously with insoluble proteinaceous glues. Biofouling of ship hulls increases drag, reducing the speed of sailing ships and increasing the fuel consumption of modern vessels (Fig. 1). Removing biofoulants is a huge maintenance expense, and new strategies are always being sought to deter or prevent attachment. In the present study, we used novel techniques to investigate barnacles and the adhesive they secrete, with a view to developing targeted, non-toxic solutions to preventing biofouling of U.S. Navy ships.

KEEPING THEM AT BAY

As early as about 400 B.C. there are reports of mariners applying oil laced with arsenic and sulfur onto wooden vessels to prevent biofouling, while the Greeks are reported to have used lead sheathing. Copper sheathing provided better antifouling properties;

the British Navy first explored this on the wooden frigate H.M.S. *Alarm* in 1758. In 1781, the U.S. Navy ship *Alliance* was coppered, as was the *Constitution* in 1785.¹ Serious problems due to the corrosive action of copper with iron prevented its direct application to ironclad hulls, and electrochemical protection of the copper with sacrificial metals like zinc eliminated its antifouling properties.



FIGURE 1
Fouling of ship hulls results in damage to surface treatments and increased drag. This ship is encrusted with bryozoans (pink patches), an invertebrate animal.

For over a century, the U.S. Navy has explored and used paints to protect ship hulls from fouling and corrosion. Modern examples include tributyltin and copper ablative paints, the latter widely implemented on naval vessels. Environmental and regulatory concerns about toxic leachates have accelerated Navy science and technology exploration of both non-leaching “antifouling” and non-toxic “foul release” strategies as future surface treatments for naval ships and underwater structures, to avoid releasing toxins into oceans and harbors. Strategies currently being researched include coatings with novel surface chemistries or textures, coatings with tethered biocides, and elastomeric release coatings. Each of these approaches provides a different surface functionality to challenge foulants like barnacles, tubeworms, and algae.

STUCK ON YOU!

Barnacles are among the more pervasive marine foulants, with over 1000 species known. Despite studies by preeminent biologists such as Charles Darwin — whose 19th-century taxonomy remains a standard work — much is still unknown about barnacle biology. These crustaceans typically attach to rocks in the water and in intertidal zones, but also to piers, buoys, and ships (Fig. 2). Barnacles settle as larval cyprids, and adhere by exuding a permanent, protein-based adhesive. Once settled, the cyprid metamorphoses into the sessile adult. Barnacles are gregarious foulants — chemical signals from curing adhesives are believed to

guide other cyprids to settle close to existing barnacles in order to promote reproduction.²

But how does the barnacle make its adhesive? How and where is it stored? If the barnacle is stuck on a rock substrate, how does it expand its space between base and side plates in order to grow? How does it release its glue to tack down the new growth? Understanding the biology and chemistry of barnacle adhesion is of great interest in the areas of marine biofouling prevention and materials science of adhesives: if we understand how the glue cures, we can more effectively develop strategies directly targeted at defeating these pervasive biofoulants.

The authors have developed a multidisciplinary approach to learn how barnacles secrete and cure their adhesive glue. Our team, with scientists from the Naval Research Laboratory and Duke University Marine Laboratory, includes specialists in biology, chemistry, and materials science. Studying *Balanus amphitrite*, or the little striped barnacle, we are developing new tools to examine the barnacle/substrate interface, glue releasing structures, and adhesive curing chemistry. Our experimental approach includes the first application of computer-aided X-ray tomography — CAT scans — to visualize the shell structure in 3D where the glue is secreted; and development of new biochemistry and surface chemistry approaches to elucidate the structure and hydration state of the adhesive protein, as well as its cross-linking, or curing, mechanism. Significantly, we discovered that the mechanism used by barnacles to cure their adhesive proceeds, in part, by a coagulation process similar to blood clotting in mammals.²



FIGURE 2

Barnacles are sessile crustaceans that are common in fouling communities (left). They adhere and grow on all kinds of organic and inorganic marine surfaces ranging from stationary rocks and piers to moving objects including lobsters, whales, and ships. The image in the center is a photograph of a hard-shelled barnacle (about 1 cm in diameter) from the top, revealing the interlocking side plates and movable top plates. The top plates protect the barnacle from predators when it is not extending its feeding appendages and seal seawater inside during low tide conditions. On the right is an X-ray tomogram rendering of a barnacle shell (without the top plates) showing the side and base plate structures. The cutaway reveals hollow, fluid-filled openings in the shell carrying ions important for shell mineralization and proteins found in the adhesive.

LOOKING UNDER THE HOOD

Buried adhesive interfaces provide a challenge to the researcher — how can we access and evaluate the adhesive curing process occurring underwater, underneath the hard calcified shell of an organism settled on a rock or ship hull (Fig. 3)? We have tackled this problem by two approaches. First, we have grown barnacles on silicone foulant-release panels, enabling us to remove them at will and turn them over to examine the adhesive directly. We have also grown barnacles on, or transferred them to, laboratory substrates that allow various spectroscopies to access the adhesive interface.

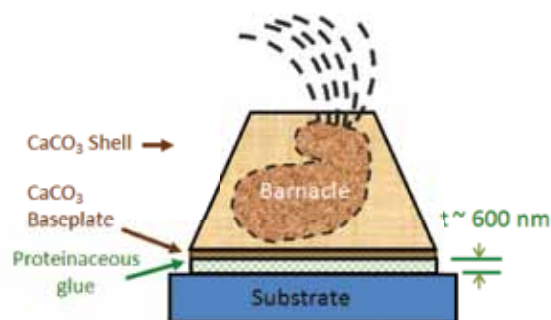


FIGURE 3

Cross-section diagram of a barnacle. The barnacle cures its glue not only underwater but underneath a protective shell. The animal is attached to the shell and feeds by sweeping the water with fringed structures called cirri — essentially it is stuck down on its head and eats with its feet.

We have employed a wide range of spectroscopies (on different substrates) at wavelengths spanning X-ray (polystyrene and polymethylmethacrylate [PMMA]), UV (CaF_2), visible (glass, CaF_2 , and polystyrene), and IR (germanium). The substrates supporting the barnacles are selected for transparency at the specified spectral wavelength. These methods have enabled us to evaluate the structure and chemistry of live barnacles (in vivo) by direct, in place (in situ) spectroscopy of the adhesive interfaces, and after removal from surfaces (ex situ) (Fig. 4). This provides a window into the live barnacle adhesive interface with a wide variety of materials science and chemistry tools. We have also found that it is possible to make three-dimensional microtomograms or “digital dissections” of living barnacles in air or submerged in water (Fig. 5). These tomography images are revealing much about the nature of the barnacle shell that was never before attainable (Fig. 6).

THE BARNACLE’S CURE-ALL

Barnacles adhere to surfaces by secreting and curing a liquid, protein-containing adhesive. The barnacle secretes its liquid glue from under the periphery of the

shell in growth cycles that result in rings of cured glue resembling the growth bands in a tree stump (see the photomicrograph in the upper center panel of Fig. 4). Liquid glue is released at the junction of the calcified base and lateral plates, and cures rapidly within minutes to hours, although the exact curing rate is not yet known. The lateral plates mate at the periphery and are interlocked to the base plate by mace-like structures (Fig. 6). The adhesive curing occurs under a protective calcium carbonate-rich shell that is simultaneously growing upward and outward to present a fresh surface for the liquid adhesive. The cured protein adhesive layer is less than a micron thick (typically ~ 600 nanometers [nm]), and the animal is further protected by calcifying a base plate shell on top of this adhesive (Fig. 3).

We have found that barnacle glue secretion and curing occur by a mechanism similar to that of blood clotting, suggesting that it is a specialized form of wound healing.² As the barnacle grows, it cracks open its shell at the periphery (see Fig. 6), allowing the adhesive to leak out and cure. At least two enzymes are involved in the adhesive curing process. These enzymes are molecules that activate protein chemistry, allowing proteins to unfold, rearrange, assemble, and lock in place after assembly. Like coagulated blood, cured barnacle glue is composed of nanofibrils intertwined in an insoluble mesh.³ Topographic imaging by atomic force microscopy (AFM) revealed that the fibrils are very thin (2 to 25 nm in diameter) and unbranched (Fig. 7). The fibrillar mesh differs from coagulated blood, however, in the way the protein folds; this folding is referred to as secondary structure. The proteins comprising the fibrils are linear chains of amino acids that can fold into coiled, globular, or hairpin structures. The sequence of amino acids results in specific, reproducible folding under normal biological conditions. Our IR, UV, and circular dichroism (CD) spectroscopy analyses indicate that the protein fibrils are most likely folding into repetitive, alternating hairpin folds that form ladder-like structures. These ladder-like folding motifs are known as amyloid structure and are most often associated with disease states, like Alzheimer’s, in humans. In individuals with diseases like Alzheimer’s, proteins do not fold into their normal functional conformation, but instead fold and aggregate into insoluble domains. Barnacle glue appears to be an example of a recently recognized class of proteins comprising naturally occurring amyloid with a functional purpose.³

COMING UNGLUED

Why is barnacle glue insoluble? Our results point to the barnacle using multiple, simultaneous methods to cure its glue into an insoluble adhesive. Folding the

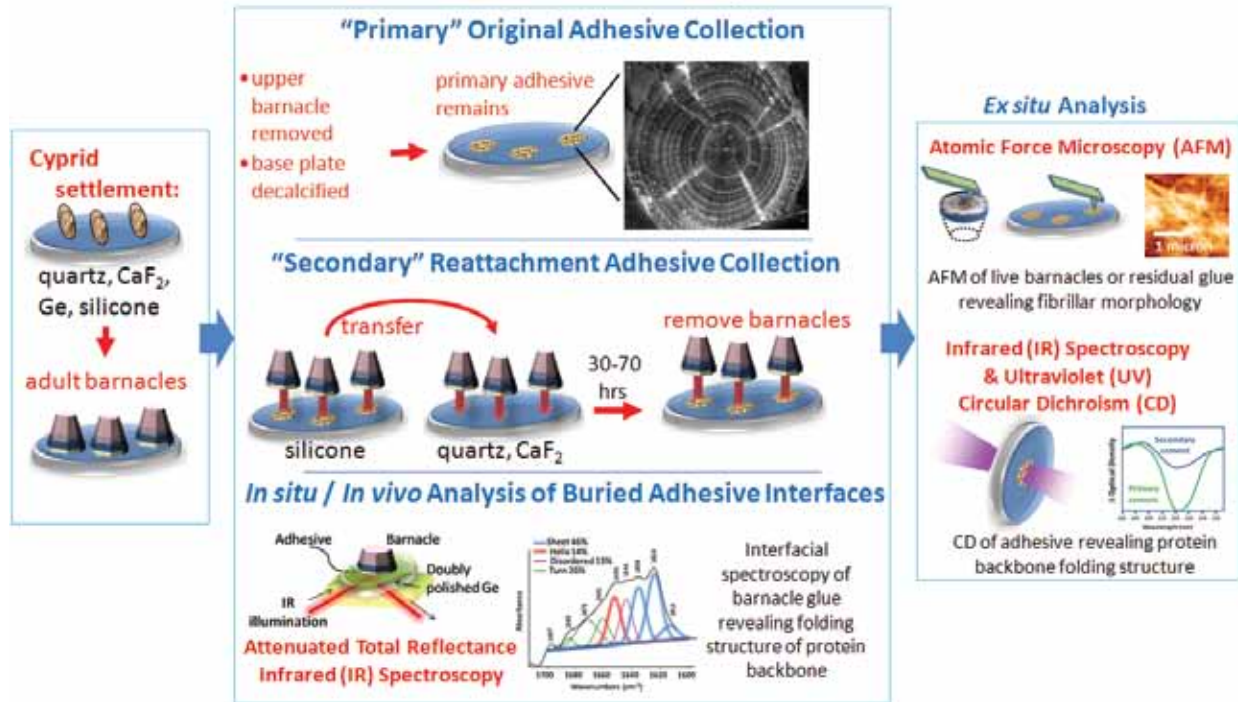


FIGURE 4 Barnacle glue analysis. To facilitate optical spectroscopies, we settle barnacle cyprid larvae on a variety of surfaces including quartz, calcium fluoride, germanium, and silicone rubber (left panel). The latter, silicone rubber, is a model fouling release surface that allows barnacles to be removed intact for examination. We are able to examine the original adhesive applied by the barnacle (upper center panel) after removing the animal and decalcifying the base plate; this glue is called “primary” adhesive. Some experiments require removal and reattachment of barnacles from silicone release coatings to other surfaces (middle center panel). This reattachment glue is called “secondary” adhesive. We have demonstrated that its morphology and chemistry are the same as the primary adhesive. Topographic analysis and transmission spectroscopies can be performed through the substrates or directly on the adhesive (right panel). Finally, spectroscopy of the buried interface of live barnacles (lower center panel) is performed using reflectance IR geometries. These spectroscopies have revealed the folding structure and hydration level (water content) of the protein adhesive.

protein chains into hairpin structures can strengthen the fibrils. Biochemical assays on liquid glue extracted from barnacles² point to permanent chemical bonds between protein chains that form in response to enzymes secreted by the barnacle similar to those in blood clotting, to enhance glue curing. The result is an insoluble mesh of tough fibers that resists our attempts to dissolve it, and resists the efforts to remove the protein during hull scraping.

We are just beginning to learn how barnacles cure their adhesive. Our studies of the adhesive from interfaces between live barnacles and model laboratory substrates (as shown in the lowest center panel in Fig. 4) have shown that the native, intact glue is not completely dry. In fact, barnacle glue has a hydration level that we estimate to be between 25% and 50% water by weight.⁴ To better address the adhesive curing process, rate, and chemistry, we are developing approaches to access the adhesive curing in real time, rather than after the fact.

CLOSING THE BARN(ACLE) DOOR

How do we stop any or all of the above? Evidence that the glue cures in ways similar to blood clotting provides us with a path forward in devising new means to design marine coatings to resist barnacle fouling. We can now explore development of coatings that contain chemistries that interfere with and counteract the biological processes of adhesive curing. How best to implement these approaches into functional surface treatments that resist these tenacious foulants is the subject of ongoing investigations. Looking at the barnacle from the inside out has provided powerful insight into the chemistry and biomechanics of hard foulants.

As we develop improved real-time and in situ techniques for probing the barnacle and its adhesive, we look forward to grasping more of this amazing creature’s secrets. Many of the procedures we are experimenting with and developing are applicable to other marine organisms. Ultimately, they may lead us

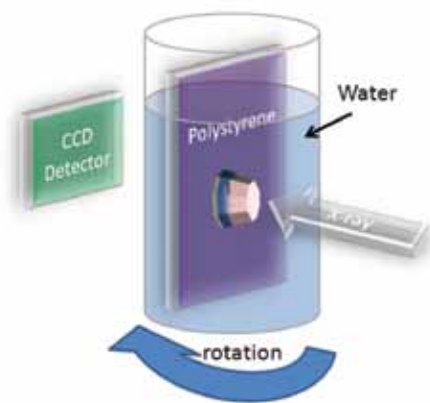


FIGURE 5
We imaged live barnacles using X-ray microtomography. Barnacles were settled on polystyrene or PMMA plastic (transparent to X-rays). Barnacles were imaged in air or submersed in seawater (above) during scans.

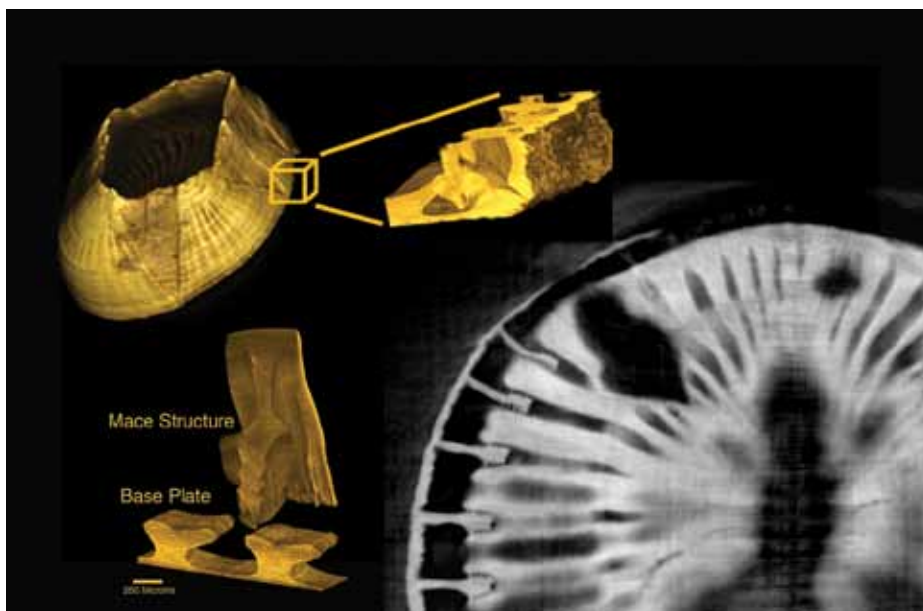


FIGURE 6
X-ray tomography showing 3D rendering of the barnacle shell (upper left) and (in the callout) a section from the growing edge where the side plates join the lower base plate. The grayscale image (lower right) shows a 2D tomograph section of the base plate viewed in plan view (from the bottom of the barnacle). Dark regions are hollow or low mass density regions, and bright regions are calcified shell. The image reveals the hollow structures in the side plates (rectangular holes at left edge), and mace-like structures found in the intersections of the side and base plates. These structures are interleaved with the base plate (lower left 3D rendering). The base plate shell is capable of growing conformally around defects in the substrate, adhesive, or adjoining animals. The dark, upside-down, spade-shaped region (in the lower right image) resulted from calcification above a thickened adhesive region under this particular barnacle.

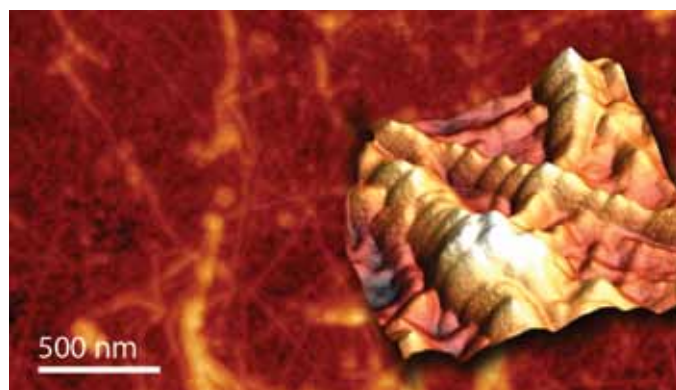


FIGURE 7
Atomic force microscopy (AFM) images of barnacle glue. Background image shows plan view image where bright and dark scale correspond to height (bright regions are higher) revealing the fibrillar morphology of the cured adhesive. The image on the right is a high-resolution AFM rendered image of the fibrillar topography (1 micron square), showing that the individual fibril crossing from left to right is segmented and is about 25 nm in diameter.

not only to the prevention of biofouling on Navy ships, but also to a broader understanding of marine biomineralization and to development of better underwater adhesives.

ACKNOWLEDGMENTS

This research was supported by the Office of Naval Research and the basic research program of the Naval Research Laboratory. We thank Mark Ingle (NAVSEA) for the image in Figure 1.

[Sponsored by ONR and NRL]

References

¹ Woods Hole Oceanographic Institute, *Marine Fouling and Its Prevention*, Chapter 11: The History of the Prevention of Fouling (Banta Publishing Co, Menasha, WI, 1952).

² G.H. Dickinson, I.E. Vega, K.J. Wahl, B. Orihuela, V. Beyley, E.N. Rodriguez, R.K. Everett, J. Bonaventura, and D. Rittschof, "Barnacle Cement: A Polymerization Model Based on Evolutionary Concepts," *Journal of Experimental Biology* **212**, 3499–3510 (2009).

³ D.E. Barlow, G.H. Dickinson, B. Orihuela, J.L. Kulp III, D. Rittschof, and K.J. Wahl, "Characterization of the Adhesive Plaque of the Barnacle *Balanus amphitrite*: Amyloid-Like Nanofibrils Are a Major Component," *Langmuir* **26**(9), 6549–6556 (2010). DOI: 10.1021/la9041309.

⁴ D.E. Barlow, G.H. Dickinson, B. Orihuela, D. Rittschof, and K.J. Wahl, "In situ ATR-FTIR Characterization of Primary Cement Interfaces of the Barnacle *Balanus amphitrite*," *Biofouling* **25**, 359–366 (2009).

“Let’s show ‘em what we’re made of”

might be an effective battle cry for human warfighters, but when considering the materials on which these warfighters rely, relating material composition to properties and performance has been an extremely difficult task. Knowing that relationship, however, is crucial for those using computational design to make better, more reliable materials for specific Naval applications. In the last few years, breakthroughs in 3D characterization, which uses information from experimentally measured images, and analysis of the reconstructed material microstructures have resulted from the availability of faster and more accurate measurement tools. Researchers in the Multifunctional Materials Branch of NRL’s Materials Science and Technology Division, using serial sectioning techniques that they devised, along with optical microscopy and electron backscatter diffraction (EBSD), collect and analyze 3D data from a variety of polycrystalline alloy microstructures to relate structure to properties and attempt to correlate such phenomena as material failure, corrosion behavior, mechanical response, and phase transformations to microstructure. Recent data sampling of a large reconstructed volume from a titanium alloy revealed a correlation between crystallography, applied load, and mechanical response. These data are applied to predictive models and simulations that in turn drive the development of materials that will function as designed under real-world conditions.

Structure–Property Relationships in a 3D Polycrystalline Microstructure

A.C. Lewis, D.J. Rowenhorst, G. Spanos, and A.B. Geltmacher
Materials Science and Technology Division

S.M. Qidwai
Science Applications International Corporation

This article provides a brief review of the three-dimensional materials characterization, analysis, and simulation tools developed in the Multifunctional Materials Branch of the Naval Research Laboratory. This innovative research combines serial sectioning, electron backscatter diffraction (EBSD), and finite element modeling to examine the role of microstructure on material behavior. An emphasis of this research is the determination of structure–property correlations in polycrystalline microstructures, as well as the identification of critical microstructural features for failure in polycrystalline microstructures. Recently, using data sampling from a large reconstructed volume of a titanium alloy, a correlation between crystallography and mechanical response was observed. This type of data is used as input for the efficient computational design of Naval materials and structures.

INTRODUCTION

To design new Naval materials that meet specific performance criteria, an in-depth understanding of the relationships between processing, microstructure, properties, and performance is required. It is now well known that the three-dimensional (3D) microstructure of materials dictates their mechanical performance and physical properties, and to develop accurate predictive models of processing and performance of advanced Naval materials, it is critical to understand the morphology and evolution of real 3D microstructures.

In recent years, 3D characterization and analysis of material microstructures have advanced rapidly, as the speed and accuracy of computational and measurement tools have increased. Three-dimensional microstructures, reconstructed from experimentally measured images, can now be used as input for simulations of mechanical response, corrosion behavior, and phase transformations.

Techniques developed in the Multifunctional Materials Branch at NRL have been applied to a variety of polycrystalline alloy microstructures for the collection and analysis of 3D data, and the application of this data to predictive models and simulations to develop an understanding of microstructure–property relationships. The overall goal of this research is to provide a framework for efficient and accurate design of materials by developing the tools for the prediction of material response under service conditions. Recently, to develop a general framework for understanding the relationships

between material microstructure and response, a beta titanium alloy has been investigated at the micro-scale to study structure–property correlations and determine critical microstructural features that cause initiation of failure.

THREE-DIMENSIONAL MICROSTRUCTURE RECONSTRUCTION

The three-dimensional microstructure of the beta titanium alloy (Timet 21s) was reconstructed using serial sectioning with optical microscopy and electron backscatter diffraction (EBSD). The microstructure of beta titanium is prototypical of many metallic systems, including stainless steels and high-performance aluminum alloys, thus investigation of this microstructure provides important insights into the behavior of many alloy systems of interest to the Navy. In the serial sectioning process, a fixed amount of material is removed from the sample surface through automated polishing. The sample is then etched to reveal contrast between the microstructural features, and finally images are collected using light optical microscopy. The serial sectioning process is repeated multiple times with a practical limit of a few hundred sections. The process results in a “stack” of images, which can be reconstructed to create the 3D microstructure.

Figure 1 illustrates the serial sectioning laboratory at NRL, where the data were collected. For this study, sectioning was performed on a semiautomatic polisher, which was calibrated to remove 1.5 μm of material

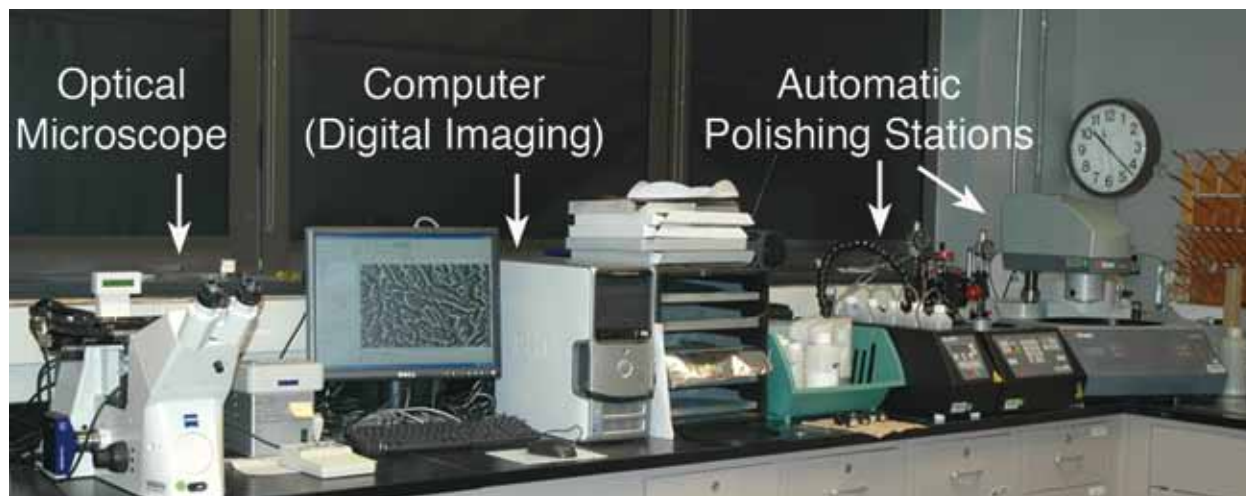


FIGURE 1
Serial Sectioning Laboratory setup at NRL.

per section. After final polishing and etching, a series of tiled light optical micrographs was taken for each section at 500 \times magnification (see Fig. 2). These image tiles are stitched together to form a single image of that section, representing a large field of view (approximately 1 mm by 0.5 mm), while simultaneously maintaining a high image resolution (<0.6 μm per pixel). Over 200 such image montages were collected and aligned using fiducial marks placed at the edges of the region of interest, resulting in a dataset measuring approximately 1 mm by 0.5 mm by 0.3 mm.

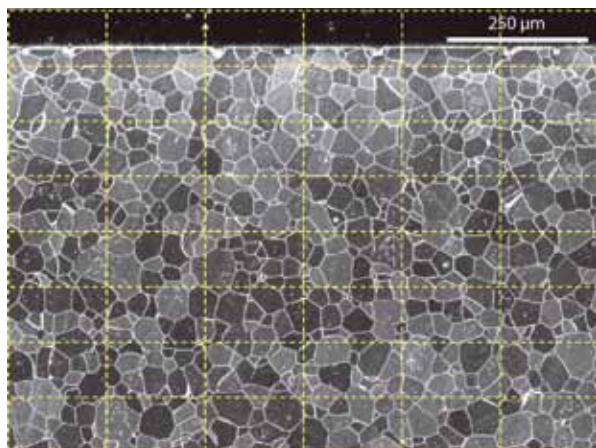


FIGURE 2
Micrograph showing beta titanium grains, from one of the 200 sections that make up the 3D dataset. The yellow lines approximate the size of the individual image tiles that were stitched together to form this image.

After every tenth optical micrograph was collected, EBSD was used to measure the crystallographic orientation of each grain. This technique allows the user to scan an electron beam over a polished surface and measure the crystallographic orientation at each point. This results in a “map” of the crystallography of the

specimen. The alignment of these EBSD images to the optical micrographs (and, thus, to the final 3D reconstruction) was accomplished by a semi-automatic alignment routine that matched the position of the center of area of a grain in the optical micrographs of a section with the equivalent center of area of the same grain in the EBSD map for that section. After the two images (EBSD map and optical micrograph) were aligned, the measured crystallographic orientations were then corrected for the EBSD image rotation, and an average crystallographic orientation was assigned to each grain in the 3D reconstruction.

The reconstructed 3D dataset for the beta titanium alloy is shown in Fig. 3. The dataset consists of over 4300 individual grains, and for each grain, the true 3D size, shape, and crystallography have been measured. From this data, a number of microstructural param-

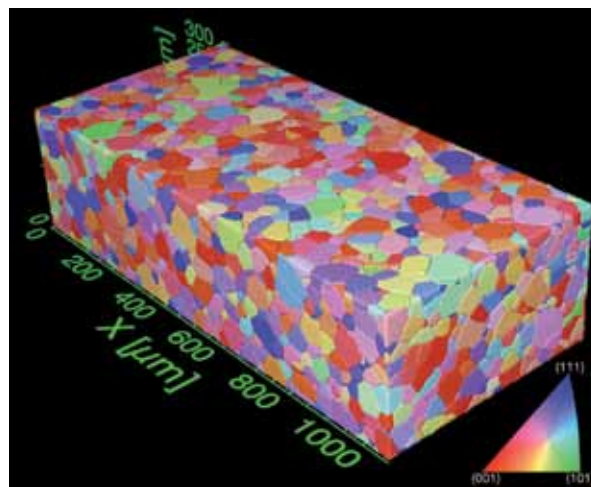


FIGURE 3
3D reconstruction of the beta titanium microstructure. Each grain is colored according to the crystallographic direction parallel to the z-axis (legend at lower right).

eters can be measured or derived, including the true 3D grain size distribution, number of grain neighbors or grain faces, grain boundary curvatures, crystallographic texture, and crystallographic interface normal distributions.¹

3D IMAGE-BASED FINITE ELEMENT ANALYSIS

In addition to the microstructural and crystallographic information that can be obtained from the 3D dataset, the reconstructed volume can be used as input into simulations of phase transformations, grain growth, or local mechanical response. One of the challenges in producing predictive simulations of materials performance is that typically very little is known about the initial conditions of the microstructure. Many researchers use algorithms to create a virtual microstructure that appears similar to real microstructures, but often these virtual microstructures lack important microstructural details that significantly affect the results of the models. By using the actual 3D representation of the microstructure as our initial condition for simulations, however, we have a perfect representation of the initial state of the microstructure with no additional assumptions or approximations.

The 3D reconstructed microstructures just described have been used as input for image-based finite element modeling (FEM) of mechanical response. Although computation power currently limits FEM simulations based on crystal plasticity to smaller datasets (consisting of up to about a few hundred grains), the results from these simulations are very powerful in that they can be used to determine critical microstructural features where local plasticity failure is likely to initiate.

For ease of computation and analysis, a subvolume containing approximately 100 grains was selected from the larger dataset, and is shown in Fig. 4(a). For this specimen, data were sampled from the original high-resolution dataset so that every third voxel (i.e., volumetric pixel) in the x - and y -directions and every second voxel in the z -direction were represented, to create a volume measuring 136 by 128 by 137 μm , represented by approximately 200,000 voxels. As shown in Fig. 4(b), an FEM mesh was generated that consisted of eight-noded brick elements, with each element corresponding to one voxel in the sampled microstructure. The finite element simulations were performed using ABAQUS[™] finite element software with customized anisotropic linear elasticity and crystal plasticity constitutive relationships for the body centered cubic (bcc) beta titanium.

Figure 4(c) is a contour plot of the response of the beta titanium microstructure subvolume. This plot shows the cumulative shear strain as a result of 0.7% applied uniaxial strain in the x -direction, which allows for qualitative visualization of the areas in the

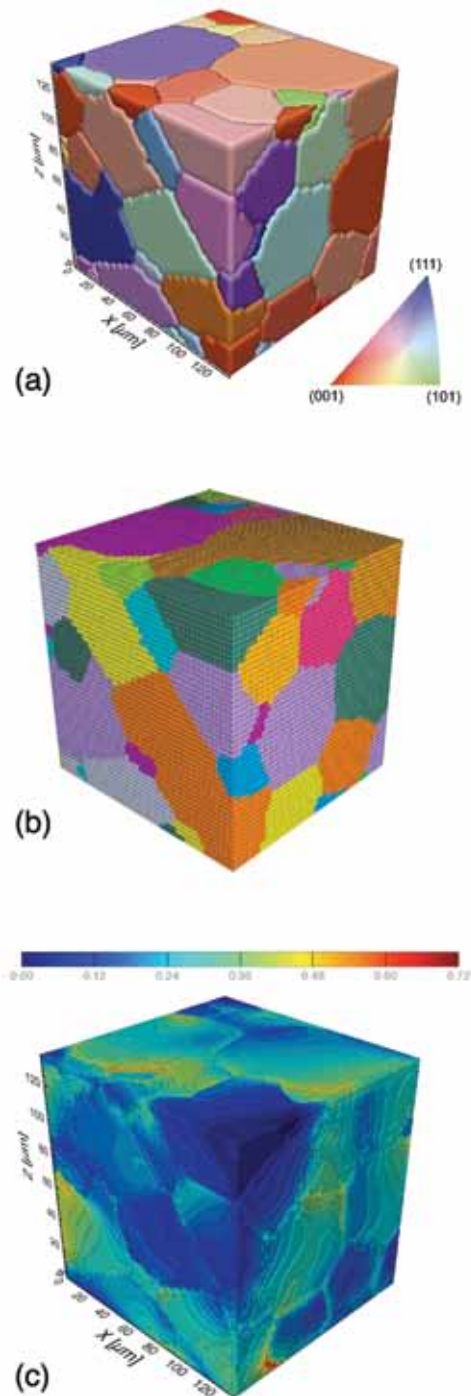


FIGURE 4

(a) Reconstruction of a subset of the titanium microstructure. (b) Finite element mesh of the reconstructed subset. (c) Contour plot of cumulative shear strain in the titanium subset, as a result of a uniaxial tensile load applied in the global x -direction. Figure adapted from Ref. 3.

microstructure with high local stresses. Plotting the data in this fashion, and relating mechanical response to microstructural features (by mapping back to the 3D reconstruction) allows for identification of features

where failure initiates, and can be used to aid in materials design. One example of such a critical microstructural feature identified by this technique is the initiation of plastic flow at grain boundaries between grains with a high degree of misorientation.²

DATA SAMPLING FOR LARGE-SCALE ANALYSIS

Because of the large amounts of memory and computation time required for the simulation of mechanical response of a volume as large as that shown in Fig. 3, it is prudent to sample multiple smaller subvolumes from the larger volume and analyze the responses of these subvolumes in combination to elucidate specific correlations. To investigate the relationship between grain orientation and mechanical response, five subvolumes, each containing approximately 100 grains, were selected from the larger volume. Figure 5 shows the location of these subvolumes within the reconstructed microstructure. The mechanical response of each subvolume was simulated separately, applying the same loading conditions.

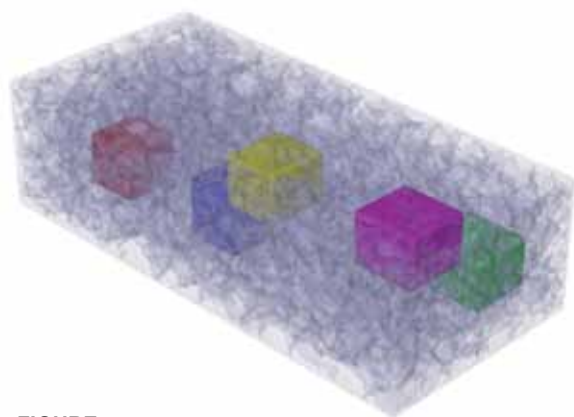


FIGURE 5
3D reconstruction of polycrystalline beta titanium microstructure, showing the location of five randomly selected subvolumes.

To visualize the complex 3D interactions within the microstructure, the scalar mean effective stress for each individual grain was calculated and plotted vs the crystallographic orientation of the grain in each of the five subvolumes. Figure 6 shows one such plot, for the case of uniaxial tensile strain applied in the x -direction. In this figure, the location of each data point on the unit triangle corresponds to the crystallographic direction in that grain that is aligned with the loading axis. (For example, data for a grain with its $\langle 001 \rangle$ axis aligned with the global x -direction would be plotted in the lower left corner of the unit triangle.) The value of effective stress is indicated by the color of each data point, according to the scale bar in the figure, with the lower stresses shown in blue and the higher stresses

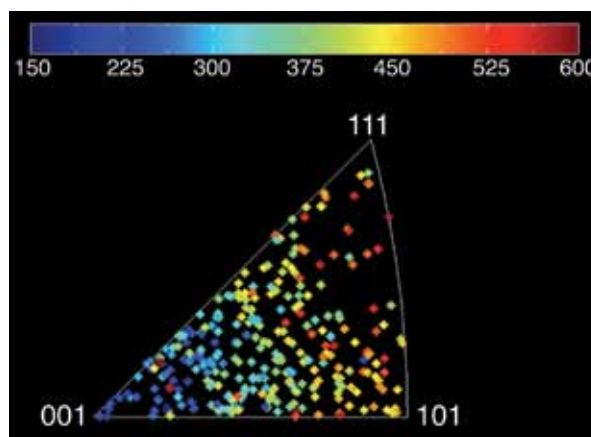


FIGURE 6
Mean effective stress (MPa) vs crystallographic axis aligned with the loading direction for the five subvolumes under uniaxial tension in the global x -direction.

in red. A correlation between crystallography and mechanical response can be seen from this plot; grains with a $\langle 001 \rangle$ direction aligned with the loading axis have a lower effective stress in response to the applied load, whereas grains with $\langle 101 \rangle$ and $\langle 111 \rangle$ directions aligned with the loading axis have a higher effective stress.

By sampling the data in this manner, it was possible to increase the number of data points without increasing the size of the model beyond the computational limits for the simulation. This method allows for calculation of properties for a statistically significant number of grains, while keeping data sets and file sizes manageable. This type of data can be used to build reliable statistical structure–property correlations that can guide design of materials intended for specific Naval applications.

SUMMARY AND CONCLUSIONS

Three-dimensional materials characterization, analysis, and simulation tools developed in the Multifunctional Materials Branch have been applied to examine the role of microstructure on material behavior. These tools are used to determine structure–property correlations in Naval materials, and to facilitate efficient computational materials design. In this study, this is demonstrated for a titanium alloy, where data sampling from a large reconstructed volume was used to reveal a correlation between crystallography, applied load, and mechanical response.

ACKNOWLEDGMENTS

This work was jointly sponsored by the Office of Naval Research and the Defense Advanced Research Projects Agency (DARPA) as part of the Dynamic 3-D

Digital Structure Program. Finite element simulations were performed through the DoD High Performance Computing Modernization Program.

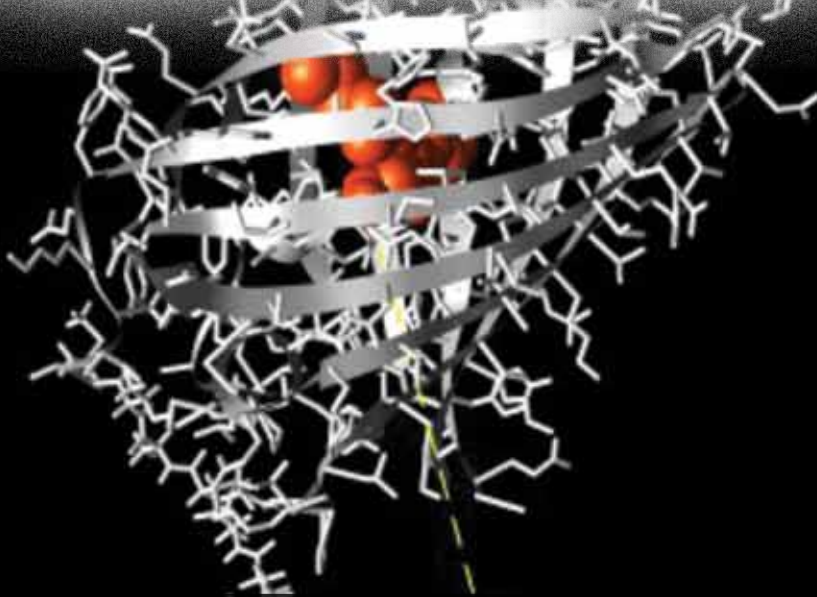
[Sponsored by ONR and DARPA]

References

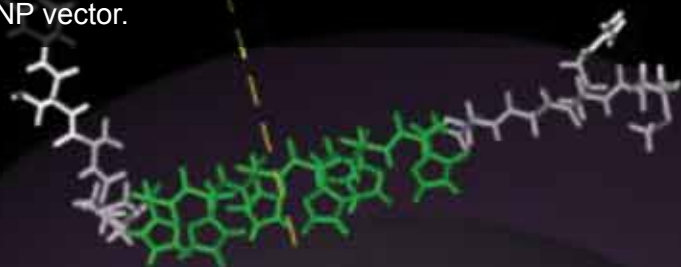
- ¹ D.J. Rowenhorst and G. Spanos, "Crystallographic and Morphological Analysis by Combining EBSD and Serial Sectioning," *Microscopy and Microanalysis* **13**, 1 (2007).
- ² M.A.S Qidwai, A.C. Lewis, and A.B. Geltmacher, "Using Image-based Computational Modeling to Study Microstructure–Yield Correlations in Metals," *Acta Materialia* **57**, 4233 (2009).

- ³ G. Spanos, D.J. Rowenhorst, A.C. Lewis, and A.B. Geltmacher, "Combining Serial Sectioning, EBSD Analysis, and Image-Based Finite Element Modeling," *MRS Bulletin* **33**, 597–602 (June 2008).

It's Alive!...Sort of



What do you get when you combine the organic and the inorganic? Not Frankenstein's monster, the Six Million Dollar Man, or Robocop, but rather the most amazing new materials, if you think small (very, very small). The novel classes of nanomaterials that a team of NRL biomolecular and optical sciences researchers are creating and investigating are composed of biomolecules, such as proteins, peptides, and nucleic acids, integrated with inanimate nanoparticles (NPs) derived from metals, metal oxides, noble metals, and semiconductors. Due to their size, NPs exhibit unique quantum-confined photophysical, electronic, and chemical qualities not present in the parent bulk materials. These hybrid biological-NP functional composites have the best of both worlds, exhibiting properties and performing activities that neither component alone has or could achieve, and therefore show untold potential to both biotechnology and national defense. NRL scientists, in response to the President's National Nanotechnology Initiative, are developing the chemistry by which the biomolecules are assembled on the NPs and thus control their properties. In the work described in this article, a fluorescent protein, mCherry, was assembled on a central luminescent semiconductor nanocrystal or quantum dot (QD) to produce an optically active biosensor that can measure enzyme activity by exploiting resonance energy transfer within the bio-NP composite. Once perfected, these types of composite nanomaterials should prove useful in defense applications including the detection and remediation of explosives and chem/bio threats, improved battlefield diagnostics and therapeutics, and lightweight electronic and energy harvesting materials. Biotechnological applications include targeted drug delivery, improved pharmaceuticals, targeted diagnostics, improved imaging, sensing of molecular-scale events inside cells, or even the combination of multiple applications on a single NP vector.



Monitoring Enzyme Activity with Hybrid Semiconductor Quantum Dot–Fluorescent Protein Assemblies

K. Boeneman, J.R. Deschamps, and I.L. Medintz
Center for Bio/Molecular Science and Engineering

M.H. Stewart
Optical Sciences Division

Creating new functional nanomaterials by integrating biomolecules such as proteins with inorganic nanoparticles has been tasked to the Department of Defense as a critical long-term priority under the National Nanotechnology Initiative. NRL continues to be a leader in this field by developing chemistries that allow biomolecules to be assembled on nanoparticles with control over their properties. These abilities are highlighted by the approach described here to assemble a fluorescent protein–semiconductor quantum dot (QD) optical sensor that can measure enzymatic activity by exploiting resonance energy transfer within the complex. The fluorescent protein, mCherry, was grown in bacteria and engineered to express both a polyhistidine tag that facilitates high-affinity QD coordination and a sequence that can be cleaved by the protease, caspase 3. The latter is an enzyme involved in programmed cell death, which can be triggered by exposure to biothreat agents. Protein self-assembly onto the QDs completes the active sensor, which is capable of detecting caspase 3 activity with significantly better sensitivity than other available assays.

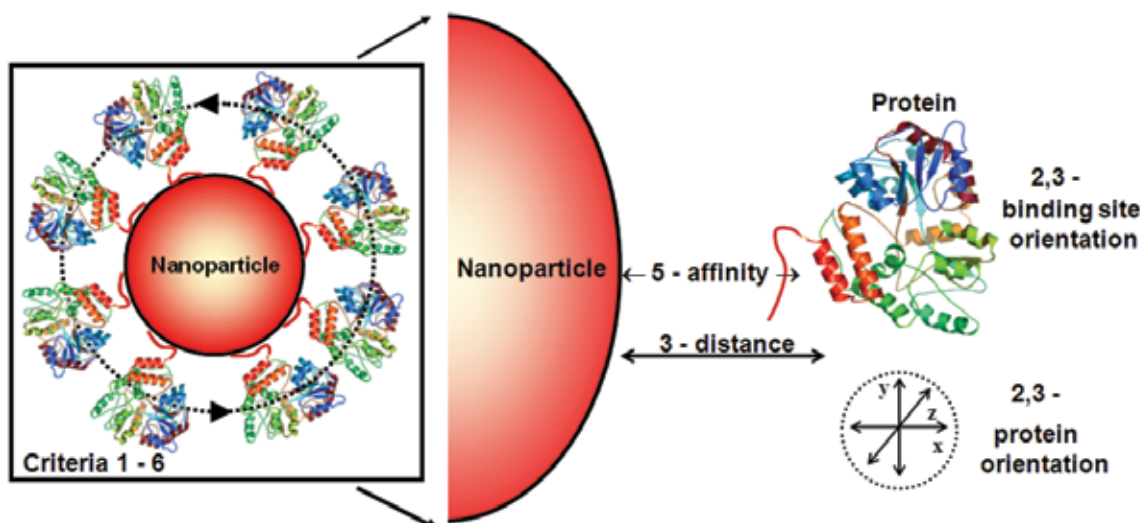
INTRODUCTION

Nanotechnology offers the potential for developing new classes of materials that can significantly impact biotechnology and national defense. Nanoparticles (NPs) derived from metals, metal oxides, noble metals, and semiconductors display unique photophysical, electronic, and chemical properties that are not present in the parent bulk material. Biologicals, including proteins, peptides, nucleic acids, and the like are capable of synthesis, catalysis, scaffolding, self-assembly, biorecognition, and energy harvesting. Integrating both into hybrid biological–NP functional composites will provide new classes of materials capable of far more than each component alone. For biotechnology, combining NPs with biologicals provides opportunities for targeted drug delivery, improved pharmaceuticals, targeted diagnostics, improved imaging, sensing of molecular-scale events inside cells, or even the combination of multiple applications on a single NP vector. Defense applications include active sensors for the detection and remediation of explosives and chem/bio threats and improved battlefield diagnostics and therapeutics along with lightweight electronic and energy harvesting materials. Department of Defense (DoD) research objectives outlined in the President's National Nanoscience Initiative include exploiting interactions between NPs and naturally occurring biomolecules for next-generation defense-related applications along with

developing methods for the inexpensive and controlled assembly of such composites.¹ Here we describe the recent development of a novel, optically active biosensor capable of monitoring enzymatic activity, that consists of a central semiconductor nanocrystal serving as a scaffold for the controlled assembly of a fluorescent protein.

INTERFACING BIOLOGICALS WITH NANOMATERIALS

NPs are similar in size as midsize to large proteins and can therefore serve as stable scaffolds for the central attachment and display of multiple copies of the same or even different biomolecules. It is helpful to envision the ultimate criteria desired from chemistries used in forming these types of composite materials as they directly impact subsequent activity (see Fig. 1). Ideally, the chemistry would attach a biomolecule to a NP (1) in a homogenous manner, (2) with control over its orientation, (3) with control over its distance from the NP, and (4) with control over the number of biomolecules per NP. The goal is to uniformly display the biomolecules on the NP surface with their active regions all clearly available for subsequent interactions. (5) Controlling the affinity for the NP surface is becoming increasingly important as it can also allow attachment and release of biologicals from the NP in response to external stimuli. It would be ex-

**FIGURE 1**

Schematic of a nanoparticle–protein bioconjugate and the criteria desired for optimized bioconjugation. Figure adapted from Ref. 2.

tremely beneficial if these chemistries would be generally applicable to (6) allow any biomolecules to be attached to any NP while still maintaining the above-described attributes.² There are relatively few available bioconjugation methods that satisfy even some of these criteria, and research at NRL is focused on addressing this specific need.

MATERIALS AND TECHNIQUES

Quantum Dots

Nanocrystalline semiconductor quantum dots (QDs) have remarkable photoluminescent (PL) properties that make them especially attractive for use in biological sensing and imaging applications.³ These include excellent photo- and chemical stability, high quantum yields, and large absorption cross-sections, which are coupled to size-tunable narrow emission spectra spanning from the UV to near-IR depending upon the constituent semiconductor materials used. The latter properties are especially useful in biology as they allow multiple differentially emissive QD populations to be effectively excited using a single wavelength, far removed from their respective emissions. This enables simultaneous monitoring of different QD emissions and allows tracking and potential correlation of complex spatiotemporal cellular events. High-quality CdSe/ZnS core/shell QDs emitting in the visible range are reproducibly prepared via thermal decomposition of organometallic precursors in organic solvents. Post-synthetic chemical modification of the nanocrystal surface is required to render the QD suspensions stable in aqueous media for biological applications and is usually accomplished by one of two principal routes:

(1) ligand-exchange with multifunctional hydrophilic surface capping ligands, or (2) use of amphiphilic polymers that interdigitate with the native organic surface.³ The Optical Sciences Division at NRL has long been a leader in developing ligands based on the first route for providing biologically compatible QDs. They have pioneered the combination of appending multidentate thiols, which provide high-affinity QD surface interactions, with either small charged groups such as in the dihydrolipoic acid (DHLA) utilized here or short polyethylene glycol (PEG) segments, both of which mediate solubility and provide compact, pH-stable QDs.⁴

Fluorescent Proteins and Self-Assembly to Quantum Dots

Numerous organisms express naturally fluorescent proteins. The first to be extensively characterized was green fluorescent protein (GFP) isolated from the luminescent jellyfish *Aequorea victoria*. Mutational engineering of this, and similar proteins, has resulted in variants with numerous fluorescent emissions and enhanced stability, which have established them as powerful tools in bioimaging and sensing applications. Here we create a self-assembled QD hybrid with a fluorescent protein termed mCherry that originated in Roger Tsien's laboratory (2008 Nobel Prize laureate in medicine for work on GFP). mCherry was first cloned from coral as a tetramer and then extensively engineered into the current, stabilized monomeric version. To conjugate proteins to QDs, we exploit metal-affinity coordination between polyhistidine residues and the ZnS shell of the QD.⁵ This requires that the proteins be recombinantly engineered to express a polyhistidine sequence at one of their termini. The same sequence allows the proteins

to also be easily purified using commercial Ni-chelate media. We have extensively characterized self-assembly between QDs and both polyhistidine-appended proteins and peptides and have found the interaction to be rapid and stable (equilibrium binding constant $K_d \sim 1 \times 10^9 \text{ M}^{-1}$) across a wide range of pHs.⁵ More importantly, the ratio of proteins assembled per QD is easily controlled through the molar amounts added together.

Förster Resonance Energy Transfer (FRET)

FRET is a process in which an excited state donor fluorophore transfers energy nonradiatively to an acceptor fluorophore. FRET requires that the donor emission wavelengths overlap with the acceptor absorption spectrum; that is, that they share spectral overlap, and the two molecules must be relatively close to each other, usually within 100 Å. FRET is characterized by a detectable loss in donor fluorescence intensity, which is sometimes coupled to an increase in the acceptor's emission intensity. Measuring these changes provides the FRET efficiency and allows estimation of the nanoscale distance separating the two fluorophores; this is why FRET is sometimes referred to as a molecular-scale spectroscopic ruler. QDs make superior FRET donors as their unique photophysical properties provide numerous advantages that are cumulatively unavailable to organic dyes functioning in the same role. When a QD donor interacts with dye acceptor(s), FRET efficiency, E , is calculated using the relationship

$$E = nR_0^6 / (nR_0^6 + r^6), \quad (1)$$

where R_0 is the donor-acceptor separation distance corresponding to 50% energy transfer, r is the actual donor-acceptor separation distance, and n is the number of acceptors centrosymmetrically arranged around a QD donor.⁶

Proteases

Proteases are enzymes that cleave specific peptidyl sequences and are involved in almost all cellular processes. Pathogens, such as the *Plasmodium* malaria parasite and *Yersenia pestis*, the cause of pneumonic plague, express specific proteases to aid in entry into host cells, to degrade host proteins for nutritional demands or to counter immune defenses, while *Clostridium botulinum* and influenza A use host proteases to activate essential virulence factors. More than 500 human proteases function as housekeeping proteins to degrade unneeded substrates during developmental processes or, in the specific case of caspase 3, to initiate apoptosis or programmed cell death, which sometimes occurs in response to pathogenic activity. When inhibited, the absence of protease activity can result in diseases and cancer.

SENSOR DESIGN, ENGINEERING, AND CASPASE 3 ASSAYS

Sensor structure and assay function are schematically depicted in Fig. 2. mCherry expressing a terminal His₆ sequence self-assembles to the surface of QDs, resulting in FRET quenching of the QD and sensitized emission from the mCherry-acceptor. A cleavage site engineered in the linker sequence separating the QD from the mCherry is recognized and cleaved by added caspase 3, which reduces FRET efficiency and provides signal transduction. Experimental work proceeded in three phases: (1) modeling and protein engineering, (2) characterization of QD-mCherry self-assembly, and (3) caspase 3 assays.⁷

Modeling and Protein Engineering

The mCherry gene is encoded in a commercial expression plasmid appended to a 35-residue linker that includes a His₆ tag and several other functional sequences. Prior to recombinant modification and protein expression, we modeled the putative QD-mCherry complex to ascertain if the assay as envisioned would function *in silico* (see Fig. 3). We apply this process to many of our QD-bioconjugate designs to optimize their function and it also represents one of the unique interdisciplinary capabilities available to NRL. The linker was first analyzed for native structure to evaluate caspase 3 accessibility when the His₆ sequence was assembled onto the QD. A comparison of more than 25 crystallographic protein sequences in the Protein Data Bank (PDB, www.rcsb.org) containing this N-terminal linker found no structure implying the sequence is present in a random-coil conformation. An area requiring the least modification in the linker was chosen for insertion of the caspase 3 cleavage site, which consists of the sequence DEVD. Constraints were applied to produce an extended linker conformation with the His₆ region in contact with the QD surface and the mCherry placed at the linker's other terminus. Placing the structure of caspase 3 near the DEVD portion of the linker and evaluating the possible binding interactions confirms that there is nothing intrinsically disfavored about the composite structure that should prevent caspase 3 binding or proteolysis. Site-directed mutagenesis was used to introduce DEVD (substrate 1) and an extended serine-glycine flanked SGDEVDSG sequence (substrate 2) into the linker. The proteins were expressed in bacteria and purified using standard techniques.

Characterization of Quantum Dot-mCherry Self-Assembly

Following protein expression, we verified that mCherry-His₆ does indeed efficiently self-assemble to

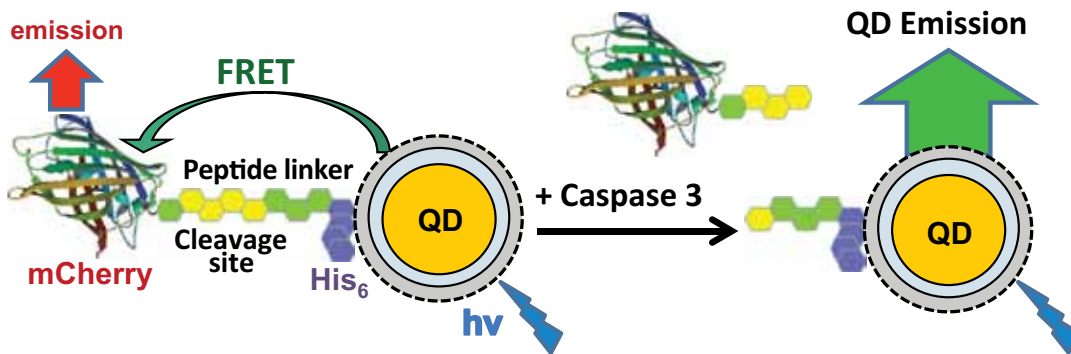


FIGURE 2
Schematic of the QD–mCherry FRET biosensor for monitoring caspase 3 activity. mCherry appended with an N-terminal linker expressing the caspase 3 DEVD cleavage site and a His₆ sequence self-assemble to the QDs, resulting in FRET quenching of the QD and sensitized emission from the mCherry-acceptor. Caspase 3 recognizes and cleaves the linker, reducing FRET efficiency and providing signal transduction. Figure adapted from Ref. 7.

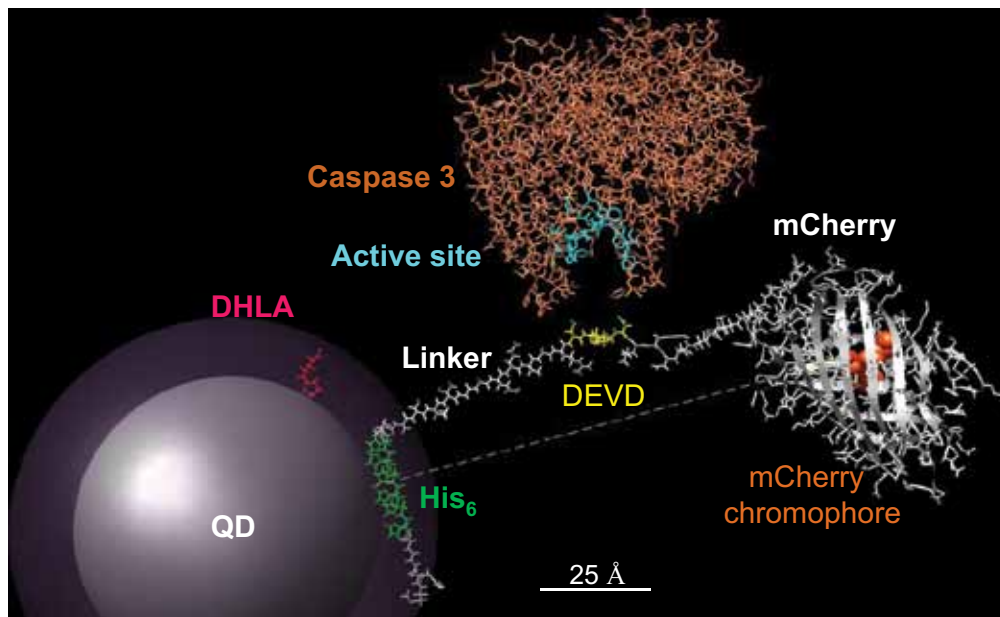
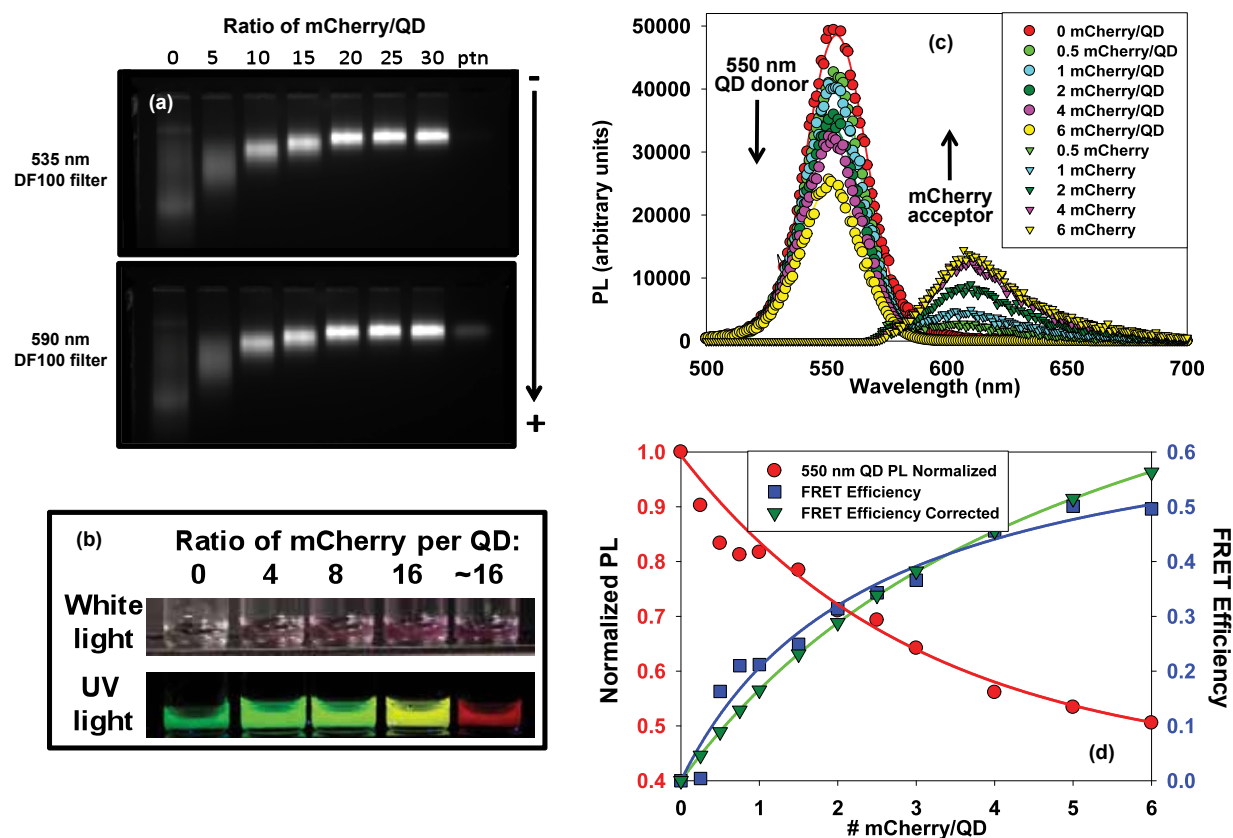


FIGURE 3
Model of mCherry self-assembled to a QD. The QD is simulated by a sphere of 29 Å radius, while the dihydroliopic acid (DHLA) surface functionalizing ligand is represented in an energy minimized conformation by an outer sphere extending a further 11 Å. Three-dimensional coordinates for mCherry (2H5Q) and caspase 3 (3EDQ) were obtained from the Protein Data Bank. mCherry with its chromophore highlighted is appended to the extended linker and coordinated to the QD via the His₆ sequence. The caspase 3 DEVD cleavage site is shown in yellow. Caspase 3 (pale orange) and specifically its active site (cyan) are afforded unhindered access to the cleavage site.

QDs and engage in FRET. Figure 4(a) shows results in which the indicated ratios of mCherry were assembled to 550-nm emitting QDs, chosen due to favorable spectral overlap, and then separated in an agarose gel. The conjugates were visualized with different filters to isolate the FRET-sensitized emission. A clear loss in QD mobility is noted as the assembled mCherry ratio per QD increases along with corresponding increases in mCherry sensitization, especially as compared to directly excited mCherry alone. These data serve to confirm both self-assembly and FRET interactions. Figure

4(b) presents images of QDs assembled with increasing mCherry under both white light and UV excitation. With the latter, QD PL loss along with FRET excitation of mCherry manifest as an increasingly yellow composite emission rather than just the original QD (green) or mCherry (red) fluorescence. Deconvoluted and background-subtracted spectra tracking progressive QD donor PL loss and corresponding mCherry acceptor sensitization are shown in Fig. 4(c) along with plots of the data as a function of mCherry valence in Fig. 4(d). These plots also serve as calibration curves for

**FIGURE 4**

(a) Agarose gels of QDs self-assembled with 5 to 30 equivalents of mCherry. Lane '0' contains unmodified QD, while 'ptn' contains 30 equivalents of mCherry alone. Images captured with 535 nm and 590 nm filters to highlight QD and mCherry emission, respectively. (b) Images of QD/mCherry self-assembly reactions under visible and UV illumination. (c) Deconvoluted spectra from 550 nm QDs self-assembled with an increasing mCherry substrate 1. Data are corrected for mCherry direct excitation. (d) Plots of normalized QD PL vs mCherry valence n (red), FRET efficiency (blue), efficiency corrected for heterogeneity using a Poisson distribution function (green) as obtained with Eq. (1). Figure adapted from Ref. 7.

the subsequent caspase 3 assays. Average QD–mCherry separation values of 5.6 nm were derived within the self-assembled complex using Eq. (1) for the unmodified parent mCherry and separation distance increased to 6.5 nm with extended substrate 2 protein.⁷

Caspase 3 Assays

Confident in mCherry's ability to self-assemble to QDs and engage in FRET, we evaluated their efficacy in targeted proteolytic assays. Figure 5 highlights representative plots of enzymatic velocity derived from monitoring changes in FRET when increasing concentrations of QD–mCherry conjugates were exposed to recombinant human caspase 3 enzyme. To extract kinetic data from the FRET changes observed during the assay, we use the previously determined ratios of mCherry to QD emissions as a calibration curve (above). Use of this ratiometric data is less sensitive to changes in reagent concentration and also allows us to transform proteolysis-induced FRET recovery data into quantitative values. Corresponding Michaelis constants

K_M and maximal velocity V_{max} were estimated using the Michaelis–Menten formula and were found to be comparable to other caspase 3 assay formats. Importantly, this reflects that there are no significant changes in enzyme activity when interacting with a nanocrystal–protein complex. However, the QD assay used 5 to 10 times less substrate and three orders of magnitude less enzyme than comparable formats and was capable of detecting enzyme levels down to the picomolar range.⁷

SUMMARY AND CONCLUSIONS

Here we describe the development of a biosensor that is a self-assembled hybrid of a naturally occurring protein with an inorganic semiconductor nanoparticle. This optically active biosensor provides specific and sensitive quantitative monitoring of enzymatic proteolysis. As demonstrated here, this approach has multiple advantages: a choice in pairing QD emission to a fluorescent protein acceptor, bacterial expression of the protease substrate in a fluorescent form, facile self-

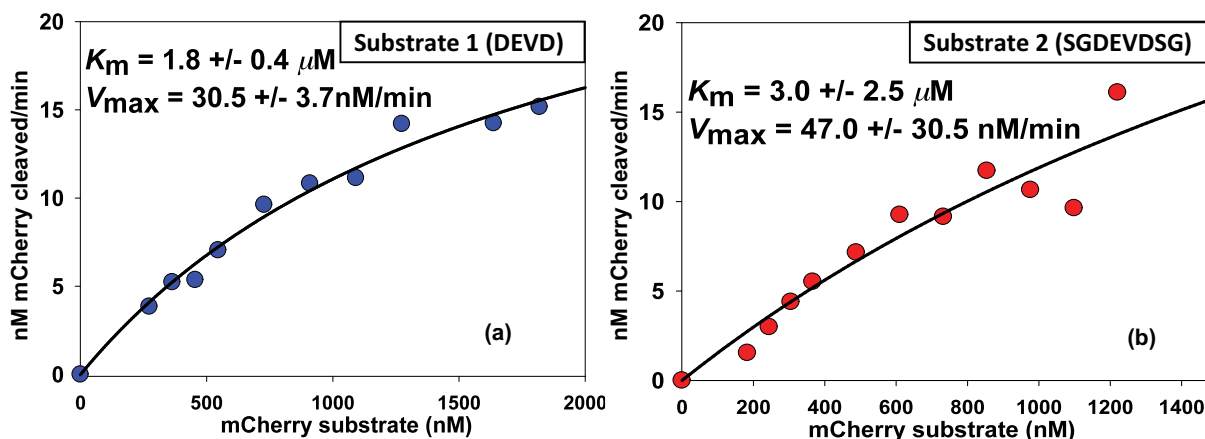


FIGURE 5

Caspase 3 assay results for QD–mCherry substrate 1 (a) and extended substrate 2 (b) along with corresponding kinetic values. Figure adapted from Ref. 7.

assembly to form the final active sensor, reduced use of enzyme/substrate, and the possibility of *in vivo* utilization. Additionally, the linker's cleavage sequence can easily be modified to be recognized by other proteases, thus allowing the sensor to monitor many different enzyme targets. Importantly, this hybrid sensor demonstrates that many of the DoD nanotechnology research goals are indeed feasible, and significant progress is being made toward them at NRL.

ACKNOWLEDGMENTS

The authors acknowledge ASEE and NRC fellowships, the Defense Threat Reduction Agency (DTRA), the Army Research Office (ARO), the Office of Naval Research (ONR), NRL, and the NRL Institute for Nanoscience for financial support. Molecular graphics images were produced using the UCSF Chimera package from the Resource for Biocomputing, Visualization, and Informatics at the University of California, San Francisco (supported by NIH P41RR-01081). This work was recently published in the *Journal of the American Chemical Society* (Ref. 7). Dr. K. Boeneman won a Young Investigator of the Year Award for her presentation of this work at the 2009 Biophotonics West, International Society for Optics and Photonics (SPIE) Annual Meeting held in San Jose, CA.

[Sponsored by DTRA and ARO]

References

¹National Science and Technology Council, Nanoscale Science, Engineering, and Technology Subcommittee (NSTC/NSET), *The National Nanotechnology Initiative: Research and Development Leading to a Revolution in Technology and Industry*, Supplement to the President's FY2008 Budget, Appendix A (http://www.nano.gov/NNI_08Budget.pdf), July 2007.

²I.L. Medintz, "Universal Tools for Biomolecular Attachment to Surfaces," *Nature Materials* **5**, 842 (2006).

³I.L. Medintz, H.T. Uyeda, E.R. Goldman, and H. Mattoussi, "Quantum Dot Bioconjugates for Imaging, Labeling, and Sensing," *Nature Materials* **4**, 435–446 (2005).

⁴K. Susumu, H.T. Uyeda, I.L. Medintz, T. Pons, J.B. Delehanty, and H. Mattoussi, "Enhancing the Stability and Biological Functionalities of Quantum Dots via Compact Multifunctional Ligands," *J. Am. Chem. Soc.* **129**, 13987–13996 (2007).

⁵K.E. Sapsford, T. Pons, I.L. Medintz, S. Higashiya, F.M. Brunel, P.E. Dawson, and H. Mattoussi, "Kinetics of Metal-Affinity Driven Self-Assembly Between Proteins or Peptides and CdSe-ZnS Quantum Dots," *J. Physical Chem. C* **111**, 11528–11538 (2007).

⁶A.R. Clapp, I.L. Medintz, J.M. Mauro, B. Fisher, M.G. Bawendi, and H. Mattoussi, "Fluorescence Resonance Energy Transfer between Quantum Dot Donors and Dye Labeled Protein Acceptors," *J. Am. Chem. Soc.* **126**, 301–310 (2004).

⁷K. Boeneman, B. Mei, A. Dennis, G. Bao, J.R. Deschamps, H. Mattoussi, and I.L. Medintz, "Sensing Caspase 3 Activity with Quantum Dot-Fluorescent Protein Assemblies," *J. Am. Chem. Soc.* **131**, 3828–3829 (2009).

Seismic Oceanography Allows a New View of the Ocean

In their efforts to better understand the oceans' small-scale processes and the mixing of coastal and deep ocean water, NRL scientists and their international colleagues are developing seismic oceanography (SO), a new technique for observing oceanic water masses. The technique was discovered serendipitously when researchers realized that seismic systems that were designed to image sub-seafloor geologic structures were also providing images of oceanic water layers.

SO, in using lower frequency sound waves than those used in acoustic oceanography, represents a new way of measuring the vertical temperature gradient throughout the water column, both vertically and laterally, and at orders of magnitude finer resolution than that offered by traditional methods. In their experiments in March 2009 in the Adriatic Sea, the researchers acquired data in the Adriatic littorals and combined seismic and oceanographic data, then used the relationship between oceanic temperature contrasts and acoustic reflectivity to generate a 5- to 10-m resolution temperature gradient. If optimal field parameters are developed, and signal processing techniques are refined, SO can be incorporated as a practical standard research or operational oceanographic tool.

Seismic Oceanography — A New View of the Ocean

W.T. Wood and D.A. Lindwall
Marine Geosciences Division

J.W. Book and J. Wesson
Oceanography Division

S. Carniel
C.N.R. – Institute of Marine Sciences, Venice, Italy

R.W. Hobbs
University of Durham, UK

NRL scientists are collaborating with international colleagues in developing a new way of observing water masses in the ocean: seismic oceanography. Using low-frequency seismic systems designed to image sub-seafloor geologic structures, thermohaline contrasts between water masses can be mapped, characterized, and quantified. Seismic oceanography uses the relationship between oceanic temperature contrasts and acoustic reflectivity to generate a quantitative measure of vertical temperature gradient throughout the water column at vertical and lateral resolution of 5 to 10 meters, several orders of magnitude finer than traditional methods. Such resolution opens up a new window on small-scale processes and mixing of the coastal and deep ocean. In 2009, we executed an ambitious field effort in the Adriatic Sea (ADRIASEISMIC-09) to acquire seismic data together with state-of-the-art oceanographic data as a way to compare the datasets and evaluate the limits and capabilities of seismic methods to characterize ocean processes. This was only the third such combined field effort ever performed, and the first in shallow water, thus adding to the useful development of this new approach. Incorporating seismic oceanography into standard oceanographic practice will require integrating field acquisition practices and developing new signal processing algorithms, with the potential benefit of gaining a new view of ocean structure.

A FAMILIAR TOOL FOR GEOPHYSICISTS USED IN A NEW WAY

Seismic oceanography (SO) is a new discipline born out of the accidental discovery that seismic systems designed to image sub-seafloor geologic structures, such as hydrocarbon traps, were also providing images of water layers in the ocean.^{1,2} The ocean is very “thin” (general aspect ratio is 1000 to 1), but subtle differences in density of this thin “sheet of water” caused by temperature and salinity variations drive much of its motion and variability. Thus, much of observational oceanography is focused on accurately measuring horizontal changes in density that both drive ocean flows and come about as consequences of ocean flow dynamics.

Seismic reflections from ocean layers are about 1000 times weaker than reflections from sediment interfaces, and for decades geophysicists had been looking right through them without ever noticing them. The reflections require careful processing of high-quality seismic data to see and interpret, but can

show subtle details in the water mass boundaries that occur on lateral scales of only a few meters (Fig. 1). Standard wire-line oceanography measurements, such as expendable bathythermograph (XBT) or conductivity-temperature-depth (CTD) casts, typically have measurement spacing of 1 to 10 kilometers; so the seismic oceanographic records with measurements every 5 to 10 meters, both horizontally and vertically, allow measurement of the ocean water masses at horizontal resolutions rarely seen. Because of the aspect ratio of the ocean, obtaining oceanographic measurements at similar resolutions both vertically and horizontally is very unusual, and so represents a new way of observing ocean phenomena.

WHAT CAUSES THE REFLECTIONS?

Seismic oceanography can be thought of as a type of acoustic oceanography (AO) but it differs in a very important way. The lower frequency sound waves used in SO, about 10 to 200 Hz, are coherently reflected (not refracted or incoherently scattered) directly by the

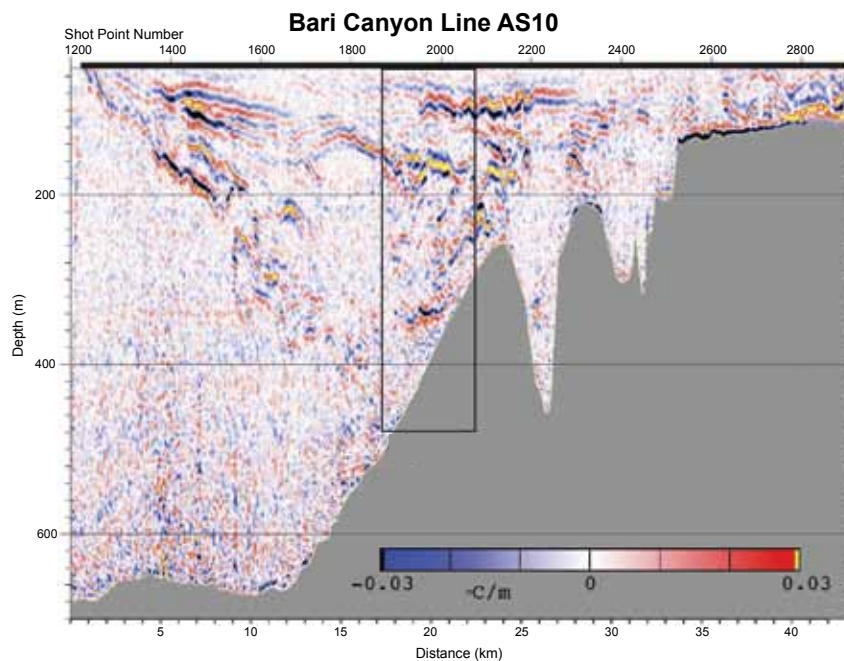


FIGURE 1
This calibrated seismic image is a cross section of the ocean in the Bari Canyon region of the Adriatic Sea, extending from deep water (left) up on to the continental shelf (right). The colors represent band-limited (smoothed) vertical temperature gradient (see Fig. 3). In this display, large, rapid temperature contrasts between water masses manifest as strong events. The boxed area was measured with a microstructure profiler (see Fig. 4) at a later time. Warmer colors indicate an upward warming (positive dT/dz), and cooler colors indicate an upward cooling (negative dT/dz).

thermohaline boundaries between water masses. These frequencies are affected by vertical changes on the scale of meters to tens of meters. Conversely, the sound waves commonly used in AO are at frequencies about 1000 times higher, 10 to 200 kHz, and are affected by features on the scale of microns to millimeters, such as suspended impurities or biota in the water column.³ Although the scatterers seen in AO records (e.g., from acoustic Doppler current profilers, ADCPs) may be associated with physical boundaries, the AO records do not contain the information to quantify the magnitude of physical property contrasts between water mass boundaries as do SO records.

The acquisition geometry for SO is shown in Fig. 2. A ship moving at 4 to 6 knots tows a controlled sound source and a linear array of tens to thousands of hy-

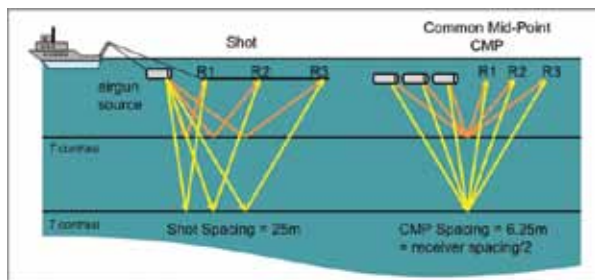


FIGURE 2
Seismic data are acquired while towing a source and a receiving array. Each channel in the array consists of 16 individual hydrophones whose signals are summed in real time to produce a single record of pressure vs time. Individual source-receiver records are rearranged post-acquisition into common midpoint (CMP) bins such that reflection points coincide. Time differences are removed (normal move-out correction) and CMP records are summed to enhance the signal-to-noise ratio.

drophones, both at a depth of a few meters. The sound source is typically an air gun, a device that explosively releases compressed air, creating a sound pulse in the ocean with a duration of 10 to 20 milliseconds. The sound pulse reflects off of near-horizontal interfaces such as sediment layers in the earth or vertical sound speed changes in the ocean, and is then recorded at the hydrophone array. Typically, the source is fired every 25 meters (about every 12 seconds). The hydrophone array contains 10 to 20 individual hydrophones that are summed to generate a single channel record, and may contain dozens to hundreds of channels, with each one providing an independent measurement of ocean reflectivity.

The reflectivity is controlled by the contrast in acoustic impedance — the product of sound speed and density. In most places in the ocean, the sound speed has a much greater effect on the acoustic impedance than does the density. Thus a seismic reflection image is effectively an image of the sound-speed contrasts as a function of depth in the water column.^{4,5} The reflections are strong or weak as the vertical temperature change is large and rapid or small and slow, respectively.

CONVERTING SEISMIC REFLECTIVITY TO TEMPERATURE CHANGE

Because acoustic impedance contrasts are dominated by temperature contrasts, there is a simple scaling factor that can be multiplied with the recorded reflectivity to yield a good approximation of the vertical temperature contrast. That is, the seismic image (a cross-section of impedance contrasts) is essentially

a scaled, band-limited measurement of the vertical change in temperature, and can yield a cross-sectional image of the vertical change in temperature (Fig. 1). However, the band-limited nature of seismic data means that there will always be sidelobes that prevent a simple, exact, one-to-one correspondence between vertical temperature change and seismic reflectivity.

Figure 3 shows graphically how the temperature and reflectivity are related. The black curve is the observed water temperature from an XBT cast, and the red curve is its vertical derivative, i.e., the temperature gradient with water depth (dT/dz). We have displayed

on the far right side of Fig. 3. The similarity of the blue and purple curves is what allows the seismic data to be used as a quantitative estimate of the thermal gradient (dT/dz , red curve). Matching the amplitudes of these curves provides the scaling factor that converts the observed seismic reflectivity into an estimate of vertical temperature gradient seen in Fig. 1.

Although the correlation between expected and observed reflectivity (blue and purple curves in Fig. 3) is very good down to 200 meters water depth, the correlation degrades below 200 m for this particular example. Note also in Fig. 3 the poor lateral continuity of reflec-

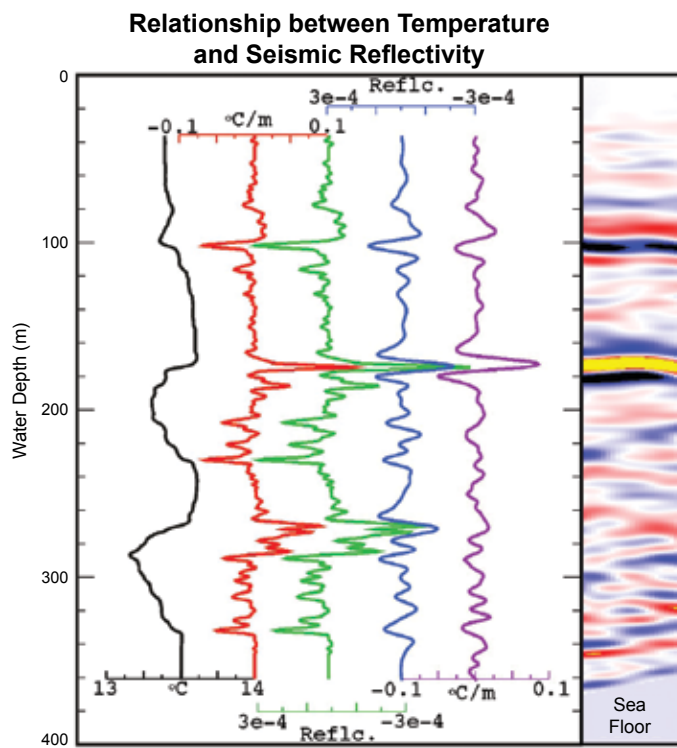


FIGURE 3

This display shows the steps relating the temperature profile with seismic reflectivity. (Black) Temperature measured from XBT 169 at shot point 2016 on line AS10 in the Bari Canyon, Adriatic Sea (see Fig. 1). (Red) Depth derivative of temperature from bottom, up. (Green) Impedance contrasts calculated from temperature and empirically derived salinity. (Blue) Impedance contrasts filtered to match the band of the seismic data. (Purple) Observed seismic data. (Far right) A series of seismic traces from the area in which the XBT was acquired. The large negative and positive events at 105 and 175 meters, respectively, correlate well to temperature contrasts in the XBT. Figure 1 shows these events to be laterally continuous. Conversely, the reflection events at about 320 meters depth are not as laterally continuous and do not correlate as well with predictions from the XBT.

the curves in this figure using the oceanographic convention of viewing dT/dz from the bottom up, opposite from the seismic reflectivity measurement made from the top down (source to target).

The salinity (not shown) is estimated from an empirical relationship derived from CTD profiles acquired in this same area within a day or two of the seismic records. Temperature and estimated salinity profiles are then used to calculate sound speed and density profiles, from which the acoustic impedance contrasts (green curve) can be calculated. The blue curve is the same estimated profile of impedance contrasts, but filtered to match the frequency band of the seismic data. The purple curve is a single column of data or trace of the observed seismic data (near shot point 2016 in Fig. 1). Finally, a group of several traces, displayed with color representing amplitude (i.e., a subset of Fig. 1) is shown

tions in the plot of the seismic data (also seen in Fig. 1, around shot point 2000) at these depths. The poor correlation near shot point 2000 may be due to a significant difference in the lateral sampling range of the XBT and the seismic wave. While the XBT samples water over a tiny range (less than 1 cm in diameter), the reflection of a broadband spherical seismic wave is affected by the portion of the reflector within the first Fresnel zone (70 to 200 meters at the frequencies used).

A REAL-WORLD APPLICATION

By early 2009, seismic reflections from water mass boundaries had been reported and several analyses had been done using combined seismic and XBT data.^{2,6,7} However, dedicated SO field programs with full seismic and oceanographic measurements had only been

performed in the Kuroshio Extension in the western Pacific^{8,9} and in the Mediterranean outflow area of the eastern Atlantic.¹⁰ In both cases, the water column objectives were in blue water, greater than 200 meters deep.

In March 2009, NRL and several international collaborators conducted the ADRIASEISMIC-09 exercise to collect both seismic data and high-resolution oceanographic measurements in the Adriatic Sea, the first such exercise to include shallow (<200 m) water. During the exercise, we adopted SO techniques to follow the North Adriatic Dense Water (NAddW) masses flowing southward from the coastal shelf into a deep basin. This is a complex process as the cold and fresh bottom shelf water suddenly encounters a warmer and saltier water resident in the deep basin, with which it mixes as it descends down the sill slope or through local canyon systems. The strong temperature contrasts that this generates, and the relatively fast action of the processes, were well suited for testing SO in shallow waters with the use of a “light” seismic system that

could be deployed quickly, using only two small air guns. The project used two generator-injector air guns for the source, and a 1200-meter, 96-channel hydrophone array for the receiver.

However, since SO measurements alone are not sufficient to fully characterize such complex processes, the resulting seismic reflection data were combined with a series of more “classical” physical oceanography measurements, e.g., CTD profiles, ADCP measurements of ocean currents, 232 XBT casts simultaneous with SO sections, and — for the first time — microstructure (very high resolution) measurements acquired via a free-falling turbulence profiler (101 casts). The microstructure measurement provides data on a full suite of important oceanographic variables at vertical resolutions on the order of millimeters, providing a calibration for how SO-measured vertical temperature changes connect to small-scale dynamical factors.

Figure 4 shows one example of a microstructure data section (vertically averaged over 1 meter) taken along a portion of the same pathway of the SO section

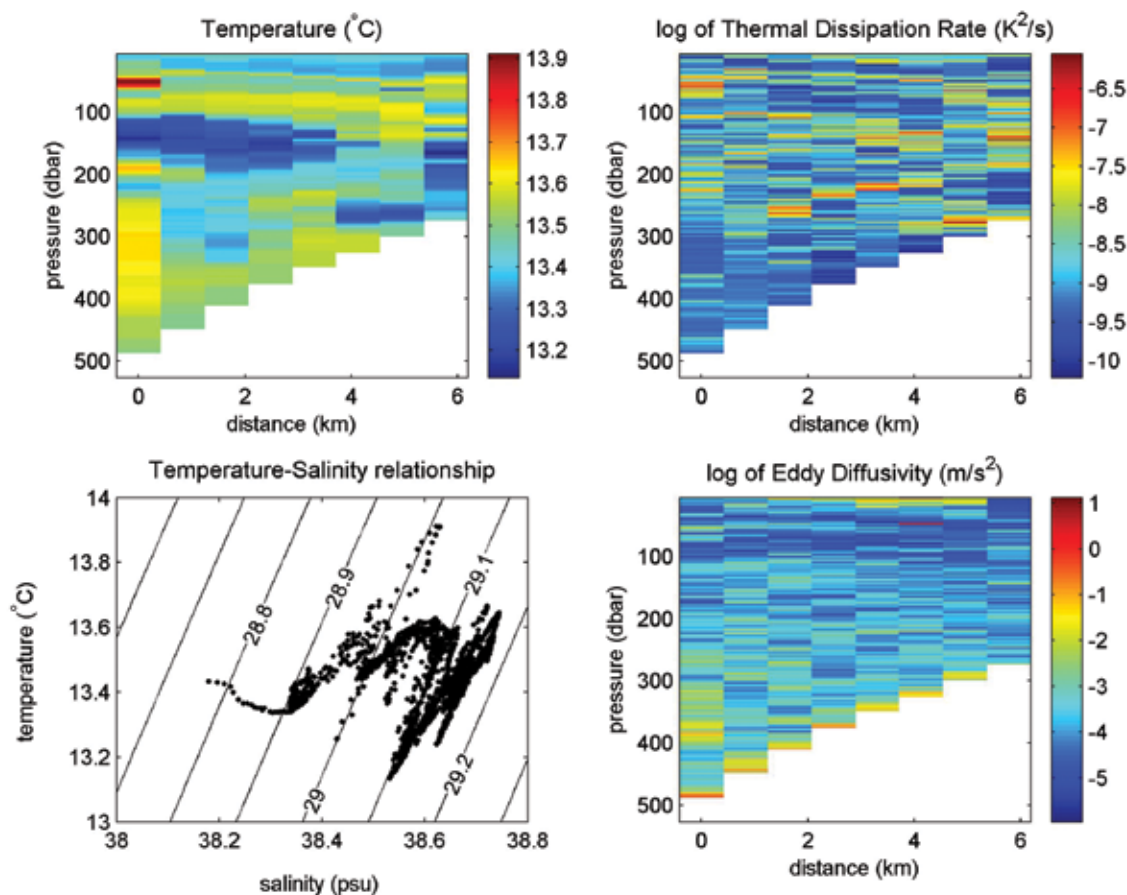


FIGURE 4

Measured temperature (upper left), measured salinity (lower left with potential temperature), calculated thermal dissipation rate from measured microstructure temperature (upper right), and calculated eddy diffusivity from measured current shear (lower right) along a repeated section to the northeast of Bari Canyon (box in Fig. 1). The zig-zag structures along isopycnals (contours of constant potential density) in the temperature-salinity diagram are characteristics of intrusions and interleaving. The thermal dissipation rates and eddy diffusivity values are displayed using a logarithmic scale.

shown in Fig. 1. The left-hand panels show how temperature and salinity variations in this region combine to interleave waters of similar densities but different temperatures. The SO technique resolves these temperature boundaries well. Interestingly, in this particular case, neither the thermal dissipation rate, nor the eddy diffusivity, the “mixing capability” caused by eddies, are tracking these broader-scale water mass boundaries. The thermal dissipation rate and eddy diffusivity shown in the right-hand panels in Fig. 4 highlight gradients of smaller vertical scale than those observable with SO, thus complementing the SO measurements. Overall, the ADRIASEISMIC-09 exercise provides compelling evidence for the need to gather a full range of measured oceanographic variables to complement and interpret the high-lateral-resolution vertical temperature changes seen with SO.

THE WAY FORWARD

The high-quality ADRIASEISMIC-09 data set we acquired demonstrates that SO can be carried out from oceanographic vessels of medium size with relatively light equipment, and that the seismic approach can be performed also in relatively shallow basins. This is an important finding, as the use of a large seismic vessel would have prohibited the kind of oceanography sampling that is necessary for any study characterizing dense shelf water movement.

SO is now at a turning point in its development. NRL and others have demonstrated that high-resolution SO observations are possible, but two aspects will likely determine if SO will be incorporated as a practical, standard research or operational oceanographic tool: (1) development of optimal field parameters and (2) development of signal processing. Field acquisition parameters such as source strength, streamer length, and others will affect the ease of deployment, quality of the data, weather windows, and the level at which SO and more familiar physical oceanography measurements might interfere with each other.¹¹ Also, SO records are so different from existing oceanographic records that to optimally incorporate them with CTD data, sea surface temperature measurements from satellites, turbulence measurements, and other data has required, and will require, significant algorithm development.^{5,6,12,13} Although some important achievements have been made in qualitatively interpreting SO data, the full potential to use this new view of the ocean’s thermal structures to quantitatively address questions on ocean dynamics has yet to be realized. To this end, the ADRIASEISMIC-09 dataset is a very important resource. For the first time, all applicable ocean variables were sampled at very high resolution together with seismic images, allowing us to explore the limits

and capabilities of seismic methods for characterizing various ocean processes.

[Sponsored by NRL]

ACKNOWLEDGMENTS

The authors gratefully acknowledge the Master and crew of the R/V *Urania* (Italian National Research Council, C.N.R.), the seismic acquisition of Giovanni Bortoluzzi (C.N.R.—Institute of Marine Sciences, Bologna) and Exploration Electronics LTD, and the microstructure acquisition and processing of Hartmut Prandke (ISW Wassermesstechnik). The seismic data were processed at NRL and also by E. Midgley (Univ. of Durham) using Seismic Unix processing software.

References

- ¹J. Gonella and D. Michon, “Deep Internal Waves Measured by Seismic-Reflection Within the Eastern Atlantic Water Mass,” *Comptes Rendus de l’Académie des Sciences, Ser II* **306**(12), 781–787 (1988).
- ²W.S. Holbrook, P. Paramo, S. Pearse, and R.W. Schmitt, “Thermohaline Fine Structure in an Oceanographic Front from Seismic Reflection Profiling,” *Science* **301**(5634), 821–824 (2003).
- ³See, for example, H. Medwin and C.S. Clay, *Fundamentals of Acoustical Oceanography* (Academic Press, Boston, 1998), Ch. 1.
- ⁴B. Ruddick, H.B. Song, C.Z. Dong, and L. Pinheiro, “Water Column Seismic Images as Maps of Temperature Gradient,” *Oceanography* **22**(1), 192–205 (2009).
- ⁵P.C. Papenberg, D. Klaeschen, G. Krahnmann, and R.W. Hobbs, “Ocean Temperature and Salinity Inverted from Combined Hydrographic and Seismic Data,” *Geophys. Res. Lett.* **37**, L04601 (2010).
- ⁶P. Nandi, W.S. Holbrook, S. Pearse, P. Paramo, and R.W. Schmitt, “Seismic Reflection Imaging of Water Mass Boundaries in the Norwegian Sea,” *Geophys. Res. Lett.* **31**, L23311 (2004).
- ⁷W.T. Wood, W.S. Holbrook, M.K. Sen, and P.L. Stoffa, “Full Waveform Inversion of Reflection Seismic Data for Ocean Temperature Profiles,” *Geophys. Res. Lett.* **35**, L04608 (2008).
- ⁸Y. Nakamura, T. Noguchi, T. Tsuji, S. Itoh, H. Niino, and T. Matsuoka, “Simultaneous Seismic Reflection and Physical Oceanographic Observations of Oceanic Fine Structure in the Kuroshio Extension Front,” *Geophys. Res. Lett.* **33**, L23605 (2006).
- ⁹T. Tsuji, T. Noguchi, H. Niino, T. Matsuoka, Y. Nakamura, H. Tokuyama, S. Kuramoto, and N. Bangs, “Two-dimensional Mapping of Fine Structures in the Kuroshio Current Using Seismic Reflection Data,” *Geophys. Res. Lett.* **32**, L14609 (2005).
- ¹⁰R. Hobbs et al. (2007), GO—Geophysical Oceanography: A new tool to understand the thermal structure and dynamics of oceans, D318 Cruise Rep., Durham Univ., Durham, U.K. (available at <https://www.bodc.ac.uk/data/>)

information_and_inventories/cruise_inventory/report/d318.pdf).

¹¹See, for example, L. Geli, E. Cosquer, R.W. Hobbs, D. Klaeschen, C. Papenberg, Y. Thomas, C. Menesguen, and B.L. Hua, "High Resolution Seismic Imaging of the Ocean Structure Using a Small Volume Airgun Source Array in the Gulf of Cadiz," *Geophys. Res. Lett.* **36**, L00D09 (2009).

¹²W.S. Holbrook and I. Fer, "Ocean Internal Wave Spectra Inferred from Seismic Reflection Transects," *Geophys. Res. Lett.* **32**, L15604 (2005).

¹³P. Paramo and W.S. Holbrook, "Temperature Contrasts in the Water Column Inferred from Amplitude-versus-Offset Analysis of Acoustic Reflections," *Geophys. Res. Lett.* **32**, L24611 (2005).

Looking Hurricanes in the Eye

If we could better understand the role of aerosols, in particular manmade ones, in tropical cyclone (TC) formation and intensity, we could better numerically model and forecast TCs, and perhaps avoid some of the catastrophic losses of life and property that they cause to both civilian and military populations. In particular, the danger that TCs pose to Naval personnel and ships is immense. For example, during World War II, Typhoon Cobra in December 1944 claimed the lives of 790 sailors, sank three destroyers, and damaged many other ships and aircraft.

NRL researchers from the Marine Meteorology Division are seeking a more precise knowledge of the dynamics and physics of cloud-storm interaction by studying high-resolution, full-physics atmospheric numerical model forecasts of TCs; Hurricane Isabel (2003) data are presented in this article for illustration. In looking into the eyes of the hurricanes, they are met with icy stares: in fact, it appears that the complex interaction of ice nucleation in hurricanes caused by aerosol particles with storm dynamics and thermodynamics can have significant impact on the intensity of hurricanes and typhoons. These particles occur naturally (e.g., windborne sand) but also originate in manmade sources, such as aircraft emissions. NRL's model forecasts suggest that high ice nuclei concentration at low temperatures leads to excessive amounts of small ice particles at upper levels of the storms, which limits vertical motion in the eyewall and constrains storm intensification. Clearly, gaining a better understanding of the microphysical processes that control TC intensity will lead to a better understanding of global weather patterns in general and the part that humanity plays in climate change.

The Impact of Ice Nuclei Concentration on Hurricane Modeling

Y. Jin, J.D. Doyle, Q. Zhao, S. Wang, and S.W. Chang
Marine Meteorology Division

Uncertainties due to aerosol interactions with radiative and cloud processes are not only a prominent issue for climate change research, but may even have important consequences for tropical cyclones as well. Suspended particulates can convert into condensation and ice nuclei, which can impact cloud-radiation interactions as well as latent heat release, resulting in complex interactions with atmospheric dynamics, especially in strongly forced systems such as tropical cyclones. Using high-resolution, full physics atmospheric numerical model forecasts of Hurricane Isabel (2003), we demonstrate that the intensity and structure prediction of tropical cyclones is highly sensitive to the ice nuclei concentration. Excessive ice particles at upper levels directly limit the development of vertical motion in the eyewall and constrain the intensification of storms. An improved understanding of ice nucleation processes and their representation in numerical models is needed to fully address aerosol-cloud interactions in tropical cyclones, as well as issues related to tropical cyclone characteristics and climate change.

INTRODUCTION

Tropical cyclones (TCs), which include hurricanes in the Atlantic basin and typhoons in the Western Pacific, are one of the most destructive natural phenomena on Earth since they are often accompanied by severe winds, torrential rainfall, extreme ocean waves, storm surges, and flooding. Tropical cyclones have a huge societal impact through potentially catastrophic property damage and loss of life. Hurricanes and tropical storms accounted for 46.3% (or \$137B) of all catastrophic losses from 1987 to 2006 according to the Insurance Information Institute. The potential impact of tropical cyclones on Navy operations can also be enormous. An extreme example is the infamous Typhoon Cobra, also known as Halsey's Typhoon after Admiral William Halsey, which struck the Pacific Fleet in December 1944 during World War II. Three destroyers were lost, and 790 sailors perished. During Hurricane Isabel of 2003, a total cost of \$105.6 million was incurred for the sortie and return of 40 Navy ships and 150 airplanes (information provided by LT Anderson, Navy Maritime Forecast Center). The expeditionary capability of Navy operations and safety of Navy personnel require more accurate tropical cyclone forecasts, as emphasized recently by the Oceanographer of the Navy, RADM David Tittley.¹

Although there has been steady improvement in TC track prediction in the past two decades, there has been little progress in improving TC intensity and

structure forecasts due to reasons ranging from lack of observations under high wind conditions to inaccurate representations of TC dynamics and physics in numerical weather prediction (NWP) models. One of the most contentious topics in the climate change debate is the climatological frequency and intensity of TCs in a globally warmed climate. While examination of long-term observational records has sometimes led to contradictory conclusions, unfortunately the current state of the art of numerical models is not yet sophisticated enough to reach a physics-based determination.

Recent research, including work being led at NRL, points to the importance of processes associated with small ice particles within the storms that have a strong influence on TC intensity and structure. Improved understanding of these key processes governing the ice particles and their complex interplay with cloud droplets, and of the cooling and heating impacts from microphysical processes in the eyewall and surrounding areas, is essential for accurate hurricane intensity and structure forecasts. Moreover, recent studies (for instance, see Ref. 2) underscore the important role of aerosols of both natural and anthropogenic origin in cloud ice and precipitation processes, and in particular their impact on hurricane intensity and structure changes. The research described here is focused on the sensitivity of hurricane intensity and structure forecasts to the ice nucleation processes, more specifically, the ice nuclei concentration, using the Navy's recently developed COAMPS** - TC (Coupled Ocean and Atmosphere

*COAMPS is a trademark of the Naval Research Laboratory.

Mesoscale Prediction System – Tropical Cyclone), which is a limited area model that has been designed to predict the TC track, intensity, and structure.

ROLE OF ICE NUCLEI

Under most atmospheric conditions, ice particles form by heterogeneous nucleation, which occurs via four different pathways: deposition, condensation freezing, immersion, and contact freezing. Aerosol particles (AP) are needed to act as ice nuclei (IN) in all four major modes. Any given AP of a certain size and chemical property can be IN for any one or all four of the nucleation modes under certain temperature and moisture conditions. One main source of IN is mineral dust, which often originates from the Sahara and Gobi Deserts and can be transported over great distances. Emissions from aircrafts, such as soot, can also be very efficient IN when the particle surface contains chemicals conducive for hydrogen bonds with water molecules. Despite decades of efforts in advancing IN measurements, and examination of nucleation processes through field campaigns, laboratory tests, and theoretical work, fundamental discrepancies remain in the IN characteristics derived from experimental and theoretical considerations (see, for example, Ref. 3).

Due to the difficulty in explicitly representing IN and their complicated interactions with the atmospheric environment in NWP models, the IN concentration typically is parameterized using a simple function of temperature (and moisture in some approaches). The complexity of the nucleation processes and the lack of observations distinguishing various ice nucleation pathways lead to large uncertainties in IN formulations, as evidenced by the nearly dozen IN formulations commonly employed in NWP models. Two of the most frequently used formulations are based on the research of Fletcher (1962)⁴ and Cooper (1986).⁵ Fletcher's formulation (shown in red in Fig. 1) was derived after synthesizing IN observations at a dozen locations worldwide. The observed IN counts, from which the Fletcher formulation was derived, vary by more than an order of magnitude between locations, underscoring the variability of IN characteristics. Cooper's formulation (shown in blue in Fig. 1) was based on in situ measurements of ice crystals in continental clouds. Note that the variability between these two formulations exceeds an order of magnitude. The Cooper formulation produces as much as two orders of magnitude more IN at warmer temperature ($>20^{\circ}\text{C}$) than does Fletcher's, whereas Fletcher's has more than an order of magnitude more IN at colder temperatures. The differences between the two sets of measurements represent variations in the IN concentrations broadly corresponding to clean or polluted environments. Also evident in Fig. 1 is the implied temperature threshold,

below which IN no longer increases with decreasing temperature. Observations of ice nucleation at cold temperatures ($<-30^{\circ}\text{C}$) are rare and a temperature threshold is often introduced in NWP models to reduce excessive ice particle concentration at very low temperatures. The uncertainty related to IN calculations is exacerbated when significant differences in the temperature threshold exist not only between the Fletcher and Cooper formulations, but also among the similar formulations implemented in various other microphysics representations. The differences among the various formulations can be as large as 13 K.

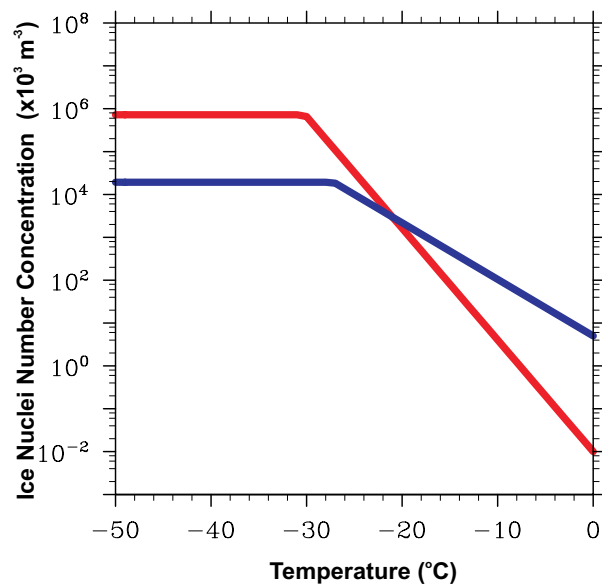


FIGURE 1
Number of ice-forming nuclei (10^3 m^{-3}) as a function of temperature from the Cooper (blue) and Fletcher (red) formulations.

NUMERICAL MODEL DESCRIPTION AND EXPERIMENTAL DESIGN

The COAMPS-TC system is based on COAMPS,⁶ which is under continuous development at the Naval Research Laboratory and has been used by Navy's Fleet Numerical Meteorology and Oceanography Center (FNMOC) for operational forecasting since 1998. Representations of physical processes within COAMPS-TC include: sub-grid-scale convective processes; cloud microphysical processes with prognostic equations for the mass conservation of cloud droplets, ice particles, rain, snow, graupel, and drizzle; radiative transfer processes for shortwave and longwave radiation; surface layer flux processes, and planetary boundary layer mixing. The basic COAMPS model has also been used for numerous studies of various weather phenomena at a wide range of scales from several hundred kilometers down to less than 50 m.

We performed a large number of COAMPS-TC forecast experiments for Atlantic TCs during 2002 to 2005 to further examine ice microphysical processes. Hurricane Isabel (2003) is selected here to illustrate the sensitive impact of IN on hurricane model forecasts. Hurricane Isabel reached category five on the Saffir-Simpson scale during the 120-hour forecast period starting from 0000 UTC 7 September. A triply nested grid configuration with the innermost domain following the storm motion is used. The grid spacing in the moving nest is 5 km and there are 40 vertical levels from the surface to approximately 30 km height. The innermost domain exclusively relies on the explicit microphysics predictive equations for cloud and precipitation processes, without applying a sub-grid-scale convection representation, which is applied in the outer two meshes, as commonly done in NWP models when the grid increment exceeds 5 to 10 km. Thus, the impact of varying the IN formulation on clouds and precipitation within the innermost mesh can be isolated in these experiments.

NUMERICAL MODEL RESULTS AND EVALUATION

The time evolution of the intensity of Hurricane Isabel derived from the 5-km-resolution grid forecast clearly indicates that the storm's intensity varies significantly between the forecasts using the Fletcher and Cooper IN formulations [Fig. 2(a)]. For example, the maximum surface wind using the Cooper formulation is 18 m s^{-1} stronger [Fig. 2(a)] than the experi-

ment using the Fletcher formulation near the end of the 120-hour forecast. The minimum surface central pressure differs by 20 hPa after 120-hour forecasts [Fig. 2(b)]. Furthermore, the IN impact on storm structure is evident, especially during the late forecast hours. At the 102-hour forecast time, the experiment using the Cooper formulation produces a strong storm [Fig. 3(b)] with a well-organized inner-core structure, including up to 3 m s^{-1} upward vertical motion at mid levels (4 to 6 km height) in the hurricane eyewall and high values (up to 55 dBZ) of model-derived radar reflectivity. This narrow and strong mid-level updraft apparent in the forecast using the Cooper formulation is reduced to 1 m s^{-1} and widened to a horizontal distance of about 100 km in the forecast using the Fletcher formulation [Fig. 3(a)]. Another pronounced distinction between these two forecasts is the ice concentration distribution at upper levels (10 to 15 km). Corresponding to the high IN concentration at colder temperatures (Fig. 1), the forecasts using the Fletcher approach produce an order of magnitude more ice particles than the Cooper formulation at the upper levels where temperature is colder than -20°C .

Given this apparent sensitivity of TC intensity forecasts to differences in the IN formulations, we carried out additional numerical experiments to assess the sensitivity of model forecasts to the IN concentration. Since the forecast using the Cooper formulation captures the observed storm intensity relatively well (see Fig. 2), we specify two new IN concentrations (Fig. 4) based on the Cooper formulation, with one (IN \times 10) having ten times greater IN concentration (New2,

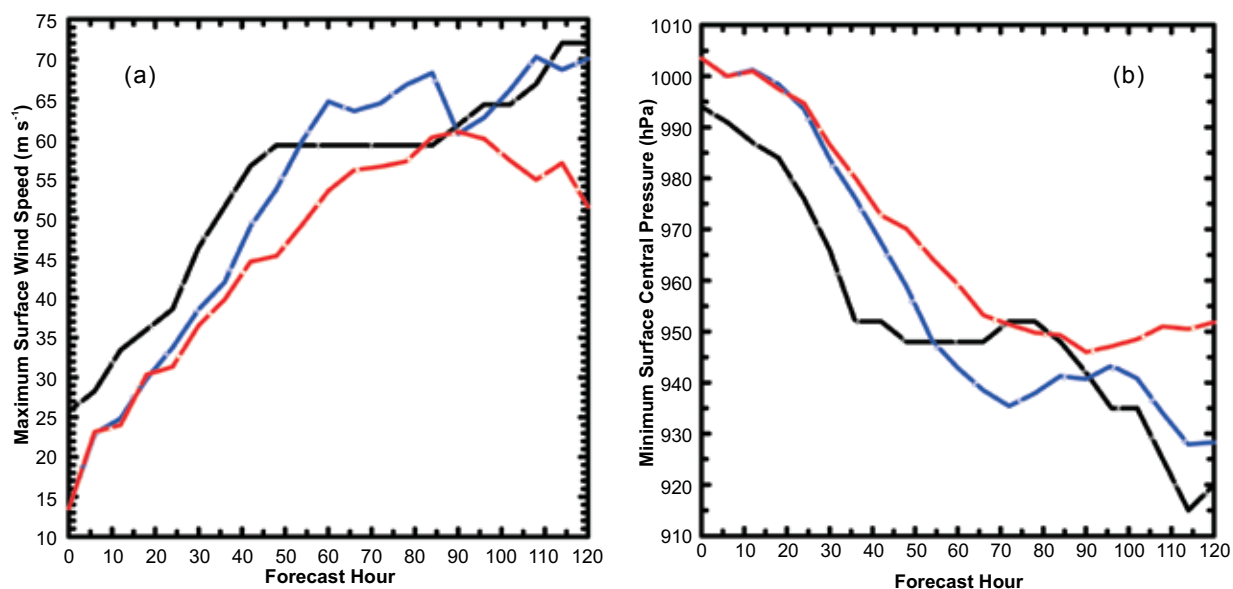


FIGURE 2

COAMPS-TC forecasts of Hurricane Isabel (2003) intensity using the Cooper (blue lines) and Fletcher (red lines) IN formulations (see Fig. 1) showing maximum surface winds (a) and minimum surface central pressure (b) over the 120-hour forecast period starting from 0000 UTC 7 September 2003. The black lines are for observed intensity from the best track data.

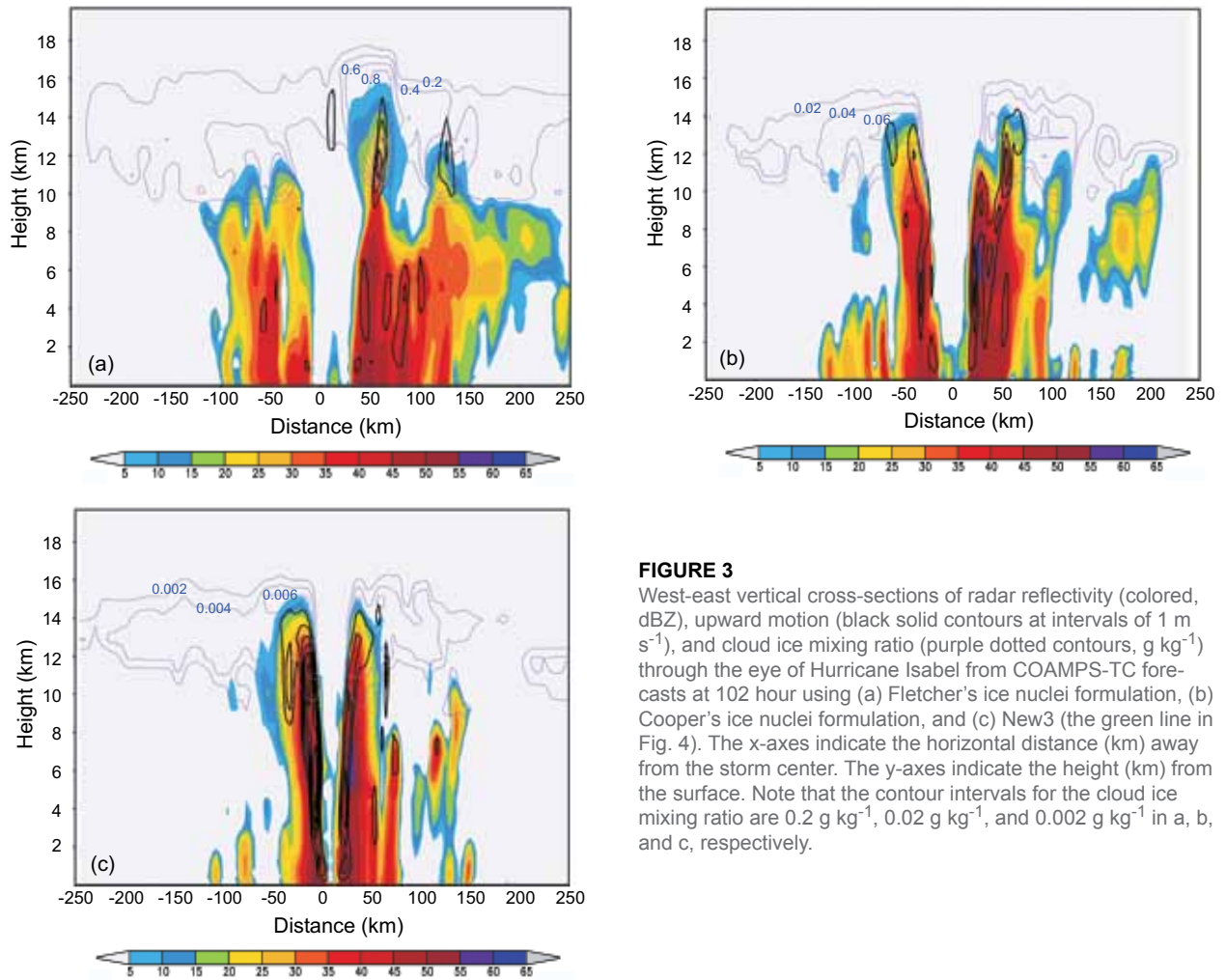


FIGURE 3

West-east vertical cross-sections of radar reflectivity (colored, dBZ), upward motion (black solid contours at intervals of 1 m s⁻¹), and cloud ice mixing ratio (purple dotted contours, g kg⁻¹) through the eye of Hurricane Isabel from COAMPS-TC forecasts at 102 hour using (a) Fletcher's ice nuclei formulation, (b) Cooper's ice nuclei formulation, and (c) New3 (the green line in Fig. 4). The x-axes indicate the horizontal distance (km) away from the storm center. The y-axes indicate the height (km) from the surface. Note that the contour intervals for the cloud ice mixing ratio are 0.2 g kg⁻¹, 0.02 g kg⁻¹, and 0.002 g kg⁻¹ in a, b, and c, respectively.

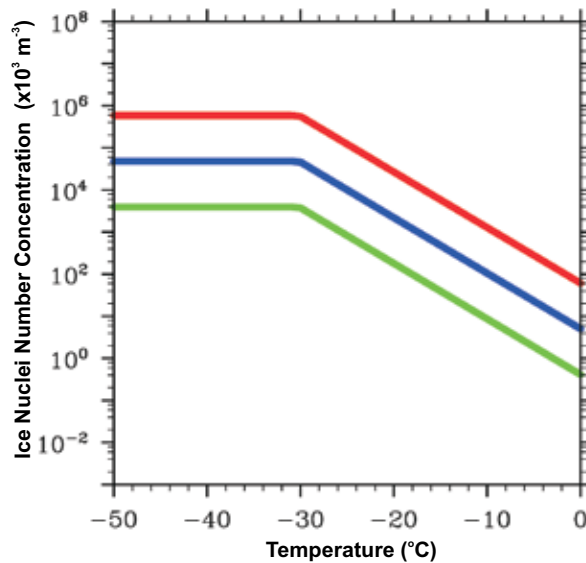


FIGURE 4

Number of ice-forming nuclei (10³ m⁻³) as a function of temperature from the Cooper (blue), New2 (red), and New3 (green) formulations.

TABLE 1 — The Minimum Surface Central Pressure (SLP) and Surface Maximum Wind (MAXW) of the 120-hour COAMPS-TC Forecasts Using the Cooper, New2, and New3 IN Formulations

| | Cooper | New2 | New3 |
|----------------------------|--------|------|------|
| Minimum SLP (hPa) | 926 | 932 | 911 |
| MAXW (m s^{-1}) | 70 | 68 | 76 |

red line) and the other experiment (IN/10) with IN reduced by a factor of ten than what Cooper's would yield at the same temperature (New3, green line). Table 1 lists the differences in the storm peak intensity among these tests. The IN \times 10 experiment produces a storm that has similar intensity (Table 1) and structure (not shown) as the test using the original Cooper formulation. The similarity between the Cooper and the IN \times 10 experiment suggests that for a given environmental condition (i.e., temperature, moisture, and winds), the storm system is not particularly sensitive to the increased IN concentration and indicates that perhaps a "saturated" state is achieved with respect to IN. On the other hand, the forecast storm using the IN/10 configuration deviates substantially from the storm evolution relative to the control Cooper forecast, not only with regard to the intensity (see Table 1), but also interestingly the storm structure as well [Fig. 3(c)]. Consistent with the IN specification and our expectations, the cloud ice at upper levels in the IN/10 storm is about 10 times less than that in the Cooper storm and about 100 times less than the storm using the Fletcher formulation. While the minimum surface central pressure and surface maximum wind speed values from the IN/10 forecasts during the first 36 forecast hours are very similar to those in the control experiment using the Cooper formulation, the cloud ice in the IN/10 experiment is 10 times less than in the control. The persistently reduced concentration of cloud ice in IN/10 has an important bearing on the subsequent storm development. The IN/10 storm eventually obtains more vigorous convection at mid levels in the eyewall, with updrafts exceeding 6 m s^{-1} (twice as much as that in the control forecast using the Cooper formulation) and similarly stronger upward vertical motion at upper levels (11 to 13 km) as well. The inner core size of IN/10 decreases significantly from that of the storm using the control Cooper formulation, and exhibits symmetric structures with narrower updrafts and high radar reflectivity on both sides of the storm.

A budget analysis reveals that the large mass of excessive cloud ice at upper levels using the Fletcher formulation limits the vertical motion in the inner core region and directly constrains the development of updrafts, as well as the intensification of the storm. Another possible reason for the weakened storm using the Fletcher formulation is that the widespread ice particles

at upper levels [see Fig. 3(a)] can potentially initiate precipitation in the region outside the eyewall. The aerosol-invigorated convection in the outer region may in turn lead to decreased graupel and snow production in the eyewall [indicated by the lower radar reflectivity in the eyewall in Fig. 3(a)] and further reduce the associated latent heat release in the inner core, consistent with recent studies (see, for example, Ref. 2).

SUMMARY AND DISCUSSION

The primary objective of this research is to evaluate the impact of ice nuclei concentration on hurricane intensity and structure derived from numerical model forecasts. Our model forecasts of Hurricane Isabel clearly suggest that high IN concentration at low temperature ($< -25 \text{ }^\circ\text{C}$) leads to excessive ice particles at upper levels in the hurricane inner core region, resulting in much weakened updrafts, reduced near-surface wind speeds, and a broader inner core of the hurricane. In the outer regions of the storm, denser and more widespread ice clouds form when high IN concentration exists. It follows from this study that aerosols, acting as ice nuclei, can have a profound impact on the development of hurricanes and weather in general. Our results suggest there indeed is a plausible link between concentrations of atmospheric particulates generated by either natural or anthropogenic sources and TC intensity, which highlights the complex and multifaceted nature of the interdependence between TC characteristics and climate change. As we continue to advance our ability to numerically predict tropical cyclones, in part through the inclusion of more sophisticated and truthful representations of microphysical processes, we expect to gain much-needed insight into the mechanisms that control the intensity of tropical cyclones, as well as a new understanding of tropical cyclone characteristics in the changing global environment.

ACKNOWLEDGMENTS

The authors would like to thank many scientists in the Marine Meteorology Division for their efforts in developing and evaluating COAMPS and COAMPS-TC. We also acknowledge suggestions and comments from Jerome Schmidt.

[Sponsored by ONR]

References

- ¹D. Titley, "USN Meteorological and Hydrological Services Update," presented at the 89th Amer. Meteor. Soc. Annual Meeting, Phoenix, AZ, January 10–16, 2009.
- ²A. Khain, B. Lynn, and J. Dudhia, "Aerosol Effects on Intensity of Landfalling Hurricanes as Seen from Simulations with the WRF Model with Spectral Bin Microphysics," *J. Atmos. Sci.* **67**, 365–384 (2010).
- ³W. Cantrell and A. Heymsfield, "Production of Ice in Tropospheric Clouds: A Review," *Bull. Amer. Meteor. Soc.* **86**, 795–807 (2005).
- ⁴N.H. Fletcher, *The Physics of Rainclouds* (Cambridge University Press, 1962).
- ⁵W.A. Cooper, "Ice Initiation in Natural Clouds," in *Precipitation Enhancement: A Scientific Challenge*, ed. R.R. Braham, Jr., Meteorological Monograph Series, Vol. 21, No. 43 (American Meteorological Society, Boston, MA, 1986), pp. 29–32.
- ⁶R.M. Hodur, "The Naval Research Laboratory's Coupled Ocean/Atmosphere Mesoscale Prediction System (COAMPS)," *Mon. Wea. Rev.* **125**, 1414–1430 (1997).

132

Measurements and Modeling of Acoustic Scattering from Unexploded Ordnance (UXO) in Shallow Water
D.C. Calvo, B.H. Houston, J.A. Bucaro, L. Kraus, H.J. Simpson, and A. Sarkissian

134

Scalable Wideband Frequency-Response for Free-Field, Littoral, and Seismic Applications
S. Dey and W.G. Szymczak

Measurements and Modeling of Acoustic Scattering from Unexploded Ordnance (UXO) in Shallow Water

D.C. Calvo,¹ B.H. Houston,¹ J.A. Bucaro,² L. Kraus,³
H.J. Simpson,¹ and A. Sarkissian¹

¹Acoustics Division

²Excet, Inc.

³Global Strategies Group

Introduction: The gradual development of coastal areas throughout the world in proximity to military training ranges and areas of past conflict has created a need to locate underwater unexploded ordnance (UXO). These ordnance, which may have veered off course and failed to detonate when they were initially released, may still pose a risk of explosion if they are subject to handling. This complicates the process of converting areas formerly restricted to military

training, for instance, into areas with general under-sea and surface activities such as fishing, boating, or diving. Searches for UXO can be costly and time consuming due to the large areas of water that need to be covered and the possibility that UXO are buried in the seafloor.

Probing the ocean bottom with sound waves offers an effective means of searching for UXO because sound pulses can propagate relatively long distances underwater and penetrate the seafloor. The use of low-frequency sound, which for this application is 2 to 30 kHz, has distinct advantages for this application. Sound waves in the lower end of this spectrum can easily penetrate the seafloor and inside the UXO, causing it to respond with structural acoustic scattering signatures different from other objects. This is in contrast to high-frequency sonar, which is useful for creating highly resolved images of an object lying on the ocean bottom but is less effective if the object is

buried. These structural acoustic clues help in classifying whether an echo from an object corresponds to UXO or to an object that poses no risk.

We are using controlled laboratory tank experiments and computer modeling to gain a fundamental understanding of how low-frequency sound waves interact with UXO at various burial depths and in the presence of seafloor roughness. An example UXO we have examined is a 5 in. diameter rocket warhead (Fig. 1). It consists of a thick-walled steel shell with interior compartments located at its ends and an inert filler material throughout most of its body.

Measurements: The experimental geometry features a line of monopole acoustic sources that synthesizes a cylindrical wavefront that ensonifies the UXO. Both source and receiver are at a low altitude above the sand and can rotate independently about the UXO in a horizontal plane to measure the variation of scattering with incidence angle (e.g., broad-side or end-on) and reception direction (e.g., backscattering or forward scattering). A measurement¹ of backscattering target

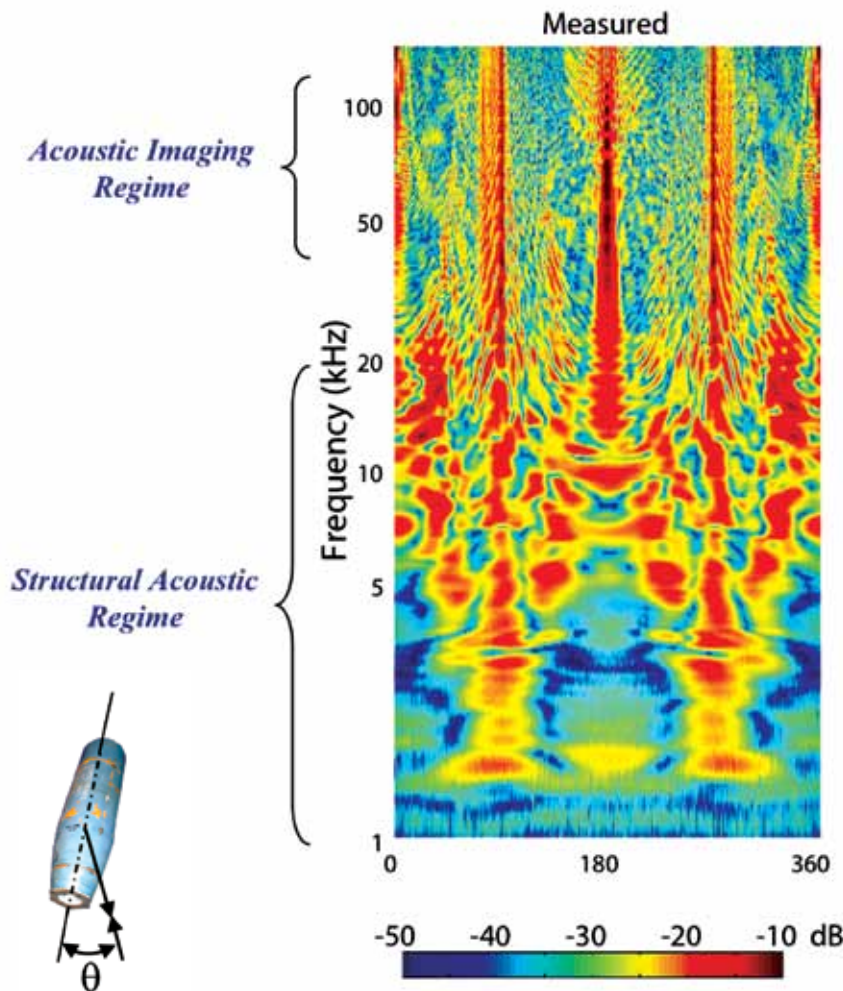


FIGURE 1 Measured backscattering target strength over a wide bandwidth of frequencies and ensonification angles for a 5-in. rocket UXO (inset) in a free-field of water.

strength as a function of frequency and incidence angle is shown in Fig. 1 for the UXO in a free-field of water (no sand is present). This figure represents a characteristic mosaic of this object that changes for objects

having less internal structure or symmetry. It therefore provides clues as to whether the sonar has encountered a UXO or a less threatening object. Extensive measurements for a variety of UXO with and without sand present have been made for both monostatic¹ and bistatic² geometries.

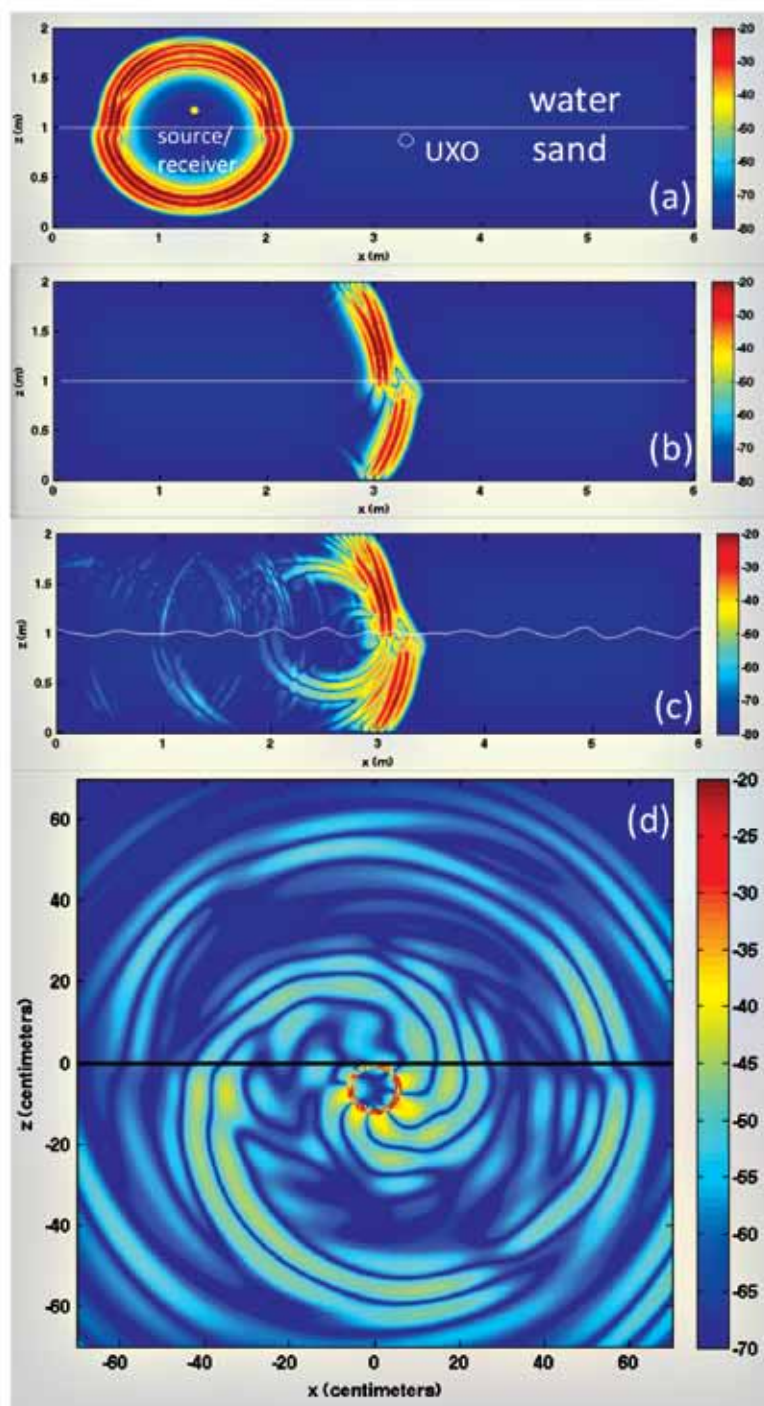


FIGURE 2

Snapshots of a computer simulation of the experiment showing the cylindrical sound pulse shortly after it has been emitted by the acoustic source (a) followed by two images (b and c) at a later instant: one with a flat and one with a roughened interface. A zoomed view of an isolated backscattered field is shown in (d) for a flush-buried UXO and a flat interface.

Modeling: Computer modeling is helpful for interpreting phenomena seen in experiments and predicting the performance of potential search systems. Our computer modeling tools include a 2D time-domain code using the elastodynamic finite integration technique (EFIT) and a 3D finite-element code (STARS3D). To examine the limits of using a 2D model, we consider the case of broadside incidence, and model the UXO two-dimensionally by sectioning the geometry to expose a circular cross-section.

Results of using the EFIT model for a geometry used in our tank experiments are shown in Fig. 2. For this case, the UXO is located below the water-sand interface. Figures 2(a) and (b) show how the leading “head” sound pulse travels quickly through the sand and reaches the UXO first, followed by the slower arrival conveyed by the water. A comparison of arrivals at the UXO position for a flat vs a rough interface is shown in Figs. 2(b) and (c) for the same instant. Figure 2(c) illustrates how roughening the interface lengthens the bottom-penetrating pulse and increases its angular spread.

A snapshot of a scattered field, which is the difference between the pressure field with and without the UXO present, is shown in Fig. 2(d) for a flush-buried UXO. A leaky structure-borne circumferential wave persists for a considerable time that in reality depends on the amount of attenuation present. The swirling appearance is caused by the depth-dependence of the incident wave.

We also model variation in bistatic scattering in a vertical plane using the geometry depicted in Fig. 3. In addition to resonances, strong forward scattering is evident, consistent with

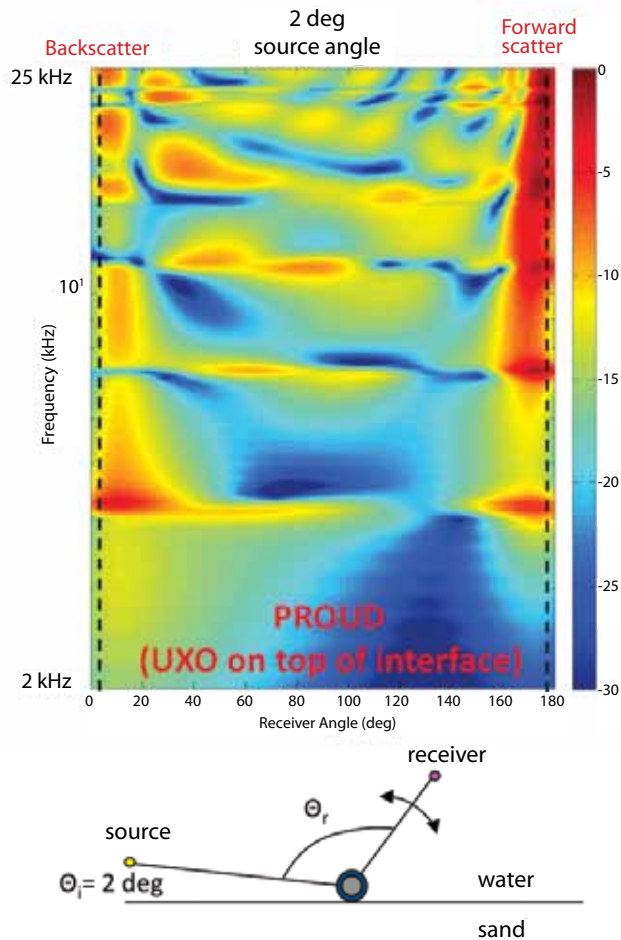


FIGURE 3
Simulated bistatic target strength as a function of frequency and receiver angle for scattering in a vertical plane for the 5-in. rocket UXO. Strong forward scatter is evident.

recent experimental measurements.² Our modeling work is also characterizing the statistical variation of the target strength as a function of sand roughness spectral parameters.³

Impact: This work has made the first systematic measurements of scattering from a variety of UXO in the low-frequency structural acoustics regime. The modeling efforts have shown that the essential scattering features and their dependence on burial depth can be accurately quantified. Both measurements and modeling are valuable input to object classification algorithms of potential use in UXO cleanup efforts both in the United States and throughout the world.

[Sponsored by ONR and SERDP]

References

- ¹ J.A. Bucaro, B.H. Houston, M. Saniga, L.R. Dragonette, T. Yoder, S. Dey, L. Kraus, and L. Carin, "Broadband Acoustic Scattering Measurements of Underwater Unexploded Ordnance (UXO)," *J. Acoust. Soc. Am.* **123**, 738–746 (2008).
- ² J.A. Bucaro, H. Simpson, L. Kraus, L.R. Dragonette, T. Yoder, and B.H. Houston, "Bistatic Scattering from Submerged Unexploded Ordnance Lying on a Sediment," *J. Acoust. Soc. Am.* **126**, 2315–2323 (2009).
- ³ D. Calvo, B.H. Houston, J.A. Bucaro, L. Kraus, H. Simpson, and A. Sarkissian, "Scattering by Unexploded Ordnance

(UXO) with Variable Burial Depth and Seafloor Roughness: A Parametric Study," *J. Acoust. Soc. Am.* **126**, 2167 (2009).

Scalable Wideband Frequency-Response for Free-Field, Littoral, and Seismic Applications

S. Dey¹ and W.G. Szymczak²

¹*GTEC, Inc.*

²*Acoustics Division*

Introduction: Rapid and accurate computations of wideband frequency-domain numerical solutions are key to many structural-acoustics and seismic applications, such as acoustic radiation and scattering; automotive noise; seismic scattering; noise, vibration, and harshness (NVH) analysis; interior-noise prediction for aircrafts; and aero-acoustics.

The wave-dependent nature of such problems can lead to large dispersion errors in numerical simulation at mid-to-high frequencies unless proper discretization strategies are used. For solutions in the frequency-domain, high-order (*hp*-version) finite element approximations offer significant accuracy

advantage over low-order methods.¹ High-order, 3D discretizations for large-scale problems may contain millions of unknown solution coefficients. The solution of the resulting system of linear algebraic equations for thousands, or even hundreds, of frequencies is a significant computational effort even on parallel computing platforms.

We have developed a scalable parallel-computing scheme based on multipoint Padé approximations,² to accelerate the frequency-sweeping of large-scale p-finite-element approximations for wave-dependent problems. Application to 3D problems of Navy interest shows significant reduction in computational effort.

Modeling Approach: To obtain the time-harmonic response, we model the structural-acoustics problem in the frequency-domain. The elastic domain is treated as a 3D linear (visco)elastic material whose dynamic response is governed by the Navier equations of elasticity. The linear-acoustic response of the fluid domain satisfies the Helmholtz equation. For littoral applications, we treat the sediment (bottom) as a damped acoustic fluid. We solve a fully coupled system of equations with appropriate compatibility conditions at the fluid-elastic interface requiring the continuity of the normal stress and pressure and that of the normal particle acceleration. We handle the infinite extent of the exterior domain by using the so-called perfectly matched layer (PML) technique.

We use a p-finite-element discretization method resulting in a frequency-dependent system of linear algebraic equations. For a wideband frequency sweep, for N discrete circular-frequencies given by $\{\omega_1, \omega_2, \dots, \omega_N\}$, we need the solutions of systems represented by the following equation:

$$A(\omega_i)u_i = b(\omega_i), \quad (1)$$

where A and b are the frequency-dependent coefficient matrix and the right-hand-side vector, respectively, and u represents the unknown solution coefficients. We use a generalized multipoint Padé-based reconstruction that requires u and

$$\frac{d^k u}{d\omega^k}, k = 1, 2, \dots, K$$

at a few coarse frequencies $\{\omega_1^0, \omega_2^0, \dots, \omega_M^0\}$ with $M \ll N$. Once the coarse frequency solutions and their K derivatives with respect to frequency are known, the solution at any frequency may be reconstructed as

$$u(\omega^0 + \delta\omega) \approx \sum_{l=0}^{l=L} p_l(\delta\omega)^l / \sum_{m=0}^{m=M} q_m(\delta\omega)^m. \quad (2)$$

Here $K = \lceil (L + M + 1) / p_n \rceil$ depends on the degree of numerator and denominator of the Padé approximation and p_n is the number of coarse frequencies used in

the reconstruction. K is typically less than or equal to 10.

Taking k -successive derivatives of Eq. (1) with respect to ω and rearranging the terms gives

$$Au^{(k)} = b^{(k)} - \sum_{j=0}^{k-1} \binom{k}{j} A^{(k-j)} u^{(j)}, \quad (3)$$

where the superscript within brackets is the degree of the derivative. One can immediately note that the solution of $u^{(k)}$ is simply the solution of k additional right-hand sides for the original system matrix. Equation (3) implies that there is no cost of additional matrix factoring beyond that needed to solve the regular system.

Application and Results: Figure 4 shows the reconstruction of the bistatic scattering response for a spherical elastic shell for 256 frequencies using just three coarse frequencies. In both cases, $L = 9$, $M = 10$. This problem has 70,616 complex-valued unknown coefficients. The total time to compute the direct response for 256 frequencies in serial is 70,439 seconds. The reconstruction for using two and three coarse frequencies (one processor per coarse frequency) is 219 and 277 seconds, respectively. This implies a speedup of 321 and 254 using two and three processors, respectively.

Figure 5 depicts a cut through the 3D finite element mesh for scattering from a fully buried elastic shell. Figure 6 compares the reconstruction of the backscattering response using two, four, and eight coarse frequency points for a band of 512 frequencies. One can observe the convergence of the Padé-based reconstruction to the direct computation of the frequency-response by solving for all the frequencies. The reconstructed result using eight coarse frequency points is virtually indistinguishable for the direct response computation. The computational cost of the reconstruction-based approach, in this example, is less than the direct computation by a factor of 64.

The presented examples demonstrate the effectiveness of the approach in producing huge computational savings while preserving the accuracy of the reconstructed responses for large-scale structural acoustics.

[Sponsored by ONR]

References

- ¹ S. Dey and D.K. Datta, "A Parallel hp -FEM Infrastructure for Three-dimensional Structural Acoustics," *International Journal for Numerical Methods in Engineering* **68**(5), 583–603 (2006).
- ² P. Avery, C. Farhat, and G. Reese, "Fast Frequency Sweep Computations Using a Multi-point Padé-based Reconstruction Method and an Efficient Iterative Solver," *International Journal for Numerical Methods in Engineering* **69**(12), 2848–2875 (2007).

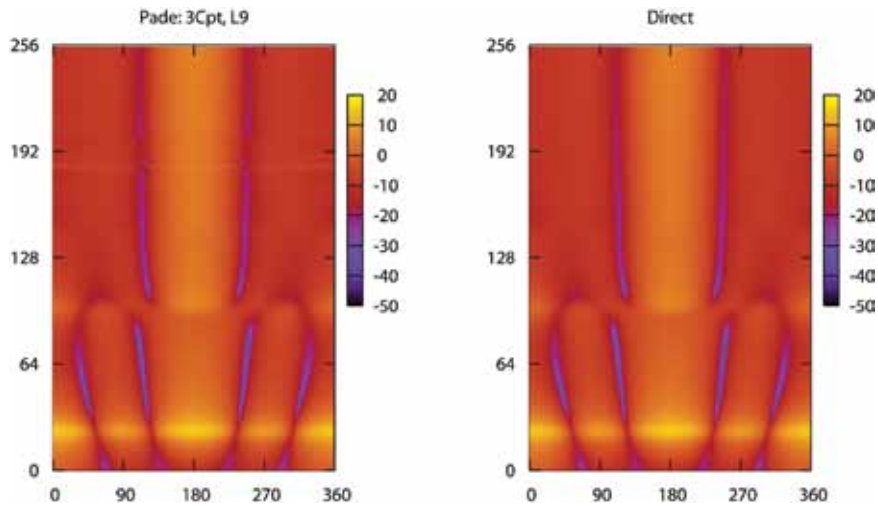


FIGURE 4
Padé-based reconstruction of bistatic-scattering response for a spherical shell (left) in free-field compared to direct computation (right).

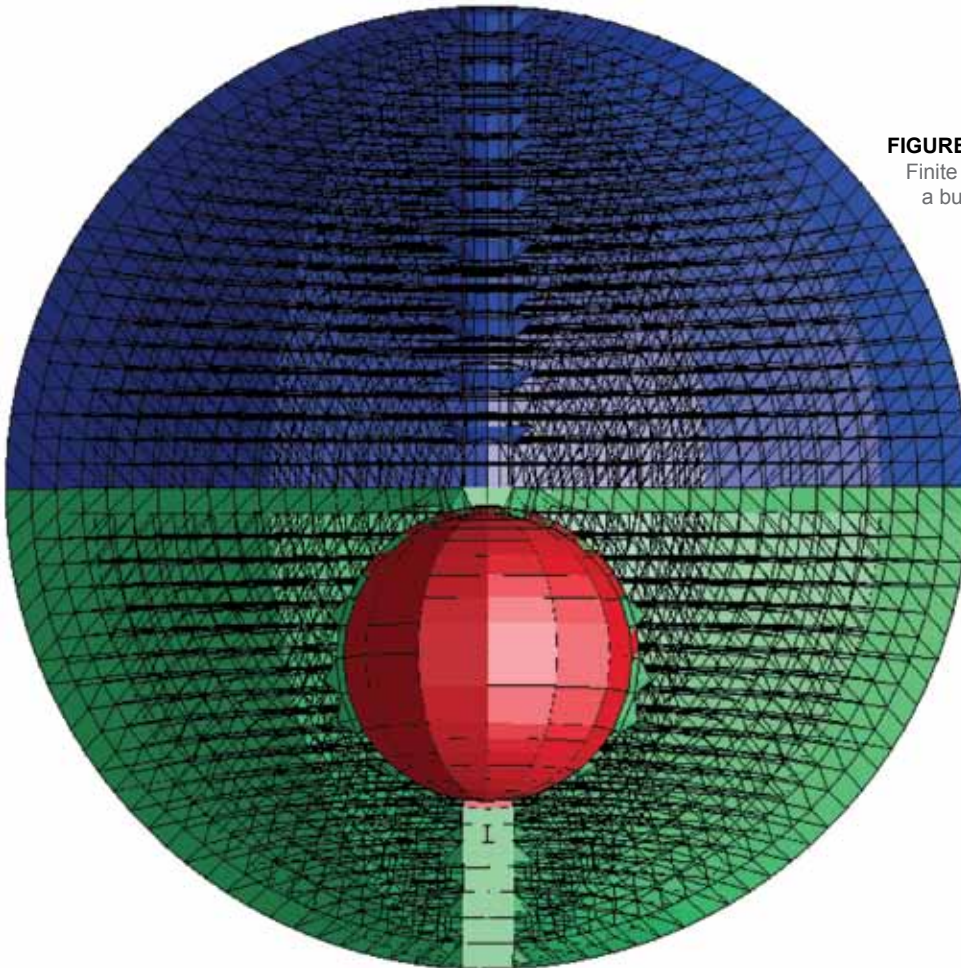
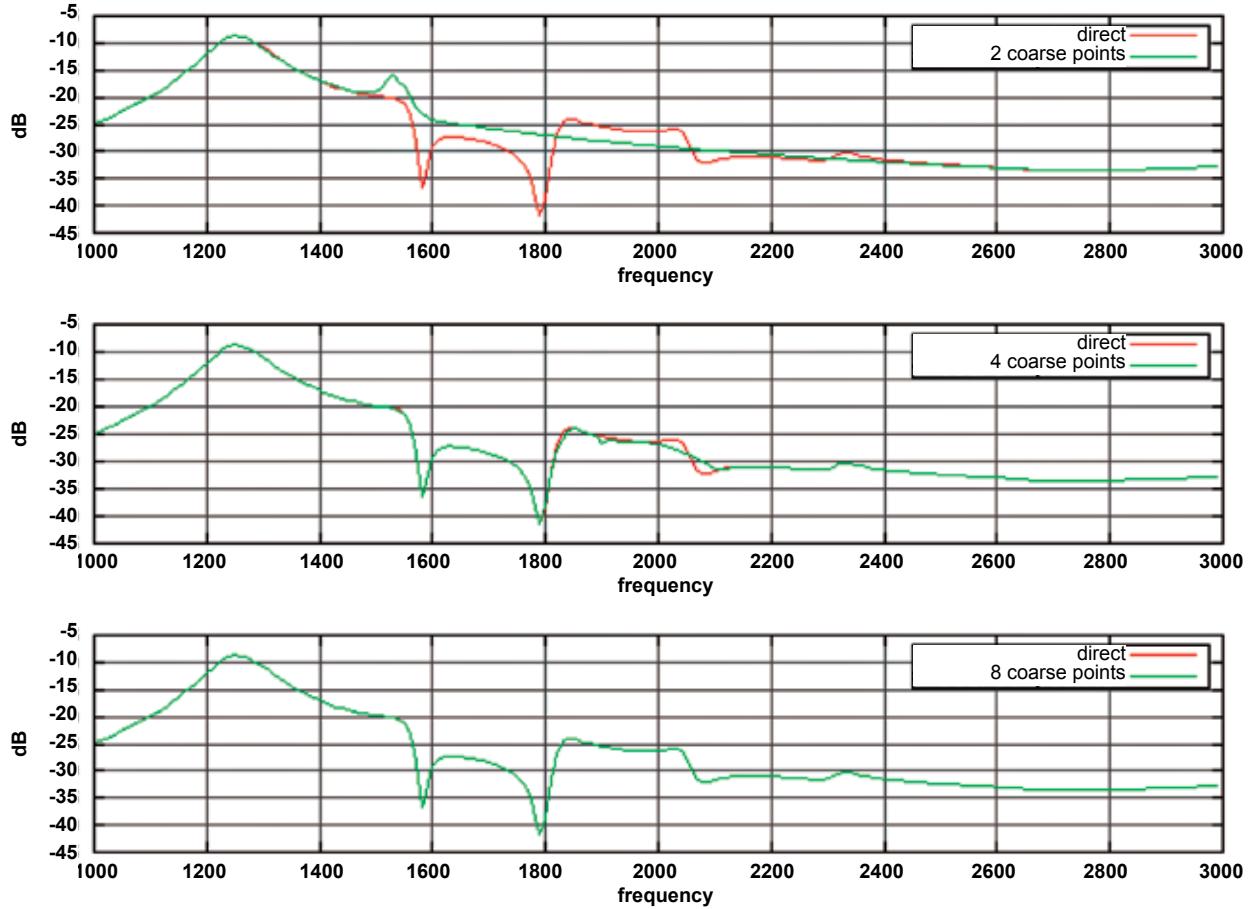


FIGURE 5
Finite element model for scattering from a buried elastic target.

FIGURE 6

Convergence of the Padé-based of the scattering response for the finite element model shown in Fig. 5.



140

Optical Depth Assimilation for Operational Dust and Pollution Prediction
J.S. Reid, J. Zhang, D.L. Westphal, E.J. Hyer, C.A. Curtis, N.L. Baker, J.R. Campbell, and P. Xian

142

Measurements of Water Vapor from the Lower Stratosphere to the Upper Mesosphere
G.E. Nedoluha, R.M. Gomez, and B.C. Hicks

143

Long-Range Optical Communications Link
M.R. Suite, B.B. Xu, C.I. Moore, H.R. Burris, L.M. Thomas, W.S. Rabinovich, J.L. Murphy, R. Mahon, P.G. Goetz, and M.S. Ferraro

Optical Depth Assimilation for Operational Dust and Pollution Prediction

J.S. Reid,¹ J. Zhang,^{1,2,3} D.L. Westphal,¹

E.J. Hyer,^{1,2} C.A. Curtis,¹ N.L. Baker,¹

J.R. Campbell,^{1,2} and P. Xian^{1,4}

¹*Marine Meteorology Division*

²*UCAR Visiting Scientist Program*

³*University of North Dakota*

⁴*ASEE Postdoctoral Fellowship program*

Synopsis: The Marine Meteorology Division has developed and delivered the world's first operational system for the assimilation of aerosol optical depth (AOD) data from satellite sensors into an aerosol forecast model. This system, the NRL Atmospheric Variational Data Assimilation System–Aerosol Optical Depth (NAVDAS-AOD), is used to improve the Navy Aerosol Analysis and Prediction System (NAAPS), used by Department of Defense (DoD) and civilian users to forecast severe visibility-reducing dust, smoke, and pollution events. Implementation of NAVDAS-AOD at the Fleet Numerical Meteorology and Oceanography Center (FNMOC), which assimilates quasi-operational NASA Moderate Resolution Imaging Spectroradiometer (MODIS) data, has nearly halved errors in Navy aerosol forecasts.

Introduction and Rationale: Dust, smoke, and pollution forecasting has become an important application area for the Department of Defense. Whereas the DoD was traditionally concerned about aerosol effects on electro-optical (EO) propagation issues related to navigation, air operations, and ordnance delivery, recent applications include directed energy and EO surveillance and reconnaissance systems. Recent emphasis in poor-visibility areas such as the Arabian Gulf, Asia, and Africa has placed even greater demands on aerosol characterization and forecasting systems. Simultaneously, the broader research community has renewed interests in aerosol particles due to their impact on meteorology, geochemical cycles, and climate.

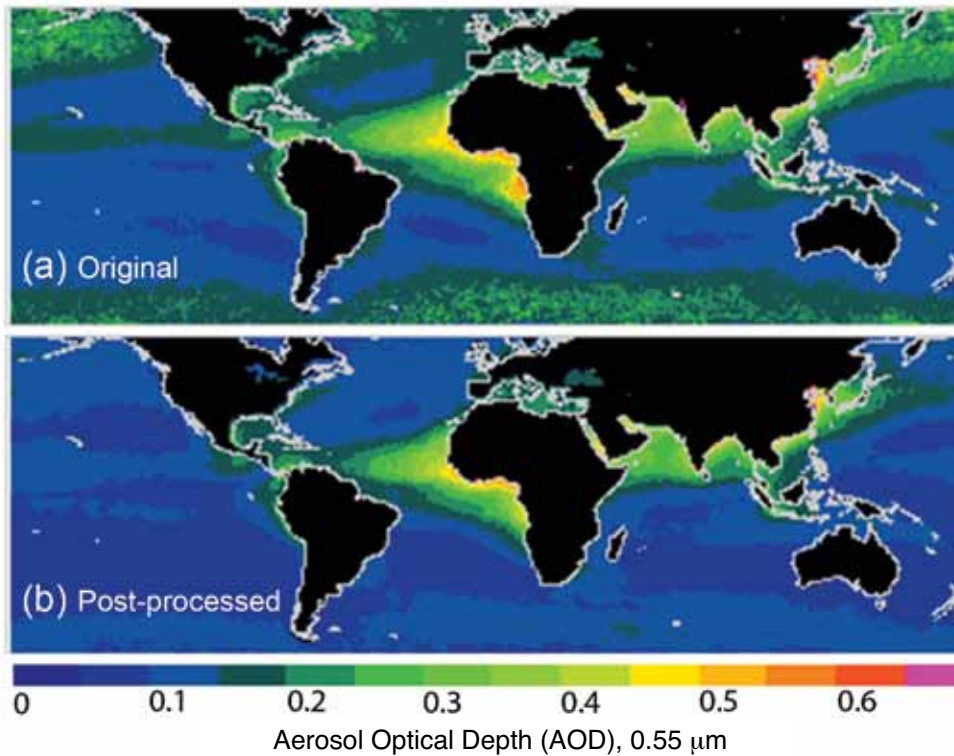
The Marine Meteorology Division has pioneered the field of global aerosol forecasting. Important firsts include (1) the development of NAAPS, the first operational global aerosol forecast model; (2) the first global use of satellite-based fire data for use in estimating forest fire and agriculture emissions; and (3) the world's first quasi-operational aerosol model verification system. These systems are used by DoD customers for operational visibility prediction, as well as by a host of civilian operational and scientific users.

Recently, NASA MODIS aerosol products have become reliably available in near real time.

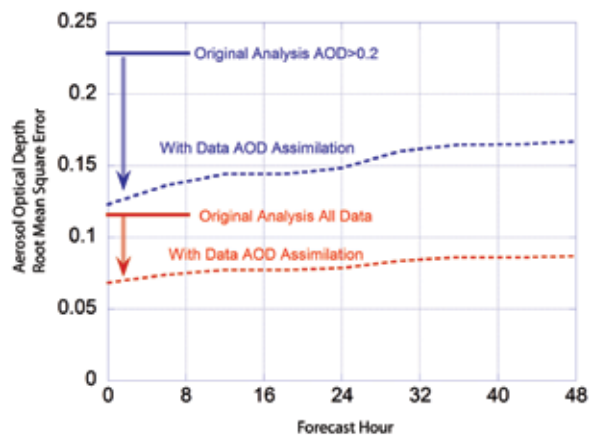
Unsurpassed for its efficacy and nearly daily coverage over the globe, the NASA MODIS products suite provides the bulk of global aerosol monitoring. Even so, before these data can be incorporated in models, several technical challenges related to product error characterization and aerosol redistribution must be met. NRL has met these challenges and devised the world's first operational aerosol optical depth system, the NAVDAS-AOD, which was transitioned to FNMOC in 2009.

System Overview: NAVDAS-AOD has three primary components: data acquisition and preprocessing, variational analysis, and feedback into NAAPS. The process begins with the acquisition of satellite aerosol optical depth data. While other data sources are or will be available, initial focus has been on near-real-time MODIS retrievals from the Terra and Aqua spacecraft, generated by the joint NASA/NOAA Near Real Time Processing Effort (NRTPE). These satellites give near-global coverage of AOD at a nadir resolution of 10×10 km and are downloaded from NRTPE with data latency of approximately 6 hours.

The most significant challenge in developing NAVDAS-AOD was the development of the preprocessor.¹ Before model assimilation can take place, error characterization must be understood and, preferably, systematic biases be removed. Remaining systematic high biases in particular can be very damaging as these will create isolated "plumes" in the analysis that will then propagate in the forecast. Major sources of systematic bias in satellite AOD include (1) cloud contamination, in which cloud edges are misidentified as dust or pollution, subsequently leading to a high bias; (2) lower boundary conditions, where white-capping and glint on the ocean surface or bright desert surfaces are misinterpreted as aerosol particles, which reduce the top of atmosphere signal to noise; and (3) microphysical bias, where the optical properties of the aerosol particles are different from what is derived or assumed in the retrieval. Through a series of validation and verification studies, NRL developed a preprocessor that screens, aggregates, performs empirical corrections, and assigns final uncertainties for these types of biases. The resulting global data field over ocean is dramatically different from the original data (Fig. 1). While on average the preprocessor reduces AOD by 20% to 30% over oceans, significant cloud-related bias is removed from the southern oceans and North Pacific (approximately 50% correction). Microphysical bias results in an approximate 10% to 20% correction for areas of significant pollution and dust loading, respectively. Correcting for ocean surface wind speed also proved important for the background marine environment.


FIGURE 1

Comparison of mean aerosol optical depth (AOD) for 2007 from the NASA MODIS instrument (a) before and (b) after pre-processing. Note significant changes in the southern oceans and North Pacific due to the removal of cloud artifacts. Also note more subtle changes in dust in the Arabian Gulf and off the African and Asian coasts due to correction of micro-physics errors.


FIGURE 2

Average NAAPS root-mean-square error improvement for aerosol optical depth (AOD) at coastal Sun photometer sites. Given are the original $T = 0$ analyses (solid), and error by forecast hour with AOD data assimilation (dashed).

After preprocessing, revised data undergoes 2D variational analysis with the NAAPS model via the core NAVDAS system.² The resulting 2D global AOD analysis is then fed back into NAAPS in three dimensions, based on the initial model vertical distribution. When observed AODs are significantly larger than in the NAAPS model, vertical redistribution follows a climatology based on the NASA Cloud Aerosol Lidar and Infrared Pathfinder Satellite Observation (CALIPSO) data set.

Based on comparisons with the NASA Aerosol Robotic Network (AERONET) network of Sun photometers, NAVDAS-AOD has reduced NAAPS root-mean-square errors by 25% to 40% for both the analysis and the 48-hour forecasts over the world coastal sites (Fig. 2). Some sites, such as those near Africa, see even greater improvements.

Other versions of the preprocessor and NAVDAS-AOD under development include the application of overland AOD, conversion to 3D variational analysis, and the addition of other passive and active sensors (e.g., CALIPSO).

[Sponsored by ONR]

References

- ¹ J. Zhang and J.S. Reid, "MODIS Aerosol Product Analysis for Data Assimilation: Assessment of Over-ocean Level 2 Aerosol Optical Thickness Retrievals," *J. Geophys. Res.* **111**, D22207 (2006), doi:10.1029/2005JD006898.
- ² J. Zhang, J.S. Reid, D.L. Westphal, N. Baker, and E.J. Hyer, "A System for Operational Aerosol Optical Depth Data Assimilation Over Global Oceans," *J. Geophys. Res.* **113**, D10208 (2008), doi:10.1029/2007JD009065.

Measurements of Water Vapor from the Lower Stratosphere to the Upper Mesosphere

G.E. Nedoluha, R.M. Gomez, and B.C. Hicks
Remote Sensing Division

Introduction: Water vapor in the stratosphere (~15 to 50 km) and mesosphere (~50 to 90 km) is the primary source of the OH radical and other hydrogen compounds, and is therefore important in ozone chemistry. In addition, water vapor entering the stratosphere is extremely sensitive to temperatures at the tropical tropopause, and is therefore relevant to our understanding of how and where air rises from the troposphere into the stratosphere. Also, because water vapor is an important greenhouse gas, measuring the amount of water vapor in the atmosphere is extremely useful for understanding global climate change.

WVMS Instruments: The ground-based Water Vapor Millimeter-wave Spectrometer (WVMS) instruments have been measuring water vapor from ~40 to 80 km and total column water vapor since the early 1990s from Network for the Detection of Atmospheric Composition Change (NDACC) sites at Mauna Loa, Hawaii (19.5°N, 204.4°E), Lauder, New Zealand (45.0°S, 169.7°E), and Table Mountain, California (34.4°N, 242.3°E). These instruments retrieve water vapor profiles by measuring the pressure-broadened 22 GHz water vapor lines, and are preferably deployed at dry, high-altitude sites, where the water vapor in the dry stratosphere and mesosphere can be observed through a minimal amount of tropospheric (surface to ~15 km) water vapor.

While these ground-based microwave measurements of water vapor in the upper stratosphere and mesosphere from 40 to 80 km are ideal for long-term change detection,¹ they do not always detect shorter-term multiyear variations such as the increase in stratospheric water vapor that was observed by the NRL Polar Ozone and Aerosol Measurement (POAM) satellite instrument in 2001.² We have, therefore, incorporated state-of-the-art technologies, including fast Fourier transform (FFT) spectrometers, to extend the range of the WVMS measurements to cover the atmosphere from 26 to 80 km.

Successful Deployment of New Instrument: The first successful deployment of such an instrument has been to the Table Mountain site (Fig. 3), where from December 2008 to May 2009, WVMS measurements showed good agreement with coincident Microwave Limb Sounder (MLS) water vapor measurements from the Aura satellite. Figure 4 shows the spectrum of the measurements made by this WVMS system on January

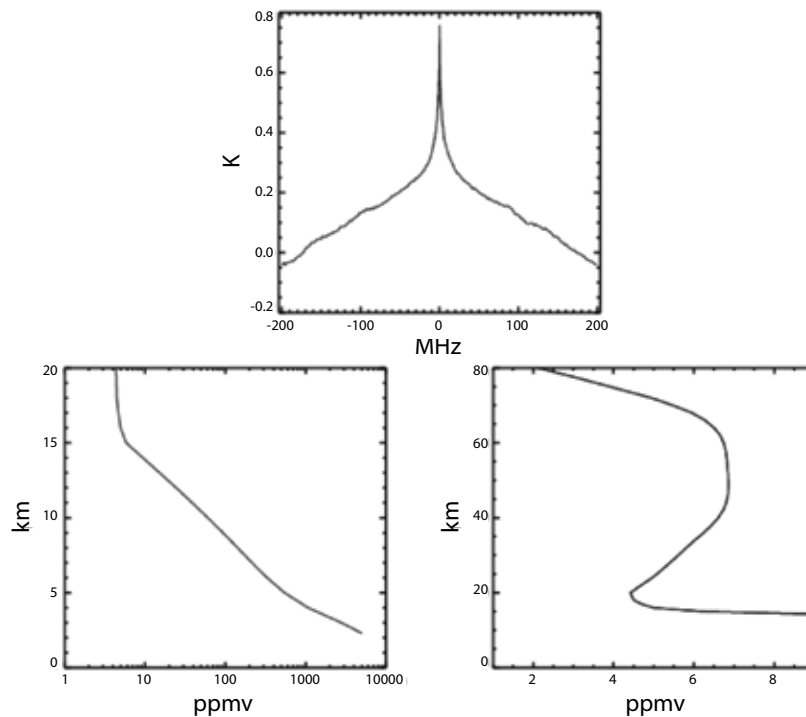
28, 2009. The measurements are integrated over the entire day in order to obtain adequate signal-to-noise. Also shown in this figure is the water vapor profile from 0 to 20 km (note the log scale) and from 0 to 80 km. The water vapor profile between ~10 km and ~26 km comes primarily from climatology, since the measurement is not sensitive in this range.

During the December 2008 to May 2009 period, WVMS measurements were also compared with radiosondes launched from the nearby Edwards AFB and Vandenberg AFB, and the new WVMS measurements showed skill at detecting variations in mid-tropospheric water vapor. The WVMS instrument at Table Mountain also participated in the NASA Measurements of Humidity in the Atmosphere and Validation Experiments (MOHAVE) campaign in September 2009, where it was compared with balloons, lidars, GPS total column measurements, and several satellite measurements.

Future of Water Vapor Measurements: The Mauna Loa site has been prepared for simultaneous deployment of a new WVMS instrument alongside the existing instrument. These instruments will be compared for approximately 1 year in order to ensure that there is no disruption to the long-term trend data taken from the Mauna Loa site. While until now the



FIGURE 3
The WVMS instrument at Table Mountain.

**FIGURE 4**

Top: Brightness temperature spectrum as measured by the WVMS instrument on January 28, 2009. A baseline has been subtracted. Bottom left: Water vapor in the troposphere. The profile begins at the 2.3 km altitude of the measurement site. Bottom right: The water vapor profile from 0 to 80 km. Note how much drier the stratosphere and mesosphere are as compared to the surface.

WVMS instruments have been used together with satellite data to measure changes in water vapor, it is not clear whether satellite measurements of water vapor in the stratosphere and mesosphere will be available in the future. WVMS instruments may, therefore, be the primary source of data for future water vapor trends in this region of the atmosphere.

Acknowledgments: The WVMS project is funded by NASA under the Upper Atmospheric Research Program and by ONR.

[Sponsored by NASA and ONR]

References

- ¹ G.E. Nedoluha, R.M. Gomez, B.C. Hicks, J.E. Wrotny, C. Boone, and A. Lambert, "Water Vapor Measurements in the Mesosphere from Mauna Loa Over Solar Cycle 23," *J. Geophys. Res.* **114**, D23303 (2009), doi:10.1029/2009JD012504.
- ² W.J. Randel, F. Wu, H.Vömel, G.E. Nedoluha, and P. Forster, "Decreases in Stratospheric Water Vapor after 2001: Links to Changes in the Tropical Tropopause and the Brewer-Dobson Circulation," *J. Geophys. Res.* **111**, D12312 (2006), doi:10.1029/2005JD006744.

Long-Range Optical Communications Link

M.R. Suite,¹ B.B. Xu,¹ C.I. Moore,¹ H.R. Burris,¹ L.M. Thomas,¹ W.S. Rabinovich,² J.L. Murphy,² R. Mahon,² P.G. Goetz,² and M.S. Ferraro²

¹Space Systems Development Department

²Optical Sciences Division

Introduction: The Electro-Optics Technology Section and the Photonic Materials and Devices Section successfully demonstrated a high-speed, long-range, free-space optical laser communication (lasercom) link between Fort Story and Fort Monroe, in Virginia, during the Trident Spectre 2009 exercise. The total range of the link was 28 km — a range approaching Earth curvature line-of-sight limited range (Fig. 5). The link gives a fully bidirectional fast Ethernet link (100 Mbps) with packet error rates less than 1% at all times. Lasercom provides an alternate data path to standard radio frequency communication links. The Trident Spectre exercise demonstrated that lasercom can provide the U.S. Navy and Marine Corps with greatly increased connectivity, low probability of intercept and detection, and path diversity to increase overall communications reliability.

Capabilities: Dual Mode Optical Interrogator (DMOI) lasercom terminals developed by Novasol, Inc., in collaboration with NRL were used for the Trident Spectre exercise. These terminals use free-space propagation of eye-safe telecommunication wavelength lasers (wavelength of 1550 nm) through the atmosphere to enable fiberless optical communications. The DMOI terminals are designed to automatically track moving targets and can themselves be operated on moving platforms. Optical communications electronics developed jointly by NRL and Smart Logic, Inc., were connected to the DMOI terminals to enable the 100 Mbps fast Ethernet data links between DMOI terminals. Communications terminals of this



FIGURE 5
Image showing endpoints of the free-space optical (FSO) link.

type can be used to connect networks separated by large distances without laying optical fiber, which is either costly for fixed locations or impossible for mobile platforms.

For the Trident Spectre 2009 exercise, one DMOI was installed at the top of the Cape Henry Lighthouse at Fort Story in Virginia Beach, Virginia. Across the Chesapeake Bay, a second DMOI was installed in an observation tower atop the historic Fort Monroe battlement. Similar communications terminals were used on USS *Comstock* during Trident Warrior 2008 (Fig. 6) to enable real-time bidirectional communications during Maritime Interdiction Operations (MIO) exercises on USNS *Yukon*. Similar NRL demonstrations were performed during the Trident Warrior 06 and Seahawk 07 exercises and for many years at NRL's lasercom test facility at the Chesapeake Bay Detachment.

Results: Several types of data at varying rates were transferred over the course of the Trident Spectre 2009 exercise. Multiple computers and high-resolution Internet protocol video cameras (2560 × 1920 pixels at Fort Story and 2048 × 1536 pixels at Fort Monroe) were connected to the optical link at Fort Story and

Fort Monroe through standard Ethernet switches. Laptop computers on either end were used to simultaneously display the multiple camera feeds, enable full net meeting functionality (duplex voice communication, chat, remote desktop, etc.), run packet error rate testing software, and conduct high-speed file transfers (greater than 100 MB transfers in approximately 45 s). The typical bandwidth used for simultaneous operation of all data sources was greater than 50 Mbps, with peak demonstrated data throughput of 91 Mbps. Using a special file transfer protocol developed at NRL, ABPACK, more than 1500 files were successfully transmitted via the link. Packet error rate testing was performed simultaneously with other network traffic over the course of the 3 days of testing with a measured average packet error rate of 0.2%. As demonstrated by the low average packet error rate, errors were rare and had no impact on network performance.

Summary: The Trident Spectre 2009 28-km direct lasercomm link was a complete success. The data link was established early each day of the 3-day demonstration and remained on throughout the day. Network



FIGURE 6
Michele Suite and the DMOI underway aboard
USS *Comstock* (LSD 45).

conductivity between Fort Story and Fort Monroe was maintained throughout the day, allowing a standard network connection between the two sites that typically do not have high-speed communications. All standard Ethernet traffic was successfully transmitted through the link, resulting in a highly reliable link that required almost no user intervention — as desired for any communication link. Use of this link or similar lasercom links for future Trident Spectre exercises and other exercises requiring high-speed conductivity is likely. The success of lasercom in numerous NRL demonstrations and its capabilities to augment standard radio frequency communications have pushed this technology to the point where operational military use of lasercom systems is probable in the very near future.

[Sponsored by ONR]

148

Elastomer-Steel Laminate Armor

C.M. Roland, D. Fragiadakis, and R.M. Gamache

151

Contaminant Monitoring in Ground and Surface Water

B.J. White, B.J. Melde, P.T. Charles, A.P. Malanoski, and M.A. Dinderman

153

Synfuel from Seawater

H.D. Willauer, D.R. Hardy, F. DiMascio, R.W. Dorner, and F.W. Williams

Elastomer-Steel Laminate Armor

C.M. Roland,¹ D. Fragiadakis,¹ and R.M. Gamache²

¹Chemistry Division

²Naval Surface Warfare Center, Indian Head

Introduction: The final countermeasure against bombs and bullets is mitigation of the effects of the blast or ballistic impact. The rise of terrorism has led to increased efforts to develop better armor, including lighter materials to expand the range of applications, for example to civilian infrastructure. Elastomeric coatings applied to building foundations minimize fragmentation from a bomb blast. This helps the building retain its structural integrity and also minimizes collateral damage (flying debris is the second leading cause of injury to occupants of a bombed building). Elastomers also increase the resistance to ballistic penetration when applied to hard substrates. This approach was an early method of “up-armoring” Marine Corps Humvees during Operation Iraqi Freedom. The initial coatings were elastomeric polyurea, which is easy to process and generally regarded as a mechanically “tough” material. However, since the operating mechanism of the coatings was unknown, the material could not be optimized.

The physics of ballistic penetration is complex, with the nature of the interaction and its effects dependent on the properties of both target and projectile. Moreover, rubber is viscoelastic, so that its mechanical behavior varies with deformation frequency.¹ This rate dependence can drastically alter the response — from liquid-like, to rubbery, to a glassy state — as the perturbation frequency increases. Since elastomers are also highly nonlinear (their properties depend on the magnitude of the strain), analysis of impact penetration can be difficult, requiring deconvolution of these effects.

Damage mitigation from elastomeric coatings likely relies on a variety of mechanisms. We have identified one important factor, in turn enabling critical aspects of the performance to be identified. The result has been the discovery of new and improved elastomeric coatings. Teaming with the Naval Surface Warfare Center, Indian Head Division (NSWC-IH), this led to the development of a laminate design that provides superior resistance to ballistic penetration, in combination with lower weight.

Ballistic Impact Response: The average strain rate for ballistic impact is the ratio of the projectile speed to the coating thickness, typically about 10^5 s^{-1} . The rate of motion of the segments (repeat units) of the chain molecules comprising the elastomer depends on temperature. For common elastomers, such as those

in tires, at room temperature these segmental motions occur at GHz and higher frequencies. However, for certain elastomers (including polyurea) they can be much slower. If this rate is on the order of the strain rate imposed by the impacting projectile, the polymer response will change from rubbery to glassy behavior (Fig. 1).² This impact-induced viscoelastic transition of the rubber is crucial for impact mitigation because the greatest energy dissipation occurs when segmental motion of the molecules occurs on the time scale of the external perturbation, causing the kinetic energy of the bullet to be converted to heat within the coating. Our tests showed that elastomers meeting this criterion had significantly higher penetration velocities (V_{50} , also known as the ballistic limit) for blunt projectiles.

Laminate Structures: Armor is always a compromise between performance and weight, and thinner elastomer coatings have lower V_{50} . However, there is a threshold around 3 mm, above which the performance changes weakly with thickness (Fig. 2). This means that the surface of the coating is dissipating a disproportionate amount of the impact energy. The near invariance of V_{50} to thickness can be exploited with a multilaminate structure. Various combinations of elastomer-steel layers were incorporated into armor structures; multiple layers always outperform single bilayers (Table 1).³

This approach was extended by making the coating itself a laminate of rubber and aluminum. With negligible increase in weight, this increases V_{50} by over 60% (Table 1). Using conventional “Rolled Homogeneous Armor,” more than twice the thickness would be required to achieve equivalent performance. A laminate construction forces a longer path-length for the incoming shock wave, due to impedance mismatching between the elastomer and metal. The multiple reflections break up the wave into a series of lower-amplitude waves. This is seen in the profuse, fragmented damage of the target (Fig. 3).

Summary: Elastomeric coatings can enhance the resistance of steel armor to high-speed projectiles. The requisite property is that the impact frequency be within the range of rates of segmental motion of the polymer molecules. Multiple bilayers further increase the ballistic limit by breakup and attenuation of the pressure wave due to impedance mismatching. Reduced weight, facile installation, use of commercially available materials, and multihit capability are among the advantages of the elastomeric coating, whose applications extend beyond military armor to include such uses as railway car and tanker protection, explosion barriers, and fragmentation protection panels.

[Sponsored by ONR]

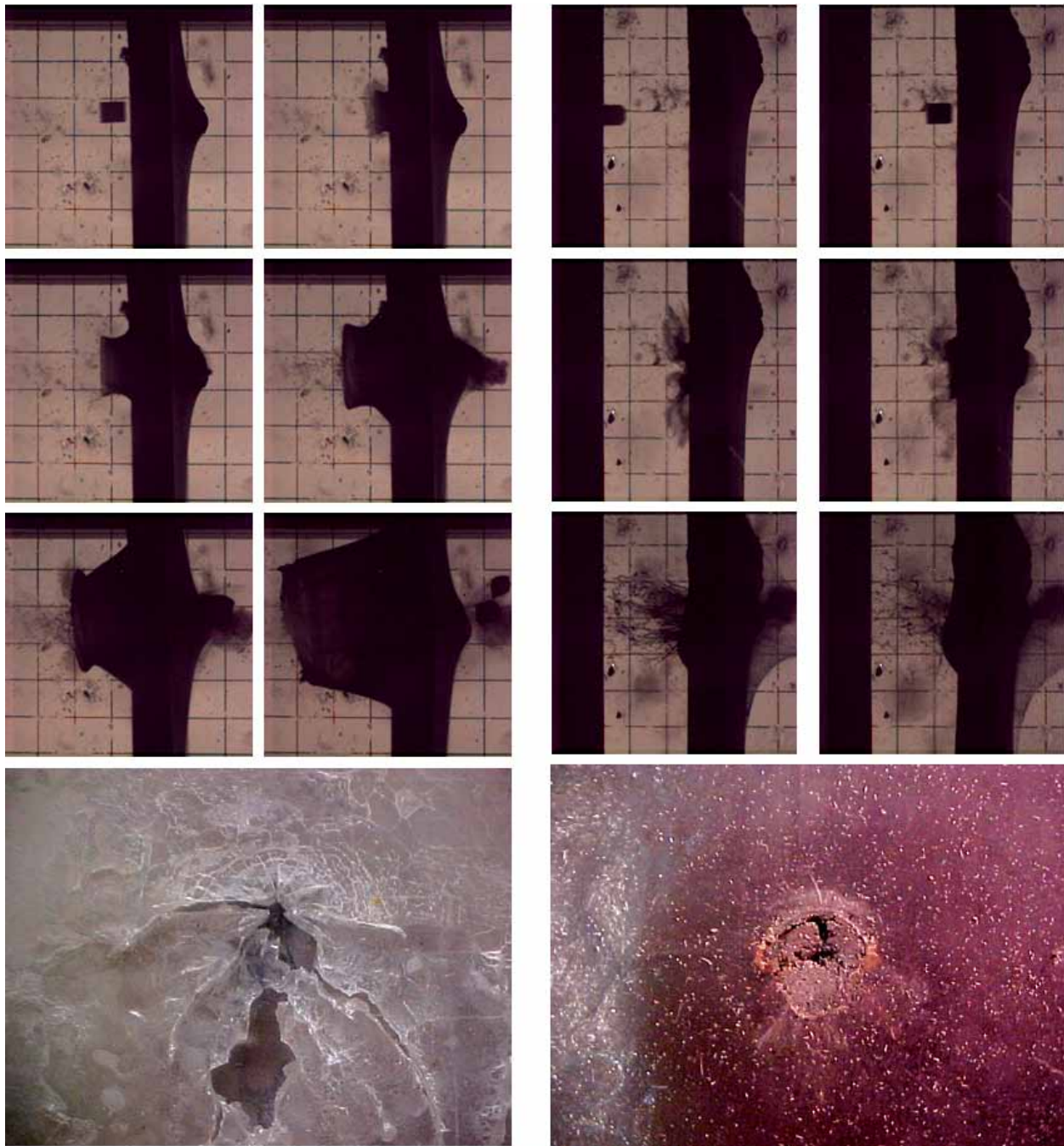


FIGURE 1

Left: Six high-speed photographs (top) of the impact response of a conventional elastomer responding in rubbery fashion with (bottom) substantial cracking. Right: The photographs (top) show the elastomer undergoing an impact-induced viscoelastic transition with (bottom) failure via shear-dominated separation of a cylindrical section of material having a cross section matching that of the blunt projectile. The projectile arrives from the left with a speed of ~ 900 m/s. The grid lines are spaced 25 mm apart.

References

- ¹ C.M. Roland, "Mechanical Behavior of Rubber at High Rates," *Rubber Chem. Technol.* **79**, 429–459 (2006).
- ² R.B. Bogoslovov, C.M. Roland, and R.M. Gamache, "Impact Induced Glass Transition in Elastomeric Coatings," *Appl. Phys. Lett.* **90**, 221910 (2007).
- ³ C.M. Roland, D. Fragiadakis, and R.M. Gamache, "Elastomer-Steel Laminate Armor," *Composite Struc.* **92**, 1059–1064 (2010).

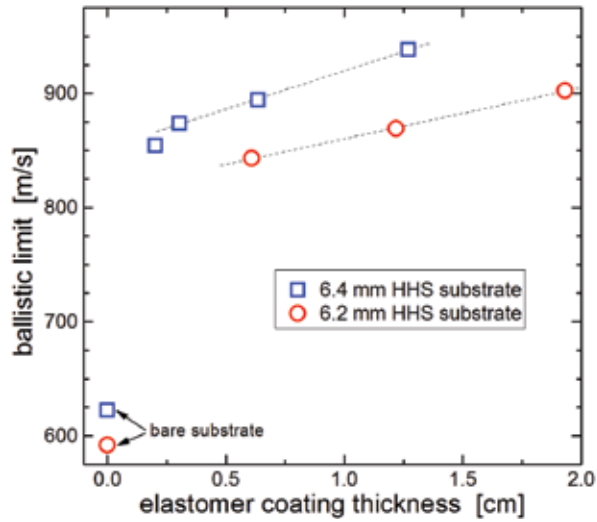


FIGURE 2
Variation in V_{50} for two steel plates as a function of the thickness of the elastomer coating (HHS = High Hard Steel). The dashed lines are the fits to the linear portion of the data, extrapolation of which gives a V_{50} much larger than that measured for the uncoated steel substrate.

TABLE 1—Effect of Front-Surface Elastomer Layers on Ballistic Limit of Steel Plates

| construction | steel layers | elastomer layers | areal density [†] (kg/m ²) | V_{50} (m/s) [®] |
|--------------|--------------------------|-----------------------------------|-------------------------------------------------|-----------------------------|
| single layer | one 12.7 mm [†] | none | 99 | 1097 ± 15 |
| single layer | one 12.7 mm [#] | none | 99 | 1184 ± 5 |
| bilayer | one 12.7 mm [#] | one 12.7 mm | 113 | 1483 ± 7 |
| four layers | two 6.4 mm [#] | two 6.4 mm | 113 | 1819 ± 2 |
| eight layers | four 3.2 mm [#] | four 3.2 mm | 113 | 1579 ± 7 |
| bilayer | one 12.7 mm [#] | one 6.4 mm | 106 | 1365 ± 6 |
| four layers | two 5.3 mm [#] | two 3.2 mm | 90 | 1457 ± 1 |
| single layer | one 5.3 mm [#] | none | 42 | 622 ± 7 |
| 21 layers | one 5.3 mm [#] | 6.1 mm total (21 soft) | 48 | 869 ± 1 |
| 21 layers | one 5.3 mm [#] | 6.1 mm total (11 soft / 10 hard)) | 51 | 1006 ± 5 |

[†]weight per unit area

[®] MIL-STD-662-F using 0.50 cal fragment simulating projectiles

[†]Rolled Homogeneous Armor

[#]High Hard Steel (MIL-A-46100)



FIGURE 3
Profuse damage accompanying penetration of laminate with 21 alternating elastomer and aluminum layers.

Contaminant Monitoring in Ground and Surface Water

B.J. White, B.J. Melde, P.T. Charles,
A.P. Malanoski, and M.A. Dinderman
Center for Bio/Molecular Science and Engineering

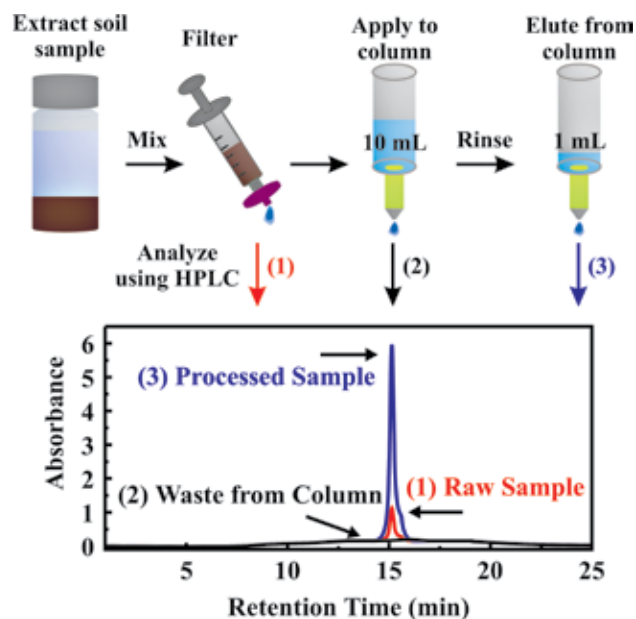
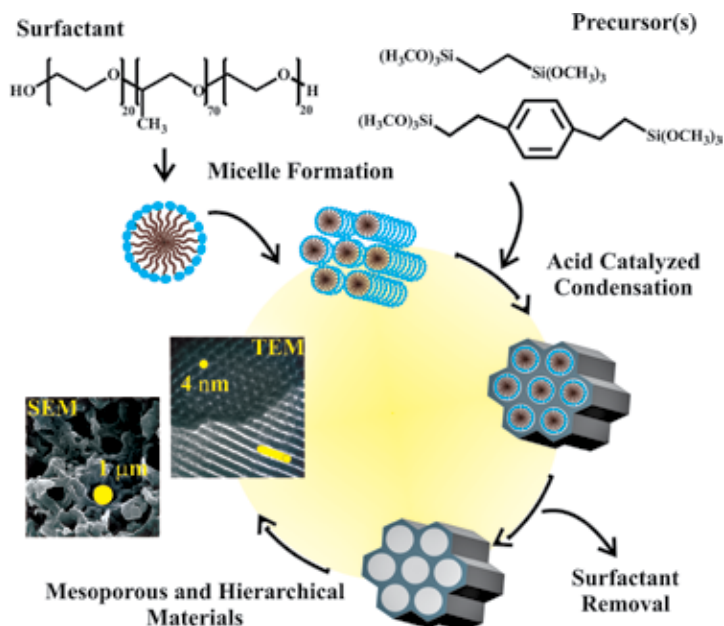
Contamination of Ordnance Ranges: The nitroenergetic compounds RDX (hexahydro-1,3,5-trinitro-1,3,5-triazine), HMX (octahydro-1,3,5,7-tetra-nitro-1,3,5,7-tetrazocine), TNT (2,4,6-trinitrotoluene), DNT (2,4-dinitrotoluene), and nitroglycerin (trinitroglycerin) are used as explosives and propellants in common ordnance. These compounds are present in the soil, ground water, and surface water at many U.S. Department of Defense (DoD) testing and training facilities as a result of the activities, both current and former, at those sites. Many of these compounds are cardioactive as well as suspected or confirmed carcinogens. There is concern regarding the ecological impact and the threat posed to personnel as a result of the persistence and distribution of nitroenergetic compounds.

Methods for monitoring levels of these compounds are needed to provide relevant data on the expansion of contaminated areas and the resulting threat to surrounding populations and wildlife. Monitoring the presence of such contaminants in the environment is challenging due to the rapid diffusion of targets into the surrounding matrix. Preconcentration of targets is often necessary to provide levels that are detectable by currently available technologies. Preconcentration involves processing a large volume of sample in order to provide a high concentration in a smaller volume. It is also often desirable to remove nontarget analytes from samples to prevent their interfering with evaluation of targets.

Novel Materials for Monitoring Contamination Levels: Preconcentration by solid-phase extraction (SPE) involves adsorbing targets onto a solid support. Desorption of target is accomplished either through a thermal process or through elution from the support using a solvent, resulting in more target in a smaller volume. Selective and semiselective adsorption can also help to eliminate nontarget compounds from the

FIGURE 4

Synthesis of porous sorbent materials. Synthesis begins with the formation of surfactant micelles in solution. The siloxane precursors are condensed around the organized micelles, which act as a template for the pore structure. After extraction of the surfactant, an organized system of pores of 2 to 8 nm diameter remains, as shown in the transmission electron microscopy (TEM) image. Coupling this templating process with a phase-separation process during synthesis produces the large pores (~1 μm) shown in the scanning electron microscopy (SEM) image.

**FIGURE 5**

Preconcentration of TNT. The sorbents have been applied to the preconcentration of TNT from soil extracts for enhanced detection. First, the soil is mixed with water to solubilize the contaminants. The particulate is then removed from the sample using filtration. A large volume of the resulting solution is applied to the sorbent column. Targets are then eluted from the column in a small volume of solvent. HPLC analysis shows the level of TNT to be quite low in the raw soil extract (1). The level of target washing through the column is undetectable (2). The concentration of TNT in the column eluent is significantly enhanced over that in the raw sample (3).

resulting sample. Our efforts in developing SPE materials have focused on periodic mesoporous organosilicas (PMOs), which are materials that combine organic groups with inorganic silica components to produce sorbents with the properties of both.^{1,2} The materials are rugged and stable, withstanding temperatures of up to 200 °C and a wide range of solvents and pH levels. The materials are synthesized as shown in Fig. 4. First, a surfactant is placed into solution at a

concentration high enough to force the formation of organized groups of molecules called micelles. Siloxane precursors, which have alternating organic and silicate groups, are then added to the solution. The conditions for condensation (polymerization) of the siloxanes are controlled through the concentrations of water, alcohol, acid, and additives in the solution. After curing, the surfactant can be washed out of the materials, leaving a porous framework with structure on two

length scales. As shown in Fig. 4, the resulting powders consist of particles that have large (~1 μm) spherical pores. In addition, there are much smaller pores (~5 nm) in the walls of the spherical pores. The small pores provide the desired high concentration of binding sites. The larger pores provide reduced resistance to liquid flow and increased connectivity throughout the structure.

Preconcentration of Contaminants: The powders can be packed into columns to provide a method for target preconcentration. When a volume of solution, ground water, surface water, or soil extract is passed through the column, the sorbent binds targets from the matrix. The column is then rinsed with water to remove any nontarget compounds. Finally, the sample is eluted from the column in a small volume of solvent such as acetonitrile. The result is that the target originally contained in 10 mL of water is now in 1 mL of solvent, an order of magnitude enhancement in concentration. As shown in Fig. 5, target that was undetectable in the raw solution is detected in the processed sample. Here, high performance liquid chromatography (HPLC) has been used for analysis of samples, but the same approach can be applied to in situ detection technologies. For example, the sorbents can be used to preconcentrate targets prior to analysis by portable electrochemical detectors or ion mobility spectrometers.

Applications: This sorbent technology was originally developed with a view toward environmental monitoring in areas on or near DoD sites of potential contamination. The techniques described can, however, be applied to monitoring in other situations, for example in the search for underwater unexploded ordnance (UXO). While the primary targets of interest have been nitroenergetics, the techniques described can also be used to synthesize sorbents applicable to the preconcentration of other targets of interest such as perchlorates, solvents, and organophosphates. The materials and approaches described provide enhanced capability to detection techniques that have traditionally been limited to laboratory applications, offering the potential to put protective detection capabilities on site and in the hands of military personnel.

[Sponsored by NRL and SERDP]

References

- ¹ B.J. Johnson, B.J. Melde, P.T. Charles, D.C. Cardona, M.A. Dinderman, A.P. Malanoski, and S.B. Qadri, "Imprinted Nanoporous Organosilicas for Selective Adsorption of Nitroenergetic Targets," *Langmuir* **24**(16), 9024–9029 (2008), doi:10.1021/la800615y.
- ² B.J. Melde, B.J. Johnson, M.A. Dinderman, and J.R. Deschamps, "Macroporous Periodic Mesoporous Organosilicas

with Diethylbenzene Bridging Groups," *Microporous and Mesoporous Materials* **130**, 180–188 (2010) doi:10.1016/j.micromeso.2009.11.003.

Synfuel from Seawater

H.D. Willauer,¹ D.R. Hardy,¹ F. DiMascio,²
R.W. Dorner,³ and F.W. Williams¹

¹Chemistry Division

²Office of Naval Research

³NRL/NRC Postdoctoral Research Associate

Introduction: NRL's Navy Technology Center for Safety and Survivability is developing a novel ocean-based capability that combines carbon dioxide and hydrogen captured from seawater for the synthesis of jet fuel at sea. In-theater, synthetic fuel production is a "game changing" proposition that will offer the Navy significant logistical and operational advantages by reducing dependence on increasingly expensive fossil fuels and by reducing fuel logistic tails and their vulnerabilities. From an environmental perspective, such a process could be considered carbon dioxide neutral since carbon dioxide is removed from the ocean and converted into a liquid hydrocarbon fuel. Upon combustion of the fuel, carbon dioxide is returned to the atmosphere where it re-equilibrates with the ocean to complete the natural carbon cycle. In addition, the synthetic hydrocarbon fuel would replace petroleum-derived fossil fuel to eliminate the emissions (sulfur and nitrogen oxides) that are produced from the combustion of these fuels by the Navy.

Carbon Capture: The world's oceans contain approximately 100 mg/L of carbon dioxide, of which 2% to 3% of the carbon dioxide is dissolved carbon dioxide gas in the form of carbonic acid, 1% is carbonate, and the remaining 96% to 97% is bound as bicarbonate. On a weight per volume basis, carbon dioxide concentration in the ocean is about 140 times greater than in air, thus making this source of carbon ideal for a synthetic fuel process at sea. However, developing the technologies to capture sufficient quantities of carbon dioxide from seawater fast enough and efficiently is a significant research challenge. NRL researchers have made breakthroughs in the development of an electrochemical cell that is able to extract all the dissolved gas and ionically bound carbon dioxide from seawater. The ion exchange materials incorporated into the cell re-equilibrate carbonate and bicarbonate in the seawater to carbon dioxide gas. The ion exchange materials offer the ability to operate at high flow rates and can be used in a wide variety of salt water compositions, which makes them ideal for this sea-based application.

In addition to carbon dioxide, the cell can produce a portion of the hydrogen needed for the hydrocarbon synthesis process with no additional energy penalty. The process efficiency, the ability to produce a portion of the hydrogen needed for the synthesis process, and the ability to regenerate the ion exchange material without the use of caustic chemicals, have made this technology superior to membrane and anion exchange processes previously developed and tested by NRL for use at sea.

Synfuel Production: The key challenge with using carbon dioxide as a chemical feedstock for production of liquid fuel is its great chemical stability. One of the few avenues open for chemical reaction is that with hydrogen. Carbon dioxide has been thought of as having too high an energy barrier for polymerization, even in the presence of a catalyst. To overcome these challenges, novel approaches in catalyst development by NRL researchers have led to thermodynamic improvements in the heterogeneous catalysis of the carbon dioxide and hydrogen to hydrocarbons. A two-step approach by NRL is shown in Fig. 6. In the first step of the approach, a key breakthrough is the development of an iron-based catalyst. Using this catalyst, we have achieved carbon dioxide conversion levels

up to 42% and have decreased unwanted methane production from 97% to 26% in favor of longer-chain unsaturated hydrocarbons. Further modification of the catalyst support has also led to increases in carbon dioxide conversion levels up to 50%. The second step of the approach, which is the subject of current efforts, involves the oligomerization of the olefins to jet fuel by a second solid acid catalyst such as zeolite.

The Future of Synfuel at Sea: We are now set to begin experiments to transition the carbon capture electrochemical cell from the laboratory to a littoral environment where carbon dioxide and hydrogen can be produced in quantities far above those achieved at the laboratory scale. There are many challenges to scaling this technology, including design, ion exchange material regeneration, process efficiency, water fouling, and power requirements. We are also facing great challenges in the effort to oligomerize olefins to a jet fuel fraction by solid acid zeolite catalysts. By modifying the pore size and acidity of the catalyst surface, we envision control over the liquid fuel fraction and yield.

[Sponsored by ONR and NRL]

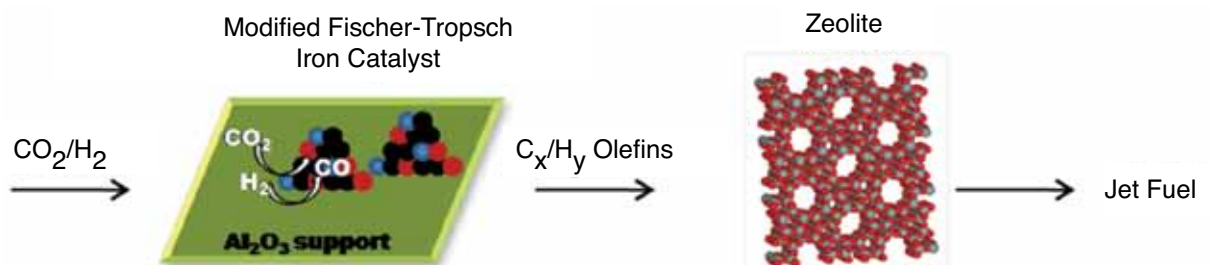


FIGURE 6
Carbon dioxide and hydrogen conversion over a modified Fischer-Tropsch iron catalyst.

156

Improvements to Towed Decoys to Enhance Aircraft Survivability

G. T. Roan

159

Adaptive Jamming Cancellation in Radar

V. Gregers-Hansen, R. Mital, and J. Cook

162

Laser System for Protection of Navy Ships

P. Mak and C. Maraviglia

165

Particle Filters for Multipath Mitigation

M. Hock and K. Lee

167

A New Gallium Nitride-based Switch for High Efficiency Power Electronics

T.J. Anderson, M.J. Tadjer, M.A. Mastro, J.K. Hite, K.D. Hobart, C.R. Eddy, Jr., and F.J. Kub

Improvements to Towed Decoys to Enhance Aircraft Survivability

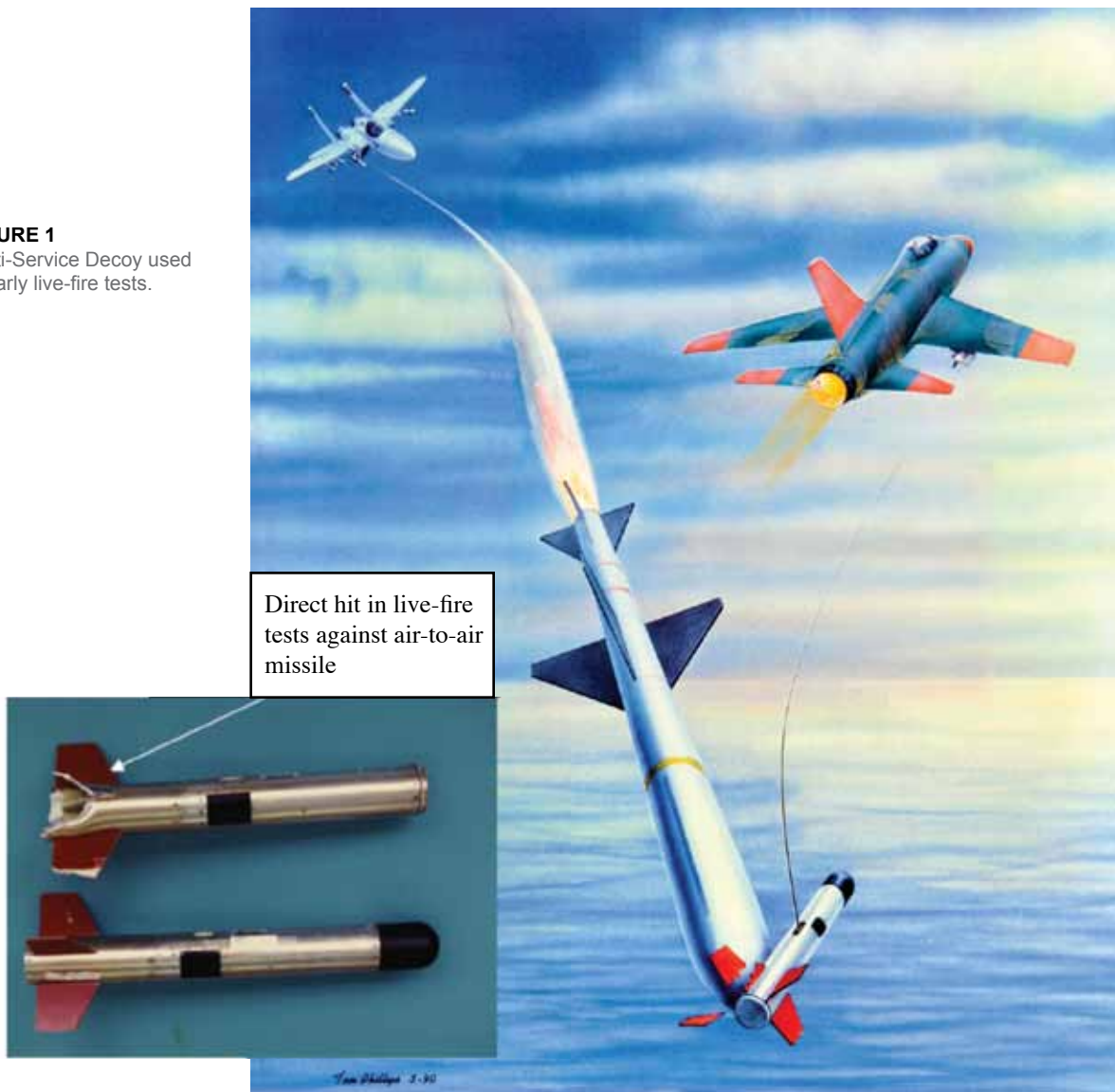
G.T. Roan

Tactical Electronic Warfare Division

Introduction: The towed decoy, which was developed by the Naval Research Laboratory in the early 1980s, has proven itself to be an effective countermeasure to radar-guided antiaircraft weaponry. The first-generation towed decoys repeat the radar signal electronically using a transmitter physically separated in angle from the defending aircraft. The repeater decoy then acts as a beacon for the radar to divert the weapon away from the aircraft. Figure 1 shows a

photograph of the NRL prototype, the Multi-Service Decoy, which was struck by an air-to-air missile in an early live-fire test. This proof of principle led to the production of the AN/ALE-50 Advanced Airborne Expendable Decoy that is currently operational on Air Force F-16 and B-1 and Navy F/A-18 aircraft. A second-generation towed decoy will soon become operational on the Navy's F/A-18 E/F Super Hornet: the AN/ALE-55 Fiber Optic Towed Decoy (FOTD) of the Integrated Defensive Electronic Countermeasures (IDECM) System. With an FOTD, a more complex electronic countermeasures waveform can be generated onboard the aircraft and communicated to the decoy through the towline. Unfortunately, both towed decoys have been beset with problems on the Super

FIGURE 1
Multi-Service Decoy used
in early live-fire tests.



Hornet because during combat maneuvers, the towline is exposed to hot engine exhaust gases that can far exceed 500 °C. The hot gases lead either to mechanical failure of the towline or optical fiber or to electrical failure of the wiring in the towline in some portions of the aircraft's flight envelope. As a result, availability of the decoy is significantly limited while the aircraft is maneuvering. NRL's Tactical Electronic Warfare Division (TEWD), working with the Chemistry and the Materials Science and Technology Divisions and with industry, has developed a range of improvements to the towline components, the launcher, and the decoy itself to enhance decoy survivability and therefore aircraft survivability during combat operations.

Recent Research and Development: A decoy towline that includes an optical fiber is shown notionally in Fig. 2. Polyimide is normally used as wire insulation because of the requirements for high dielectric strength and for sufficient flexibility to pass a minimum bend radius of 6 mm. NRL researchers have focused on two materials with improved capability to function in the exhaust plume: a thermo-oxidatively stable polymer known as poly(carborane-siloxane-acetylene), or PCSA,¹ and silica microtubing. A 12 μm coating of PCSA over a 75 μm coating of polyimide raised the functional temperature of a pair of polyimide wires from 500 °C to 630 °C with a 5000 V potential difference, with little or no reduction in flexibility. PCSA was developed by NRL and is manufactured by Triton Systems Incorporated under NRL direction. Higher temperatures of operation have been achieved using small-diameter (~350 μm) silica tubing with a wire in the center that is quite flexible (less than 6 mm bend radius) and yet capable of carrying electrical current at 5000 V at temperatures of up to 1000 °C.

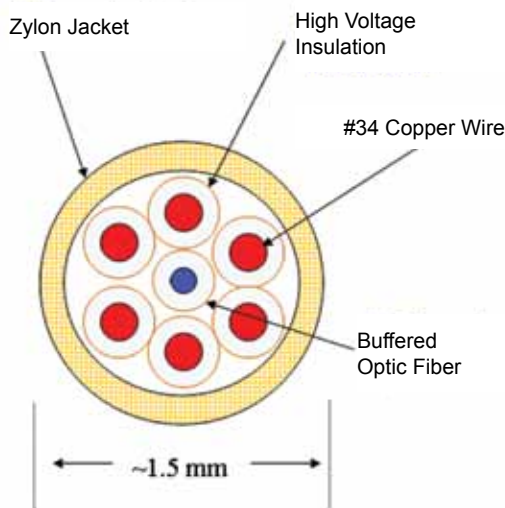


FIGURE 2
Notional towline for a fiber optic towed decoy.

Unfortunately, the silica-insulated wire has been too brittle to be used in the current towline, but modifications to the launcher under consideration may enable its use in the near future. The silica-insulated wire is manufactured by Polymicro under an NRL patent.²

Researchers at both NRL and Meggitt Defense Systems are working to improve the tensile strength of the towline in the exhaust plume. In the current towline, Zylon, also known as PBO, provides adequate tensile strength at low temperature but it loses 50% tensile strength at 500 °C, and it weakens in the presence of water vapor and in sunlight. NRL is experimenting with towlines made using carbon fibers that have a higher tensile strength than Zylon at room temperature, and in a flame test at 1200 °C, a carbon fiber towline under 400 N of tension survives for 37 s as opposed to 2 s for Zylon. Unfortunately, carbon fibers burn in air, and a means to slow the combustion rate remains under investigation. Alternatively, Meggitt has constructed a hybrid towline using a noncombustible ceramic fiber called Nextel. Nextel is weaker than either Zylon or carbon fiber at room temperature, but a hybrid Nextel/Zylon towline maintains a tensile strength of 445 N at a temperature of 650 °C where Zylon decomposes. Two test flights have been carried out on an F/A-18 E/F using the hybrid Nextel/Zylon towline with promising results.

NRL and Meggitt Defense Systems are developing modifications to the decoy launcher to reduce the stress applied to the towline. The F/A-18 E/F decoy launcher has a capacity for three single-use (expendable) decoy canisters, each containing a decoy, several hundred feet of towline, and the spool and brake assembly within a volume of 7 cm by 7 cm by 48 cm. In the standard launcher, the decoy is ejected at a velocity of 9 m/s using an explosive charge called a squib and the decoy is severed (not recovered) at the end of a mission. This explosive deployment places a high load on the towline at launch. Meggitt has developed a new magazine that slides into the existing launcher on the Super Hornet and ejects the decoy at a lower velocity (~5 m/s) using a spring. Once ejected from the launcher, the decoy is accelerated by the airstream drag as the towline spools from a free spinning reel assembly. Due to the low friction of the free spinning reel and the high acceleration of the decoy and towline by airstream drag, the decoy is fully deployed in less time than the standard launch using a squib, and with reduced strain on the towline. The strain on the towline is further reduced through a change to the AN/ALE-55 decoy fin assembly. The new magazine is also capable of recovering the decoy after a mission, potentially saving the Navy millions of dollars through reuse of decoys.

Future Navy decoys will benefit from ongoing research into wide bandgap semiconductors (WBGs) such as silicon carbide (SiC) and gallium nitride (GaN). Current towed decoys, the AN/ALE-50 and AN/ALE-55, use a vacuum tube known as a traveling wave tube (TWT) to supply the RF power over a wide frequency range. Under a WBGs program sponsored by the Office of Naval Research (ONR) and the Defense Advanced Research Projects Agency (DARPA), microwave monolithic integrated circuit (MMIC) devices are being produced for use in solid-state power amplifiers that can now compete with the TWT in power and bandwidth. The MMIC operate at voltages between 20 and 50 V as compared to 2000 to 5000 V for a TWT, which is advantageous because a low-voltage towline is much less expensive to build than a towline carrying several thousand volts. Potentially, a solid-state RF power amplifier would cost thousands of dollars less than the TWT equivalent due to the economy of large-scale integrated circuit manufacturing.

In a demonstration project, NRL TEWD teamed with Cree, Inc., and Keragis Corporation to build a

prototype of a solid-state decoy using GaN MMIC. Cree³ developed the high-power GaN MMIC on a GaN/SiC substrate that measures 4 mm by 3 mm by 0.05 mm. Six of the MMIC devices were inserted into a novel, 5-cm-diameter cylindrical power combiner, built by Keragis, which provides an excellent thermal path to the airstream for dissipation of the heat generated by the power MMIC. Figure 3 shows the solid-state towed decoy with the two power combiners.

Summary: NRL research led to the development of the towed decoy for the self-protection of Navy and Air Force aircraft from modern radar-guided weapons. Recent multidisciplinary research and development is adding to the operational capabilities of the towed decoy with new towlines capable of operating in a high-temperature exhaust plume, improved methods of deployment and recovery, and solid-state decoys with better reliability and lower lifecycle cost.

Acknowledgments: The author gratefully acknowledges the support of this work by the Office of Naval Research under Program Element 0603123N.

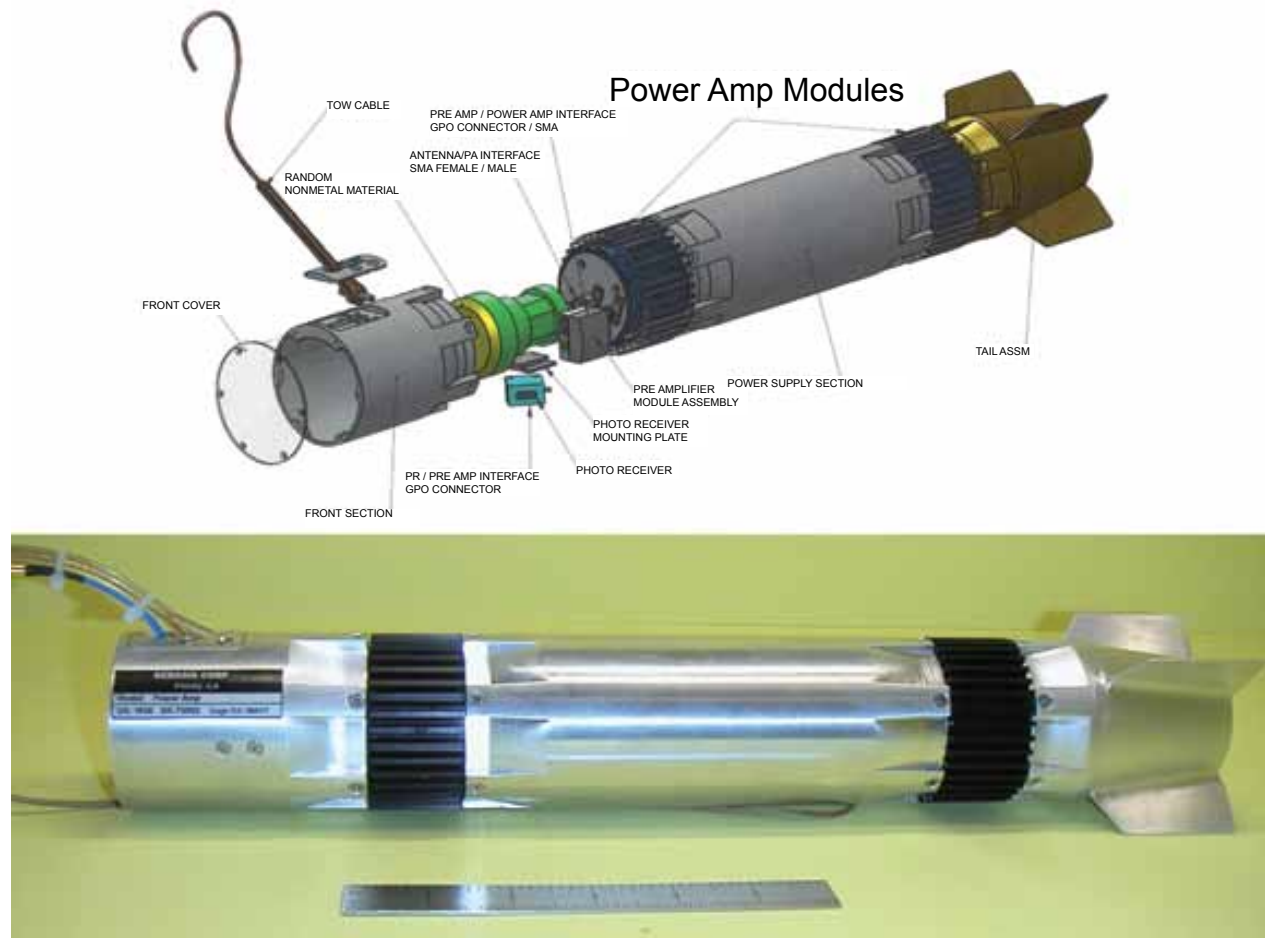


FIGURE 3 Solid state towed decoy prototype with a pair of GaN solid state amplifiers.

The author also acknowledges the contributions of NRL coresearchers Teddy Keller and Manoj Kolel-Veetil of the Chemistry Division, and Ron Tonucci and Harry Jones of the Materials Science and Technology Division.

[Sponsored by ONR]

References

- ¹ M.K. Kolel-Veetil and T.M. Keller, "Polymeric Protection of Navy Fighter Jet Towlines," *2007 NRL Review*, pp. 147–148 (2008).
- ² R.J. Tonucci and G. Roan, "High Voltage High Temperature Wire," United States Patent 7,002,072, Feb. 21, 2006.
- ³ J.W. Milligan, S. Sheppard, W. Pribble, A. Ward, and S. Wood, "SiC and GaN Wide Bandgap Technology Commercial Status," International Conference on Compound Semiconductor Manufacturing Technology, April 14–17, 2008, Chicago, IL.

Adaptive Jamming Cancellation in Radar

V. Gregers-Hansen, R. Mital, and J. Cook
Radar Division

Introduction: The new core mission for the Navy is integrated air and missile defense (IAMD). This combines conventional anti-air warfare (AAW) against aircraft and missiles, with ballistic missile defense (BMD) against short- and medium-range ballistic missile threats to Navy sea-based assets or high-value land-based targets. New radars designed to support this mission must meet difficult requirements for very long range detection and discrimination of lethal objects, and provide high-precision weapons control. All of these requirements must be achieved while incurring little to no degradation in performance in the presence of anticipated intense electronic attack (EA) while operating in an environment of heavy clutter and interference. While the entire gamut of EA techniques must be considered in the radar design, the specific threat of high-power barrage noise jamming

from long-range standoff jammers is of particular concern.

Traditional radar approaches dealing with the standoff jamming threat consist of a combination of low antenna sidelobes and adaptive nulling techniques. Because in many cases low antenna sidelobes alone cannot mitigate standoff jammers, adaptive jamming cancellation systems are added to the radar to reduce jamming residues to an acceptable level.¹ Adaptive jamming cancellation systems have often failed to meet expectations due to a lack of understanding of factors such as system bandwidth, multipath reflections, number of simultaneous jammers, and hardware tolerances and inefficiencies. A research project in the Radar Division is seeking to improve the understanding of these limitations through a high-fidelity modeling and simulation effort. This article gives a brief overview of sidelobe canceller implementations, presents the development of a suitable simulation model, and provides performance predictions for a specific sidelobe canceller design.

Jamming Scenario Assumed: A typical jamming scenario confronted by a Navy radar is illustrated in Fig. 4. The scenario includes a number of simultaneous jamming platforms ($N_j = 4$ shown), each at range R_j and with an effective radiated power density (ERP) defined in units of dBW/MHz. It is assumed that the combination of jammer ERP and its standoff range results in a jamming-to-noise ratio (JNR) in an isotropic sidelobe of JNR = 30 dB. The jammers are distributed over an angular threat sector ($\pm 30^\circ$ shown in Fig. 4) and at specified elevation angles. If any of the jammers enters the main beam region, supplementary main beam cancellation techniques would be required but this aspect of performance is not addressed here. In a typical at-sea environment, the jamming signals can enter the radar antennas via direct and indirect paths. The indirect path is the "multipath" signal defined by its relative amplitude and time delay as it enters the radar antennas.

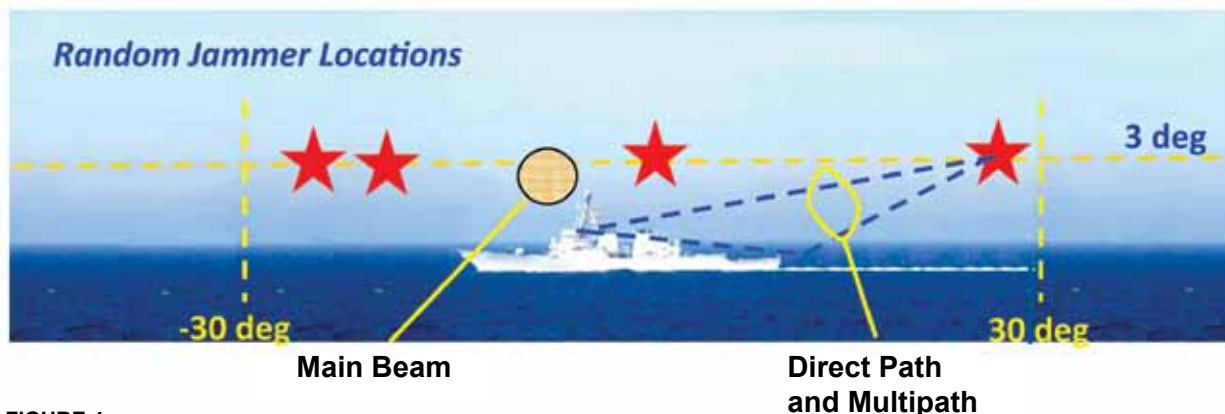


FIGURE 4

Notional jamming environment; jammers are randomly located across the $\pm 30^\circ$ angular sector but outside the main beam.

Dispersion of the received jamming across the spatial extent of the main and auxiliary antennas becomes a limiting factor on performance when jamming suppression over a wide bandwidth is required. The effect of dispersion is greatest for jammers furthest away from array boresight.

Sidelobe Canceller (SLC) Simulation: The objective of an SLC system is to suppress jamming received through the sidelobes of a radar antenna. Using a number of additional antenna elements, usually designated as the auxiliary (AUX) antennas, it is possible to place nulls in the directions of the interfering signals by subtracting weighted versions of the signal received in the AUX antennas. A simple block diagram of a sidelobe cancellation system is shown in Fig. 5. For the simulation results presented in the next section, a main antenna array with a 4 m diameter ($D = 4$ m) is assumed. This figure shows $N_A = 4$ AUX antennas placed along the perimeter of the main array at locations that are selected randomly within each of four quadrants. For practical reasons, no auxiliary antennas are usually located inside the main array. The maximum number of nulls that can be placed in the direction of jammers is equal to the number of AUX antennas. Also shown in Fig. 5 is the use of “fast taps” at the output of each AUX antenna spaced in time by Δ seconds. These fast taps ($L = 3$) do not

allow the sidelobe canceller to suppress additional jammers, but they can improve cancellation performance, particularly against wide bandwidth jamming and multipath. Thus, a total of $N_A \cdot L$ channels weighted by an identical number of complex weights ($\tilde{w} = (w_1, w_2, \dots, w_{N_A \cdot L})$) are used to suppress the jamming received in the main channel. The computation of these adaptive weights is based on a number N_s of complex samples collected simultaneously from the main and AUX channel using a suitable algorithm. For the results presented here, use of the near optimal sample matrix inversion technique is assumed.

In the sidelobe canceller simulation, all channels are bandpass filtered in Gaussian filters of bandwidth B . The jamming entering the radar antennas has a rectangular bandwidth of width $4 \cdot B$ and is sampled at its respective Nyquist rate. This complex-sampling rate of $4 \cdot B$ is maintained through the signal processor. The simulation of the sidelobe canceller system shown in Fig. 5 takes into account all group and phase delays based on jammer angular locations and antenna phase centers. While the phase centers of the AUX antennas are accurately characterized by their physical location, the phase center of the main antenna in the sidelobe region is a random variable determined by the specific sidelobe characteristics in the jammer direction. In the simulation, a horizontal linear array of elements is used to represent the actual circular array in the

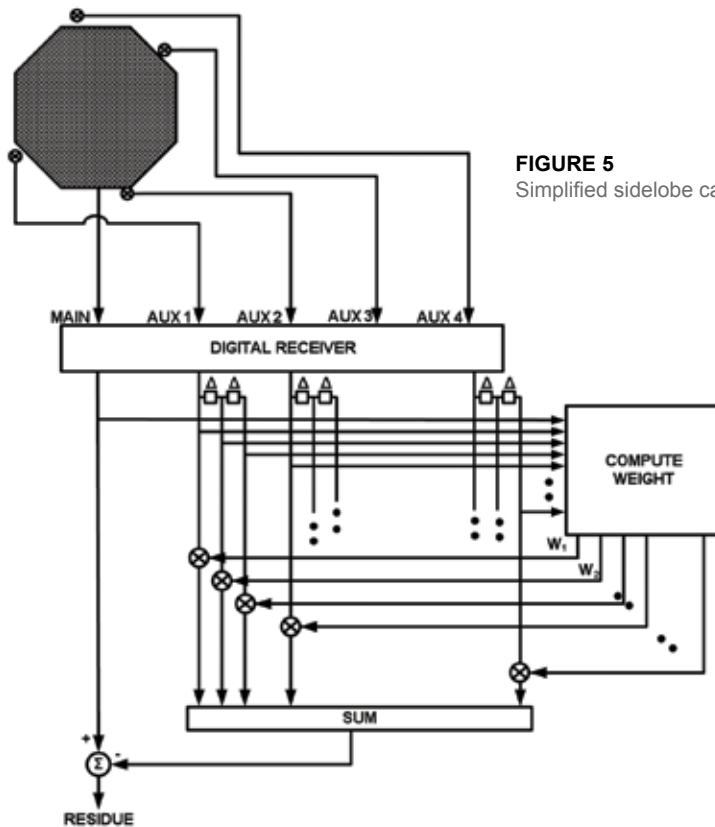


FIGURE 5
Simplified sidelobe canceller block diagram.

simulation. This approximation is valid since the jammers are all at almost the same elevation angle but widely distributed in azimuth. Using this simplification, the array can be represented by a linear array of $N_{EL} = 88$ elements rather than about 6000 as needed to populate a 4 m diameter array at S-band. The linear array is weighted by a 50 dB Taylor function, and random amplitude and phase errors are added at each element to result in a median sidelobe level of around -10 dBi. The AUX antenna gain is assumed to be $G_{AUX} = 8$ dB. Both main antenna sidelobes and the AUX gain pattern are modulated by the same element pattern. With this representation of the main antenna, its impulse response from any jammer directions is simply given by the element weights with a time-tap spacing given by the projection of the element spacing on the jammer direction. From this tapped delay line representation, the frequency response of the array to the jamming can be calculated using the *chirp-transform* technique. The operation of the coherent

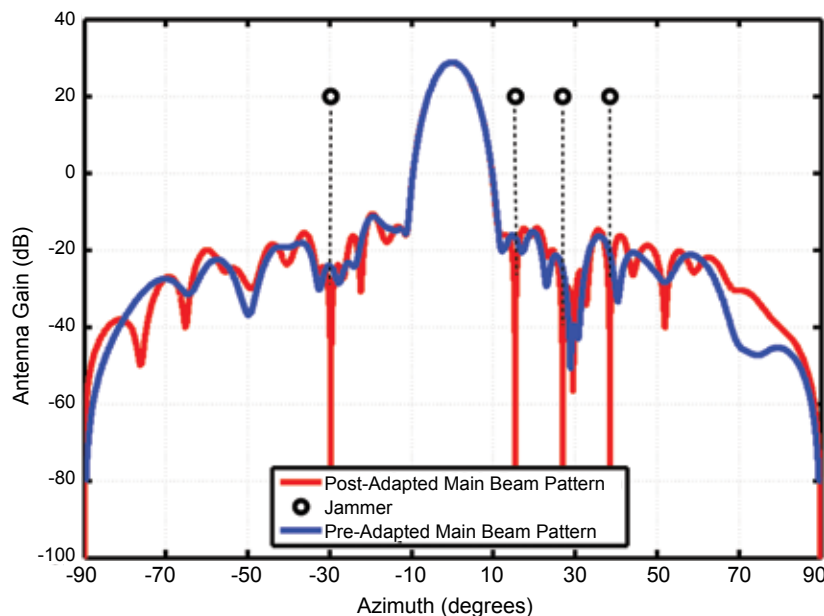


FIGURE 6
Illustration of nulling of four jammers by adaptive sidelobe cancellation (SLC).

sidelobe canceller is illustrated in Fig. 6, showing the effective sidelobe pattern of the main antenna in the presence of four jammers before and after jamming cancellation.

Simulation Results: The performance results assume a scenario with four standoff jammers as previously described. It is desired to design a sidelobe cancellation system that will suppress jamming over a $B = 50$ MHz bandwidth such that the *jamming-plus-thermal noise to thermal noise* ratio is less than 5

dB with a 90% probability. Figure 7 shows four key performance trade-offs leading to such a design. In Fig. 7(a), the number of auxiliary antennas is varied between two and eight for a relatively narrow bandwidth of $B = 1$ MHz. With only $N_A = 2$ or 3 AUX antennas, performance is poor because the system has insufficient degrees of freedom to create nulls in four directions simultaneously. For $N_A = 4$, performance is much improved but ill conditioning results in occasional larger residues. Therefore, the number of AUX antennas for our design example was chosen as $N_A = 6$.

Figure 7(b) shows the effect of increasing the system bandwidth beyond the 1 MHz value assumed for Fig. 7(a). It can be seen that for a 50 MHz bandwidth, performance is significantly worse than the requirement due to time-delay and dispersion effects.

In Fig. 7(c), fast time taps have been added to the basic sidelobe canceller, as shown in Fig. 5. The tap spacing was 2 ns ($\sim 0.1/B$), and the number of equidistant taps was varied from one to four. It can be seen that $L = 3$ results in a sidelobe canceller design meeting the requirement.

Finally, Fig. 7(d) shows the effect of the number of samples from each channel used to calculate the weights. All previous results used a large number of samples ($N_s = 8092$) to approximate optimum performance. In Fig. 7(d), the number of samples was reduced to as few as 64. To avoid significant performance degradation due to inadequate sample support, use of at least $N_s = 128$ samples is required.

Conclusion: A modeling and simulation effort to predict the performance of a sidelobe canceller has been described. As an example of the use of this model, a sidelobe canceller design for suppression of

jamming from $N_j = 4$ independent jamming sources with a system bandwidth of 50 MHz to a residue level of less than 5 dB above thermal noise with a 90% probability was considered. The resulting design requires four AUX antennas, three fast taps per channel spaced by 2 ns, and at least 128 training samples per channel.

Other features of the simulation model developed under this project include the modeling of multipath effects from the sea surface, also known as “hot clutter,” and main beam jamming cancellation using high-gain AUX antennas. A complete description

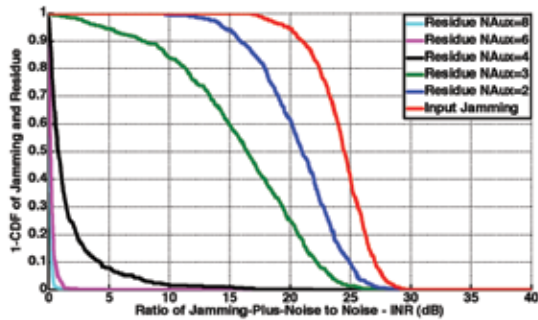


FIGURE 7(a)
Effect of number of auxiliary antennas on SLC performance for $N_J = 4$ jammers and bandwidth $B = 1$ MHz.

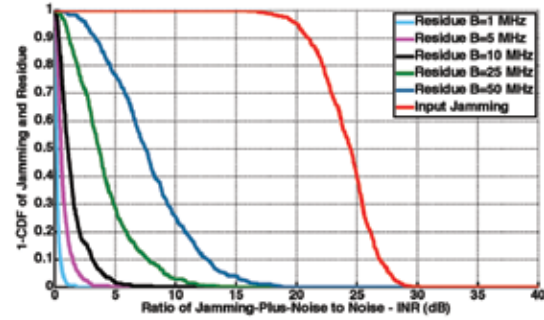


FIGURE 7(b)
Effect of radar bandwidth on SLC performance for a fixed number of jammers and auxiliary antennas ($N_J = 4$ and $N_A = 6$).

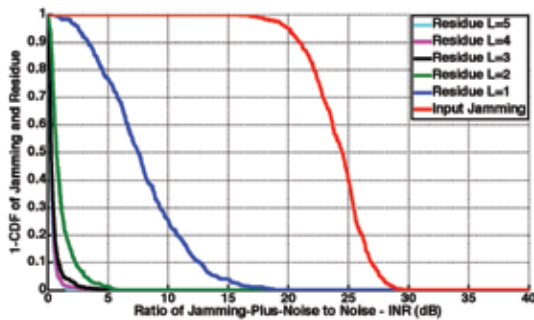


FIGURE 7(c)
Effect of the number of fast taps with 2-ns spacing on SLC performance for $N_J = 4$ jammers, $N_A = 6$ auxiliary antennas, and a $B = 50$ MHz system bandwidth.

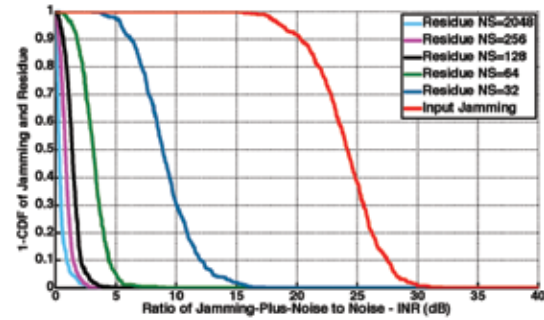


FIGURE 7(d)
Effect of number of training samples on SLC performance for $N_J = 4$, $N_A = 6$, 3 fast taps with 2-ns spacing, and a 50 MHz bandwidth.

of this work will be included in a forthcoming NRL Report.

[Sponsored by NRL]

Reference

¹ R.A. Monzingo and T.W. Miller, *Introduction to Adaptive Arrays* (John Wiley & Sons, New York, NY, 1980).

Laser System for Protection of Navy Ships

P. Mak and C. Maraviglia
Tactical Electronic Warfare Division

Introduction: Antiship missiles (ASM) are an acknowledged threat to U.S. Navy ships. Many of these missiles are TV-guided, infrared-guided, or have an operator-in-the-loop in the terminal phase of their engagement. Improved ship survivability against these optically guided and imaging threats requires the development of a laser-based, multiband countermeasure (CM) capability that will also enable an onboard/offboard response against advanced threats if necessary. We describe here the development, fabrication, and testing of a laser-based, smart jamming electro-optic/infrared (EO/IR) CM system called SHIELDS

(Shipboard Integrated Electro-optic Defense System), which is designed to counter currently deployed and emerging ASM threats.

System Description: NRL's research on laser-based IRCM for ship defense since the late 1980s had generated a set of EO/IR CM requirements based upon which Lockheed Martin developed and fabricated SHIELDS. SHIELDS was designed to perform the following functions when engaging an ASM: acquire the missile threat after a target handoff from a radar or an IR search and track system; track the target; turn the lasers on for active tracking and target interrogation; perform smart jamming; and evaluate CM effectiveness. SHIELDS comprises the following subsystems: a multifunction IR camera, a high-frame-rate visible camera, a multiband IR/visible laser system (MIRVLS), a stabilized optical pointer, an optical assembly/turret, and a universal processor (UP). Most of these components are form and function compatible with the shipboard version to ease technology transition.

The IR camera has a narrow field of view (FOV) and a high-resolution focal plane array (FPA) for target detection and tracking. It is also used for active detection/tracking and target interrogation when engaging an in-band threat. The high sensitivity and

resolution of the camera provide a shipboard capability to evaluate the effectiveness of soft-kill or hard-kill CM by monitoring the target's response to the CM. The camera has a variable frame rate to meet various performance requirements. The TV camera has the same FOV and a high-resolution detector FPA. It performs the same functions as the IR camera.

The key components of MIRVLS, developed by BAE Systems, are a thulium fiber laser, a holmium-doped YAG laser, and two wavelength converters. The fiber laser pumps the YAG laser, which sequentially pumps an IR wavelength converter and a visible wavelength converter to generate IR and visible outputs, respectively. The pulsed laser is comprised of three modules: a shoe box sized optical head, the fiber laser, and an electronic control unit. The laser output waveform is controlled by the pump diodes in the fiber laser. The laser functions are active target tracking, target interrogation, and jamming.

The field of regard of the EO/IR sensors and laser beam steering are controlled by a stabilized optical pointer (SOP). The SOP has a gimballed mirror assembly (GMA) that can rotate to any position within 360° in 0.6 s. With this agile component, SHIELDS will be capable of engaging multiple targets rapidly. The SOP will provide horizontal coverage against sea-skimming threats and is stabilized for a surface combatant up to sea state 5.

To minimize the SOP size and the complexity of the SHIELDS optical train, all of the transceiver and

optical components are integrated into a common optical path. This common path includes the external window, SOP pointing mirror, MIRVLS, EO/IR cameras, and beam-combining elements. All alignment-critical components are mounted rigidly to an optical bench, which is supported at four corners by shock/vibration isolators. The optical assembly and the SOP are installed inside a turret as shown in Fig. 8. The Rotating Environmental Hood (REH) is slaved to the SOP/GMA azimuth position and provides mechanical isolation from external forces (such as wind load and hood friction).

The functions of the UP are threat management, acquisition, tracking, SOP motion control, EO/IR closed-loop CM, system control, and interfaces to other SHIELDS subsystems. The UP has six VME boards. Core SHIELDS processing is performed by a two-board commercial-off-the-shelf module (for motion control) and two custom boards that combine the strengths of the PowerPC with an array of very high-density field programmable gate arrays to perform SHIELDS track processing and countermeasure functions.

All of the aforementioned subsystems, components, a host computer, data acquisition system, mass data storage, and associated power supplies and controls are installed in an 8-ft × 8-ft × 20-ft shelter as shown in Fig. 9, which also includes a SHIELDS system block diagram. The turret sits inside the shelter during system checkout, laser alignment or adjustment, and

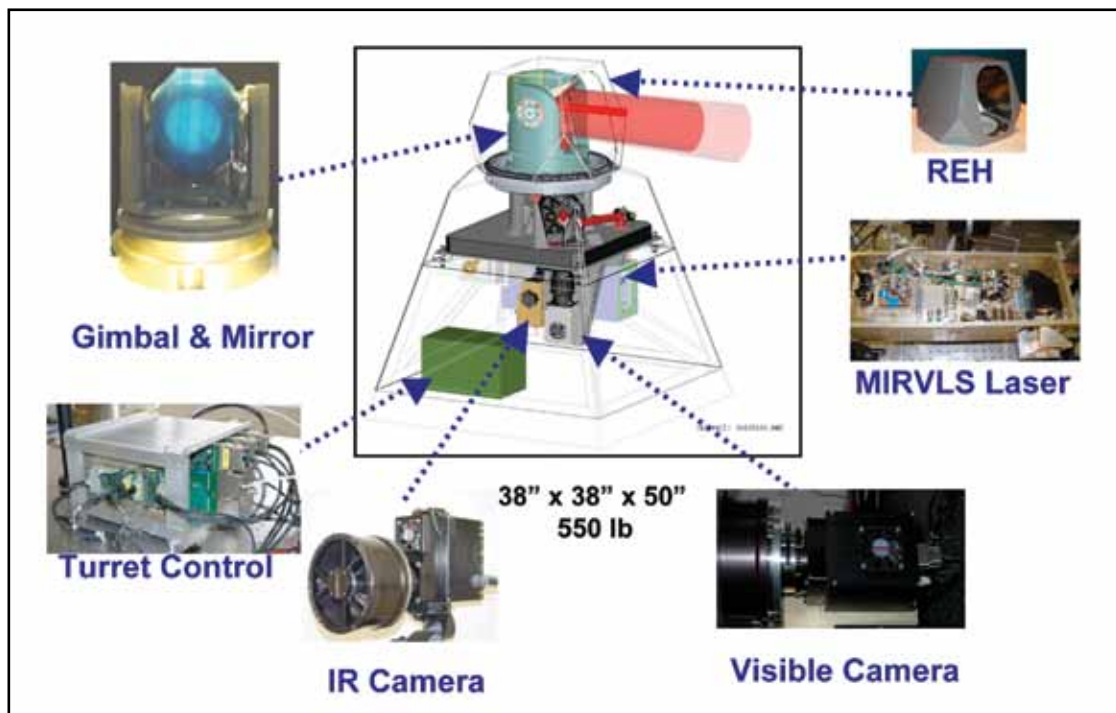


FIGURE 8
SHIELDS turret and its transceiver and optics components.

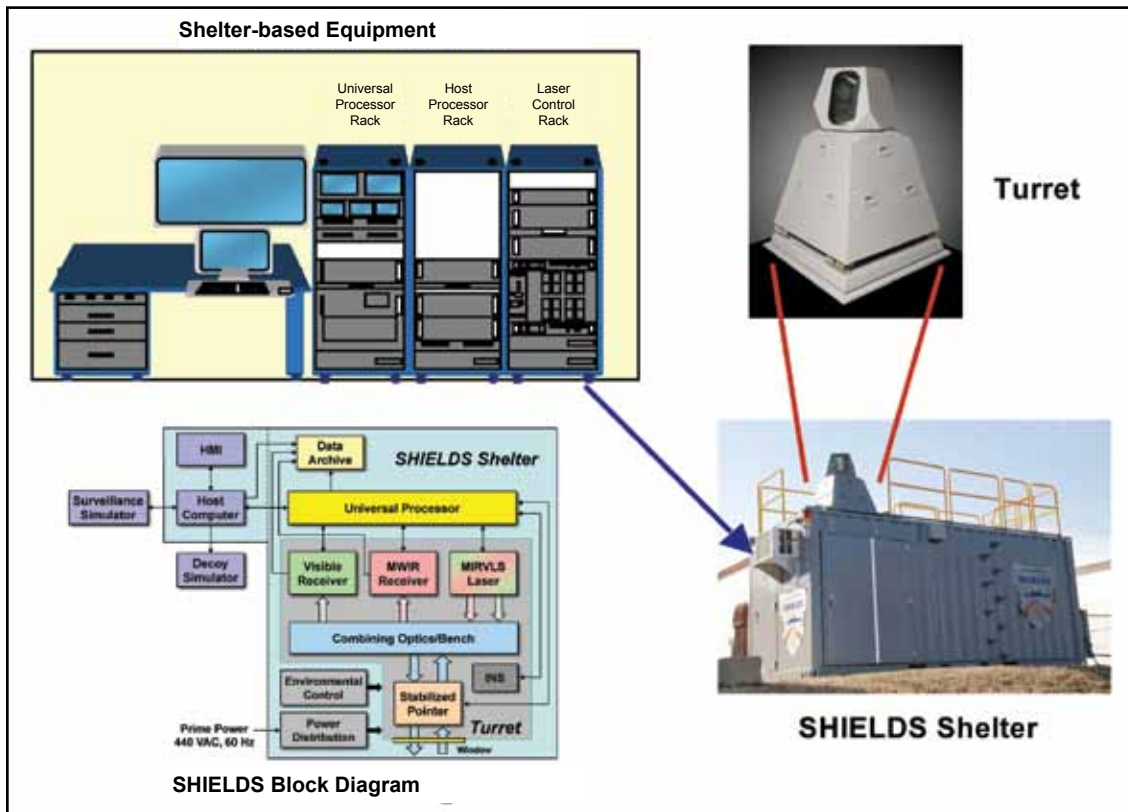


FIGURE 9
SHIELDS shelter and system block diagram.

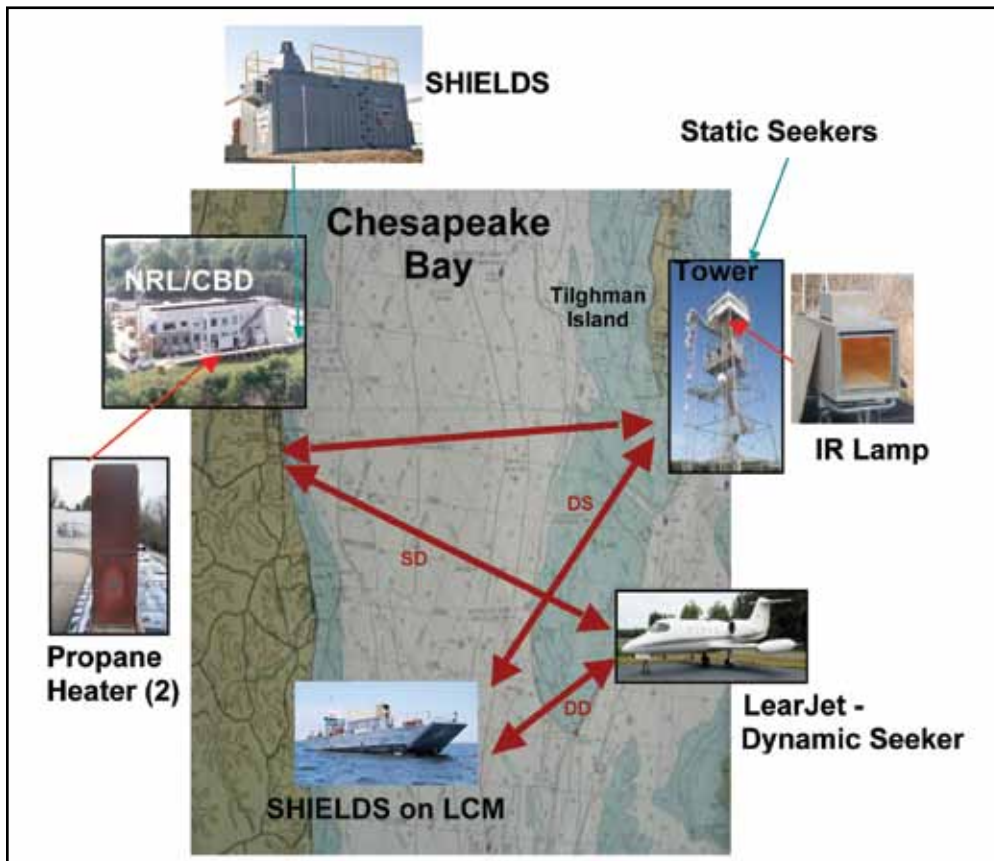


FIGURE 10
SHIELDS field trials at NRL/CBD.

system storage. The side door of the shelter allows the turret to be operated inside the shelter if needed. The turret was raised to the roof of the shelter during SHIELDS field trials.

Field Demonstrations: In 2009, NRL designed and conducted four phases of field trials, as illustrated in Fig. 10, at the NRL Chesapeake Bay Detachment (CBD) to evaluate the effectiveness of SHIELDS against ASM seekers. In the static-on-static (SS) phase, the SHIELDS shelter was moved to a concrete pad at NRL/CBD, about 120 ft above the bay, and the seekers were installed in a test tower 75 ft above the bay on Tilghman Island (TI) over 10 km away. In the static-on-dynamic (SD) phase, the static SHIELDS engaged a test asset that was captive-carried on a Learjet. In the dynamic-on-static (DS) phase, SHIELDS was installed on NRL's Landing Craft, Mechanized (LCM), which was then maneuvered out to the Chesapeake Bay to test against the seekers mounted in the TI tower. These three sets of testing led to the dynamic-on-dynamic (DD) phase, which involved SHIELDS on a moving LCM and engaging captive-carried seekers flown on a Learjet.

NRL selected a wide array of test assets that represent operational and future-generation optically guided ASM threat technologies for SHIELDS testing. The test assets included four IR- and two TV-guided seekers. Two of the IR seekers are FPA-based simulators developed by NRL. The other two IR seekers are surrogates of threat systems. The visible band seekers are used in operational missile systems.

The result of the field trials was the first-ever demonstration of shipboard closed-loop IRCM (CLIRCM) and closed-loop EOCM (CLEOCM) capabilities against airborne ASM seekers from a maneuvering ship on water. Successful CLIRCM and CLEOCM tests conducted at tactically significant ranges against EO/IR ASM seekers included target handoff, acquisition, coarse and fine track, active target acquisition, active track, target interrogation and classification, optical breaklock, and lock transfer that simulated onboard/offboard IRCM.

Conclusion: NRL has developed and demonstrated laser-based EO/IR CM technology that is ready for shipboard transition. Required SHIELDS upgrades include component ruggedization for harsh shipboard environments and SHIELDS interface to combat systems.

[Sponsored by ONR]

Particle Filters for Multipath Mitigation

M. Hock and K. Lee

Tactical Electronic Warfare Division

Introduction: The Navy requires high-precision electronic support (ES) angle measurements so that closely spaced targets at the horizon can be separated, identified, and tracked. It is especially important to have high-precision angle estimates for cueing shipboard radars, for tracking emitters passively, and for correlating ES and radar reports. When the received signal is corrupted by multipath, conventional angle estimation algorithms can produce angle estimates that are many tens of degrees in error. In recent years, some new angle estimation algorithms such as modified subspace methods and maximum likelihood techniques have been developed to address this problem. But these existing algorithms still have some limitations. The objective of this research is to improve the capability to track low-angle targets over the sea surface by developing new elevation angle tracking algorithms based on particle filters. The multipath problem is highly nonlinear and particle filters are a new approach suited to nonlinear problems.

Multipath Problem at Sea: Figure 11 illustrates the multipath problem at sea. The ES antenna on the ship receives two strong signals from the same target.¹ One signal arrives along a direct path from the target and the second signal is reflected off the ocean surface. The direct and reflected signals have nearly the same magnitude when the sea surface is smooth and the target is at low elevation. The two signals are also coherent and there is severe interference between them. There is also a third component to the multipath signal, referred to as diffuse scattering, which is a sum of small reflections from the irregular sea surface.

We assume that measurements are obtained from an interferometer direction finding (DF) sensor in this research. Performance of the interferometer is seriously degraded by multipath.

State Space Model for Tracking Under

Multipath: The core of the research involves reformulating existing models of multipath interference to fit them into the state-space framework of particle filters. The general form of the discrete-time state-space model is specified by the following state equation and measurement equation:

$$x_k = f(x_{k-1}, w_{k-1})$$

$$z_k = h(x_k, v_k)$$

where x_k is the state vector, z_k is the measurement

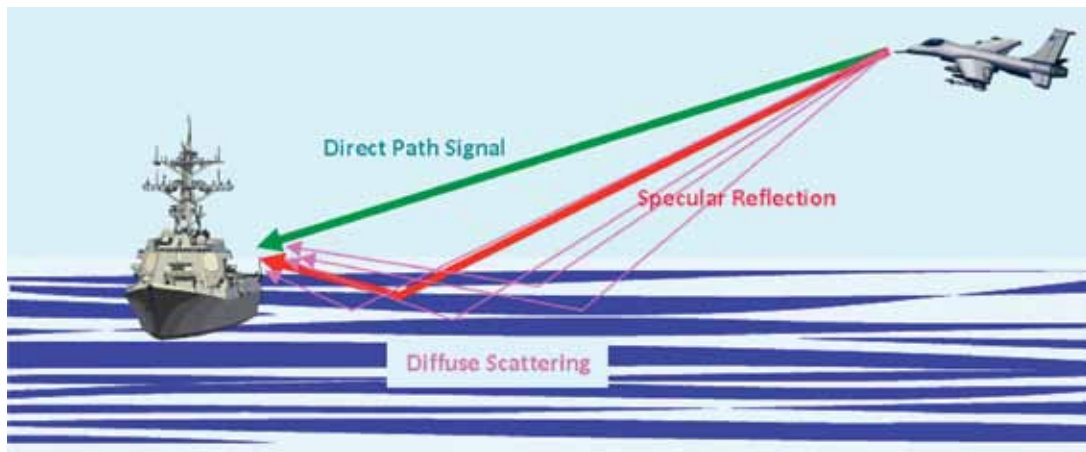


FIGURE 11
Multipath over the sea surface.

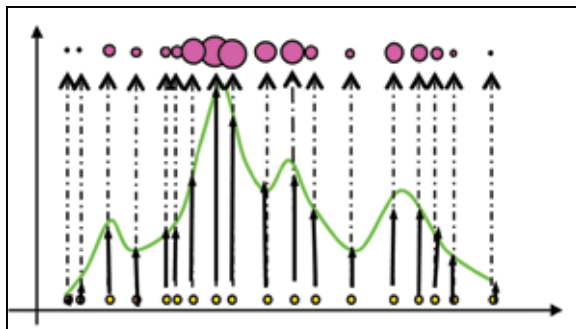


FIGURE 12
Particle representation of a probability density function.

vector, w_k is process noise, and v_k is measurement noise. In the multipath problem, the function f is a kinematic model of target motion and the function h is a nonlinear deterministic model of the multipath interference. Several multipath models with different levels of detail are being formulated. The most appropriate model for a particular application depends on the degree of information that is available concerning the position of the antenna array and sea state. When full information is available, the most detailed model can be applied.

Particle Filters: Particle filters² are signal processing techniques that are used to estimate the state of nonlinear dynamic systems. They can be applied to any state-space model and are a generalization of the traditional Kalman filter used for linear systems. The key idea of the particle filter is to represent a complex probability density function by a set of samples (“particles”) and associated weights. The concept is shown in Fig. 12, where the green line represents a complex density, black dots represent particles, and pink dots represent associated weights. A large number of particles can provide a close approximation to the density.

The particles and weights are updated after each measurement is received and the estimate of the state is made based on the weighted particle set. A number of variants of the particle filter have been developed. In our research we have applied both sequential importance resampling (SIR) particle filters and cost-reference particle filters.³ Cost-reference particle filters have some advantages for implementation in that they do not require knowledge of the measurement noise distribution and can be designed with a structure suitable for parallel processing.

Testing with Measured Data: Prerecorded field data are being used to evaluate the algorithms and to identify needed enhancements. The available data sets were collected from a scenario with an inbound low-elevation target approaching the sensor from various azimuth angles. Figure 13 shows a typical result comparing true elevation and estimated elevation. The data set is processed by a conventional direction finding algorithm and the NRL particle filter. The conventional method does not provide accurate elevation angle estimates and it also generates outliers, denoted by the black x’s, that lie outside the viewing range of the graph. The particle filter generates more accurate and smoother estimates without any outliers.

Summary: Particle filters are being applied to improve the capability to track low-elevation targets over a smooth sea surface. The research involves developing state-space models for target elevation under multipath conditions and implementing particle filters. Because the particle filter incorporates both a kinematic model of target motion and a model of multipath signal propagation, the particle filter algorithms demonstrate superior performance to the conventional method with real data.

[Sponsored by NRL and ONR]

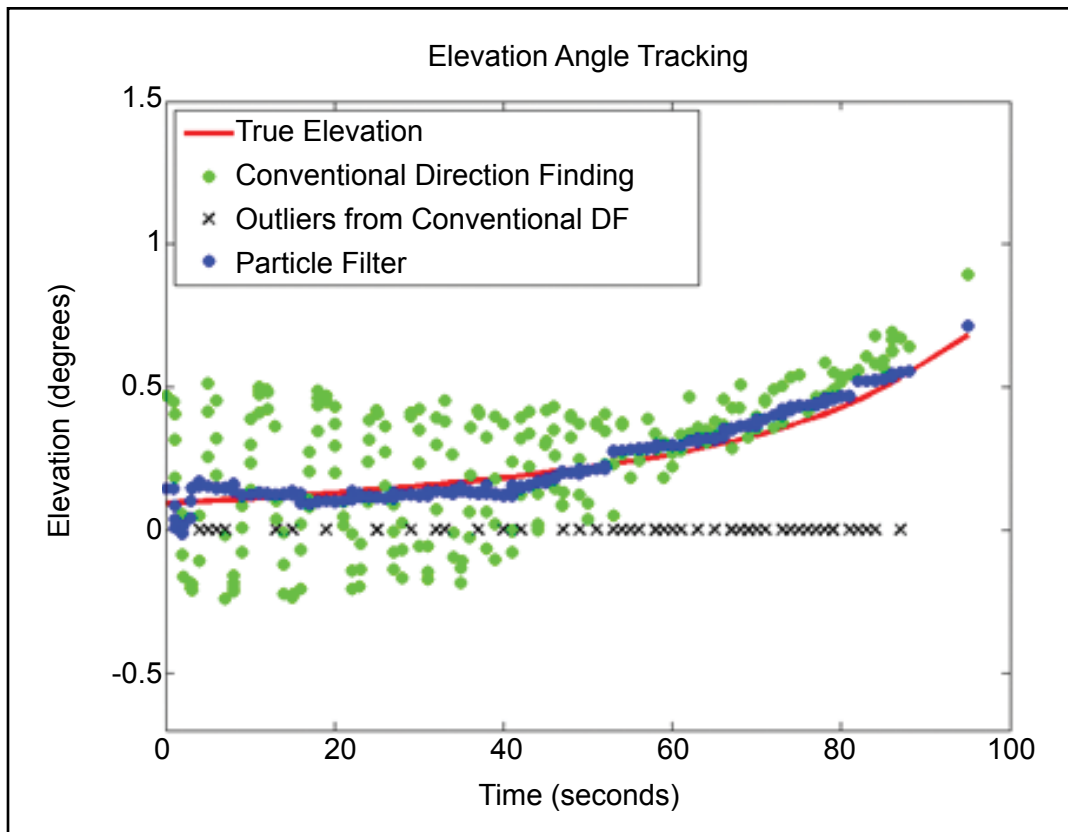


FIGURE 13
Elevation estimates from the conventional DF and the particle filter.

References

- ¹ L. Blake, *Radar Range-Performance Analysis* (Artech House, Norwood, MA, 1986).
- ² B. Ristic, D. Arulampalam, and N. Gordon, *Beyond the Kalman Filter* (Artech House, Boston, MA, 2004).
- ³ J. Miguez, S. Xu, M. Bugallo, and P. Djuric, "Particle Filtering for Systems with Unknown Noise Probability Distributions," Proceedings of the 2003 IEEE Workshop on Statistical Signal Processing, St. Louis, MO, pp. 522–525, Sept. 2003.

A New Gallium Nitride-based Switch for High Efficiency Power Electronics

T.J. Anderson,¹ M.J. Tadjer,² M.A. Mastro,¹ J.K. Hite,¹ K.D. Hobart,¹ C.R. Eddy, Jr.,¹ and F.J. Kub¹

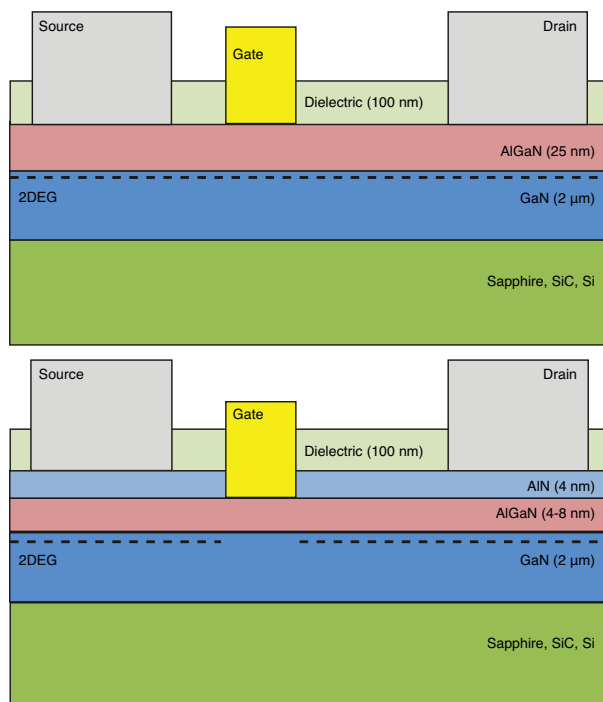
¹Electronics Science and Technology Division

²University of Maryland

Introduction: A long-sought goal for gallium nitride (GaN)-based transistor research has been the development of a reliable, fast, efficient, normally-off power switch. Such a device would have a wide range of immediate military power converter applications, such as high-power satellite communications and radar, unmanned underwater vehicles, ship drive

components, and hybrid vehicle inverters. As a wide bandgap semiconductor, GaN is attractive for its high mobility, high power capability, and chemical and thermal stability, but GaN transistors typically have normally-on (depletion mode) characteristics, which offer limited fail-safe properties. The NRL Power Electronics Branch has realized the first enhancement-mode aluminum gallium nitride (AlGa_N)/GaN high electron mobility transistor (HEMT) fabricated by a selective wet etch approach,¹ shown compared to a conventional depletion mode transistor in Fig. 14.

Development of a Selective Etch: The first key discovery was a chemically selective etch for aluminum nitride (AlN) over gallium-containing compounds such as AlGa_N and GaN. Wet etching of AlN using heated AZ400K photoresist developer has been reported in the literature,² but its effectiveness in etching AlGa_N or GaN is not understood. AZ400K is a potassium borate based solution with a pH around 13, which is already commonly used in diluted form in virtually every step in semiconductor fabrication. We have verified, using scanning electron microscopy (SEM) and X-ray photoelectron spectroscopy (XPS), that AlN does in fact etch at a slow rate in near-boiling

**FIGURE 14**

Cross-section diagram of a conventional IHEMT (top) compared to the new AlN/ultrathin AlGaIn/GaN HEMT (bottom).

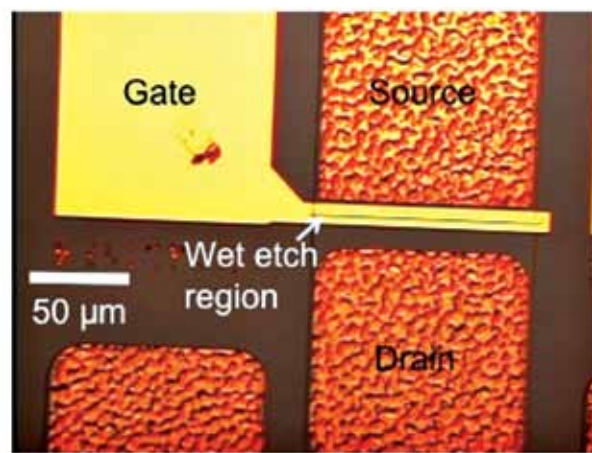
AZ400K, while AlGaIn and GaN are very stable for up to 1 hour in this solution.

Development of Device Structure: The second key component of this work was the engineering of the device structure to implement AlN layers to take advantage of the etch stop discovery, since most HEMTs use strictly AlGaIn/GaN materials. Theory predicts that the gate voltage for transistor turn-on (threshold voltage) is directly related to the AlGaIn barrier thickness. Calculations show that normally-off operation can be achieved by using a thin AlGaIn barrier (roughly less than 6 nm, but the exact thickness depends upon the AlGaIn stoichiometry). The problem is that the HEMT device is based on the principle of a strain-induced two-dimensional electron gas forming at the AlGaIn/GaN interface. The thin layers required for normally-off operation do not produce enough strain to generate appreciable carrier density, thus current flow is severely limited. Therefore, most efforts toward enhancement-mode operation have focused on retaining thicker AlGaIn (20 to 25 nm) to keep a high electron density, then selectively thinning the AlGaIn under the gate of the device to remove the charge and turn off the channel under zero gate bias. The only known method to achieve this is plasma etching,³⁻⁵ which can create damage in the material, impacting leakage currents and reliability. The NRL

team realized that by adding an AlN layer on top of an ultrathin AlGaIn layer, strain and resulting channel electron density can be reintroduced to compensate for the thinner AlGaIn barrier. By combining this engineered layer approach with the discovered wet etching method, a solution to the normally-off GaN HEMT was achieved.

Device Fabrication and Characterization: AlN/AlGaIn/GaN layer structures were grown on sapphire substrates by metal organic chemical vapor deposition (MOCVD). The layer structure included an initial 2-μm undoped GaN layer on an AlN nucleation layer, followed by either 8- or 4-nm Al_{0.3}Ga_{0.7}N layers, followed by a 4-nm AlN cap layer. The sheet resistance for both samples was ~1100 Ω/square, and the sheet carrier concentration was $\sim 6 \times 10^{12} \text{ cm}^{-2}$ with a mobility of $\sim 1000 \text{ cm}^2/\text{V}\cdot\text{s}$ at room temperature for both samples, as determined by Hall measurements. HEMT devices were fabricated following standard compound semiconductor processes, starting with mesa etching, followed by ohmic metal deposition and annealing, deposition of a dielectric etch mask for the wet etch to define the gate area, then the AZ400K etch process, and finally gate metal deposition. Figure 15 is an optical image of a completed device.

Electrical Measurements: After completing fabrication of the devices on the 4-nm AlN/8-nm AlGaIn/2-μm GaN wafer, the field effect transistor (FET) current vs voltage (I-V) curves were measured and the threshold voltage was extracted as a function of etch time, as shown in Fig. 16. The constant threshold voltage implies that the AlGaIn barrier is intact, and the thickness does not change with etch time, clearly supporting the etch stop hypothesis. Based on the initial positive results, a wafer was grown with a

**FIGURE 15**

Optical image of a functioning device. Magnification is 40x.

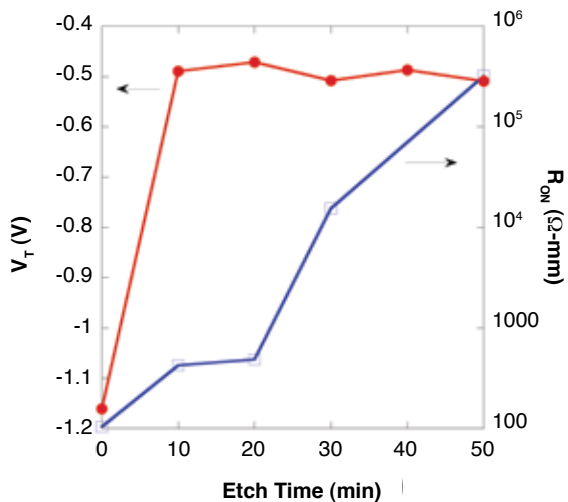


FIGURE 16
Threshold voltage (V_T) and on-resistance as a function of etch time.

4-nm-thick AlGaIn layer, which was expected to yield a positive threshold voltage based on fundamental calculations. Following the previously described standard fabrication process, a threshold voltage of +0.21 V was extracted from the FET I-V curves, as shown in Fig. 17. This value is consistent with reports of structures using comparable AlGaIn thickness,⁶ and with theoretical calculations based upon other measured device parameters.

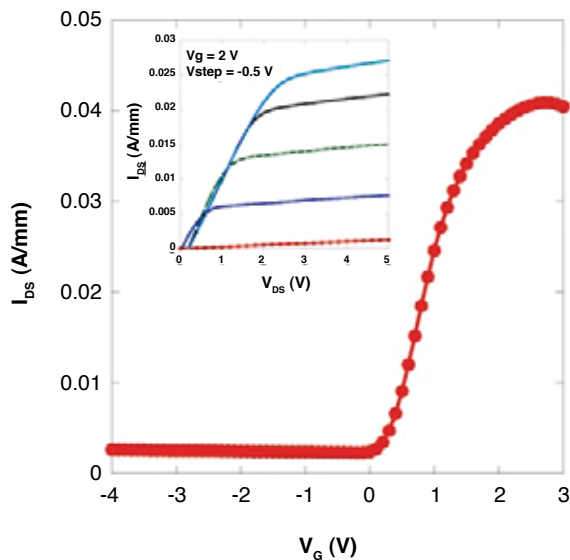


FIGURE 17
 V_{GS} - I_{DS} curve for 4-nm AlN/4-nm AlGaIn/2- μ m GaN structure. The drain bias was 5 V, and extracted V_T was +0.21 V. The V_{DS} - I_{DS} curve is shown in the inset.

Summary: NRL has achieved the first normally-off GaN HEMT fabricated through device structure engineering and a wet chemical recess etch of the gate region. The achievement employed a device structure incorporating an AlGaIn/GaN HEMT with an ultra-thin AlGaIn layer for positive threshold voltage, capped with a thin AlN layer to increase channel charge. Subsequently, a selective wet chemical etch was used to open the AlN layer and stop cleanly on the AlGaIn surface, resulting in a normally-off device. The selective wet etch approach improves manufacturability since etch stop layers can be built in to the device structure. This will improve reliability and process control, which represents a significant development toward commercialization of GaN power switches.

Acknowledgments: The authors are sincerely grateful to the microwave HEMT device group at NRL (S. Binari et al.) for insightful discussions and equipment use, the NRL Institute for Nanoscience for equipment use and support, and G. Jernigan of the Electronics Science and Technology Division for XPS characterization. JKH acknowledges the support of the American Society for Engineering Education/Naval Research Laboratory Postdoctoral Fellowship Program.
[Sponsored by ONR]

References

- T.J. Anderson, M.J. Tadjer, M.A. Mastro, J.K. Hite, K.D. Hobart, C.R. Eddy, Jr., and E.J. Kub, "An AlN/Ultrathin AlGaIn/GaN HEMT Structure for Enhancement-Mode Operation Using Selective Etching," *IEEE Electron Device Lett.* **30**(12), 1251–1253 (2009).
- S.J. Pearton, J.C. Zolper, R.J. Shul, and F. Ren, "Processing Defects and Devices," *J. Appl. Phys.* **86**(1), 1–78 (1999).
- W. Saito, Y. Takada, M. Kuraguchi, K. Tsuda, and I. Omura, "Recessed-gate Structure Approach toward Normally-off High Voltage AlGaIn/GaN HEMT for Power Electronics Applications," *IEEE Trans. Electron. Devices* **53**(2), 1–7 (2006).
- M. Kuraguchi, Y. Takada, T. Suzuki, M. Hirose, K. Tsuda, W. Saito, Y. Saito, and I. Omura, "Normally-off GaN MISFET with Well-controlled Threshold Voltage," *Phys. Status Solidi A* **204**(6), 2010–2013 (2007).
- S. Maroldt, C. Haupt, W. Pletschen, S. Müller, R. Quay, O. Ambacher, C. Schippel, and F. Schwierz, "Gate-recessed AlGaIn/GaN Based Enhancement-mode High Electron Mobility Transistors for High Frequency Operation," *Jap. J. Appl. Phys.* **48**(4), 04C083/1–04C083/3 (2009).
- Y. Ohmaki, M. Tanimoto, S. Akamatsu, and T. Mukai, "Enhancement-mode AlGaIn/AlN/GaN High Electron Mobility Transistor with Low On-state Resistance and High Breakdown Voltage," *Jap. J. Appl. Phys.* **45**(44), L1168–L1170 (2006).

172

CT-Analyst® Deployed for the 2009 Presidential Inauguration
J. Boris, G. Patnaik, K. Obenschain, M. Ronas, C. Williams, and J. Delaney

174

Beyond-line-of-sight Tactical Communications Relay (BTCR)
M. Rugar, J. Doffoh, and B. Vorees

176

Coastal Environmental Hyperspectral Imaging from the Space Station
*M.R. Corson, R.L. Lucke, D.R. Korwan, W.A. Snyder, C.O. Davis,
N.R. Mcglothlin, S.D. Butcher, and D.L. Wood*

CT-Analyst® Deployed for the 2009 Presidential Inauguration

J. Boris,¹ G. Patnaik,¹ K. Obenschain,¹ M. Ronas,²
C. Williams,³ and J. Delaney⁴

¹Laboratory for Computational Physics and Fluid Dynamics

²Center for Computational Science

³ITT Corporation

⁴National Medical Response Team

The Problem: Airborne contaminants in cities, ports, and bases, whether released accidentally or deliberately as a chemical, biological, or radiological (CBR) agent, present potentially lethal, round-the-clock threats to civilian and military personnel. A crisis manager or warfighter must make immediate life-and-death decisions about how to respond to such an emergency based on incomplete knowledge of the source and the contaminant plume's evolution. The critical speed-vs-accuracy dilemma has always been: Do we make quick decisions (a few seconds) based on crudely computed estimates about the spreading threat, or do we wait a long time (several minutes) for more accurate computations of how the contaminant cloud will evolve? A coordinated defensive response within 3 to 5 minutes of a contaminant's release can reduce casualties by a factor of four or five. Unfortunately, most urban plume predictions take 10 to 15 minutes today.

Even without the dire time constraint, computing wind-driven contaminant transport (CT) over a city or large facility challenges current-day modeling^{1,2} because unsteady, turbulent, buoyant flow physics must be solved over large, complex geometry areas. These challenges can be met using a computational fluid dynamics (CFD) model called FAST3D-CT developed at NRL originally for aerospace applications based on NRL's Flux-Corrected Transport (FCT) algorithms and many years of related basic fluid dynamics and atmospheric research. Although the runs take up to a day on big computers, the advantages of using the heavily validated³ FAST3D-CT model include accurately computing around the buildings while solving the dynamic, turbulent CT problem in cases where experiments are impossible or impractical. Although there is now a reliable computational ground truth, the dilemma has been to make this prediction capability useful in emergencies.

The Achievement: To resolve this speed-vs-accuracy dilemma, NRL invented a methodology to make 3D CFD instantly useful for crisis managers in operational situations. In the laboratory well ahead of time, we carry out detailed simulations of airflow

over the entire urban geometry of interest and save out wind-field databases for a full set of wind conditions and a number of test sources. The relevant information from these databases is compressed into 18 tables called Dispersion Nomographs™ to be used on PCs, one nomograf for each of 18 wind directions over the city. The implementation of this approach for crisis management is called CT-Analyst^{®1,2} (Contaminant Transport Analyst). CT-Analyst takes full account of the building geometry on the airflow and is both faster and more accurate than other existing or proposed systems.

Figure 1 shows CT-Analyst as it appears interactively for a fictitious scenario with four distinct toxic chemical sources in downtown Washington, D.C. The notations near each source are added for clarity. Sources of different size can be released at different times and locations with extents and shapes controlled by the nearby buildings. When a source location is not known, a few local observations of the agent can be combined to estimate the unknown source location. This operation, called "backtrack," is illustrated for the lower left source in the figure. Figure 1 would require hours to compute using other "urban" methods but took ~0.4 s to compute using CT-Analyst. Extensive testing and validation of the CT-Analyst methodology has been performed,² one example of which is illustrated for Washington, D.C., in Fig. 2. This figure addresses the question of whether the underlying CFD computations, as reflected through the CT-Analyst predictions, are computed with a fine enough grid. For Washington, D.C., the FAST3D-CT runs were performed with 3-m, 6-m, and 12-m grids, and the results show that even 12-m spatial resolution is adequate for operational use.

The Impact: NRL's CT-Analyst system is the first operational *instantaneous* emergency assessment system for airborne contaminant threats in cities. Using CT-Analyst, the accuracy of CFD simulations can be recovered nearly instantly, with little loss of fidelity, by a crisis manager or a warfighter in the field. CT-Analyst is deployed for daily use with Federal emergency managers, police, and fire officials in Washington, D.C., and Chicago, Illinois. It was deployed during Operation Iraqi Freedom and was selected by the Missile Defense Agency for urban dispersion and consequence management.

CT-Analyst was deployed as the nation's crisis management model and used at the HazMat Reachback Center (HRC), hosted by NRL for the 2009 Presidential Inauguration under the auspices of the U.S. Secret Service and the National Medical Response Team. The HRC was designated to provide the crisis and consequence assessment for the Washington,

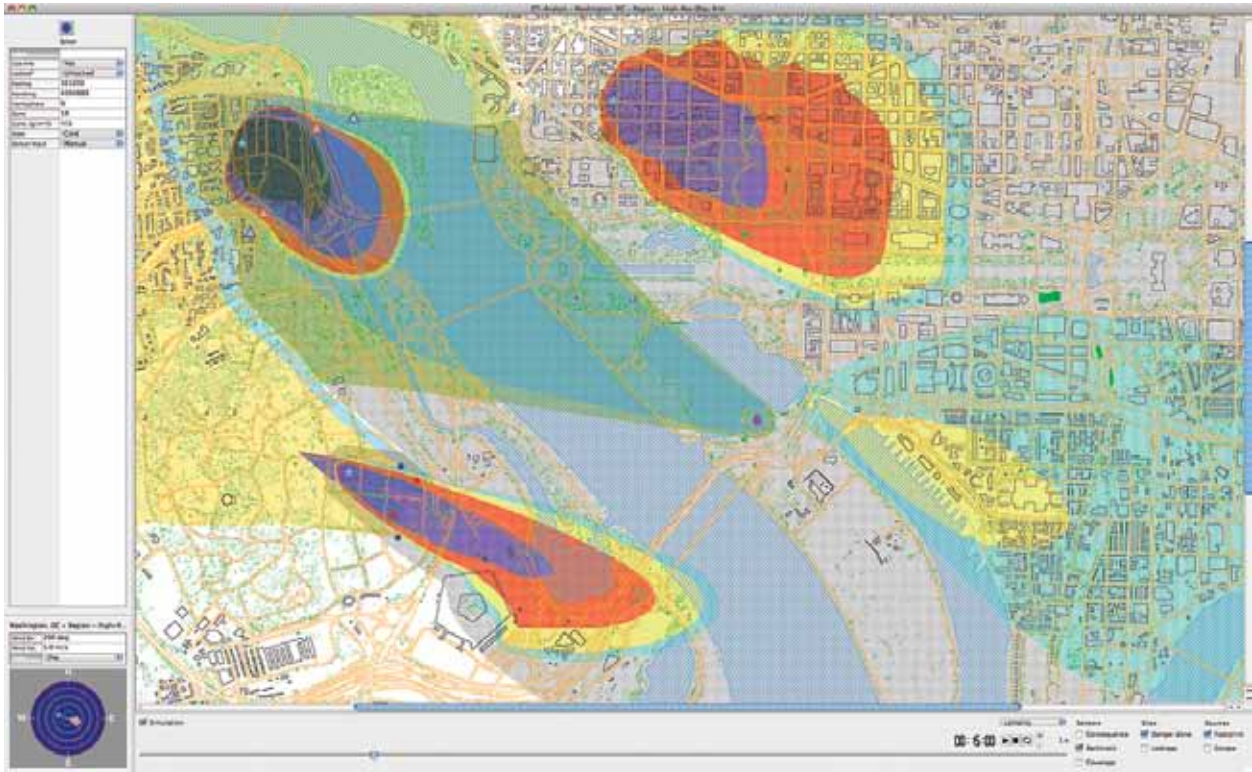


FIGURE 1
 The entire CT-Analyst graphical user interface display predicting lethality for a scenario involving four separate toxic chemical releases in the mall area of Washington, DC. Notations have been added giving the amounts released and release times of the four sources. An upwind site danger zone and sensor fusion for a backtrack computation are also shown. Computation for this entire display takes about 0.4 s.

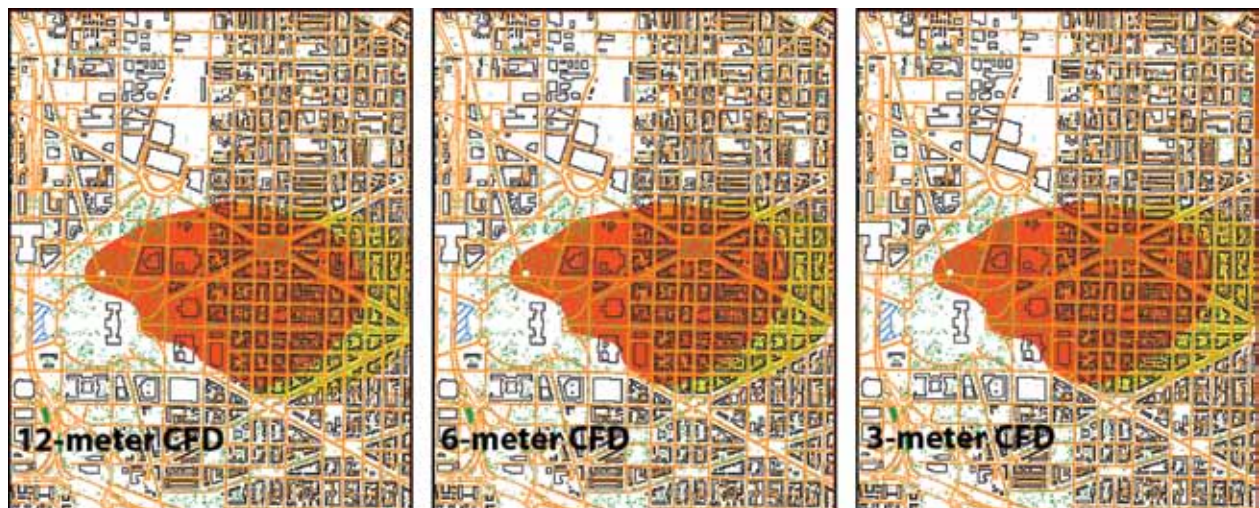


FIGURE 2
 CT-Analyst display of a plume envelope for a release near Union Station in Washington, DC, using CFD computed at three different spatial resolutions. The yellow region in each panel shows where the plume is above the ground and has not yet touched down. Very little practical difference can be seen in the three different resolution predictions.

**FIGURE 3**

Hazardous Materials Reachback Center for the 2009 Presidential Inauguration. Experts from a number of agencies came together at NRL to provide situation and consequence assessments for any real or postulated release of hazardous materials in Washington, DC, during the Presidential Inauguration activities and subsequent events.

D.C., area in the event of an airborne contaminant release. The ViPR video teleconferencing capability was employed to transmit graphical results straight to the D.C. multi-agency operations center. Participants at NRL included the FBI, Secret Service, National Medical Response Team, D.C. fire and police personnel, Army and Marine chemical incident support teams, the National Oceanic and Atmospheric Administration (NOAA), the Department of Homeland Security (DHS), and the Defense Threat Reduction Agency (DTRA). Although no actual HazMat incidents took place, in numerous drills the results of the initial assessments by CT-Analyst were provided to the HRC commander, typically within a minute or two.

Acknowledgments: The authors wish to thank Adam Moses, Mi-Young Obenschain, Lisa Williams, and Theodore Young, Jr., of the Laboratory for Computational Physics and Fluid Dynamics contaminant transport team, and also Kat Adams, John Cook, Vadim Gamezo, Jason Geder, David Kessler, David Mott, Alexei Poludnenko, Ravi Ramamurti, Doug Schwer, Teddy Holt, and Annette Williams. Special thanks are due Hank Dardy, Basil Decina, Bob Doyle, Will Hawkins, Darmesh Shah, and others from the Center for Computational Science who supported the HRC. Further thanks are due Carey Cox, Bo Cybyk, Jack Fulton, John Iselin, Sandy Landsberg, Charles Lind, Julie Pullen, and Rob Scott for their technical discussions and contributions to various components that became part of this effort. Aspects of the work discussed here were supported by ONR through NRL and in the past by the DoD High Performance Computing Modernization Office, Naval Surface Warfare Center

(NSWC) Crane, DARPA, DTRA, the Missile Defense Agency (MDA), the Technical Support Working Group (TSWG), and DHS.

[Sponsored by the National Medical Response Team]

References

- ¹ J. Boris, K. Obenschain, G. Patnaik, and T. Young, Jr., "CT-Analyst: Fast and Accurate CBR Emergency Assessment," Proceedings of the First Joint Conference on Battle Management for Nuclear, Chemical, Biological, and Radiological Defense, Williamsburg, VA, November 4–8, 2002.
- ² J. Boris, "The Threat of Chemical and Biological Terrorism: Preparing a Response," *Comp. Science and Engineering* 4, 22–32 (2002).
- ³ G. Patnaik, J. Boris, M.-Y. Lee, T. Young, B. Leidl, F. Harms, and M. Schatzmann, "Validation of an LES Urban Aerodynamics Model with Model and Application Specific Wind Tunnel Data," The Seventh Asia-Pacific Conference on Wind Engineering, Taipei, Taiwan, November 8–12, 2009.

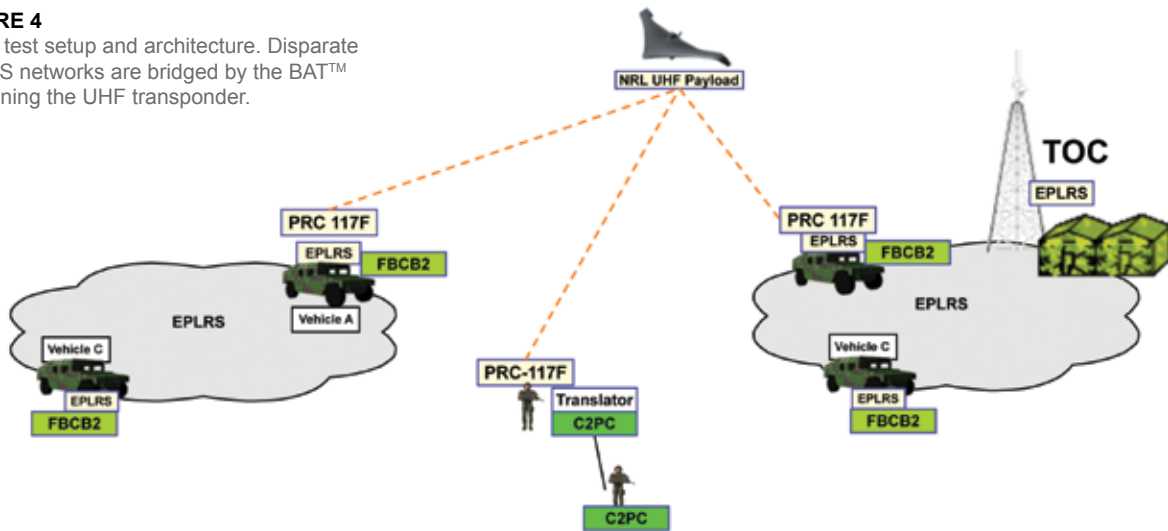
Beyond-line-of-sight Tactical Communications Relay (BTCR)

M. Rupar, J. Doffoh, and B. Vorees
Information Technology Division

Introduction: A joint Navy and Army team, led by the Naval Research Laboratory, has demonstrated a beyond-line-of-sight tactical communications relay (BTCR) capability to extend tactical networks for the Army and Marine Corps (USMC) using an NRL-developed surrogate UHF satellite transponder flown in a small unmanned aerial system (UAS) at low altitudes. This link extension integrated disparate networks and supported networked interaction between

FIGURE 4

Relay test setup and architecture. Disparate EPLRS networks are bridged by the BAT™ containing the UHF transponder.



simulated Army and USMC units using organic communications assets.

The objective of this effort, sponsored by the Office of the Secretary of Defense (OSD), was to develop and demonstrate communications range extension in an operational scenario for a Tier II UAS. In FY09, an NRL-developed surrogate UHF satellite transponder was integrated into the BAT™, a UAS built by Northrop Grumman, to provide tactical network range extension. The Army Communications–Electronics Research, Development, and Engineering Center (CERDEC) and NRL demonstrated this technology as part of the C4ISR On-The-Move (OTM) Event 2009 (E09) at Ft. Dix, New Jersey.

The demonstration objective was to link disparate Enhanced Position Location Reporting System (EPLRS)-based networks via NRL's UHF transponder on the BAT™ (Fig. 4). The Army and USMC situational awareness (SA) applications were to interact over this architecture.

NRL was responsible for technical and project management. CERDEC personnel partnered with NRL, and the Project Manager C4ISR OTM provided Army networking hardware and vehicles and hosted the demonstration.

The successful interaction between the two SA tools, the USMC's Command and Control PC (C2PC) and the Army's Force XXI Battle Command, Brigade-and-Below (FBCB2), was accomplished by software developed by SPAWAR-Pacific. This software, as part of SPAWAR-Pacific's Software Interoperability Environment (SIE), enabled bidirectional exchange of tactical data between existing FBCB2 and C2PC systems. SPAWAR-Pacific personnel supported this effort.

Preliminary Testing: Initial testing of the UAS-mounted transponder with tactical radios (PRC-117F and PSC-5) was conducted in El Centro, California. A Viasat e-mail program (Vmail), Multi-Generator (MGEN) Tool Kit (an NRL application for measuring IP network performance), and C2PC/FBCB2 message traffic were all exercised over the link. Figure 5 shows MGEN throughput over the transponder using PRC-117Fs transmitting at 42 kbps. One node (base) was stationary, while the other node was mobile. These tests proved the viability of a Tier II UAS as a communications link in an environment using tactical resources.

C4ISR OTM Event: The BTCR demonstration was part of the C4ISR OTM event in August 2009. Four Army vehicles with tactical routers were configured to form two distinct EPLRS-linked local area networks, one of which also included the Army's Tactical Operations Center (TOC). A vehicle in each EPLRS network was outfitted with PSC-5 and PRC-117F radios to allow the two local area networks to communicate via the transponder.

A third vehicle, outfitted with the two tactical radios, simulated a dismounted USMC unit. This vehicle operated C2PC with the SIE Translator and communicated with the other units via the UHF transponder.

BTCR successfully demonstrated the transmission of voice and data over the UAS-mounted transponder. A variety of command and control messages were successfully communicated between the two SA applications over that link. Table 1 shows the results of the tested VMF (variable message format) messages. Traffic was initiated from the TOC and sent out to

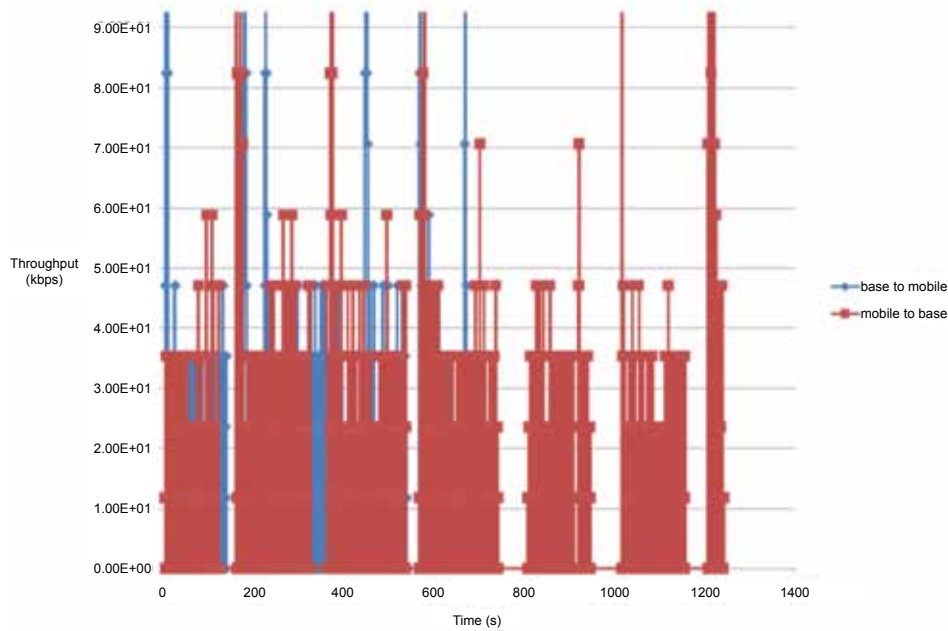


FIGURE 5
Throughput test results for MGEN at 42 kbps via the UAS-mounted transponder.

TABLE 1—Applications Performance for BTRC

| Reception at Destinations | | | | |
|---------------------------|-------|-------|-------|-------|
| Origin: TOC | PM 12 | PM 13 | PM 17 | PM 81 |
| Position Report | YES | YES | YES | YES |
| Spot Report | YES | YES | YES | YES |
| Free Text | YES | YES | YES | YES |
| Overlay | YES | YES | YES | YES |
| Call for Fire | YES | YES | YES | YES |

the other nodes in the network. The simulated USMC node is labeled PM 81. The three other nodes, PM 12, PM 13, and PM 17, were all simulated Army forces.

Conclusion: BTRC successfully demonstrated the supporting of tactical IP networks over a surrogate UHF satellite transponder flown in a small (Tier II) UAS, the networking of Army nodes in separate EPLRS clouds through that UHF link, the moving of meaningful traffic through that network over the UHF link, and the demonstration of an SA message Translator that allowed USMC messages generated by C2PC to be injected into the Army’s FBCB2 (and vice versa).

This program successfully demonstrated the viability and interoperability of a new series of technology with the use of existing tactical communications on a platform that will greatly contribute to the overall common operational picture (COP).

[Sponsored by OSD]

Coastal Environmental Hyperspectral Imaging from the Space Station

M.R. Corson,¹ R.L. Lucke,¹ D.R. Korwan,¹ W.A. Snyder,¹ C.O. Davis,² N.R. Mcglothlin,³ S.D. Butcher,³ and D.L. Wood³
¹Remote Sensing Division
²Oregon State University
³Praxis Inc.

Introduction: Environmental characterization of the coastal ocean is a critical element in planning and executing naval operations in coastal areas. The coastal ocean is complicated, with in-water constituents including organic and inorganic dissolved and suspended matter that affect visibility, and various bottom types and depths that affect mobility. Accurate maps of bathymetry, in-water constituents, water optical properties, and bottom characteristics significantly enhance the speed and safety of operations from warfighting to humanitarian relief. In the mid 1990s, scientists at the Naval Research Laboratory began an ambitious program to develop instrumentation and techniques to produce these maps using remotely sensed hyperspectral imagery taken from aircraft platforms. In contrast to a conventional color camera, which images in only three wavelength bands, a hyperspectral camera for coastal characterization typically images in 50 to 100 contiguous wavelength bands, and this extra information can be exploited to understand and quantify the complicated coastal ocean environment.^{1,2}

Development of the Spaceborne Hyperspectral Imager: Spaceborne environmental hyperspectral imaging is a natural next step for the NRL program, building on its extensive foundation of airborne experience. Space offers repeat access to many different coastal types worldwide, access that would be completely impractical using aircraft. Naval forces require coastal environmental information worldwide, and the spaceborne imager coupled with ground truth provides data to determine which retrieval algorithms work on particular coastal types, and the range of errors in the retrieved environmental products.

In March 2007, the DoD Space Test Program manifested the NRL Hyperspectral Imager for the Coastal Ocean (HICO), which is sponsored by the Office of Naval Research under its Innovative Naval Prototype program, to be launched to the International Space Station. To take advantage of the Space Station opportunity, HICO had to be designed, built, calibrated, and delivered for payload integration in 18 months. A small but dedicated team of scientists and engineers in NRL's Remote Sensing Division accomplished this feat ahead of schedule in 16 months. Figure 6 shows the flight imager in the laboratory during calibration.



FIGURE 6
The HICO flight imager in the laboratory. The imager is incorporated into a larger payload module that attaches to the Japanese Exposed Facility on the International Space Station.

As an Innovative Naval Prototype, the HICO program has two primary goals. The first goal is to demonstrate a new capability to satisfy Naval needs. HICO demonstrates the ability to characterize the complicated coastal environment from space, providing a new capability that complements current methods. For this demonstration, HICO is optimized for coastal ocean imaging with design and performance requirements based on decades of airborne experience at NRL and at other laboratories. An important performance requirement is high

signal-to-noise ratio for water scenes. Water scenes have low albedo and are viewed through the atmosphere, which, due to scattered sunlight, is significantly brighter than the underlying coastal scene. The atmospheric signal must be removed from the image because it contains no information about the water scene, and this process degrades the signal-to-noise ratio after atmospheric removal. HICO has a signal-to-noise ratio greater than 200 to 1 for water-penetrating wavelengths when viewing a 5% albedo scene from space. HICO scenes are approximately 42 by 190 km, sufficient to capture the scale of coastal dynamics. HICO's ground sample distance, the size of a pixel on the water surface, is approximately 90 m, providing sufficient resolution for this proof-of-concept demonstration.

The second goal of the Innovative Naval Prototype program is the demonstration of methods to reduce cost and schedule. HICO addresses this by using commercial-off-the-shelf (COTS) components where feasible. The HICO spectrometer, CCD camera, and telemetry and control computer are COTS hardware. Because the camera and computer are not designed to operate in a vacuum, they are housed in hermetically sealed enclosures containing nitrogen gas. The camera enclosure also includes a small fan for forced convection. A novel use of a COTS component in HICO is a commercial motorized rotary stage, intended for use in laboratory vacuum systems, to point the imaging line of sight.

Environmental Products from HICO on the Space Station: On September 10, 2009, HICO was launched from the Tanegashima Space Center in Japan to the International Space Station and attached to the Exposed Facility of the Japanese Kibo module using Kibo's remote manipulator arm, as shown in Fig. 7. HICO was activated on September 24, and after a brief checkout, began imaging coastal sites worldwide. An example product of the new HICO capability to produce environmental maps from spaceborne imagery is shown in Fig. 8. The left image in Fig. 8 is a conventional color image of Andros Island and adjacent ocean in the Bahamas, acquired by HICO on the Space Station and constructed using three HICO wavelength bands. The false-color image on the right is a preliminary bathymetry map of the ocean surrounding the island, retrieved from the fully spectral HICO image.

Summary: The Hyperspectral Imager for the Coastal Ocean demonstrates a new capability for environmental characterization of the coastal ocean from space. Environmental maps produced from HICO data for coastal types worldwide will be compared to in situ



FIGURE 7
The payload module containing HICO is positioned by the Japanese remote manipulator arm prior to attachment to the Exposed Facility (NASA photograph).

measurements to understand and validate the accuracy of the HICO products. The HICO program is the first step in providing a valuable new tool for Naval operations in the coastal zone.

[Sponsored by ONR]

References

- ¹A.F.H. Goetz, G. Vane, J. Solomon, and B.N. Rock, "Imaging Spectrometry for Earth Remote Sensing," *Science* **228**, 1147–1153 (1985).
- ²C.O. Davis, K.L. Carder, B.-C. Gao, Z.P. Lee, and W.P. Bissett, "The Development of Imaging Spectrometry of the Coastal Ocean," *IEEE Proceedings of the International Geoscience and Remote Sensing Symposium* **4**, 1982–1985 (2006).

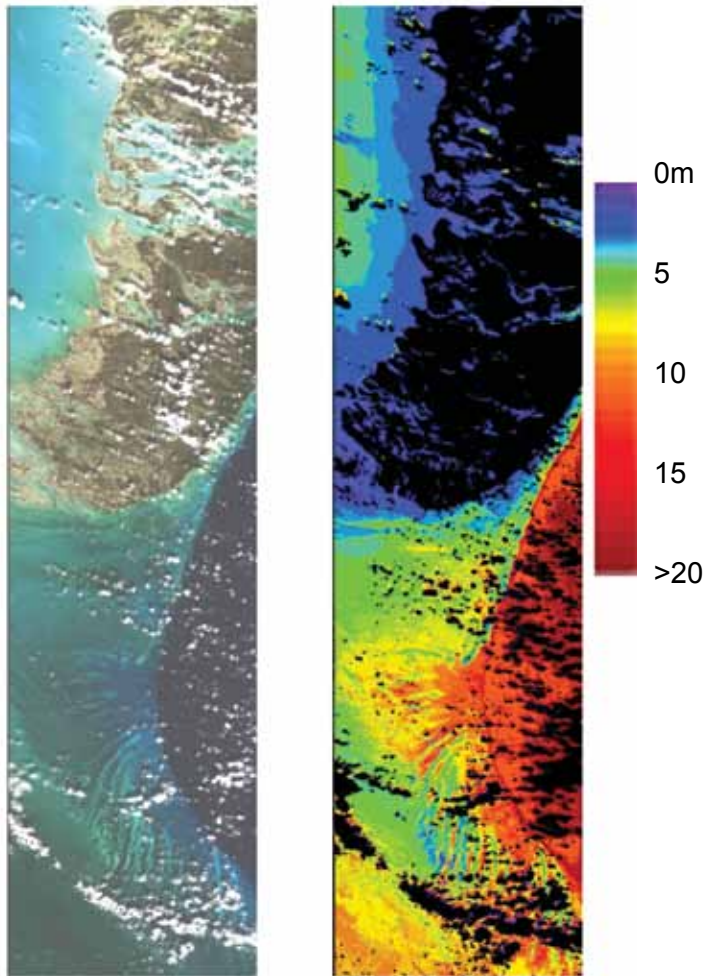


FIGURE 8
Left: Color image of Andros Island, Bahamas, constructed using three HICO wavelength bands. Right: False-color bathymetry map retrieved from the fully spectral HICO data. Land and clouds are masked black. Imaged area is approximately 42 by 190 km.

180

Nanostructured Magnets for Improved Energy Efficiency

M.A. Willard, K.E. Knipling, and M. Daniil

181

High Performance Antireflection Structured IR Fibers

J.S. Sanghera, C. Florea, L.E. Busse, L.B. Shaw, F.H. Kung, and I.D. Aggarwal

183

Broad-Spectrum Pathogen Surveillance

A.P. Malanoski, T.A. Leski, L. Cheng, Z. Wang, D.A. Stenger, and B. Lin

187

Plasma Processing of Ion Energy-sensitive Materials

S.G. Walton, E.H. Lock, M. Baraket, D.R. Boris, R.F. Fernsler, S.H. North, C.R. Taitt, J.T. Robinson, F.K. Perkins, and P.E. Sheehan

189

Standoff Detection of Trace Explosive Residues by Resonant Infrared Photothermal Imaging

C. Kendziora, R.A. McGill, R. Furstenberg, M. Papantonakis, V. Nguyen, G. Hubler, and J. Stepnowski

Nanostructured Magnets for Improved Energy Efficiency

M.A. Willard,¹ K.E. Knipping,¹ and M. Daniil²

¹Materials Science and Technology Division

²George Washington University

Introduction: Reducing our reliance on fossil fuels by the widespread hybrid and electric transportation options has resulted in a recent surge in sustainable energy research and infrastructure, especially in electricity generation from replenishable energy sources (e.g., wind, solar, hydro, and geothermal). In parallel with this infrastructure investment, it is also essential to develop technologies that avoid squandering these newly tapped resources by improving the efficiency of energy production, distribution, and consumption. By reducing the losses inherent to power generation, conditioning, and conversion, energy efficiency will be improved, adding to our overall energy sustainability. The Navy's effort to produce "all-electric ship" technologies requires improvements in these areas to achieve the highest possible shipboard power density. Significant gains can be achieved by development of smaller, lighter, and more efficient power converters and magnetic filters. A main challenge to the energy efficiency of these components is the loss generated by the magnetic core materials from hysteretic, acoustic, or eddy current sources. This article discusses NRL's alloy research regarding the fabrication and characterization of novel nanostructured soft magnetic alloys exhibiting low core losses and designed for use in power applications.

Nanotechnology Solution: Nanocrystalline soft magnetic alloys are a class of premiere magnetic materials exhibiting a large saturation magnetization and small coercivity, resulting in a highly efficient core material for alternating current applications.¹ These materials consist of nanoscale magnetic crystallites embedded within an intergranular amorphous matrix (schematically shown in Fig. 1). The partially crystalline material with refined grain size results in a desirable combination of large saturation induction, high permeability, and low core losses, unobtainable in conventional soft magnetic alloys. The improved performance is only possible when grains are smaller than a fundamental magnetic length scale called the exchange correlation length (L_{ex}) and the operation temperature is sufficiently low such that the magnetic coupling between grains is maintained. A current technical challenge is meeting both of these objectives in a cost-effective way.

Materials Processing: Achieving the optimal magnetic performance for energy efficiency and size/

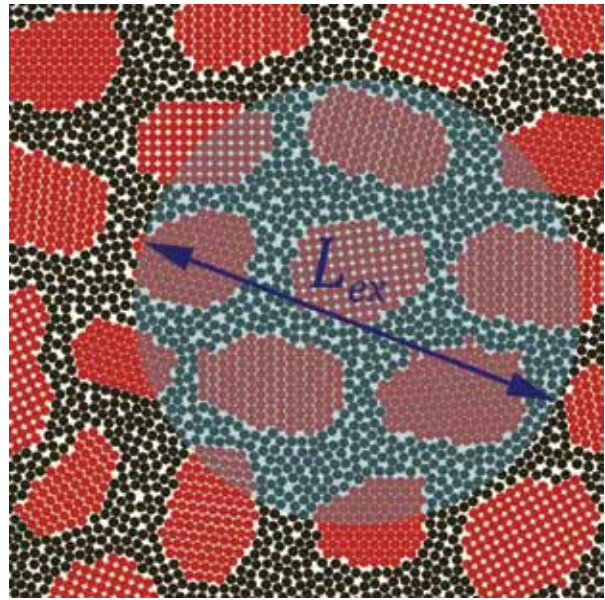


FIGURE 1

Schematic diagram showing relationship between nanocrystalline grains (red) and exchange correlation length (light blue).

weight reduction requires non-equilibrium processing to achieve the necessary nanoscale microstructure. Two steps are used to prepare these materials. First, a rapid solidification process is used to create an amorphous alloy (i.e., material with disordered atomic-scale structure) in the form of long, thin ribbons. These materials are subsequently annealed above 500 °C to produce the ultrafine grains necessary for low core losses. Alloys with composition $(\text{Fe}_{1-2x}\text{Co}_x\text{Ni}_x)_{88}\text{Zr}_7\text{B}_4\text{Cu}_1$ have been recently designed and produced at NRL using a single-wheel, melt-spinning process (see Fig. 2) in which a molten alloy of the desired composition is expelled through a jet-cast orifice onto a rapidly rotating copper wheel (~50 m/s), solidifying the melt at a rate exceeding 10^5 °C/s.

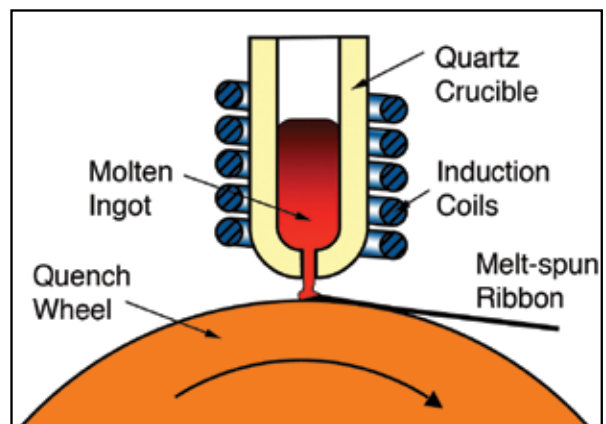


FIGURE 2

Schematic diagram of the melt-spinning technique for forming amorphous ribbons from a molten alloy.

Magnetic Performance: Due to their refined grain size and intergranular amorphous phase, these nanostructured alloys possess low hysteretic and core losses. Using state-of-the-art magnetometers at NRL, magnetic hysteresis loop measurements were collected at temperatures up to 600 °C (see Fig. 3). From these measurements, the important performance metrics — the saturation magnetization and the coercivity — were determined and compared with other soft magnets. Large values of saturation magnetization are desirable because less core material is required for a given flux density in application, while small values of coercivity result in lower losses and better energy efficiency. The magnetic properties of a state-of-the-art (Fe,Co)-based nanocrystalline material specifically designed for high-temperature applications is shown in Fig. 3. Our new alloys have comparable saturation magnetization values with much lower coercivity, resulting in improved energy efficiency. Moreover, the small Co content of the alloys improves the cost effectiveness considerably.

Summary: The newly developed nanocrystalline alloy, with composition $\text{Fe}_{77}\text{Co}_{5.5}\text{Ni}_{5.5}\text{Zr}_7\text{B}_4\text{Cu}_1$, shows

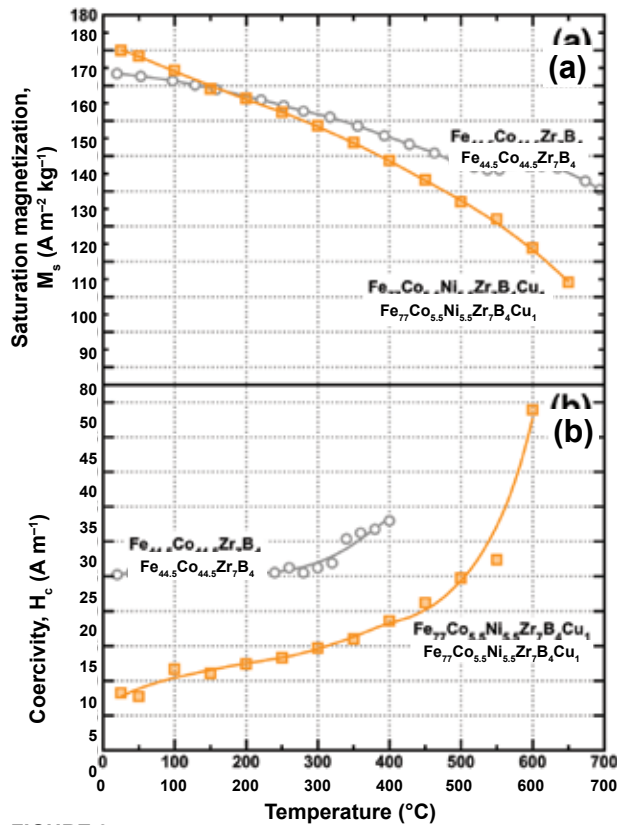


FIGURE 3 Temperature dependence of (a) saturation magnetization and (b) coercivity for a nanocrystalline alloy developed at NRL ($\text{Fe}_{77}\text{Co}_{5.5}\text{Ni}_{5.5}\text{Zr}_7\text{B}_4\text{Cu}_1$) and a state-of-the-art alloy designed for high-temperature use ($\text{Fe}_{44.5}\text{Co}_{44.5}\text{Zr}_7\text{B}_4$).²

improved losses through the broad temperature range from room temperature to 500 °C.² These materials are suitable for Naval power applications at frequencies up to 100 kHz and for use in high-temperature environments or at room temperatures without the necessity for oil cooling (i.e., green technology).

[Sponsored by ONR]

References

- ¹ M.A. Willard and M. Daniil, "Nanostructured Soft Magnetic Materials," in *Nanoscale Magnetic Materials and Applications*, eds. J.P. Liu et al. (Springer, New York, 2009) pp. 373–398.
- ² K. Knipling, M. Daniil, and M.A. Willard, "Fe-based Nanocrystalline Soft Magnetic Alloys for High Temperature Applications," *Appl. Phys. Lett.* **95**, 222516 (2009); I. Skorvanek et al., *Phys. Status Solidi A* **196**, 217–220 (2003).

High Performance Antireflection Structured IR Fibers

J.S. Sanghera,¹ C. Florea,² L.E. Busse,¹ L.B. Shaw,¹ F.H. Kung,³ and I.D. Aggarwal¹

¹Materials Science and Technology Division

²Global Defense Technology & Systems, Inc.

³University Research Foundation

The Problem: Infrared optical fibers are being developed for numerous applications in the 2 to 12 μm wavelength region. These include laser power delivery for infrared missile protection systems as well as infrared active devices such as lasers, filters, and wavelength converters. However, the choice of materials that can be used to draw optical fibers for this region is limited to high-index materials, such as chalcogenide glasses. These materials have high refractive indices (2.4 to 2.8) and, hence, the light experiences high reflection losses when it enters and exits the fiber (around 32% loss for two faces). Thin film antireflective (AR) coatings can be used to reduce these reflection losses, but they damage at relatively low laser peak power intensities ($<0.3 \text{ GW/cm}^2$) compared to the glass ($>1 \text{ GW/cm}^2$). This problem worsens when multilayer coatings are used for the purpose of broadband antireflection performance.

The Solution: An alternative approach to reducing the reflection loss is to build a structure into the surface of the optic itself in which the refractive index effectively varies gradually and continuously from air to the value of the bulk. These structures are generally subwavelength and periodic, typically consisting of a collection of identically shaped features, such as graded cones or depressions, that minimize diffraction and

interference effects.¹ The distances between the features, as well as their dimensions, are designed so that they are smaller than the wavelength of light. If these surface structures are periodic, they are often referred to as a “moth eye” surface structure; otherwise, they are called “random” surface structures. The term “moth eye” is derived from nature, where it was observed that the eye of nocturnal insects such as moths reflected little or no visible light regardless of the angle at which incident light struck the eye surface.² This phenomenon is now well understood and is attributed to the tiny protrusions on the surface of the eye (Fig. 4). It is now possible to create artificial moth-eye structures in the visible and other wavelengths to significantly reduce the reflection loss from an optical interface between air and a window or a refractive optical element. Oxide glasses with moth-eye surface structures have also demonstrated remarkably higher resistance to damage from high-intensity laser illumination³ when compared to the glasses with AR coatings. This bodes well for transmitting high-power mid-IR laser energy through suitable structures produced on the endfaces of IR fibers.

Basic Theory: It is important to design and model these antireflective microstructures for the chalcogenide glasses to identify the shape and height of the features that will minimize reflection losses in the infrared region. Two basic guidelines have been clearly established in the literature: the period of the pattern needs to be smaller than the shortest wavelength in the range of interest, and the height of the features needs to be about half of the largest wavelength in the range of interest. A simple model that yields good results is the effective index method, in which the antireflective structure is sectioned into thin slices and light transmission is estimated at each interface. The key point is that each slice contains a different ratio of air and chalcogenide glass, and this ratio changes continuously and smoothly from the top to the bottom of the microstructure. We used this model to design a suitable AR structure for the IR fibers.

Experimental Details: Typically, subwavelength periodic patterns can be obtained directly in the material through photo- or e-beam lithography and etching, or through an embossing approach in which the desired structure is first built in a robust material (such as metal shim) that is then used to replicate the structure in the desired material. Given the practical ease of the embossing method as previously demonstrated

in stamping vinyl records, we built a specialized chamber to allow for alignment and stamping of the fiber against the shim (Fig. 5). Temperature was used to control the glass viscosity, which in turn dictated the pressure required to stamp the characteristic features onto the surface of the fiber.

The stamping process was correlated with fiber transmission measurements before and after the embossing process. We compared the measured transmission at a single wavelength (3.39 μm) available from a standard HeNe laser to that obtained over the full wavelength range of interest (2 to 5 μm) using an FTIR spectrometer.

Results: Figure 6 shows an infrared fiber cable that has been stamped on both endfaces. (A) and (B) highlight two different types of features that have been demonstrated: (A) shows a positive moth-eye structure with glass protrusions, and (B) shows a negative moth-eye structure with depressed features. These structures have reduced reflection losses so that the transmission through the cable has increased from 68% to over 90%, and furthermore, the transmission was improved over a large spectral bandwidth (2 to 5 μm). In addition, the fiber cable has successfully transmitted the full output power without damage from an infrared laser used in missile protection systems. With optimized design

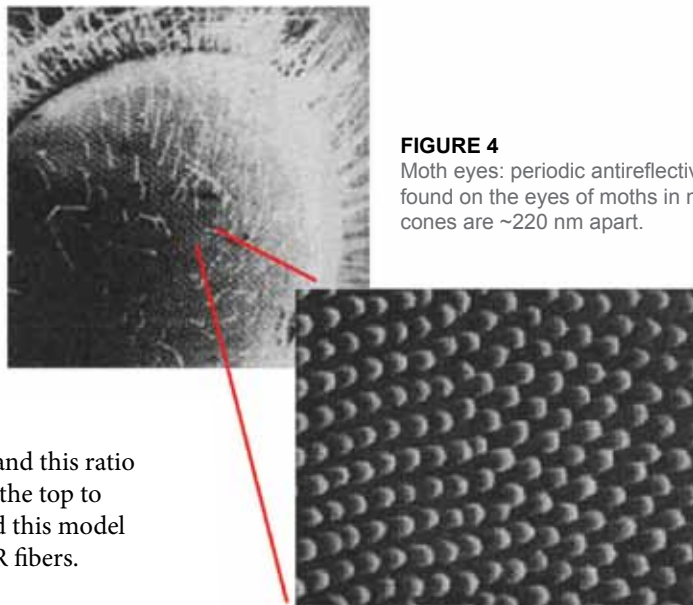


FIGURE 4
Moth eyes: periodic antireflective structures found on the eyes of moths in nature. The cones are ~ 220 nm apart.

of the structure, it will be possible to further improve performance and demonstrate transmission above 95% over the full range of interest.

[Sponsored by ONR]

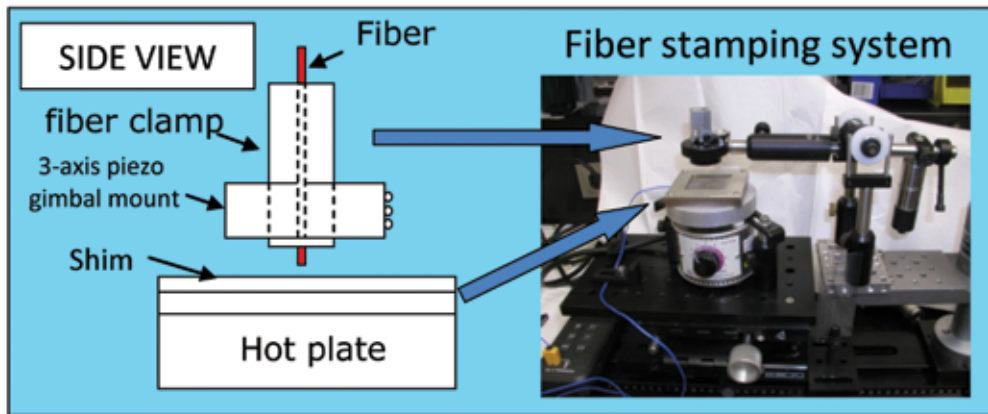
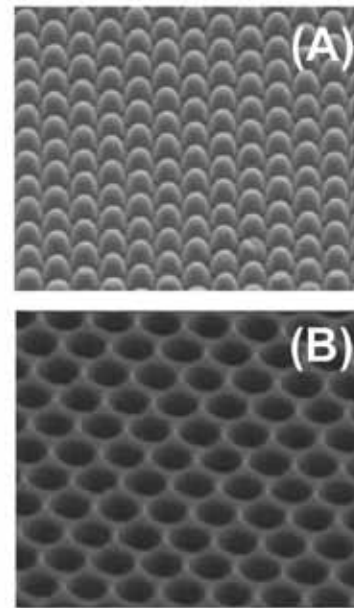


FIGURE 5
A stamping system designed to emboss the antireflective moth-eye structure onto the endface of infrared fibers using a custom-made metal shim.



FIGURE 6
An embossed flexible IR fiber cable with two examples of structures that can be stamped onto the fiber endface: (A) positive moth-eye structure with glass protrusions and (B) negative moth-eye structure with depressed features.



References

- ¹ J.J. Cowan, "Aztec Surface-relief Volume Diffractive Structure," *J. Opt. Soc. Am.* **7**, 1529 (1990).
- ² P.B. Clapham and M.C. Hutley, "Reduction of Lens Reflexion by the 'Moth Eye' Principle," *Nature* **244**, 281 (1973).
- ³ W.H.E. Lowdermilk and D. Milam, "Graded-index Antireflection Surface for High-power Laser Applications," *Appl. Phys. Lett.* **36**, 891 (1980).

Broad-Spectrum Pathogen Surveillance

A.P. Malanoski, T.A. Leski, L. Cheng, Z. Wang,
D.A. Stenger, and B. Lin
Center for Bio/Molecular Science and Engineering

Introduction: A comprehensive resequencing microarray, the Tropical and Emerging Infections (TessArray® RPM-TEI 1.0 array), has been developed

to identify and distinguish between biothreat organisms of interest and genetically close, related species. The approach was confirmed from testing a subset of target organisms, such as Ebola viruses and Lassa viruses, at the U.S. Army Medical Research Institute of Infectious Diseases (USAMRIID) at Ft. Detrick, Maryland. Most potential biothreat organisms are endemic in some part of the world. Using the resequencing pathogen microarray (RPM) for detection in locations such as West Africa can support indigenous monitoring as it provides sequence information. An ongoing collaboration with Njala University aims to establish a broad-spectrum pathogen surveillance capability in the Republic of Sierra Leone, West Africa, using RPM technology combined with a geographic information system (GIS). This has the potential to improve public health efforts in an infected area as well as provide monitoring of the changes occurring to a biothreat organism in its natural location.

Background: Monitoring biothreat agents has become an important issue since the anthrax attacks of October 2001. Most potential biothreat organisms are indigenous to some part of the world, such as Lassa and Ebola viruses in parts of Africa, or Hantavirus in South America.¹ This complicates monitoring of biothreat agents, as the target organisms are not fixed but evolving. In order to mitigate this risk, it is critical to monitor target organisms in their natural environment as part of any pathogen surveillance. In addition, these organisms pose a serious threat not only to regions that are not normally subjected to their presence but also to local populations that are regularly exposed to them. It becomes clear that it is essential to monitor pathogens in their indigenous environment, so that we can gain understanding of the natural reservoir, transmission mode, and the epidemic and temporal dynamics of the organisms. Furthermore, monitoring of biothreat agents in remote populations can be integrated with local surveillance needs if the testing method provides sufficient information. A diagnostic solution we have developed, high density RPM, which tests for many pathogens simultaneously with high sensitivity and specificity, meets these needs (Fig. 7). The solution has the necessary capability to provide genetic sequence information for the organism(s) detected. A lab has been set up in Bo, Sierra Leone, that has the capability to run this diagnostic.

Resequencing Microarrays: RPM provides these capabilities because of its unique combination of features. The core aspect of this method is the high-density nature of the microarray that allows 1 million individual bases to be interrogated. Groups of contiguous bases (100 to 1000 bases) from a specific virus or bacteria strain can be selected that allow related strains (85% sequence similarity) to also be detected. We recently developed in silico modeling of the platform to improve and simplify the microarray design process.² Using this knowledge, it was possible to design in only six weeks an optimal resequencing

microarray, TessArray® RPM-TEI 1.0, for the detection of most Centers for Disease Control and Prevention (CDC, Atlanta, Georgia) category A, B, and C biothreat agents. Validating most of the array with the actual organisms would require a biosafety level 3 facility, which would be costly and time consuming. An alternative using synthetic targets was used to validate the microarray. Overall, the testing results of RPM-TEI 1.0 arrays, performed using target sequences matching the sequence used to generate the microarray probes, demonstrated excellent detection capabilities of RPM for biothreat agents. A number of genetically diverse

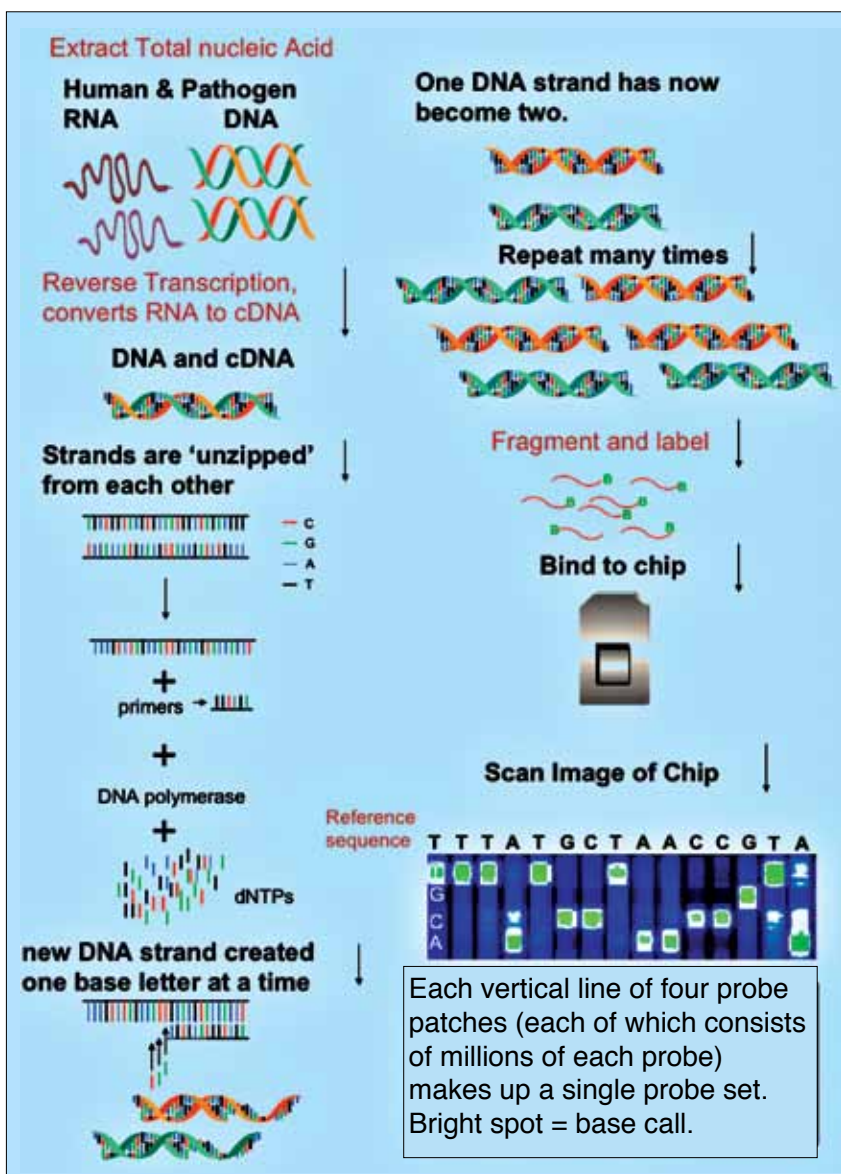


FIGURE 7

Schematic flow diagram of the RPM diagnostic. Total nucleic acids are extracted from a sample, then amplification is carried out to increase the detection sensitivity of the target of interest. Amplified products are subjected to fragmentation and labeling before being hybridized to the microarray. Hybridized microarrays are processed and then scanned to generate the images, which are analyzed to determine a sequence.

viruses were used to confirm these capabilities with experiments conducted in the Virology Division of USAMRIID and carried out according to a standard protocol for testing unknown samples (Table 1).

Sierra Leone: This project aims to create a pathogen surveillance GIS that will use diagnostic data from RPM arrays at Mercy Hospital in Bo, Sierra Leone. Pathogen surveillance must keep track of many factors, such as how a pathogen is transmitted (vector), antibiotic resistance, where it originates, and what it is (biotype/serotype), which have geographic and temporal components that can naturally be stored and related to each other in a GIS. However, implementing a disease-surveillance GIS in Sierra Leone is greatly complicated by the absence of both fine-scale maps in Sierra Leone and the conditions at Mercy Hospital. Power, communications, and computer resources are all required to properly run the RPM diagnostic and to integrate the results into a GIS system. As part of equipping the lab at Mercy Hospital with the RPM platform, a C-band satellite dish was installed, a battery system interfaced with diesel and solar units was set up to provide hybrid power and independence from a single energy source, and the various equipment required for the platform were installed. Collaborators from Njala University have used GPS units to start filling in the missing map information (Fig. 8).

Conclusion: The RPM technology, with its capability of simultaneously testing for many pathogens while providing sequence information, makes it ideal for use where many pathogens have similar initial symptoms and early detection is important. Engaging nations in Africa, Asia, and South America, where many biothreat agents are native, in using this

technology provides advanced tools to support their own efforts to improve public health while providing important information for protecting against biothreat agents.

Acknowledgments: The funding for developing the RPM-TEI 1.0 array was provided by the Office of Naval Research. We also appreciated partial support from Tessarae, LLC through a Cooperative Research and Development Agreement (NCRADA-NRL-06-406). The assistance provided by Drs. Sofi Ibriam and Mahamed Aitichou, and Mr. Justin P. Hardick, Ms. Sarah Strand, and Ms. Raquel Abella during the validation of RPM-TEI chips was also greatly appreciated. We are also grateful for the support provided by the Office of the Secretary of Defense (OSD) Coalition Warfare Office for the “Pathogen Surveillance in West Africa” project. Luke Cheng was supported through the Department of Navy (DoN) Science and Engineering Apprenticeship Program (SEAP).

[Sponsored by ONR, OSD, and Tessarae LLC]

References

- ¹D.G. Bausch, A.G. Sprecher, B. Jeffs, and P. Boumandouki, “Treatment of Marburg and Ebola Hemorrhagic Fevers: A Strategy for Testing New Drugs and Vaccines under Outbreak Conditions,” *Antiviral Res.* **78**(1), 150–161 (2008).
- ²A.P. Malanoski, B. Lin, and D.A. Stenger, “A Model of Base-call Resolution on Broad-Spectrum Pathogen Detection Resequencing DNA Microarrays,” *Nucleic Acids Res.* **36**(10), 3194–3201 (2008).

TABLE 1—Selected Agents Tested Using TessArray RPM-TEI 1.0 Array

| Organism | Taxon | Concentration | RPM Result |
|----------------------------|--------------|-------------------------|-------------------------------------------------------|
| Ebola Zaire | Filoviridae | 1 – 10 ⁻⁴ ng | Zaire Ebola virus strain Zaire 1995 |
| Ebola Reston | | 1 – 10 ⁻³ ng | Reston Ebola virus strain Pennsylvania |
| Ebola Ivory Coast | | 10 ⁻¹ ng | Cotê d’Ivoire Ebola virus |
| Ebola Zaire strain Mayinga | | 10 ⁻¹ ng | Zaire Ebola virus strain Mayinga |
| Marburg Ravn | | 10 ⁻¹ ng | Lake Victoria Marburg virus - Ravn |
| Marburg Musoke | | 10 ⁻¹ ng | No detection |
| Marburg Ci67 | | 10 ⁻¹ ng | Marburg virus strain M/Germany/Marburg/1967/Ratayczak |
| Lassa Josiah | Arenaviridae | 1 – 10 ⁻³ ng | Lassa virus strain Josiah |
| Lassa Z148 | | 1 – 10 ⁻³ ng | Lassa virus strain Z148 |
| Lassa Acar | | 10 ⁻¹ ng | Lassa virus |
| Lassa Weller | | 10 ⁻¹ ng | Lassa virus strain Weller |
| Lassa Pinneo | | 10 ⁻¹ ng | Lassa virus |

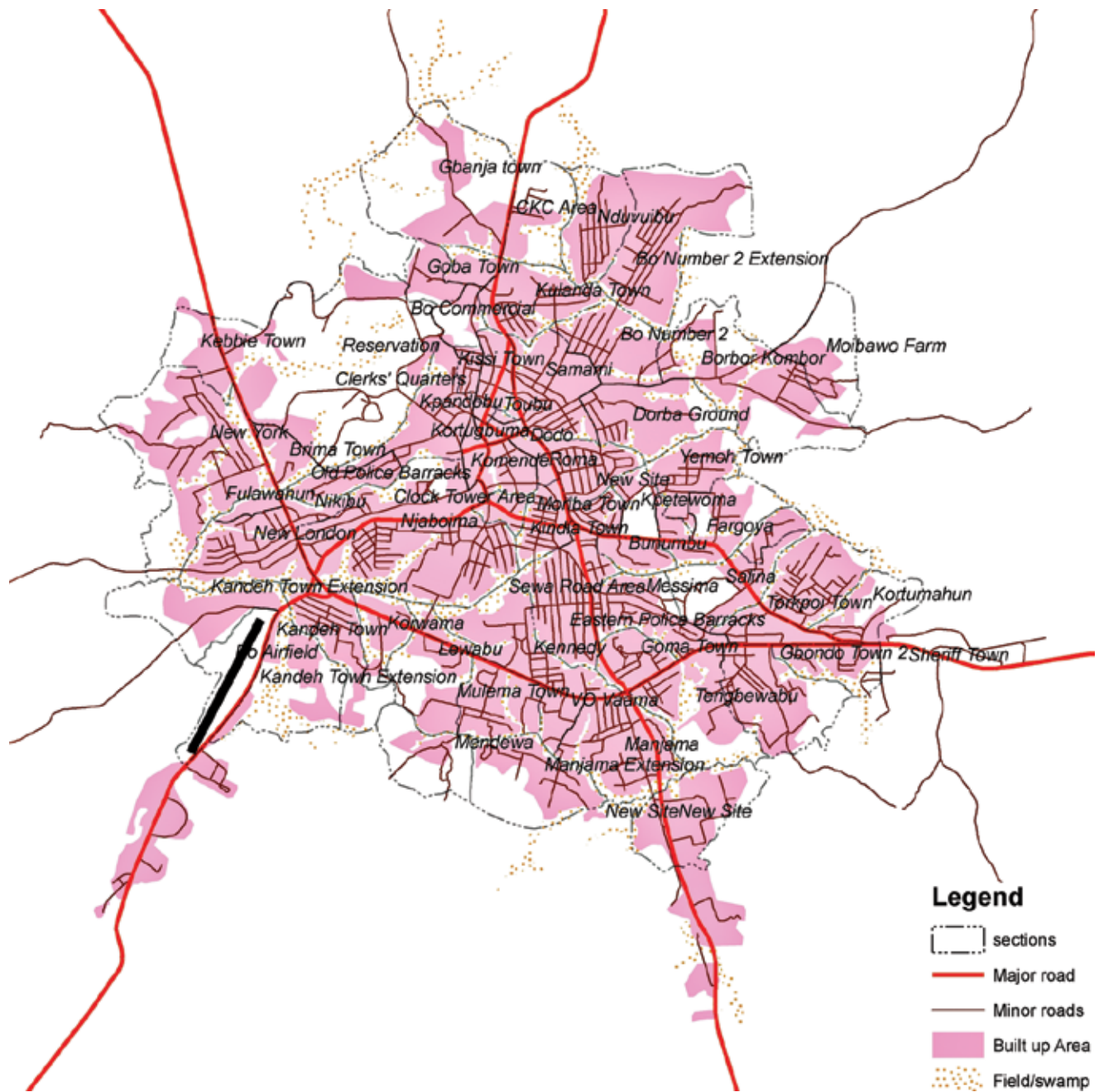


FIGURE 8
 Map of Bo, Sierra Leone. This image was made by integrating remote imagery and GPS handheld units. Major and minor roads, built-up areas, fields, and town sections are all indicated.

Plasma Processing of Ion Energy-sensitive Materials

S.G. Walton,¹ E.H. Lock,¹ M. Baraket,¹ D.R. Boris,¹
R.F. Fernsler,¹ S.H. North,² C.R. Taitt,² J.T. Robinson,³
F.K. Perkins,³ and P.E. Sheehan⁴

¹Plasma Physics Division

²Center for Bio/Molecular Science and Engineering

³Electronics Science and Technology Division

⁴Chemistry Division

Plasma Processing: Plasmas are a critical tool for the production and modification of materials. These partially ionized gases comprising electrons and positive ions can create or modify large areas with precision down to the nanoscale. Consequently, plasmas have been the semiconductor industry's tool of choice to produce the complex circuitry found in the electronic devices we take for granted. Every plasma has its own profile of reactive species including electrons, ions, excited neutrals, reactive neutral fragments (radicals), and photons. This profile depends considerably on the background gas and can be adjusted precisely. By adjusting this profile, the plasma will remove material, deposit material, or change the chemical makeup of the surface to which it is exposed. Despite a string of successes, serious concerns remain over the use of plasmas in producing and modifying materials used in next-generation electronic, sensing, and energy applications. More specifically, ions with large kinetic energies can produce unwanted effects. For polymers, ion-induced surface roughness can render the material unusable, and in the case of monolayer films like graphene, etching must be avoided.

The plasma processing system developed in NRL's Plasma Physics Division averts these issues because of its ability to deliver ions with very low kinetic energies (Fig. 9). To understand this, one must recognize that most plasmas are sustained by applying electric fields. The applied field couples mainly to the electrons, increasing their energy so that some fraction of the population is energetic enough to ionize the gas. While the electrons are energetic, the ions remain at or near the background gas temperature. In order to prevent the more mobile electrons from leaving, the plasma self-organizes to maintain a positive potential such that electron losses are reduced. Nearly all of this potential arises at the plasma-substrate interface, and so positive ions impacting the substrate arrive with energies well in excess of the electrons. Our approach to plasma generation uses a high-energy electron beam to ionize, excite, and dissociate the background gas. Because electric fields are not required, the plasma electrons have very little energy and so the plasma potential is small as well. In fact, ions arrive at the surfaces with energies of only a few eV, a value that is at or below the bond strength of polymeric materials and graphene. We have successfully functionalized polymer substrates of interest in biothreat detection and diagnostic technologies and treated graphene for electronics and sensing applications without damaging the material.

Chemical Functionalization of Microtitre Plates:

With colleagues in the Center for Bio/Molecular Science and Engineering, we have developed a method for chemically functionalizing commercial, polystyrene microtitre plates to facilitate biomolecule immobilization. The multi-well microtitre plate is a standard

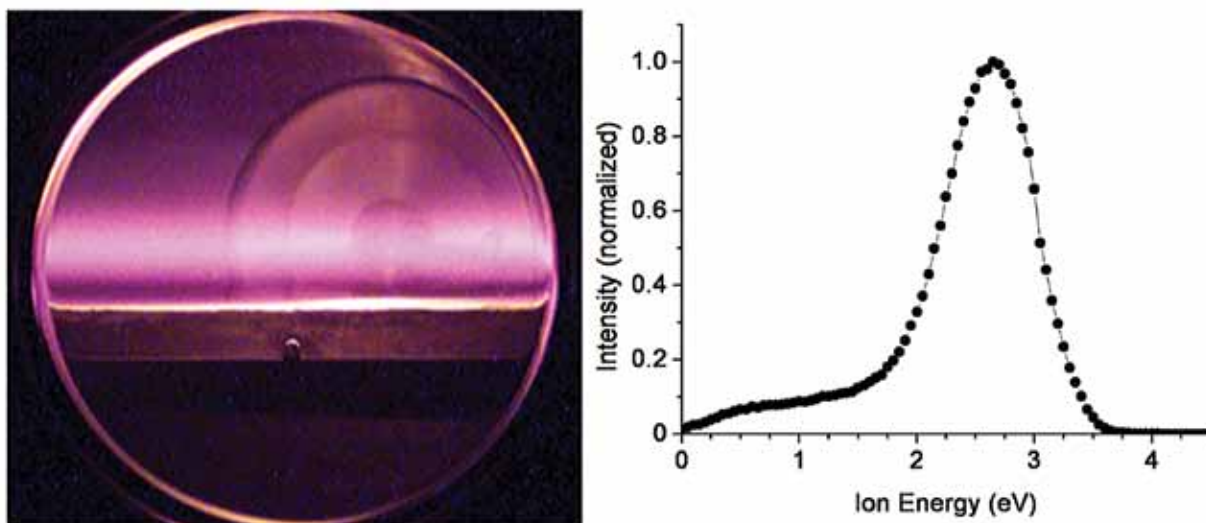
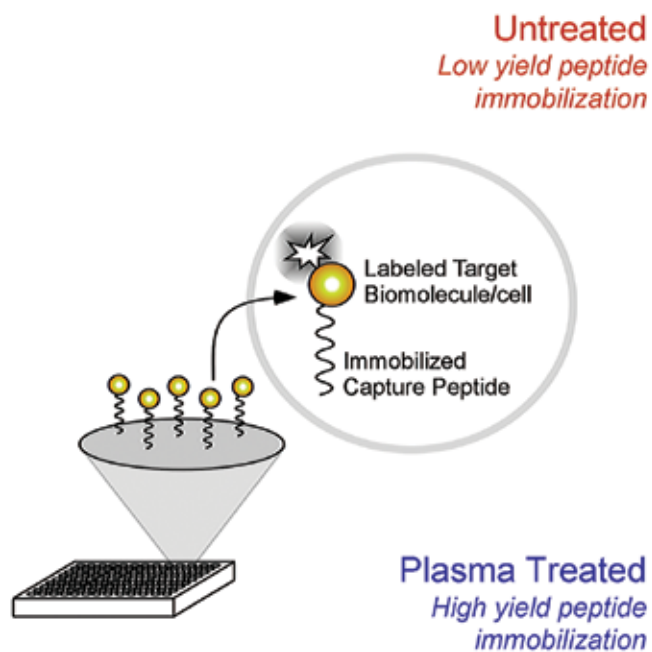


FIGURE 9

NRL's plasma processing system (left) and an ion energy distribution measured at an adjacent processing stage (right). The range of ion energies is below the bond strength of many materials and is a critical feature in the success of the system.

tool used for the development of diagnostic tests and other biological detection schemes. Depending on the target agent, specific “capture” biomolecules are immobilized on the plate surface. While nonspecific adsorption is the most commonly used method for immobilization of proteins, many biomolecules do not retain their enzymatic or binding activities when immobilized in this fashion. Specifically, covalent immobilization allows for a stable and oriented display of these biomolecules. Using our plasma processing system, we introduce chemical functionalities to the plate surfaces, which allow for virtually any type of covalent attachment chemistry without changing the surface morphology. In Fig. 10, we demonstrate differential binding properties of a bacterial biomarker, lipopolysaccharide (LPS), to a variety of antimicrobial peptides (AMPs) immobilized onto plate surfaces that have been treated with plasma (bottom) and those that have not (top). Although the example of Fig. 10 is specific to oxygen, the plasma-based approach is flexible and allows us to introduce a variety of chemical moieties for covalent attachment.



Chemical Functionalization of Graphene:

Graphene is a single monolayer of sp^2 bonded carbon, with superlative electrical, mechanical, and thermal properties. However, to increase the range of potential graphene-based applications, precise control over surface functionalities is required. With colleagues in the Chemistry and Electronics Science and Technology Divisions, we have developed an approach that can decorate the surface of graphene with various functional groups without adversely disrupting the graphene honeycomb structure. Figure 11 shows chemical and structural characteristics before and after adding oxygen functional groups. The oxidized graphene has distinct chemical signatures associated with the addition of oxygen as well as a significantly increased D-peak, indicating the transformation from sp^2 to sp^3 carbon. However, the sp^2 carbon and the graphitic-induced G band remain. Importantly, after high-temperature annealing to remove the functionalities, the pretreatment characteristics are recovered, indicating little or no damage to the graphene structure as a result of the treatment. Here again, the

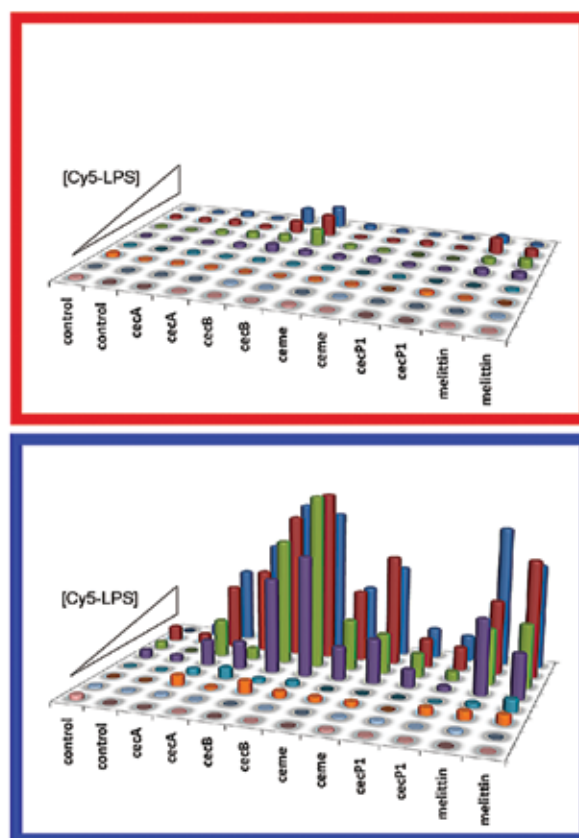


FIGURE 10

Fluorescence from untreated (top) and plasma treated (bottom) microtitre plates indicating the binding of a fluorescently labeled bacterial biomarker, lipopolysaccharide (LPS), to a variety of antimicrobial peptides. Plasma treatment introduces chemical moieties that promote the covalent immobilization of peptides, thereby increasing the LPS capture yield and the associated signal strength by up to 40 times compared to the untreated plates.

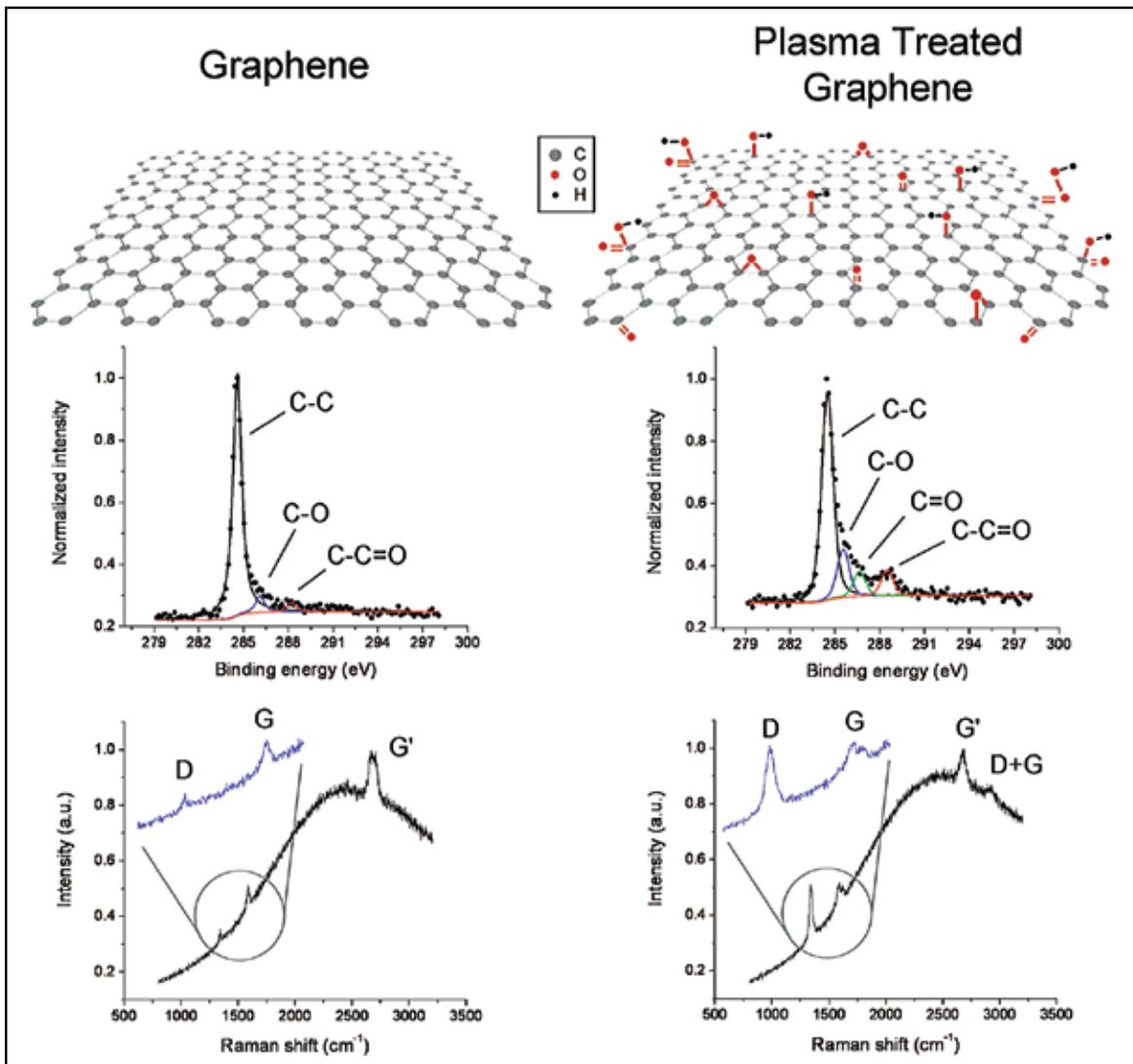


FIGURE 11

A representation of graphene functionalization (top) along with supporting surface diagnostics. X-ray photoelectron spectroscopy (XPS) measurements (middle) show an increase in the oxygen functionalities bound to carbon after exposure to an argon/oxygen plasma. The presence of those species alters the carbon bond structure, as indicated by the increase in the D band signal in the Raman spectrum (bottom).

system's flexibility enables us to tailor the functional group by simply changing the operating gas mixture.

[Sponsored by NRL/ONR and DTRA]

Standoff Detection of Trace Explosive Residues by Resonant Infrared Photothermal Imaging

C. Kendziora,¹ R.A. McGill,¹ R. Furstenberg,¹ M. Papantonakis,¹ V. Nguyen,¹ G. Hubler,¹ and J. Stepnowski²

¹Materials Science and Technology Division

²Nova Research Inc.

Counter-IED Motivation: Motivated by improvised explosive device (IED) and homeland security concerns, explosives detection is a critical research area for the Navy, the Department of Defense (DoD), and the Department of Homeland Security (DHS). An emerging thrust is to potentially replace point detection of trace residues (which requires physical contact) with standoff capability from a safe distance. Ideally, a standoff technique should be safe to use around people, nondestructive, selective, rapid, and adaptable to new types of threats. NRL's Materials Science and Technology Division has demonstrated a novel resonant infrared (IR) photothermal approach that has the potential to meet these goals. In this technique,

light of a specific infrared wavelength is directed to the surface of interest and the thermal response is viewed with an infrared camera. Comparing the thermal image as a function of incident wavelength with the absorption spectrum of explosives reveals the presence and location of trace residues. By varying the incident wavelength, other analytes of interest (e.g., drugs and chemical agents) could also be imaged. Field testing of an NRL-built system was successfully performed at the Yuma Proving Ground in Yuma, Arizona.

Infrared Signature Based Technical Approach:

The infrared region of the electromagnetic spectrum between 2 and 12 μm is often referred to as the “fingerprint region” for chemical identification because the patterns of absorption bands are highly material specific. Figure 12 illustrates the IR transmission for three explosives analytes of interest — RDX, TNT, and DNT — and water vapor in air at atmospheric pressure.¹ This selective absorption property is exploited in the NRL Remote Explosives Detection (RED) approach by shining light from an infrared quantum cascade laser (QCL) at a wavelength that is selectively absorbed by trace explosives on the surface of interest. Due to the low vapor pressure of explosives, these traces can persist in particle form for months or longer.

Figure 13 shows the schematic diagram for the NRL RED technology.² The 6.25 μm wavelength is selectively absorbed by the nitrogen–oxygen stretch vibration common to most high explosives. The 6.25 μm light is transmitted through humid air due to a narrow gap in the water vapor absorption spectrum. Additional laser wavelengths can be added to increase sensitivity and selectivity, or to detect other analytes of interest. Signal collection is performed in the long-wave IR (LWIR) transparent region of the spectrum from 8 to 12 μm . The figure also shows an example differential image (laser “on” minus laser “off”) where both TNT and RDX are detected using 6.25 μm wavelength light from a QCL.³ The red circle indicates the area illuminated by the beam.

Field Testing at Yuma Proving Ground: A multi-disciplinary team of physicists, chemists, and engineers from the Division designed, assembled, and field-tested a cart-based system to test the RED technology under a variety of ambient parameters, including temperature, sunlight, humidity, dust, wind, and standoff distance.⁴ Figure 14 shows the assembled RED cart system during testing at the Yuma Proving Ground. The red arrow in the figure traces the approximate path of the invisible IR laser beams from the cart to the sample tripod 10 m away. The cart system actually features four lasers (two on resonance and two off resonance) to increase the detection sensitivity and selectivity. The beams are

collimated at a 12 mm diameter to optimize use of the available laser power. The laser output powers were in the eye-safe (Class 1) range so that users and observers did not have to wear laser goggles. The thermal imager used on the cart was an inexpensive uncooled bolometer array. The collection optic was a standard commercial germanium lens.

The experiment consisted of directing the laser beam (and co-aligned collection optics) toward a surface of interest using a mirror gimbal. A sequence of four laser pulses took approximately 1 s while the thermal images were collected. Comparing the frames with the laser on to those with the laser off yielded the signal due to the RED process. During this testing, the explosives TNT, RDX, PETN, C4, Tetryl, Comp B, PBX4, and PE4 were successfully detected as far as 30 m away. This distance is not a fundamental limitation for the technique, and improvements to the system are ongoing.

This field test demonstrated that the RED technique is not limited by daylight, variable temperature, humidity, or sand. It was able to detect all eight explosives species tested at 10 m or greater distance using eye-safe laser powers. The capability to perform stand-off detection of trace explosives using eye-safe lasers is of great importance in the counter-IED mission for Navy, DoD, and DHS applications. This technology is being further developed to make the system more compact and rugged, and to increase system sensitivity, selectivity, and standoff distance capability.

[Sponsored by the OSD Rapid Reaction Technology Office and NRL/ONR]

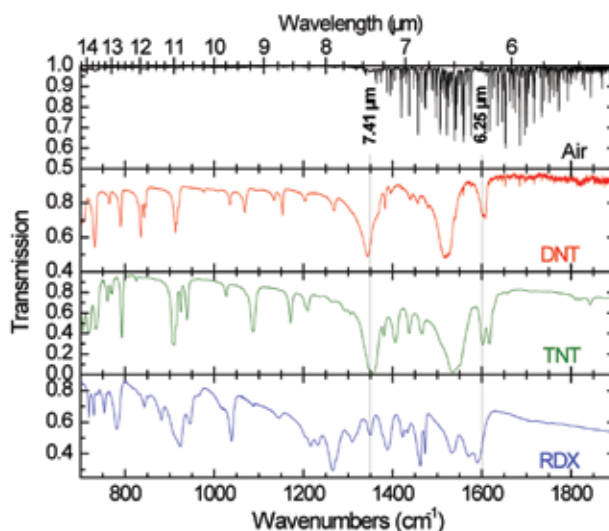
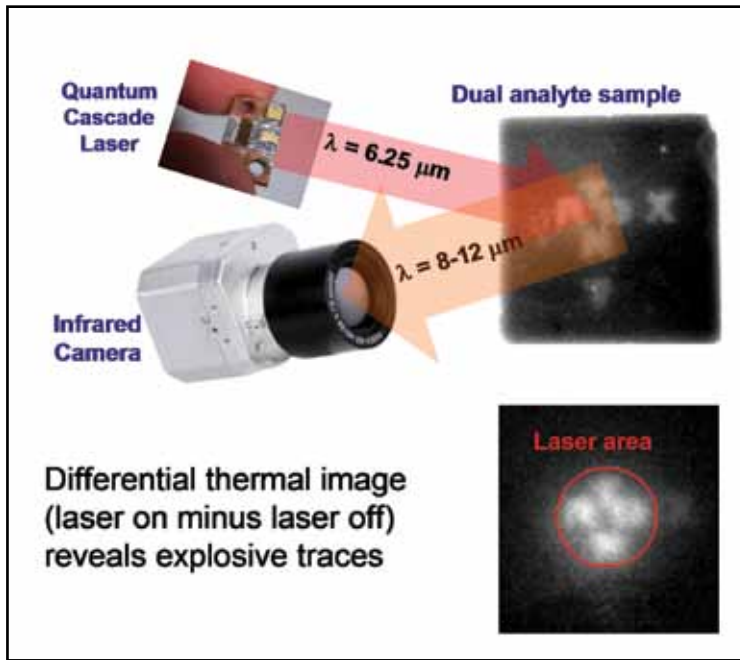


FIGURE 12 The infrared transmission spectra of the explosives RDX, TNT, and the decay product DNT. Dips in the spectra correspond to absorption bands. Absorption bands common among the explosives, such as those shown at 6.25 and 7.41 μm , are highlighted with vertical lines.

**FIGURE 13**

The RED technology. An IR beam from the QCL is selectively absorbed by the trace explosives on a surface, causing a slight heating. This heat signal is detected and imaged using an IR camera.

**FIGURE 14**

The NRL cart system during testing at the Yuma Proving Ground. The sample tripod is positioned at 10 m standoff distance. The red arrow illustrates the approximate path of the invisible infrared beam.

- ⁴ R. Furstenberg, C. Kendziora, M. Papantonakis, S.V. Stepnowski, J. Stepnowski, V. Nguyen, M. Rake, and R.A. McGill, "Stand-off Detection of Trace Explosives by Infrared Photo-thermal Spectroscopy," *IEEE Conf. on Technol. for Homeland Security*, 2009, 978-1-4244-4179-2, 465-471 (2009).

References

- ¹ R. Furstenberg, C.A. Kendziora, J. Stepnowski, S.V. Stepnowski, M. Rake, M.R. Papantonakis, V. Nguyen, G.K. Hubler, and R.A. McGill, "Stand-off Detection of Trace Explosives via Resonant Infrared Photothermal Imaging," *Appl. Phys. Lett.* **93**, 224103 (2008).
- ² R.A. McGill et al., "Detection of Chemicals With Infrared Light," U.S. Patent Application No. 12/255,103, filed Oct. 21, 2008, Publication No. US2010/0044570 A1, Feb. 25, 2010.
- ³ M.R. Papantonakis, C. Kendziora, R. Furstenberg, S.V. Stepnowski, M. Rake, J. Stepnowski, and R.A. McGill, "Stand-off Detection of Trace Explosives via Resonant Infrared Photothermal Imaging," *Proc. SPIE* **7304**, 730418-8 (2009).

194

Spectral Tuning of Organic Nanocolloids

C.M. Spillmann, J. Naciri, G.P. Anderson, M. Chen, and B.R. Ratna

196

Spin Rotation for Quantum Information

S.E. Economou, A. Greilich, and T.L. Reinecke

198

Sheet of Carbon Atoms Points Way to Ultra-fast Transistors

D.K. Gaskill, P.M. Campbell, G.G. Jernigan, J.B. Boos, J.G. Tischler, E.R. Glaser, J.C. Culbertson, J.L. Tedesco, R.L. Myers-Ward, C.R. Eddy, Jr., N.A. Papanicolaou, J.G. Champlain, D. Park, and R. Bass

200

Functionalized CMOS Nanomechanical Resonators for Chem-Bio Sensing

J.W. Baldwin, M. Zalalutdinov, J.S. Burgess, and B.H. Houston

Spectral Tuning of Organic Nanocolloids

C.M. Spillmann, J. Naciri, G.P. Anderson,
M. Chen, and B.R. Ratna
Center for Bio/Molecular Science and Engineering

Introduction: There is a need within the Navy and Department of Defense for the development of multifunctional and smart materials on the nanoscale. Such materials are relevant to several focus areas of importance to the Navy, including the advancement of nanoscience technology and chemical and biological detection. As part of this vision, NRL is studying the controlled self-assembly and interaction of molecules to create tunable and functional organic nanostructures. Liquid crystal (LC) is a mesophase of matter ideal for incorporating tunable functionality at different length scales due to its ability to inherently self-organize. We use the self-assembly of polymerizable LCs to control the molecular aggregation of stable fluorescent chromophores to create a unique class of organic fluorescent nanocolloids (FNCs) and demonstrate tuned fluorescent emission spectra of nanocolloid populations under single wavelength excitation.

Nanocolloid Synthesis and Characterization: Fluorescent nanocolloids are synthesized using three components: an LC cross-linking agent that exhibits a stable nematic phase, a homologue of the organic chromophore perylene, and polymerizable surfactant. The perylene derivative, PERC11, is chosen due to its strong absorption and fluorescence, and outstanding (photo)chemical and thermal stability. The surfactant

capping agent has a carboxylic head group that allows for chemical coupling of the FNC surface to biomolecules of interest. The end result is FNCs composed of a cross-linked network of LC molecules with controlled dye aggregates distributed throughout the interior of the nanocolloid and capped by a functional surfactant.

Using an established two-phase miniemulsion procedure, stable spherical nanocolloids suspended in water are produced with diameters ranging from 50 to 300 nm, as determined from dynamic light scattering and scanning electron imaging. The mole ratio of dye to LC cross-linking agent is varied from 0.6% to 4.8%, and yet within this small range we are able to tune the fluorescent emission of the FNCs over much of the visible spectrum (Fig. 1).

Spectroscopic Characterization: The absorption spectra of FNCs containing 0.6 and 4.8 mol% PERC11 reveal a shift from the 0–0 vibronic transition to the 0–1 and 0–2 transitions of the dye as it assembles into larger aggregates. We also observe a red-shift in the fluorescent emission spectrum as the dye concentration is increased in FNC populations excited at 488 nm. This effect is the result of a shift in the vibronic states of the dye aggregate due to the stacking of the π - π molecular orbitals. Confocal images of four different FNC populations deposited on a substrate demonstrate the tuned emission spectra of the FNCs [Fig. 2(a)]. Spectral analysis of individual colloids reveals that the PERC11 molecular aggregates at a given concentration are uniformly distributed throughout the FNC population [Fig. 2(b)].

Control experiments with non-LC cross-linking agents reveal that control of PERC11 aggregation in

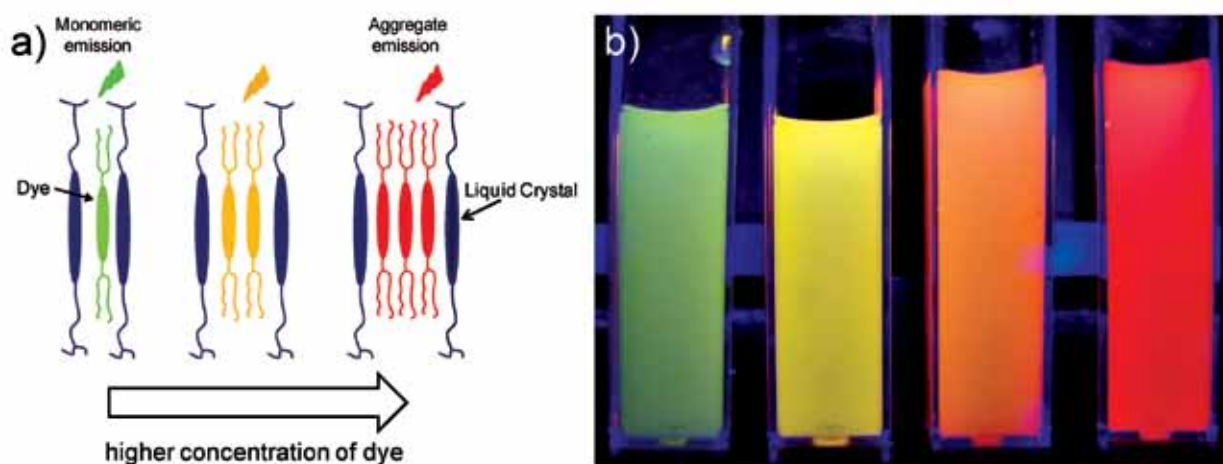


FIGURE 1

(a) Schematic of dye and cross-linking agent interaction. Control of PERC11 aggregation in FNCs is dictated by the ratio of dye to the nematic cross-linking agent DACTP11. A low ratio of dye to DACTP11 results in a monomeric emission spectrum, while increasing the ratio leads to aggregate formation and a red-shift in the emission spectrum. (b) Four FNC populations suspended in water under UV excitation with 0.62 (green), 1.54 (yellow), 2.54 (orange), and 4.84 (red) mol% of PERC11 to DACTP11.

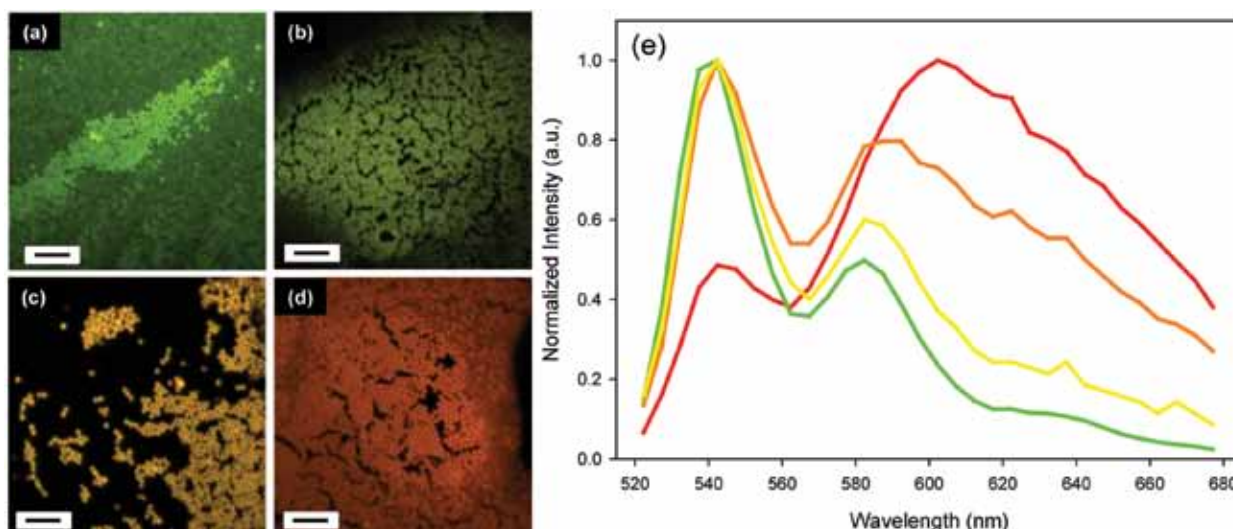


FIGURE 2 Confocal images and emission spectra of FNC samples deposited and dried on silicon substrate correspond to FNC samples with (a) 0.62, (b) 1.54, (c) 2.54, and (d) 4.84 mol% PERC11. (e) Average spectral emission of FNCs in images (a) through (d). Scale bars in images (a) through (d) equal 2 μm .

FNCs is driven by three parameters. The first is miscibility of the molecular components in the temperature range used to synthesize the nanocolloids. The second parameter is π - π molecular interactions between the dye and the LC cross-linking molecule. Our results show that a liquid crystal molecule with sufficient core-core interactions with perylene controls the aggregation of dye molecules. The third parameter is the ratio of the molecular species. Adjusting the mole ratio of PERC11 relative to the LC cross-linker controls the dye aggregation and tunes the fluorescent emission spectra

of FNCs. The quantum yield of the FNCs varied from ~ 1.0 to 0.6 as the emission spectra shifted from green to red, respectively, and indicates that confinement of the dye and dye aggregates by the LC cross-linking agent does not significantly alter with quantum yield in the FNCs.

Fluorescent Tracer in Bioassays: To demonstrate the functionality of FNCs, we bioconjugate the surface to primary amines of NeutrAvidin (NA). The FNC-NA complexes are used as fluorescent tracers in a fluid

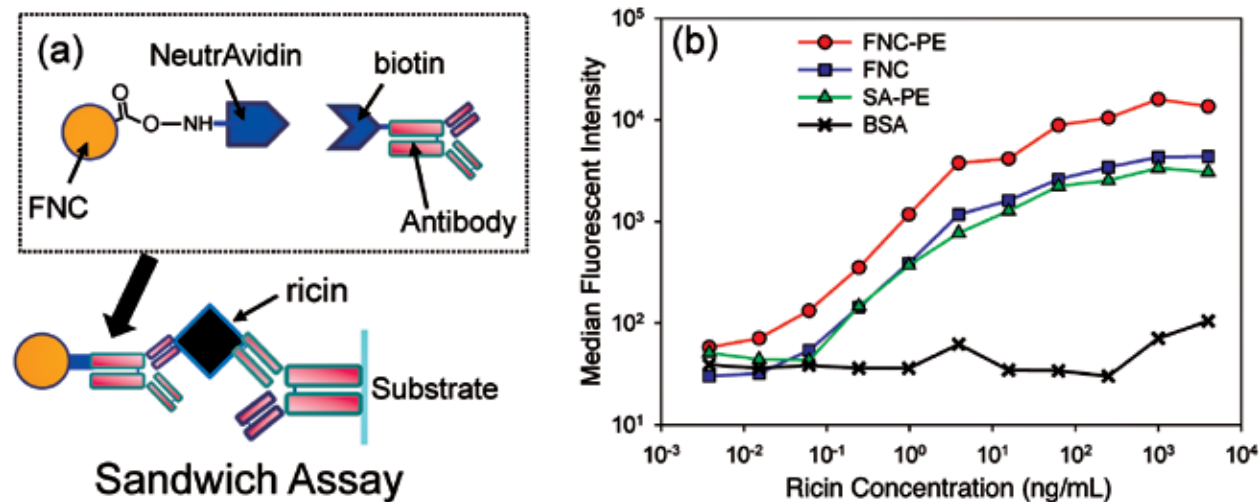


FIGURE 3 Fluid array immunoassay with FNCs. (a) Schematic representation of FNC-NA coupling to biotinylated anti-ricin antibody to complete a sandwich immunoassay. (b) Intensity of FNC-NA conjugated to anti-ricin antibodies tracked as a function of ricin concentration. FNCs (blue) matched signal strength of standard streptavidin-phycoerythrin (SA-PE) bound to anti-ricin (green). Fluorescent intensity of FNC-NAs amplified by addition of biotinylated phycoerythrin (FNC-PE) to NeutrAvidin on a nanocolloid surface (red). Microspheres coated with bovine serum albumin (BSA) were included as control for nonspecific binding (black).

array immunoassay to detect the highly toxic protein ricin. A schematic setup of the FNC preparation and assay is shown in Fig. 3(a). The FNCs match the fluorescent intensity for streptavidin-phycoerythrin (SA-PE), a standard label for the assay [Fig. 3(b)]. The utility of using nanoparticles as a scaffold to amplify the assay is demonstrated by subsequent addition of biotinylated PE (Bt-PE), which upon binding to the unoccupied NA on the nanoparticles results in a four-fold increase in fluorescent intensity. These encouraging initial results portend the usefulness of FNCs in a wide range of fluorescent bioassays.

Summary: We demonstrate the concentration-dependent spectral tuning of perylene in a nanocolloid system. Manipulation of π - π molecular orbital interactions in the presence of an LC component controls the dye stacking and emission spectrum. We find that the molecular structure of the LC cross-linking agent and its phase behavior play a critical role in controlling the perylene molecular aggregates. The organic nanocolloids are highly fluorescent, exhibit a long shelf life, and are easy to bioconjugate. The simplicity of the synthetic approach and ease of surface functionalization provide opportunity to design other novel multifunctional nanocolloids beyond the FNCs described here.

[Sponsored by NRL and DTRA]

Spin Rotation for Quantum Information

S.E. Economou,¹ A. Greulich,² and T.L. Reinecke¹

¹Electronics Science and Technology Division

²University of Maryland, College Park

Introduction: Quantum information technologies, which include quantum communications and quantum computing, offer revolutionary opportunities for highly secure communications and for real-time processing of large data arrays in battle environments, which are important to the Department of Defense. The fundamental properties of quantum mechanics, such as entanglement and measurement-induced “collapse” of a quantum state, can prevent eavesdropping over quantum communication channels and can enable the solution of problems that grow exponentially difficult with classical computation.

Optical Spin Rotations: Electron spins in solids are among the leading candidates as quantum bits (qubits) for storage and processing of quantum information, with the direction of the spin — up or down — forming the two states of the qubit. The basic logic operation required for quantum information

processing is the coherent rotation of the spin qubit. This is more general than simply changing the spin state from an initial prescribed state to a final one; instead, we need to be able to perform a given operation without knowledge of the input state of the qubit. This makes any protocol harder to design and implement. In our theoretical work,¹ we developed the design of a spin rotation protocol using fast optical laser pulses. This work provided a straightforward prescription for the experimental implementation of spin rotations, which had not been demonstrated at that time. This approach is fast and experimentally simple, and takes advantage of the special properties of optical pulses that have a hyperbolic secant temporal shape.

The spin can be represented by a 3D vector on a unit sphere (Bloch sphere), as shown in Fig. 4. Any rotation of a vector can be described by two quantities, the axis of rotation and the angle of rotation. A spin state that is parallel to the axis of rotation will not be rotated by said rotation, but in quantum mechanics it will acquire a phase. In the self-assembled III-V semiconductor quantum dots of interest in quantum information, there are preferred directions. The direction along which the quantum dot is grown sets the quantization axis for optical polarization selection rules. We use an external magnetic field to determine a second preferred direction, the energy quantization axis. To implement an arbitrary spin rotation, the two axes should not be parallel. We choose them to be orthogonal and refer to them as z and x respectively. We exploit the two inequivalent directions and, by adjusting the pulse polarization, induce phases to the corresponding spin states. This phase is precisely the angle of spin rotation.

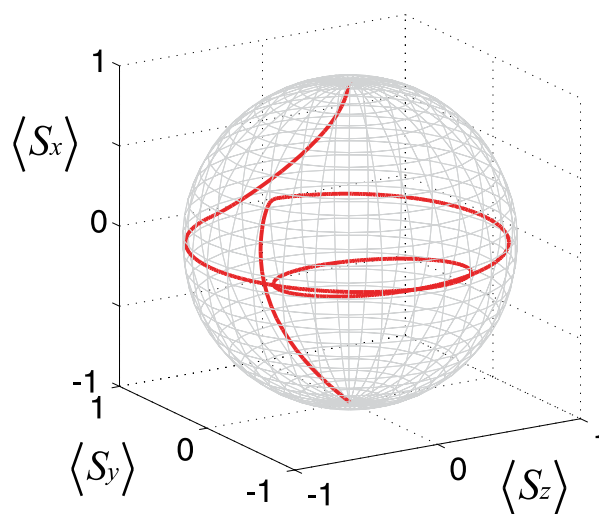


FIGURE 4 Calculation of the trajectory of the spin vector undergoing a rotation about the y axis composed of three rotations (z - x - z). The tip of the spin vector is shown (red).

The experimental demonstration of these ideas was carried out in our recent joint work with an experiment² on an ensemble of InAs quantum dots, each charged with an excess electron. A sequence of three pulses was used: a pump, a control, and a probe. The pump laser sets the spins in a well-defined initial state (z) perpendicular to the external magnetic field B , which points along the x axis. Under the influence of this magnetic field, the spins precess in the yz plane, as shown by the black line in Fig. 5(a). An appropriately chosen control laser pulse circularly polarized along the z axis will induce rotations of the spin about the z direction. Therefore, the effect of this rotation will be most evident when the control pulse finds the spin pointing along the y direction. The probe measures the z direction of the spin by optical absorption. Since the

spin vector is precessing in a circle, its z projection will be oscillating in time, as shown in Fig. 5(b).

In the theory,¹ the angle of rotation depends on the detuning of the control pulse (the difference in optical frequency between the transition resonance and the pulse) for fixed pulse duration and pulse intensity. Thus only the control pulse frequency needs to be tuned in order to change the rotation angle. To demonstrate experimentally the predicted dependence of the spin rotation on the detuning, we fixed the intensity and time of incidence of the control pulse and varied the detuning. The measured z component of the spin is shown in Fig. 5(b) for several values of the detuning. The measured dependence of the rotation angle on the detuning is in very good agreement with the predicted one, as shown in Fig. 5(c).

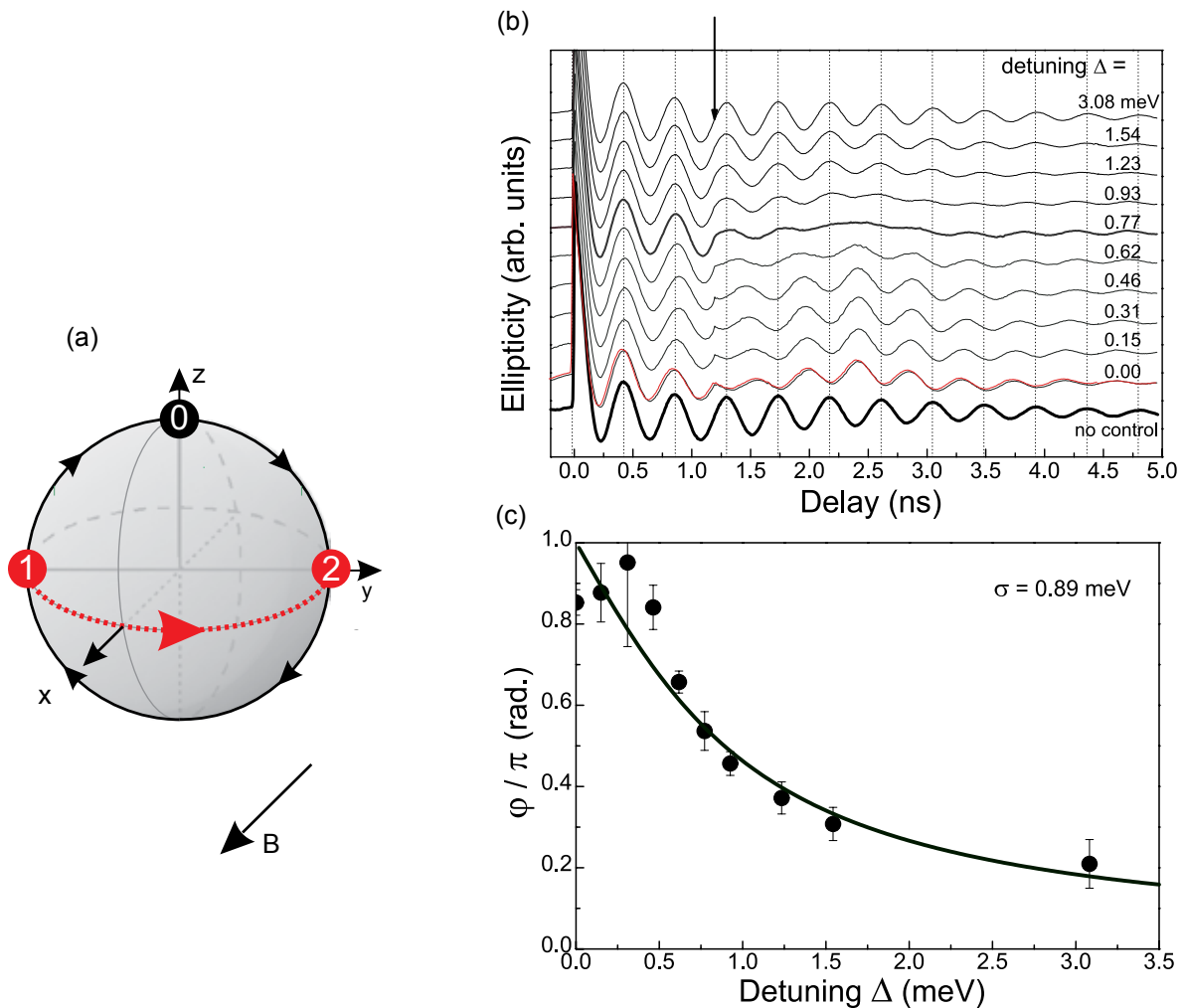


FIGURE 5

(a) Sketch of the spin vector tip precessing about the B field (x axis) and rotated about the z axis, from $-y$ to y . (b) Experimental data of the z projection of the spin as a function of time. The arrow denotes the time of incidence of the control pulse. The change in phase and amplitude of the z projection is due to the rotation of the spin. (c) Experimental dependence of rotation angle on the detuning of the control pulse (points) plotted against theoretical prediction (curve) with no adjustable parameters.

Conclusions: We have designed theoretically and demonstrated experimentally an optical technique to implement arbitrary spin rotations in semiconductor quantum dots. These single qubit gates form the fundamental logic operations in quantum information processing devices, which once built will have important implications for how the Navy processes information.

[Sponsored by NRL and ONR]

References

- ¹S.E. Economou and T.L. Reinecke, “Theory of Fast Optical Spin Rotation in a Quantum Dot Based on Geometric Phases and Trapped States,” *Phys. Rev. Lett.* **99**, 217401 (2007).
²A. Greilich, S.E. Economou, S. Spatzek, D.R. Yakovlev, D. Reuter, A.D. Wieck, T.L. Reinecke, and M. Bayer, “Ultrafast Optical Rotations of Electron Spins in Quantum Dots,” *Nature Physics* **5**, 262–266 (2009).

Sheet of Carbon Atoms Points Way to Ultra-fast Transistors

D.K. Gaskill, P.M. Campbell, G.G. Jernigan, J.B. Boos, J.G. Tischler, E.R. Glaser, J.C. Culbertson, J.L. Tedesco, R.L. Myers-Ward, C.R. Eddy, Jr., N.A. Papanicolaou, J.G. Champlain, D. Park, and R. Bass
Electronics Science and Technology Division

Introduction: Graphene is a two-dimensional sheet of carbon atoms arranged in a hexagonal pattern (similar to a “chicken-wire fence”), and due to its unusual properties is of great interest to the electronics community. For example, the electrons and holes in graphene act as if they have zero effective mass and travel at velocities faster than in any semiconductor. This property could be used to make a transistor that switches faster than any other made. Through a program in NRL’s Institute for Nanoscience, researchers in the Electronics Science and Technology Division (ESTD) have developed a method to make wafer-scale graphene, known as epitaxial graphene (EG). These efforts resulted in NRL teaming with HRL, Inc., in DARPA’s Carbon Electronics for RF Applications (CERA) program, where the team fabricated EG field effect transistors that defined the state of the art for graphene in several performance metrics. The characteristics of these devices have been used to predict that the ultimate switching speed of suitably scaled graphene transistors should be a trillionth of a second or faster. Such ultra-fast THz electronic devices are of great interest to the U.S. Navy for various applications, including low noise amplifiers (LNAs), where ultra-fast switching cannot easily be achieved with existing electronics technology.

Epitaxial Graphene: For many years it has been known that heating silicon carbide (SiC) substrates to temperatures in excess of 1300 °C in ultra-high vacuum could sublime Si atoms, resulting in a carbon-rich surface. Recently, it has been understood that when this process takes place on the basal plane of hexagonal SiC, the residual carbon will reconstruct to form the graphene hexagonal lattice. NRL discovered that for improved graphene properties, the starting substrate surface must be prepared to be atomically smooth and free of underlying defects — this was achieved by etching the SiC substrate in hydrogen at elevated temperatures. After the subsequent sublimation of silicon, EG formation on the substrate surface was confirmed by graphene’s relatively unique Raman spectral fingerprint. Figure 6 shows EG on the Si-polar face of a SiC substrate. Epitaxial graphene also grows on the C-polar face of SiC, albeit faster. Analysis of the film in Fig. 6 showed that the flat “terraces” between the raised “atomic steps” were covered with a single layer of graphene, about 3.3 Å thick, whereas the steps were covered with about two layers of graphene.

The electrical properties of EG were characterized by the van der Pauw Hall technique using small (10 by 10 μm²) test structures. The 300 K Hall data for EG on the Si-face (blue) and C-face (red) of the SiC substrate are shown in Fig. 7. As can be seen, the mobility of graphene can be higher than that of conventional semiconductors, such as silicon. In addition, the data in Fig. 7 predict that EG will have extremely high

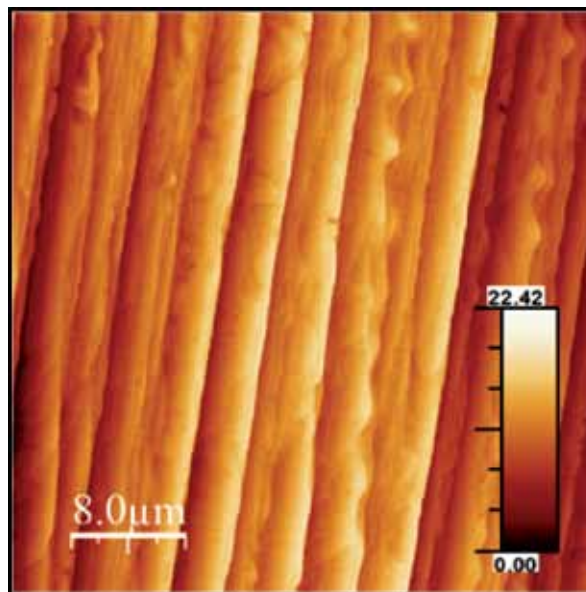
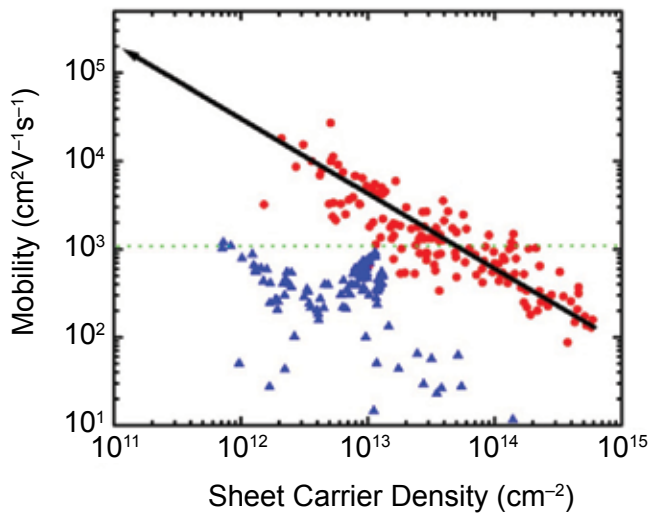


FIGURE 6
 Atomic force micrograph of epitaxial graphene on the Si-face of SiC. The scale units are nm. The surface is dominated by terraces delineated by nearly vertical steps.

mobilities for low sheet charge densities, approaching $200,000 \text{ cm}^2 \text{ V}^{-1} \text{ s}^{-1}$ for densities of 10^{11} cm^{-2} . To learn more about EG electrical transport properties, far-infrared magneto transmission (FIR-MT) measurements were carried out at 4 K. Absorption features are easily observed in the FIR-MT spectra and examples at various magnetic fields (B) are shown in Fig. 8. The strongest absorption feature (arrow) is due to a Landau level transition, $L_{-1(0)} \rightarrow L_{0(1)}$, that shifts in energy in proportion to the square root of B, as shown in the inset of Fig. 8. This square root dependence on B is consistent with carriers acting as if they have zero effective mass, one of the relatively unique properties of graphene.



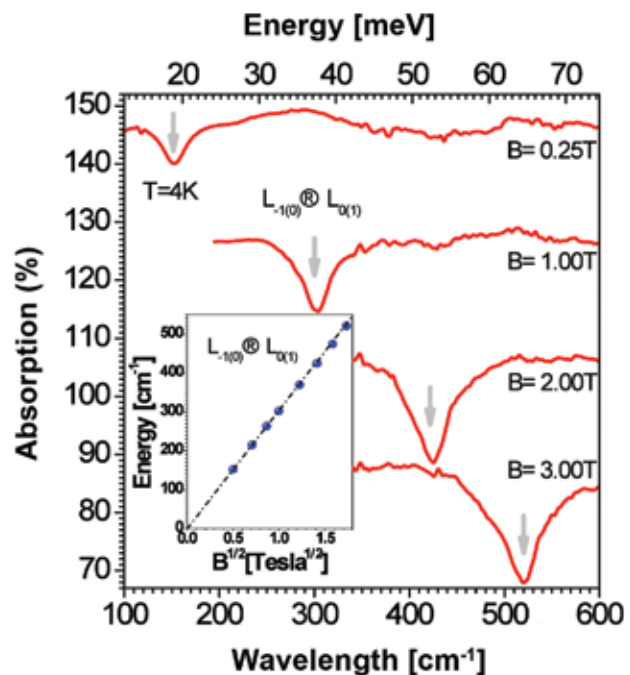
In addition, the width of the absorption for different magnetic fields can be used to place a lower bound on the mobility of EG. Analysis of the line width of the strongest absorption feature showed that the sample contained regions with mobilities of at least $250,000 \text{ cm}^2 \text{ V}^{-1} \text{ s}^{-1}$, a value consistent with the extrapolated value found in Fig. 7.²

The first EG experiments were carried out on small portions of SiC substrates and this later was transitioned to larger, wafer-sized samples. The critical parameter for graphene growth was the temperature uniformity across the “2-inch” (50.8 mm) diameter Si-face SiC wafers. Otherwise, EG was continuous

FIGURE 8
The far-infrared magneto transmission spectra of epitaxial graphene on C-face of SiC as a function of magnetic field B. The major absorption, denoted by the arrows, is due to Landau level transition, $L_{-1(0)} \rightarrow L_{0(1)}$. The absorption shifts in energy as the square root of B, shown in the inset, which is a characteristic of graphene and different from other semiconductors that shift linearly in B.

FIGURE 7

The 300 K mobility of $10 \times 10 \mu\text{m}^2$ van der Pauw Hall samples as a function of (single) sheet carrier concentration for EG on Si-face (blue) and on C-face (red) SiC. It can be observed that the values for C-face epitaxial graphene extrapolate to approximately $200,000 \text{ cm}^2 \text{ V}^{-1} \text{ s}^{-1}$ for sheet density of 10^{11} cm^{-2} (black arrow). The dotted green curve marks the mobility of silicon.



over the entire wafer with morphology similar to that shown in Fig. 6 and thicknesses as described earlier for the smaller samples.

Graphene Transistors: Another advantage of graphene is that silicon device fabrication techniques can be used with only minor modification to create graphene devices. This means that the etching, metalization, and dielectric gate deposition “tools” currently used in the silicon fabrication world can be employed to fabricate graphene devices. In addition, by using EG on wafers, literally dozens of experiments can be conducted at one time to optimize essential fabrication techniques. For these reasons, EG wafers provided by ESTD in collaboration with HRL in the CERA program quickly enabled significant progress in making graphene transistors. For example, wafers of this type yielded superior properties such as excellent resistivity uniformity of 2.8% and record 300 K Hall mobilities of $\approx 2700 \text{ cm}^2 \text{ V}^{-1} \text{ s}^{-1}$. Shown in Fig. 9 (top) is

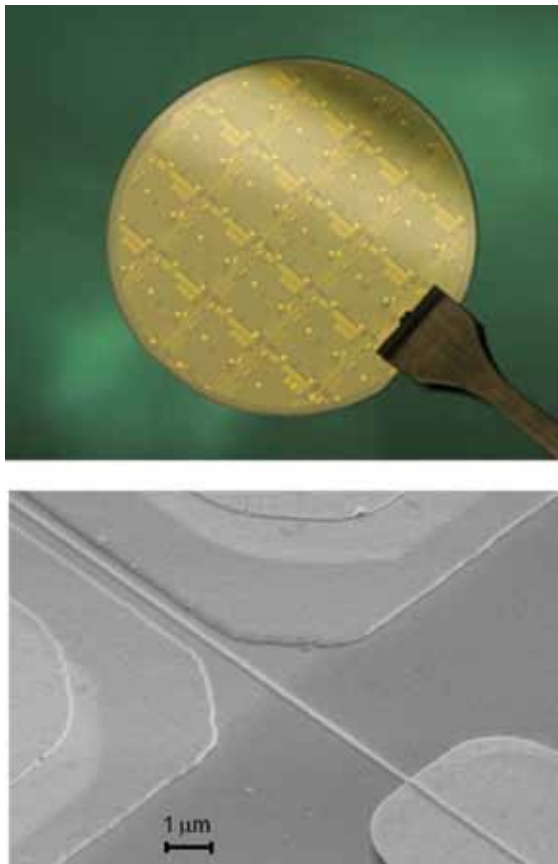


FIGURE 9
(Top) Epitaxial graphene processed into field effect transistors on a 50.8 mm diameter SiC wafer in collaboration with HRL, Inc., and in conjunction with the DARPA CERA program. (Bottom) Epitaxial graphene field effect transistor fabricated at ESTD. The gate length is 130 nm and the source–drain spacing is 1 μm .

processed EG on a 2 in. diameter SiC wafer. Devices from EG wafers yielded field effect transistors exhibiting state-of-the-art ambipolar behavior, $I_{\text{on}}/I_{\text{off}}$ ratios and peak transconductances.³ Frequency performance metrics were established for these devices ($L_g = 2 \mu\text{m}$) such as cut-off frequency–gate length product ($f_T \cdot L_g$) of 10 GHz μm and f_{max} of 14 GHz. In addition, gate delay was found to be 2 ps μm^{-1} , which is very encouraging for superior high-speed gate-switching performance for small gate lengths.

ESTD recently began fabricating EG transistors and initial results yielded cut-off frequencies of 20 GHz for 130 nm gate lengths. A scanning electron micrograph of this device is shown in Fig. 9 (bottom). Although these speeds fall short of the expected potential of graphene-based transistors, this is an important first step along the path to create LNAs that reduce power consumption by a factor of six and increase the frequency of operation by a factor of two over existing state-of-the-art devices.

[Sponsored by ONR and DARPA]

References

- J.L. Tedesco, B.L. VanMil, R.L. Myers-Ward, J.M. McCrate, S.A. Kitt, P.M. Campbell, G.G. Jernigan, J.C. Culbertson, C.R. Eddy, Jr., and D.K. Gaskill, “Hall Effect Mobility of Epitaxial Graphene Grown on Silicon Carbide,” *Appl. Phys. Lett.* **95**, 122102 (2009). 1 μm
- G.G. Jernigan, B.L. VanMil, J.L. Tedesco, J.G. Tischler, E.R. Glaser, A. Davidson III, P.M. Campbell, and D.K. Gaskill, “Comparison of Epitaxial Graphene on Si-face and C-face 4H SiC Formed by Ultrahigh Vacuum and RF Furnace Production,” *Nano Letters* **9**(7), 2605–2609 (2009).
- J.S. Moon, D. Curtis, M. Hu, D. Wong, C. McGuire, P.M. Campbell, G. Jernigan, J.L. Tedesco, B. VanMil, R. Myers-Ward, C. Eddy, Jr., and D.K. Gaskill, “Epitaxial-Graphene RF Field-Effect Transistors on Si-Face 6H-SiC Substrates,” *IEEE Electron Device Lett.* **30**(6), 650–652 (2009).

Functionalized CMOS Nanomechanical Resonators for Chem-Bio Sensing

J.W. Baldwin, M. Zalalutdinov, J.S. Burgess, and B.H. Houston
Acoustics Division

Introduction: The canine olfactory system remains the most successful detector in use today for vapor sensing of explosives. For the lowest detectable concentrations (~ 1 ppb), in order to have a sufficient number of analyte molecules interacting with the olfactory neural receptors, the canine inhales as much as 10^{-12} to 10^{-13} g of analyte.¹ Our goal is to use arrays of low-cost complementary metal oxide semiconductor (CMOS) nanomechanical resonators with their extremely small mass and high surface/volume

ratio as a competitive and complementary technique for vapor sensing applications (i.e., for explosives, chemical warfare agents, and biomolecules). We have demonstrated that femtogram (fg) sensitivity, 10^{-15} g, is achievable in air under ambient conditions using functionalized CMOS nanomechanical resonators.² This research program has been focused on integrating nanomechanical resonators with all-electrical transduction in CMOS, essentially linking arrays of nanoelectromechanical-resonator systems (NEMS) with the information/signal processing capabilities of very large scale integration (VLSI) systems, and addressing the key outstanding problem of targeted functionalization.

A lack of selective functionalization on the resonator surface using vapor adsorptive functional groups specific towards target analyte molecules has been an impediment to the realization of resonator-based nanomechanical systems for mass sensing. When located on structural elements or microchannel walls, analyte-specific functional groups greatly limit the minimum detectable level of the overall device. In addition, traditional spin-cast polymer films used for preconcentrators and cantilever-based sensors present the problem of being many times thicker than the nanomechanical resonator, essentially burying the resonator in the adsorptive polymer. To address these problems, we use a monolayer functionalization scheme based on a UV-mediated reaction between terminal alkenes and a hydrogen terminated surface,³ e.g., silicon or diamond, using a quartz mask to irradiate only the areas to be functionalized.

This ability to functionalize only the resonator and not the surroundings on a large scale is of great importance for attaining the highest sensitivity, and the monolayer functionalization technique maintains the high quality factor (Q) of the resonator. This opens the possibility of patterning arrays of NEMS, with each element having its own unique functional group, allowing for increased analyte selectivity for the overall device using a pattern recognition scheme. Moreover, we believe that the use of integrated arrays of such resonators, which according to current beliefs mimics the function of canine nose, enables an enhanced vapor sensing performance to be practically realized.

Design and Functionalization: The ideal resonator structure would have small mass, high quality factor, large surface area, and enough rigidity to withstand the wet chemistry processing associated with the surface functionalization. In order to be considered for field-type applications, the resonator sensor must have a built-in transduction mechanism, preferably an all-electrical operation. In this article, we present an arch-bridge resonator designed for integration with CMOS electronics and fabricated within an unmodified

flow of a standard CMOS process.² The double-layer polysilicon (gate layer) is used as a structural material for the arch resonator, whereas the thermally grown field oxide serves as a sacrificial layer. The all-electrical operation of the arch resonator, shown in Fig. 10, is enabled by the thermoelastic excitation and piezoresistive readout of the mechanical vibrations.

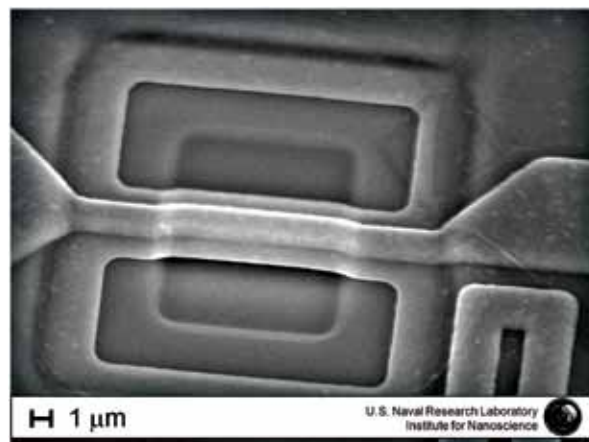


FIGURE 10
Arched bridge nanomechanical resonator with piezoresistive transduction and thermoelastic actuator implemented.

Figure 11 shows the reaction scheme for functionalizing the resonator with a hexafluoroisopropanol (HFIPA) group. The chip is first completely hydrogenated in a hydrogen plasma before contacting the surface with the terminal allyl. After contacting, a UV-transparent mask can be used to irradiate the features of interest, thus leaving the areas exposed to the UV light functionalized with the HFIPA group as seen in the X-ray photoelectron spectroscopy (XPS) spectra in Fig. 11.

Sensor Performance: The CMOS nanomechanical resonator in Fig. 10 was functionalized with the HFIPA group shown in Fig. 11 with no detectable degradation of the Q in air. A model analyte was chosen to show the hydrogen bond interaction between triethylamine (TEA) and the functionalized surface HFIPA, and to measure the level of detection that this device provides. Figure 12 shows the response of the resonator towards TEA, methanol, and water vapor. A mass flow controller (MFC)-controlled impinger, which delivers saturated vapor in nitrogen to a dilution chamber, is used to deliver the analyte vapor to the CMOS chip (5 by 5 mm) located in a flow cell (17 mL).

The plot in Fig. 12 was obtained by pulsing a single vapor at 100 standard cubic centimeters per minute (SCCM) for 2 min, 50 SCCM for 2 min, and 20 SCCM for 2 min, with a purge cycle of N_2 at 5 standard liters

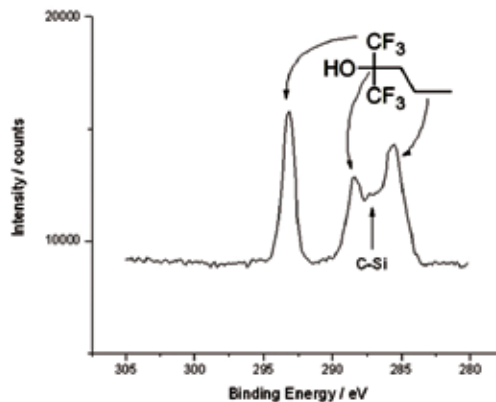
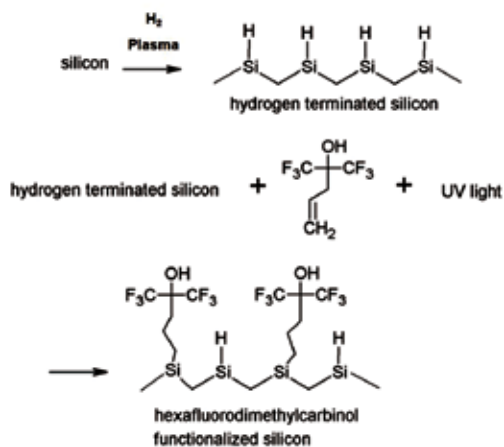


FIGURE 11
Functionalization scheme and XPS results of monolayer coverage on silicon surface.

per minute (SLM) for 2 min between each exposure. The process was repeated for each analyte individually (water 28%, methanol 153%, and TEA 69%). No detectable adsorption of water and methanol was observed. The HFIPA functional group is hydrophobic due to the fluorination, and by design we would not expect physisorption of these two analytes. However, TEA is expected to hydrogen bond to the HFIPA group and is detected in our system. Adsorption was flow rate dependent. At 100 SCCM, 252 fg were adsorbed and detected, while at 20 SCCM, only 63 fg were detected. This shows the importance of using a microfluidic cell so that more analyte can be brought to the surface of the resonator in a shorter time.

The mass responsivity of this system (R) was estimated to be 1.26×10^{-18} g/Hz. A 1-fg detection level is projected for TEA, based upon the 1 kHz readout bandwidth. The resonator showed a selective response towards the TEA over typical solvent molecules.

Accomplishments: We have developed high-frequency and high-quality-factor NEMS resonator designs within commercially available, low-cost CMOS processes. These resonators have all-electrical drive and detection schemes incorporated into their design. We have accomplished the selective surface functionalization by depositing a vapor adsorptive monolayer of hexafluorodimethylcarbinol on nanomechanical resonators and measuring their response to various vapors. A 1-fg detection level was projected, based on the frequency stability of the resonator in air and the signal-to-noise ratio in the electromechanical transduction. The HFIPA-functionalized resonator showed a selective response to TEA over typical solvent molecules. We plan to expand the breadth of polymers specific to different analytes and to enhance the sensitivity levels by scaling down the dimensions of the resonators.

[Sponsored by ONR]

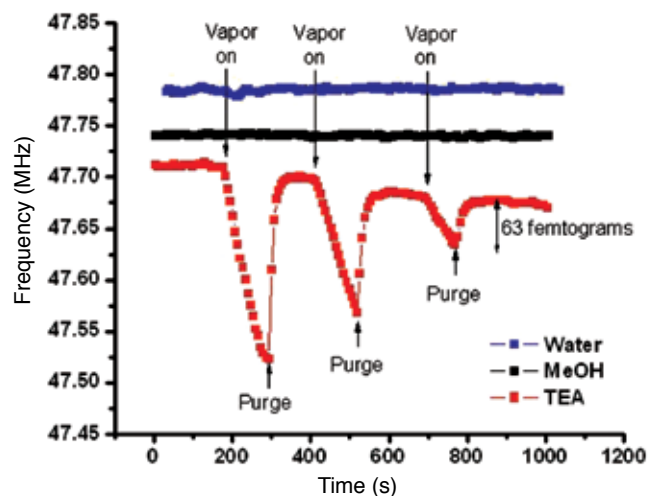
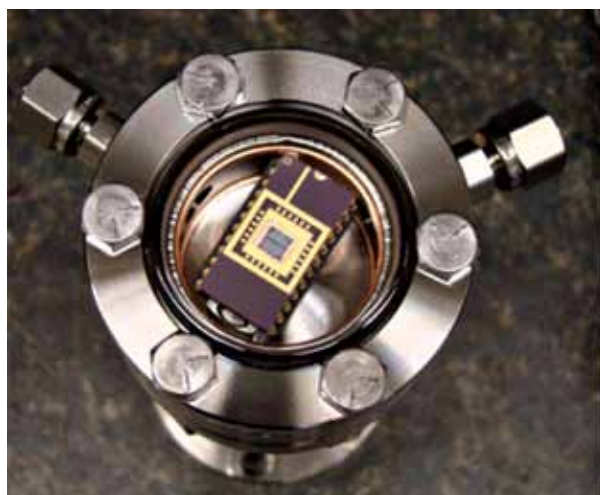


FIGURE 12
Prototype flow cell (left) with functionalized CMOS chip inside. Femtogram mass sensitivity and selectivity of triethylamine using functionalized arched bridge resonator (right).

References

- ¹ M. Krausa, and A.A. Reznev, eds., *Vapour and Trace Detection of Explosives for Anti-terrorism Purposes*, NATO Science Series II, Mathematics, Physics and Chemistry, V. 167 (Kluwer, Dordrecht, Netherlands, 2003).
- ² J.W. Baldwin, M.K. Zalalutdinov, B.B. Pate, and B.H. Houston, "Patterned Functionalization of Nanomechanical Resonators for Chemical Sensing," Navy Case Number 99,430, provisional application number 61/102,470; J.W. Baldwin, M.K. Zalalutdinov, B.B. Pate, M.J. Martin, and B.H. Houston, "Optically Defined Chemical Functionalization of Silicon Nanomechanical Resonators for Mass Sensing," *Nanotechnology* 2008, 8th IEEE Conference on Nanotechnology, Arlington, TX, 18–21 August 2008, pp. 139–142, doi:10.1109/NANO.2008.48; M.K. Zalalutdinov, J.D. Cross, J.W. Baldwin, B.R. Ilic, W. Zhou, B.H. Houston, and J.M. Parpia, "CMOS-Integrated RF MEMS Resonators," *Journal of Microelectromechanical Systems* **19**(4), 807–815(2010).
- ³ M.R. Linford, P. Fenter, P.M. Eisenberger, and C.E.D. Chidsey, "Alkyl Monolayers on Silicon Prepared from 1-alkenes and Hydrogen-terminated Silicon," *J. Am. Chem. Soc.* **117**(11), 3145–3155 (1995); T. Strother, W. Cai, X. Zhao, R.J. Hamers, and L.M. Smith, "Synthesis and Characterization of DNA-modified Silicon (111) Surfaces," *J. Am. Chem. Soc.* **122**(6), 1205–1209 (2000).

206

The ASW Reach-back Cell Ocean Analysis System
J.D. Dykes and P. Fanguy

208

Marine Sediment Strength from Dynamic Probes
A. Abelev, K.R. Tubbs, and P.J. Valent

211

Characterizing River Environments by Combining Imagery and Models:
What We Can Do Now and In the Future
C.A. Blain, A.D. Weidemann, R.P. Mied, R.S. Linzell, and P. McKay

The ASW Reach-back Cell Ocean Analysis System

J.D. Dykes¹ and P. Fanguy²

¹*Oceanography Division*

²*QinetiQ North America*

Introduction: Obtaining a real-time characterization of the 3D structure of the ocean is important in supporting naval operations, particularly in anti-submarine warfare (ASW). The oceanographers and forecasters of the ASW Reach-back Cell (RBC), located at the Naval Oceanographic Office (NAVOCEANO) at Stennis Space Center, Mississippi, analyze ocean and atmospheric data using state-of-the-art computing hardware and software to build a comprehensive picture of the environment in operational areas of interest. Along with the growing technology comes the ever-increasing volume of measurements in the ocean and atmosphere and rapidly expanding data assimilation and numerical modeling prediction capability. These challenging conditions call for a user interface with a concise set of software tools that help the user stay organized and not be overwhelmed by a wide variety of methods and technologies in order to handle the abundance of data. The ASW Reach-back Cell Ocean Analysis System (ARCOAS) is designed to fulfill such requirements.

Software Approach: ARCOAS is a user interface designed on top of ArcMAP version 9.3, a powerful software package using geographic information system (GIS) technology developed by Environmental System Research Institute (ESRI), Inc. A highly flexible programming language used in Microsoft Office applications, Visual Basic for Applications (VBA), is also built into ArcMAP and provides a rapid development path for invoking the powerful GIS functionality of ArcMAP coupled with helpful graphics classes of Microsoft Office components. Thus, ARCOAS is designed and built with an object-oriented approach that incorporates listeners, dialog boxes, interactive displays, and clickable buttons, all put together to offer the user tools tailored to the work at hand. ARCOAS is not just a cleverly coded graphical user interface (GUI) made of classes and modules: it also offers an environment and language in which the oceanographer is familiar and comfortable, while providing environmental information in a common geographic reference frame.

Applications: The primary focus of the oceanographers in the ASW RBC is to assess the level and confidence in the data and model output depicting the

current and predicted structure of the ocean. One goal is to provide a level of certainty to other users of the data and model output as it affects their applications (e.g., algorithms for ocean acoustics) and their own interpretations on which critical mission decisions are made. The first step is to quickly locate the data with respect to the Earth, a step at which a GIS is inherently quite proficient. Figure 1 shows a world map view rendering available domains from numerical models such as (1) the global Navy Coastal Ocean Model (NCOM)¹ run at NAVOCEANO; (2) the Coupled Ocean and Atmosphere Mesoscale Prediction System (COAMPS[®])² run at Fleet Numerical Meteorology and Oceanography Center (FNMOC) in Monterey, California; and (3) WAVEWATCH III³ run at FNMOC and NRL Stennis. Once located, data can be visualized as shown in Fig. 2, where the view is zoomed to a model domain to focus on the locations of the plotted profiles and the layer rendering the model output of surface water temperature. Other items rendered are (1) locations of environmental measurements such as Expendable Bathythermographs (XBTs) and Argo floats collecting ocean profiles of temperature and salinity; (2) remotely sensed data ground tracks depicting sea surface height (SSH) variations measured by radar altimeters on polar orbiting satellite platforms; and (3) multichannel sea surface temperature (MCSST) data derived from brightness temperatures measured from satellites.

Although Fig. 2 shows a myriad of observation points within this region of interest, further analysis can be performed on specific observation data using a guided process of elimination and selection. Figure 3 shows a plot of measured and modeled time-coincident temperature and salinity profiles at a specific location for comparison. More interesting is the comparison of the overlaid sonic layer depths (SLD) derived from the plotted profiles. SLD is highly sensitive to variations of the thermohaline structure, which directly affects performance of acoustic systems supporting ASW.

Conclusion: Additional capabilities provided in the user-interface structure of ARCOAS include layer mathematics, animations, cross-sections, various drawing functions, a highly configurable setup utility, exporting presentable graphics, and model performance statistics. ARCOAS will serve as a well-tested prototype for further development to increase flexibility by integrating the Department of Defense Commercial Joint Mapping Toolkit (C/JMTK) to build run-time system tools that can be used in other frameworks besides ArcMAP. As we satisfy more functional requirements with further improvements and

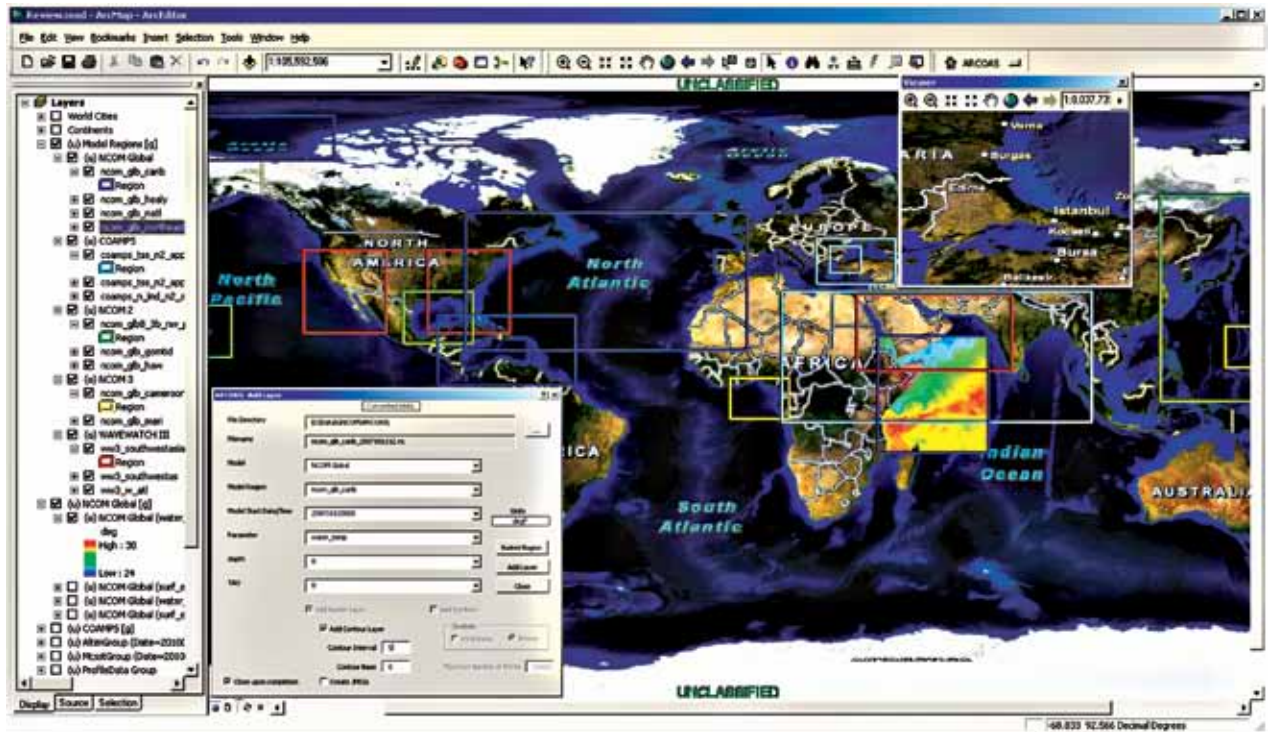


FIGURE 1
Global view of atmospheric and ocean prediction model domains available for analysis. The color-coded boxes correspond to domains organized in groups, in this case by type of model, including global NCOM subsections, COAMPS, and WAVEWATCH III. The table of contents on the left indicates what is displayed. The inset dialog box is the interface for bringing up a data layer from output of a model domain. In this case, a region in the northeastern Indian Ocean was selected and a raster data layer of surface temperature from NCOM is displayed.

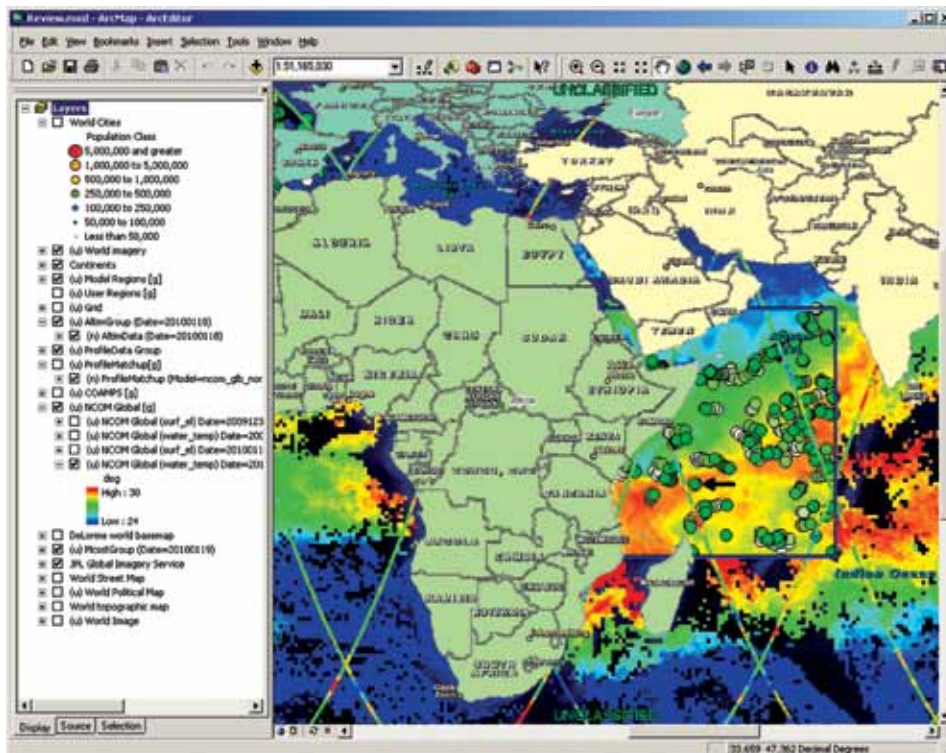


FIGURE 2
A plot of the raster layer referred to in Fig. 1 of surface temperature from global NCOM in the northeastern Indian Ocean and the satellite-derived MCSST, showing that they are fairly consistent with each other. Also plotted are the measured SSH variations along ground tracks from a radar altimeter for one day and profile locations limited to the NCOM domain. Greener points are more recent profiles. The selected point indicated by the arrow corresponds to the plots in Fig. 3.



FIGURE 3
Profiles of measured and modeled temperature and salinity plotted from a selected point indicated by the arrow in Fig. 2. The SLD levels overlaid on the profile plots are calculated based on both measured and modeled parameters and show how sensitive SLD is to the ocean thermohaline structure.

follow this new development path, ARCOAS has the potential to be useful for more general meteorological and oceanographic applications in support of Navy operations.

[Sponsored by SPAWAR]

References

- 1 C.N. Barron, A.B. Kara, R.C. Rhodes, C. Rowley, and L.F. Smedstad, "Validation Test Report for the 1/8° Global Navy Coastal Ocean Model Nowcast/Forecast System," NRL/MR/7320--07-9019, Naval Research Laboratory, Stennis Space Center, MS, 2007.
- 2 R.M. Hodur, "The Naval Research Laboratory's Coupled Ocean/Atmosphere Mesoscale Prediction System (COAMPS)," *Mon. Wea. Rev.* **125**, 1414–1430 (1997).
- 3 H.L. Tolman, "Development of a Multi-grid Version of WAVEWATCH III," Tech. Note 256, NOAA/NWS/NCEP/MMAB, 2007.

Marine Sediment Strength from Dynamic Probes

A. Abelev, K.R. Tubbs, and P.J. Valent
Marine Geosciences Division

Background: Rapid assessments of undrained shear strength of marine sediments are often of great interest in various branches of offshore civil and petroleum engineering, and especially for the Navy.

Dynamic free-fall penetrometers offer a potential for such rapid strength assessment, but have typically been employed in conjunction with mostly empirical relationships to investigate the undrained shear strengths of sediments. In this work, we analyze the behavior of one such commonly used penetrometer: the STING (Sea Terminal Impact Naval Gauge). It consists of a main sensor assembly with an attached straight shaft of 19 mm diameter and up to 3 m long, with a flat cylindrical plate, called the "foot" hereafter (of several different diameters from 25 to 70 mm) at the rod tip (see Fig. 4). The probe is deployed in free-fall and penetrates foot-first on impact into the sediments (usually soft clayey sediments). The native processing algorithm, based on interpretations of the deceleration time-history of impact, typically suffers from unreliable and inaccurate derivation of the undrained shear strength of sediments — a fundamental strength descriptor, highly important in a wide variety of applications and problems involving marine sediments. An example of using this algorithm is shown in Fig. 4 for a series of drops with different foot diameters at the same location. These data are compared with the standard lab-derived vane test results, representing an accurate measurement of the undrained shear strength of soil. While some records match the lab data well, others deviate significantly, often overpredicting by a factor of five or more. These inconsistencies are typical of a wide range of soils and locations explored.

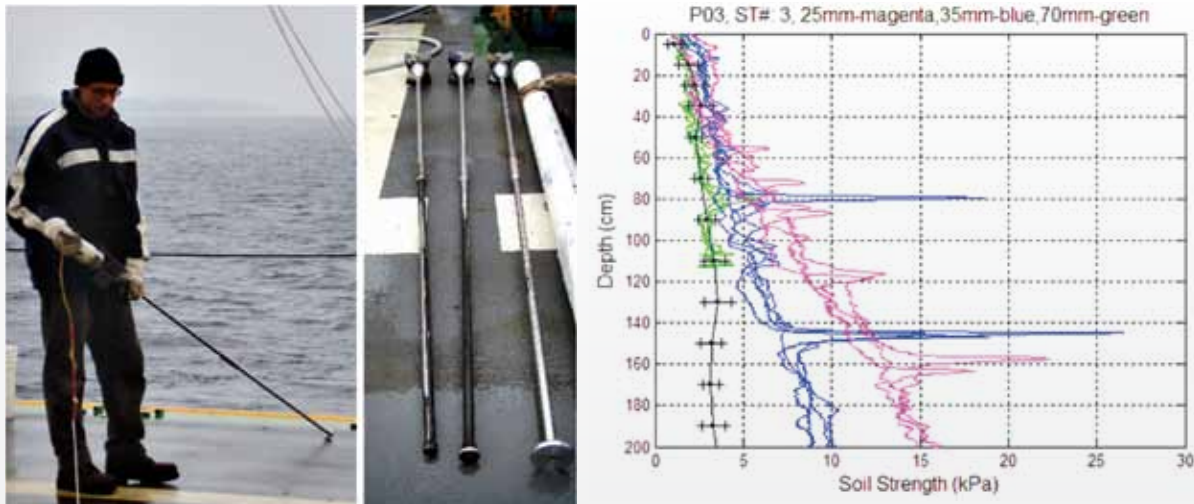


FIGURE 4

(Left to right) STING penetrometer before deployment; several different foot diameters including 25, 35, and 70 mm; and un-drained shear strength results from one location processed using STING native algorithms (green, blue, magenta), compared with lab standard vane tests (black curve with error bars representing standard deviation).

Analysis of Bearing Resistance: Analysis of probe impact burial can be conducted using various approaches. One may attempt to produce full dynamic solutions, including large sediment deformation and flow around the penetrating STING, full elasto-plastic constitutive formulations, and rate effects. One such analysis is explored in Ref. 1 using a finite element approach and including ALE (Arbitrary Lagrangian-Eulerian) remeshing scheme. Alternatively, one could use a simplified pseudo-static approach² that computes a static collapse load for a pre-embedded STING penetrometer at a series of depths, ranging from the sediment-water interface and down to a depth of about 3 m (maximum STING embedment data available). Although this analysis neglects the effects of prior strains and deformations occurring during the penetration process and assumes the sediment to be at the in situ stress state, it has proven to be useful interpreting penetrations of other probes, such as the XBP (eXpendable Bottom Profiler) probe.

In this work, and similar to that described in Ref. 2, we solve the basic equation of motion, based on the known (and probe-recorded) deceleration time series to derive the overall sediment resistance force, while accounting for buoyancy effects. This sediment resistance force depends strongly on the rate of deformation of the soil, plastically flowing around the penetrating probe.^{3,4} We account for these effects using constant coefficients, appropriate to the general materials under consideration, i.e., soft cohesive marine muds. Thus, transitioning from dynamic to pseudo-static sediment force, we approximate the problem of the bearing capacity of foundations, representing the sediment

resistance via a nondimensional bearing capacity factor. This factor, in turn, is derived from a series of numerical solutions (pseudo-static) using FLAC3D finite-difference code. These solutions are then represented analytically, by standard curve-fitting, as a function of the foot diameter, embedment depth, and velocity of the probe, allowing for an easy inversion routine to be implemented. An elasto-plastic constitutive model of soil resistance is used, with elastic parameters chosen with utmost care. The single-parameter soil failure model (undrained shear strength) is then derived using the obtained numerical solutions and measured probe decelerations, and adjusted for burial depth and probe velocity. The results of numerical analysis are given in Fig. 5, showing distribution of von Mises (shear) stress and velocity vector and contours of soil, plastically flowing around the penetrating probe. Side friction of soil on the penetrometer rod can be shown to be ignored without major loss of validity. Figure 6 shows the final prediction of the shear strength using original STING software and the new method developed here. Aside from a small initial portion of the curve, the improvement in prediction is significant. Further details of this work can be found in Ref. 5.

Acknowledgments: The help of the crews and research teams in obtaining the field data at sea is greatly appreciated.

[Sponsored by NRL and ONR]

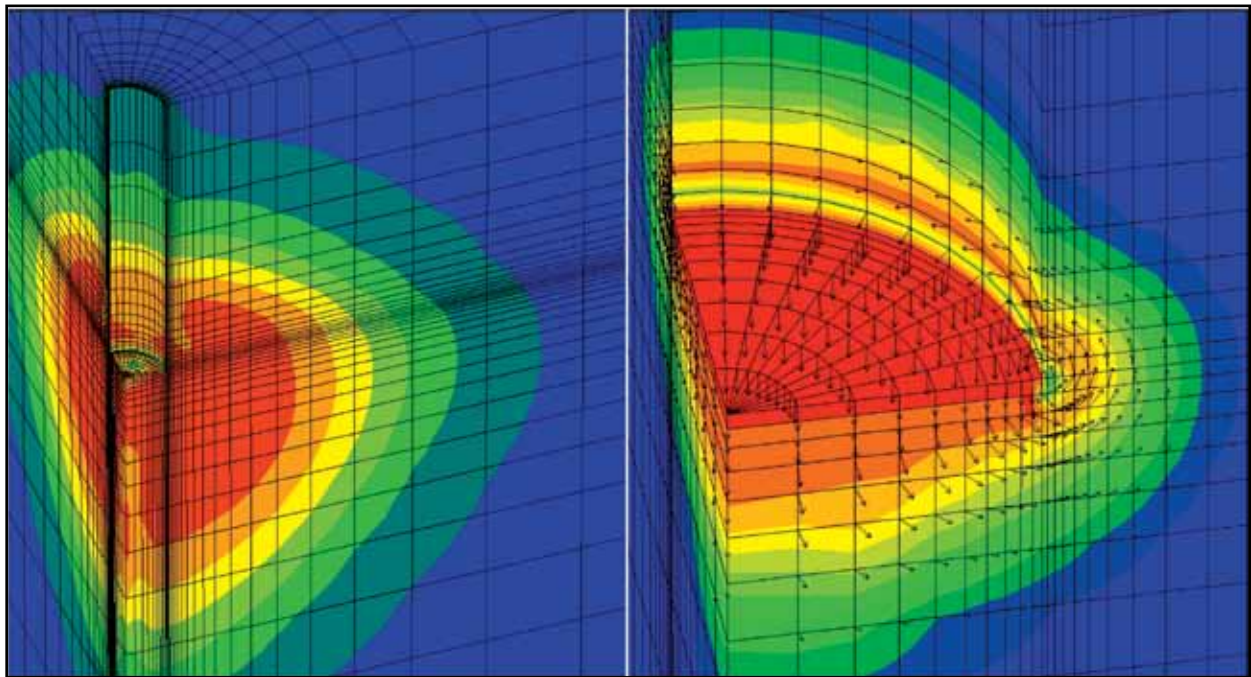


FIGURE 5

Typical results of numerical analysis of STING at a particular embedment depth, showing contours of the von Mises (shear) stress (left) and soil velocity vectors and contours (right), identifying a well-developed failure in the soil and formation of a distinct flow pattern around the foot of the penetrometer.

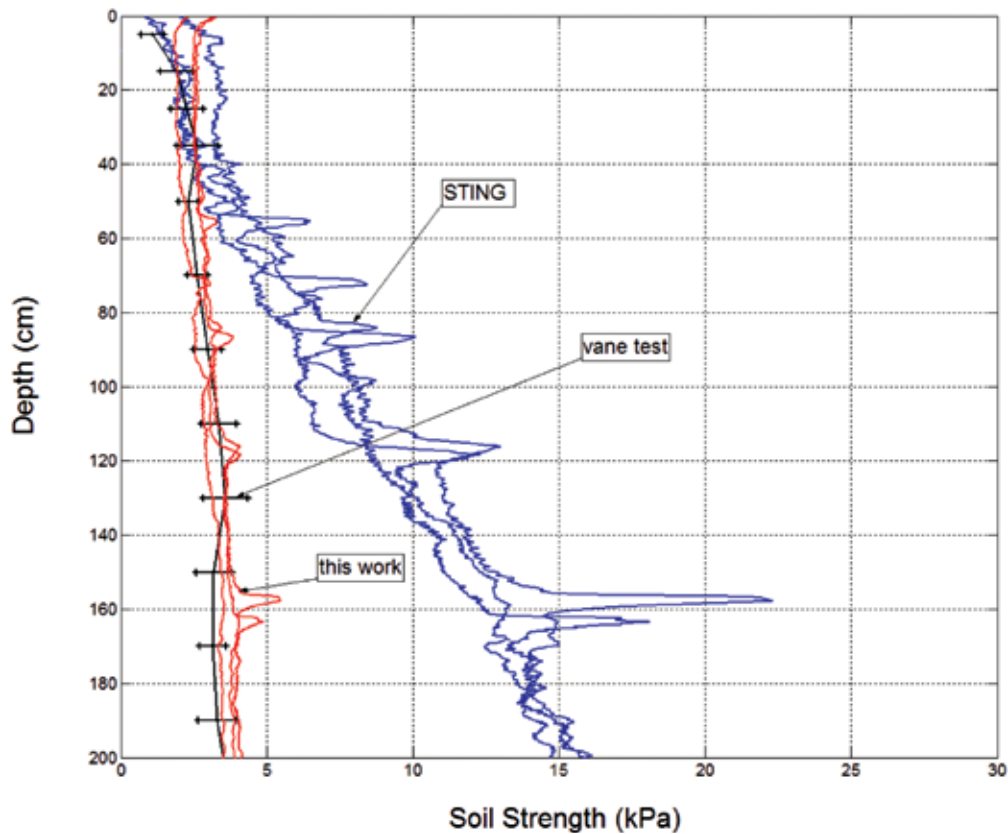


FIGURE 6

STING-processed (blue) and FLAC3D-computed (red) undrained shear strength computation from a location in the Gulf of Mexico, compared with the lab-measured vane test results (black solid lines with error bars representing the standard deviation).

References

- ¹ A. Abelev, J. Simeonov, and P.J. Valent, "Numerical investigation of Dynamic Free-fall Penetrometers in Soft Cohesive Marine Sediments Using a Finite Element Approach," Oceans 2009, MTS/IEEE Biloxi, MS, 26–29 Oct. 2009, abstract no. 090612-059.
- ² C.P. Aubeny and H. Shi, "Interpretation of Impact Penetration Measurements in Soft Clays," *J. Geotech. Geoenviron. Eng.* **132**, 770 (2006).
- ³ C.P. Aubeny and H. Shi, "Effect of Rate-Dependent Soil Strength on Cylinders Penetrating Into Soft Clay," *IEEE J. Ocean. Eng.* **32**, 49–56 (2007).
- ⁴ G. Biscontin and J.M. Pestana, "Influence of Peripheral Velocity on Vane Shear Strength of an Artificial Clay," *Geotech. Testing J.* **24**, 423–429 (2001).
- ⁵ A. Abelev, K. Tubbs, and P.J. Valent, "Numerical Investigation of Dynamic Free-fall Penetrometers in Soft Cohesive Marine Sediments Using a Finite Difference Approach," Oceans 2009, MTS/IEEE Biloxi, MS, 26–29 Oct. 2009, abstract no. 090612-058.

Characterizing River Environments by Combining Imagery and Models: What We Can Do Now and In the Future

C.A. Blain,¹ A.D. Weidemann,¹ R.P. Mied,² R.S. Linzell,³ and P. McKay⁴

¹*Oceanography Division*

²*Remote Sensing Division*

³*QinetiQ North America*

⁴*ASEE Postdoctoral Associate*

The Navy's Push Into Riverine Environments:

In response to the increasing use of inland waterways by enemy combatants engaged in the Global War on Terror, the Navy has fielded three new riverine squadrons within the last three years. Their mission involves diverse combinations of surveillance, patrol, interdiction, and delivery of land forces into river environments. This plan to increase the number of river operations highlights the need for detailed descriptions of the water levels, flow, and geometry of a given river.

Rivers pose one of the most challenging environments to characterize because they form the interface between land and water in the coastal margin. They are geometrically complex and change continually in position and character. Predictive models of the river environment require detailed descriptions of river bank position, bed elevation, upstream fluxes, and downstream variability due to tidal modulations. To compound the difficulty, Navy river operations are most often conducted in denied areas across the globe where very little of this information is available.

Meeting the Immediate Challenge: To address the need for a predictive capability for currents and water

level in rivers in regions where knowledge of the system is limited, we devised an approach that initiates a river model from available imagery and provides a strategy to compensate for missing data. The River Simulation Tool¹ (RST) provides an intuitive interface for configuring a 2D hydrodynamic model of a river or river segment that has been remotely observed and imaged. In-water points and possible river bank locations are extracted from imagery and processed in such a way as to generate a model grid representing the river bank positions and to derive synthetic bottom depths. The RST defaults to configurations for the river model and contingencies to specify missing information, as necessary, such as upstream forcing or bathymetry. Realizing that a great deal of uncertainty can accompany application of the RST to a real river, a capability for specifying multiple inputs is available. From these multiple data sets, we can perform an ensemble of model runs to bracket the uncertainty or assess the sensitivity of predictions to unknown inputs.

The RST was applied to a segment of the upper East Pearl River in Mississippi, a region having no archived digital shoreline, but for which a Quickbird satellite image is available [Fig. 7(a)]. Applying the RST to the imagery results in an oriented shoreline [Fig. 7(b)] and a model grid with estimated bathymetry [Fig. 7(c)]. In situ data, such as bathymetry, upstream river flux, and downstream tidal variability, are known in this same region, permitting a comparison between river currents and elevation produced by an image-initiated model through the RST [Fig. 8(a)] to observed currents at one location² [Fig. 8(b)].

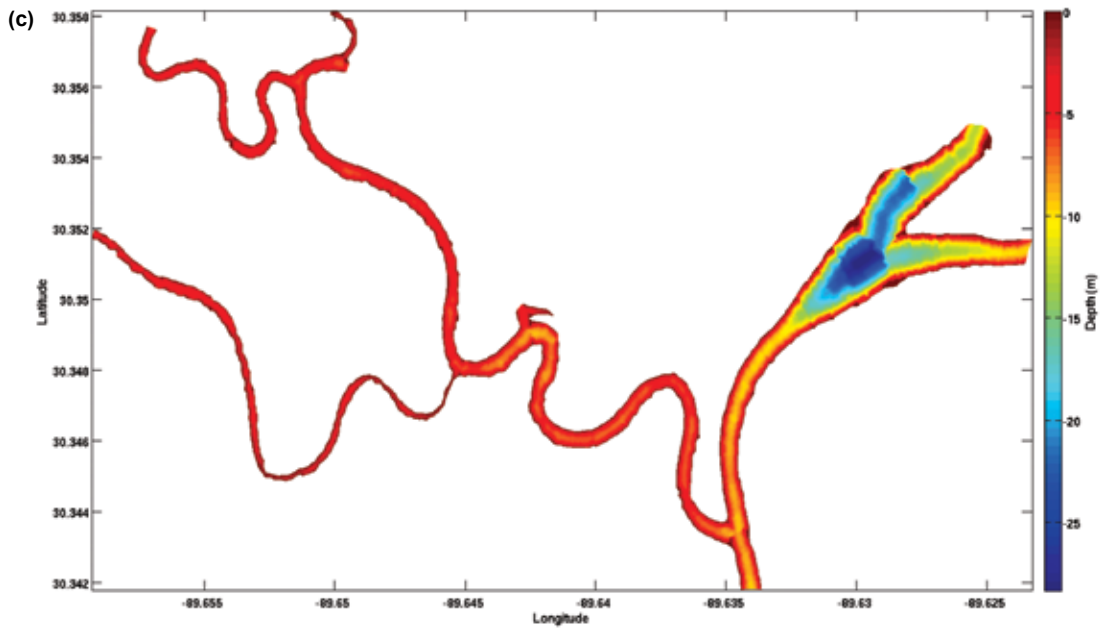
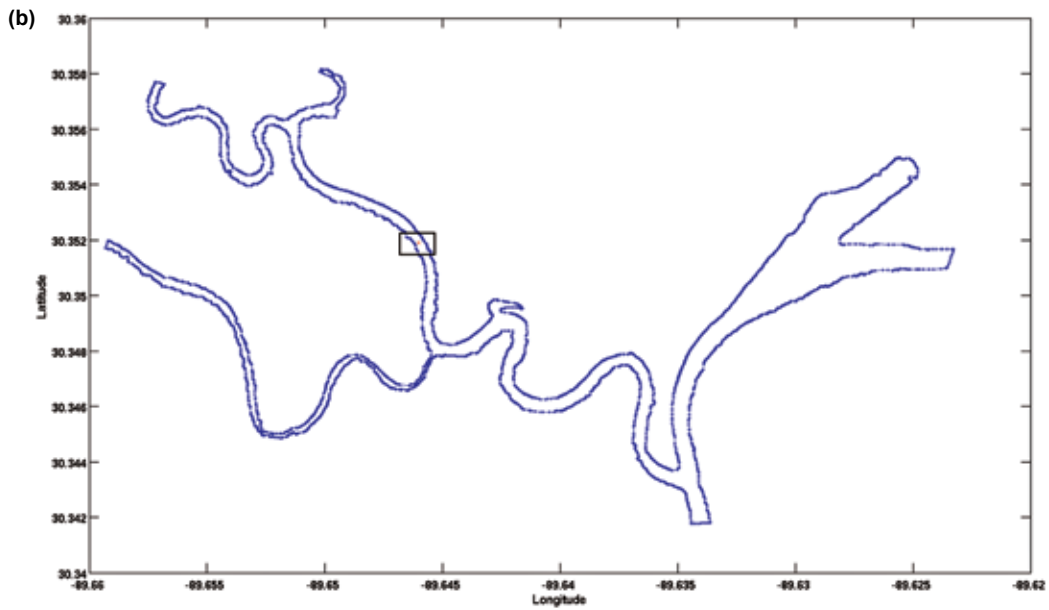
Future Capabilities: In addition to geometric information, color imagery of the river surface contains a rich assortment of features indicative of the underlying flow, such as circulation eddies or mixing zones between different water types. Imagery taken of the Potomac River, Maryland (Fig. 9), shows developing waves that are indicative of an instability between river currents of different magnitudes. Present research efforts aim first to quantify the circulation features in the surface imagery. Sensitivity analyses are then performed by applying an analytical process model to the same river reach to better understand the relationship between the surface circulation and the 3D structure of the river currents. A relationship between surface currents and 3D river currents can ultimately be used to formulate a methodology for constraining modeled river flow based on surface imagery. Such a leap in technology dramatically enhances our ability to address the needs of mission planners for riverine operations through more accurate representations of actual riverine environments.

[Sponsored by NRL and SPAWAR]



FIGURE 7

The RST is applied to the lower east Pearl River, MS. (a) Multispectral imagery from the Quickbird satellite taken on May 1, 2007; (b) shoreline coordinates processed from water points and edge data extracted from imagery; (c) the resulting 2D river model created by the RST with color contours indicating water depth.



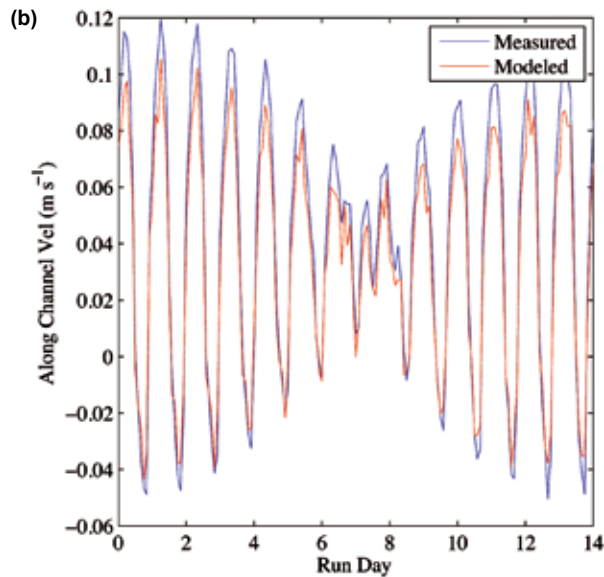
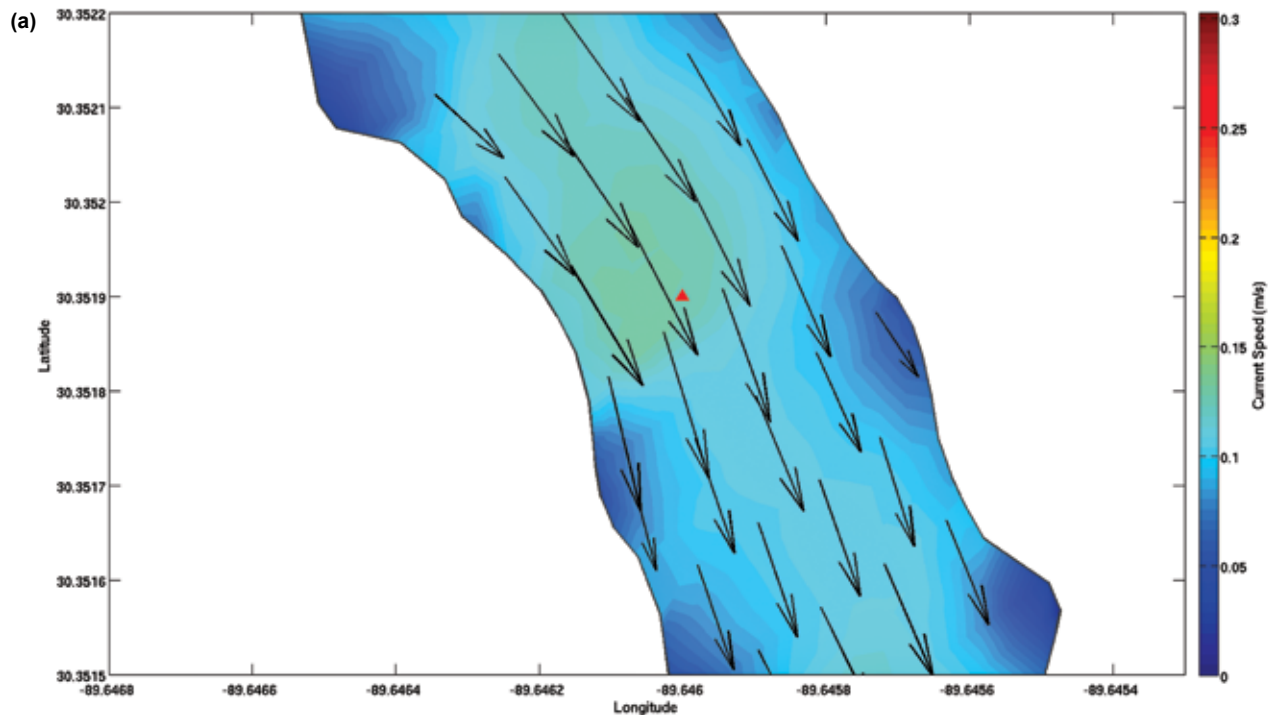


FIGURE 8

Modeled currents from the RST within a single river reach: shown are (a) the magnitude as color, and direction as arrows; and (b) a comparison to measured currents at one location.

References

- ¹ C.A. Blain, R. Linzell, A. Weidemann, and P. Lyon, "A Tool for Rapid Configuration of a River Model," MTS/IEEE Oceans'09 Conference Proceedings, Biloxi, MS, Oct. 28, 2009.
- ² P. McKay and C.A. Blain, "Toward Developing a Hydrodynamic Flow and Inundation Model of the Lower Pearl River," MTS/IEEE Oceans'09 Conference Proceedings, Biloxi, MS, Oct. 28, 2009.

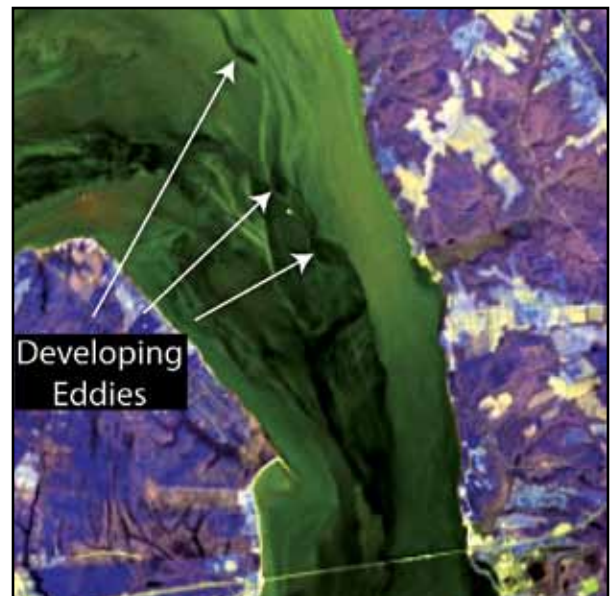


FIGURE 9

Imagery at a bend in the Potomac River, MD, taken by the ASTER satellite on April 2, 2003.

216

Asymmetric Lasercom for Small Unmanned Aerial Systems

P.G. Goetz, W. T. Freeman, J.L. Murphy, B. Mathieu, S.J. Frawley, M.R. Suite, M.S. Ferraro, W.R. Smith, B.B. Xu, R. Mahon, W.S. Rabinovich, M.A. Colbert, H.R. Burris, C.I. Moore, and W.W. Schultz

218

SWOrRD: Swept-Wavelength Optical resonance-Raman Detection of Bacteria, Chemicals, and Explosives

J. Grun, C. Manka, P. Kunapareddy, R. Lunsford, D. Gillis, S. Nikitin, Z. Wang, J. Bowles, and M. Corson

222

Single-shot Imaging Magnetometry and Spectroscopy Using Cold Atoms

F.K. Fatemi, M.L. Terraciano, M. Bashkansky, and Z. Dutton

Asymmetric Lasercom for Small Unmanned Aerial Systems

P.G. Goetz,¹ W.T. Freeman,² J.L. Murphy,¹ B. Mathieu,³ S.J. Frawley,² M.R. Suite,⁴ M.S. Ferraro,¹ W.R. Smith,⁴ B.B. Xu,⁴ R. Mahon,¹ W.S. Rabinovich,¹ M.A. Colbert,² H.R. Burris,⁴ C.I. Moore,⁴ and W.W. Schultz⁵

¹Optical Sciences Division

²SmartLogic

³Barry Design, LLC

⁴Naval Center for Space Technology

⁵Chemistry Division

Introduction: As reliance on small unmanned aerial systems (UASs) expands, and sensors requiring higher-bandwidth downlinks are developed, the need for secure high-data-rate communications increases. Laser communication (lasercom), also known as free-space optical (FSO) communication, is inherently low-probability-of-interception and detection (LPI/LPD). Lasercom has been previously demonstrated on manned aircraft; however, those systems require a high-precision pointing system and correspondingly high-accuracy navigation information hardware, both of which are prohibitively heavy for small UASs.

The work described here opens up the use of lasercom to small UASs, which could not otherwise support lasercom terminals. NRL developed an alternative to conventional lasercom terminals and applied it to small UASs. The enabling technology in these new terminals is the modulating retro-reflector (MRR). NRL has actively developed MRRs since 1998, primarily for terrestrial and shipboard applications. An MRR architecture shifts most of the power, weight, and pointing requirements to one end of the link, allowing the other end to be extremely small, low-power, and require only rough pointing.

Airborne Lasercom Transceiver Components: NRL's MRR transmitters and photoreceivers require only coarse pointing ($\pm 15^\circ$). An optical amplitude modulator is mounted in the path of a cornercube retro-reflector. The ground station's laser beam is

retro-reflected back with data impressed on the beam. MRR transmitters and photoreceivers are installed in modified, low-cost, lightweight (65 g) camera gimbals to allow hemispherical coverage.

Dakota Wingpod Lasercom System: The MRR transceiver gimbals, stabilized camera, and electronics are installed in a wingpod. Hardware providing GPS position, inertial sensing, and heading are included. An onboard processor maintains pointing to the laser ground station. An RF modem in the tail of one pod adds the capability to make hardware configuration changes while in flight for testing purposes. The final weights of the pods are 3.6 kg and 3.1 kg, including gimballed lasercom transmitter and receiver, stabilized camera, video compressor/modem, navigation data sources, antennas, pod structure, and mounting hardware. The combined power draws and weights of the components required for communication are 6 W and 1 kg, and can readily be further reduced. The pods require only power and an optional GPS antenna feed from the Dakota. Figure 1 shows the Dakota with wingpods.

Lasercom Ground Station: The lasercom ground station is based on the Dual Mode Optical Interrogator (DMOI) developed by NovaSol and NRL under the Office of Naval Research DMOI program. NRL extended the capabilities of the DMOI to allow it



FIGURE 1
Dakota UAS with MRR lasercom wingpods.

to track aircraft. Using GPS information, a gimbal provides coarse pointing, putting the aircraft into the field of view of the DMOI's fine steering mirrors, which then optically track the lasercom transceiver. The DMOI is 305 mm by 254 mm by 279 mm, requires



FIGURE 2
Dual Mode Optical Interrogator (DMOI) on tripod.

FIGURE 3
Frame captured from a 15 frames/second video stream.



100 to 180 W, and is controlled by a laptop. The laser system has been classified ANSI / IEC Class 1M, which is eye-safe out of the aperture. Figure 2 shows the DMOI on a tripod.

Flight Tests: NRL successfully completed flight tests on a Dakota UAS at Dugway Proving Ground, Utah, from June 15 to 19, 2009. Two pods were carried on the Dakota. The pods operated independently, allowing various configurations to be tested on the same flight. Maximum range was 2.5 km. The data rate on all links was 2 Mb/s. Three types of links were demonstrated:

- 1) Live video was captured on the ground using the lasercom downlink, while pointing and zoom commands were sent to the camera via the lasercom uplink. A frame captured from a 15 frames/second video stream is shown in Fig. 3.
- 2) Video was stored onboard while the aircraft was out of range, followed by download of the video files over the lasercom link when it came back in range.

- 3) An Ethernet link was established and used for two-way file transfer and communication with the aircraft.

Current and Future Work: The information gained from the flight tests is being used to develop more advanced airborne lasercom payloads. Work is currently under way to increase range while decreasing size and weight for use on expendable, long-range UASs for intelligence, surveillance, and reconnaissance (ISR).

Acknowledgments: The authors would like to thank Matt Sinfield, Jason Wooden, Mark Nielson, and Amy Secrist of the Space Dynamics Lab for assisting with integrating the wingpods and operating the Dakota, Dave Stuart for piloting the Dakota, and Yevgeniya (Jane) Case of L3 Geneva Aerospace for operating the Dakota autopilot.

[Sponsored by the OSD Rapid Reaction Technology Office]

Reference

¹ W.S. Rabinovich, R. Mahon, H.R. Burris, G.C. Gilbreath, P.G. Goetz, C.I. Moore, M.F. Stell, M.J. Vilcheck, J.L. Witkowski, L. Swingen, M.R. Suite, E. Oh, and J. Koplow, "Free-space Optical Communications Link at 1550 nm Using Multiple-Quantum-Well Modulating Retroreflectors in a Marine Environment," *Optical Engineering* 44(5), 056001(2005).

SWOrRD: Swept-Wavelength Optical resonance-Raman Detection of Bacteria, Chemicals, and Explosives

J. Grun,¹ C. Manka,² P. Kunapareddy,² R. Lunsford,² D. Gillis,³ S. Nikitin,² Z. Wang,⁴ J. Bowles,³ and M. Corson³

¹*Plasma Physics Division*

²*RSI Inc.*

³*Remote Sensing Division*

⁴*Center for Bio/Molecular Science and Engineering*

Introduction: Detection of bacteria, chemicals, or explosives with Raman scattering is fast, noncontact, does not require chemical supplies, and is adaptable to robotic vehicles — making Raman ideal for many military and civilian applications. In this technique, a laser is used to illuminate an area that may contain the sought-after substance. Some of the laser light is absorbed by the molecular vibrational and rotational states of the substance, and is re-emitted (scattered) at wavelengths slightly different than the wavelength of the illuminating laser. The spectrum of this scattered light is unique to the substance's molecular bond structure, forming a signature that can be used for identification. However, the fraction of laser light that is Raman scattered is very small, leading to insufficient sensitivity in many practical situations. Furthermore, the illuminated area may contain many different substances, each scattering its own Raman spectrum. What is measured is the sum of these spectra, which can be quite complex, so that the ability to identify the constituent substances (i.e., the method's specificity) is degraded. There remains a continuing need to improve the specificity and sensitivity of Raman detection.

When the photon energy of the illuminating laser matches one or more of the energies of the substance's vibrational and rotational states, the laser is said to be in resonance with the substance, and the scattering process is called resonance-Raman. In resonance, the amount of absorbed laser light is significantly greater, and so is the amount of scattered light: light scattered through resonance-Raman is 100 to 100,000 times more intense than light scattered through a Raman process. Thus, we expect that resonance-Raman detection would result in a much better sensitivity (~ ppm

for Raman in ideal environments), or equivalently, allow much larger distance from which detection can be made. However, this is hard to realize in practice. Current detectors use lasers operating at a single laser wavelength, which are not necessarily in resonance with the bonds of the sought-after substance, or are resonant with bonds of one substance but not with those of another.

Swept-Wavelength Optical resonance-Raman

Detection: The potential for increased sensitivity of resonance-Raman can be achieved if a way is found to illuminate the sample with more than one wavelength, chosen to be resonant with the substance's rotational and vibrational states. And, as discussed below, illuminating with more than one wavelength adds another important capability — increased selectivity in complex environments, i.e., environments that contain many different substances.

We are developing two technologies to enable practical multiwavelength resonance-Raman detection.^{1,2,3} The first technology is SWOrRD, Swept-Wavelength Optical resonance-Raman Detection, a multiwavelength resonance-Raman system that sequentially illuminates an area with a laser tunable from deep-ultraviolet to near-infrared and acquires resonance-Raman spectra at each illumination wavelength with a two-stage tunable spectrometer. All components of the SWOrRD system are synchronized, under computer control, and switching wavelengths takes less than one second. The laser has certain unique characteristics that make it especially suitable for detection: narrow bandwidth, low peak power, and high average power (see Fig.4).

A comparison of a multiwavelength resonance-Raman signature of the explosive HMX and a resonance-Raman signature of HMX acquired by illuminating with a single wavelength is shown in Fig. 5. Looking at the single illumination wavelength signature, it is easy to imagine how the distinctive features of this signature are lost once noise and the signatures of other substances are superimposed on it, resulting in a loss of specificity. The multiwavelength signature is composed of multiple spectra, each produced by illumination with a distinct laser wavelength, which are assembled to form a 2D signature, the two independent dimensions being laser-illumination wavelength and scattered wave numbers. In addition to the information contained in the single spectrum, this 2D signature contains information reflecting variations in resonance cross sections with illumination wavelength. It is therefore much more robust and harder to confuse, resulting in better specificity, especially in complex environments containing many different substances.

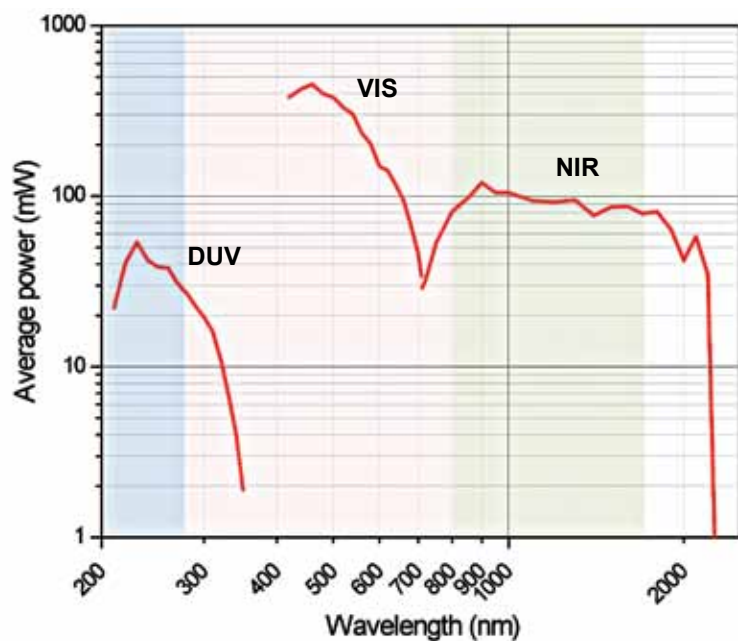
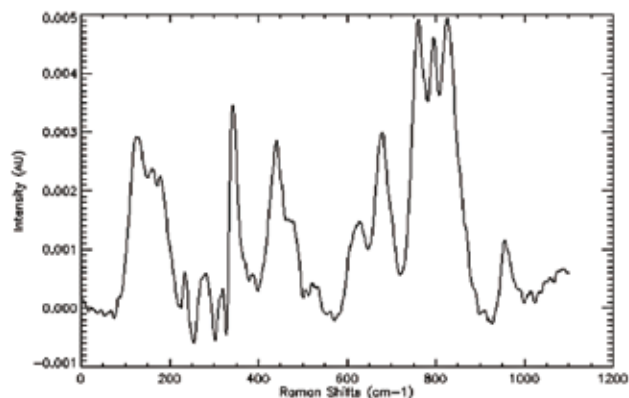
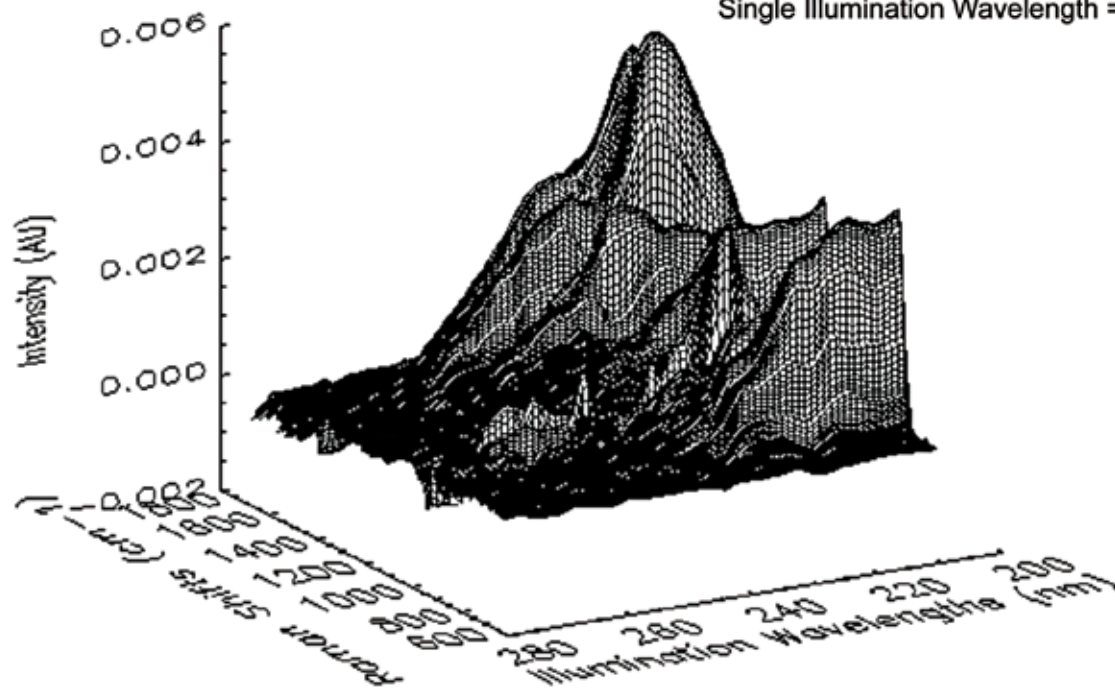


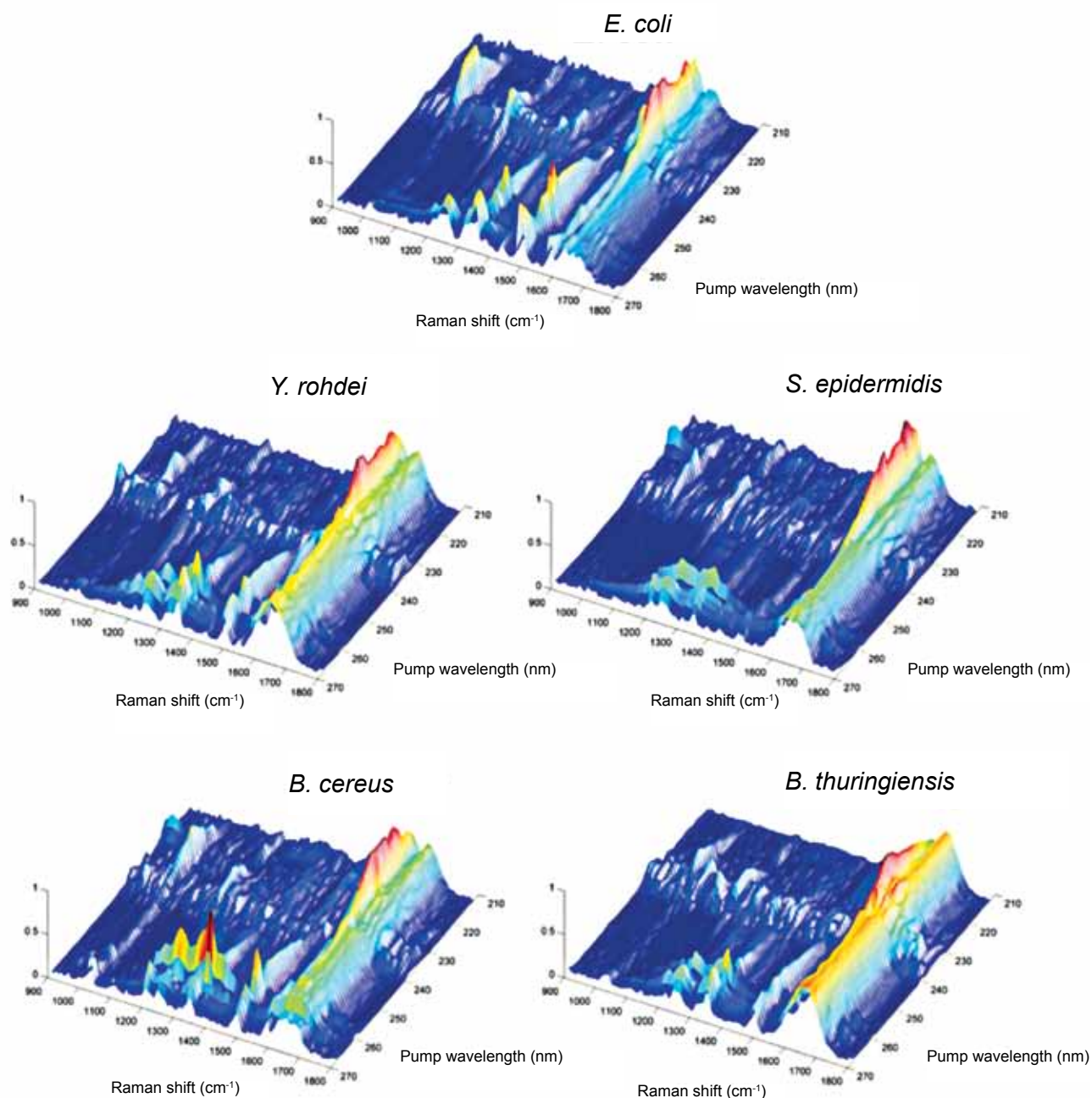
FIGURE 4
Average laser power of the SWOrD laser as a function of wavelength. The laser runs at 1 kHz, has a line width of about 4 cm^{-1} , and is tunable in less than 1 s in 0.1-nm steps.

FIGURE 5
One- and two-dimensional resonance-Raman spectra of the explosive HMX. Top right: A spectrum acquired by illumination with 261-nm laser light. Bottom left: A spectrum acquired by illuminating with multiple laser wavelengths from 210 to 270 nm.



Single Illumination Wavelength = 261 nm



**FIGURE 7**

Bacterial signatures. Two-dimensional resonance-Raman signatures of *E. coli*, *Y. rohdei*, *S. epidermidis*, *B. cereus*, and *B. thuringiensis*.

determines which library signatures make up the field-measured signature, and thus identifies the chemical present and the amount.

Conclusion: We are currently working on developing SWOrRD technology to the point where it is practical to field, and are also adopting it for medical applications. Two-dimensional signatures of bacteria, explosives, chemicals used to manufacture explosives, pharmaceuticals, and assorted chemicals that may occur in the environment are being measured. The

ORASIS code is being adopted so it can take a measured signature of a complex mixture and decompose it into constituent signatures, such as those shown in Figs. 6 and 7.

[Sponsored by DTRA]

References

- ¹ J. Grun, C.K. Manka, S. Nikitin, D. Zabetakis, G. Comanescu, D. Gillis, and J. Bowles, "Identification of Bacteria from Two-Dimensional Resonant-Raman Spectra," *Analytical Chemistry* 79(14), 5489–5493 (2007).

- ² G. Comanescu, C.K. Manka, J. Grun, S. Nikitin, and D. Zabetakis, "Identification of Explosives with Two-Dimensional Ultraviolet Resonance Raman Spectroscopy," *Applied Spectroscopy* **62**, 833–839 (2008).
- ³ S. Nikitin, C. Manka, and J. Grun, "Modified Solc Notch Filter for Deep Ultraviolet Applications," *Appl. Opt.* **48**(6), 1184–1189 (2009).
- ⁴ J. Bowles, P. Palmadesso, J. Antoniadis, M. Baumbach, and L.J. Rickard, "Use of Filter Vectors in Hyperspectral Data Analysis," *Proc. SPIE* **2553**, 148–157 (1995).

Single-shot Imaging Magnetometry and Spectroscopy Using Cold Atoms

F.K. Fatemi,¹ M.L. Terraciano,¹ M. Bashkansky,¹ and Z. Dutton²

¹*Optical Sciences Division*

²*Radar Division and BBN Technologies*

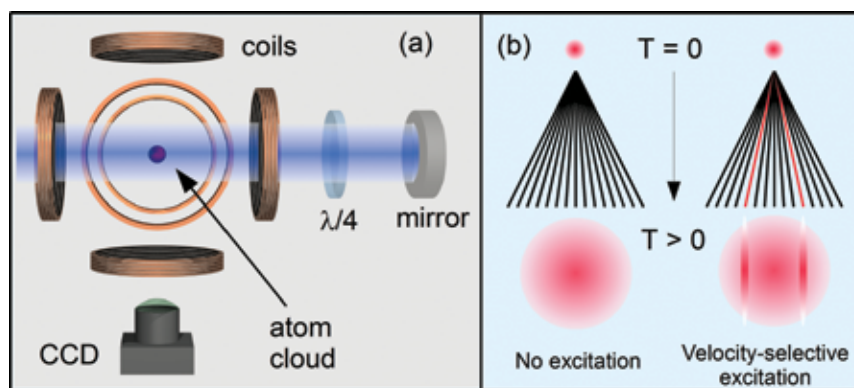
Introduction: Ultracold ($T \sim 100$ microKelvin) atoms are promising candidates for next-generation inertial sensors and magnetometers, but there are several technical challenges to optimizing their performance. The atoms must be initiated efficiently into specific electronic states, and good knowledge and control of magnetic fields is required. To address these issues, we have developed a simple, single-shot technique for imaging ambient magnetic fields with submillimeter spatial resolution over a few centimeters, and for simultaneous measurement of the atomic internal state distribution. This allows real-time optimization of experimental parameters. Such diagnostics previously required time-consuming measurements that prevented real-time evaluation. Our technique requires no hardware beyond what is already used in a typical cold atom setup.

Background: A typical cold atom trap [Fig. 8(a)] confines approximately 10^7 rubidium atoms in a 1 mm diameter volume. When the atoms are released, the cloud freely expands with a distribution of velocities [Fig. 8(b)]. At a later time, the atoms have dispersed spatially according to their velocities so that a fluorescence image of the expanded cloud represents the velocity distribution: under normal conditions, this expanded cloud has a smooth Gaussian profile. In our technique, we can selectively excite atoms within a narrow velocity class because the excitation laser frequency is Doppler-shifted into resonance only for specific velocities. Resonant velocity-selected atoms show up in the image as increased fluorescence [Fig. 8(b), right]. The associated Doppler shifts are proportional to the external fields, and can be used to measure the populations of magnetic sublevels.

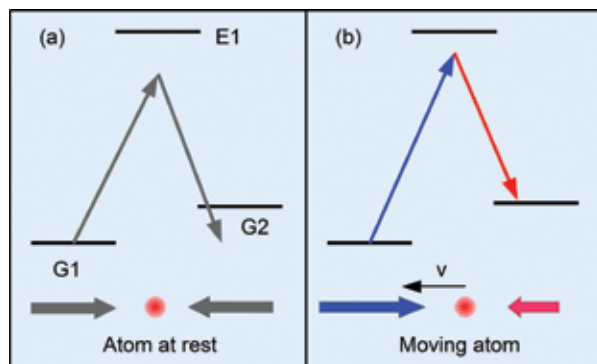
Stimulated Raman Transitions: Velocity selection can occur when atoms are placed in a counterpropagating laser field through stimulated Raman transitions between two ground states, G1 and G2 (see Fig. 9). For an atom at rest, each beam appears to have the same frequency [Fig. 9(a)]. For atoms in motion, however, one beam will be Doppler-shifted to a higher frequency while the other is red-shifted [Fig. 9(b)]. If the apparent frequency difference matches the energy level spacing in the atom, Raman transitions will occur only for that velocity class. In our technique, the two energy levels are magnetic sublevels, which are Zeeman-shifted linearly by a magnetic field. Transitions occur in atoms with Doppler shifts that compensate for the Zeeman shift. Thus, using these two-photon transitions, there is a simple linear relationship between the magnetic field strength and the positions of excited atoms on the camera. The participating energy levels are narrow and capable of discriminating atomic velocities to within 1 mm/s, which corresponds to a magnetic field sensitivity on the order of 1 nT.

Imaging Magnetometry: As an example of the technique, we show background-subtracted images of the expanded atom cloud for different magnetic field strengths. For the images in Fig. 10(a), the fields are spatially uniform. Even without calibration, one can easily use this technique in real time to null magnetic fields simply by zeroing the separation between these stripe features [see the bottom left image of Fig. 10(a)]. If there are spatially varying magnetic fields present, with gradient B' , the resonance condition is also spatially varying and the gradient is intuitively captured in the fluorescence image. For the figures in Fig. 10(b), the atoms were placed in a linear quadrupole field, which occurs at the center of an anti-Helmholtz coil pair. Reference 1 gives a quantitative analysis of this technique.

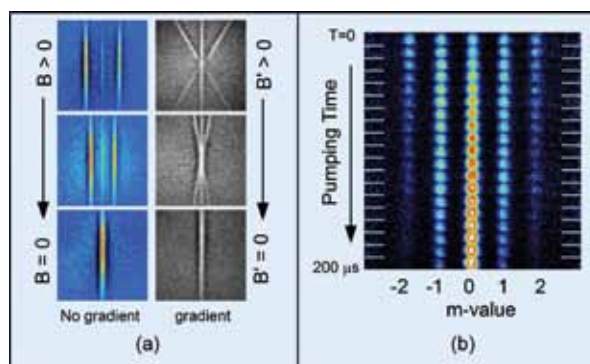
Raman Spectrography: The technique can be slightly modified to measure the population of each magnetic sublevel of a hyperfine manifold simultaneously. By using Raman beams that couple the hyperfine manifolds, which have opposite Zeeman shifts, the selected velocity is also dependent on the magnetic sublevel.² This technique is ideally suited for optimizing optical pumping into a desired sublevel or for measuring sublevel-dependent processes. In Fig. 10(b), we show images of the sublevel distribution as a function of optical pumping pulse duration in a magnetic field. The atoms are in the $F = 2$ hyperfine level, which has $2F + 1$ magnetic sublevels, and are initially equally distributed between $m_F = -2$ to $m_F = 2$, but optical pumping moves the atoms into $m = 0$ in 200 μ s.

**FIGURE 8**

(a) Experiment layout. A cold atom cloud (red circle) is released from a magneto-optical trap and exposed to a retroreflected Raman beam. A CCD camera images the expanding atom cloud from an orthogonal direction, and Helmholtz coils control the magnetic field. (b) Schematic of atom cloud expansion without (left) and with excitation. Resonant velocities (red lines) appear as stripes of increased fluorescence in the image.

**FIGURE 9**

Level diagrams for atoms at rest (a) and in motion (b). The Raman beams are shifted into resonance only for atoms with the correct Doppler shift.

**FIGURE 10**

Background-subtracted fluorescence images of expanding atom clouds after Raman excitation. (a) Magnetometry: The separation between features is directly proportional to the scalar magnetic field (left). Gradient fields, B' , appear as spatially varying resonances (right). (b) Montage of spectrographs of magnetic sublevels for increasing optical pumping pulse durations. The unpolarized sample (top) is pumped into the $m = 0$ state after $200 \mu\text{s}$.

in this example. Reference 2 gives an analysis of this technique.

Summary: We have presented a single-shot technique for imaging magnetic fields over a region with submillimeter spatial resolution using cold atoms. A slight modification allows the technique to measure the populations of several atomic internal states simultaneously. Because the measurements are made in a single shot, they provide useful diagnostics for real-time optimization of cold atom sensors.

[Sponsored by ONR]

References

- ¹ M.L. Terraciano, M. Bashkansky, and F.K. Fatemi, "A Single-shot Imaging Magnetometer Using Cold Atoms," *Opt. Express* **16**, 13062–13069 (2008).
- ² F.K. Fatemi, M.L. Terraciano, M. Bashkansky, and Z. Dutton, "Cold Atom Raman Spectrography Using Velocity-selective Resonances," *Opt. Express* **17**, 12971–12980 (2009).

226

Real-time Surface Wave Information by Coherent Radar
P.A. Hwang, M.A. Sletten, and J.V. Toporkov

227

Shipboard AIS and Radar Contact Reporting (SARCR)
R. L. Nichols

Real-time Surface Wave Information by Coherent Radar

P.A. Hwang, M.A. Sletten, and J.V. Toporkov
Remote Sensing Division

Introduction: The technique for extracting wave period and wave direction from radar backscattering intensity reached a mature stage by the 1980s,¹ but the determination of wave height has been hindered by the complex nature of the modulation transfer function relating the radar return to surface wave properties. In contrast to backscattering intensity, the coherent radar Doppler signal characterizes the radial velocity of the surface roughness that scatters back the radar waves. The oscillatory component of the Doppler signal is dominated by the surface wave motion. The principal wave period can be derived from the peak frequency of the Doppler spectrum and the significant wave height from the Doppler variance. Analyses of coherent radar measurements collected from the ocean show that with radar range coverage on the order of ten dominant wavelengths, the spectral peak wave period and significant wave height can be determined from as little as 1 s of data.² This new development offers rapid acquisition of critical surface wave information for naval operations and research of the ocean environment.

Doppler Processing: Two approaches can be used to derive the Doppler velocity from the coherent radar return. The first is to obtain the signal phase through Hilbert transformation of the radar return and then compute the time derivative of the signal phase. This method is basically the covariance approach to spectral moment estimation from pulse pairs, thus is called the “pulse pair” approach. The second is by spectral processing of short segments of the complex radar return signal, typically through fast Fourier transformation (FFT), and is called the “FFT” approach. The Doppler frequency computed by the pulse pair method is the equivalent of the mean Doppler frequency defined by the first moment of the Doppler frequency spectrum derived from the FFT method. Figure 1 shows an example of the spatio-temporal

images of the Doppler velocity fields of the surface roughness modulated by large-scale ocean surface waves using the coherent radar returns processed by the two methods.

Wave Analysis: Applying spectral analysis to the spatial series of the Doppler velocity record yields a wave number spectrum of the surface wave velocity. The surface displacement spectrum is related to the wave velocity spectrum in a deterministic fashion following the surface wave theory. Figure 2(a) shows examples of the wave number spectra processed with the Doppler velocity using 1 and 5 s of radar data. For comparison, the corresponding spectrum computed with 20 min of accelerometer data measured by a nearby wave buoy is also shown. Interestingly, the Doppler velocity spectra computed with 1 and 5 s of

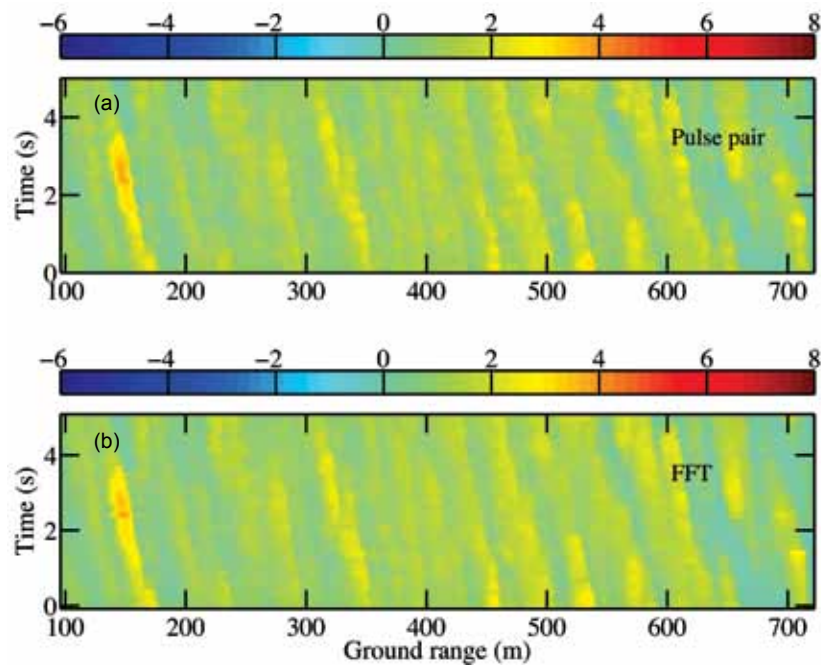
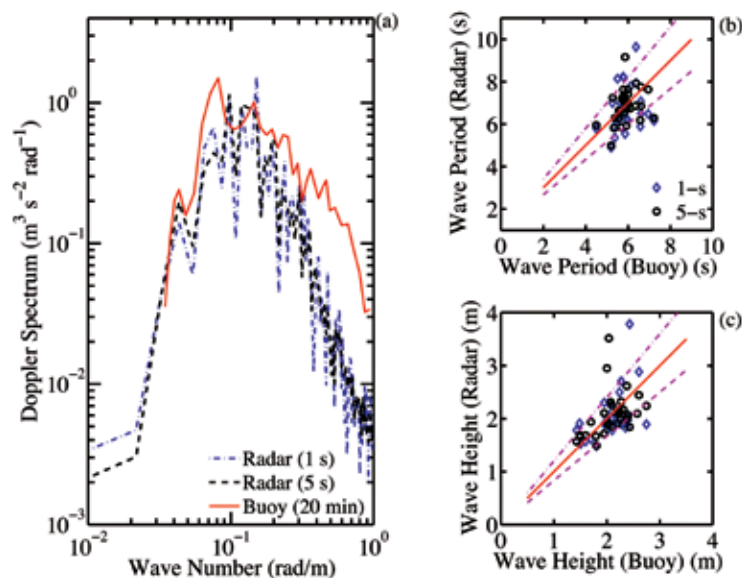


FIGURE 1
 An example of the spatio-temporal images of the Doppler velocity field derived from (a) pulse pair and (b) FFT approaches. The unit of the colorbar scale is m/s.

radar data are very similar; both are in good agreement with the buoy measurement, especially in the energetic spectral peak region.

For naval operations in the sea, as well as for ocean surface wave research involving air-sea interaction, the key parameters of the surface wave field are the significant wave height and spectral peak period. Together with the wind speed, the three environmental variables form the dimensionless parameters quantifying ship response, maneuvering, wave impact, growth of wind-generated waves,


FIGURE 2

Comparison of (a) wave number spectra, (b) peak wave period, and (c) significant wave height, obtained by radar (1 and 5 s of data) and wave buoy (20 min of data). Line segments of 1:1, 1.2:1, and 1:1.2 slopes are superimposed for reference.

and air-sea exchanges of momentum and energy. The spectral peak wave period is readily obtained from the Doppler spectrum. The significant wave height can be computed from the fluctuation component of the radar Doppler velocity. The results are presented in Figs. 2(b) and (c). The peak wave period derived from the present procedure is about 1 s longer than in situ buoy measurements. Accounting for this bias, most wave period and wave height results are confined within the envelopes bounded by $\pm 20\%$ from perfect agreement. For reference, line segments of 1:1, 1.2:1, and 1:1.2 slopes are superimposed in the figure.

[Sponsored by ONR]

References

1. I.R. Young, W. Rosenthal, and F. Ziemer, "Three-dimensional Analysis of Marine Radar Images for the Determination of Ocean Wave Directionality and Surface Currents," *J. Geophys. Res.* **90**, 1049–1059 (1985).
2. P.A. Hwang, M.A. Sletten, and J.V. Toporkov, "A Note on Doppler Processing of Coherent Radar Backscatter from the Water Surface: With Application to Ocean Surface Wave Measurements," *J. Geophys. Res.*, **115**, C03026 (March 2010) doi:10.1029/2009JC005870.

Shipboard AIS and Radar Contact Reporting (SARCR)

R.L. Nichols
Space Systems Development Department

Background: Guarding coastal approaches has always been a national priority but the events of September 11, 2001, have heightened the emphasis on filling important gaps in our ability to secure the

nation against various threats. A key element of the national strategy for improving security is to provide enhanced Maritime Domain Awareness (MDA). The strategy is aimed at ensuring that decision-making authorities have information necessary to identify and react to potential threats to national security arising in the maritime domain. Threats must be identified as early and as far offshore as possible, requiring awareness of activity not only in our territorial waters, but also in the Contiguous Zone (from 12 to 24 nautical miles from the coast), in the Exclusive Economic Zone (EEZ — out to 200 nautical miles), and even on the high seas. The paucity of dedicated sensors to provide persistent coverage of our coastal waters and commercial shipping lanes hampers the development of in-depth maritime domain situational awareness.

The Naval Research Laboratory recognized that to meet this MDA challenge, new approaches need to be explored. The approach taken by the Mission Development Branch of the Space Systems Development Department was to explore the possibility of using nontraditional sensor sources, i.e., those being used by commercial vessels during their normal transits. NRL proposed the Shipboard Automatic Identification System (AIS) and Radar Contact Reporting (SARCR) system to the U.S. Department of Homeland Security (DHS) Science and Technology Directorate, Borders and Maritime Security Divisions, Maritime Security Technology Program, which funded this effort in FY09. The effort proposed was to design, develop, integrate, test, and install 15 rapid prototype systems. These systems are capable of capturing the ship's onboard radar-generated tracks and simultaneously collect radiated AIS messages and relay all the collected data via a commercial Iridium satellite communications (SATCOM) link to the John A.

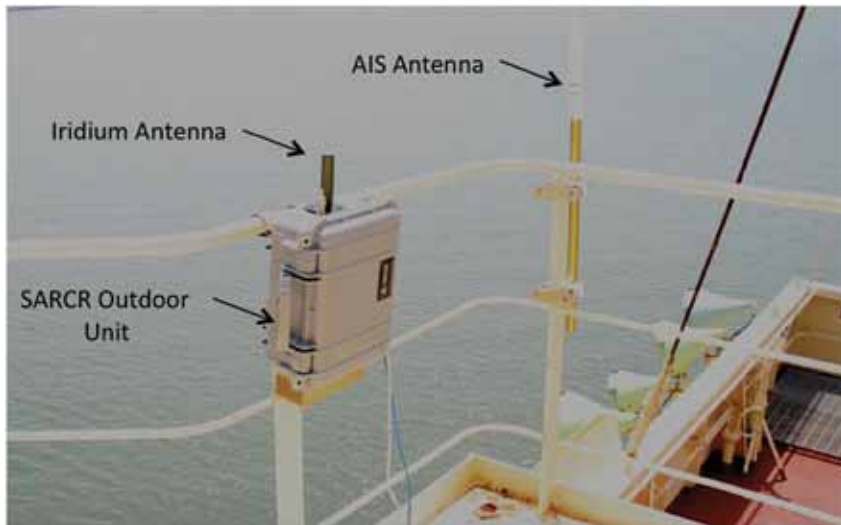


FIGURE 3
The SARCR Outdoor Unit deployed.

Volpe National Transportation Systems Center for distribution to Government and commercial users via the Maritime Safety and Security Information System (MSSIS).

Aid (ARPA) tracker via an International Standard International Electrotechnical Commission (IEC) 61162-1 RS-232/422 interface¹ and to the Outdoor Unit (Fig. 3) via either an Ethernet or an internal ZigBee wireless card located in each unit. The Outdoor Unit is fully integrated, containing an AIS receiver, a GPS receiver, an Iridium modem, and the associated antennas for each system.

System Overview: The SARCR system consists of two subunits, an Indoor and an Outdoor Unit, built with off-the-shelf hardware. The Indoor Unit interfaces to the ship's radar Automatic Radar Plotting

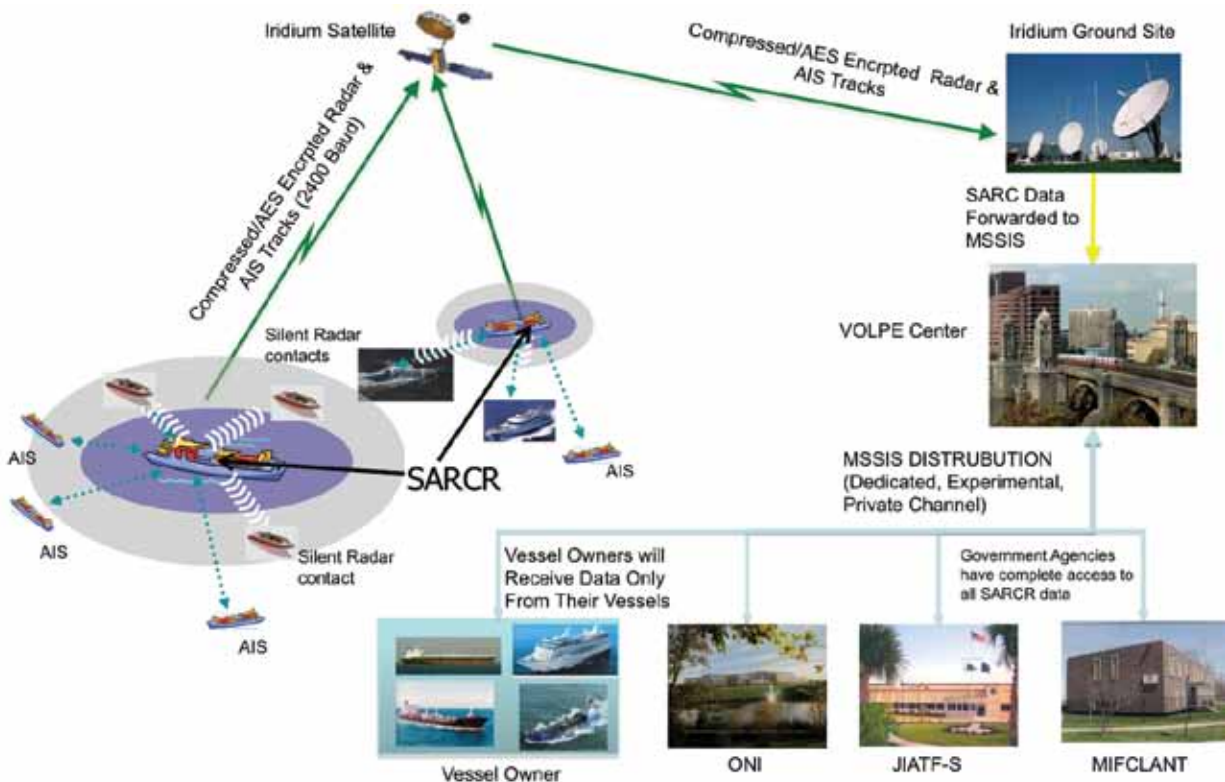


FIGURE 4
SARCR concept of operations.

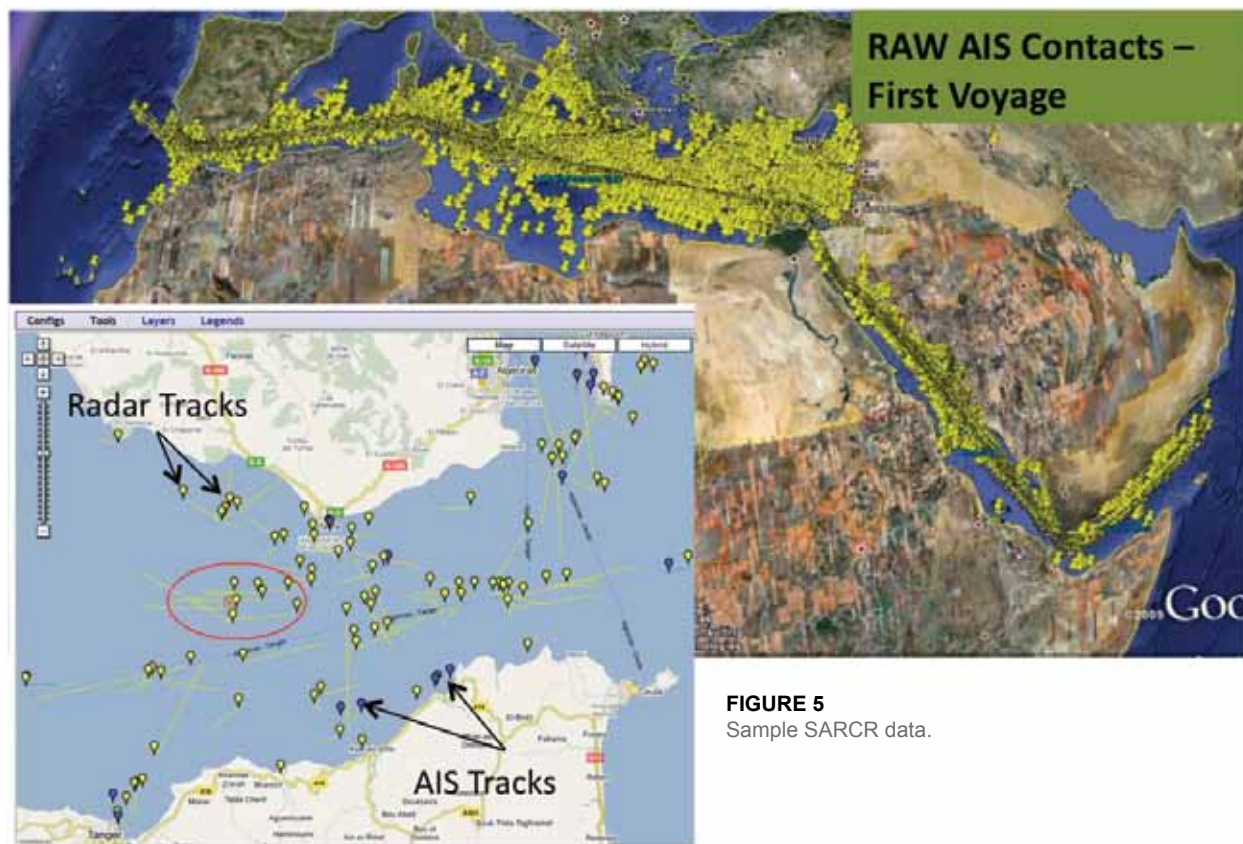


FIGURE 5
Sample SARCR data.

Functional Description: IEC-61162-1-formatted target track messages (TTM) from the ship’s radar ARPA tracker are collected by the Indoor Unit and forwarded to the Outdoor Unit. The Outdoor Unit then extracts a target’s range and bearing along with time data from the TTM message and converts the data into latitude and longitude. Once the position has been calculated, a modified IEC-61162-1 message containing the positional data and time is created. This message is forwarded to the communications software module in the Outdoor Unit. The Outdoor Unit’s communications module then evaluates it as either a new track or an update track. At the same time, the Outdoor Unit is receiving AIS messages and forwarding them to the communications module to undergo the same evaluation.

Every minute, the communications module builds a series of data packets containing all the new radar and AIS tracks and track updates, which are compressed, software-encrypted using 256 bit software encryption, and transmitted continuously (24/7/365) via a 2400 baud Iridium satellite modem link to land-based processing centers. To maintain connectivity across the Iridium satellite link to the land-based processing center, NRL developed an ACK-NAK and a packet-tracking scheme that has allowed for an average data loss of less than 3%. The land-based processing center decrypts, decompresses, and distributes the

received data via the Internet to the owner of the participating vessel from which the data originated and to U.S. agencies, Office of Naval Intelligence (ONI), Joint Inter-Agency Task Force South (JIATF-S), and U.S. Coast Guard’s Maritime Intelligence Fusion Center – Atlantic (MIFCLANT). The team has installed one unit on a commercial vessel (as shown in Fig. 3), and will have installed the remaining units by the end of FY10. The concept of operations and a sample of data are seen in Figs. 4 and 5, respectively.

[Sponsored by DHS S&T Directorate, Maritime Security Technology Program]

Reference

¹ International Electrotechnical Commission 61162-1, International Standard Third Edition 2007-04, *Maritime Navigation and Radiocommunication Equipment and Systems - Digital Interfaces; Part 1: Single Talker and Multiple Listeners* (2007).

232

High-Yield Z-Pinch Thermonuclear Neutron Source

A.L. Velikovich, R.W. Clark, J. Davis, J.L. Giuliani, Y.K. Chong, C.A. Coverdale, and D. Flicker

234

Rapid Air Traffic Modeling and Prediction

C.R. Kaplan, E.S. Oran, N. Alexandrov, and J.P. Boris

High-Yield Z-Pinch Thermonuclear Neutron Source

A.L. Velikovich,¹ R.W. Clark,² J. Davis,¹
J.L. Giuliani,¹ Y.K. Chong,¹ C.A. Coverdale,³
and D. Flicker³

¹Plasma Physics Division

²Berkeley Research Associates, Inc.

³Sandia National Laboratories

Introduction: Neutron beams are useful for many applications, from noninvasive imaging and characterization of materials to producing medical isotopes and detecting hidden explosive devices. Some applications require high-energy neutrons created in fusion nuclear reactions between deuterium (D) and tritium (T). To achieve thermal fusion, deuterium or DT plasma must be heated to about 10^8 K, which is a challenging task. One of the pathways to controlled thermonuclear fusion is inertial confinement fusion (ICF). High-energy ICF lasers, such as OMEGA at the University of Rochester and the National Ignition Facility (NIF) at Lawrence Livermore National Laboratory, as well as ICF pulse power facilities, such as the Z accelerator at Sandia National Laboratories, compress and heat deuterium or DT-filled capsules by strong laser or X-ray radiation. The highest thermonuclear DD neutron yield of the pre-NIF era is about 3×10^{11} , obtained by direct capsule illumination with laser beams on OMEGA and by X-ray compression on Z. In the future, NIF will deliver ~ 180 kJ of X-ray energy to the capsule. DT neutron yield corresponding to “breakeven” (the same energy input as released in a DT reaction) is 6×10^{16} . Neutron yields above 6×10^{16} can only be produced when the fusion energy release

exceeds the input, indicating ignition and fusion energy gain. On the other hand, a DD plasma at the same temperature and density would produce a fusion neutron yield about two orders of magnitude less due to lower reaction cross section, that is, about 6×10^{14} . Deuterium fusion neutron yields of this magnitude could only be expected from ignition-scale ICF facilities, only one of which, NIF, has been built so far.

Z-pinch Neutron Sources: A DD fusion neutron yield of about 3×10^{13} , exceeding the previous ICF record by two orders of magnitude, has recently been obtained on Z without a capsule implosion. A deuterium gas column was imploded in cylindrical geometry by a 15 MA, 100-ns-long current pulse, as illustrated by Figs. 1(a) and (b). The most powerful, fast, multi-MA current driver in the world, shown in Fig. 1(c), is much smaller and simpler to operate than ignition-class lasers.

Non-thermonuclear DD fusion neutrons have been produced in Z-pinch plasmas at pinch currents up to about 2 MA for many years. They were generated by relatively small quantities of “beam” deuterium ions accelerated in the strong electric fields accompanying the development of instabilities in the pinch. Their collisions with the cold “target” deuterium ions produced fusion neutrons. This “beam-target” mechanism of neutron production does not scale well to high currents and plasma densities, showing little promise for producing neutron yields above 10^{13} .

New opportunities for nuclear fusion in Z-pinch plasmas emerged at higher-current facilities. Analysis and modeling of the experimental results on Z done at NRL¹ led to an unexpected conclusion: a substantial part of the observed fusion neutrons must have been

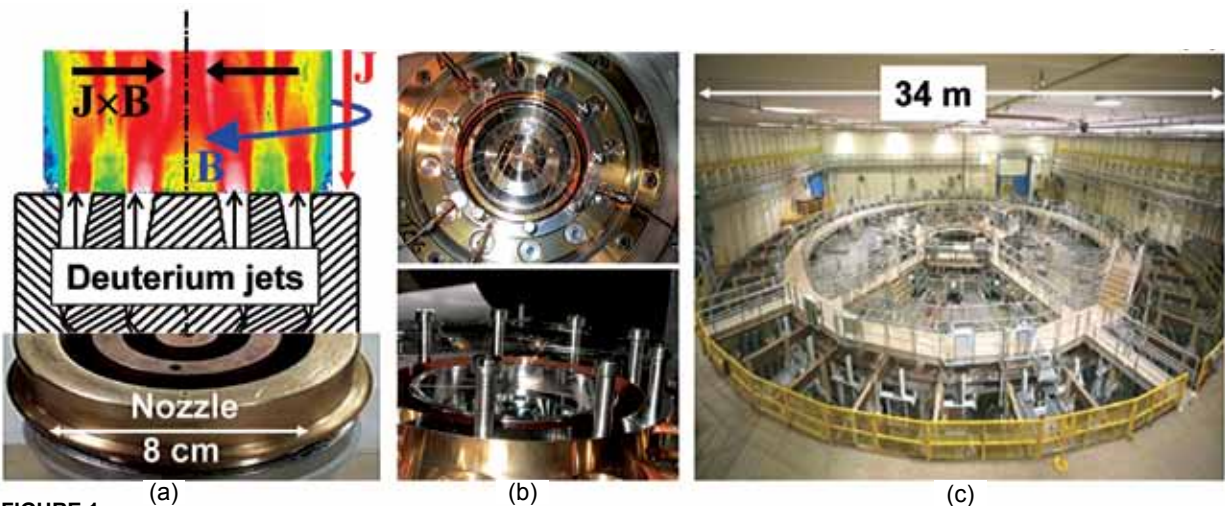


FIGURE 1

(a) An annular gas jet injected from a supersonic nozzle between the anode and cathode of the Z accelerator and then radially imploded by the $\mathbf{J} \times \mathbf{B}$ force to produce a tight, hot Z-pinch column on axis. (b) The nozzle installed on Z by L-3 Communications/Pulse Sciences. Thin wire mesh defines the anode. (c) Photo of the Z accelerator at Sandia National Laboratories, which after its refurbishment completed in 2007, can drive current pulses up to 26 MA and 100 to 300 ns.

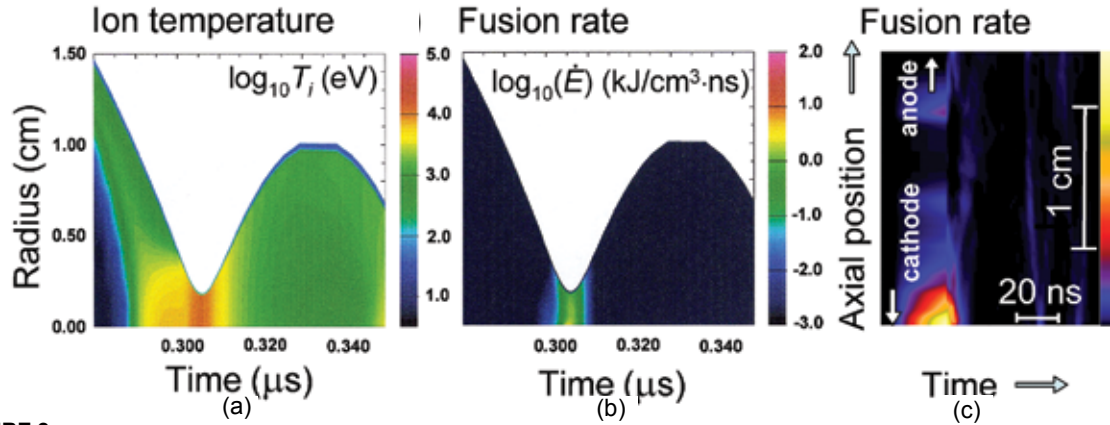


FIGURE 2

Simulated plasma heating and neutron production in deuterium gas-puff Z-pinch implosions on Z. Time histories of the ion temperature (a) and the DD fusion reaction rate (b) are from the 1D simulations. Radially integrated, time-resolved fusion rate (c) is from a 2D simulation.

of thermonuclear origin. Deuterium-pinch plasma imploded on Z by a 15 MA current is heated to about 10^8 K, has a sufficiently large mass, and is inertially confined long enough to produce over 10^{13} neutrons via the thermal mechanism. Figures 2(a) and (b) show the simulated time history of the ion temperature and the fusion energy and neutron production rate. The ions in the converging compressed deuterium plasma shell are heated by shock waves and adiabatically. As the ion temperature approaches 10^8 K, the fusion reaction starts producing neutrons. Figure 2(c) shows the axial nonuniformity of the neutron production in Z

experiments, with most of the neutrons coming from near the cathode. The thermonuclear fusion mechanism implies that the neutron yield scales with the pinch current as I^4 .

Figure 3 compares the results of experiments on two different high-current facilities at Sandia² with the I^4 scaling and simulation results. Radiation-hydro simulations take into account only the thermal mechanism of neutron production, which is seen to be sufficient to account for all observed neutron yield. Kinetic simulations done in 2009 with a code capable of capturing the contribution of the “beam-target” mechanism to the neutron production, estimate it to be about 50% of the total, the remaining 50% of neutrons being of thermal origin. Also shown is the predicted neutron yield in the new experiments with deuterium pinches designed at NRL for the refurbished Z facility, ZR. Our simulations predict DD neutron yields of about 4×10^{14} , that is, in the ignition-scale range. Extrapolating these results to higher driving currents, we can expect fusion ignition and energy gain in DT Z-pinch plasma at about 50 MA.

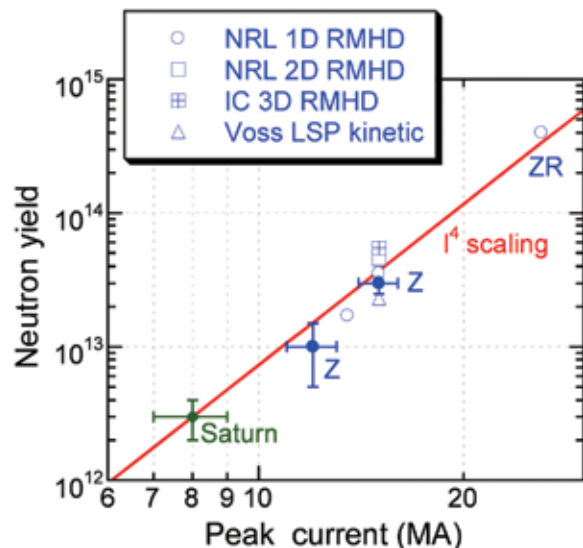


FIGURE 3

Neutron yield measured in gas-puff implosions on Saturn and Z accelerators at Sandia National Laboratories compared to the results of simulations of Z implosions done independently at NRL, Imperial College (IC, London, UK), and Voss Scientific, LLC (Albuquerque, NM). Radiative-magnetohydrodynamic (RMHD) simulations (NRL, IC) model only the thermonuclear contributions to the DD neutron yield, whereas the kinetic simulation (Voss) accounts for the beam-target mechanism of neutron production.

Summary: A deuterium Z-pinch can become the most powerful, cost-efficient, and energy-efficient laboratory source of thermal fusion neutrons, in the same way as fast Z-pinches are the most powerful laboratory X-ray sources. As stated in a *Nature Physics* “Research Highlights” article reviewing this work, the simulations and experiments “suggest that the technology has matured to a stage where useful fluxes [of neutrons] could soon be generated.”²³

Acknowledgments: The work presented here is part of a larger program on radiation effects and electronics survivability testing involving many scientists from NRL, Sandia National Laboratories, and industry. [Sponsored by DOE/NNSA]

References

¹ A.L. Velikovich, R.W. Clark, J. Davis, Y.K. Chong, C. Deeney, C.A. Coverdale, C.L. Ruiz, G.W. Cooper, A.J. Nelson, J. Franklin, and L.I. Rudakov, "Z-pinch Plasma Neutron Sources," *Phys. Plasmas* **14**, 022701 (2007).
² C.A. Coverdale, C. Deeney, A.L. Velikovich, J. Davis, R.W. Clark, Y.K. Chong, J. Chittenden, S. Chantrenne, C.L. Ruiz, G.W. Cooper, A.J. Nelson, J. Franklin, P.D. LePell, J.P. Apruzese, J. Levine, and J. Banister, "Deuterium Gas-puff Z-pinch Implosions on the Z Accelerator," *Phys. Plasmas* **14**, 056309 (2007).
³ Research Highlights, *Nature Physics* **3**, 217 (April 2007).

Rapid Air Traffic Modeling and Prediction

C.R. Kaplan,¹ E.S. Oran,¹ N. Alexandrov,² and J.P. Boris¹

¹Laboratory for Computational Physics and Fluid Dynamics

²NASA Langley Research Center

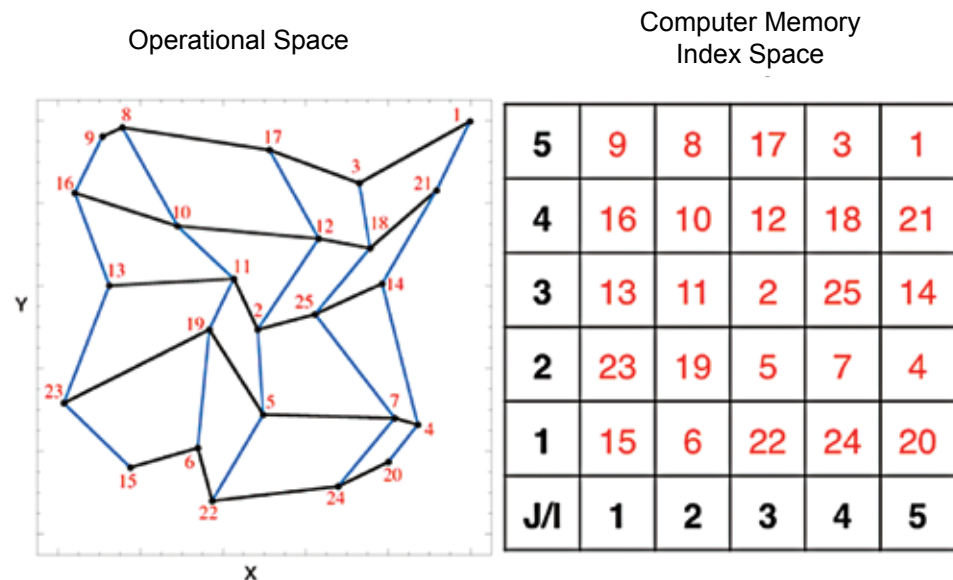
Introduction: Optimization and control of the air traffic system is vital to our national economy and homeland security. In order to develop strategies to design and control the increasingly complex aspects of air transportation, we must have a fast research tool for modeling all aspects of the air-traffic system, ranging from local groups of aircraft to global optimizations of entire traffic systems, including baggage, passengers, and aircraft. We are currently developing a dynamic global model, the Air Traffic Monotonic Lagrangian Grid (ATMLG), for simulating the air traffic flow as a platform for evaluating approaches to air systems control and optimization. ATMLG can be used to test control strategies for conflict prevention and traffic-flow management, or to evaluate the reaction of the system to local and global perturbations, such as weather. For example, ATMLG could be used to determine the most efficient

FIGURE 4

The figure shows a simple 2D MLG containing the x and y physical locations of 25 labeled nodes. The black (horizontal) lines show the x-links and the blue (vertical) lines show the y-links. The table shows the grid indices in computer memory of the nodes shown in the figure. That is, node 15 is indexed at I = 1, J = 1; node 6 is indexed at I = 2, J = 1, etc.

way to reroute air traffic after local conditions, such as thunderstorms, have caused disturbances throughout the entire air-traffic system. This work is applicable to both military and civil aviation, as well as to other systems where many objects are moving in complex paths relative to each other, such as swarms of mobile sensors and space debris.

Monotonic Lagrangian Grid (MLG): The MLG was originally developed at NRL in the mid 1980s,¹ and has since been used as the underpinning for various particle dynamics simulations. The MLG is a data structure for storing the positions and other data needed to describe *N* moving objects, where *N* can be very large. The MLG algorithm sorts and orders objects on a grid structure in real (operational) space and indexing (computer memory) space. As an example, Fig. 4 depicts a small, two-dimensional (2D) MLG. The image on the left shows the 25 MLG nodes (objects) in operational space, while the table on the right shows the grid indices in computer memory of each node. Although the nodes are irregularly spaced (left figure), they are indexed regularly in the MLG by a monotonic mapping between the grid indices and the operational locations. A computer program based on the MLG data structure does not need to check *N*-1 possible distances to find which nodes are close to a particular node. Rather, the indices of the neighboring nodes are automatically known because the MLG node indices vary monotonically in all directions with the Lagrangian node coordinates. This is the major advantage of the MLG data structure for air traffic modeling. Extensive searches to find nearby aircraft are eliminated, allowing many more aircraft to be safely tracked on modest computers in real time.



Conflict Prevention and Resolution Research:

We have combined the MLG with algorithms for conflict prevention, circumventing restricted zones, and updating aircraft trajectories, for various test-case scenarios. Conflict prevention algorithms include those for preventing collisions and for maintaining adequate separation distance between aircraft. Figure 5 shows results from a simulation to evaluate “rules” to determine the best way to circumvent a restricted area with a minimum amount of flight delay time. The red square regions, which could, for example, represent an area of bad weather, were placed in the center of the computational domain, and aircraft approaching that area were required to avoid it according to the rules for that scenario. For example, in scenario (a), aircraft approaching the region from the northeast, entering the region at face a, are rerouted to the west (shown by the blue arrow). Aircraft approaching from the northwest are rerouted to the east (shown by the red arrow).

In scenario (b), all aircraft are rerouted in a clockwise direction. In scenario (c), aircraft were routed to the numbered way-points. The bar chart in Fig. 5 indicates that the rules defined in scenario (c) result in the least delay time.

We have also used ATMLG to investigate ways to maintain a safe separation distance between many aircraft in complex airspace.² This is particularly important to the design of the Next Generation Air Transportation System, in which it is proposed that aircraft in high-altitude airspace will use automated self-separation maintenance methods. For a hypothetical problem, we tracked the total number of conflict-avoidance moves for each aircraft. This includes the initial primary maneuver when two aircraft first approach each other, and any subsequent secondary maneuvers required as a result of the primary maneuver. That is, after each aircraft is redirected to maintain a 3-km separation distance, we then check to ensure

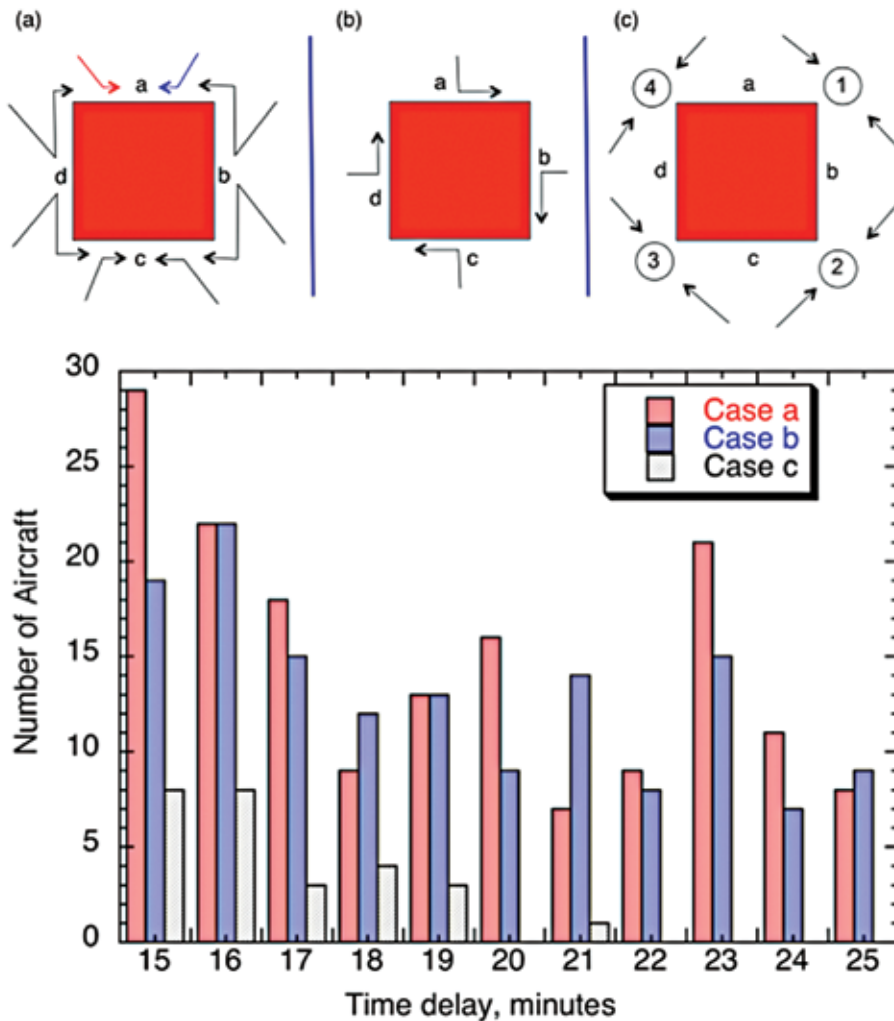


FIGURE 5 Simulation results to evaluate “rules” to determine the best way to circumvent a restricted area with minimum flight delay time.

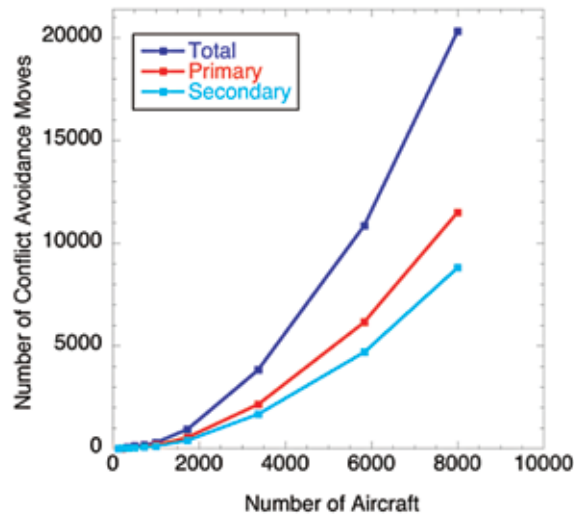


FIGURE 6

The number of moves to maintain a safe separation distance increases exponentially with the number of aircraft in the simulation.

that the modified trajectories do not create subsequent potential conflicts. Figure 6 shows that the total number of conflict avoidance maneuvers increases exponentially with the number of aircraft in the simulation, and that there are almost as many secondary maneuvers as primary maneuvers.

Discussion: We have developed ATMLG as a tool to rapidly test ideas and algorithms for preventing conflicts and maintaining adequate separation distance among aircraft. The fast sorting algorithm in the MLG enables rapid simulation of various air-traffic scenarios, and future implementations of ATMLG can be used as the basis for active design of the air transportation system.

Acknowledgments: The authors gratefully acknowledge support from NASA Langley Research Center (LaRC) under Interagency Agreement IA1-910 between LaRC and the Laboratory for Computational Physics and Fluid Dynamics.

[Sponsored by NASA]

References

- ¹ J. Boris, "A Vectorized 'Near Neighbors' Algorithm of Order N Using a Monotonic Logical Grid," *J. Computational Physics* **66**(1), 1–20 (1986).
- ² C.R. Kaplan, E.S. Oran, N. Alexandrov, and J.P. Boris, "The Monotonic Lagrangian Grid for Fast Air-Traffic Evaluation," AIAA Paper 2010-597, American Institute of Aeronautics and Astronautics, Reston, VA, 2010.

238

Joint Milli-Arcsecond Pathfinder Survey (JMAPS) Fine Attitude Determination Approach
T.W. Lim, F.A. Tasker, and P.G. DeLaHunt

240

TacSat-4, Advanced UHF SATCOM
M. Hurley, W. Raynor, M. Johnson, K. Weldy, E. Becker, C. Amend, M. Nurnberger, T. Duffey, R. Skalitzky, T. Specht, E. Bradley, R. Baldauff, J. Armingier, J. Barnds, K. Akins, J. Hicks, E. Sydow, G. Sandhoo, D. Bentz, B. Davis, and E. Gruner

242

Integrating the Sun-Earth System for the Operational Environment (ISES-OE)
J.L. Lean, J.D. Huba, S.E. McDonald, S. Slinker, D.P. Drob, J.T. Emmert, R.R. Meier, J.M. Picone, G. Joyce, J. Krall, A. Stephan, K.A. Roach, H. Knight, S.P. Plunkett, C.-C. Wu, B.E. Wood, Y.-M. Wang, R.A. Howard, J. Chen, P.A. Bernhardt, and J.A. Fedder

245

Origins of Solar Energetic Particle (SEP) Variability
Y.-K. Ko and A.J. Tylka

248

Technology Development for High Integrity GPS (HiGPS)
O.J. Oaks

Joint Milli-Arcsecond Pathfinder Survey (JMAPS) Fine Attitude Determination Approach

T.W. Lim, F.A. Tasker, and P.G. DeLaHunt
Spacecraft Engineering Department

Introduction: The Joint Milli-Arcsecond Pathfinder Survey¹ (JMAPS) is a Department of the Navy space astrometry mission to conduct an all-sky, bright star astrometric and spectrophotometric survey. The primary goal of the mission is to update the bright star catalog currently used by Department of Defense, NASA, and commercial star tracker manufacturers for spacecraft attitude determination. Secondary goals include the development and flight demonstration of an advanced detector such as the H4RG-10 CMOS-Hybrid detector/readout sensor. The JMAPS spacecraft configuration and instrument specifications are shown in Fig. 1.

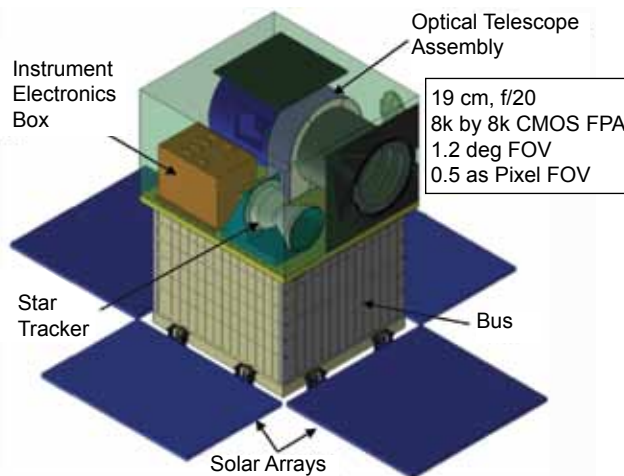


FIGURE 1
JMAPS space vehicle design (from Ref. 1).

To support the mission star catalog accuracy of 1 milli-arcsecond (mas) in position, 1 mas/year in proper motion, and 1 mas in parallax, the instrument line-of-sight must maintain its pointing stability of 50 mas (1σ) during observation. This stringent requirement is met in part by using the instrument as a fine attitude determination star tracker to produce an unprecedented 10 mas (1σ) attitude determination accuracy at a 5 Hz rate. The approach developed at NRL to accomplish this objective is presented.

JMAPS Fine Attitude Determination: Instrument fine attitude determination starts with the current spacecraft attitude estimates determined

by the Kalman filter that combines star tracker and gyro measurements and estimates the attitude at 5 as (1σ) accuracy. Using the spacecraft attitude and the onboard star catalog, guide stars in the instrument field of view (FOV) are identified. Guide star windows are then placed around the expected star locations as shown in Fig. 2. Typically, a 64 pixel by 64 pixel guide star window will be placed for an initial acquisition. The size of the guide star window decreases as the instrument fine attitude becomes available. Fine attitude determination is performed by comparing the measured centroid locations of the guide stars to their expected locations at the centers of the windows.

Thanks to the small size of the guide star window, which is less than 64 pixels or 32 as, the process of refining attitude estimates through the instrument measurements is considered a small angle attitude update with respect to a reference attitude. This permits application of small angle attitude determination methods in addition to well-known, general-purpose algorithms such as TRIAD, QUEST, and q-method.² Using the small angle assumption, a new computationally efficient algorithm³ was developed based on the homogeneous transformation (HT) that has typically been used to describe robot manipulator kinematics.

Simulations and Results: The performance of the HT algorithm is evaluated and compared to well-known algorithms TRIAD, q-method, and QUEST. Only two guide stars are employed to compare the HT algorithm against the TRIAD algorithm since it (TRIAD) is limited to operating on two stars at a time. Ten guide stars are used to evaluate the HT algorithm in comparison to q-method and QUEST. Focal plane star images are simulated with random centroiding errors as well as attitude biases and the algorithms are applied to estimate the attitude correction. As an example of the results, Fig. 3 shows the cross-boresight axis accuracy, defined as the standard deviation of 500 attitude estimates subtracted from the truth value. Standard deviations are shown for 20 different guide star patterns within the FOV. The left-hand plot in Fig. 3 shows the results among q-method, QUEST, and HT algorithms using 10 guide stars, while the right-hand plot reflects the comparison between TRIAD and HT algorithms using two guide stars only. All methods produce similar results for 10 guide stars and the HT algorithm performs better with two guide stars against TRIAD. Attitude estimation errors decrease with a larger number of guide stars.

Summary: Simulations establish that the unprecedented goal of 10 mas (1σ) attitude determination accuracy can be met with the JMAPS instrument and

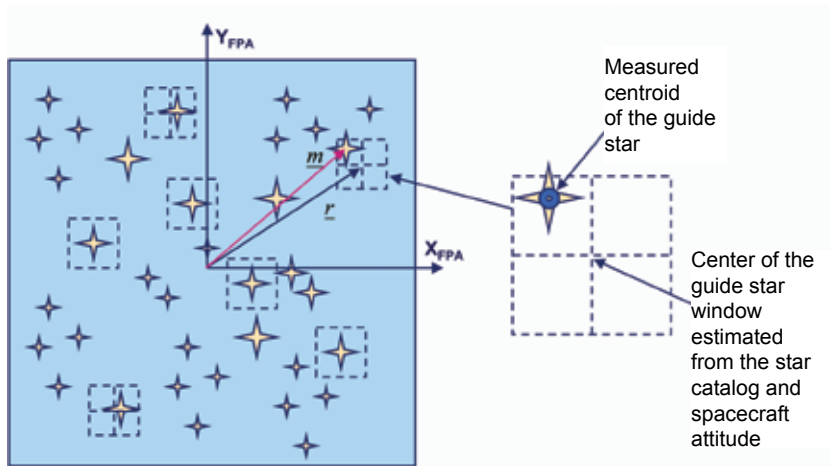


FIGURE 2
Guide stars and their windows in the focal plane array (FPA).

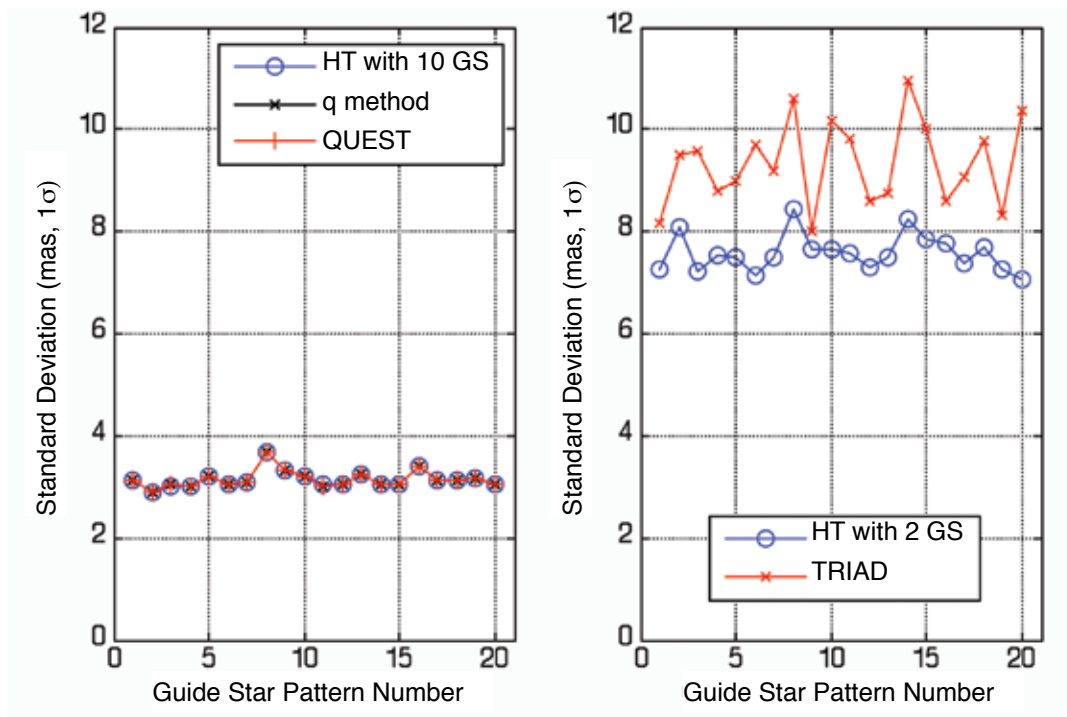


FIGURE 3
Standard deviation of cross-boresight attitude error estimates with 10 guide stars (left) and with 2 guide stars (right).

various attitude determination algorithms. In particular, the HT algorithm provides attitude determination accuracy comparable to the existing TRIAD, q-method, and QUEST algorithms while requiring less than half the computation cost of the other methods. The HT algorithm can produce attitude estimates when at least two guide stars are available and take as many as available guide stars in the instrument FOV, offering flexibility with instrument operation as a star tracker.

[Sponsored by ONR]

References

¹ B.N. Dorland, R.P. Dudik, Z. Dugan, and G.S. Hennessy, “The Joint Milli-Arcsecond Pathfinder Survey (JMAPS): Mission

Overview and Attitude Sensing Applications,” AAS Paper 09-181, 19th AAS/AIAA Space Flight Mechanics Meeting, Savannah, GA, Feb. 9–12, 2009.

² M.D. Shuster and S.D. Oh, “Three-Axis Attitude Determination from Vector Observations,” *J. Guidance, Control and Dynamics* 4(1), 70–77 (1981).

³ T.W. Lim, F.A. Tasker, and P.G. DeLaHunt, “The Joint Milli-Arcsecond Pathfinder Survey (JMAPS) Instrument Fine Attitude Determination Approach,” AAS Paper 10-031, 33rd AAS Guidance and Control Conference, Breckenridge, CO, Feb. 2010.

TacSat-4, Advanced UHF SATCOM

M. Hurley,¹ W. Raynor,¹ M. Johnson,¹ K. Weldy,¹
E. Becker,¹ C. Amend,¹ M. Nurnberger,¹ T. Duffey,¹
R. Skalitzky,¹ T. Specht,¹ E. Bradley,¹ R. Baldauff,¹
J. Arminger,¹ J. Barnds,¹ K. Akins,¹ J. Hicks,¹
E. Sydow,¹ G. Sandhoo,¹ D. Bentz,² B. Davis,³
and E. Gruner³

¹Spacecraft Engineering Department

²Harris Corp.

³Space-Ground System Solutions

Mission Summary and Status: TacSat-4 is a Navy-led joint mission¹ to augment current satellite communications (SATCOM) capabilities and to advance Operationally Responsive Space (ORS) systems. The TacSat-4 mission was selected by a joint process culminating in a flag and general officer vote by Army, Navy, Air Force, Marine Corps, and U.S. Strategic Command. TacSat-4 provides 10 ultra high frequency (UHF) channels, which can be used for any combination of communications, data exfiltration, or Blue Force Tracking (BFT). TacSat-4's unique orbit augments geosynchronous SATCOM by providing near-global, but not continuous, coverage including the high latitudes. TacSat-4 improves on current SATCOM by providing communications-on-the-move for existing radios



FIGURE 4

TacSat-4 during bus-to-payload mating.

without requiring antenna pointing. TacSat-4 provides flexible up and down channel assignments, which increases the ability to operate in some interfered environments. The Virtual Mission Operations Center (VMOC) tasking system coupled with the orbit allows dynamic reallocation, within 24 hours during normal operations, to different theaters worldwide, enabling rapid SATCOM augmentation when unexpected operations or natural events occur.

In October 2009, NRL engineers completed the spacecraft (see Fig. 4). TacSat-4 is awaiting launch in the fall of 2010 on a Minotaur-IV launch vehicle from Kodiak, Alaska. If military utility is confirmed during the first year of flight operations, TacSat-4 flight operations will be extended for at least 2 more years, and a follow-on acquisition of one to four spacecraft will be considered to augment existing UHF SATCOM. A constellation of four spacecraft provides three or more theaters with 24/7 coverage.

NRL is the program manager, with the Office of Naval Research funding the payload, management, and first year of operations as the lead sponsor. The Office of the Secretary of Defense Office for Technology/ Director of Defense Research and Engineering funded the standardized spacecraft bus. The Operationally Responsive Space Office and Air Force's Space and Missile Systems Center (SMC) are providing the launch on a Minotaur-IV. NRL's Blossom Point Ground Station will perform operations in coordination with Naval Network Warfare Command and the Global and Regional SATCOM Centers.

Enabling Technologies: Multiple technologies were used to provide this capability on a small satellite (less than 500 kg) and to provide users straightforward access to the flexible UHF SATCOM "COMMx" payload with dynamic tasking. The spacecraft is shown in Fig. 5 with the COMMx payload and spacecraft bus clearly labeled. Technologies of note include the 12-ft deployable payload antenna, the payload's thermal subsystem, a standardized spacecraft bus, and the Virtual Mission Operations Center.

Enabling Technology — Payload Antenna: The most visible and one of the most challenging subsystems was the 3-m (12-ft) diameter payload antenna. This UHF antenna operates over a frequency range of 240 to 420 MHz. Challenging requirements on the antenna included a 60 lb mass allocation, stowed mode of greater than 60 Hz and deployed mode at greater than 5 Hz, ability to withstand 1 MRad of total ionized dose (TID) radiation, a temperature range of ± 150 °C, and low passive intermodulation (PIM). PIM is generated by loose or "dirty" metal-to-metal contacts in the RF field. If PIM were to occur, it effectively raises

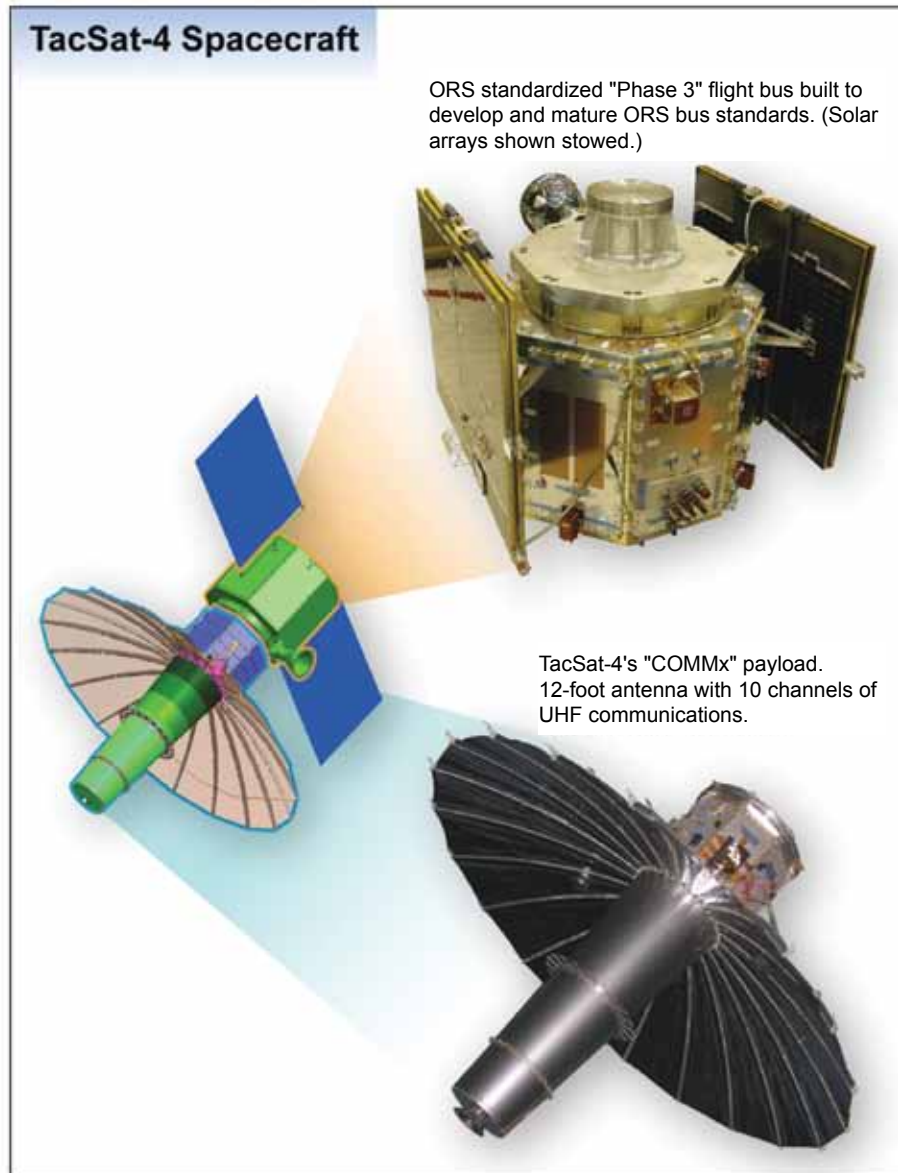


FIGURE 5
The TacSat-4 spacecraft.

the noise floor of an antenna, quickly reducing the performance to unacceptable levels for a system with multiple simultaneous channels (TacSat-4 has 10 channels). The antenna design took advantage of relatively loose surface “flatness” requirements and used a novel Kapton®-Copper flex circuit for the reflector material, as well as several capacitive coupling techniques. The detailed design and test results are documented in Ref. 2.

Enabling Technology — Thermal Subsystem:

The challenges facing the COMMx Thermal Control System (TCS) were extensive, most notably the heat dissipation of 600 W within the small payload volume of approximately 1 m diameter by 1 m high. To support

TacSat-4’s performance, mass, volume, and integration requirements, a Central Thermal Bus (CTB) design was implemented. The essence of the CTB approach is to package all heat-dissipating devices close to each other at a central location inside the spacecraft while using a cooling technology to (a) collect the waste heat, (b) transport it to the spacecraft radiators, and (c) reject it to space at a place where heat removal is the most efficient (i.e., the coldest sink). The CTB uses both constant conductance heat pipes (CCHP) and loop heat pipe (LHP) technology in conjunction with an LHP temperature control method and thermal diode designs. The TacSat-4 implementation has proven the design through testing and model comparisons. Once launched, this thermal design will be one of

the most advanced thermal systems on-orbit. Several papers^{3,4} provide design-level detail about this thermal system.

Enabling Technology — Standardized Spacecraft

Bus: The TacSat-4 program was also used as a path-finder to develop and test new spacecraft bus standards for the DoD. NRL and the Johns Hopkins University (JHU) Applied Physics Laboratory (APL) collaborated with an industry team of more than 10 companies to develop, mature, and document standards for small spacecraft systems. The spacecraft bus was built by NRL and APL to mature ORS bus standards developed by an Integrated (government and industry) System Engineering Team, the “ISET Team,” with active representation from AeroAstro, Air Force Research Laboratory, APL, ATK Space, Ball, Boeing, Design Net Engineering, General Dynamics AIS, Microcosm, Microsat Systems Inc., Massachusetts Institute of Technology Lincoln Laboratory, Orbital Sciences, NRL, SMC, Space System Loral, and Raytheon. Reference 5 discusses the approach used, including how performance thresholds were established, the iterative application, and maturation of those standards through building the flight bus.

Enabling Technology — Virtual Mission

Operations Center: The VMOC is an automated mission operations center that increases user access for tasking requests, STRATCOM apportionment changes (i.e., user priority changes), and dynamic payload capability management. The VMOC leverages the latest web technologies to provide these capabilities. VMOC has been developed and demonstrated since 2003 and is currently moving into an operations mode on the SIPRNET, supporting both TacSat-4 and ORS-1. VMOC is now the baseline tool for payload tasking and asset visibility of all ORS spacecraft.⁶

Conclusion: NRL and our partners have overcome many technical challenges to enable TacSat-4’s advanced SATCOM capabilities for the Navy and DoD. TacSat-4 is now complete and awaits launch in late 2010.

[Sponsored by ONR]

References

- ¹ K. Weldy, A. Hurley, C. Amend, E. Becker, M. Nurnberger, K. Akins, C. Ford, M. Johnson, W. Raynor, and M. Hurley, “TacSat-4 Mission and the Implementation of Bus Standards,” Proceedings of the 22nd Annual AIAA Utah State Small Satellite Conference, Logan, UT, Aug. 11–14, 2008, SSC08-III-2.
- ² C. Amend, M. Nurnberger, P. Oppenheimer, S. Koss, and B. Purdy, “A Novel Approach for a Low-Cost Deployable Antenna,” Proceedings of the 40th Aerospace Mechanisms Symposium, NASA Kennedy Space Center, FL, May 12–14, 2010, NASA/CP-2010-216272.

³ R.W. Baldauff, W.J. Arming, and T.T. Hoang, “Design and Analysis of the Thermal Control System for the TacSat-4 Spacecraft COMMX Payload,” *2009 NRL Review*, pp. 114–124.

⁴ R. Baldauff, W. Arming, and T. Hoang, “Design and Analysis of the Thermal Control System for the TacSat-4 Spacecraft, COMMX Payload,” Aerospace International Two Phase Conference, Oct. 2009 (this paper includes more detailed presentation and figures of the thermal system).

⁵ G. Sandhoo, A. Rogers, P. Stadter, E. Finnegan, M. Hurley, M. Johnson, W. Raynor, P. Schwartz, and J. Griswold, “Standards for Responsive Small Satellites,” European Space Agency 4S Symposium, Small Satellites Systems and Services, Rhodes, Greece, 26–30 May 2008.

⁶ E. Miller, O. Medina, M. Hurley, and J. Barlow, “Virtual Mission Operations Center and the ORS Ground System Enterprise,” AIAA-RS7-2009-6001, AIAA 7th Responsive Space Conference, Los Angeles, CA, April 27–30, 2009.

Integrating the Sun-Earth System for the Operational Environment (ISES-OE)

J.L. Lean,¹ J.D. Huba,² S.E. McDonald,¹ S. Slinker,² D.P. Drob,¹ J.T. Emmert,¹ R.R. Meier,¹ J.M. Picone,¹ G. Joyce,² J. Krall,² A. Stephan,¹ K.A. Roach,¹ H. Knight,¹ S.P. Plunkett,¹ C.-C. Wu,¹ B.E. Wood,¹ Y.-M. Wang,¹ R.A. Howard,¹ J. Chen,² P.A. Bernhardt,² and J.A. Fedder³

¹*Space Science Division*

²*Plasma Physics Division*

³*Icarus Research, Inc.*

Introduction: NRL’s Space Science and Plasma Physics Divisions have commenced an ambitious joint venture: Integrating the Sun-Earth System for the Operational Environment (ISES-OE). The primary goal of this program is to quantitatively understand the space environment above 100 km altitude. This highly variable region can impact Naval operations by disrupting communications and navigation. Central to the ISES effort is an ensemble of multiyear simulations with Sun-Earth system models that calculate ionospheric composition,¹ neutral composition,² and winds,³ along with electrodynamic integration of the surrounding space plasma.⁴ ISES-OE uses additional NRL models and observations of solar extreme ultraviolet (EUV from 0 to 120 nm) spectral irradiance,⁵ ambient solar wind,⁶ and coronal mass ejections.⁷ Large databases of drag-derived and remotely sensed neutral thermospheric densities constructed with NRL algorithms⁸ and GPS-derived total electron content (TEC) are being analyzed to provide model validation on time scales as long as the 11-year solar cycle. Figure 6 sketches the ISES components.

An Expanded Operational Domain — the Sun-Earth System: Accompanying the expansion of Naval

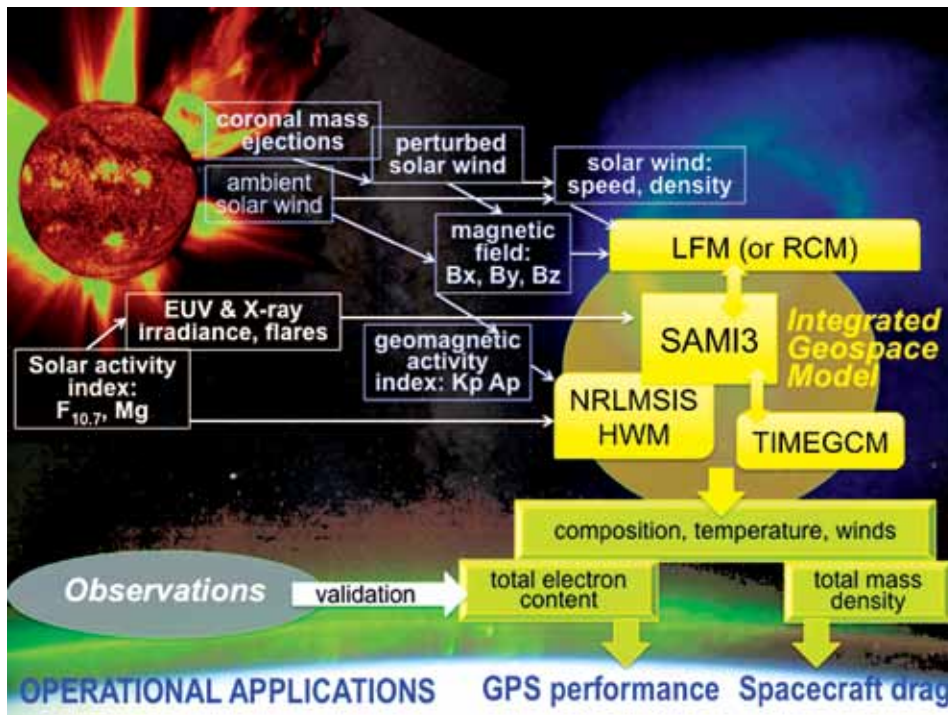


FIGURE 6

In this schematic of ISES program elements, the components of the integrated geospace model are identified in yellow, with the SAMI3 ionospheric model (along with the NRLMSIS and HWM empirical models) at the core. Physical integration is underway with TIMEGCM, RCM, and LFM to physically couple the thermosphere, plasmasphere, and magnetosphere, respectively. Drivers of geospace fluctuations occur in two primary forms, via solar EUV photons (orange) and particles and plasma in the solar wind (purple). Observations of ionized and neutral densities in the thermosphere and ionosphere provide model validation.

activities beyond the surface of the Earth is a growing awareness of adverse space environment impacts on sophisticated military systems. Earth-orbiting spacecraft support myriad Fleet operations for which command, control, communications, and computer systems (C4) are crucial. Charged particles in the F layer (200 to 400 km) transmit, reflect, retard, and refract kHz to MHz radio waves that enable C4 capabilities. Neutral gases impede the motion of the more than 15,000 Earth-orbiting objects that the U.S. Space Command tracks. Because the space environment fluctuates widely, robust knowledge of geospace fosters tactical advantage in Naval operations by reducing uncertainties in communications and navigation, radar accuracy, targeting precision, orbit prediction, and space situational awareness.

The Changing Ionosphere and Atmosphere:

Charged and neutral densities in the F region can increase by an order of magnitude or more in response to changing solar activity. From the minimum to maximum of the Sun's 11-year activity cycle, TEC increases from ~10 to more than 40 TECU (1 TECU = 10^{16} electrons per m^2). Correspondingly, the maximum reflected radio frequency increases from 3 to 12 MHz. Figure 7 illustrates the changes of 5 to 10 TECU in global TEC as a result of changing irradiance (as the Sun rotates on its axis over 27 days), and of annual and semiannual oscillations (AO and SAO). Regional fluctuations can exceed the global changes by an order of magnitude. The geographical maps in Fig. 8 illustrate how the local TEC maximum tracks the subsolar point

throughout the day, with subequatorial enhancements (the equatorial anomaly) resulting from electrodynamic and winds.

Integrated Geospace Models: The enormity of geospace (a volume four orders of magnitude larger than the Navy's terrestrial operating environment) precludes adequate observational specification. The needed space-based measurements are sparse and intermittent. Global coverage is attainable only with numerical models, but integrated geospace models are in their infancy. Simulations that integrate the thermosphere, ionosphere, plasmasphere, and magnetosphere began only in 2001, three decades after numerical models of terrestrial weather integrated the lower atmosphere, oceans, and land.

Because electron, ion, and neutral particle variations in the ionosphere and thermosphere (from ~90 to 600 km) are the prime source of space impacts on the operational environment, the core of the ISES integrated model is NRL's state-of-the-art ionospheric model, SAMI3,^{1,4} and its embedded thermosphere. Unique among ionospheric models for its numerical sophistication, SAMI3 solves continuity and momentum equations for seven ion species on a non-orthogonal, non-uniform, single mesh fixed grid that extends to ~8 Earth radii (R_E). The model, which includes a dynamo electric field and accounts for collisionless plasma processes above 2000 km, couples electrostatically with the surrounding plasmasphere and magnetosphere.⁴

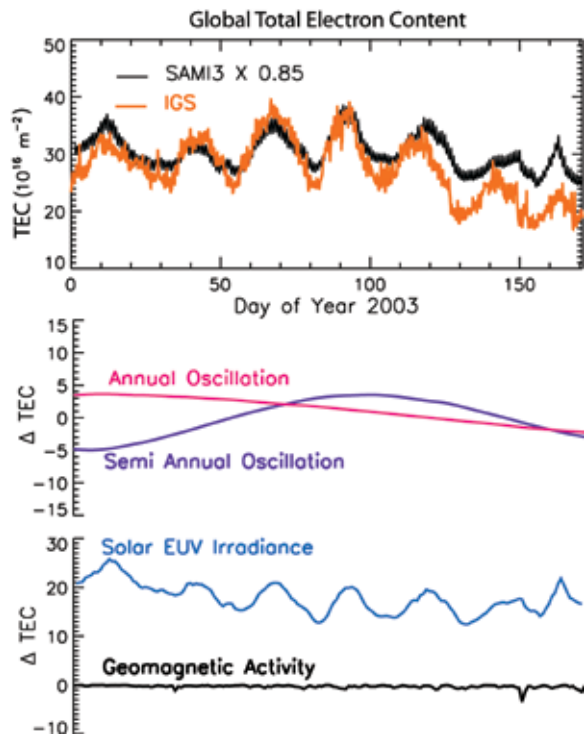
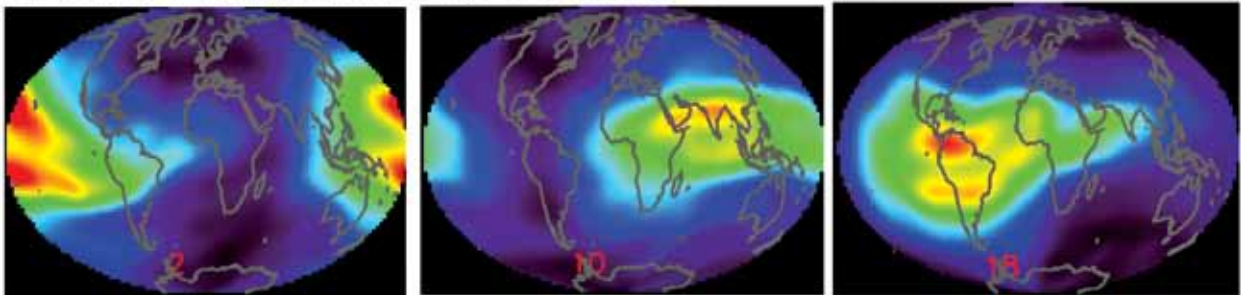


FIGURE 7
 Shown are 2-hourly values of global ionospheric total electron content (TEC) during the first six months of 2003, derived from GPS observations by the International GPS Service (IGS) and simulated with the baseline ISES model. Also shown (in the middle panel) are the changes attributable to the semi-annual and annual oscillations, and (in the lower panel) the solar and geomagnetic activity.

Observed — International GPS Service



Modeled — SAMI3 with NRLMSIS and HWM

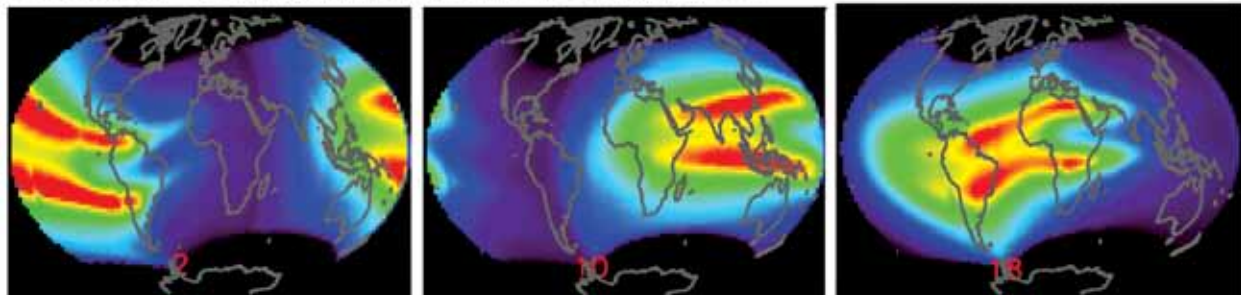


FIGURE 8
 Ionospheric total electron content, 31 March 2003. The diurnally driven variations in ionospheric electron content at 2, 10, and 18 hours UT (near midnight, noon, and dusk at 0° longitude) are shown from observations in the upper panel, and simulated by SAMI3 in the lower panel. There are distinct differences in the observed and modeled equatorial anomaly, identified as the high ridges on either side of the magnetic equator.

Model Simulations and Validation: The ISES program expands integrated Sun–Earth system modeling beyond the current community focus on severe, transient geomagnetic storms. ISES also addresses the more persistent and dominant influences of solar irradiance variations changes and the AO and SAO. Underway are simulations of the entire descending phase of solar cycle 23 (i.e., from 2002 to 2008) using a range of model configurations with measured and modeled solar-heliospheric drivers (Fig. 6).

Initial comparisons (Fig. 7) between observed and modeled TEC suggest that modeled TEC are overall higher with weaker monthly and seasonal variations. Probable explanations are that the adopted solar EUV irradiances are too high, and that the AO and SAO in neutral densities are not adequately predicted. The differences (Fig. 8) in the regional structure of the equatorial anomaly likely relate to the model's lack of electrodynamic integration with the surrounding thermosphere and plasmasphere. Future simulations will use a more advanced ISES model in which SAMI3 is integrated with first-principles simulations of the thermosphere (TIMEGCM), the plasmasphere (RCM), and the magnetosphere (LFM). Ultimately, the ISES-OE program will produce a fully integrated and validated geospace model for further exploration and quantification of the complex operational space environment.

[Sponsored by ONR and NASA]

References

- ¹ J.D. Huba, G. Joyce, and J.A. Fedder, "Sami2 is Another Model of the Ionosphere (SAMI2): A New Low-latitude Ionosphere Model," *J. Geophys. Res.* **105**(A10), 23,035–23,054 (2000).
- ² J.M. Picone, A.E. Hedin, D.P. Drob, and A.C. Aikin, "NRLMSISE-00 Empirical Model of the Atmosphere: Statistical Comparisons and Scientific Issues," *J. Geophys. Res.* **107**(A12), 1468 (2002), doi:10.1029/2002JA009430.
- ³ D.P. Drob, J.T. Emmert, G. Crowley, J.M. Picone, G.G. Shepherd, W. Skinner, P. Hays, R.J. Niciejewski, M. Larsen, C.Y. She, J.W. Meriwether, G. Hernandez, M.J. Jarvis, D.P. Sipler, C.A. Tepley, M.S. O'Brien, J.R. Bowman, Q. Wu, Y. Murayama, S. Kawamura, I.M. Reid, and R.A. Vincent, "An Empirical Model of the Earth's Horizontal Wind Fields: HWM07," *J. Geophys. Res.* **113**, A12304 (2008), doi:10.1029/2008JA013668.
- ⁴ J.D. Huba, G. Joyce, S. Sazykin, R. Wolf, and R. Spiro, "Simulation Study of Penetration Electric Field Effects on the Low- to Mid-latitude Ionosphere," *Geophys. Research Lett.* **32**, L23101 (2005), doi:10.1029/2005GL024162.
- ⁵ J.L. Lean and T.N. Woods, "Solar Spectral Irradiance: Measurements and Models," in *Evolving Solar Activity and the Climates of Space and Earth*, eds. C.J. Schrijver and G.L. Siscoe (Cambridge Univ. Press, 2010), pp. 269–298.
- ⁶ Y.M. Wang, N.R. Sheeley, Jr., J.L. Phillips, and B.E. Goldstein, "Solar Wind Stream Interactions and the Wind Speed-Expansion Factor Relationship," *Astrophys. J.* **488**, L51 (1997).
- ⁷ R.A. Howard, J.D. Moses, A. Vourlidas, J.S. Newmark, D.G. Socker, S.P. Plunkett, C.M. Korendyke, J.W. Cook, A. Hurley, and J.M. Davila, "Sun Earth Connection Coronal and Heliospheric Investigation (SECCHI)," *Space Science Reviews* **136**(1-4), 67–115 (2008).

- ⁸ J.T. Emmert, R.R. Meier, J.M. Picone, J.L. Lean, and A.B. Christensen, "Thermospheric Density 2002–2004: TIMED/GUVI Dayside Limb Observations and Satellite Drag," *J. Geophys. Res.* **111**, A10S16 (2006), doi:10.1029/2005JA011495.

Origins of Solar Energetic Particle (SEP) Variability

Y.-K. Ko and A.J. Tylka
Space Science Division

The SEP Radiation Hazard: Solar energetic particle (SEP) events are significant natural radiation hazards for Navy and DoD space-based assets. These episodic outbursts of high-energy protons and ions from the Sun damage solar panels, interfere with sensors, and cause a variety of single-event-effects (SEEs) in spacecraft electronics. Unless vulnerable systems are safe-moded prior to the event, these effects can interrupt or degrade performance not only during an event, but also for an extended period of time after the SEP event is over. Unlike other components of the natural space-radiation environment, SEPs are highly variable in intensity, duration, the distribution of particle energies, and ionic composition.¹ These variable factors, in turn, determine the nature of the radiation hazard posed to satellite systems. Discovering and modeling the factors that drive this variability is the prime objective of SEP research at NRL, with the ultimate goal of a physics-based predictive model of the SEP radiation hazard that can be employed by satellite operators.

SEPs and Fast CMEs: An extensive body of evidence indicates that large SEP events are produced by very fast coronal mass ejections (CMEs), which explode outward from the Sun at speeds exceeding 1000 km/s. As illustrated in Fig. 9, these very fast CMEs drive shocks through the corona and interplanetary medium. Interactions between the shock and suprathermal seed particles produce the high-energy SEPs that endanger spacecraft. In particular, the shock expands and crosses many magnetic field lines, which emerge from different source regions on the Sun. Since the SEPs are charged particles, they travel outward along the magnetic field lines, provided that cross-field diffusion is small. Thus, the SEPs subsequently observed at Earth should retain some signature of the source regions from which the magnetic field lines and the seed particles emerged.

SEPs and Source Regions: We have recently discovered evidence that ties SEP compositional

variability to specific structures on the solar surface.² By employing heliospheric magnetic-field mapping techniques developed by NRL Space Science Division scientists,³ we first traced the solar wind magnetic field lines that guide the SEPs from Sun to Earth back to their origination point at the Sun. We then used data from NASA's Wind and ACE spacecrafts to analyze the elemental composition of SEPs and the solar wind.

Figure 10 shows the synoptic Carrington maps of the Sun for eight SEP events from 2004 to 2006. Marked on each are the source location of the CME that produced the SEP event and the footpoint of the magnetic field line that connected the Sun to Earth at the time of the SEP event. In the four examples at the left, this footpoint is from a coronal hole (CH); in the four examples on the right, this footpoint is from an active region (AR). A "coronal hole" is a structure on the solar surface that appears as a dark patch in the extreme ultraviolet (EUV) or X-ray image of the Sun. An "active region" is another structure on the Sun with bright magnetic loops when seen in EUV and X-rays, and with strong underlying magnetic field. The solar wind, which carries open magnetic field lines from the Sun out into the heliosphere, can originate from either coronal holes or active regions.

The left panel of Fig. 11 shows hourly averaged iron-to-oxygen (Fe/O) ratios at 5 to 10 MeV/nucleon from these and four other SEP events in 2004 to 2006, correlated against the Fe/O measured simultaneously in the thermal solar wind. (Fe/O provides a particularly sensitive measure of heavy-ion variability in SEPs and the solar wind.) In the correlation plot, data points associated with AR sources are displayed as red symbols; data points associated with CH sources are black.

The right panels of Fig. 11 show the histograms generated from these data, color coded as before. Although the SEP distributions are by no means bimodal, a larger SEP Fe/O preferentially appears when the footpoint is from an AR, and a smaller SEP Fe/O preferentially appears when the footpoint is from a CH. In contrast, the solar-wind particles that emerge from ARs and CHs have almost identical Fe/O distributions.

Implications: These results are the first successful example of tracking SEP compositional variation back to differences in the source of the guiding magnetic field. These results indicate that near-real-time mapping of the interplanetary magnetic field from Earth to its solar-source structure may provide a means of forecasting the heavy-ion content of SEP events, a particularly important concern for SEEs. New puzzles are the processes that cause the compositional difference between SEPs and the solar wind, and why these processes are different for active regions and coronal holes. Thus, this discovery provides not only a new window on SEP variability, but also on the physics of solar regions that give rise to the solar wind.

[Sponsored by ONR]

References

- ¹ A.J. Tylka and M.A. Lee, "A Model for Spectral and Compositional Variability at High Energies in Large, Gradual Solar Particle Events," *Astrophys. J.* **646**, 1319-1334 (2006).
- ² Y.-K. Ko, A.J. Tylka, C.K. Ng, and Y.-M. Wang, "Solar Wind Source Regions and Variability in Heavy-Ion Composition in Gradual Solar Energetic Particle Events," submitted to *Astrophys. J.*, 2010.
- ³ Y.-M. Wang, M. Pick, and G.M. Mason, "Coronal Holes, Jets, and the Origin of ³He-rich Particle Events," *Astrophys. J.* **639**, 495-509 (2006).

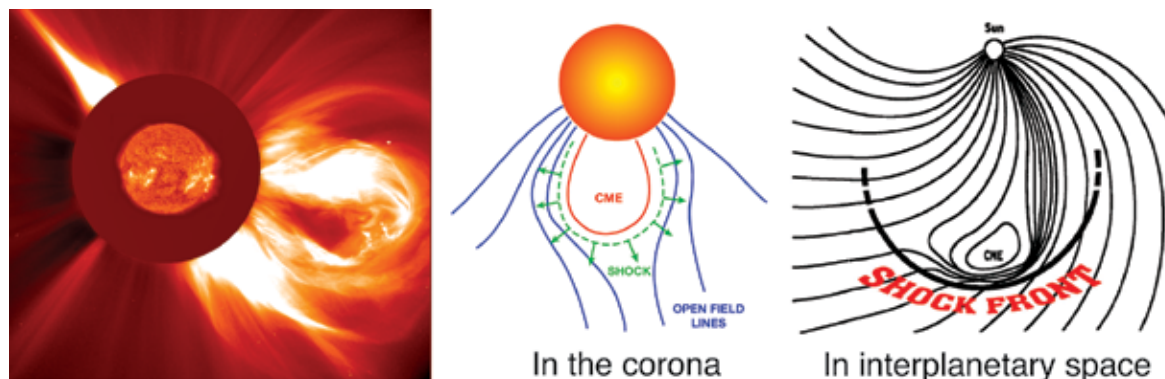


FIGURE 9

(Left) A coronal mass ejection, as imaged from the Sun-Earth L1 Lagrangian point by NRL's Large Angle and Spectrometric Coronagraph (LASCO) aboard the Solar and Heliospheric Observatory (SOHO) spacecraft. Two cartoons of the CME and the CME-driven shock, as viewed from above the ecliptic plane, while in the corona (center) and in interplanetary space (right), moving through the heliospheric magnetic field.

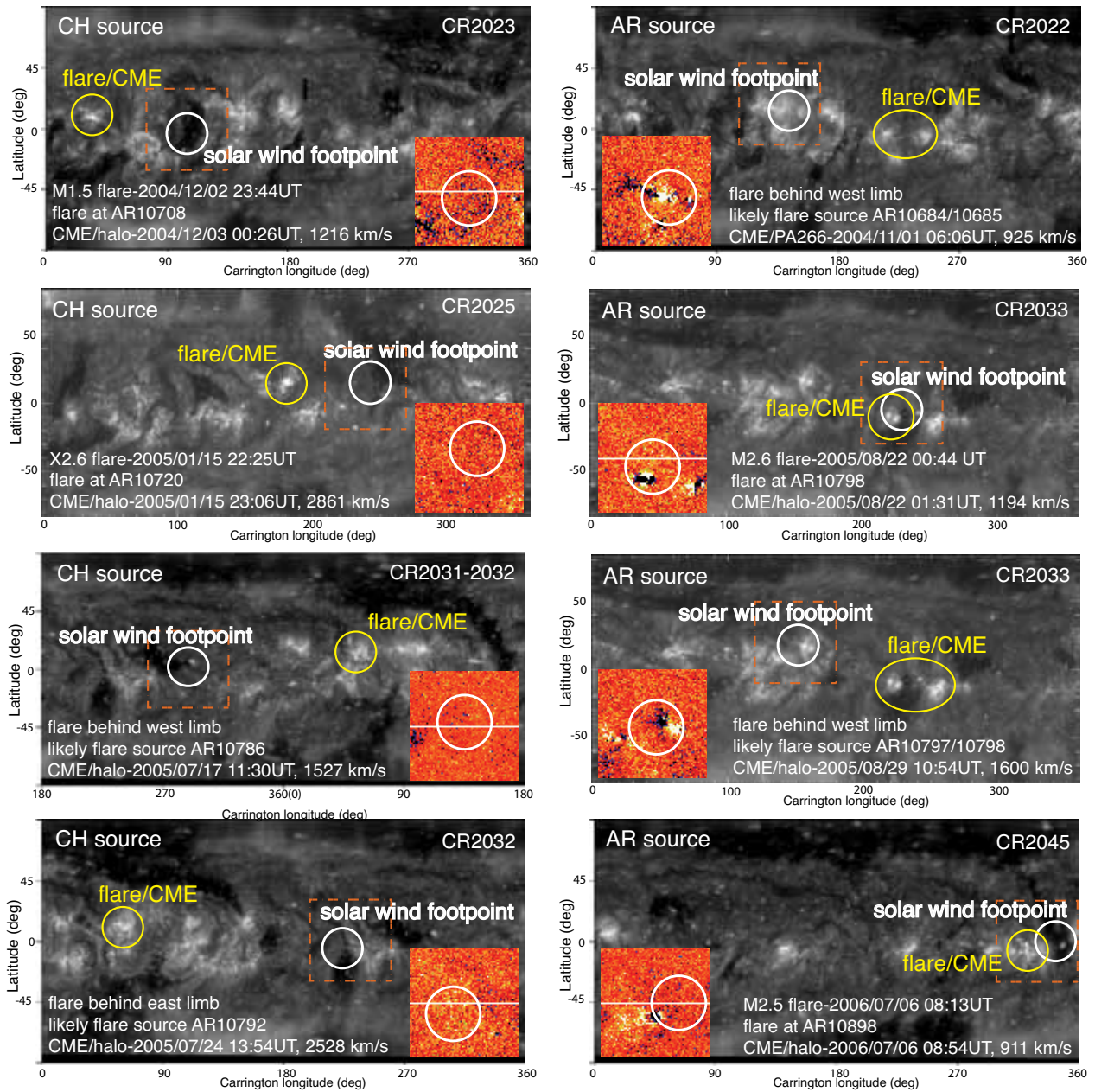


FIGURE 10

Carrington maps for eight SEP events, with the eruption point of the CME and the footprint of the Sun-Earth magnetic field line marked for coronal-hole (left) and active-region (right) sources. The Carrington maps are constructed from images taken by the NRL-participating Extreme Ultraviolet Imaging Telescope (EIT) aboard SOHO. The insets are corresponding magnetic field synoptic charts (cropped to the same area as the orange-dashed square on the EIT maps, and white/black patches representing positive/negative field) from the Michelson Doppler Imager (MDI) aboard SOHO.

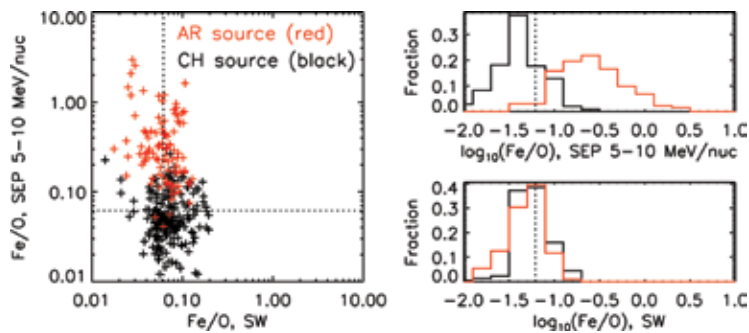


FIGURE 11

(Left) Correlation plot of hourly averaged SEP Fe/O at 5 to 10 MeV/nucleon vs simultaneous measurements of the solar-wind Fe/O, measured by the Wind and ACE spacecraft, respectively, both of which were also at L1. Red points correspond to active-region (AR) sources, black points to coronal-hole (CH) sources. (Right) Histograms of the SEP (top) and solar-wind (bottom) Fe/O, with same color coding.

Technology Development for High Integrity GPS (HiGPS)

O.J. Oaks

Space Systems Development Department

Background: The Naval Research Laboratory is investigating the capability to augment GPS navigation and time synchronization using the existing constellation of Iridium satellites. The technology concept, HiGPS, is based on prior work and demonstrations provided by The Boeing Company. NRL is leveraging experience and expertise gained from the early NRL Timing and Navigation Technology Satellite development programs and more than 30 years experience supporting GPS development and operation to exploit the concept of providing a robust anti-jam capability for navigation and time synchronization. The concept aids GPS in using the Iridium communications satellite signals. NRL has teamed with prime contractor Boeing and subcontractors Iridium, Coherent Navigation, and Rockwell Collins to provide the GPS anti-jam enhancement in the very near future. This requires technology development of a signal-in-space, ground infrastructure, and user equipment that will support the HiGPS augmentation concept. The signal-in-space development leverages on the existing Iridium satellite communication signals and the infrastructure that supports them. The technology development effort is ongoing and several milestone achievements have demonstrated the potential to deliver anti-jam navigation and time synchronization capability in the near future. In June 2008, a successful test was performed at NRL that provided time synchronization to military communications equipment while being jammed, and in June 2009, a successful test was performed at NRL that demonstrated anti-jam capability for navigation. The objective is to develop the anti-jam technology that can be transitioned to operation in 2011.

Iridium is a communications satellite system of 66 space vehicles in low Earth orbit (LEO). The constellation consists of 6 planes of 11 satellites in polar orbits that provide continuous global Earth coverage. Compared with GPS, Iridium has a lower altitude and a higher transmitted power, and therefore provides a significantly stronger received signal that can be exploited for aiding the GPS signals in navigation and time synchronization applications. The Iridium satellite onboard communications electronics is reprogrammable and can be configured to transmit signals that are suitable for navigation and to aid time synchronization. The Iridium ground control is being expanded to support the new signal-in-space that will be delivered to GPS users that have the HiGPS augmentation capability. The objective is to provide Iridium aiding

signals in areas where GPS may be denied by interference or jamming. The concept uses ground reference stations outside the area of interference that simultaneously receive Iridium and GPS signals. The reference stations derive data that relate GPS to the Iridium signals and allow precise prediction of the GPS signal. This information is sent as augmentation data to users via the lower-altitude, higher-power Iridium satellites. The users process this information to enable reception of the GPS signals in a high-noise environment. This augmentation capability has the potential to provide more robust navigation and time synchronization, including higher jamming and interference rejection, faster acquisition times, and improved accuracy.

Technology Components and System Concept:

The technology system components under development consist of reference stations, the HiGPS designed signal-in-space, the user equipment designed to combine the HiGPS augmentation data with the GPS signals, and an operations center with a ground network connected to the reference stations and Iridium satellite control station. Figure 12 presents a simplified system concept. The first-generation HiGPS signal-in-space that has been deployed is the Enhanced Narrowband signal, so named because it has the same characteristic 40 kHz narrow bandwidth of the Iridium communications signals. The ranging accuracy using this signal is several microseconds because of the narrow bandwidth. A near-term, future-generation Advanced Waveform signal is under development that will have a bandwidth greater than 7 MHz, which will provide a ranging accuracy more like the GPS signal of several nanoseconds. The augmentation data modulated on the HiGPS signal includes the GPS broadcast data, the Iridium satellite ephemerides, and Iridium-to-GPS carrier phase difference data. The HiGPS receivers remove the GPS broadcast data from the received GPS signals, allowing a longer integration time for coherently tracking the GPS carrier signal. The integration time is increased from 20 ms to 5 s, providing a 30 dB improvement in signal-to-noise. Iridium ephemerides are required to perform an initial geolocation using only the Iridium signal. For cold-start acquisition in a GPS-denied environment, the HiGPS receiver must first acquire the Iridium signal, obtain the augmentation data, and compute an initial position using measurements from the Iridium signal. Once the data are obtained and the geolocation is sufficient, the HiGPS receiver can then acquire and track the GPS signals in a high-noise environment. The carrier phase difference data are used to aid the receiver in acquiring and maintaining carrier phase-lock on the GPS signal.

The data are precise to 20 picoseconds, which is a fraction of a carrier cycle and provides submeter

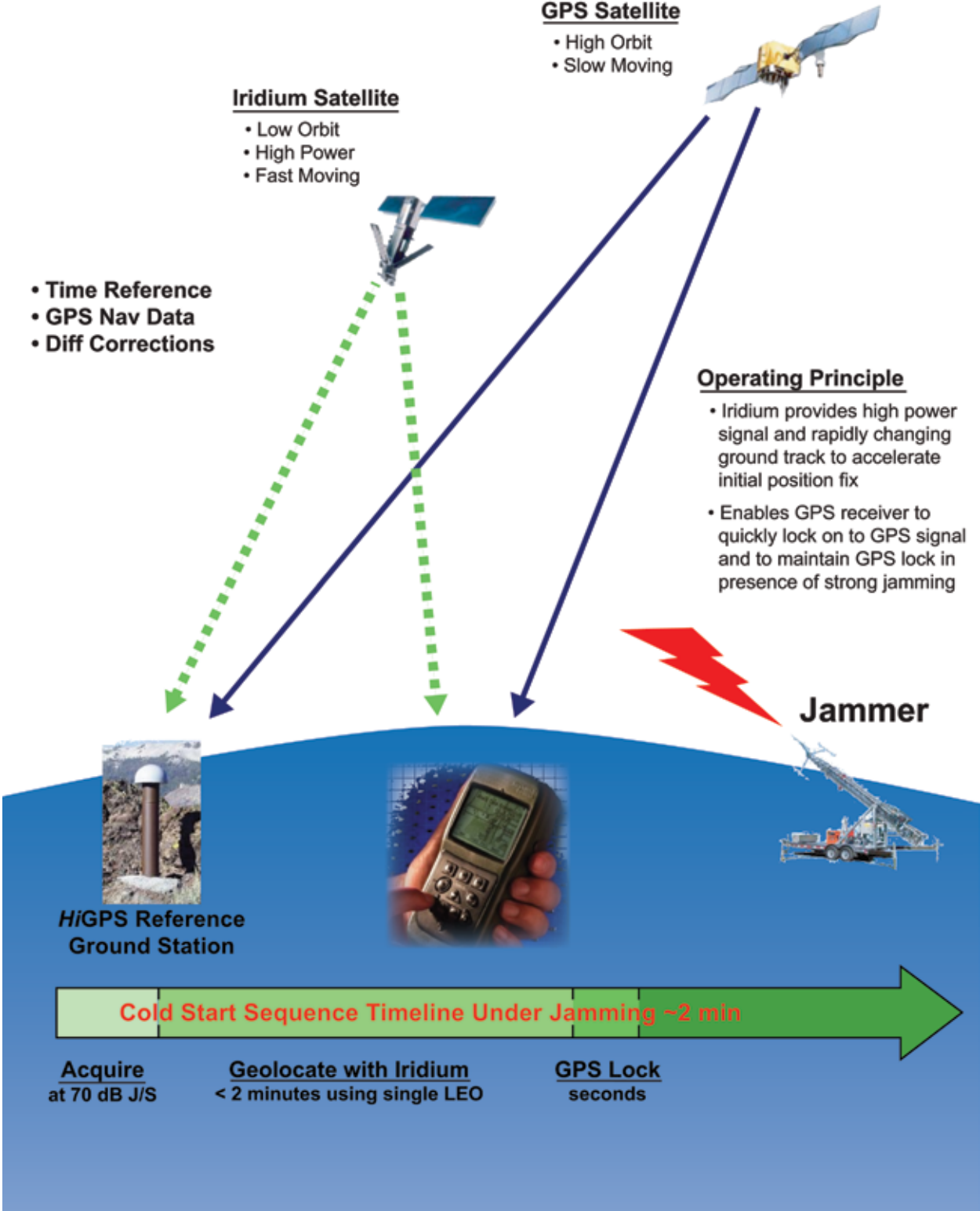


FIGURE 12
HiGPS operational concept.

accuracy in the position solution. A first-generation prototype HiGPS receiver has been completed along with reference stations that have been deployed to support technology demonstrations.

Technology Demonstrations Enabling Use of GPS in a Jammed Environment: An initial tracking demonstration was performed in 2007 that demonstrated the feasibility of the concept. The results achieved greater than 20 dB improvement in anti-jam performance with submeter accuracy in position. In this demonstration, the receiver was already tracking Iridium and GPS before the jamming was turned on and the time of operation was limited to 30 s. Since that time, the HiGPS Program has been further developing the technology to provide acquisition in a jammed environment and more continuous operation across many Iridium satellites. In June 2009, a test was performed at NRL that demonstrated the ability to provide the HiGPS signal over an area of operation and to acquire GPS signals in a jammed environment. Figure 13 is a screen shot of the command console showing deployment of the HiGPS signal over the test area at NRL. The signals were provided over NRL

in a matter of seconds after the command was sent. The reference station for the test was in Philadelphia, Pennsylvania, and the operation center was in southern California. The test used the first-generation deployed ground infrastructure network. Figure 14 is a series of pictures that show acquisition of the GPS signals in a jammed environment, which was performed at NRL during the demonstration tests. The focus of the test was on acquisition and not tracking. The acquisition performance achieved an anti-jam improvement greater than 30 dB over the currently fielded GPS receivers with an accuracy of several meters and a time to first GPS determined position of roughly two minutes. This performance will improve as the technology is refined during 2010. The current focus of the HiGPS Program is to merge the tracking capability demonstrated in 2007 with the acquisition capability demonstrated in 2009. The 2010 and 2011 efforts include demonstrating the complete system capability in field tests and initiating a plan to transition the technology to the warfighter.

[Sponsored by ONR]



FIGURE 13

The HiGPS signal-in-space is uploaded from Fairbanks, AK, via crosslinks to the Iridium satellite, which provides the signal to the NRL test area within seconds of commanding.

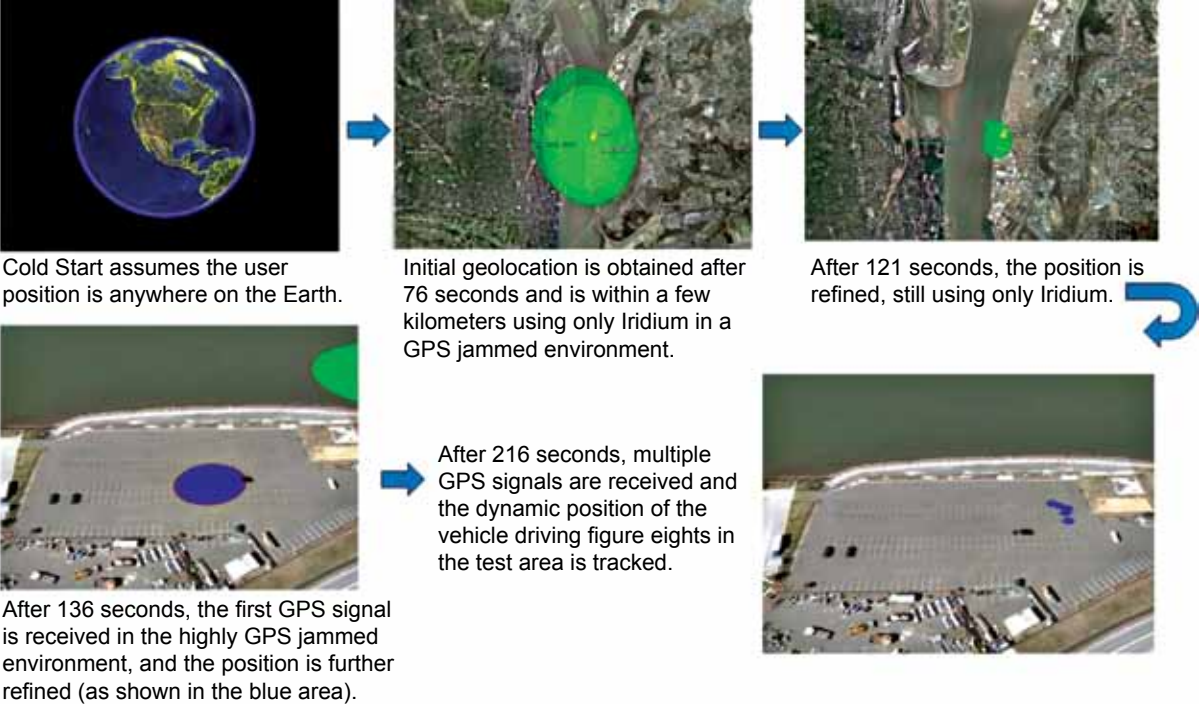


FIGURE 14
Demonstration of GPS acquisition in a jammed environment.

Programs for Professional Development

274

Programs for NRL Employees — Graduate Programs, Continuing Education, Professional Development, Equal Employment Opportunity (EEO) Programs, and Other Activities

276

Programs for Non-NRL Employees — Recent Ph.D., Faculty Member, and College Graduate Programs, Professional Appointments, and College and High School Student Programs

278

Employment Opportunities



PROGRAMS FOR NRL EMPLOYEES

The Human Resources Office supports and provides traditional and alternative methods of training for employees. NRL employees are encouraged to develop their skills and enhance their job performance so they can meet the future needs of NRL and achieve their own goals for growth.

One common study procedure is for employees to work full time at the Laboratory while taking job-related courses at universities and schools local to their job site. The training ranges from a single course to undergraduate, graduate, and postgraduate course work. Tuition for training is paid by NRL. The formal programs offered by NRL are described here.

GRADUATE PROGRAMS

The **Advanced Graduate Research Program** (formerly the Sabbatical Study Program, which began in 1964) enables selected professional employees to devote full time to research or pursue work in their own or a related field for up to one year at an institution or research facility of their choice without the loss of regular salary, leave, or fringe benefits. NRL pays all travel and moving expenses for the employee. Criteria for eligibility include professional stature consistent with the applicant's opportunities and experience, a satisfactory program of study, and acceptance by the facility selected by the applicant. The program is open to employees who have completed six years of Federal Service, four of which have been at NRL.

The **Edison Memorial Graduate Training Program** enables employees to pursue graduate studies in their fields at local universities. Participants in this program work 24 hours each workweek and pursue their studies during the other 16 hours. The criteria for eligibility include a minimum of one year of service at NRL, a bachelor's or master's degree in an appropriate field, and professional standing in keeping with the candidate's opportunities and experience.

To be eligible for the **Select Graduate Training Program**, employees must have a Bachelor's degree in an appropriate field and must have demonstrated ability and aptitude for advanced training. Students accepted into this program devote three academic semesters to graduate study. While attending school,

they receive one-half of their salary and benefits, and NRL pays for tuition and travel expenses.

The **Naval Postgraduate School (NPS)**, located in Monterey, California, provides graduate programs to enhance the technical preparation of Naval officers and civilian employees who serve the Navy in the fields of science, engineering, operations analysis, and management. NRL employees desiring to pursue graduate studies at NPS may apply for a maximum of six quarters away from NRL, with thesis work accomplished at NRL. Participants continue to receive full pay and benefits during the period of study. NRL also pays for tuition and travel expenses.

In addition to NRL and university offerings, application may be made to a number of noteworthy programs and fellowships. Examples of such opportunities are the **Capitol Hill Workshops**, the **Legislative Fellowship (LEGIS) program**, the **Federal Executive Institute (FEI)**, and the **Executive Leadership Program for Mid-Level Employees**. These and other programs are announced from time to time, as schedules are published.

Research conducted at NRL may be used as **thesis material for an advanced degree**. This original research is supervised by a qualified employee of NRL who is approved by the graduate school. The candidate should have completed the required course work and should have satisfied the language, residence, and other requirements of the graduate school from which the degree is sought. NRL provides space, research facilities, and supervision but leaves decisions on academic policy to the cooperating schools.

CONTINUING EDUCATION

Undergraduate and graduate courses offered at local colleges and universities may be subsidized by NRL for employees interested in improving their skills and keeping abreast of current developments in their fields.

NRL offers **short courses** to all employees in a number of fields of interest including administrative subjects, and supervisory and management techniques. Laboratory employees may also attend these courses at nongovernment facilities.

For further information on any of the above Graduate and Continuing Education programs, contact the Workforce Development and Management Branch (Code 1840) at (202) 404-8314 or via email at Training@hro.nrl.navy.mil.

The **Scientist-to-Sea Program (STSP)** provides opportunities for Navy R&D laboratory/center personnel to go to sea to gain first-hand insight into operational factors affecting system design, performance, and operations on a variety of ships. NRL is a participant of this Office of Naval Research (ONR) program. Contact (202) 404-7635.

PROFESSIONAL DEVELOPMENT

NRL has several programs, professional society chapters, and informal clubs that enhance the professional growth of employees. Some of these are listed below.

The **Counseling & Referral Service (C/RS)** helps employees to achieve optimal job performance through counseling and to resolve problems such as family and work-related stress and relationship difficulties, and behavioral, emotional, and substance use problems that may adversely impact job performance. C/RS provides confidential assessments and short-term counseling, training workshops, and referrals to additional resources in the community. Contact (202) 767-6857.

The **NRL Women in Science and Engineering (WISE) Network** was formed in 1997 through the merger of the NRL chapter of WISE and the Women in Science and Technology Network. Luncheon meetings and seminars are held to discuss scientific research areas, career opportunities, and career-building strategies. The group also sponsors projects to promote the professional success of the NRL S&T community and improve the NRL working environment. Membership is open to all S&T professionals. Contact (202) 404-4389 or (202) 767-4697.

Sigma Xi, The Scientific Research Society, encourages and acknowledges original investigation in pure and applied science. It is an honor society for research scientists. Individuals who have demonstrated the ability to perform original research are elected to membership in local chapters. The NRL Edison Chapter, comprising approximately 400 members, recognizes original research by presenting awards annually in pure and applied science to outstanding NRL staff members. The chapter also sponsors lectures at NRL on a wide range of scientific topics for the entire NRL community. These lectures are delivered by scientists from all over the nation and the world. The highlight of the Sigma Xi lecture series is the Edison Memorial Lecture, traditionally featuring a distinguished scientist. Contact (202) 767-9522.

The **NRL Mentor Program** was established to provide an innovative approach to professional and career training and an environment for personal and professional growth. It is open to permanent NRL employees in all job series and at all sites. Mentorees are matched with successful, experienced colleagues having more technical and/or managerial experience who can provide them with the knowledge and skills needed to maximize their contribution to the success of their immediate organization, to NRL, to the Navy, and to their chosen career fields. The ultimate goal of the program is to increase job productivity, creativity, and satisfaction through better communication, understanding, and training. NRL Instruction 12400.1A provides policy and procedures for the program. Contact (202) 404-8314 or Training@hro.nrl.navy.mil.

Employees interested in developing effective self-expression, listening, thinking, and leadership potential are invited to join the Forum Club, a chapter of **Toastmasters International**. Members of this club possess diverse career backgrounds and talents and to learn to communicate not by rules but by practice in an atmosphere of understanding and helpful fellowship. NRL's Commanding Officer and Director of Research endorse Toastmasters. Contact (202) 404-4670.

EQUAL EMPLOYMENT OPPORTUNITY (EEO) PROGRAMS

Equal employment opportunity (EEO) is a fundamental NRL policy for all employees regardless of race, color, national origin, sex, religion, age, sexual orientation, or disability. The NRL EEO Office is a service organization whose major functions include counseling employees in an effort to resolve employee/management conflicts, processing formal discrimination complaints, providing EEO training, and managing NRL's affirmative employment recruitment program. The NRL EEO Office is also responsible for sponsoring special-emphasis programs to promote awareness and increase sensitivity and appreciation of the issues or the history relating to females, individuals with disabilities, and minorities. Contact the NRL Deputy EEO Officer at (202) 767-2486 for additional information on any of their programs or services.

OTHER ACTIVITIES

The award-winning **Community Outreach Program** directed by the NRL Public Affairs Office fosters programs that benefit students and other community citizens. Volunteer employees assist with and judge science fairs, give lectures, provide science demonstrations and student tours of NRL, and serve as tutors, mentors, coaches, and classroom resource teachers. The program sponsors African American History

Month art and essay contests for local schools, student tours of NRL, and an annual holiday party for neighborhood children in December. Through the program, NRL has active partnerships with three District of Columbia public schools. Contact (202) 767-2541.

Other programs that enhance the development of NRL employees include sports and theater groups and the **Amateur Radio Club**. The **NRL Fitness Center** at NRL-DC, managed by Naval Support Activity Washington Morale, Welfare and Recreation (NSAW-MWR), houses a fitness room with treadmills, bikes, ellipticals, step mills, and a full strength circuit; a gymnasium

for basketball, volleyball, and other activities; a game room; and full locker rooms. The Fitness Center is free to NRL employees and contractors. NRL employees are also eligible to participate in all NSAW MWR activities held on Anacostia Naval Annex and Washington Navy Yard, less than five miles away. The **NRL Showboaters Theatre**, organized in 1974, is “in the dark.” Visit www.nrl.navy.mil/showboaters/Past_Productions.php for pictures from past productions such as Annie Get Your Gun, Gigi, and Hello Dolly. Contact (202) 404-4998 for Play Reader’s meetings at NRL.

PROGRAMS FOR NON-NRL EMPLOYEES

Several programs have been established for non-NRL professionals. These programs encourage and support the participation of visiting scientists and engineers in research of interest to the Laboratory. Some of the programs may serve as stepping-stones to federal careers in science and technology. Their objective is to enhance the quality of the Laboratory’s research activities through working associations and interchanges with highly capable scientists and engineers and to provide opportunities for outside scientists and engineers to work in the Navy laboratory environment. Along with enhancing the Laboratory’s research, these programs acquaint participants with Navy capabilities and concerns and provide a path to full-time employment.

RECENT PH.D., FACULTY MEMBER, AND COLLEGE GRADUATE PROGRAMS

The **National Research Council (NRC) Cooperative Research Associateship Program** selects associates who conduct research at NRL in their chosen fields in collaboration with NRL scientists and engineers. Appointments are for one year (renewable for a second and possible third year).

The **NRL/ASEE Postdoctoral Fellowship Program**, administered by the American Society for Engineering Education (ASEE), aims to increase the involvement of highly trained scientists and engineers in disciplines necessary to meet the evolving needs of naval technology. Appointments are for one year (renewable for a second and possible third year).

The **Naval Research Enterprise Intern Program (NREIP)** is a ten-week program involving NROTC colleges/universities and their affiliates. The Office of Naval Research (ONR) offers summer appointments at Navy laboratories to current sophomores, juniors, seniors, and graduate students from participating

schools. Application is online at www.asee.org/nreip through the American Society for Engineering Education. Electronic applications are sent for evaluation to the point of contact at the Navy laboratory identified by the applicant. Students are provided a stipend of \$7,500 (undergraduates) or \$10,000 (graduate students).

The American Society for Engineering Education also administers the **Navy/ASEE Summer Faculty Research and Sabbatical Leave Program** for university faculty members to work for ten weeks (or longer, for those eligible for sabbatical leave) with professional peers in participating Navy laboratories on research of mutual interest.

The **NRL/United States Naval Academy (USNA) Cooperative Program for Scientific Interchange** allows faculty members of the U.S. Naval Academy to participate in NRL research. This collaboration benefits the Academy by providing the opportunity for USNA faculty members to work on research of a more practical or applied nature. In turn, NRL’s research program is strengthened by the available scientific and engineering expertise of the USNA faculty.

The **National Defense Science and Engineering Graduate Fellowship Program** helps U.S. citizens obtain advanced training in disciplines of science and engineering critical to the U.S. Navy. The three-year program awards fellowships to recent outstanding graduates to support their study and research leading to doctoral degrees in specified disciplines such as electrical engineering, computer sciences, material sciences, applied physics, and ocean engineering. Award recipients are encouraged to continue their study and research in a Navy laboratory during the summer.

For further information about the above six programs, contact (202) 404-7450.

PROFESSIONAL APPOINTMENTS

Faculty Member Appointments use the special skills and abilities of faculty members for short periods to fill positions of a scientific, engineering, professional, or analytical nature at NRL.

Consultants and experts are employed because they are outstanding in their fields of specialization or because they possess ability of a rare nature and could not normally be employed as regular civil servants.

Intergovernmental Personnel Act Appointments temporarily assign personnel from state or local governments or educational institutions to the Federal Government (or vice versa) to improve public services rendered by all levels of government.

COLLEGE AND HIGH SCHOOL STUDENT PROGRAMS

The student programs are tailored to high school, undergraduate, and graduate students to provide employment opportunities and work experience in naval research. These programs are designed to attract applicants for student and full professional employment in fields such as engineering, physics, mathematics, and computer sciences. The student employment programs are designed to help students and educational institutions gain a better understanding of NRL's research, its challenges, and its opportunities. To participate in these programs, the student must be continuously enrolled in school on at least a half-time basis at a qualifying educational institution.

The **Student Career Experience Program (SCEP)** employs students in study-related occupations. The program is conducted in accordance with a planned schedule and a working agreement among NRL, the educational institution, and the student. Primary focus is on the pursuit of undergraduate and graduate degrees in engineering, computer science, or the physical sciences. Applications are accepted year-round.

The **Student Temporary Employment Program (STEP)** is a one year temporary employment program that may be renewed. This program enables students to earn a salary while continuing their studies and offers them valuable work experience. They must be continuously enrolled in school on at least a half-time basis at a qualifying educational institution. Applications are accepted year-round.

The **Summer Employment Program (SEP)** employs students for the summer that are enrolled in a qualifying educational institution on at least a half-time basis studying paraprofessional and technician position in engineering, physical sciences, computer sciences, and mathematics. Applications are due the 2nd Friday in February.

The **Student Volunteer Program** helps students gain valuable experience by allowing them to voluntarily perform educationally related work at NRL. Applications are accepted year-round.

For additional information on these student programs, contact (202) 767-8313.

For high school students, the **DoD Science & Engineering Apprenticeship Program (SEAP)** offers students grades 9 to 12 the opportunity to serve for eight weeks as junior research associates in a DoD laboratory. Under the direction of a mentor, students gain a better understanding of the challenges and opportunities of research through participation in scientific programs. Criteria for eligibility are based on science and mathematics courses completed and grades achieved; scientific motivation, curiosity, and capacity for sustained hard work; a desire for a technical career; teacher recommendations; and achievement test scores. For additional information, contact (202) 767-2365 or SEAP@hro.nrl.navy.mil.

NRL EMPLOYMENT OPPORTUNITIES

for Highly Innovative, Motivated, and Creative Professionals

NRL offers a wide variety of challenging S&T positions that involve skills from basic and applied research to equipment development. The nature of the research and development conducted at NRL requires professionals with experience. Typically there is a continuing need for electronics, mechanical, aerospace, and materials engineers, metallurgists, computer scientists, and oceanographers with bachelor's and/or advanced degrees and physical and computer scientists with Ph.D. degrees.



■ **Biologists.** Biologists conduct research in areas that include biosensor development, tissue engineering, molecular biology, genetic engineering, proteomics, and environmental monitoring.

■ **Chemists.** Chemists are recruited to work in the areas of combustion, polymer science, bioengineering and molecular engineering, surface science, materials, synthesis, nanostructures, corrosion, fiber optics, electro-optics, microelectronics, electron-device technology, and laser physics.

■ **Electronics Engineers and Computer Scientists.** These employees may work in the areas of communications systems, electromagnetic scattering, electronics instrumentation, electronic warfare systems, radio frequency/microwave/millimeter-wave/infrared technology, radar systems, laser physics technology, radio-wave propagation, electron device technology, spacecraft design, artificial intelligence, information processing, signal processing, plasma physics, vacuum science, microelectronics, electro-optics, fiber optics, solid state, software engineering, computer design/architecture, ocean acoustics, stress analysis, and expert systems.

■ **Materials Scientists/Engineers.** These employees are recruited to work on materials, microstructure characterization, electronic ceramics, solid-state physics, fiber optics, electro-optics, microelectronics, fracture mechanics, vacuum science, laser physics and joining technology, and radio frequency/microwave/millimeter-wave/infrared technology.

■ **Mechanical and Aerospace Engineers.** These employees may work in areas of spacecraft design, remote sensing, propulsion, experimental and computational fluid mechanics, experimental structural mechanics, solid mechanics, elastic/plastic fracture mechanics, materials, finite-element methods, nondestructive evaluation, characterization of fracture resistance of structural alloys, combustion, CAD/CAM, and multi-functional material response.

■ **Oceanographers, Meteorologists, and Marine Geophysicists.** These employees work in the areas of ocean and atmospheric dynamics, air-sea interaction, upper-ocean dynamics, oceanographic bio-optical modeling, oceanic and atmospheric numerical modeling and prediction, data assimilation and data fusion, retrieval and application of remote sensing data, benthic processes, aerogeophysics, marine sedimentary processes, advanced mapping techniques, atmospheric physics, and remote sensing. Oceanographers and marine geophysicists are located in Washington, DC, and at the Stennis Space Center, Bay St. Louis, Mississippi. Meteorologists are located in Washington, DC, and Monterey, California.

■ **Physicists.** Physics graduates may concentrate on such fields as materials, solid-state physics, fiber optics, electro-optics, microelectronics, vacuum science, plasma physics, fluid mechanics, signal processing, ocean acoustics, information processing, artificial intelligence, electron-device technology, radio-wave propagation, laser physics, ultraviolet/X-ray/gamma-ray technology, electronic warfare, electromagnetic interaction, communications systems, radio frequency/microwave/millimeter-wave/infrared technology, computational physics, radio and high-energy astronomy, solar physics, and space physics.

For more information and current vacancy listings,
visit <http://hroffice.nrl.navy.mil/>

General Information

280

Technical Output

281

Key Personnel

282

Contributions by Divisions, Laboratories, and Departments

285

Subject Index

288

Author Index

289

Map/Quick Reference Telephone Numbers

TECHNICAL OUTPUT

The Navy continues to be a leader in initiating new developments and applying these advancements to military requirements. The primary method of informing the scientific and engineering community of the advances made at NRL is through the Laboratory's technical output — reports, articles in scientific journals, contributions to books, papers presented to scientific societies and topical conferences, patents, and inventions.

The figures for calendar year 2009 presented below represent the output of NRL facilities in Washington, D.C.; Bay St. Louis, Mississippi; and Monterey, California.

In addition to the output listed, NRL scientists made more than 2244 oral presentations during 2009.

| Type of Contribution | Unclassified | Classified | Total |
|------------------------------------------------------------------------------------|--------------|------------|-------|
| Articles in periodicals, chapters in books, and papers in published proceedings | 1425* | 0 | 1425* |
| NRL Formal Reports | 9 | 5 | 14 |
| NRL Memorandum Reports | 46 | 0 | 46 |
| Books | 0 | 0 | 0 |
| Patents granted | 51 | | 51 |
| Statutory Invention Registrations (SIRs) | 0 | | 0 |

*This is a provisional total based on information available to the Ruth H. Hooker Research Library on April 2, 2010. Additional publications carrying a 2009 publication date are anticipated. Total includes refereed and non-refereed publications.

KEY PERSONNEL

Area Code (202) unless otherwise listed
Personnel Locator - 767-3200
DSN-297 or 754

| Code | Office | Phone Number |
|-----------------------------------------------------------------|------------------------------------------------------------------------------------|--------------|
| EXECUTIVE DIRECTORATE | | |
| 1000 | Commanding Officer | 767-3403 |
| 1000.1 | Inspector General | 767-3621 |
| 1001 | Director of Research | 767-3301 |
| 1001.1 | Executive Assistant | 767-2445 |
| 1002 | Chief Staff Officer | 767-3621 |
| 1004 | Head, Technology Transfer | 767-3083 |
| 1006 | Head, Office of Program Administration and Policy Development | 767-3091 |
| 1008 | Office of Counsel | 767-2244 |
| 1030 | Public Affairs Officer | 767-2541 |
| 1100 | Director, Institute for Nanoscience | 767-3261 |
| 1200 | Head, Command Support Division | 767-3621 |
| 1220 | Head, Security | 767-0793 |
| 1400 | Head, Military Support Division | 767-2273 |
| 1600 | Commander, Scientific Development Squadron One | 301-342-3751 |
| 1800 | Director, Human Resources Office | 767-3421 |
| 1830 | Deputy EEO Officer | 767-5264 |
| 3005 | Deputy for Small Business | 767-6263 |
| 3540 | Head, Safety Branch | 767-2232 |
| BUSINESS OPERATIONS DIRECTORATE | | |
| 3000 | Comptroller/Associate Director of Research | 767-2371 |
| 3200 | Head, Contracting Division | 767-5227 |
| 3300 | Head, Financial Management Division | 767-3405 |
| 3400 | Head, Supply and Information Services Division | 767-3446 |
| 3500 | Director, Research and Development Services Division | 404-4054 |
| SYSTEMS DIRECTORATE | | |
| 5000 | Associate Director of Research | 767-3425 |
| 5300 | Superintendent, Radar Division | 404-2700 |
| 5500 | Superintendent, Information Technology Division/ NRL Chief Information Officer* | 767-2903 |
| 5600 | Superintendent, Optical Sciences Division | 767-7375 |
| 5700 | Superintendent, Tactical Electronic Warfare Division | 767-6278 |
| MATERIALS SCIENCE AND COMPONENT TECHNOLOGY DIRECTORATE | | |
| 6000 | Associate Director of Research | 767-3566 |
| 6100 | Superintendent, Chemistry Division | 767-3026 |
| 6300 | Superintendent, Materials Science and Technology Division | 767-2926 |
| 6400 | Director, Laboratory for Computational Physics and Fluid Dynamics | 767-3055 |
| 6700 | Superintendent, Plasma Physics Division | 767-2723 |
| 6800 | Superintendent, Electronics Science and Technology Division | 767-3693 |
| 6900 | Director, Center for Bio/Molecular Science and Engineering | 404-6000 |
| OCEAN AND ATMOSPHERIC SCIENCE AND TECHNOLOGY DIRECTORATE | | |
| 7000 | Associate Director of Research | 404-8690 |
| 7100 | Superintendent, Acoustics Division | 767-3482 |
| 7200 | Superintendent, Remote Sensing Division | 767-3391 |
| 7300 | Superintendent, Oceanography Division | 228-688-4670 |
| 7400 | Superintendent, Marine Geosciences Division | 228-688-4650 |
| 7500 | Superintendent, Marine Meteorology Division | 831-656-4721 |
| 7600 | Superintendent, Space Science Division | 767-6343 |
| NAVAL CENTER FOR SPACE TECHNOLOGY | | |
| 8000 | Director | 767-6547 |
| 8100 | Superintendent, Space Systems Development Department | 767-0410 |
| 8200 | Superintendent, Spacecraft Engineering Department | 404-3727 |

*Additional Duty

CONTRIBUTIONS BY DIVISIONS, LABORATORIES, AND DEPARTMENTS

Radar Division

159 Adaptive Jamming Cancellation in Radar
V. Gregers-Hansen, R. Mital, and J. Cook

222 Single-shot Imaging Magnetometry and Spectroscopy Using Cold Atoms
F.K. Fatemi, M.L. Terraciano, M. Bashkansky, and Z. Dutton

Information Technology Division

174 Beyond-line-of-sight Tactical Communications Relay (BTCCR)
M. Rupar, J. Doffoh, and B. Vorees

Optical Sciences Division

216 Asymmetric Lasercom for Small Unmanned Aerial Systems
P.G. Goetz, W.T. Freeman, J.L. Murphy, B. Mathieu, S.J. Frawley, M.R. Suite, M.S. Ferraro, W.R. Smith, B.B. Xu, R. Mahon, W.S. Rabinovich, M.A. Colbert, H.R. Burris, C.I. Moore, and W.W. Schultz

222 Single-shot Imaging Magnetometry and Spectroscopy Using Cold Atoms
F.K. Fatemi, M.L. Terraciano, M. Bashkansky, and Z. Dutton

181 High Performance Anti-Reflection Structured IR Fibers
J.S. Sanghera, C. Florea, L.E. Busse, L.B. Shaw, F.H. Kung, and I.D. Aggarwal

143 Long-Range Optical Communications Link
M.R. Suite, B.B. Xu, C.I. Moore, H.R. Harris, L.M. Thomas, W.S. Rabinovich, J.L. Murphy, R. Mahon, P.G. Goetz, and M.S. Ferraro

Tactical Electronic Warfare Division

162 Laser System for Protection of Navy Ships
P.S. Mak and C. Maraviglia

156 Improvements to Towed Decoys to Enhance Aircraft Survivability
G.T. Roan

165 Particle Filters for Multipath Mitigation
M. Hock and K. Lee

Chemistry Division

88 Marine Biofouling: Grasping Barnacle Cement Curing from the Inside Out
K.J. Wahl, R.K. Everett, D.E. Barlow, G.H. Dickinson, B. Orihuela, and D. Rittschof

216 Asymmetric Lasercom for Small Unmanned Aerial Systems
P.G. Goetz, W.T. Freeman, J.L. Murphy, B. Mathieu, S.J. Frawley, M.R. Suite, M.S. Ferraro, W.R. Smith, B.B. Xu, R. Mahon, W.S. Rabinovich, M.A. Colbert, H.R. Burris, C.I. Moore, and W.W. Schultz

148 Elastomer-Steel Laminate Armor
C.M. Roland, D. Fragiadakis, and R.M. Gamache

153 SynFuel from Seawater
H.D. Willauer, D.R. Hardy, F. DiMascio, R.W. Dorner, and F.W. Williams

187 Plasma Processing of Ion Energy-sensitive Materials
S.G. Walton, E.H. Lock, M. Baraket, D.R. Boris, R.F. Fernsler, S.H. North, C.R. Taitt, J.T. Robinson, F.K. Perkins, and P.E. Sheehan

Materials Science and Component Technology Directorate

88 Marine Biofouling: Grasping Barnacle Cement Curing from the Inside Out
K.J. Wahl, R.K. Everett, D.E. Barlow, G.H. Dickinson, B. Orihuela, and D. Rittschof

97 Structure-Property Relationships in a 3D Polycrystalline Microstructure
A.C. Lewis, M.A. Siddiq Qidwai, D.J. Rowenhorst, G. Spanos, and A.B. Geltmacher

189 Standoff Detection of Trace Explosive Residues by Resonant Infrared Photothermal Imaging
C. Kendziora, R.A. McGill, R. Furstenberg, J. Stepnowski, M. Papantonakis, V. Nguyen, and G.K. Hubler

180 Nanostructured Magnets for Improved Energy Efficiency
M.A. Willard, K.E. Knippling, and M. Daniil

Laboratory for Computational Physics and Fluid Dynamics

172 CT-Analyst® Deployed for the 2009 Presidential Inauguration
J.P. Boris, G. Patnaik, K. Obenschain, M. Ronas, C. Williams, and J. Delaney

234 Rapid Air Traffic Modeling and Prediction
C.R. Kaplan, E.S. Oran, N. Alexandrov, and J.P. Boris

Plasma Physics Division

218 SWOrRD: Swept-Wavelength resonance-Raman Detection of Bacteria, Chemicals, and Explosives
J. Grun, C. Manka, P. Kunapareddy, R. Lunsford, D. Gillis, S. Nikitin, Z. Wang, J. Bowles, and M. Corson

187 Plasma Processing of Ion Energy-sensitive Materials
S.G. Walton, E.H. Lock, M. Baraket, D.R. Boris, R.F. Fernsler, S.H. North, C.R. Taitt, J.T. Robinson, F.K. Perkins, and P.E. Sheehan

232 High-Yield Z-Pinch Thermonuclear Neutron Source
A.L. Velikovich, R. W. Clark, J. Davis, J.L. Giuliani, Y.K. Chong, C.A. Coverdale, and D. Flicker

242 Integrating the Sun-Earth System for the Operational Environment (ISES-OE)
J.L. Lean, J.D. Huba, S.E. McDonald, S. Slinker, D.P. Dorb, J.T. Emmert, R.R. Meier, J.M. Picone, G. Joyce, J. Krall, A. Stephan, K.A. Roach, H. Knight, S.P. Plunkett, C.-C. Wu, B.E. Wood, Y.-M. Wang, R.A. Howard, J. Chen, P.A. Bernhardt, and J.A. Fedder

Electronics Science and Technology Division

187 Plasma Processing of Ion Energy-sensitive Materials
S.G. Walton, E.H. Lock, M. Baraket, D.R. Boris, R.F. Fernsler, S.H. North, C.R. Taitt, J.T. Robinson, F.K. Perkins, and P.E. Sheehan

196 Spin Rotation for Quantum Information
S.E. Economou, A. Greilich, and T.L. Reinecke

198 Sheet of Carbon Atoms Points Way to Ultra-fast Transistors
D.K. Gaskill, P.M. Campbell, G.G. Jernigan, J.B. Boos, J.G. Tischler, E.R. Glaser, J.C. Culbertson, J.L. Tedesco, R.L. Myers-Ward, C.R. Eddy, Jr., N.A. Papanicolaou, J.C. Champlain, D. Park, and R. Bas

167 A New Gallium Nitride-based Switch for High Efficiency Power Electronics
T.J. Anderson, M.J. Tadjer, M.A. Mastro, J.K. Hite, K.D. Hobart, C.R. Eddy, Jr., and F.J. Kub

Center for Bio/Molecular Science and Engineering

104 Monitoring Enzyme Activity with Hybrid Semiconductor Quantum Dot-Fluorescent Protein Assemblies
J.R. Deschamps, K. Boeneman, M.H. Stewart, and I.L. Medintz

218 SWOrRD: Swept-Wavelength resonance-Raman Detection of Bacteria, Chemicals, and Explosives
J. Grun, C. Manka, P. Kunapareddy, R. Lunsford, D. Gillis, S. Nikitin, Z. Wang, J. Bowles, and M. Corson

187 Plasma Processing of Ion Energy-sensitive Materials
S.G. Walton, E.H. Lock, M. Baraket, D.R. Boris, R.F. Fernsler, S.H. North, C.R. Taitt, J.T. Robinson, F.K. Perkins, and P.E. Sheehan

183 Broad-Spectrum Pathogen Surveillance
A.P. Malanoski, T.A. Leski, L. Cheng, Z. Wang, D.A. Stenger, and B. Lin

151 Contaminant Monitoring in Ground and Surface Water
B.J. White, B.J. Melde, P.T. Charles, A.P. Malanoski, and M.A. Dinderman

194 Spectral Tuning of Organic Nanocolloids
C.M. Spillman, J. Naciri, G.P. Anderson, M.-S. Chen, and B.R. Ratna

Acoustics Division

200 Functionalized CMOS Nanomechanical Resonators for Chem-Bio Sensing
J.W. Baldwin, M.K. Zhalutdinov, J.S. Burgess, and B.H. Houston

132 Measurements and Modeling of Acoustic Scattering from Unexploded Ordnance (UXO) in Shallow Water
D.C. Calvo, B.H. Houston, J.A. Bucaro, L. Kraus, H.J. Simpson, and A. Sarkissian

134 Scalable Wideband Frequency-Response for Free-Field, Littoral and Seismic Applications
S. Dey and W.G. Szymczak

Remote Sensing Division

- 218 SWOrRD: Swept-Wavelength resonance-Raman Detection of Bacteria, Chemicals, and Explosives
J. Grun, C. Manka, P. Kunapareddy, R. Lunsford, D. Gillis, S. Nikitin, Z. Wang, J. Bowles, and M. Corson
- 176 Coastal Environmental Hyperspectral Imaging from the Space Station
M.R. Corson, R.L. Lucke, D.R. Korwan, W.A. Snyder, C.O. Davis, N.R. Mcglothlin, S.D. Butcher, and D.L. Wood
- 142 Measurement of Water Vapor from the Lower Stratosphere to the Upper Mesosphere
G.E. Nedoluha, R.M. Gomez, and B.C. Hicks
- 226 Real-time Surface Wave Information by Coherent Radar
P.A. Hwang, M.A. Sletten, and J.V. Toporkov
- 211 Characterization River Environments by Combining Imagery and Models: What We Can Do Now and in the Future
C.A. Blain, A.D. Weidemann, R.P. Mied, R.S. Linzell, and P. McKay

Oceanography Division

- 211 Characterization River Environments by Combining Imagery and Models: What We Can Do Now and in the Future
C.A. Blain, A.D. Weidemann, R.P. Mied, R.S. Linzell, and P. McKay
- 206 The ASW Reach-back Cell Ocean Analysis System
J.D. Dykes and P. Fanguy

Marine Geosciences Division

- 113 Seismic Oceanography — A New View of the Ocean
W.T. Wood, J.W. Book, S. Carniel, R.W. Hobbs, D.A. Lindwall, and J. Wesson
- 208 Marine Sediment Strength from Dynamic Probes
A. Abelev, D.R. Tubbs, and P.J. Valent

Marine Meteorology Division

- 122 The Impact of Ice Nuclei Concentration on Hurricane Modeling
Y. Jin, D. Doyle, Q. Zhao, S. Wang, and S.W. Chang

- 140 Optical Depth Assimilation for Operational Dust and Pollution Prediction
J.S. Reid, J. Zhang, D.L. Westphal, E.J. Hyer, C.A. Curtis, N.L. Baker, J.R. Campbell, and P. Xian

Space Science Division

- 242 Integrating the Sun-Earth System for the Operational Environment (ISES-OE)
J.L. Lean, J.D. Huba, S.E. McDonald, S. Slinker, D.P. Dorb, J.T. Emmert, R.R. Meier, J.M. Picone, G. Joyce, J. Krall, A. Stephan, K.A. Roach, H. Knight, S.P. Plunkett, C.-C. Wu, B.E. Wood, Y.-M. Wang, R.A. Howard, J. Chen, P.A. Bernhardt, and J.A. Fedder
- 245 Origins of Solar Energetic Particle (SEP) Variability
Y.-K. Ko and A.J. Tylka

Space Systems Development Department

- 248 Technology Development for High Integrity GPS (HiGPS)
O.J. Oaks
- 227 Shipboard AIS and Radar Contact Reporting
R.L. Nichols
- 143 Long-Range Optical Communications Link
M.R. Suite, B.B. Xu, C.I. Moore, H.R. Harris, L.M. Thomas, W.S. Rabinovich, J.L. Murphy, R. Mahon, P.G. Goetz, and M.S. Ferraro

Spacecraft Engineering Department

- 240 TacSat-4, Advanced UHF SATCOM
M. Hurley, B. Raynor, M. Johnson, K. Weldy, E. Becker, C. Amend, M. Nurnberger, T. Duffey, B. Skalitzky, T. Specht, E. Bradley, B. Baldauff, J. Armingier, J. Barnds, K. Akins, J. Hicks, E. Sydow, G. Sandhoo, D. Bentz, B. Davis, and E. Gruner
- 238 Joint Milli-Arcsecond Pathfinder Survey (JMAPS) Fine Attitude Determination Approach
T.W. Lim, F.A. Tasker, and P.G. DeLaHunt

SUBJECT INDEX

- 3-MV Tandem Pelletron Accelerator Facility, 54
- 3D analysis, 97
- Acoustic Reverberation Simulation Facility, 78
- Acoustic Seafloor Characterization System, 70
- Acoustics Division, 64
- Adaptive pulse compressor, 29
- Administrative Services, 81
- Advanced diesel fuels, 37
- Advanced Graduate Research Program, 274
- Advanced Silicon Carbide Epitaxial Research Laboratory (ASCERL), 60
- Aerosol particles, 122
- Air-traffic modeling, 234
- Airborne electronic countermeasures, 156
- Airborne technologies, 216
- Amateur Radio Club, 276
- ANDE-2, 14
- Anechoic chamber, 50
- Anti-jam technology, 248
- Anti-jamming techniques, 216
- Anti-ship missile (ASM), 162
- Antifouling, 88
- Antisubmarine warfare, 206
- APEX-2, 62
- Armor, 148
- Atmospheric Prediction System Development Laboratory, 72
- Automatic Identification System, 227
- Autonomous Systems and Robotics Laboratory, 46
- Barnacle, 88
- BAT™, 174
- Behavioral Detection Laboratory, 46
- Beyond line of sight, 174
- Biofouling, 88
- Biothreat agents, 183
- Blossom Point Satellite Tracking and Command Facility, 76, 85
- Bus standards, 240
- Calibration Facility, 66
- Carbon capture, 153
- Carbon dioxide, 153
- Cavitation-resistant alloys, 31
- Center for Bio/Molecular Science and Engineering, 62
- Chemical Vapor and Plasma Deposition Facility, 52
- Chemistry Division, 52
- Chesapeake Bay Detachment (CBD), 83
- Class 10 clean room, 74
- Class 100 clean room, 42
- Class 1000 clean room, 74
- CMOS, 200
- Coherent radar, 226
- Cold atoms, 222
- Community Outreach Program, 275
- Compact Antenna Range, 44
- Compound Semiconductor Processing Facility, 60
- Computational Electromagnetics (CEM) Facility, 44
- Coronal mass ejections, 245
- Counseling & Referral Service (C/RS), 275
- Coupled ocean-wave atmosphere model, 37
- Cryptographic Technology Laboratory, 46
- CT-Analyst®, 56
- Cyber Defense Development Laboratory, 46
- Deep Towed Acoustics/Geophysics System, 70
- Delayed Burgers' equation, 35
- Deployable antenna, 240
- DoD Science & Engineering Apprentice Program (SEAP), 277
- Dual Mode Optical Interrogator (DMOI), 143
- Dynamic penetration, 208
- Edison Memorial Graduate Training Program, 274
- Elastomers, 148
- Electra, 58
- Electrical, Magnetic, and Optical Measurement Facility, 54
- Electro optical (EO) propagation, 140
- Electron beam lithography, 42
- Electronics Science and Technology Division, 60
- Energy materials, 180
- Environmental Acoustic Recording Systems (EARS) buoys, 64
- Environmental hyperspectral imaging, 176
- Environmental monitoring, 150
- Enzyme, 104
- EO/IR countermeasure system, 162
- Epicenter, 60
- Epitaxial graphene, 198
- Equatorial spread F modeling, 33
- Ex-USS Shadwell (LSD-15), 52, 85
- Fine attitude determination algorithm, 238
- Finite element simulations, 97
- Fitness Center, 276
- Fluorescence, 104
- Fluorescent nanocolloids, 194
- Focal Plane Array Evaluation Facility, 48
- Focused Phased Array Imaging Radar, 66
- Fragment simulating projectiles, 148
- Free Surface Hydrodynamics Laboratory (FSSL), 66
- Free-space optical communications, 216
- Freespace Laser Communications Laboratory, 46
- Gamble II, 58
- GaN HEMT, 167
- Geoacoustic Model Fabrication Laboratory, 64
- Geographic information system, 183, 206
- Global aerosol forecasting, 140
- Global Awareness Data-exfiltration International Satellite (GLADIS), 76
- GPS, 23
- Graphene biomolecule, 187
- Ground water, 150
- Heat pipes, 240
- HERSCHEL, 14
- Heterogeneous laminate armor, 31
- HICO, 12, 35, 66, 176
- High Energy Laser Laboratory, 58
- High Performance Computing, 46
- HiGPS, 248
- HREP, 12
- Hurricane, 122
- Ice nuclei, 122
- Immersive Simulation Laboratory, 46
- In Situ Sediment Acoustic Measurement System, 70
- Inertial confinement fusion, 232
- Information Technology Division, 46
- Infrared fibers, 181
- Infrared, 189
- Institute for Nanoscience, 42
- Intelligence surveillance, 216
- Ion Tiger, 16
- IR Missile-Seeker Evaluation Facility, 48
- Iridium, 227, 248
- ISES-OE, 242
- Jamming, 159
- JCTD, 30
- Jet noise reduction, 32
- JMAPS, 238
- Laboratory for Advanced Materials Synthesis (LAMS), 60
- Laboratory for Autonomous Systems Research, 20
- Laboratory for Computational Physics and Fluid Dynamics, 56
- Laminar Flow Clean Room, 78
- Large Area Plasma Processing System (LAPPS), 58
- Large Area Scintillation Array (LASA), 74
- Laser fusion, 8
- Laser power delivery, 181
- Lasercom, 143, 216
- Liquid crystal, 194
- Littoral, 134
- Low antenna sidelobes, 159
- Low-elevation tracking, 165
- Low-power digital neutron detector, 34
- LPI/LPD techniques, 216
- Magnetic materials, 180
- Magnetic Resonance Facility, 52
- Magnetolectronics Fabrication Facility, 54

- Magnetometry, 222
 Marine Corrosion and Coatings Facility, 52, 85
 Marine Geosciences Division, 70
 Marine Meteorology Division, 72
 Maritime Domain Awareness (MDA), 227
 Materials development, 150
 Materials Processing Facility, 54
 Materials Science and Technology Division, 54
 Materials Synthesis/Property Measurement Facility, 52
 Mechanical Characterization Facility, 54
 Mentor Program, 275
 Mercury, 58
 Methane hydrates, 8
 Micro/Nanostructure Characterization Facility, 54
 Microbial fuel cells, 10
 MicroSTAR-H x-ray generator, 62
 Microstructures, 97
 Microtitre plate, 187
 Middle atmosphere, 142
 Midway Research Center, 76, 84
 Millimeter-Wave Vacuum Electronics Synthesis Facility (MWVESF), 60
 Minuteman InfraLynx Communications System (MICS), 76
 MISSE7, 13
 Mixing, 113
 Mobile Ad Hoc Networking, 46
 Mobile Atmospheric Aerosol and Radiation Characterization Observatory (MAARCO), 72
 Mobile imaging and spectroscopic threat identification (MISTI), 38
 Model forecasts, 122
 Monotonic Lagrangian Grid (MLG), 234
 Monterey (NRL-MRY), 82
 Moth eyes, 181
 Moving Map Composer Facility, 70
 Multipath, 165
 Nanomaterials, 180
 Nanomechanical resonators, 200
 Nanometer Characterization/Manipulation Facility, 52
 Nanoscale electrode materials, 9
 Nanotechnology, 104
 National Defense Science and Engineering Graduate Fellowship Program, 276
 National Research Council (NRC) Cooperative Research Associateship Program, 276
 Naval alloys, 97
 Naval Key Management Laboratory, 46
 Naval Postgraduate School (NPS), 274
 Naval Research Enterprise Intern Program (NREIP), 276
 NAVDAS-AOD, 140
 Navy Fuel Research Facility, 52
 Navy Prototype Optical Interferometer (NPOI), 66
 Navy/ASEE Summer Faculty Research and Sabbatical Leave Program, 276
 Neutron source, 232
 Nike, 58
 Nitroenergetic compounds, 150
 NOGAPS-ALPHA, 74
 NP-3D EW flying laboratory, 50
 NRL/ASEE Postdoctoral Fellowship Program, 276
 NRL/United States Naval Academy (USNA) Cooperative Program for Scientific Interchange, 276
 NRLFCU, 41
 Numerical modeling, 208
 Numerical weather prediction, 122
 Observation impact monitoring system, 38
 Ocean Dynamics and Prediction Computational Network Facility, 68
 Ocean temperature, 113
 Oceanography Division, 68
 Oceanography, 206
 Operational deployment, 172
 Operationally Responsive Space (ORS), 240
 Optical detection, 189
 Optical Fiber Preform Fabrication Facility, 48
 Optical instrument, 238
 Optical Sciences Division, 48
 ORASIS, 218
 Particle filters, 165
 Pathogen surveillance, 183
 Periodic mesoporous organosilicas (PMOs), 34
 Photovoltaics, 9
 Plasma Physics Division, 58
 Plasma processing, 187
 Plume modeling, 172
 Polymer fuel cell, 16
 Pomonkey Facility, 84
 Protein, 104
 Pure spin currents, 32
 Quantum cascade laser, 189
 Quantum dot, 104
 Quantum information, 196
 Radar Division, 44
 Radio Frequency Anechoic Chamber, 78
 RAIDS, 12
 Railgun Materials Testing Facility, 58
 Raman spectroscopy, 222
 Rapid threat assessment, 172
 Reconnaissance, 216
 Remote explosives detection (RED), 189
 Remote Sensing Division, 66
 Resequencing pathogen microarray (RPM), 183
 Resonance-Raman, 218
 RF communication relay, 174
 River current, 211
 River Simulation Tool (RST), 211
 Riverine environments, 211
 Rough sand interface, 132
 Ruth H. Hooker Research Library, 81
 Salt Water Tank Facility, 64
 SARCR, 227
 SATCOM, 174
 Satellite Data Processing Laboratory, 72
 Satellite navigation, 248
 Scansfish, 68
 Scientific Development Squadron One (VXS-1), 83
 Scientist-to-Sea Program (STSP), 275
 Seafloor probe, 208
 Sediment strength, 208
 Seismic, 113
 SEITE I and II, 15
 Select Graduate Training Program, 274
 Semiconductors, 196
 Sensor, 104
 SEPTR, 68
 Service Oriented Architecture Laboratory, 46
 SHIELDS, 162
 Shipboard, 162
 Showboaters Theatre, 276
 Sidelobe canceller (SLC) simulation, 159
 Sigma Xi, 275
 SIMPLEX VI and VII, 15
 Single event effects, 245
 Single-domain antibodies, 62
 Slocum glider, 68
 Solar Coronagraph Optical Test Chamber (SCOTCH), 74
 Solar energy particles, 245
 Solid-state decoy, SA6
 SONoMAGnetic LABoratory (SOMALAB), 64
 Sound speed, 113
 Space Physics Simulation Chamber, 58
 Space Science Division, 74
 Space Solar Cell Characterization Facility (SSCCF), 60
 Space Systems Development Department, 76
 Spaceborne hyperspectral imager, 176
 Spacecraft attitude determination, 238
 Spacecraft Engineering Department, 78
 Spacecraft Robotics Engineering and Controls Laboratory, 78
 Spectral tuning, 194
 Spin control, 196
 Spin Test Facility, 78
 SSULI, 11
 Static Loads Test Facility, 78
 Stennis Space Center (NRL-SSC), 82
 Structured acoustics, 132, 134
 Student Career Experience Program (SCEP), 277
 Student Temporary Employment Program (STEP), 277
 Student Volunteer Program, 277
 Summer Employment Program (SEP), 277
 Sun-Earth systems, 242
 Superconductors, 10
 Supramolecular assembly, 194
 Surface Characterization Facility, 48
 Surface water, 151
 Surface wave, 226
 SWOrRD facility, 58, 218
 Synchrotron Radiation Facility, 52
 Synfuel, 153
 Table-Top Terawatt (T3) laser, 58
 Tac-Sat4, 39, 240
 Tactical Electronic Warfare Division, 50
 Tactical radios, 174
 Technical Information Services, 80
 Technology Transfer Office, 80

Thermal Fabrication and Test Facility, 78
Thin-Film Materials Synthesis and Processing Facility, 54
Time transfer, 248
Toastmasters International, 275
Towed decoy, 156
Towline, 156
Transistor, 198
Trident Spectre 2009, 143
Tropical and emerging infections, 183
Tunable multi-wavelength, 218
Two-color manipulation of spins, 33
Two-photon excitation emission, 30
UHF SATCOM, 240
UHF transponder networks, 174
Ultra-low-loss Infrared Fiber-Optic Waveguide Facility, 48
Ultrafast Laser Facility (ULF), 60
Ultrafast optics, 196
Underwater acoustic communication, 36
Underwater acoustics, 132
Unexploded ordnance (UXO), 132
Unmanned aerial vehicles, 216
Unmanned air vehicle, 16
Vacuum Ultraviolet Solar Instrument Test facility, 74
Vertical Microstructure Profiler (VMP), 68
Very high angular resolution Imaging Spectrometer (VERIS), 74
Vibration Test Facility, 78
Visual Analytics Laboratory, 46
VMOC, 240
Voice Communications Laboratory, 46
Warfighter Human System Integration Laboratory, 46
Water Vapor Millimeter-wave Spectrometer (WVMS), 66, 142
Water vapor, 142
Wet etch, 167
Wideband, 134
Women in Science and Engineering (WISE) Network, 275
Z-pinch, 232

AUTHOR INDEX

- Abelev, A., 208
 Aggarwal, I.D., 181
 Akins, K., 240
 Alexandrov, N., 234
 Amend, C., 240
 Anderson, G.P., 194
 Anderson, T.J., 167
 Armingier, J., 240
 Baker, N.L., 140
 Baldauff, B., 240
 Baldwin, J.W., 200
 Baraket, M., 187
 Barlow, D.E., 88
 Barnds, J., 240
 Bashkansky, M., 222
 Bass, R., 198
 Becker, E., 240
 Bentz, D., 240
 Bernhardt, P.A., 242
 Blain, C.A., 211
 Boeneman, K., 104
 Book, J.W., 113
 Boos, J.B., 198
 Boris, D.R., 187
 Boris, J.P., 172, 234
 Bowles, J., 218
 Bradley, E., 240
 Bucaro, J.A., 132
 Burgess, J.S., 200
 Burriss, H.R., 143, 216
 Busse, L.E., 181
 Butcher, S.D., 176
 Calvo, D.C., 132
 Campbell, J.R., 140
 Campbell, P.M., 198
 Carniel, S., 113
 Champlain, J.C., 198
 Chang, S.W., 122
 Charles, P.T., 151
 Chen, J., 242
 Chen, M.-S., 194
 Cheng, L., 183
 Chong, Y.K., 232
 Clark, R.W., 232
 Colbert, M.A., 216
 Cook, J., 159
 Corson, M.R., 176, 218
 Coverdale, C.A., 232
 Culbertson, J.C., 198
 Curtis, C.A., 140
 Daniil, M., 180
 Davis, B., 240
 Davis, C.O., 176
 Davis, J., 232
 DeLaHunt, P.G., 238
 Delaney, J., 172
 Deschamps, J.R., 104
 Dey, S., 134
 Dickinson, G.H., 88
 DiMascio, F., 153
 Dinderman, M.A., 151
 Doffoh, J., 174
 Dorner, R.W., 153
 Doyle, D., 122
 Drob, D.P., 242
 Duffey, T., 240
 Dutton, Z., 222
 Dykes, J.D., 206
 Economou, S.E., 196
 Eddy, Jr., C.R., 167, 198
 Emmert, J.T., 242
 Everett, R.K., 88
 Fanguy, P., 206
 Fatemi, F.K., 222
 Fedder, J.A., 242
 Fernsler, R.F., 187
 Ferraro, M.S., 143, 216
 Flecker, D., 232
 Florea, C., 181
 Fragiadakis, D., 148
 Frawley, S.J., 216
 Freeman, W.T., 216
 Furstenberg, R., 189
 Gamache, R.M., 148
 Gaskill, D.K., 198
 Geltmacher, A.B., 97
 Gillis, D., 218
 Giuliani, J.L., 232
 Glaser, E.R., 198
 Goetz, P.G., 143, 216
 Gomez, R.M., 142
 Gregers-Hansen, V., 159
 Greilich, A., 196
 Grun, J., 218
 Gruner, E., 240
 Hardy, D.R., 153
 Hicks, B.C., 142
 Hicks, J., 240
 Hite, J.K., 167
 Hobart, K.D., 167
 Hobbs, R.W., 113
 Hock, M., 165
 Houston, B.H., 132, 200
 Howard, R.A., 242
 Huba, J.D., 242
 Hubler, G.K., 189
 Hurley, M., 240
 Hwang, P.A., 226
 Hyer, E.J., 140
 Jernigan, G.G., 198
 Jin, Y., 122
 Johnson, M., 240
 Joyce, G., 242
 Kaplan, C.R., 234
 Kendziora, C., 189
 Knight, H., 242
 Knipling, K.E., 180
 Ko, Y.-K., 245
 Korwan, D.R., 176
 Krall, J., 242
 Kraus, L., 132
 Kub, F.J., 167
 Kunapareddy, P., 218
 Kung, F.H., 181
 Lean, J.L., 242
 Lee, K., 165
 Leski, T.A., 183
 Lewis, A.C., 97
 Lim, T.W., 238
 Lin, B., 183
 Lindwall, D.A., 113
 Linzell, R.S., 211
 Lock, E.H., 187
 Lucke, R.L., 176
 Lunsford, R., 218
 Mahon, R., 143, 216
 Mak, P.S., 162
 Malanoski, A.P., 151, 183
 Manka, C., 218
 Maraviglia, C., 162
 Mastro, M.A., 167
 Mathieu, B., 216
 McDonald, S.E., 242
 McGill, R.A., 189
 Mcglothlin, N.R., 176
 McKay, P., 211
 Medintz, I.L., 104
 Meier, R.R., 242
 Melde, B.J., 151
 Mied, R.P., 211
 Mital, R., 159
 Moore, C.I., 143, 216
 Murphy, J.L., 143, 216
 Myers-Ward, R.L., 198
 Naciri, J., 194
 Nedoluha, G.E., 142
 Nguyen, V., 189
 Nichols, R.L., 227
 Nikitin, S., 218
 North, S.H., 187
 Nurnberger, M., 240
 Oaks, O.J., 248
 Obenschain, K., 172
 Oran, E.S., 234
 Orihuela, B., 88
 Papanicolaou, N.A., 198
 Papantonakis, M., 189
 Park, D., 198
 Patnaik, G., 172
 Perkins, F.K., 187
 Picone, J.M., 242
 Plunkett, S.P., 242
 Rabinovich, W.S., 143, 216
 Ratna, B.R., 194
 Raynor, B., 240
 Reid, J.S., 140
 Reinecke, T.L., 196
 Rittschof, D., 88
 Roach, K.A., 242
 Roan, G.T., 156
 Robinson, J.T., 187
 Roland, C.M., 148
 Ronas, M., 172
 Rowenhorst, D.J., 97
 Rupar, M., 174
 Sandhoo, G., 240
 Sanghera, J.S., 181
 Sarkissian, A., 132
 Schultz, W.W., 216
 Shaw, B., 181
 Sheehan, P.E., 187
 Siddiq Qidwai, M.A., 97
 Simpson, H.J., 132
 Skalitzy, B., 240
 Sletten, M.A., 226
 Slinker, S., 242
 Smith, W.R., 216
 Snyder, W.A., 176
 Spanos, G., 97
 Specht, T., 240
 Spillman, C.M., 194
 Stenger, D.A., 183
 Stephan, A., 242
 Stepnowski, J., 189
 Stewart, M.H., 104
 Suite, M.R., 143, 216
 Sydor, E., 240
 Szymczak, W.G., 134
 Tadjer, M.J., 167
 Taitt, C.R., 187
 Tasker, F.A., 238
 Tedesco, J.L., 198
 Terraciano, M.L., 222
 Thomas, L.M., 143
 Tischler, J.G., 198
 Toporkov, J.V., 226
 Tubbs, K.R., 208
 Tylka, A.J., 245
 Valent, P.J., 208
 Velikovich, A.L., 232
 Vorees, B., 174
 Wahl, K.J., 88
 Walton, S.G., 187
 Wang, S., 122
 Wang, Y.-M., 242
 Wang, Z., 183, 218
 Weidemann, A.D., 211
 Weldy, K., 240
 Wesson, J., 113
 Westphal, D.L., 140
 White, B.J., 151
 Willard, M.A., 180
 Willauer, H.D., 153
 William, C., 172
 Williams, F.R., 153
 Wood, B.E., 242
 Wood, D.L., 176
 Wood, W.T., 113
 Wu, C.-C., 242
 Xian, P., 140
 Xu, B.B., 143, 216
 Zalalutdinov, M.K., 200
 Zhang, J., 140
 Zhao, Q., 122

NAVAL RESEARCH LABORATORY

4555 Overlook Ave., SW • Washington, DC 20375-5320

LOCATION OF NRL IN THE CAPITAL AREA



Quick Reference Telephone Numbers

| | NRL Washington | NRL- SSC | NRL- Monterey | NRL CBD | NRL VXS-1 Patuxent River |
|-------------------|-------------------|----------------|------------------|----------------|-----------------------------|
| Hotline | (202) 767-6543 | (202) 767-6543 | (202) 767-6543 | (202) 767-6543 | (202) 767-6543 |
| Personnel Locator | (202) 767-3200 | (228) 688-3390 | (831) 656-4763 | (410) 257-4000 | (301) 342-3751 |
| DSN | 297- or 754- | 828 | 878 | — | 342 |
| Direct-in-Dialing | 767- or 404- | 688 | 656 | 257 | 342 |
| Public Affairs | (202) 767-2541 | (228) 688-5328 | (202) 767-2541 | — | (202) 767-2541 |

Additional telephone numbers are listed on page 281.

General information on the research described in this *NRL Review* can be obtained from the Public Affairs Office, Code 1030, (202) 767-2541. Information concerning Technology Transfer is available from the Technology Transfer Office, Code 1004, (202) 767-7230. Sources of information on the various educational programs at NRL are listed in the *NRL Review* chapter entitled "Programs for Professional Development."

For additional information about NRL, the *NRL Fact Book* lists the organizations and key personnel for each division. It contains information about Laboratory funding, programs, and field sites. The *Fact Book* can be obtained from the Technical Information Services Branch, Code 3430, (202) 404-4963. The web-based *NRL Major Facilities* publication, which describes each NRL facility in detail, can be accessed at <http://www.nrl.navy.mil>.

NRL REVIEW STAFF

SENIOR SCIENCE EDITOR

John D. Bultman

COORDINATOR

Jonna Atkinson

CONSULTANT

Kathy Parrish

DESIGN, LAYOUT, AND GRAPHIC SUPPORT

Jonna Atkinson
Heather Miller

EDITORIAL ASSISTANCE

Saul Oresky
Kathy Parrish
Claire Peachey

PHOTOGRAPHIC PRODUCTION

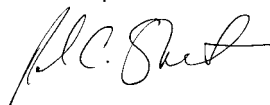
Jamie Baker
Gayle Fullerton
James Marshall
Jon Smallwood

REVIEWED AND APPROVED

NRL/PU/3430--10-529

RN: 11-1226-1046

April 2011



Paul C. Stewart, Captain, USN
Commanding Officer



www.nrl.navy.mil

www.nrl.navy.mil

2010 NRL REVIEW
